Low resolution structure and packing investigations of collagen crystalline domains in tendon using Synchrotron Radiation X-rays, Structure factors determination, evaluation of Isomorphous Replacement methods and other modeling.

Saad Mohamed

UNIVERSITE
JOSEPH FOURIER
SCIENCES. TECHNOLOGIE. MEDECINE

THESE PRESENTEE PAR

SAAD Mohamed

POUR OBTENIR LE TITRE DE DOCTEUR
DE L'UNIVERSITE JOSEPH FOURIER-GRENOBLE I
(ARRETES MINISTERIELS DU 5 JUILLET 1984 ET DU 30 MARS 1992)

Spécialité : Cristallographie et RMN Biologiques

Low Resolution Structure and Packing Investigations of Collagen Crystalline Domains in Tendon using Synchrotron Radiation X-Rays. (Structure Factors Determination, Evaluation of Isomorphous Replacement Methods and other Modelling.)

DATE DE SOUTENANCE: **le 22 Octobre 1994**

COMPOSITION DU JURY

Président :	Dr. G. Zaccai, directeur de Recherche au CNRS
Directeur de Thèse :	Prof. A. Miller, Président de l'Université de Stirling (Ecosse)
Rapporteurs :	Prof. W. Traub, Institut Weizmann (Israel)
	Dr. H. Chanzy, Directeur de Recherche au CNRS
Examinateurs :	Prof. J. Vicat, Université Joseph Fourier
	Prof. M. Van Der Rest, ENS LYON

Thèse préparée dans les Laboratoires de l'Installation Européenne de Rayonnement Synchrotron à Grenoble

Remerciements

Ce travail de thèse a été préparé sous la direction du professeur Andrew Miller de l'université d'Edimbourg, Ecosse, qui a mis à ma disposition les données de diffraction de tendon réalisées au synchrotron de Daresbury. La préparation des échantillons et les expériences ont été réalisées auparavant par les soins des Drs. Tim et Linda Wess du laboratoire du Prof. Miller. Je leur suis ici reconnaissant pour leur contribution à la partie expérimentale de cette thèse.

Je remercie aussi le professeur Carl-Ivar Brändén directeur de recherche à l'Installation Européenne de Rayonnement Synchrotron qui a accepté de prendre sous sa responsabilité les aspects administratifs et pratiques de mon travail. Le professeur Brändèn a mis à ma disposition toute sa compétence ainsi que les moyens matériels pour la poursuite sérieuse de ma thèse. Il m'a aussi permis d'avancer dans de nouveaux projets d'études structurales sur la Dystrophine humaine dont la fonction est tant attendue. Je lui dois ici toute ma gratitude.

Je remercie aussi l'Association Francaise contre les Myopathies pour son soutient pendant mes études.

Ce travail a aussi bénéficié d'une collaboration très étroite avec Didier Richard, informaticien à l'Institut Laue Langevin, pour la partie traitement d'images. Une grande partie des outils infographiques a été réalisée par ses soins notamment par l'écriture et l'adaptation de programmes pour les besoins spécifiques du traitement des données de fibres.

Je remercie aussi particulièrement le Dr. H. Müller de l'ESRF pour avoir accepté de relire, de corriger et et de suggérer les modifications necessaires.

Je remercie aussi tous les membres du personnel, les secrétaires et les documentalistes de l'EMBL, de l'ILL et de l'ESRF qui , par leurs aides pratiques m'ont permis de travailler dans de bonnes conditions.

Je remercie les membres et examinateurs de mon jury : Dr. G. Zaccai, Prof. W. Traub, Dr. H. Chanzy, Prof. J. Vicat pour les soins qu'il a apporté à la correction du manuscript ainsi que Prof. M. Van Der Rest.

à Nabil et Abderahmane ...

Table des matières

Résumé français

A. Qu'est ce que le collagène ?
Caractérisation des formes fibreuses du collagène.

Le Collagène est le constituant majeur de toutes les protéines des organismes vertébrés. Le pourcentage du collagène dans les organismes de mammifères ainsi que dans beaucoup d'espèces invertébrés est d'au moins 25%. C'est une protéine qui existe dans le monde animal sous une large variété de formes. Ainsi, on peut le trouver sous forme de filaments très fins, de feuillets transparents ou bien sous la forme de fibres épaisses très rigides. Le collagène est présent dans divers tissus comme les épidermes, les tendons, le cartilage, les os, la cornée ainsi que dans les lames basales.

On peut dire de façon simplifiée que le rôle principal du collagène est de contenir ainsi que de servir de support et d'intercalaire pour les tissus. La fonction essentiellement structurale du collagène est principalement due à la résistance mécanique des fibres de collagène. Cette fonction structurale est assurée grâce à une conformation moléculaire unique au niveau de la séquence d'acides aminés où l'on retrouve une très grande régularité dans la distribution des résidus et de façon périodique. Du fait de cette séquence unique, il résulte un alignement spécifique lors de l'assemblage extracellulaire ainsi que la formation de liaisons covalentes qui sont déterminantes pour la force extensible des fibres de collagène.

Le collagène est une protéine spéciale du fait de son caractère très ordonné et de sa résistance mécanique accrue. On le trouve sous forme de réseau structural flexible pour contenir d'autre tissus comme la peau et les gaines musculaires, ou bien sous la forme de cordage assurant la conjonction entre deux tissus comme les tendons et les ligaments. On le trouve aussi sous forme de réseau structural rigide comme dans les os, ou bien comme surface de jointure à très faible effet de friction dans les articulations ainsi que dans des tissus élastiques de transport de fluides comme les vaisseaux sanguins.

Différents types génétiques de collagène existent dans les espèces animales supérieures. Ceux-ci ont déjà été caractérisés par des études biochimiques qui ont ainsi permis de trouver des types différents de collagène dans chaque tissu (Miller E.J. *et.al.*, 1982). Ainsi le collagène de type I, qui est aussi le plus abondant, est le composant exclusif du tendon et des os. Par contre le collagène dit de type II est celui qu'on trouve dans d'autres tissus comme la peau ou les tissus vasculaires en même temps que le collagène de type III. Quant au collagène de type II on le trouve comme composant majeur du cartilage. Toutefois, les types I, II et III de collagène qui forment la matrice extracellulaire ont toujours une forme fibreuse périodique dans l'arrangement des molécules. Par contre, les autres types de collagènes, dits de type IV et V et que l'on trouve dans d'autres tissus n'ont pas cette structure fibreuse et périodique.

Les molécules de collagène sont formées de trois chaînes polypeptidiques qu'on appelle les chaînes-α

qui possèdent toutes les trois une séquence répétitive de la forme Gly-X-Y le long de la séquence primaire, les lettres X et Y désignent quant à elles tout autre acide aminé. Le collagène de type I possède deux types de chaînes polypeptidiques comme celles définies ci-dessus. Ces chaînes sont appelées α1(I) et α2(I) et s'associent dans un rapport stoechiométrique de 2. Chaque chaîne α1(I) possède 1014 résidus présents dans les deux chaînes peptidiques. Les dimensions des chaînes-α avant de leur repliement en triple hélice sont approximativement de 3000Å par 15 Å.

La conformation moléculaire du collagène en triple hélice a été déduite grâce à l'analyse de la séquence primaire ainsi qu'aux études de diffraction aux grands angles des rayons X. Le pas dans chacune des hélices gauches du collagène est de 2.9 Å approximativement. Les trois hélices sont ensuite enroulées les unes sur les autres autour du même axe pour former une super hélice droite qui constitue la molécule de collagène. Chaque brin de cette super hélice possède trois acides aminés par tour avec une distance inter résidu de 2.86Å. Ces trois chaînes sont à leur tour reliées par une translation axiale de 2.86Å et une rotation azimutale de 108°. Par conséquent, chaque brin est aussi un super enroulement de la chaîne polypeptidique avec une hauteur hélicoïdale de 30 résidus (voir figure I.2 p. 23). Le domaine central du collagène possède un résidu glycine tous les trois résidus, mais les extrémités de la molécule qu'on appelle les télopeptides ne possèdent pas cette régularité. Le repliement hélicoïdal de ces deux extrémités est donc interdit. Par exemple la chaîne α1(I) bovine possède 1014 résidus dans la partie centrale avec une glycine tous les trois résidus. L'extrémité N-terminale (N-télopeptide) possède 16 résidus et l'extrémité C-terminale (C-télopeptide) 25 résidus sans cette régularité (Fietzek & Kuhn, 1976; Helseth *et.al.*, 1979). 20% des autres acides aminés dans la molécule de collagène sont des prolines ou des hydroxyprolines dont l'importance pour la stabilisation ainsi que pour les propriétés du collagène sont maintenant discutées.

Le collagène (Rich *et. al.*, 1961; Traub et Piez, 1971) est l'une des rares protéines qui est de nature fibreuse plutôt que globulaire et volumineuse comme les autres structures protéiques. Nous avons vu que l'unité de base du collagène est formée de trois chaînes polypeptidiques différentes, chacune étant une hélice tertiaire gauche. La super hélice droite formée par l'enroulement des trois brins possède un caractère répétitif et une hauteur qui semblent être liés à la structure primaire de la chaîne polypeptidique. Les trois chaînes polypeptidiques sont maintenues ensemble par des liaisons hydrogènes qui sont seulement possibles du fait que les résidus glycines occupent toutes les troisièmes positions dans chacune des trois chaînes. Ainsi la séquence répétitive de la glycine et le couplage des chaînes par des liaisons hydrogènes sont les facteurs qui permettent aux trois chaînes de s'intégrer ensemble dans une super hélice stable. La figure I.1 p. 22 montre comment trois chaînes hélicoïdales gauches de type 3_1 peuvent être amenées à former une triple hélice de type collagène. Les hélices gauches 3_1 étant préférées à toutes autres structures secondaires à cause de leur contenance élevée en acides aminés prolines et hydroxyprolines. De ce fait le collagène est unique parmi les autres protéines car il est le seul à posséder un pourcentage très élevé de prolines et d'hydroxyprolines. De plus les restrictions stériques et de rotation propres à la stéréochimie de ces deux résidus font que la structure hélicoïdale gauche 3_1 soit en fait la plus probable. Finalement et au vu de cette description simple des molécules de type collagène nous pouvons conclure que la stabilité

de cette molécule dépendrait des facteurs suivants: (a) la quantité de résidus prolines et hydroxyprolines présents dans chaque chaîne polypeptidique ainsi que la distribution de ces résidus le long de la structure primaire, (b) la séquence glycine dans chacune des trois chaînes, et (c) le nombre et le mode de liaisons hydrogènes qui relient les trois chaînes.

Les tendons, tissus dont la fonction mécanique est évidente dans les organismes vertébrés, sont formés par des micro fibres, elles mêmes composées d'un arrangement régulier de molécules de collagène de type I. Depuis plusieurs décennies, des études biochimiques ainsi que des études de microscopie électronique et de diffraction de rayons X ont abouti à une caractérisation plus ou moins complète de la structure primaire ainsi que de la structure secondaire et tertiaire. Cependant, l'empilement et plus généralement l'organisation moléculaire du collagène dans le tendon ainsi que les spécificités de cette structure au niveau des interactions biochimiques ne sont pas encore résolus et nécessitent une étude structurale plus approfondie.

B. Avantages et buts de l'étude structurale des fibres de collagène au rayonnement synchrotron

Le rayonnement synchrotron est de plus en plus utilisé pour des études structurales de molécules d'intérêt biologique et plus particulièrement des fibres. Tous les laboratoires de rayonnement synchrotron sont actuellement équipés de dispositifs expérimentaux adaptés aux études structurales par diffraction de fibres (Nave *et.al.*, 1985). D'une façon générale, les cristaux ayant des grandes mailles cristallographiques (virus, ADN etc....) représentent une classe importante et à part. Ils représentent des structures pour lesquelles aucune analyse structurale n'est possible sans l'usage du faisceau X synchrotron (Ealick & Walter, 1993; Fisher & Johnson, 1993; Logan *et.al.*, 1993; Pflugl *et.al.*, 1993). En effet, la nature peu divergente du faisceau de rayons X synchrotron permet de séparer plusieurs ordres de diffraction rapprochés pour des mailles cristallines supérieures à 200Å. Des études très récentes sur des mégastructures sont d'ailleurs très représentatives de l'intérêt croissant que suscite le rayonnement synchrotron au niveau de la résolution structurale de molécules ou d'assemblages moléculaires géants et qui dépendraient exclusivement de la disponibilité des sources de rayonnement synchrotron.

En ce qui concerne les études de diffraction de fibres, les problèmes généralement rencontrés sont de natures différentes et concernent aussi bien les conditions expérimentales que l'analyse des données de diffraction. La diffusion diffuse qui résulte du désordre moléculaire ou de mouvements atomiques corrélés au sein du réseau cristallin ainsi que la très faible intensité des tâches de diffraction des échantillons biologiques sont les exemples les plus courants de difficultés rencontrées dans l'analyse des donnés de diffraction de fibres. Par contre, lors de l'usage du faisceau intense de rayons X synchrotron, nous obtenons généralement un rapport signal sur bruit des tâches de diffraction qui permettent d'observer sur les clichés des caractéristiques, qui d'ordinaire, sont difficilement observables dans les expériences avec des sources de rayons X classiques. Ainsi les expériences de diffraction sur des fibres de collagène avec le rayonnement synchrotron semblent être très

prometteuses pour une caractérisation structurale à basse résolution de ce matériau.

Le but principal de cette étude est d'évaluer les potentialités de la méthode du remplacement isomorphe pour obtenir les phases des données de diffraction de collagène natif et de ses dérivés lourds. Les problèmes majeurs rencontrés auparavant dans les études avec des sources de rayons X classiques ainsi que les solutions que je propose d'utiliser sont présentés ci-dessous:

1) Toute étude cristallographique nécessite la définition préalable d'un système cristallin unique (réseau de Bravais et groupe de symétrie) sur la base duquel les taches dans les clichés de diffraction seront indexées. Plusieurs systèmes ont déjà été proposés dont un récemment par Kajava (1991). Je consacrerai le chapitre 3 à la comparaison de ce nouveau modèle avec le modèle triclinique établi auparavant par Fraser et MacRae sur la base de données expérimentales. Pour cela j'ai écrit un programme de calcul du cliché de diffraction pour les deux modèles et j'ai comparé les résultats des deux modèles aux clichés expérimentaux. La maille triclinique de Fraser & MacRae est ainsi confirmée en utilisant des techniques d'amélioration et d'addition d'images qui ont permis de visualiser les détails dans les clichés de diffraction et de voir ainsi toutes les taches de diffraction même les plus faibles.

2) L'espacement des réflexions successives dans la direction des indices l du réseau réciproque, c'est à dire dans la direction parallèle à l'axe de la fibre dans le plan du film, est très petit. Les différents ordres sont entremêlés comme le montre la figure II.12 p. 41. Ceci est dû à la taille inhabituelle de la maille élémentaire du collagène qui fait à peu prés 678Å dans la direction de l'axe c ($c^* = 0.0015Å^{-1}$) et qui complique le processus d'intégration des réflexions. La solution serait de faire des mesures avec des distances échantillon-détecteur supérieures à celles déjà utilisées, mais on perd ainsi dans la résolution car les réflexions d'ordres supérieurs ne sont plus enregistrées sur les films à moins d'utiliser des détecteurs de surface plus grande (comme les récentes "image-plates").

3) L'axe de rotation des domaines cristallins dans la fibre n'est pas parallèle à un axe du réseau réciproque. Ceci exclu donc l'usage des méthodes de rotation de monocristaux. De plus, l'absence de précision dans la mise au point expérimentale de l'inclinaison de la fibre par rapport au faisceau de rayons X rend encore plus difficile l'indexation des ordres successifs dans la direction de l'indice l.

4) L'élargissement des taches, dû à la taille réduite des microcristaux dans l'échantillon, n'est pas défini pour chaque réflexion, par conséquent chaque tache sera intégrée manuellement.

5) Le bruit de fond ainsi que la diffusion diffuse sur les films et plus particulièrement sur les axes méridional et équatorial sont très importants. L'usage de plusieurs film dans une même cartouche permet de collecter les taches très intenses sur le dernier film où le bruit de fond et la diffusion diffuse sont fortement atténués.

6) Les domaines cristallins dans le tendon sont aussi désorientés de 1 ou 2 degré selon la direction polaire (voir figure II.3 p. 30). Il en résulte que les tâches de diffraction sont arquées, principalement dans la direction de l'axe Z. Ces arcs sont dépendants de la position des taches sur le film et leur effet n'a pas pu être simulé par les programmes de prédictions (mais ceci est

en cours de réalisation). De plus une correction supplémentaire, dite facteur de Lorentz, doit être apportée à chaque intensité intégrée. Elle est nécessaire pour corriger certains effets géométriques propres à la diffraction par les fibres.

7) L'intensité des taches de Bragg des fibres de collagène possède une dynamique très importante surtout en ce qui concerne les intensités sur les axes principaux (c'est à dire le méridien et l'équateur) du cliché de diffraction quand on les compare à celles des autres régions du film. Pour cela on utilise plusieurs films dans une même cartouche pour mesurer les intensités faibles sur les premier films et celles qui sont très fortes sur les derniers. Ceci pose un problème d'alignement et d'orientation des différents films exposés dans la même cartouche. Le chapitre 5 montre la méthode de traitement numérique des images permettant de déterminer l'origine du cliché de diffraction et la réorientation des différents films d'une même cartouche. Ainsi les données relatives à une expérience seront collectées de façon plus rapide et plus sûre produisant un jeu de facteurs de structure pour le tendon natif et pour chaque dérivé lourd. La saturation des pics aussi a toujours été contrôlée avant de procéder à l'intégration.

Le but principal de ce travail est de collecter le maximum de données quantitatives (c'est à dire des facteurs de structures) des fibres de collagène du tendon afin de permettre une étude structurale à basse résolution et d'élucider ainsi le problème de l'empilement des molécules dans les domaines ordonnés de collagène. La méthode du remplacement isomorphe par des atomes lourds sera testée puisque c'est la méthode la plus couramment utilisée dans les études structurales aux rayons X des protéines. Nous attendons de cette méthode qu'elle conduise à la compréhension du mode d'empilement des molécules dans les cristaux de collagène et ce, à très basse résolution, en fournissant les phases des réflexions natives. En effet la solution des phases pour les facteurs de structures de la structure native est le problème crucial et seule la méthode du remplacement isomorphe permet de le résoudre de façon mathématique. Par ailleurs, aucune autre source d'information expérimentale sur les phases n'est applicable comme par exemple la méthode directe qui n'est possible qu'avec un nombre d'atomes très faible dans la structure. De plus, les clichés de diffraction avec des dérivés lourds ont été réalisés au synchrotron de Daresbury (Angleterre) et l'on voit de façon perceptible des changements dans l'intensité des taches de Bragg diffractées. Ceci prouve que la méthode des dérivés isomorphes (MIR) peut être riche en informations.

Après une introduction aux méthodes générales utilisées en cristallographie des fibres aux rayons X une partie de ce travail concernera la mesure de la taille moyenne des domaines cristallins le long de l'axe de la fibre. Nous savons que le tendon est constitué de plusieurs domaines microscopiques ayant une structure cristalline et la caractérisation de la taille de ces domaines ouvre de nouvelles perspectives grâce au propriétés du rayonnement synchrotron. En effet, si l'on arrive à isoler un des domaines monocristallins du tendon qui fasse des dimensions de l'ordre de quelques microns alors une étude cristallographique à haute résolution est possible par les méthodes du cristal tournant en utilisant ces domaines monocristallins. Ceci est uniquement possible grâce à l'avènement de sources synchrotrons très intenses qui permettent de réaliser des expériences avec des faisceaux de rayons X

très focalisés dont les dimensions peuvent atteindre le domaine submicronique au niveau de l'échantillon (voir à ce sujet l'ESRF Beamline Handbook).

Ensuite, la périodicité unidimensionnelle du collagène dans le tendon étant établie d'après l'observation des données sur l'axe meridional, nous supposerons que le tendon est de nature cristalline et essayerons de résoudre sa structure à basse résolution. Le système cristallin sera celui déjà défini par d'autres auteurs et c'est sur la base de ce système que mes données de diffraction seront interprétées. Pour cela j'ai écrit un programme de calcul numérique qui fait des prédictions du cliché de diffraction par des fibres; les différents paramètres expérimentaux y sont considérés comme l'inclinaison de la fibre par rapport au faisceau direct ou la désorientation polaire des domaines cristallins dans le tendon. Des moyens informatiques et de traitement d'images sont à ma disposition pour travailler sur des images de films après numérisation. Le traitement d'images a bénéficié d'une contribution de D. Richard, informaticien à l'institut Laue-Langevin (Grenoble) qui a développé des outils graphiques et numériques puissants.

C. Méthodes et techniques d'études structurales des fibres et les améliorations obtenues dans ce travail

La diffraction des rayons X par des fibres biologiques naturelles a longtemps été une technique de caractérisation qualitative des tissus étudiés. Les informations obtenues par ce biais étaient limités à l'observation de taches discrètes sur le cliché de diffraction qui indiquaient un arrangement périodique des molécules sans pour cela permettre de résoudre des structures 3-D. Certains travaux à très basse résolution ont cependant été possibles grâce à des synthèses de Fourier à une dimension mais où les phases des réflexions étaient négligées. Une telle synthèse de Fourier tenant compte des amplitudes seulement et pour des données à une dimension est valable pour quelques ordres de réflexion seulement car on peut dans ce cas tolérer des approximations sur les valeurs numériques des phases. Dans le cas du collagène nous avons obtenu des clichés de diffraction à moyenne résolution qui montrent clairement l'existence d'un ordre cristallin à trois dimensions. Nous avons en plus des taches méridionales très intenses et un ensemble de taches plus faibles réparties sur des lignes verticales et dont l'intersection avec l'équateur est en accord avec des périodicités latérales pour l'arrangement moléculaire. Plus tard je montrerai que toutes ces taches sont prévisibles quand on calcule les taches de Bragg obtenues avec un réseau de Bravais triclinique auquel on fait subir une rotation complète autour de l'axe de la fibre.

Les fibres sont des systèmes formés de molécules allongées qui sont plus ou moins alignées le long de l'axe de la fibre. Ces molécules forment des domaines cristallins plus ou moins étendus et les différents domaines ont une désorientation azimutale aléatoire autour de l'axe de la fibre (voir figure II.3 p. 30). Les clichés de diffraction dans ce cas sont similaires à ceux obtenus dans les méthodes du cristal tournant. Les expériences de diffraction avec des fibres sont généralement réalisées en mettant les fibres dans le faisceau de rayons X et un film détecteur à une distance convenablement choisie par l'expérimentateur. Les fibres sont normalement perpendiculaires au faisceau direct et on obtient sur le

détecteur deux axes principaux: la direction parallèle à l'axe de la fibre et passant par le centre est appelée le méridien et l'axe qui lui est perpendiculaire et dans le plan du film est appelé l'équateur. Souvent on incline la fibre légèrement vers la source du faisceau primaire ce qui permet d'enregistrer des ordres supérieurs sur le méridien et d'augmenter ainsi la résolution de l'expérience. La diffraction enregistrée sur l'équateur donne une information sur l'ordre latéral des molécules. Celle-ci est souvent moins bonne que la diffraction observée sur le méridien car on y observe des taches très faibles et plutôt diffuses superposées à un bruit de fond très intense. Elle montre en tout cas que l'ordre dans la direction latérale est moins important que celui dans la direction parallèle à la fibre. La diffraction sur le méridien nous permet quant à elle d'étudier la structure en projection sur l'axe parallèle à l'axe de la fibre. La figure II.2 p. 29 montre le dispositif expérimental schématique pour réaliser une expérience de diffraction avec des fibres.

Pour toute étude structurale aux rayons X, il est d'abord nécessaire de définir les caractéristiques géométrique exacte de la fibre. Des études préalables au microscope électronique (Hulmes *et.al.*, 1981) ont démontré l'existence de micro domaines formant des fibres de très petite taille dans le tendon. Ces domaines sont des groupements réguliers de molécules de collagène de diamètre de 200 à 300 nm et sont comparables aux particules cristallines dans une poudre. Les orientations azimutales de ces domaines sont aléatoires et prennent toutes les valeurs possibles entre 0 et 2π. Ainsi les fibres sont analogues aux poudres mais les orientations s'effectuent de préférence autour d'un seul axe, l'axe de la symétrie cylindrique. Les domaines cristallins de collagène dans le tendon possèdent aussi une distribution d'orientations polaires (figure II.3 p. 30) de faible amplitude dont une estimation à 1 ou 2 degrés a été faite par Fraser et Suzuki (1976). La maille unité du cristal de collagène est une maille triclinique définie par les six paramètres habituels a^*,b^*,c^*,α^*, β^* et γ^*. Aussi, vu la symétrie cylindrique du problème le réseau réciproque sera décrit dans un système de coordonnés sphérique polaire ou l'axe vertical Z joue un rôle évident (figure II.4 p. 30). La géométrie de diffraction et les différentes relations sur les vecteurs du réseau réciproque sont montrés dans les figures II.5 et II.6 p. 31.

Les études structurales sur les protéines par synthèse de Fourier ont bénéficiées de quatre techniques majeures pour le calcul des structures. Ces techniques sont: 1) le calcul des cartes de Patterson 2) les méthodes directes 3) la méthodes du remplacement isomorphe et 4) la diffusion anomale. Alors que les deux premières méthodes ne s'appliquent pas pour des macromolécules de la taille du collagène, il est vraisemblable que la méthode du remplacement isomorphe sera capable de produire des cartes de densité au moins à basse résolution et ceci sera l'objet principal de notre étude.
L'intégration et l'obtention des facteurs de structures pour le collagène natif et de ses dérivés restent le problème à résoudre car il n'existe pas de logiciel connu qui permette d'analyser les films de diffraction. Beaucoup de difficultés sont propres à la diffraction par les fibres du fait de la géométrie particulière soit au niveau du positionnement expérimental de l'échantillon soit à un niveau plus méthodologique comme la géométrie du réseau réciproque. En plus des erreurs statistiques, qui

limitent la précision sur les taches de diffraction observées, il existe des erreurs qui empêchent l'enregistrement systématique d'intensités intégrées. Par exemple, les effets d'absorption, d'extinction, de polarisation, les réflexions superposées, les effets de désordre et de défaut de structure, les effets d'aberration géométrique, ainsi que le bruit de fond intense et le facteur de Lorentz (Arndt & Willis, 1966). Nous diverses corrections que j'ai jugées importantes pour une étude structurale à basse résolution seront exposées en détails plus loin (figure II.7 p. 37 et II.15 p. 46). Une section spéciale est consacrée à l'étude des réflexions superposées qui sont le problème critique dans la diffraction des fibres. Je montrerai, après calcul des positions de taches de Bragg, que certaines réflexions sont utilisables même à haute résolution mais que d'autres seront superposées. La superposition des taches de diffraction des fibres est problématique surtout dans la région équatoriale où les données à basse résolution sont importantes pour comprendre l'arrangement latéral des molécules dans la maille cristallographique. Il existe aussi un phénomène important dans les expériences de diffraction par des fibres qui est le bruit de fond très intense sur le film. Celui-ci qui est encore plus intense lorsque l'on utilise le rayonnement X synchrotron et trouve son origine dans des effets divers à l'intérieur de l'échantillon. Il doit être soustrait de façon correcte lors de l'intégration des taches de Bragg des fibres. J'ai pour cela utilisé un processus manuel d'intégration des taches de Bragg de façon à caractériser le bruit de fond de façon plausible pour chaque réflexion. Toutefois, la correction majeure que j'ai appliquée lors de la collecte de données sur le tendon est le facteur de Lorentz. Une justification en est donnée dans un paragraphe traitant spécialement de cette correction. La correction de Lorentz est extrêmement importante pour la diffraction par les fibres et doit tenir compte d'une géométrie spéciale à chaque expérience.

Finalement, j'utiliserai la méthode du remplacement isomorphe pour deux raisons principales. La première, est que la plupart des structures biomoléculaires résolues l'ont été grâce à cette technique et deuxièmement, parce que les expériences réalisées par T. et L. Wess montrent, de façon évidente, des changements significatifs dans les clichés de fibres. L'ensemble des expériences contient des clichés pour le collagène natif plusieurs dérivés lourds contenant respectivement l'élément Au, I, Pt ainsi que deux autres expériences: une avec de l'acide phosphotungstique (PTA) et une avec du polyéthylène glycol (PEG). L'acide phosphotungstique est d'habitude utilisé dans les études de macromolécules en microscopie électronique pour le contraste qu'il introduit. Son usage est recommandé dans les expériences de diffraction de rayons X avec les très grosses molécules biologiques pour s'assurer qu'une modification sensible est introduite dans les intensités diffractées. Quand à l'iode, il est admis que les sites de fixation de cet élément dans la maille unité sont très peu nombreux car l'iode est supposé se fixer de préférence sur la tyrosine (d'après Miller et Wess, communication orale). Or il existe un seul résidu tyrosine dans la séquence primaire du collagène et de plus la tyrosine se trouverait à une seule extrémité de la molécule. Les autres dérivés lourds sont supposés marquer le collagène en plusieurs sites d'où une difficulté supplémentaire dans l'interprétation ultérieure des cartes de Patterson.

D. Résultats

Plusieurs modèles pour l'empilement des molécules de collagène dans le tendon ont été proposés depuis plusieurs dizaines d'années. Ces modèles étaient obtenus à partir de l'interprétation des clichés classiques de microscopie électronique ou bien de l'analyse semi-qualitative des clichés de diffraction (avant l'utilisation du rayonnement synchrotron) de rayons X (Woodhead-Galloway *et. al.*, 1975; Veis & Yuan, 1975; Smith, 1968; Miller & Parry,1973; Nemetschek & Hosemann, 1973). Cependant aucun de ces modèles ne pouvait être conforme à tous les résultats expérimentaux et il a fallu attendre les *travaux de Fraser et MacRae (1981) pour obtenir un jeu de paramètres cristallographiques calculés* à partir des clichés de diffraction de tendon marqué à l'acide phosphotungstique. La maille triclinique ainsi obtenue tenait compte des réflexions méridionales et équatoriales et a été calculée par la méthode des moindres carrés. J'ai supposé cette maille comme étant la mieux adaptée pour une étude cristallographique à basse résolution mais auparavant il a fallu la vérifier. En 1991 Kajava a proposé une nouvelle maille cristallographique (voir table III.2 p. 52). Cet auteur prétend être en accord avec les expériences précédentes. Dans le chapitre 3 j'ai comparé le modèle de Kajava et celui obtenu auparavant en faisant des prédictions des taches de Bragg des deux modèles et en les comparant aux résultats des dernières expériences obtenues au synchrotron. Il en résulte que le modèle proposé par Kajava est faux car la maille dans ce cas est très grande et ne produit pas les réflexions très faibles supplémentaires comme l'affirme Kajava. De plus le modèle classique dont les paramètres sont listés dans la table III.1 p. 52 semble donner la meilleure interprétation des clichés de diffraction en le superposant aux films obtenus avec du tendon marqué à l'acide phosphotungstique. J'ai pour cela utilisé des techniques d'analyse et de filtrage numérique d'images afin de supprimer le bruit de fond des clichés de diffraction et de permettre de voir toutes les taches de diffraction y compris celles de très faible intensité. L'étude structurale à 3 dimensions se fera donc sur la base de ce modèle.

Dans le Chapitre 4, j'ai pu montré que les domaines ordonnés dans le tendon sont assimilables à des domaines monocristallins de taille moyenne longitudinale d'environ 1 µm. Après examen de la théorie de diffraction par des cristaux de petites tailles, j'ai utilisé dans le chapitre 4 les techniques de caractérisation des cristaux dans les méthodes de poudres pour calculer l'élargissement des taches de Bragg sur le méridien et de calculer ainsi la taille des cristaux selon la direction parallèle à l'axe de la fibre. J'ai utilisé pour cela deux méthodes différentes mais qui ont donné les mêmes résultats. Tout d'abord, j'ai enregistré le profil du faisceau direct qui donne une mesure de la divergence *instrumentale de l'expérience. Ensuite j'ai mesuré les ordres 1 à 9 du collagène qui ont nécessité une* mesure aux très petits angles des ordres de diffraction pour une maille qui fait 678Å le long de la fibre et j'ai soustrait la correction obtenue par le faisceau direct. L'équation d'Scherrer stipule qu'un élargissement de la forme

$$B(2\theta)=\frac{0.94\lambda}{L\cos\theta}$$

intervient lors de la diffraction par des poudres de monocristaux où **B(2θ)** désigne l'élargissement de la raie selon la direction 2θ sur le film et **L** désigne la taille moyenne des cristaux selon la perpendiculaire à la direction définie par les indices hkl de la raie. Une autre méthode, complètement différente (dite de Stokes-Wilson) donne une formule identique à une constante près, mais où l'élargissement de raie est calculé à partir de l'aire de la courbe délimitant le profil de la raie. La taille selon la direction parallèle à l'axe de la fibre des cristaux de collagène ainsi calculée est de 1µ environ. Quand on sait que l'axe c de la maille triclinique définie pour le collagène fait à peu prés 678Å nous obtenons des domaines cristallins formés par approximativement 15 mailles cristallographiques. Ce résultat est curieux quand on sait que le calcul de Scherrer ou de Stokes-Wilson part de l'hypothèse d'un nombre très grand de mailles élémentaires dans les cristaux. Je n'ai pas pu calculer la dimension moyenne dans les directions perpendiculaire à l'axe de la fibre dans le plan ab du cristal (c'est à dire aussi dans les plans hk0 du réseau réciproque) car ceci nécessite des conditions expérimentales différentes où les réflexions telles que (h,0,l) et (0,k,l) doivent être convenablement enregistrées. Néanmoins, j'ai donné les principes d'une telle expérience dans le chapitre 4 et j'ai obtenu un résultat qui caractérise de façon approximative la taille des domaines cristallins selon la direction où l'ordre est apparemment le plus évident. Cette expérience a été faite dans le but de savoir s'il est possible d'envisager des expériences de diffraction avec des petits monocristaux de collagène extrait du tendon et de permettre ainsi une étude cristallographique classique. L'usage du synchrotron avec des faisceaux extrêmement parallèles et focalisés au niveau de l'échantillon est en projet à l'ESRF (et ailleurs) où la dimension minimale déjà atteinte est de l'ordre de 10µ actuellement et où le domaine du micron est en vue.

Dans le chapitre 5 j'ai traité du problème de l'exploitation des films de diffraction par les fibres de collagène. Les expériences accumulées par l'équipe d'Edimbourg sur plusieurs années ont été faites avec l'objectif de pouvoir extraire des informations structurales sur le collagène du tendon mais surtout dans le but d'évaluer les méthodes MIR pour la diffraction des fibres. Après exposition au faisceau de rayons X, les films sont numérisés de façon habituelle avec une ouverture de 50µ. Mais là où d'autres études cristallographiques de protéines disposent des outils informatiques nécessaires à l'extraction des intensités intégrées il n'existe, à ma connaissance, aucun programme qui fasse la même évaluation pour les données de fibres. J'ai du pour cela mettre au point un outil de traitement d'image mais surtout un programme de prédiction des clichés de diffraction pour les fibres tenant compte de tous les paramètres expérimentaux. Ceux-ci sont en effet obtenus de façon approximative lors de la réalisation de l'expérience et ont nécessité un affinement plus précis notamment en ce qui concerne l'angle d'inclinaison de la fibre par rapport au faisceau direct. J'ai ensuite procédé à l'orientation et la superposition des films de façon interactive car les films exposés dans la même cartouche ont été numérisés séparément ce qui nous a fait perdre l'orientation originale des films dans la cassette. La superposition des films n'est pas obligatoire mais cela m'a permis de tester plusieurs effets sur les films successifs. La saturation des taches très intenses par exemple doit être contrôlée et dans ce cas l'intégration a été faite sur les derniers films avec une correction pour l'absorption due au chemin de la radiation dans les premiers films. Plusieurs images expérimentales et les images

calculées peuvent être juxtaposées à l'écran. Ensuite les taches sont intégrées et écrites dans un fichier intermédiaire. Le profil de la boite d'intégration peut être rectangulaire ou ellipsoïdal selon la position et la forme de la tache de Bragg qu'on désire intégrer. L'orientation des taches et leur distribution sur le film n'est pas uniforme et ceci a nécessité un traitement manuel très long de tous les films afin de garantir un jeu minimum de facteurs de structure correct pour les calculs de Fourier. Les intensités mesurées sur le film sont corrigées et le facteur de Lorentz appliqué puis les réflexions sont identifiées par leurs indices de Miller. Cependant, quelques ambiguïtés restent sur les indices de certaines taches trop rapprochées sur le film ou bien pour les taches dont il a été impossible d'attribuer des indices de Miller faute d'orientation suffisante de la fibre. Une explication détaillée sur ces effets est donnée dans le chapitre 5. Ce procédé m'a permis, toutefois, d'obtenir un jeu de facteurs de structure pour le collagène natif et trois de ses dérivés. La qualité de ces mesures étant plus ou moins reflétée par la déviation standard calculée pour chaque réflexion, ceci m'a amené à inclure dans le jeu de données des réflexions pour lesquelles, soit l'intensité était trop faible, soit il y avait une confusion entre une vraie tache de Bragg et du bruit de fond sur le film. Ces mesures étaient toutefois justifiées par le fait que premièrement, nous avons besoin pour chaque réflexion native de la même réflexion mesurée pour le dérivé lourd afin de détecter des différences isomorphes et de calculer la phase de la réflexion native et, deuxièmement, par le fait que les transformées de Fourier tiennent compte de la précision sur une réflexion en la pondérant par un poids qui est l'inverse du carré de la déviation standard. Les réflexions que j'ai obtenues pour chaque expérience sont présentées dans le chapitre 6 où j'ai donné la liste des réflexions méridionales avec une résolution allant jusqu'à 8Å. Je donne surtout la liste des réflexions, natives et dérivées, jamais obtenues auparavant qui sont sur les lignes verticales d'indices de Miller (-1,0,l) et (1,0,l). Le reste des données sera détaillé en annexes. Ces données tridimensionnelles ne sont, pour ainsi dire, qu'une première tentative suite à la mise en oeuvre d'une technique de collection de données de fibres. Certaines corrections sur les facteurs de structure peuvent s'avérer nécessaire quand à la valeur de l'amplitude mesurée qui a pu être confondue avec du bruit de fond sur le film ou bien une correction sur les indices de Miller des réflexions.

Ensuite, j'ai analysé ses réflexions avec les routines fournies par l'ensemble CCP4 de calcul cristallographique pour les protéines et j'ai obtenu quelques statistiques sur les facteurs de structures que j'ai présenté dans les tables du chapitre 6. Ces statistiques ont permis, à priori, de juger de la qualité des données collectées. Toutefois les données brutes (c'est à dire celles que j'ai produites dans les annexes après traitement des films seulement) ont subi un ensemble d'opérations à l'aide de la programmathèque de CCP4, comme la moyenne de plusieurs réflexions et la fusion des réflexions reliées par des opérations de symétrie pour donner un ensemble de réflexions minimales (corrigées) de la symétrie P1.

Ainsi, les facteurs de structure obtenus dans ce travail pour le collagène natif permettent, en l'absence de phases, de modéliser une structure et de calculer les facteurs de structure pour ensuite les comparer aux facteurs de structure expérimentaux. De plus, les mesures de diffraction aux très petits angles qui ont servi à calculer la longueur moyenne des cristaux ont aussi fourni les facteurs de structure des ordres 1 à 9 après intégration de ces ordres qui d'habitude ne sont pas enregistrés dans

les expériences de diffraction aux grand angles. L'ensemble de données que j'ai obtenues concerne donc les facteurs de structure du collagène natif, d'un dérivé contenant l'élément Iode , un dérivé contenant l'élément Au et un troisième contenant du PEG. Le PEG ne contient pas d'élément lourd mais j'ai collecté les données de ce dérivé pour tester la méthode que j'ai développée et pour évaluer la méthode MIR pour des fibres de collagène.

Par conséquent j'ai calculé des cartes de Patterson différence à basse résolution dans la maille triclinique en faisant à chaque fois une Patterson différence entre les données natives et les données des dérivés isomorphes. J'ai cherché à visualiser si des pics correspondant à des atomes lourds sont présents. Les figures en fin du chapitre 6 montrent les cartes calculées avec la résolution optimale selon les trois axes principaux de la maille triclinique. La résolution dans la direction de l'axe *b* est inférieure à celle obtenue selon l'axe *a* ce qui correspond bien au fait que nous avons plus de réflexions superposées sur les lignes verticales d'indices généraux (h,k,l) avec k≠0 (voir paragraphe sur les réflexions superposées pour la diffraction par le collagène). Toutes ces cartes (Fig. VI.26 p. 143 et Fig. VI.27 p. 144) montrent un pic très fort à l'origine mais ceci est un résultat normal dans une Patterson différence. Par contre, j'ai observé des différences entre les trois cartes où l'on voit que la carte calculée avec le dérivé Au montre plusieurs pics répartis dans le volume de la Patterson différence alors que la carte calculée avec les deux autres dérivés I et PEG ne montrent pas de pics très prononcés. La recherche des positions des atomes lourds ne sera pas pour autant très facile car nous avons d'abord des cartes à basse résolution et aussi le nombre des atomes lourds dans la maille n'est pas connu. Dans le cas où des informations sur la position des atomes lourds seraient disponibles à partir d'autres sources (par exemple par des modélisations ou des simulations) nous pourrions calculer une Patterson différence et la comparer aux cartes expérimentales obtenues dans le chapitre 6 afin de valider le modèle.

Le chapitre 7 est consacré à une étude de diffraction de fibres de collagène par simulation. J'ai d'abord construit un modèle de molécule de collagène à partir d'un brin de trois hélices trouvé dans la banque de données de coordonnées atomiques de protéines PDB. Chen *et.al.* , (1991) ont construit ce modèle de collagène en triple hélice en utilisant la modélisation moléculaire et en faisant des calculs de minimisation d'énergie en utilisant le champ de force de Kollman. Ils ont pu ainsi obtenir un modèle stable d'une séquence tripeptidique riche en glycines et prolines comme c'est le cas pour le collagène naturel. J'ai donc recueilli le modèle dans la PDB en choisissant le modèle où chaque hélice contient la séquence $(Gly\text{-}Pro\text{-}Hyp)_{16}$ et où les trois hélices sont enroulées en une triple hélice droite comme dans le collagène. La longueur du brin original est à peu près de 100Å. Ensuite, j'ai généré, à partir de ce modèle, une molécule complète de longueur 4.4xD≈3000Å où D≈678Å est une périodicité de la fibre de collagène définie dans le chapitre 1. Les télopeptides (les télopeptides sont les quelques acides aminés qui se trouvent à l'extrémité C-terminale et N-terminale de la molécule de collagène et qui ne possèdent pas la conformation en triple hélice) n'ont pas été modélisés car nous ne connaissons pas leur conformation exacte. Leurs séquences respectives, en effet, ne possèdent pas la séquence répétitive Gly-X-Y expliquée plus haut. J'ai ensuite simulé les clichés de diffraction par des fibres après avoir construit les domaines cristallins de collagène contenant le modèle ci-dessus. Le problème

fondamental était de savoir comment les molécules de collagène sont orientées dans la maille primitive qui est plus petite que la molécule de collagène. Pour cela j'ai simulé plusieurs cas de figures où la molécule modèle définie ci-dessus est un segment rigide de longueur moyenne 3000Å de densité électronique moyenne à peu prés égale à celle du collagène naturel. Cette molécule doit être contenue dans une seule maille élémentaire sous la forme de cinq fractions. Chaque fraction appartient à une molécule intégrale mais qui traverse les mailles avoisinantes. Une molécule doit avoir une extrémité qui commence, par exemple à l'origine de la maille et se prolonger par continuité jusque dans la cinquième maille au dessus (ou en dessous) en ayant ainsi une direction bien définie par rapport aux vecteurs élémentaires de la maille unité (a,b et c). Les différents empilements dans ce cas où la molécule, pour simplifier le problème, ne peut pas avoir une trajectoire sinueuse, sont obtenus lorsque la molécule pointe vers des directions différentes dans la maille unité. Ces différentes directions (voir Fig. VII.2 p. 152 et p. 153) ont été définies par Fraser *et.al.* (1981), par des règles de sélection simples introduites dans le chapitre 7. Ces règles de sélection ne doivent en aucun cas définir des orientations telles que les translations du cristal amènent un fragment de la molécule à être superposé à un autre fragment dans la maille voisine ou bien à une structure où les molécules sont empilées de façon très dense dans une seule région de la maille triclinique. De plus, le saut qui est dû au fait que le cinquième fragment de la molécule a une longueur de 0.4D seulement et qui donne l'aspect strié aux micrographies de microscopie électronique doit être évident dans tous les modèles. J'ai enfin simulé les clichés de diffraction de fibres pour trois modèles simples de collagène avec des orientations définies avec les règles mentionnées ci-dessus et un modèle où les atomes étaient placés de façon aléatoire dans la maille triclinique afin de valider les résultats. J'ai ainsi obtenu des figures de diffraction qui ressemblent fortement aux clichés expérimentaux et où l'on peut surtout noter la présence des lignes verticales de réflexions d'indices (-1,0,l) et (1,0,l) et autres mais aussi des réflexions d'indice $l \approx 75$ correspondant à la périodicité de l'hélice de base. Les effets de désorientation et de taille de domaines cristallins ont été simulés et sont en accord avec les clichés expérimentaux.

E. Conclusions

En conclusion j'ai effectué un travail de traitement et d'analyse de données 3D pour le collagène cristallin du tendon jamais réalisé auparavant. La structure du tendon est très originale du fait que c'est la seule protéine connue qui se trouve à l'état très ordonné dans l'organisme vivant. L'importance du collagène dans le monde vivant n'est plus à démontrer et les caractérisations structurales que j'ai faites permettent une meilleur compréhension du mode d'empilement des molécules dans le tendon et de leur influence sur les propriétés mécaniques de ce tissu. Une expérience aux très petits angles m'a permis de mesurer la taille moyenne longitudinale des cristaux. J'ai aussi montré que la maille cristallographique proposée par Kajava est en contradiction avec les résultats évidents des clichés de diffraction. Le nouveau modèle est en fait une structure où la maille trouvée est probablement une maille multiple. Ensuite, avec l'aide d'outils graphiques et de logiciels très puissants j'ai pu collecter des facteurs de structure pouvant mener à la détermination structurale à basse résolution. Les

méthodes d'obtention et les corrections ajoutées à ces facteurs de structure sont celles qui me sont apparues les plus adéquates mais d'autres méthodes sont possibles et doivent être mises en euvre dans le but de comparer leurs résultats à ceux de ce travail. La méthode de collecte de données a été conçue de façon à minimiser les erreurs systématiques soit sur l'intensité intégrée soit sur les indices des réflexions. Les ordres méridionaux sont collectés jusqu'à la résolution de 8Å et constituent les données mesurées avec la meilleure précision. Les jeux de réflexions situées sur les lignes verticales d'indices (-1,0,l) et (1,0,l) sont aussi déterminés pour le collagène natif et les dérivés avec une bonne précision mais les réflexions sur l'équateur sont partiellement voir complètement superposées et la précision sur les intensités intégrées est plus faible. Les autres réflexions 3D que j'ai obtenues sont déterminées avec moins de précision mais représentent un préalable en vue de la détermination structurale 3D du collagène. J'ai ainsi testé la méthode MIR à basse résolution en calculant des cartes de Patterson différence entre les dérivés et le collagène natif. Le calcul a été fait avec toutes les données obtenues sachant que les données erronées introduisent un bruit de fond global dans les synthèses de Fourier. J'ai mis en évidence les différents types de Patterson différences selon qu'on travaille avec les mesures du dérivé Iode ou celle du dérivé Or ou bien avec celles du dérivé PEG. Le dérivé Or qui est supposé contenir le plus d'atomes lourds par maille élémentaire montre quelques pics susceptibles d'être interprétés comme des pics de Patterson dus à des atomes lourds. Le dérivé Iode par contre ne montre pas la même distribution de pics marqués comme le dérivé Or et ceci nous amène à penser que la méthode MIR est une bonne approche au problème des phases.

Finalement j'ai construit un modèle de molécule de collagène contenant trois hélices riches en prolines et glycines. Les molécules ainsi construites ont servi d'approximation à la densité électronique réelle des molécules de collagène et j'ai pu construire des domaines cristallins ordonnés de maille triclinique comme définie auparavant. Des figures de diffraction de fibres ont été générées et m'ont permis d'étayer le modèle de l'empilement possible des molécules de collagène en domaines monocristallins orientés aléatoirement autour de l'axe de la fibre macroscopique. Les modèles obtenus sont en accord avec les données obtenues au microscope électronique à savoir les zones périodiques de faible et haute densité. Ce modèle m'a aussi permis d'avoir un jeu de facteurs de structure et surtout un jeu préliminaire de phases pouvant servir pour les réflexions natives ou bien pour l'obtention directe des phases expérimentales par des méthodes d'aplatissement de solvant.

Chapter 1
Introduction

A. Collagen in Life.

Collagen is the major protein constituent of all vertebrates; about 25% of the body protein of mammals and many invertebrate species is collagen. It occurs in a wide variety of forms as fine filaments, transparent sheets and thick coarse fibres and in such diverse tissues as skin, tendons, cartilage, bone, cornea and basement membrane.

Collagen exists to contain, support and interconnect tissues. The special function as a supporting framework of the body is largely dependent on the high tensile strength of collagen fibres. Collagen fulfils this function by means of a unique molecular conformation due to regular repeating units in its amino acid sequence, the subsequent highly specific alignment in the extracellular aggregation of the molecules and finally the formation of covalent cross links to provide the ultimate high tensile strength of the fibre. Collagen is an unusual protein, it is highly ordered, has a high tensile strength and is virtually inextensible to overcome mechanical problems. It is used as a flexible network to contain other tissues, e.g. skin and muscle fascia, as a rope-like material to connect one tissue to another in tendons and ligaments, as a rigid structural framework in bone, as a low-friction ball-bearing type surface in the joints and as a liquid transport system of pipes in the circulation of blood.

B. Characterisation of Fibrous Forms of Collagen.

1. Biological Characterisation.

In higher animals collagen forms a major structural component of connective tissue, including tendon, bone, cartilage, skin, vascular tissues, and basement membranes. Within a given organism, several genetically distinct types of collagen are found. These genetic types have been characterised biochemically and each kind of tissue is found to have a characteristic composition of collagen genetic types (Miller E.J. *et.al.*, 1982). The most prevalent genetic type, hereafter designated type I is found as the nearly exclusive collagenous component of tendon and bone, whereas in many other tissues, such as skin, vascular tissues, and reticular tissues, type I is found together with a lesser amount of type III collagen. Type II collagen is the major component of cartilage. The three interstitial collagens of type I, II and III form periodic fibrils and are considered to occur largely in fibrous form in the extracellular matrix. Some 18 collagen types have now been reported. Other genetic types, such as type IV and type V collagens are apparently not found as typical collagen fibrils. Type V is thought to be a minor

fibrillar component.

Collagen molecules are composed of three polypeptide chains, so called α-chains, with repeating sequences of the form Gly-X-Y along their length, where X and Y are any amino acid residues. In type I collagen there are two distinct kinds of chains α1(I) and α2(I) , which occur in a ratio of two to one respectively. Each α1(I) chain has 1014 residues present as repeating tripeptide sequence of the form $(Gly\text{-}X\text{-}Y)_n$ with 16 additional residues at the N-terminus and 25 at the C-terminus. α2(I) chain has a similar but not identical sequence. The dimensions of the three stranded α-chains is about 3000 by 15 Å. The conformation of the collagen molecule was determined to be a triple helical from amino acid sequence characteristics and from high-angle X-ray data. The rise per residue in each left-handed helical chain is about 2.9 Å, and three of these helices are supercoiled in a right-handed manner about a central axis to give the final molecular structure. In this conformation each strand has approximately three amino acids per turn with an axial translation of 2.86 Å between residues. The three chains in turn are related to each other by an axial translation of 2.86 Å and an azimuthal rotation of about 108 degrees. This means that each strand is supercoiled with a pitch of about 30 residues. Although the large central portions of the collagen chains contain glycine as every third residue, the regions at each end of the chain, called telopeptides, do not show this sequence regularity. The super helical pattern for these telopeptides is thus forbidden. The bovine α1(I) chain has 1014 residues with glycine at every third position, but has 16 residues at the N-terminal end (N-telopeptide) and 25 residues at its C-terminal end (C-telopeptide) without this regularity (Fietzek et.al, 1976; Helseth et al, 1979), 20% of the others are the imino acids

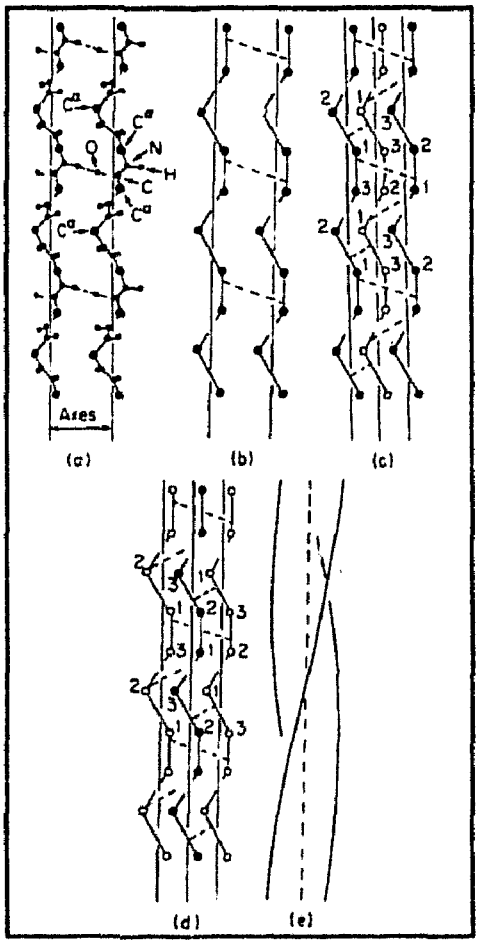

Fig. I.1 : (Rich and Crick, 1961) Diagram showing the formation of two collagen models from the polyglycine sequence:
(a)Two strands of polyglycine with black dots representing various atoms and dashed lines as hydrogen bonds.
(b)Two chains of the polyglycine sequence in which only the C^{α} atoms and hydrogen bonds are shown.

(c)The third chain shown with open circles lies behind the two shown in (b) to make a collagen-like arrangement. The numbers indicate the phasing of the residues on the polypeptide chains
(d)The third chain is added in front of the two in (b) giving rise to a second collagen-like arrangement.
(e)Solid lines represent the axes around which the polyglycine chains are coiled. This gives a view of the possible three dimensional coiled-coil structure of the molecule.

proline and hydroxyproline. Calculations on the N-telopeptide amino acid sequence have led to a proposed model for this region's secondary structure (Helseth *et.al.*, 1979).

The biosynthesis (Ramachandran and Reddi , 1976) of collagen is similar to that of other proteins but is distinguished by at least two general prominent features: the protein is first synthesised as a precursor form in which several important functions are fulfilled, then it is submitted to several post-translational modifications which occur after assembly of the three chains and which are essential for some of its structural features.

2. Conformational Studies of Collagen-like Molecules.

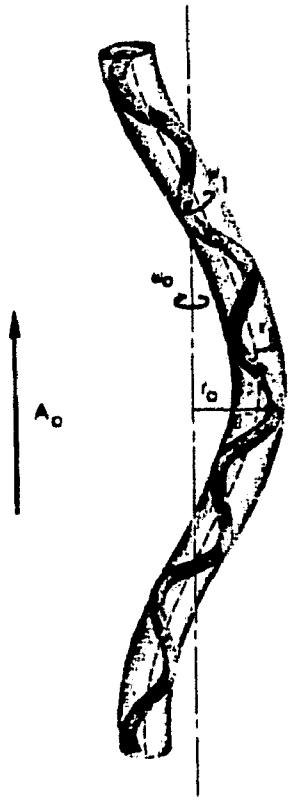

Fig. I.2: The Geometry of a coiled-coil.

Collagen (Rich & Crick, 1961; Traub and Piez, 1971) is one of the few proteins which is fibrous rather than globular in bulk molecular structure. The basic collagen molecule is composed of three distinct polypeptide chains, each of which is nearly a left-handed threefold helix. These three helical chains wrap around one another to form a single superhelix whose repeat and pitch appears to be variable and dependent upon the primary structures of the polypeptide chains. The three polypeptide chains are held together by interchain hydrogen bonds which are able to come near to one another because glycine residues are found in every third residue position of each of the three chains. Thus the repetitive glycine residue sequencing and the mode of interchain hydrogen bonding are responsible for the manner in which the three polypeptide chains fit together to form the super helix.

Fig. I.1 shows how three left-handed 3_1-helical polypeptide chains can be brought together to form a collagen-like triple helix. The left-handed 3_1-helix is preferred to any other secondary structure because of the high content of the imino acid residues proline and hydroxyproline in each of the three chains.

MANQUE PAGE 24

C. Advances expected with Synchrotron Radiation and Purpose of this Work for Fibre Structural Studies

Crystals with large unit cells represent an important class of structures for which analysis would be difficult without the availability of synchrotron radiation (Ealick & Walter, 1993; Fisher & Johnson, 1993; Logan *et.al.*, 1993; Pflugl *et.al.*, 1993). The natural low divergence of synchrotron radiation beams makes possible the resolution of many orders of diffraction for unit cells with lengths greater than 200 Å. Recent representative structures with large unit cells are illustrative of the emerging class of megastructures (viruses, DNA fibres etc...) that will be almost entirely dependent upon synchrotron radiation sources.

Diffuse scattering that results from correlated motions of atoms within a crystal lattice in addition to the weakly diffracting nature of the material are some of the problems encountered in fibre diffraction data reduction. The high signal-to-noise ratio resulting from the use of synchrotron radiation can also be used to observe features in the diffracting patterns that ordinarily are unnoticed or unappreciated in classical X-rays sources.

The major problems faced in previous data collection with conventional fibre diffraction studies are the simultaneous occurrence of the following obstacles; in the course of this thesis I will also give the possible solutions developed to overcome these problems:

1) The crystallographic interpretation of diffraction patterns requires the definition of a unique crystal system (unit cell and space group) on the basis of which the observed Bragg reflections are indexed. Different systems have already been proposed including a recently published superlattice suggested by Kajava (1991). Chapter 3 introduces a comparison between the triclinic cell with the new proposed model by computer prediction of the Bragg spots on the fibre diffraction pattern. The triclinic unit cell is validated using peak enhancement methods and image addition.

2) Close spacing of successive orders in reciprocal space in the l direction due to the unusual high value of the c axis ($c^* = 0.0015 Å^{-1}$). The solution will be the use of larger sample-detector distances but this will also reduce the resolution of the experiment unless larger area detectors are used.

3) The rotation or fibre axis is not parallel to a reciprocal lattice vector which precludes the use of crystal rotating methods. Further, the lack of precision in the measurement of the experimental fibre tilt relative to the direct beam makes it difficult the correct indexing of Bragg spots.

4) The extent of broadening of the spots due to finite crystal size is not defined for every reflection, thus intensity integration has to be carried carefully by manual setting of the correct integrating area over each peak region.

5) The presence of intense background over the films simultaneously with high diffuse scattering principally on the equator and helix layer lines. This problem will be overcome by using multiple film packs and working out the data on bottom films where strong peaks are present but background and diffuse scattering have been absorbed by top films.

6) The spots arc due to disorientation of the crystalline domains principally in the Z direction. This

arcing is position dependent in film space due to the curvature of the Ewald sphere and is not yet correctly predicted by computer simulation. A Lorentz Factor has also to be applied to the integrated intensities in order to correct for the spread out of reflections in the reciprocal space that is proper to fibre diffraction experiments.

7) High dynamic range between meridional and off meridional Bragg reflections makes it necessary to use film packs to record intensities of different magnitudes. This is especially the case for data on the two principal axis, e.g. meridian and equator where spots are intense. Chapter 5 is devoted for the use of fast digital image processing to allow for a reliable reorientation of different films and interactive peak integration. Peak saturation was always checked before the integration was carried.

The main purpose of this study was to gather quantitative data suitable for structural characterisation of collagen packing and structure in tendon fibres. The MIR method will be assessed because it is a widely used method that has often yielded good results in conventional protein crystallography. We expect that this method will provide the means to understand the packing problem in collagen crystals, at least at a low-resolution level. The phasing problem being the most difficult to solve since no other methods are available. Moreover, diffraction patterns obtained with heavy atoms added collagen fibres have been obtained and show discernible intensity changes in the diffracted spots. Hence, after an introduction to the general methods used in fibre X-ray crystallography, part of this work will deal with the mean crystal size determination in the direction along the fibre. Then, the one dimensional periodicity in tendon collagen being obvious from the observation of the meridional medium angle scattering, the tendon will be considered to be of 3-D crystalline quality and all the subsequent work will assume the packing on the basis of a triclinic crystal system defined elsewhere.

Chapter 2
Structural Studies of Collagen Fibres

A. Application of X-rays to Collagenous Structures.

1. Diffraction by Fibres.

Many naturally occurring biological materials are of fibrous nature. X-ray diffraction patterns from such materials are usually obtained by placing the fibres at right angles to the X-ray beam. In the diffraction pattern, the direction parallel to the fibre axis and through the centre of a fibre diffraction pattern is referred to as the meridian, and the direction perpendicular to this is called the equator. Fibres are usually composed of long, chain-like molecules, packed together with their axes parallel, or nearly parallel, to the fibre axis. Usually, in fibres, molecules are regularly arranged so as to form crystalline regions, but the different regions within a fibre are randomly oriented about the fibre axis. The diffraction patterns from such fibres are similar to single crystal rotation photographs.
Depending on the degree of order, various kinds of diffraction characteristic are observed.
If molecules are randomly displaced relative to each other in the direction of the fibre axis, discrete spots are only observed along the equator, and the higher layer lines have a continuous distribution of intensity along them. Whereas, random displacement by a fixed amount can give rise to discrete spots on some layer lines and a continuous streak of intensity along others. Thus, a random displacement by half the repeat period along the fibre axis will produce spots on the even numbered layer lines and streaks on the odd ones (Wilson, 1966).
Screw disorder, which is a combination of rotational and translational disorder, is common with helical molecules. This produces diffraction patterns with discrete spots in the central region but continuous streaks elsewhere along the layer lines. Discrete spots along the meridian indicate periodicities along the fibre axis.
In order to obtain information about the regions of the transform near the origins of the higher layer planes it is necessary to tilt the fibre through half the scattering angle for that region. The diffraction along the equator of the pattern gives information about the structure in projection down the fibre axis, and even if the rest of the diffraction pattern is rather diffuse, discrete spots along the equator will indicate the lateral distance between molecules.

2. Experimental Set-up for Fibre X-ray Studies.

Fibre diffraction experiments, in contrast to other protein crystallographic studies, require specific specimen preparation. Both native and reconstituted from purified collagen fibres can be examined by X-ray diffraction. A specimen of dimensions approximately 0.5x0.5x5mm is convenient to work with in that it can be easily held and stretched, but considerably smaller pieces can be used successfully. A suitable tissue can be dissected from various sources, clamped in an enclosed specimen cell with

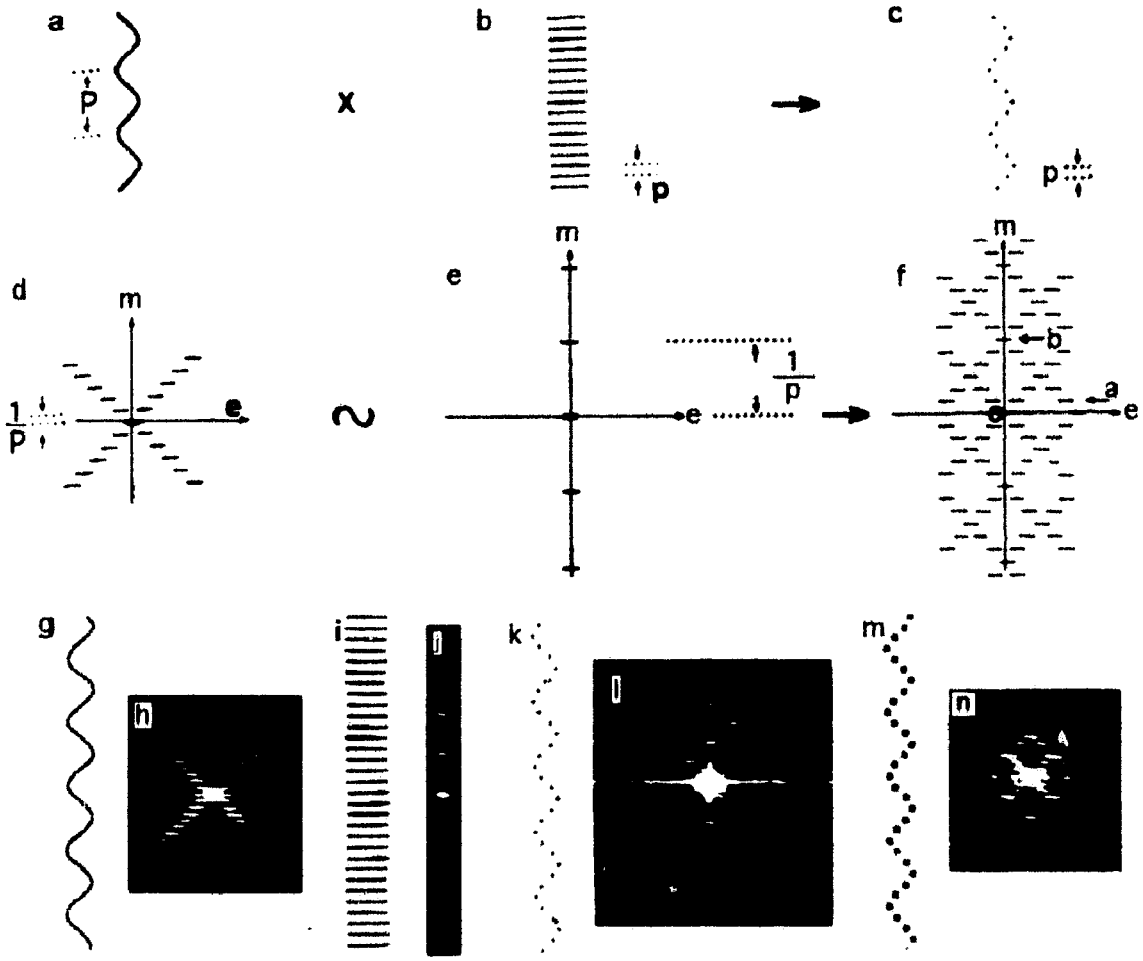

Fig. II.1: (after Vibert, 1987). A discontinuous helix (c) is the product of a continuous helix (a) and a set of planes of spacing p (b). Its transform (f) is therefore the convolution of the transforms (d) and (e) obtained from (a) and (b) respectively. (g) and (l) illustrate these effects by optical diffraction; (m) and (n) show the effect of increasing the size of the scattering unit; m and e designate meridional and equatorial axis respectively.

Mylar windows, and stretched to improve orientation. The specimen can be continuously maintained in hydrated state by keeping it in contact with water vapour or buffer solution. The general configuration of an X-Ray diffraction experiment suitable for use with connective tissues is shown in fig. II.2:

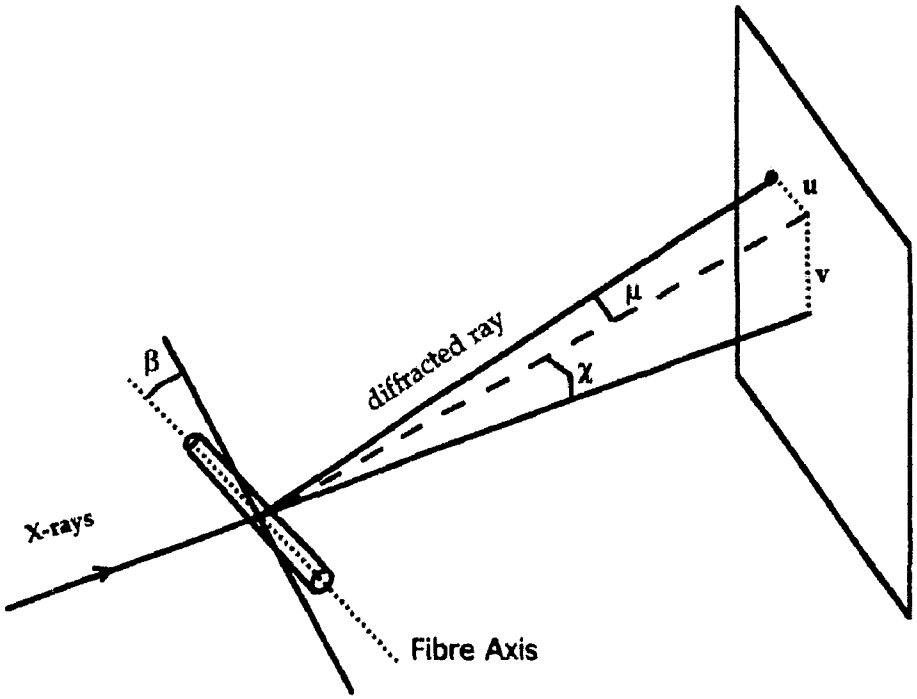

Fig. II.2:Fibre X-ray diffraction patterns are generally obtained by putting the sample at a near perpendicular direction to the incoming beam. When higher meridional orders are needed the fibre is tilted by an angle β.

Nowadays, synchrotron radiation laboratories all have dedicated experimental instrumentation for fibre diffraction experiments (Nave *et al.*, 1985).

B. X-Ray Structural Studies

1. Unit Cell and Reciprocal Lattice Geometry

Before any X-ray structural study can be started the overall geometric features in the structure need to be defined. Previous electron microscopic studies (Hulmes *et.al.*, 1981) have already demonstrated the existence of microfibrilar domains in the tendon. These domains comprise regularly grouped collagen molecules (200-300 nm) in diameter and might be compared to the crystalline domains in a powder. Azimuthal disorientation is random and take all possible values between [0,2π] and thus fibres are "powders" with one dimensional distribution of crystalline domains. Crystalline domains in tendon also may have polar disorientation but this has been shown to be of 1° or 2° in absolute magnitude (Fraser *et.al.*, 1976).

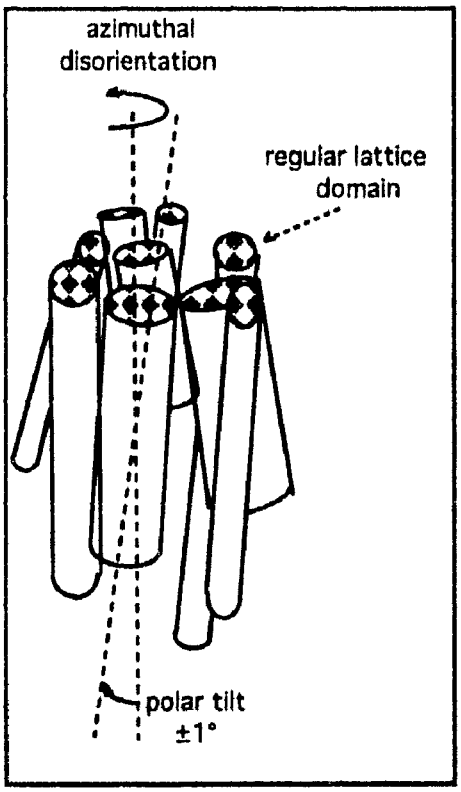

Fig. II.3: Collagen in tendon is composed of regular crystalline domains of aligned molecules. These domains have both azimuthal disorientation about the vertical axis and polar tilt of ~1°.

The interpretation of fibre diffraction patterns requires, in addition to the reciprocal cell parameters $a^*,b^*,c^*,\alpha^*,\beta^*$ and γ^*, the definition of two Euler angles for each reciprocal unit cell vector. Thus the unit cell is described in terms of eight parameters in the reciprocal spherical polar coordinates (Fraser *et.al.*, 1981) where the Z axis is parallel to the fibre axis. For convenience, the plane containing the a^*-axis is taken as the origin for azimuthal angles φ so that $\varphi_{a^*}=0$. The eight parameters needed to define the reciprocal cell and its orientation with respect to the fibre axis are then $a^*,b^*,c^*, \theta_{a^*}, \theta_{b^*}, \theta_{c^*},\varphi_{b^*}, \varphi_{c^*}$.

The reciprocal interaxial angles of the unit cell are then calculated using:

$$\cos\alpha^* = \cos\theta_{b^*}\cos\theta_{c^*} + \sin\theta_{b^*}\sin\theta_{c^*}\cos(\varphi_{b^*}-\varphi_{c^*})$$

$$\cos\beta^* = \cos\theta_{a^*}\cos\theta_{c^*} + \sin\theta_{a^*}\sin\theta_{c^*}\cos\varphi_{c^*}$$

$$\cos\alpha^* = \cos\theta_{a^*}\cos\theta_{b^*} + \sin\theta_{a^*}\sin\theta_{b^*}\cos\varphi_{b^*}$$

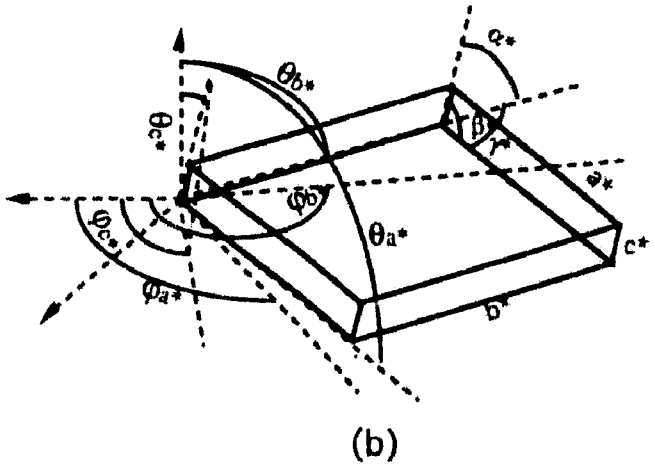

Fig. II.4: Reciprocal lattice unit cell (Z axis not to scale) showing the definitions of the unit cell parameters and relative angles to the fibre axis refined by (Fraser et.al., 1983).

For a reflection with Miller indices h,k,l, due to cylindrical symmetry of the fibre we obtain the diffraction geometry shown in figure II.5. The diffraction geometry assumes a well oriented fibre e.g. fibre axis vertical and perpendicular to the X-ray beam so that the unique information is obtained

from one quadrant of the film. But, the fibre is conventionally tilted to the X-ray beam to extend the meridional resolution limit so the four-quadrant symmetry is lost.

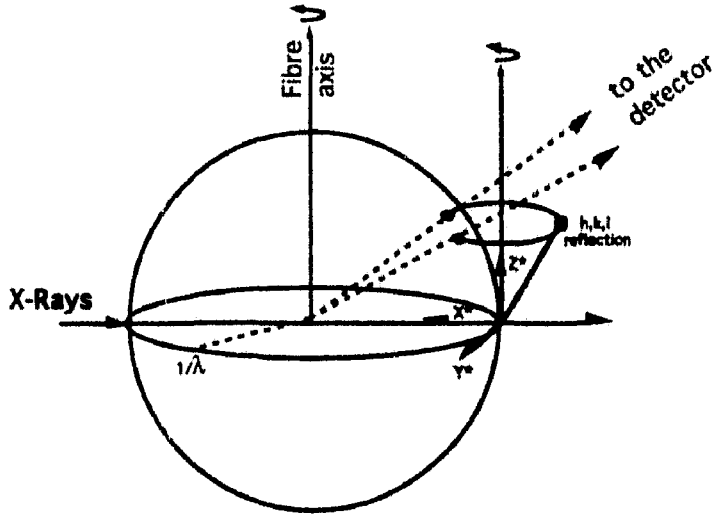

Fig. II.5 : Diffraction geometry for a fibre in reciprocal space. Due to the cylindrical symmetry, each reflection with Miller indices (h,k,l) intercepts the Ewald sphere at two symmetric points relative to the fibre axis.

2. Fibre Diffraction Equations.

Intensity data obtained from a specimen with fibre-type orientation can be conveniently summarised in terms of specimen intensity transform Is, where D is a reciprocal lattice vector (Fig. II.6). The transform has a cylindrical symmetry and convenient measure of its value, for a particular value of D, is the scattered intensity per structural repeating unit, corrected for specimen absorption, relative to the scattered intensity from a single electron at S.

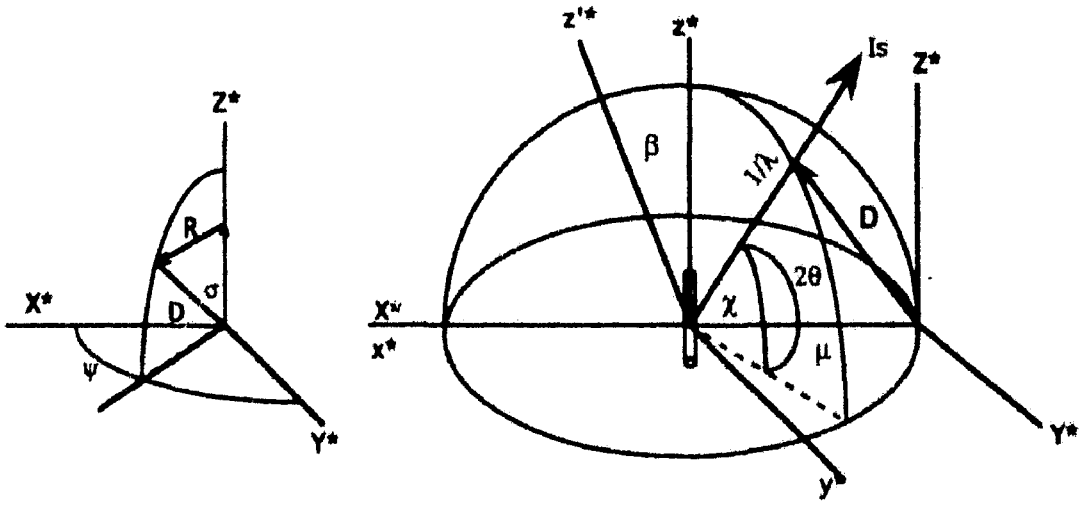

Fig. II.6

In the conventional arrangement for collecting fibre diffraction data, the specimen is irradiated with X-rays by a collimated beam of monochromatic radiation passing along xS (Fig. II.6) and the scattered

intensity is measured for a range of values of the angles μ and χ which are related to the reciprocal-space co-ordinates as follows:

$$D=\frac{\sqrt{2(1-\cos\mu\cos\chi)}}{\lambda}$$

$$Z=\frac{[\sin\beta(1-\cos\mu\cos\chi)+\cos\beta\sin\chi]}{\lambda}$$

$$R=\sqrt{D^2-Z^2}$$

$$\sin\psi=\frac{\sin\mu\sin\chi}{\lambda R}$$

$$\cos\sigma=\frac{Z}{D}$$

where β is the inclination of the fibre axis to the normal to the incident X-ray beam.

The positions of the reflections on a flat film recording camera are related to μ and χ by the equations:

$$\tan\mu=\frac{u}{r}$$

$$\tan\chi=\frac{v}{\sqrt{r^2+u^2}}$$

where r is the specimen-film distance.

$$u=\frac{2rYl}{2-\lambda^2D^2}$$

$$v=\lambda Z\sqrt{\frac{r^2+u^2}{1-\lambda^2Z^2}}$$

3. The Electron Density Equations

The most useful mean of investigation for collagen molecular structure and packing is fibre X-ray diffraction where the patterns can allow determination of the three dimensional packing of molecules, the lateral arrangement of neighbouring molecules and the determination of the unit-cell parameters. The aim of every structural analysis by the diffraction technique is to obtain an image of the structure by Fourier transform with the structure factor moduli as coefficients.

Thus scattering of X-ray by an atom is described by the atomic scattering factor

$$f(\vec{S})=\int_{Vol.of\ Atom}\rho(\vec{r})\exp 2\pi i\,\vec{r}.\vec{S}\,dv$$

where the electron density distribution of an atom is obtained from wave mechanics.

The scattering of X-rays by a molecule in turn is described in terms of the molecular transform

$$G(\vec{S})=\sum_{j=1}^{Natoms} f_j \exp 2\pi i\,\vec{r}.\vec{S}$$

The diffraction pattern is the Fourier transform of the structure and vice versa the structure is the Fourier transform of the diffraction pattern.

$$\vec{F}(\vec{S})=\sum_{j=1}^{N} f_j \exp(2\pi i \vec{r}.\vec{S})$$

$$=\int_{V\,cell} \rho(\vec{r}) \exp(2\pi i \vec{r}\vec{S}) dv$$

where $\vec{S}$ is used to denote the position in the diffraction space.
It can be shown that:

$$\rho(\vec{r})=\int_{V\,diff\,space} \vec{F}(\vec{S}) \exp(-2\pi\, i\vec{r}\,\vec{S})\, dv_s$$

The integration can be replaced by a summation since $\vec{F}(\vec{S})$ is not continuous and is non-zero at the reciprocal lattice points. Hence

$$\rho(x,y,z)=\frac{1}{V}\sum_{h=-\infty}^{\infty}\sum_{k=-\infty}^{\infty}\sum_{l=-\infty}^{\infty} \vec{F}(hkl) \exp{-2\pi i(hx+ky+lz)}$$

$$\rho_{abs}(x,y,z)=\frac{\vec{F}(0)}{V}+\frac{1}{V}\sum_{h\neq 0}^{\pm\infty}\sum_{k\neq 0}^{\pm\infty}\sum_{l\neq 0}^{\pm\infty} \vec{F}(hkl)\ \exp{-2\pi i(hx+ky+lz)}$$

The electron density $\rho_{abs}(x,y,z)$ represents the absolute electron density and thus, the structure of the crystal. Since $\vec{F}(0)$ is difficult to measure because of parasitic scatter around the incident beam one takes only the relative scattering density level, $\rho(x,y,z)$ in the structure

$$\rho(x,y,z)=\frac{1}{V}\sum_{h\neq 0}^{\pm\infty}\sum_{k\neq 0}^{\pm\infty}\sum_{l\neq 0}^{\pm\infty} |F(hkl)|\ \exp[i\,\alpha(hkl)] \exp{-2\pi i\,(hx+ky+lz)}$$

Such a Fourier synthesis has three potential sources of error : (1) errors in the phases $\alpha(h,k,l)$, (2) errors in the structure factor amplitude F(h,k,l), and (3) series termination errors also called resolution limit. Resolution errors can be particularly acute in low angle scattering studies, in which only a few reflections are recorded. Inclusion of a finite rather than an infinite number of reflections in crystal structure equation cause the Fourier transform to be abruptly truncated and the resulting series suffer from smearing in real space of the density profile. Therefore one method used to correct for termination error is to multiply the structure factors by an artificial temperature factor (Franklin et Gossling, 1953; Warren, 1969)

$$F(hkl)=F(hkl)\exp\left(-\delta\sin^2\theta/\lambda^2\right)$$

where δ is a constant. The temperature factor, given by the exponential term in the equation above causes the Fourier transform to fall gradually to a desired value at the limiting resolution, and thereby avoids the abrupt cutoff in the transform but the uncertainty of this method is the lack of objective way to assign a value to the constant δ.

Unlike the high resolution studies with globular proteins where detailed structure analysis is attained by increasing the limit of the resolution sphere to include all the diffracted intensity, fibre diffraction patterns can provide reflection data which do not contain all the required Bragg reflections in a given resolution limit. That is, the resolution in classical protein crystallography is improved by including the experimental data contained in successive resolution shells around the reciprocal space origin whereas the structure factors obtained with fibre diffraction patterns will always lack of experimentally determined reflections due to peak overlap and other limiting conditions. The incompleteness of diffraction data obtained with fibre patterns, where peak overlap takes place, will be shown later.

Hence, we might calculate Fourier maps using an incomplete data set obtained from fibre diffraction patterns but the calculated maps do not necessary have a full 3D significance. The resolution concept also will not be defined exactly as in the classical protein crystallography. A special case of Fourier calculation is obtained for example when reflection data have indices related to special lattice planes. The calculated maps are then defined as a projection of the structure on that special plane. For instance, the projection of a crystal structure down a crystallographic axis (c, say) is given by

$$\rho\ (x,y)=\int_c \rho\ (x,y,z)dz$$

such a projection is given by the transform:

$$\rho\ (x,y)=\frac{1}{A}\sum_{h=-\infty}^{\infty}\sum_{k=-\infty}^{\infty}\vec{F}(h,k,0)\exp -2\pi i(hx+ky)$$

where A is the area of the xy projection. This means that the projection of a structure may be determined from the corresponding zero level of the diffraction pattern.

4. The Phase problem.

In protein crystallography there are four widely used techniques for overcoming the phase problem: 1) The Patterson summation 2)Direct methods 3)The heavy atom isomorphous replacement method in which a heavy atom is introduced into a light atom structure and is used as a marker 4)Anomalous scattering in which phase information is obtained from the scattering of an atom whose natural absorption frequency is close to the frequency of the incident radiation.

a) Isomorphous replacement.

The isomorphous replacement method was developed for proteins by Perutz and colleagues in the 1950s. It has provided the breakthrough in the phase problem which allowed the structures of myoglobin and haemoglobin to be solved (for a complete review see the original work of Kendrew *et. al.*, 1960; Perutz *et. al.*, 1960, a complete reference for the papers is given in Blundel and Johnson). The technique involves producing a derivative crystal by soaking into a protein crystal a solution of a compound containing a heavy atom and collecting a set of diffraction data from that crystal. If the heavy atom has bound to the protein at a site or sites without affecting the protein structure itself, there will be differences in the intensities of the X-ray reflections which contain information about the phases. The positions of the heavy atoms can usually be calculated using a Patterson function whose coefficients are related to the intensity differences between the native and derivative data. Then, the knowledge of the heavy atoms positions can be combined to calculate the phases for the native protein data.

In order to calculate the electron density one needs to know $\vec{F}(hkl)$, that is one needs to know both the amplitude F(hkl) and the phase $\alpha(hkl)$ of the structure factor. This is emphasised by rewriting the electron density equation as

$$\rho\,(x,y,z)=\frac{1}{V}\sum_{h=-\infty}^{\infty}\sum_{k=-\infty}^{\infty}\sum_{l=-\infty}^{\infty}F(hkl)\,\exp i\alpha(hkl)\;\exp -2\pi i(hx+ky+lz)$$

The problem of phase determination is thus the ultimate problem in any crystal structure determination.

The Patterson function is a convolution function which may always be calculated from a set of diffraction data. It is defined as

$$P(u,v,w)=\int_{Vol.Cell}\rho\;(xyz)\,\rho\;(x+u,y+v,z+w)dv$$

The value of the function at a particular point $\vec{u}(u,v,w)$ is calculated from the product of the two values of the electron density at positions $\vec{x}$ and $\vec{x}+\vec{u}$ summed over all the unit cell.

Writing

$$\rho\;(\vec{x})=\frac{1}{V}\sum_{h=-\infty}^{\infty}\vec{F}(\vec{h})\,\exp -2\pi i\vec{h}.\vec{x}$$

$$\rho\;(\vec{x}+\vec{u})=\frac{1}{V}\sum_{h'=-\infty}^{\infty}\vec{F}(\vec{h'})\,\exp -2\pi i\vec{h'}.(\vec{x}+\vec{u})$$

then

$$P(u,v,w)=\frac{1}{V^2}\sum_{h}\sum_{h'}\vec{F}(\vec{h}).\vec{F}(\vec{h'})\,\exp -2\pi i\vec{h'}.\vec{u}\int_{V\,cell}\exp -2\pi i(\vec{h}+\vec{h'}).\vec{x}\;dv$$

The integration is equal to zero unless h=-h' when it is equal to V

$$P(\vec{u})=\frac{1}{V}\sum_{h} \vec{F_h}^2 \exp -2\pi i\vec{h'}.\vec{u}$$

Heavy atom derivatives of a macromolecular crystal can be prepared which for a minimum of two derivatives (and the native crystal) and in the absence of errors, leads to a unique determination of the phase $\alpha(h,k,l)$. This requires the site and occupancy of heavy atom to be known for the calculation of the vector $\vec{F}(\vec{S})$. In the absence of any starting phase information the heavy atom is located using an isomorphous difference Patterson synthesis P(u,v,w) where the isomorphous difference is given by

$$\Delta_{ISO}(hkl)=|\vec{F}_{PH}(hkl)| - |\vec{F}_{P}(hkl)|$$

and the Patterson function is given by

$$P(uvw)=\frac{2}{V}\sum_{hkl} \Delta^2_{ISO}(hkl) \cos[2\pi(hu+kv+lw)]$$

The largest non-origin peaks on the Patterson map should be due to the heavy atom vectors provided the derivative protein crystal is isomorphous with the unmodified or native protein crystal.
Unfortunately, experimental difficulties such as non-isomorphism, weak substitution by the heavy atom, crystal variations, etc. often mean that two heavy atom derivatives are not sufficient to determine the phases well enough to define the image. Thus, three, four or five heavy atom derivatives are usually incorporated in the calculation of the phases.

5. Systematic Corrections for Determining Structure Factor Amplitudes with Fibres.

In addition to statistical errors that limit the precision of the observed diffraction, several sources of systematic error hinder experimental recording of the integrated intensity of a reflection. Examples are absorption, extinction, polarisation, simultaneous reflections, disorder, chromatic and geometrical aberrations, background, and the Lorentz factor (Arndt *et.al.*, 1966)

a) Absorption

The intensity I of a beam passing through a crystal of thickness t is given by $I=I_0 \exp(-\mu t)$ where I_0 is the intensity of the incident beam and μ is the linear absorption coefficient (Units cm^{-1}). The path of the beam through the sample is dependent on the scattering angle 2θ. At higher scattering angles the path length increases, and the scattered radiation is exponentially reduced. These absorption effects can be significant in X-ray diffraction and are due principally to the photoelectric effect.
As the crystal thickness increases, the absorption of X-rays will diminish the amount of radiation transmitted through the crystal. At the same time the intensity of a radiation in a diffraction spot increases as the volume of the crystal increases. In low-angle diffraction the scattering angles are small enough that absorption corrections can usually be neglected. For protein crystallography with geometrically regular shaped crystals these corrections are also neglected due to isotropic distribution

of reflections in reciprocal space. However it is not only the absolute magnitude of the absorption correction which is important, but also its relative variation from reflection to reflection in particular

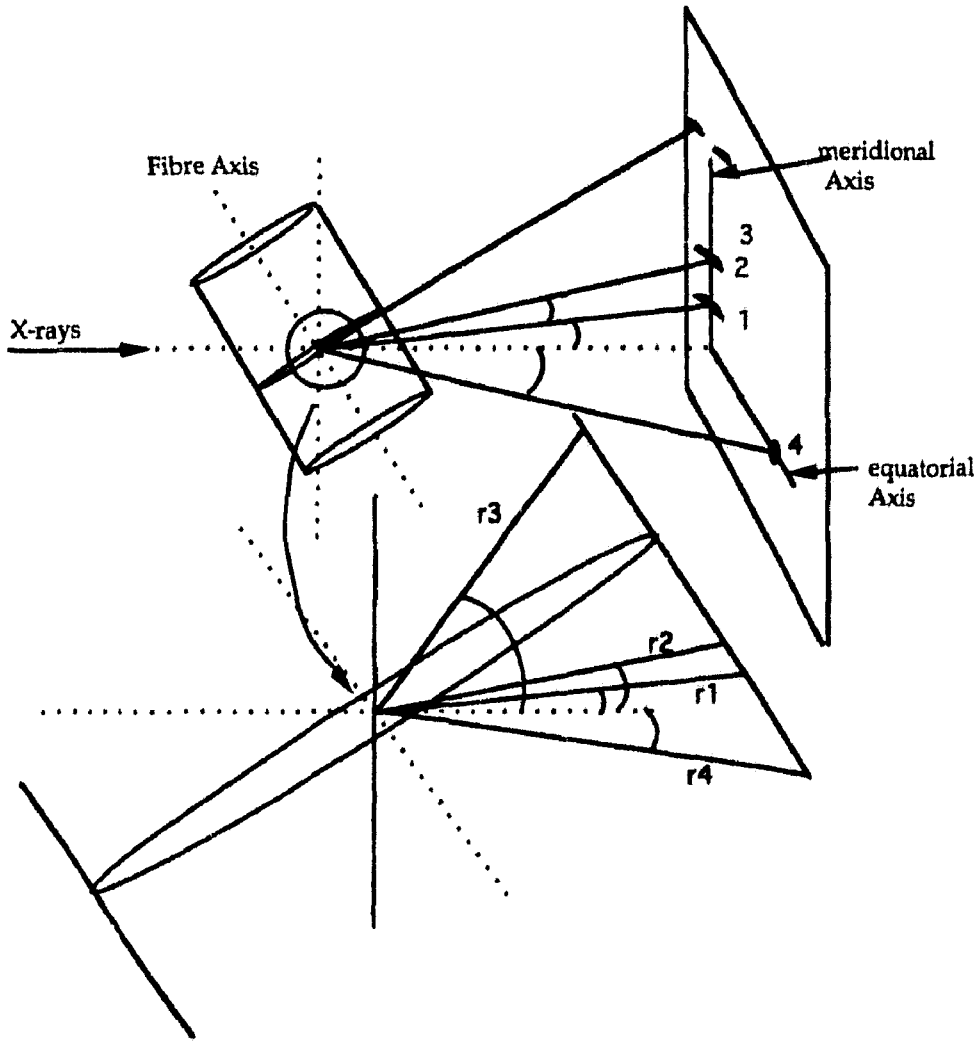

Fig. II.7 : The path of each reflection in a fibre sample is dependent on the scattering direction and on the tilt of the fibre relative to the X-rays. Diffracted rays r1 ,r2 and r3 represent meridional reflections whereas r4 is a non meridional reflection. One can see that high resolution meridional peaks may encounter more or less specimen absorption (r3≠r2≠r1). This absorption correction however was dropped because the meridional reflections are split into two symmetric reflections at high l indices.

geometry of crystals (rod shaped or disk shaped crystals). The geometry of tendon fibre is such that the corrections to be applied to the structure factors cannot be dropped without prior examination. Figure II.7 shows the paths of different diffracted rays throughout a tendon fibre. If the fibre is tilted to the X-rays, then two equivalent reflections e.g. (h,k,l) and (-h,-k,-l), do not have the same path in the sample. However, reflections belonging to the same layer line have paths which are equivalent. Figure II.9 shows a medium angle native diffraction pattern obtained with a fibre tilted by ~4.2° and the absorption effects that are obvious on meridional reflections.

The corrections for fibre absorption requires in addition, that the primary beam intensity is measured. Since we have not measured the direct beam intensity it is not possible to correct for the fibre absorption. Moreover these corrections are only important for meridional reflections as shown in the

figures above but meridional reflections are also split into two symmetric reflections with increasing l so that we can neglect this correction for high l reflections.

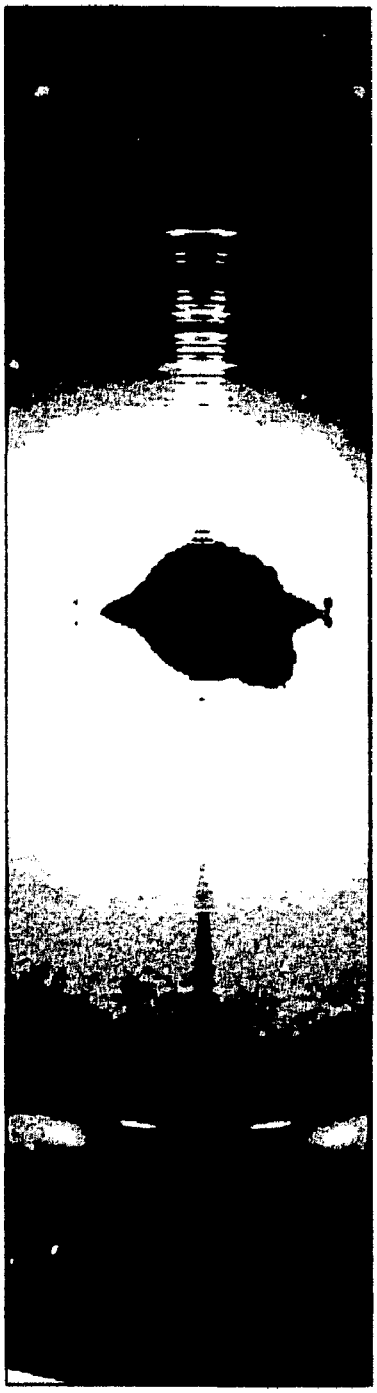

Fig. II.8 : (left) The geometry of a fibre is such that the absorption effects in the X-ray diffraction patterns are important only on the meridional axis. Parallel to that, the meridional reflections are also split into two symmetric off meridional components. Consequently the absorption correction is not necessary for meridional collagen fibre diffraction data .

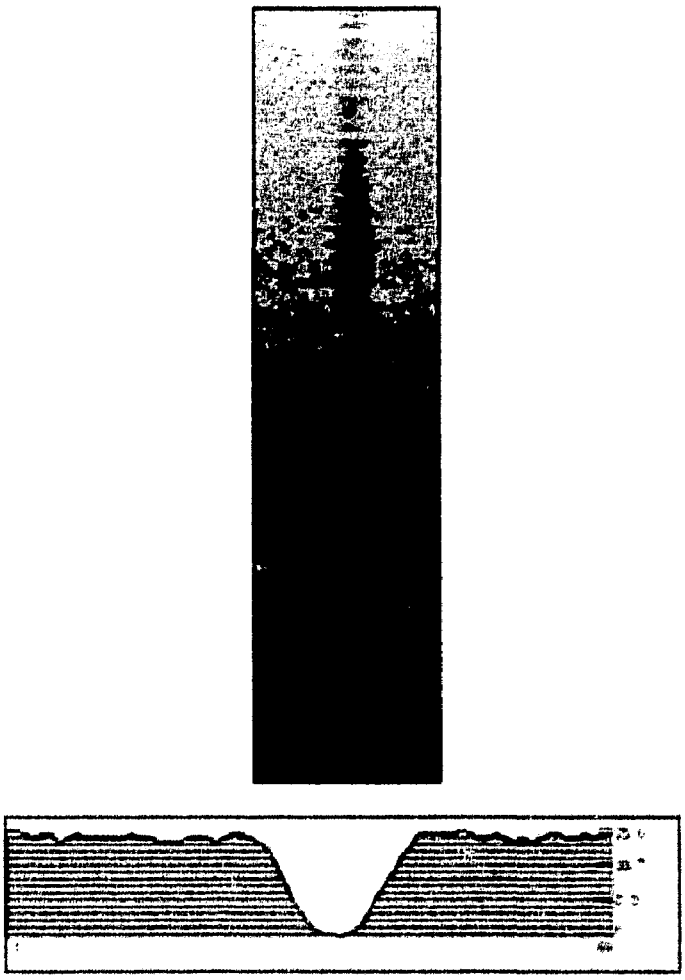

Fig. II.9: The above two figures show a section in the meridional lower part of the X-ray film where absorption is the most striking. A projection along the vertical direction shows an average difference in the recorded optical density (≈25) which is not negligible.

b) Simultaneous reflections

Simultaneous reflections are observed with rotating crystal method when two or more reflections are superimposed or very close on the film and thus their proper indexing is not precise. The intensities

then measured at the predicted position are the sum of the individual peaks.

Unless profile fitting procedures are applied to the area where overlapping peaks occur, there is no mean to associate an integrated intensity with each predicted Bragg reflection. However, this is usually not a major problem in the crystal rotating method since the rotation axis can arbitrary be set around any reciprocal cell direction and thus avoid overlap. To explain how fibre diffraction patterns are obtained I show in the figures below a set of predicted patterns calculated for different sections in the reciprocal space.

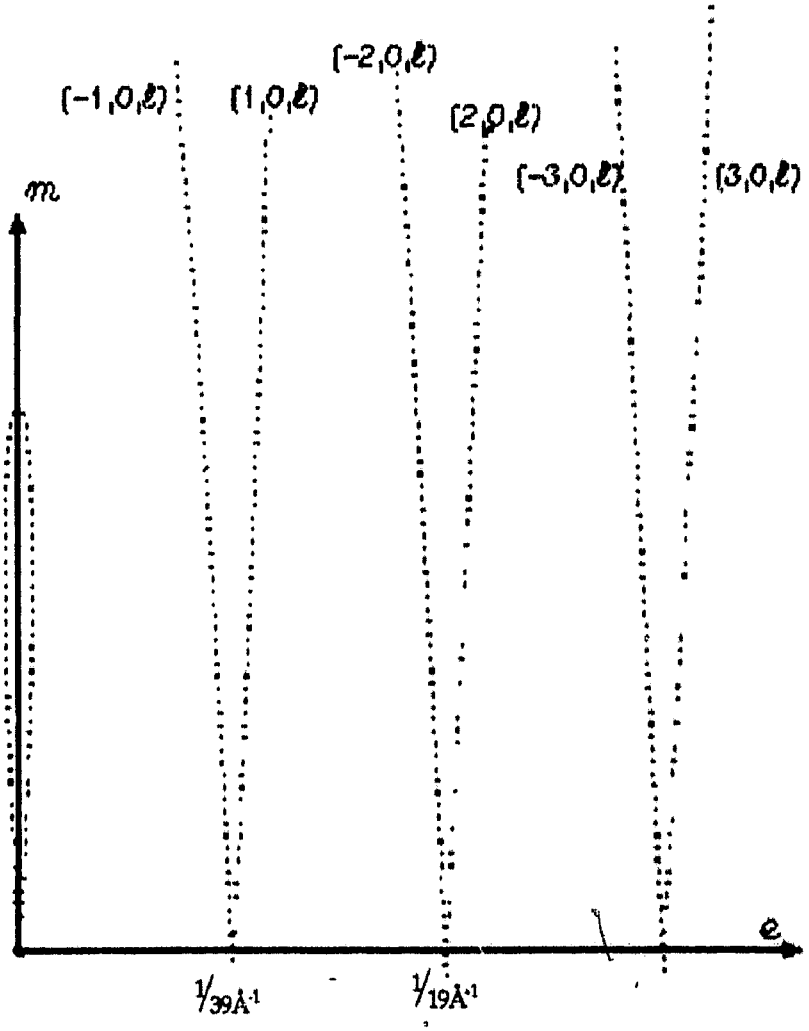

Fig.II.10 : In order to understand the medium angle X-ray fibre diffraction patterns obtained with rat tail tendon I have calculated in this figure and in the next three ones the predicted Bragg positions in the film space. The pattern shown here is for the sections of the reciprocal space with indices (h,0,l) and (-h,0,l), h ≤3, l ≤75. m designates the meridional axis and e the equatorial axis. Only one quarter of the X-ray pattern is shown for clarity. The vertical distance between two predicted spots is proportional to 1/678Å. The meridional reflections are more spliced with increasing l. Then at a value of l ≈ 50, the meridional reflection are no more recorded because the circles in reciprocal space do not intercept the Ewald sphere (compare to blind zones in crystal rotation methods). If the unit cell was tetragonal and the c axis was parallel to the fibre axis then all reflections will be superimposed and the angle between the vertical row-lines will be 0. This figure also shows that the near equatorial reflections with l≤5 are overlapped.

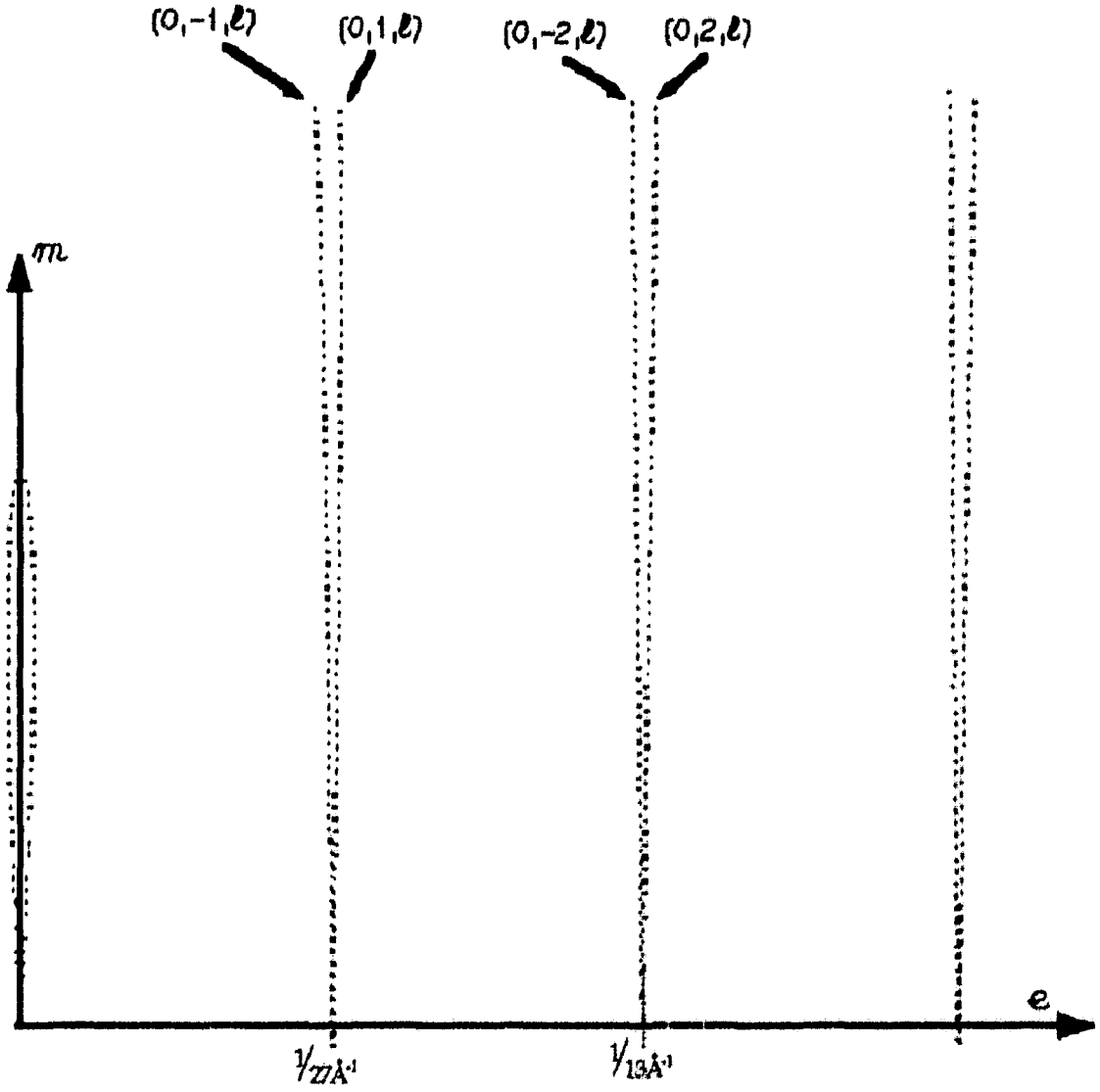

Fig. II.11: predicted Bragg positions for the reciprocal space zone with Miller indices (0,-k,l) and (0,k,l) where = 0, $k \leq 4$, $l \leq 4$.The near equatorial reflections with $l \leq 20$ are strongly overlapped.

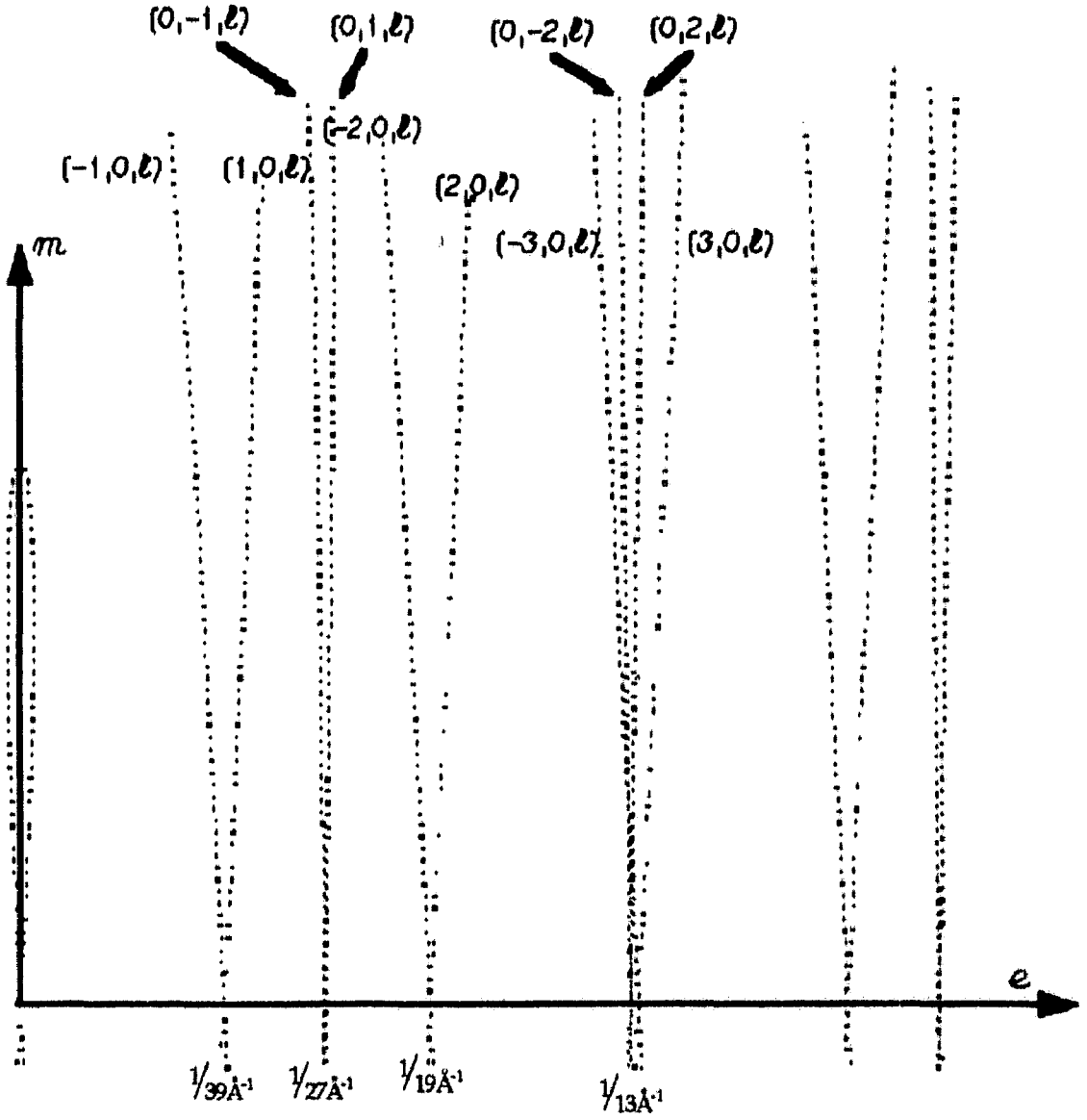

Fig. II.12: This pattern is the sum of the two previously calculated patterns obtained by simple image addition.

Fig. II.13 shows a predicted pattern in film space for a native collagen fibre. The pattern is calculated for a 0° fibre tilt and only one quadrant of the pattern is shown. The overlap of many Bragg reflections is prominent in the equatorial region but row lines of (h,k) values are split with increasing l.

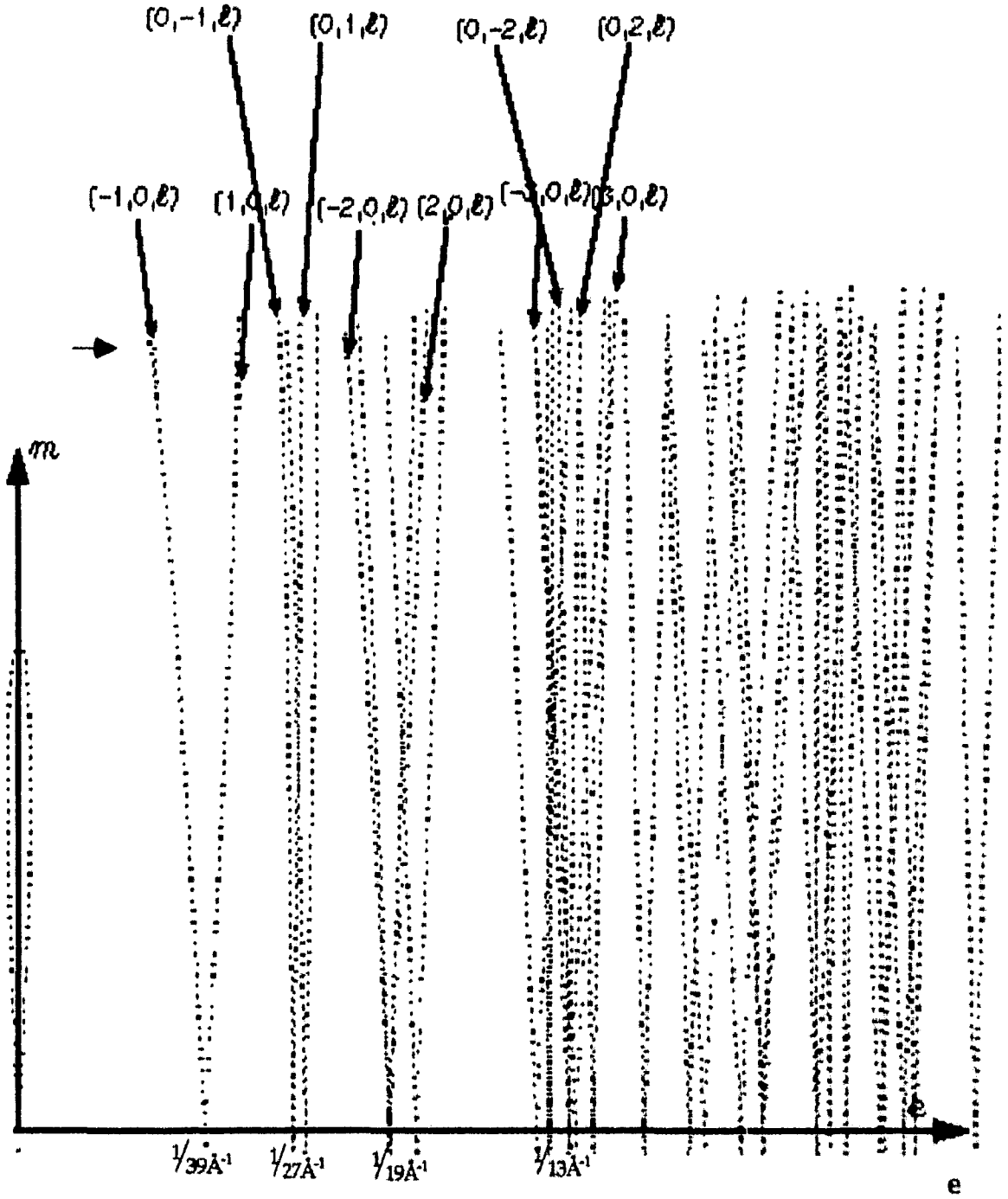

Fig. II.13 : The complete predicted pattern for collagen crystalline fibres showing the overlap of many Bragg reflections. The simulation was carried for the reciprocal space region defined by h=(-4,4), k=(-4,4) and l=(0,75). It is obtained for a 0° fibre tilt to the X-ray beam but other values for the tilt (which might resolve some overlapped peaks) are also possible. The horizontal arrow, in the region around l=75, indicates the approximate position of the (m=0, n=-1) helix layer line.

From these patterns, it is obvious that low angle orders on the equator are difficult to obtain and, consequently, only those Bragg reflections of the pattern where little overlap occurs might produce explicit integrated intensities. The Fourier transform will thus suffer from summation errors due the lack of these data. Consequently, we can not handle these missing data as termination series errors

but as a resolution hole in the Fourier series.

The first row lines in the 1/39Å region have indices (-1,0,l) and (1,0,l), and, for low l value, these are the Fourier terms in the electron density map corresponding to planes parallel to the ac plane of the direct unit cell. At low resolution these orders are important to identify the lateral arrangement of collagen molecules since for example (-1,0,1) and (1,0,1) are perpendicular to different reticular planes in the crystal. Another specific problem to the fibre diffraction data analysis is also shown in figure II.13 where successive l orders on a row line are imprecise, e.g. (h,k,l-1), (h,k,l) and (h,k,l+1) might be inaccurate due to their neighbouring. The fibre tilt relative to the X-ray beam is the major factor affecting this correct indexing.

c) Background Removal

All patterns obtained with tendon samples usually contain a considerable amount of continuous background intensity. This background is remarkably high when synchrotron radiation is used and it has different origins within the sample. The understanding of these origins is not easy and requires specific work (computer simulation, low temperature crystallography, microfocused X-ray beam etc...). However the Bragg reflections obtained in native and derivative crystalline collagen are surrounded by this background such that peak integration has to be carried carefully. This problem is usually overcome for non-fibrous proteins studies by integrating the total diffracted intensity and subtracting the value of the background estimated in the vicinity of the peaks. The process is usually performed automatically in monocrystalline proteins since the positions and shapes of the Bragg peaks are easily predictable. However, the spots in collagen fibre diffraction are too close for the background to be estimated from each peak neighbourhood.

When tilted, fibre diffraction patterns also show a difference in the distribution of continuous background between the upper and the lower part of the pattern. This was already shown in figure II.7 where the path of the diffracted rays is shorter in the upper part of the fibre.

Figure II.4 shows a comparison of the iodine labelled collagen pattern before and after background subtraction. The digital filter applied for background subtraction is a standard method to improve image quality and will be explained in a separate chapter on image analysis. I thus demonstrate with this example that the background subtraction is a decisive technique for improving the quality and the understanding of fibre diffraction patterns but is not necessary if the method is inaccurate since it can remove part of the peak intensity. I have developed and tested different techniques to subtract background from fibre patterns by applying the method suggested in the paper of Millane (Millane *et.al.*, 1985) and a method where the background was modelled by a polynomial function. The polynomial functions have taken the coefficients estimated in the film regions where there were no Bragg reflections.

Fig. II.14 : A simple background subtraction method described the text was applied to iodine patterns where I first show one half of the pattern in the upper part and then same pattern after background subtraction in the lower part. We thus obtain a more comprehensive diffraction pattern that shows discernible peaks but the

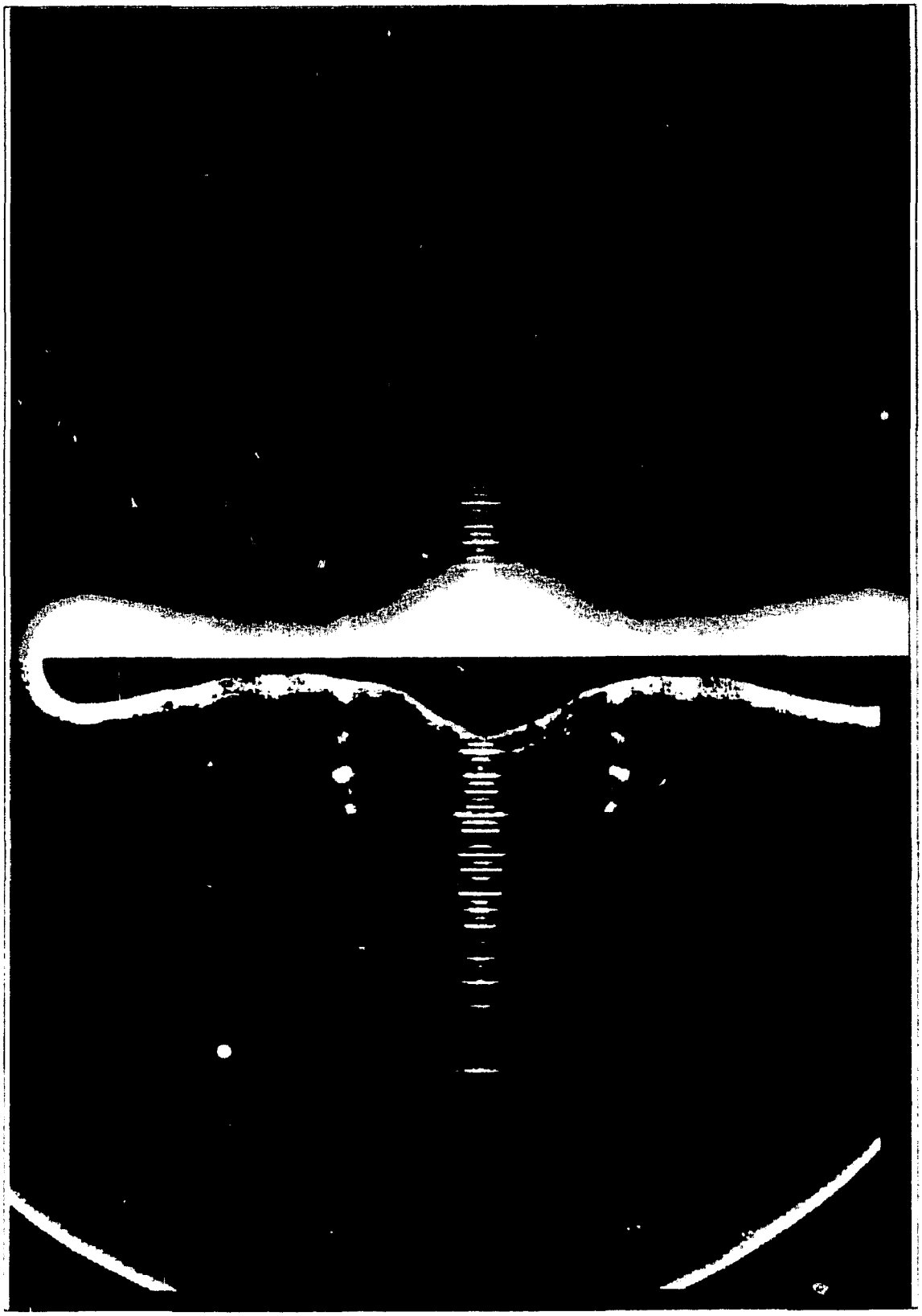

method introduces artefacts principally on the equator and near strong peaks. I have used this method especially to reveal the presence of high intensity discrete reflections in the near-equatorial and helix layer-line regions but the integration of Bragg spots was done with a local background correction

d) Polarisation and Lorentz Factor

Protein crystallographic studies often require that a monocrystal be rotated with respect to the incident beam in order to record several separate reflections. Another advantage of crystal rotation is also the rapid recording of integrated intensities before calculating structure factor amplitudes.
The integrated intensity is usually written

$$I_{int}(\vec{H}) = K\, L(\vec{H})\, P(\vec{H}) \left| \vec{F}(\vec{H}) \right|^2$$

where P is a polarisation factor and L is the Lorentz geometric correction factor. In monocrystal rotation experiment, this factor, which depends on the diffraction geometry is introduced to correct for the fact that different reflections are spending different amounts of time in the Ewald sphere to satisfy the Bragg law. Now fibre diffraction is equivalent to rotating crystal geometry in that monocrystalline domains are grouped in parallel bundles having random orientations about their long axes. The reciprocal lattice points are spread out into circles (figure II.15) with radii proportional to the distance R between the fibre axis and the intersection of the reflection with the Ewald sphere. For a given number of crystalline domains in the fibre, a greater fraction of the intensity is recorded for a reflection at smaller radius than at larger radius. Consequently, a Lorentz correction factor has also to be applied to the integrated intensity before the structure factor is calculated.
The Lorentz factor is thus the term that corrects for the fact that not all the diffracted rays from different reflections in a fibre diffraction experiment have the same opportunity of being recorded. In crystal rotating method like in fibre diffraction method, the rate of rotation of a lattice point belonging to a layer line is again inversely proportional to the reciprocal space distance R between the rotation axis in reciprocal space and the point of intersection with the Ewald sphere. The Lorentz factor in this case will be written

$$L = \frac{1}{R}$$

the relation between the intensity and the structure factor then becomes

$$\left| \vec{F}(\vec{H}) \right|^2 = L^{-1}\, I_{int}(\vec{H}) = R\, I_{int}(\vec{H})$$

where $I_{int}(\vec{H})$ is the integrated, background subtracted film intensity of reflection $\vec{H} = (h,k,l)$.
This factor is usually not defined for meridional reflections because $R \approx 0$ and is often neglected in small angle scattering experiments on one dimensional crystals for the following reasons:

1) meridional reflections always intersect the Ewald sphere at low angle
2) the correction for Lorentz factor is of the same magnitude and can be replaced by a proportionality factor
3) one dimensional Fourier summation is carried for structure factors measured in arbitrary units

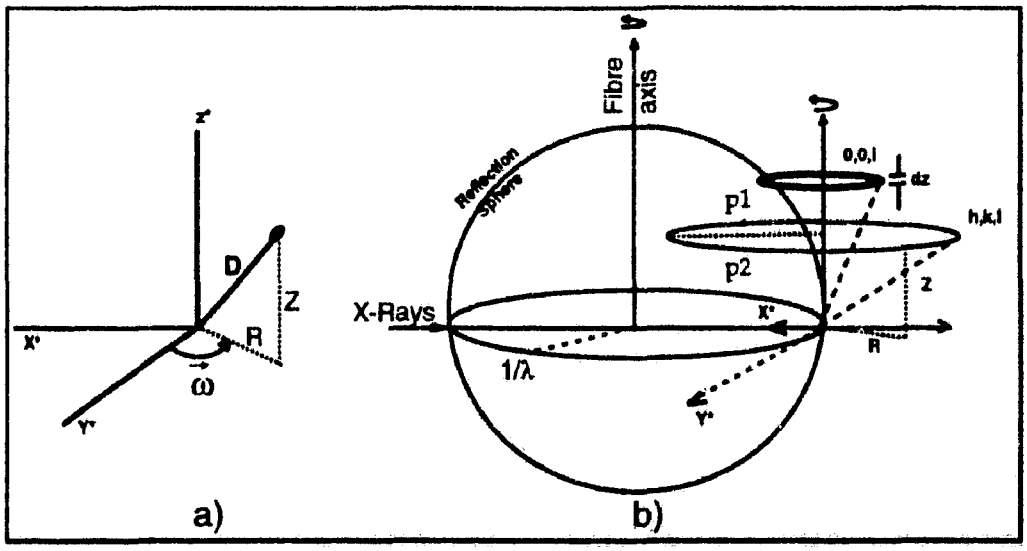

Fig. II.15: a) single crystal rotation method, where crystal is rotated at a constant angular velocity $\vec{\omega}$ requires a Lorentz factor proportional to ω to correct for integrated intensities. For ω constant, L is proportional to R b) Meridional (exaggerated) and non-meridional reflections in a fibre have reciprocal lattice points distributed on circles due to cylindrical distribution of orientation. Each reciprocal lattice point intercepts the sphere of Ewald in two location p1, p2 which are symmetric for a vertic lly aligned fibre. The Lorentz correction is L=R by use of analogy to a). If disor entation is present, reciprocal lattice points are spread into circles of finite thickn ss dz.

However, with crystalline col agen fibres, the Lorentz factor becomes an important detail for the following reasons:

a) Presence of Bragg scattering out of the meridional region.

b) Crystalline domains usually exhibit additional disorientation about the fibre axis and produce important arcing of the diffraction spots. The extent of disorientation causes the meridional reflections to be extended off the meridian. Therefore, additional geometric correction is required to calculate the structure factors from the observed integrated intensities.

Other factors like divergence of the beam, lateral size of the coherent scattering domains also influence the observed integrated intensity.

Considering all of these effects and for the purpose of this study the Lorentz correction will be examined in details to allow for the specific features of scattering by fibres.

From the general relation given above , we now can derive a special Lorentz correction

$$\left|\vec{F}(\vec{H})\right|^2 = L^{-1}\, I_{int}(\vec{H}) = R\, I_{int}(\vec{H})$$

which is correct for a reflection of regularly defined shape located on a position on the film defined by 1/R. We now need to correct for the fact that the reflection might be spread in the R direction and introduce thus the variation in the R direction by summing over step variations in that direction. Lorentz correction can thus be applied under the form of an integral of the form

$$\left|\vec{F}(\vec{H})\right|^2 \approx \int I(\vec{H})\, R\, dR$$

Now if the reflections are spread in the Z direction, we can also sum the total contribution by integrating values with small variations over Z axis, yielding

$$\left|\vec{F}(\vec{H})\right|^2 \approx \frac{2\pi}{V_r}\iint I(\vec{H})\, R\, dR dZ$$

where V_r is the volume of the reciprocal unit cell and $2\pi/V_r$ is introduced for normalisation.

C. MIR Method as Approach for X-ray Diffraction Investigations into Collagen Structure and Packing.

Since MIR methods have been the most successful procedures to solve the phase problem, one may expect that this will also enable the phasing of the data extracted from X-ray fibre diffraction patterns.

1. Native Collagen

The native collagen diffraction pattern is shown in figure II.16 where I have added background subtracted films together. The background subtraction procedure introduced some artefacts on the equator (figure II.16) but our goal was to display the weakest intensities on all of the row-lines. The reflections on the helix layer lines are also obvious but one can clearly see some weak intensities on the other row-lines. The single reflections have been collected using a method described below.

2. Isomorphous Derivatives of the Crystalline Collagen

High angle X-ray diffraction data for isomorphous derivatives for type I collagen have been obtained at the crystallographic beamline in Daresbury by Drs Wess T & L. The data set contains films for gold, platinum, iodine and phosphotungstic acid labelled collagen. X-ray diffraction patterns for PEG added collagen have also been recorded. The use of electron microscopy stains such as phosphotungstic acid and other heavy atom reagents like uranyl acetate is justified by the large number of labelling sites and the efficiency of these heavy atoms to label collagen molecules. However, these stains are better not used in phase determination studies due to the possibly high number of labelling sites, the low site occupancy as well as possible disruption of structure leading to a lack of isomorphism.

The use of iodine labelled collagen on the other hand is convenient because the position of this heavy atom is supposed to label the end of the molecule. This assumption is justified from the aminoacid sequence knowledge where tyrosine is the only residue with high affinity to iodine and is located at the N-termini of the molecule (Miller & Wess, private communication). The other heavy atom derivatives in turn may cause additional difficulties in the Patterson map interpretation due to the possibly high number of heavy atoms in the unit cell. It is obvious that, whilst in globular proteins the accessible surface and thus the fixation sites per residue number is small due to the numerous buried residues, in fibrous proteins, this surface is actually larger.

Fig. II.16 : The diffraction patterns from native collagen contain a set of well resolved spots on the meridional and equatorial axis. However, we need to collect data on the other row-lines in order to produce a 3D reflections set for Fourier synthesis. The figure shown here is an image addition of 3 films from one exposure

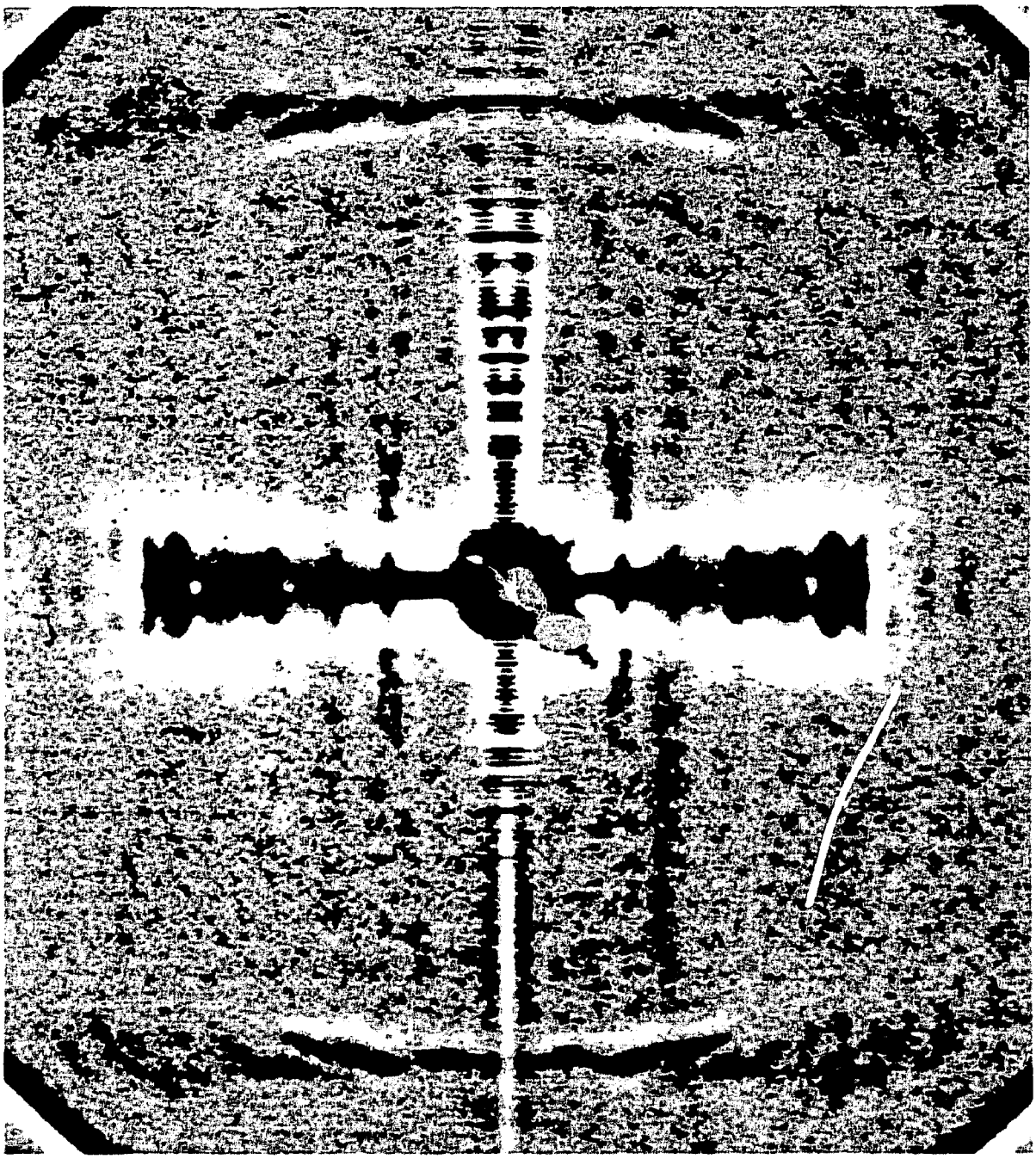

using a film pack. One thus observe additional weak intensities on the vertical row-lines and the helix layer-line which are necessary for a 3D Fourier synthesis.

Fig. II.17 : This figure shows a section of the native diffraction pattern in the region of the vertical row-lines with R ≈ 1/27Å to R ≈ 1/19Å. The reflections on the helix layer line are obvious, however I have indicated some weak reflections on those row-lines with an arrow.

The heavy atoms in principle have more access to the residues known to have high labelling affinity when those residues are distributed on the cylindrical surface of the collagen molecule. In our experiments, the number of heavy atoms added to the native structure is unknown and this makes the Patterson difference maps more complicated. Otherwise, these heavy atoms may form clusters of more than one heavy atoms bound to residues separated by a distance less than the resolution limit of the available diffraction data. But this is not a major problem since high molecular weight proteins ordinarily require the use of such clustered metals in order to observe intensity differences in the diffraction data (Blundel & Johnson, 1990).

Moreover, the heavy atom labelled collagen is assumed to be isomorphous and consequently no tests for isomorphism will be undertaken. Whilst these tests are very important in high resolution protein crystallography, it is not actually possible to test for the lack of isomorphism. Lack of isomorphism can manifest itself in many different ways some of which are impossible to identify unless the structure of the native protein crystal is already known. Possible lack of isomorphism can also be caused by the movement of a sidechain or even part of a polypeptide chain. The movement is in a way which do not disturb the rest of the protein structure but introduce a difference in the density map at a site which is different from the heavy atom substitution. Lack of isomorphism can also lead to a change in the unit cell

dimension but low resolution studies are not severely affected. The only problem arising in unit cell dimension change is the ambiguity introduced when indexing Bragg reflections. This problem is very critical in collagen pattern analysis as spots of successive l values are very close in reciprocal space. However, a special section of this work will deal with this problem later in detail.

Finally, the lattice parameters, thus the latest available refined values are those published in the paper of Fraser *et. al.* (1983) and are given in table III.1. These are assumed to be the best crystallographic parameters for the packing of collagen molecules in the crystalline domains of tendon. These parameters and the experimental native and derivative diffraction patterns obtained at Daresbury, will serve us as the starting materials for our low-resolution crystallographic study on collagen molecules in tendon. The next chapter however will fix for the adequacy of these parameters since a new set of crystal parameters have been recently published.

Chapter 3

The Crystal Unit Cell of Collagen in Tendon is Triclinic

A. Previous and New Models of Collagen Packing

Several structural models for collagen packing have been proposed over the last few decades by investigators working on the structure of tendinous collagen. Based on electron microscopy and X-ray diffraction studies there has been the two-stranded microfibrils model proposed by Woodhead-Galloway *et. al.*, 1975, the four-stranded model (Veis & Yuan, 1975), the five-stranded (Smith, 1968, Miller & Parry, 1973) and eight-stranded (Nemetschek & Hosemann, 1973).

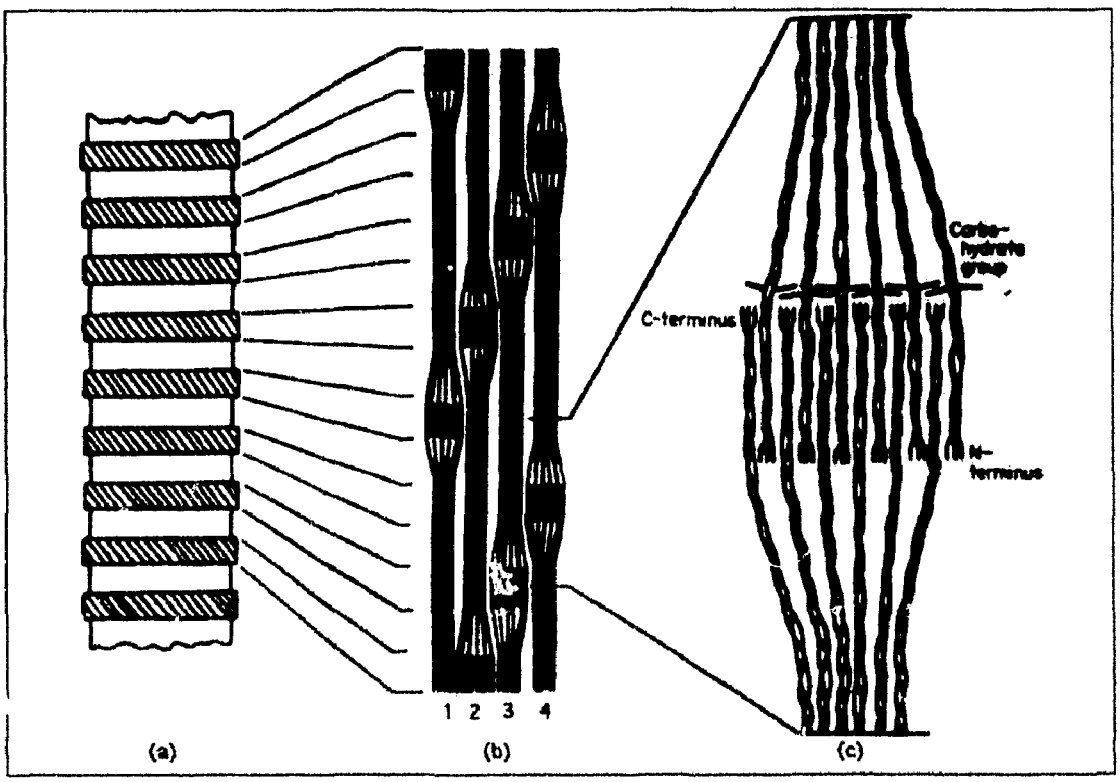

Fig. III.1 : (adapted from Kajava, 1991) Schematic representation of the levels of collagen fibril arrangement as suggested by Kajava.: (a) a characteristic cross-striated pattern of collagen fibril;(b) arrangement of the microfibrils determining the axial periodicity D of different shading observed with the electron microscope ; (c) the region of bunch overlap, where the molecules are packed hexagonally .

However, none of these proposed models has been in total agreement with the available experimental data; this holds particularly with the X-ray diffraction patterns. The present medium angle synchrotron radiation experiment applied to native and derivative collagen fibres has increased the evidence that type I collagen fibres in tendon are composed of crystalline arrays of collagen molecules. The molecules are thought to be packed in a quasi-hexagonal unit cell. Fraser *et. al.* , (1983) have refined the unit cell parameters and its orientation relative to the fibre axis using X-ray films of

PTA labelled collagen. The PTA labelled collagen has ordinarily X-ray diffraction patterns that contains a lot of high intensity and well resolved spots due to the presence of the heavy atoms. In this chapter, the triclinic unit cell (Hulmes *et. al.*, 1979, Fraser *et. al.*, 1983) will be shown to fit the experimental data at best and a computer comparison with another recently published model (Kajava,

Table III.1

Triclinic Cell	a = 39.97Å	b = 26.95Å	c = 677.9Å
Fraser & al.	$\alpha = 89.24°$	$\beta = 94.59°$	$\gamma = 105.58°$
Triclinic Cell	a = 86.5Å	b = 86.5Å	c = 2690Å
Kajava	$\alpha = 94.6°$	$\beta = 86.05°$	$\gamma = 120.0°$

1981) will show the incorrectness of this new proposed model.

Kajava proposed a model of different packing for collagen molecules at the microfibrilar level and by the way he suggested a new crystal unit cell. In his model (figure III.1) the collagen molecules are aligned in axial register to form a bunch. The bunches are aligned head to tail and penetrate by 300Å into each other to form the microfibrils. The model has an effective axial periodicity of 670Å when projected on to the fibre axis and this results from the staggering of microfibrils rather than the staggering of molecules as in the conventional model.

The main result obtained by Kajava is that he suggests a set of new crystallographic parameters for the unit cell. These parameters are listed in table III.1 together with those of the conventional model. In this new model the unit cell is larger than in all previously proposed models, and consequently, the X-ray diffraction pattern should display many additional reflections. However, this is not observed in the X-ray diffraction patterns and Kajava accounts for it by the fact that these reflections are very weak to be observed.

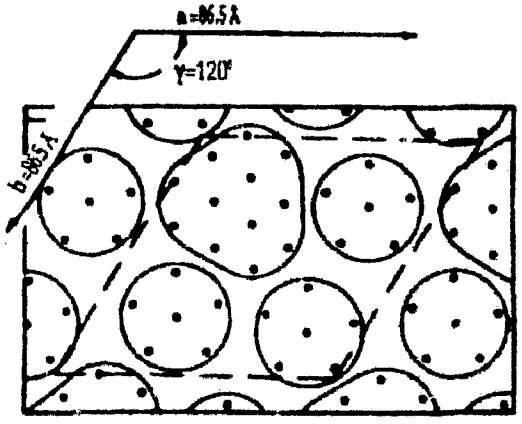

Fig. III.2 (Taken from Kajava, 1991) :Unit cell defined by Kajava for the model of collagen molecular packing. Large circles designate overlapping regions.

Kajava then calculated the low angle equatorial diffraction pattern for the packing and unit cell he proposes and compares this to the results obtained by others. He thus found an agreement between calculated diffraction data and X-ray diffraction patterns and obtained an R-factor of 26% for his

model.

So far, the Kajava model has been constructed with the assumption that some Bragg reflections which support his model are present on the X-ray diffraction patterns and have so far not been observed.

B. A Comparison of Collagen Models with Experimental Fibre Diffraction Patterns

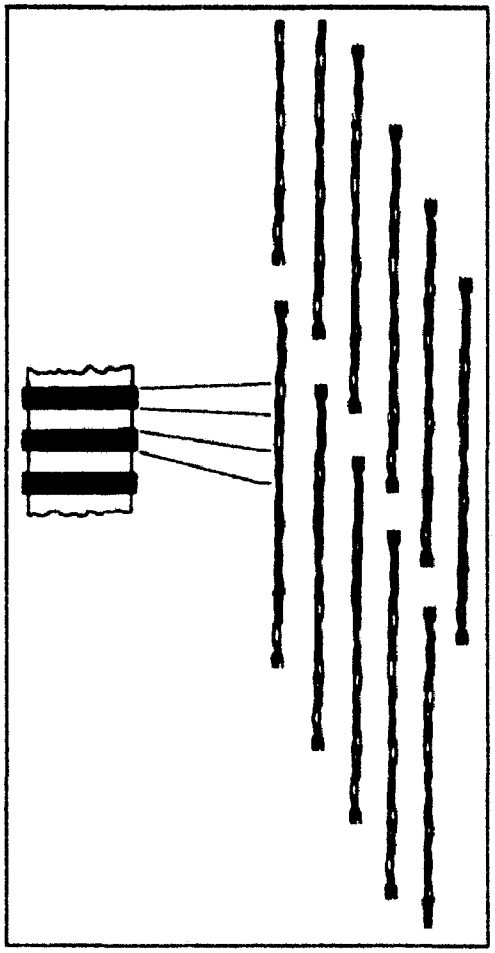

Fig. III.3 :The characteristic banding pattern observed with tendon fibrils under electron microscope is related to the staggering of collagen molecules by 678Å in the axial direction.

In order to show which model better fits the experimental data I used computed lattice prediction of the fibre diffraction patterns for both models. The calculation done in this section is only for the prediction of the positions of Bragg reflections and no intensity calculation will be done. We have at hand X-ray synchrotron radiation diffraction patterns obtained with phosphotungstic acid (PTA) labelled collagen which show high intensity peaks on the first row-lines and some other high intensity peaks on the (±1kl, ±2kl. etc...) row-lines. The data were collected using a pack of films so that all the intensity range was recorded.

The films were then scanned using a conventional photodensitometer and binary files were generated. The use of a colour computer display allowed me to display the films on an 8 bit colour scale. A fast, image display software also allowed me to handle very large arrays of data e.g. 2400x2400 pixels per film in an easy way. I thus used the high on-line memory capacity of the computers at the ESRF.

Rotation and inversion of images were also possible in order to align and superimpose films within the same pack. This enabled me to use the image addition of successive films in order to represent all the diffracted peaks on the same pattern and compare with the predicted patterns. In fact, due to the high continuous background intensity on the films, the weakest reflections in a fibre diffraction pattern are not always observed and we thus need the image digital processing to enhance those weak intensities. The steps used in this process were as follows :

1) The photodensitometer raster used for film scanning was 50μm so that I could first apply a

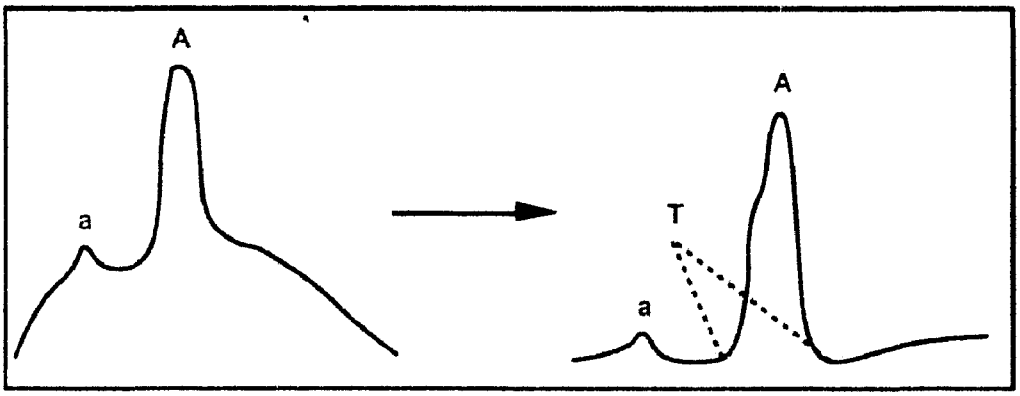

Fig. III.4. : A schematic view of the background subtraction method used. for peak enhancement purpose. The peaks (a) and (A) are the weakest and highest peak located on a continuous background. After background removal , the two peaks are situated on a zero level background but for the highest peak some negative curving in the wings (T) may occur .

smoothing filter in order to minimise the noise introduced by the photodensitometer. This was achieved after averaging each pixel value with all neighbouring pixels in a square box 3 pixel length.

2) Films were then oriented relative to each other in order to bring together the same centre and the same vertical and horiz ntal axes for all the films.

3) Then the following background subtraction method was applied but for display purposes only. It's use can not be generalised as a background removal procedure due to the artefacts it introduces in the data. That is, for each pixel in the image a value of the surrounding average intensity was first calculated on a large squared box of width ~100 pixels. This average value was then subtracted from the pixel value. The process is repeated by scanning horizontally and vertically each pixel in the image. As a result, for regions of the films where spots are very weak but located on a continuous background, the background was consequently removed

whereas for regions containing high peaks the procedure removes the surrounding background but also the peak height is truncated and some curving occurs in the direct vicinity of it (figure III.4). The method has thus a lot of artefacts but nevertheless for isolated weak peaks it is an efficient method to improve the weakest peaks. The method described above is also suitable for image addition as described in the next point.

4) Following the above procedures, the images from one pack are then added pixel by pixel so that all contributions from different films were simply added.

5) Finally, the experimental and the predicted fibre patterns were compared using simultaneous graphical display or image superposition.

C. Results and Discussion

The starting point for each fibre pattern simulation is the knowledge of the unit cell parameters, its orientation relative to the fibre axis and the diffraction geometry involved in the experiment (film sample distance, photodensitometer raster unit, fibre tilt, fibrils polar disorientation etc...). The program I have written take into consideration all of these parameters and I will show the importance of these parameters for data integration in a later section. Despite the experimental inaccuracy of these values, it was always possible to calculate a fibre diffraction pattern in film space using preliminary values. The fibre diffraction patterns were obtained by calculating for each (h,k,l) reflection, the intercept with the Ewald sphere when cylindrical rotation followed by a tilt to the X-ray beam was applied. Then I calculated the position of the Bragg reflection on the film using the equations given in section II.B.2. An arbitrary value of 255 was set for each pixel in the calculated pattern where Bragg spot was predicted and zero elsewhere. The predicted binary images were then added to the experimental diffraction patterns. Figure III.5 shows the image addition of the patterns obtained with the conventional unit cell.

Only the central region of the pattern (e.g. up to l=50) is shown in figure III.5 but the prediction was correct over the whole pattern. The overlap of predicted and experimental patterns in the region of the helix layer-line will be shown in the paragraph on data integration where fibre tilt effects will be discussed. Let us first consider the (-1,0,l) and the (1,0,l) row-lines in figure III.5 where the agreement between predicted and experimental spots is obvious for the conventional triclinic unit cell obtained by Fraser & MacRae (1981). Both row-lines are highly populated with single spots which is usual when the experiment is done with heavy atom labelled collagen. These spots however are usually not seen all at once on a single film due to the strong background intensity in the pattern central region. They are viewed all at once in the figure above because I have added all the background subtracted intensities from different film in that region. The equatorial high intensity reflections for instance are obtained from bottom films where strong continuous scattering has been absorbed by the uppermost films.

A near equatorial region of the row-lines from which important geometric features are deduced is shown in figure III.6. The angle between these two row-lines is related to the interaxial angles in the unit cell (Fraser *et.al.*, 1981). The predicted Bragg spots are roughly superimposed on the experimental reflections that is, the unit cell parameters a and b and the interaxial angles defined for the unit cell are thus correct. Fraser and MacRae, in their studies of collagen unit cell, excluded the tetragonal unit cell as a possible lattice after investigation of this region and further concluded that this angle is related to the φ_{c^*} angle in the unit cell.

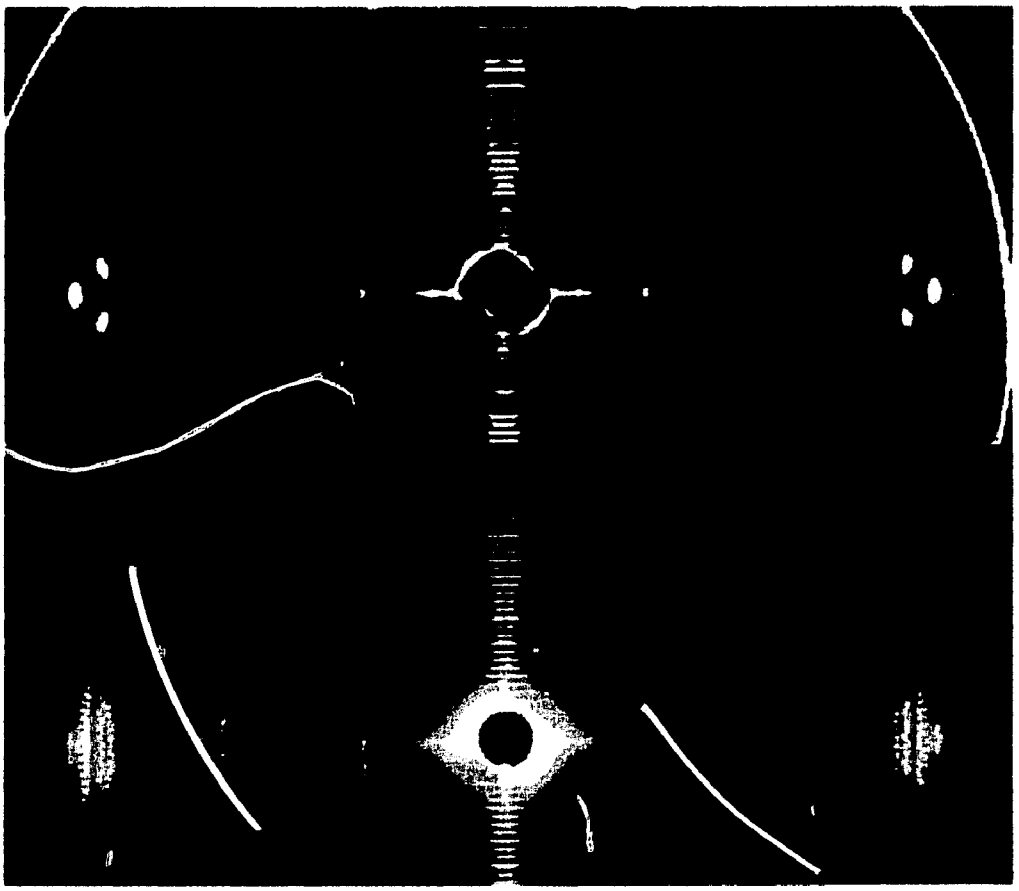

Fig. III.5 : Prediction of the Bragg spots obtained with the conventional triclinic unit cell. The method used for digital filtering and image addition is described in the text. The upper image shows PTA stained collagen pattern obtained after background subtraction and image addition. The data display on the row-line have been improved in comparison to the untreated images thanks to this technique. The lower image is the same but obtained after addition of the simulated Bragg spots where it is now obvious that the unit cell parameters used in this calculation are in good accordance to the experimental pattern.

So far the predictions for the triclinic unit cell are in good agreement with the low-resolution experimental patterns. We also observe in figure III.5 that intensities from the other row-lines are distributed on vertical sections in the X-ray pattern and they all have intercepts with the equator at observed R values R=1/27Å,R=1/19Å and R=1/13Å. The peak overlap in these regions is important and precludes their description in terms of single Bragg spots. These row-lines intensities are also very strong on the equator probably due to high diffuse scattering which causes overlap of many

Bragg reflections. Example of this strong overlap is shown by the strongest triplet reflections in the R=1/13Å region.

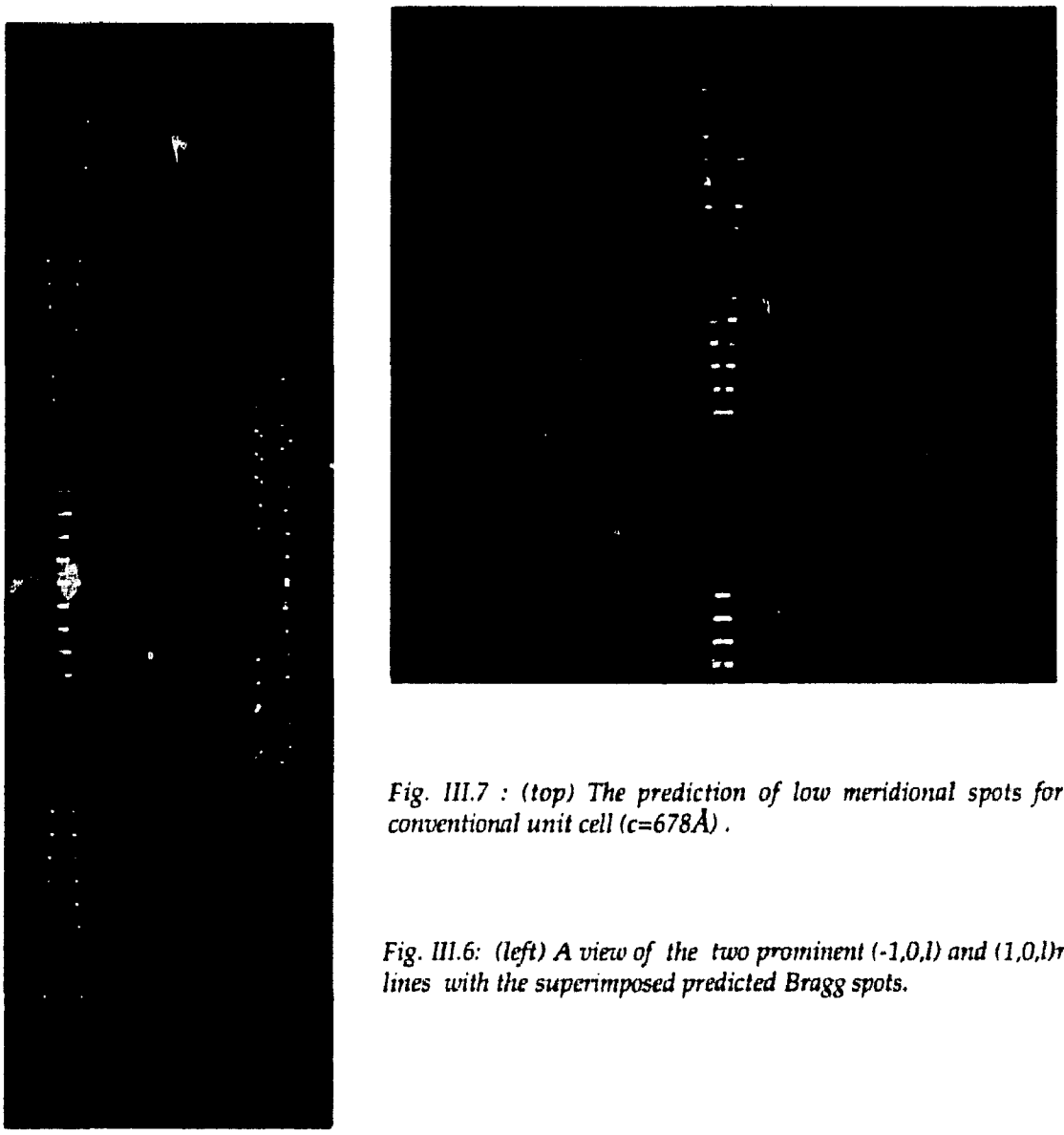

Fig. III.7 : (top) The prediction of low meridional spots for the conventional unit cell (c=678Å) .

Fig. III.6: (left) A view of the two prominent (-1,0,l) and (1,0,l)row-lines with the superimposed predicted Bragg spots.

I have then simulated the lattice Bragg reflections for the unit cell proposed by Kajava. I obtained the patterns shown in figure III.8 where the first remark is that the film is overcrowded with Bragg spots. The unit cell in that case predicts many more Bragg spots then observed on the fibre pattern. In the central region of the pattern there are three additional row-lines in the region R<1/39Å where Kajava predicts low intensity on the equator. Therefore, these regions have been carefully inspected over the films in the pack and I never observed experimental evidence for even a low intensity spots. The background subtraction and image addition procedure also have not allowed for the observation of some weak intensity peaks that complies with the new model. Moreover, the Kajava model does not fit either to the experimental positions of the observed (-1,0,l) and (1,0,l) row-lines nor to the fact that these row-lines are split according to the interaxial angle defined above. The intercept of the fourth

row-line with the equator is estimated at R≈1/40Å. Since the new model has unit cell parameters a=86.5Å, b=86.5Å, the presence of Bragg spots in that region is only due to the order n=2 of the harmonic reflection (2,0,l≈0) obtained with the conventional unit cell parameters e.g. 2/86.5 Å ≈ 1/40Å. All other predicted spots are so far not observed in the experimental pattern shown in figure III.8. I thus can conclude that the new proposed model is not obvious since the pattern prediction in that case is not consistent with the available experimental patterns. Although the calculation done by Kajava has led to a favourable R-factor on a model electron density , this can only be explained by the

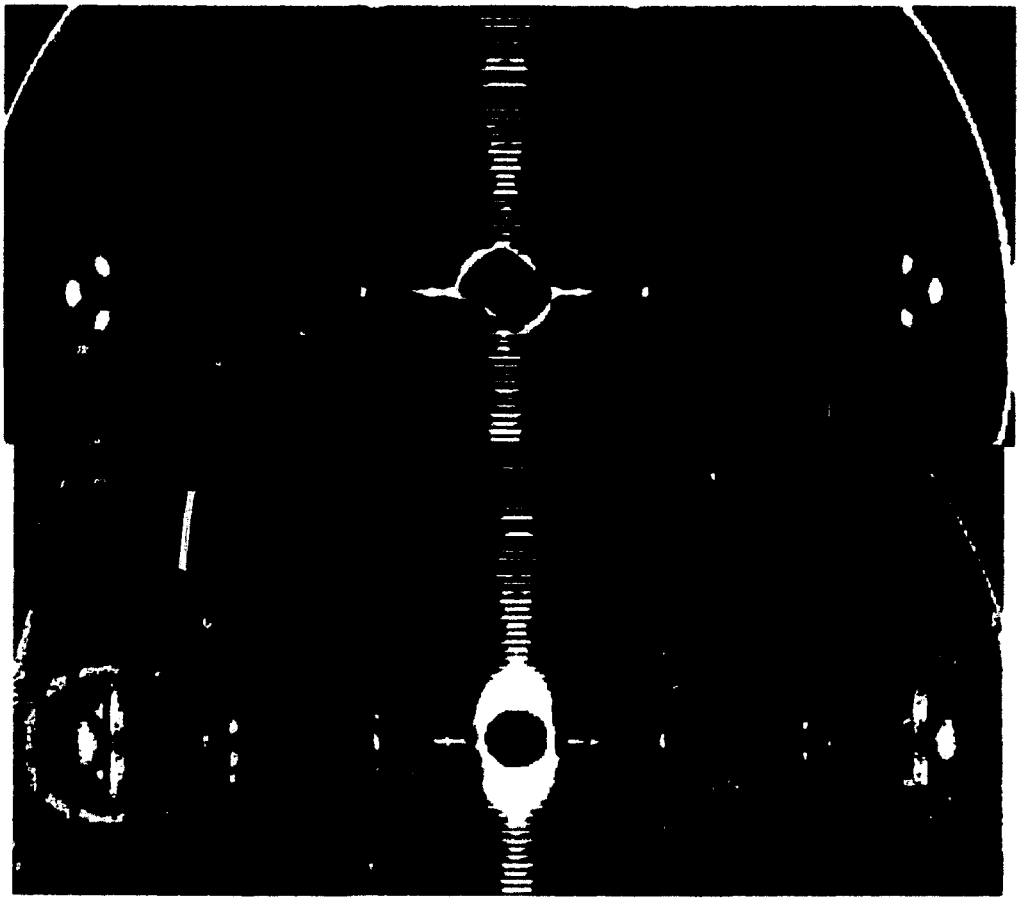

Fig. III.8: Here I show the pattern of the PTA treated fibre that has been improved to show low intensity peaks (top). Background removal and image addition techniques are explained in the text. The bottom figure shows the same pattern with the prediction done with Kajava unit cell. The X-ray films is overcrowded with predicted Bragg spots and doesn't fit the observed experimental spots. The validity of this model is discussed in the text.

low number of reflections he included in his calculation.

Now if we calculate the following ratios with the unit cell parameters he has obtained

$$\frac{a_{kajava}}{a_{triclinic}} = \frac{86.5}{39.97} \approx 2 \qquad \frac{b_{kajava}}{b_{triclinic}} = \frac{86.5}{26.95} \approx 3 \qquad \frac{C_{kajava}}{C_{triclinic}} = \frac{2690.}{677.9} \approx 4$$

we obtain roughly integer ratios so we can conclude that Kajava' s model is a non-primitive unit cell defined on the triclinic one by the vectors 2a, 3b and 4c. The volume of this unit cell is 2x3x4=24-times

greater than the primitive one. Knowing that the primitive triclinic unit cell contains one collagen molecule so the new one can contains24 collagen molecules. Figure III.2 shows the packing of collagen

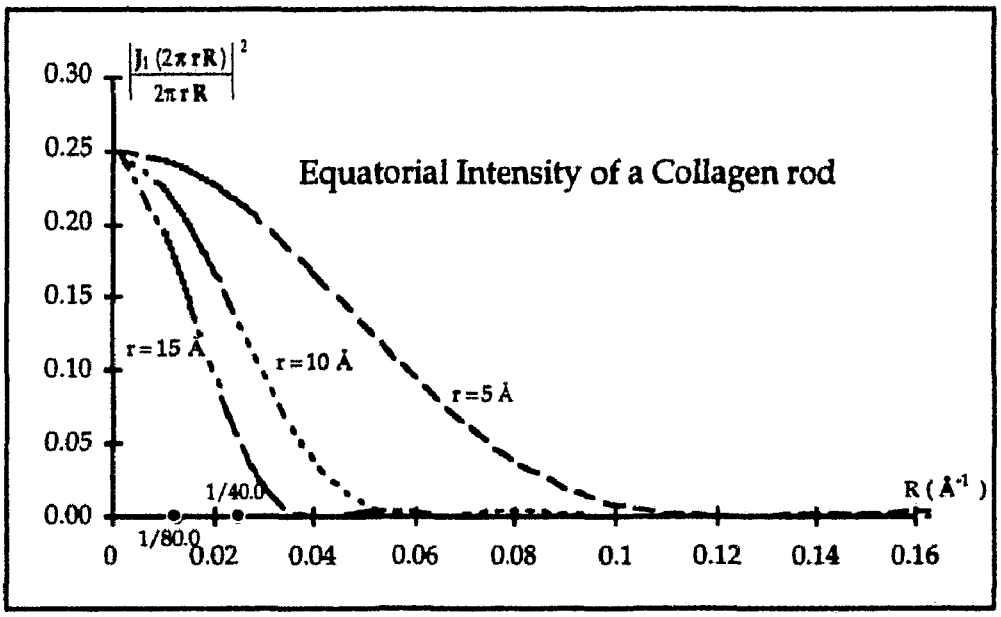

Fig. III.9 : Calculated intensity along the equatorial axis for a model collagen molecule with radius respectively r=5Å, 10Å and 15Å. The intensity calculated at R=1/80Å is remarkably higher than the intensity at R=1/40Å.

molecules in the new model. The unit cell contains 24 segments of one molecule with large circles designating bunches of penetrating molecules. The unit cell is 2690Å long in the c direction, e.g. parallel to the collagen molecule, so if we give up the hypothesis that large bunches are regions of penetrating molecules and suppose that these are also parallel collagen segments we obtain the 24-folds non-primitive unit cell.

The other condition which disables the new model is that it does not explain the absence of many reflections in the diffraction pattern. We can assume two hypothesis for the missing reflections:

a) The Bragg spots in principle, sample the molecular transform in reciprocal space at vectors defined by the Miller indices. Accordingly, the Kajava model is possible if we assume that a lot of the predicted spots to be sufficiently weak due to the molecular transform. Then this must be true on the equator since the transform of a cylindrical molecule has an intensity distribution in reciprocal space which is mainly distributed on layer lines. Hence, in the region on the equator near the origin of the film we apply Porod's law of small angle scattering from a rod shaped homogeneous molecule. We thus approximate the collagen molecule to a cylinder with uniform electron density and dimensions ≈5Å x 3000Å. The small angle scattering amplitude from such a molecule is then calculated using the cylindrical coordinate system and yields an expression in terms of Bessel function of the first order. We write

$$F_c(R) = (\Delta\rho) \int_0^r 2\pi\, r\, dr\, .\, J_0(2\pi\, r\, R)$$

where r is the radius of the molecule, $\Delta\rho$ is the electron density excess of the cylindrical molecule and R is the reciprocal coordinate. The intensity is then obtained by squaring the above structure factor amplitude after integration and we write it

$$I(R) = \left[(\Delta\rho)\, A\, .\, \frac{2\, J_1(2\pi\, r\, R)}{2\pi\, r\, R}\right]^2 \approx \left[\frac{J_1(2\pi\, r\, R)}{2\pi\, r\, R}\right]^2$$

Now, the calculation done by Kajava predicts many weak intensity reflections in the region around R≈1/80Å, whereas low angle equatorial experimental patterns show the first prominent intensity at R≈1/40Å. Therefore, I have plotted the intensity function on the low angle equatorial axis that follows

Fig. III.10 : The Kajava unit cell predicts additional row-lines in the central region of collagen X-ray pattern. Thus, following a subtraction of background from all the images in the same pack and image addition to improve the weakest intensity peaks I show here the overlap of predicted and experimental data. The Kajava model obviously doesn't fit the experimental pattern since no additional row-lines are observed in the central region. The conventional experimental row-lines are here clearly identified but the position and he split of the (-1,0,l) and (1,0,l) row-lines is also not followed by the new model.

the law obtained above in figure III.9. The collagen molecule is approximated by a cylinder with

radius of respectively r=5Å, 10Å and 15Å. The first minima calculated for each rod molecule are shown in figure III.9 and are obtained respectively at R=1/8Å for a cylinder of radius r=5Å, R=1/18Å for a radius r=10Å and R=1/25Å for r=15Å. The intensity calculated for R=1/80Å indicated by a circle on figure III.9 is thus non-zero and it has clearly a value equivalent or even higher than that obtained at R=1/40Å. Consequently, the presence of a high intensity Bragg reflection at R=1/40Å must be followed by another Bragg spot with at least an equivalent intensity at R=1/80Å for the Kajava model to be consistent with the X-ray pattern.

b) Systematic absences are usually observed with crystals belonging to the fourteen Bravais lattices and follow the special selection rules on Miller indices listed in the International Tables of Crystallography. They often indicate that the primitive unit cell is either body centred or face centred which is not actually the case for the collagen packing in Kajava's model. For example, for a reflection with indices 00l on the meridian there must be 3 systematically absent orders for the new model to agree with the meridional diffraction pattern. This means that, given a meridional reflection (0,0,l), the (0,0,l+1), (0,0,l+2) and (0,0,l+3) orders are systematically absent. We thus obtain the h=0,k=0,l=4n selection rule which is not a known extinction rule in the Crystallographic Tables.

In summary, I have shown in this chapter that the new proposed model could not be validated from the X-ray diffraction experiments whereas the conventional model is shown to fit with a better accuracy with the experimental data. The crystallographic study in the next chapters will attempt to understand the structure and packing of collagen molecules in tendon on the basis of this crystal system.

Chapter 4

Measurement of Crystalline Average Domains Size in Tendon by Means of Peak Broadening Analysis

It is a general feature of the structure of fibrous collagen that the crystalline order of an assembly of molecules in the fibre is better developed in the direction parallel to the fibre axis than perpendicular to it (Miller *et.al..*, 1981). This is shown by the meridional reflections in a fibre diagram that are always intense, sharp and with little diffuse scattering between them. Equatorial reflections conversely, are weak and always superimposed on a strong diffuse scattering which indicates that crystalline order is less perfect in this direction and that the degree of lateral disorder is important.

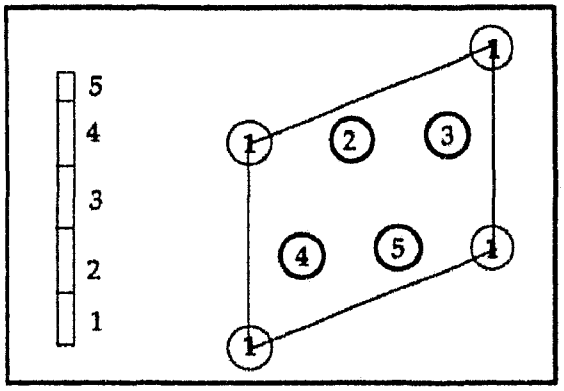

Fig. IV.1: A collagen molecule of length L= 4.4 X 677Å (D=677Å) is represented by a rod divided into 5 segments labelled 1-5. One unit cell contains one collagen molecule and crystal translations generate the whole structure by unit cell replication but the position of the relative segments in one cell must be consistent with the wholeness of one molecule. There are a lot of possible arrangements and orientations e.g. up and down molecules for the molecular segments 1-5 in the unit cell but this is not yet understood. (Adapted from Miller, 1981)

The equatorials are even sometimes not observed in native tendon and depend on sample preparation. Since the crystalline nature of collagen arrangement in native tendon has been well established it might be interesting to study the extent of this crystallinity in all directions and to relate this microscopic quantity to the macroscopic observed physical properties of tendon such as the high mechanical rigidity.

Characterisation of crystallite size is a conventional mean in powder diffraction methods. In materials science, measurement of crystal size in polycrystalline specimens by means of X-rays is based on two quite distinct effects. First, there is the general appearance of the diffraction photographs, from which it is possible to tell immediately whether the specimen consists of large or small crystals; secondly, there is the broadening of the powder lines that is produced when the crystals become very fine indeed.

The purpose of this chapter is to obtain an approximate measure of the broadening of the low 00l orders (l = 1 to 9) for crystalline collagen in rat tail tendon. These reflections are indexed on the basis of the unit cell previously described (Fraser *et.al..*, 1983; Fraser *et.al..*, 1987). The content of one unit cell is one collagen molecule represented by its 5 segments (Fig. IV.1). The crystalline domains in tendon fibres will be supposed to contain arrays of parallel molecules. The length of one molecule is about 3000Å.

The fact that the exact content of the unit cell has never been solved, proceeds from the difficulty to solve fibrous crystal structures with large c axis and also from the many Bragg reflections overlap. However the characterisation of the dimensions of crystalline domains in native fibres enable the study of monocrystalline domains extracted from the macroscopic tendon fibre using electron microscope sample preparation techniques. Such monocrystalline domains can theoretically be exposed to micro-focused high flux X-ray beams obtained with synchrotron radiation sources and allow further monocrystal structure determination.

A. Diffraction by Small Crystals.

1. Intensity Scattered from a Small Parallelopepidon Crystal.

Usually, crystal structure determination assumes crystals to be of sufficiently great dimensions for broadening due to finite crystal size to be neglected. Integrated intensities derived for structure factor calculation are function of the atomic coordinates within one unit cell with only peak broadening arising from crystal mosaicity. Thus crystal size effects are more or less neglected at the costs of the resolution limit attainable and the degree of ordering in the structure. In order to explicitly recall the parameters defining the crystal dimension the relations defining the diffracted intensity from a crystal will next be reconsidered.

The following relationships assume an unpolarised monochromatic beam of intensity I_0 and wavelength λ, falling on a very small single parallelopepidon crystal with edges $N_1\vec{a}$, $N_2\vec{b}$ and $N_3\vec{c}$. Relative to a crystal origin at O, the position of the atom of type n in unit cell $m_1 m_2 m_3$ is given by the vector $\vec{R}^{\,n}_{m} = m_1\vec{a} + m_2\vec{b} + m_3\vec{c} + \vec{r}_n$. The scattered intensity at a point P of observation, at a distance R from the small crystal in a direction specified by the unit vector $\vec{s}$ is obtained by first calculating the instantaneous electric field $\vec{E}_P$ scattered from the atom (m,n):

$$\vec{E}_P = \frac{\vec{E}_0 e^2}{m c^2 R} f_n e^{i\left\{2\pi\nu t - (2\pi/\lambda)\left[R - (\vec{s}-\vec{s_0})(m_1\vec{a} + m_2\vec{b} + m_3\vec{c} + \vec{r}_n)\right]\right\}}$$

The resultant electric field at P due to all atoms in the crystal is then obtained by summing over n to include all the atoms in a unit cell, and summing over $m_1 m_2 m_3$ to include all the unit cells

$$\vec{E}_P = \frac{\vec{E}_0 e^2}{mc^2 R} e^{2\pi i(\nu t - R/\lambda)} F \frac{e^{(2\pi i/\lambda)(\vec{s}-\vec{s_0})N_1\vec{a}} - 1}{e^{(2\pi i/\lambda)(\vec{s}-\vec{s_0})\vec{a}} - 1} \frac{e^{(2\pi i/\lambda)(\vec{s}-\vec{s_0})N_2\vec{b}} - 1}{e^{(2\pi i/\lambda)(\vec{s}-\vec{s_0})\vec{b}} - 1} \frac{e^{(2\pi i/\lambda)(\vec{s}-\vec{s_0})N_3\vec{c}} - 1}{e^{(2\pi i/\lambda)(\vec{s}-\vec{s_0})\vec{c}} - 1}$$

Then, the total diffracted intensity from a small crystal is obtained as the product

$$I_P = \vec{E}_P \vec{E}_P^{\,*} \times c/8\pi$$

B. Structural Broadening by Size Effects.

Structural broadening in diffraction experiments is due to distortions in the crystalline lattice combined with the particle size. These two effect are not easily distinguishable and mathematical analysis of the line profiles is required. However it is generally admitted that the two effects are additive. The effect of broadening due to small crystallite size on one single reflection measured at a position defined by the direction $\vec{s}$ is resumed by

$$I(\vec{s}) = I_e F^2 \frac{\sin^2(\pi/\lambda)(\vec{s}-\vec{s}_o)\ N_1\vec{a}}{\sin^2(\pi/\lambda)(\vec{s}-\vec{s}_o)\vec{a}} \frac{\sin^2(\pi/\lambda)(\vec{s}-\vec{s}_o)N_2\vec{b}}{\sin^2(\pi/\lambda)(\vec{s}-\vec{s}_o)\vec{b}} \frac{\sin^2(\pi/\lambda)(\vec{s}-\vec{s}_o)N_3\vec{c}}{\sin^2(\pi/\lambda)(\vec{s}-\vec{s}_o)\vec{c}}$$

where I_e is the intensity scattered by one electron, $N_1N_2N_3$ are the numbers of unit cells along the $\vec{a}$, $\vec{b}$ and $\vec{c}$ directions, thus defining the general shape of the crystalline particles. In general the N_1, N_2, N_3 are such large numbers that each of the three quotients differs from zero only if the three Laue equations are closely satisfied and hence the powder diffraction pattern reflections are sharp. For smaller crystals where N_1, N_2 and N_3 are small the three quotients expand, and the smaller the crystals the broader the powder pattern reflections.

1. The Scherrer Equation

This equation (Scherrer, 1918) has been derived for a particular case but has turned out to be of general applicability (Warren, 1969). First, let us assume a powder sample of small cubic crystals, all of the same size with the above defined values $N_1=N_2=N_3=N$. The crystals are assumed to be free from strains and faulting so that peak broadening is due only to the small crystallite size. For convenience the powder sample is replaced by a single crystal which takes all orientations. With the unit vectors $\vec{s}$ and $\vec{s}_o$ representing the exact Bragg law for a reflection hkl we have :

$$\vec{s}-\vec{s}_o=\lambda(h\vec{a}^*+k\vec{b}^*+l\vec{c}^*)$$

where $\vec{a}^*$, $\vec{b}^*$ and $\vec{c}^*$ are the reciprocal unit cell vectors. Let us now consider slightly different directions $\vec{s}'$ and $\vec{s}'_o$ for the diffracted and primary beam, and relate them to $\vec{s}-\vec{s}_o$ by the small difference vector $\Delta\vec{s}$ as shown in the figure below.

$$\vec{s}'-\vec{s}'_o=\vec{s}-\vec{s}_o+\Delta\vec{s}$$

Expressing the above equation of structural broadening for a reflection in terms of the general direction $\vec{s}-\vec{s}_o$ gives

$$I(\vec{s}) = I_e \; F^2 \; \frac{\sin^2(\pi/\lambda)\,\Delta\vec{s}\; N_1\,\vec{a}}{\sin^2(\pi/\lambda)\,\Delta\vec{s}\,\vec{a}} \; \frac{\sin^2(\pi/\lambda)\,\Delta\vec{s}\,N_2\,\vec{b}}{\sin^2(\pi/\lambda)\,\Delta\vec{s}\,\vec{b}} \; \frac{\sin^2(\pi/\lambda)\,\Delta\vec{s}\,N_3\vec{c}}{\sin^2(\pi/\lambda)\,\Delta\vec{s}\;\vec{c}}$$

Each of the three quotients can be approximated by a Gaussian function which has the same maximum ordinate and the same area by using a well known approximation:

$$\frac{\sin^2 Nx}{\sin^2 x} \rightarrow N^2 \exp -(Nx)^2/2$$

With this approximation, the intensity expression simplifies to

$$I(\vec{s}) = I_e F^2 N^6 e^{-(\pi/\lambda^2)N^2\left\{(\Delta\vec{s}\,\vec{a})^2+(\Delta\vec{s}\,\vec{b})^2+(\Delta\vec{s}\,\vec{c})^2\right\}}$$

Moreover, since the axes $\vec{a}^*$, $\vec{b}^*$ and $\vec{c}^*$ are assumed to be equal and orthogonal, the expression reduces to

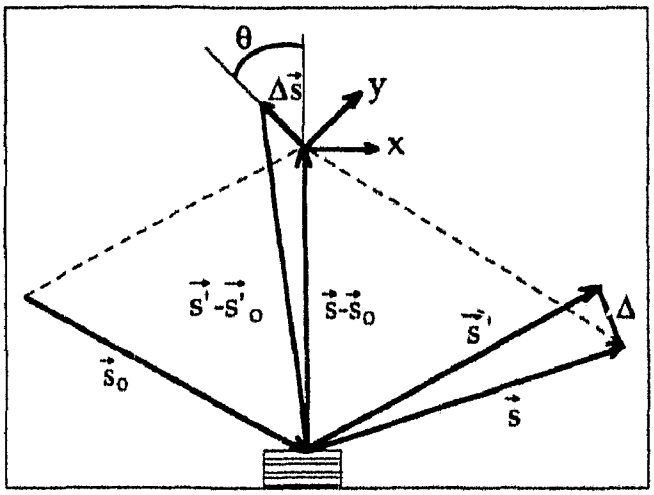

Fig. IV.2: Geometrical relations involved in the derivation of the Scherrer equation.

$$I(\vec{s}) = I_e F^2 N^6 e^{-(\pi/\lambda^2)(Na)^2(\Delta\vec{s})^2}$$

The exact Bragg law directions $\vec{s}$ and $\vec{s}_0$ are shown by figure IV.2. The above simple intensity expression is needed for a direction $\vec{s}' = \vec{s}+\Delta$ which makes a fixed angle with the Bragg law direction $\vec{s}$. Thus maintaining $\vec{s}'$ at a fixed angle from $\vec{s}$, one now wishes to find the total contribution to the intensity when the crystal is rocked through the whole region where there is any contribution. Instead of rocking the crystal, it is simpler to hold the crystal fixed and rock the $\vec{s}'-\vec{s}_0$ vector by adding the small vectors $\vec{x}$ and $\vec{y}$ which are in a plane normal to $\vec{s}-\vec{s}_0$. The difference vector $\Delta\vec{s}$ which was introduced above becomes

$$\Delta\vec{s} = \vec{x}+\vec{y}+\Delta$$

and the magnitude squared is given by

$$(\Delta\vec{s})^2=(x-\Delta\sin\theta)^2+y^2+(\Delta\cos\theta)^2$$

The intensity $I(\Delta)$ at a fixed departure Δ is proportional to the sum over all values of x and y where x and y are small values. The sum can thus be carried out from $-\infty$ to $+\infty$:

$$I(\Delta)=K I_e F^2 N^6 e^{-\pi (Na/\lambda)^2(\Delta\cos\theta)^2}\int_{-\infty}^{+\infty} e^{-\pi(Na/\lambda)^2(x-\Delta\sin\theta)^2}dx \int_{-\infty}^{+\infty} e^{-\pi(Na/\lambda)^2y^2}dy$$

by introducing the replacement $x'=x-\Delta\sin\theta$, $dx'=dx$, the integrals are independent of Δ so that the following equation results

$$I(\Delta) = K' e^{-\pi (Na/\lambda)^2 \Delta^2 \cos^2\theta}$$

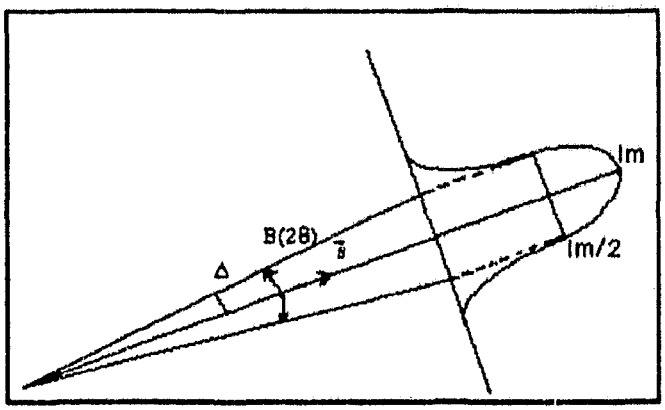

Fig. IV.3:The width B(2θ) *representing the angle in radians on a* 2θ *scale which subtends the half maximum intensity width of a powder diffraction peak.*

When $\Delta=0$, $I(\Delta)=I_m$ where I_m is the peak maximum and when $I(\Delta)=I_m/2$ the angle defined by Δ is half the angle B(2θ) which subtends the half maximum intensity width of the peak.
The value of B(2θ) is given by

$$B(2\theta)=\frac{2[(\ln 2)/\pi]^{1/2}\lambda}{N\cos\theta}$$

Letting L=Na represent the cube edge dimension of the crystals we obtain the Scherrer equation

$$\boxed{B(2\theta)=\frac{0.94\lambda}{L\cos\theta}}$$

This equation was originally derived for a sample of cubic crystals but it is often easily applied to the peak widths of non-cubic materials. It is not a bad approximation, if for each hkl reflection, the value

of L is interpreted as an average crystal dimension perpendicular to the reflecting planes.

Therefore, and on the basis of the crystalline model for collagen packing in tendon, the value of the broadening of the meridional 00l orders is the average crystallite dimension of the collagen domains in tendon in the $\vec{c}$ direction according to Scherrer equation.

For a given crystal dimension L, the Scherrer equation shows that the peak width increases as $1/\cos(\theta)$, and hence particle-size broadening becomes most pronounced at large values of 2θ.

Peak profile broadening in crystal diffraction experiments is not always due to sample size and distortions effects but usually depends on experimental settings.

In classical X-ray powder diffraction there is an additional instrumental broadening arising from effects such as slit widths of the collimation system, natural wavelength widths of the $K\alpha_1$ and $K\alpha_2$ lines in classical generators and the superposition of the non-resolved $K\alpha_1$ and $K\alpha_2$ peaks. These few examples show that corrections for instrumental broadening can be very important and should precede a peak broadening analysis.

2. The Method of Stokes and Wilson.

Stokes and Wilson (1942) introduced a more general treatment of the particle size broadening. The resulting broadening has an expression differing by a constant to the result obtained by Sherrer.

Usually, to calculate the integrated intensity of a reflection, an integration is first carried over all unit cells in the crystal and then the integration is carried over the reciprocal space. Now the integration order can be reversed and the integration carried first in the reciprocal space and than summed over the crystal unit cells. The position of a unit cell in a crystal is given by $\vec{R}_n=n_1\vec{a}+n_2\vec{b}+n_3\vec{c}$.

Expressing the diffraction vector by $(\vec{s}-\vec{s}_0)/\lambda=h\vec{a}^*+k\vec{b}^*+l\vec{c}^*$, where h, k and l are continuous variables, the intensity from one crystal is expressed by

$$I(h,k,l)=I_e F^2 \sum_n \sum_i e^{2\pi i[(n_1-n_1)h+(n_2-n_2)k+(n_3-n_3)l]}$$

The integrated intensity of a reflection is proportional to an integral of I(hkl) in reciprocal space. It is also given by an integral of $P(\theta)$, where $P(\theta)$ is the distribution with respect to 2θ of the power in a powder diffraction peak:

$$P=\int P(2\theta)\, d(2\theta)=K\iiint I(h,k,l)\, dh\, dk\, dl$$

Now let us again consider an orthorhombic crystal and the special case of a 00l reflection. The intensity is non vanishing only for very small values of the presumed continuous variables h and k, though the following limit is a good approximation

$$\left|\frac{\vec{s}-\vec{s}_0}{\lambda}\right| = \frac{2\sin\theta}{\lambda} = \left|h\vec{a}^* + k\vec{b}^* + l\vec{c}^*\right| \longrightarrow l\left|\vec{c}^*\right|$$

from the derivation of the approximate relation $2\sin\theta/\lambda \approx 1|\vec{c}^*|$ one obtains $d(2\theta)=(\lambda|\vec{c}^*|/\cos\theta)\,dl$ and after integrating with respect to dl

$$P(2\theta)=\frac{K\cos\theta}{\lambda|\vec{c}^*|}\iint I(h,k,l)\,dh\,dk$$

replacing I(hkl) by its expression and integrating from -1/2 to 1/2

$$P(2\theta)=\frac{K\,I_E F^2\cos\theta}{\lambda|\vec{c}^*|}\sum_{n_1}\sum_{n_2}\sum_{n_3}\sum_{n'_3} e^{2\pi i\,(n'_3-n_3)\,l}$$

Letting $N_3(n_1n_2)$ represent the number of cells in the row (n_1n_2), the sum over n_3 and n'_3 can be stated as

$$\sum_{0}^{N_3-1} e^{2\pi i n'_3 l}\sum_{0}^{N_3-1} e^{-2\pi i n_3 l}=\frac{\sin^2\pi N_3 l}{\sin^2\pi l}$$

At the peak maximum, the quotient takes a maximum value $N_3^2(n_1n_2)$ and the maximum in the peak profile is then given by

$$P_{max}(2\theta)=\frac{K\,I_e F^2\cos\theta}{\lambda|\vec{c}^*|}\sum_{n_1}\sum_{n_2} N_3^2(n_1n_2)$$

Carrying the integration for dh, dk from -1/2 to 1/2 and for dl, from l-1/2 to l+1/2 the total power of peak area is

$$\int P(2\theta)\,d(2\theta)=K\,I_e F^2 N$$

where N is the total number of cells in a crystal.

The integral breadth $\beta(2\theta)$ of a reflection is defined as the ratio of the peak area to the peak maximum

$$\beta(2\theta)=\frac{\int P(2\theta)\,d(2\theta)}{P_{max}(2\theta)}=\frac{\lambda N}{|\vec{c}|\cos\theta\sum_{n_1}\sum_{n_2} N_3^2(n_1n_2)}$$

$|\vec{c}|N_3(n_1n_2)$ is the crystal dimension in the $\vec{c}$ direction for the column of cells n_1n_2, let V be the volume of the crystal and N=V/abc; the integral breadth takes then the simplest form

$$\boxed{\beta(2\theta)=\frac{\lambda}{L\cos\theta}}$$

L is again the volume average of the crystal effective particle dimension in the $\vec{c}$-direction.

C. Correction for Instrumental Broadening.

In addition to the broadening due to particle size in a diffracted peak, there is always extraneous experimental broadening caused by slit widths, sample sizes and beam characteristics. All of these sources of broadening are grouped together under the name instrumental broadening and need to be suitably dealt with.

In order to correct for instrumental broadening it is usually convenient to use a standard peak observed under exactly similar conditions as the sample. The standard sample must ideally represent a perfect, i.e. strain and faults-free, crystalline particle of a size which makes effects of broadening negligible. This peak is usually obtained by mixing the powder sample under investigation and the crystal so that diffracted peak from the known crystal can be taken as the standard.

Considering the large unit cell in our collagen sample, $|\vec{c}| \approx 677$Å, it is evidently difficult to find a standard sample from the powder diffraction literature with unit cell dimension having a similar

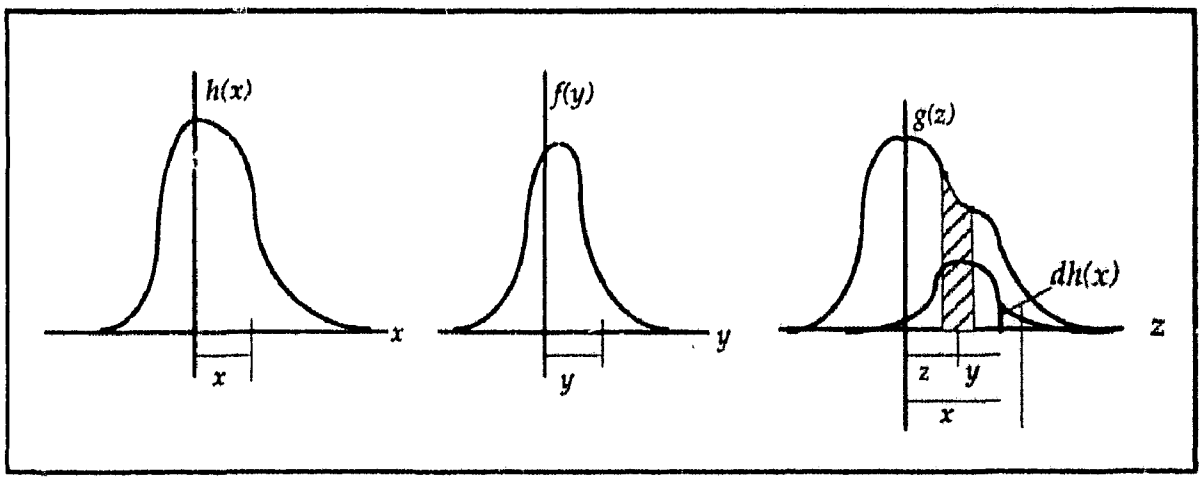

Fig. IV. 4: The three curves which are involved in the correction for instrumental broadening.

value and which could be incorporated in the tendon sample. Consequently, the only possible correction for instrumental broadening has to be calculated or modelled from the knowledge of the peak profile of the primary beam.

The principle of the correction applied to a diffracted peak can be discussed in terms of three curves as sketched in Figure IV. 4 .

Let the curve f(y) represent the broadening due to particle size only and be the function one wishes to obtain. The curve g(z) represents the effect of instrumental broadening as described before, it is the peak profile of the standard. The curve h(x) is the diffraction peak obtained from the sample, and it contains both the particle-size and instrumental broadening. The relation between the three curves is obtained by considering the cross-hatched area g(z)dz on the curve for instrumental broadening only. If there is particle size broadening then the area g(z)dz is spread out by the function f(y). Then at a

displacement y the ordinate is the contribution dh(x) at the position x=z+y on the h(x)-curve. Since the ordinates in the two curves are proportional to the peak areas,

$$\frac{dh(x)}{f(y)} = \frac{g(z)dz}{A}$$

where A is the area of the f(y) curve. One obtains the convolution product after the replacement y=x-z and calculating the ordinate of h(x):

$$h(x)=\frac{1}{A}\int g(z).f(x-z)\,dz$$

The needed experimental sample function is buried under the integral. This is the inconvenience of the method but assuming shapes for the three curves, it is possible to overcome this restriction and obtain relations between the half maximum widths of the curves.

Experimental shapes of diffraction peaks are usually approximated by analytical functions. The shape of a diffracted beam can either be Gaussian or Lorentzian (Cauchy curve) or a mixture e.g. convolution, of them. In this case, the relationship between curve widths B for these two simple functions can be resumed by

Gaussian shape	$f(y) \approx \exp(-a^2 y^2)$	$B(h)^2 = B(g)^2 + B(f)^2$
Cauchy shape	$f(y) \approx \frac{1}{1 + a^2 y^2}$	$B(h) = B(g) + B(f)$

Now for the purpose of broadening measurement the use of synchrotron radiation is of great benefit. In fact, one of the advantages of X-ray synchrotron beam is the high flux of the main beam which allows for the diffraction by monochromators while delivering high intensity beam at the sample position. These monochromators are made from large and perfect monocrystals delivering a narrow and parallel monochromatic beam at the sample. The shape of the main beam, when recorded at the film position is thus a good approximation for a standard instrumental broadening free from sample-dependent factors. However, the measurement of the direct beam by a conventional X-ray film or detector require that the intensity must be dampened to avoid detector damage. This was obtained by placing an attenuator, usually an aluminium foil in front of the detector plane.

D. Experimental Measurement of Collagen Crystallite Size

1. Experimental Requirements for Average Crystallite Size Determination

The conditions required for collagen crystal size determination are:

1) The recording of the first meridional reflections considering their low resolution

contribution to the overall geometric features in the crystal i.e. molecular form and packing. This theoretically also includes the zero and first orders.

2) Unlike the usual peak integrating procedure the primary beam and the individual

Table IV.1

l	1	2	3	4	5	6	7	8	9
r (cm)	2637.7	1318.8	879.2	659.4	527.5	439.6	376.8	329.7	293.0

meridional spots must be sampled at a reasonable number of points for curve fit procedures to yield appropriate broadening parameters.

3) The experimental set-up always requires the intercept of the main beam to preserve the detector from "seeing" the intense direct beam and thus avoid damage to the detector. When using X-ray films, this is also very advantageous to avoid back scattering from the pack holder. Back scattering would indeed cover the low orders with a parasitic saturating intensity.

Table IV.1 lists the calculated film-sample distances for the successive orders 1 to 9 to be recorded using the following relationship and a monochromatic beam (CuKα 1.54Å).

$$r = v \sqrt{\frac{1-\lambda^2 l^2 c^{*2}}{\lambda^2 l^2 c^{*2}}}$$

where r is the sample-film distance, v is the film radius (≈6 cm) and l is the highest meridional order observed.

The r value, which allows for 9 orders to be correctly recorded, lies in the range of the actually used

Table IV.2

Experiment No	Sample	Beamstop	Attenuator	Exposure time	Film No in the Pack
1	in	in	80 µm	20 mn	1st
2	in	in	80 µm	5 mn	last
3	in	in	80 µm	5 mn	3rd
4	in	out	500 µm	5 s	1st
5	out	out	Strong Peak : out Weaker Peak : 500 µm Weakest Peak : 500 µm	5 s 5 s 1 s	1st
6	in	out	500 µm	1 s	1st

small angle camera geometry.

Thus the experiments were carried out on the small angle beamline 8.2 at the SRS Daresbury with 2.26m camera distance and the sample cells when used had mica windows. The samples were fresh prepared rat tail tendons hold between two stretching clamps and maintained in hydrated state by a saline physiological solution. The wavelength was set to the CuKα (λ =1.54 Å). The recording of fibre patterns required film packs to allow for the high dynamic range of the spots. The attenuators when

used were a set of Al foils each of 40μm thickness whereas direct beam recording required an attenuator of thickness 500μm.

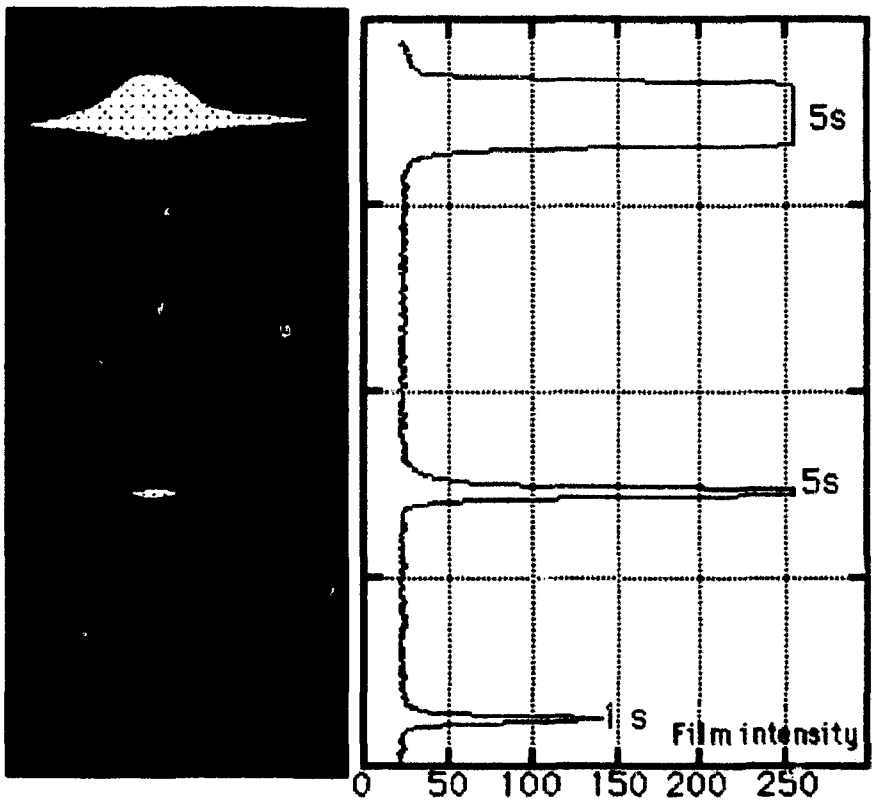

Fig. IV.5: A region of the digitised film obtained with the experiment No 5 showing two purposeless saturated peaks obtained : one with long exposure time (5s) and one when the attenuator has been removed. The third peak with 1s exposure time and the attenuator present is of the quality required for profile fitting.

X-ray films were then scanned with a conventional photodensitometer (50μm raster). The resolution of one pixel in the photodensitometer scanning for a 50μm raster was deduced from the following approximations:

$$2d\sin\theta = \lambda \xrightarrow[\theta<<]{} \theta \approx \lambda / 2d \longrightarrow d \approx \lambda / 2\theta$$

$$\theta \approx \tan\theta = \frac{50\mu m}{2.26m}$$

$$d \approx 34804 \text{ Å} \approx 3.48 \text{ μm}$$

This value for d is thus the maximum upper limit for crystal size broadening the current experiment can yield.

In order to record the low meridional orders of native collagen and the direct X-ray beam, six experiments were performed at the SRS Daresbury. The different experimental conditions are summarised in table IV.2.

2. Data Analysis.

The X-ray films obtained in the experiments listed in table IV.2 were then digitised using a conventional photodensitometer and images were inspected using computer image display. Only experiment No 3 and No 5 yielded suitable data for curve fitting procedures and are shown in figures IV.5 and IV.6.

A vertical section of the scanned film where the main beam has been recorded is shown in figure IV.5 (right) as only the profile in this section is required for the measurement of instrumental broadening. The long exposure time in experiment No 3 also allowed the effective recording of the even orders (2,4,6,8) which are naturally very weak in native tendon. The scanning of the third film in the pack enabled the recording of the non-saturated peaks for the first high orders. In order to visualise the lowest peaks (±8,±9) the intensity scale for displaying the meridionals is on a logarithmic scale. This gives the appearance as if the ±1 orders are broader and saturated but figure IV.7 shows that this is not the case and that orders ±1 are well resolved while order +1 is narrow and very close to the beamstop edge. The first order (l=-1) peak is also corrupted by some intensity issued from the scattering of the beamstop.

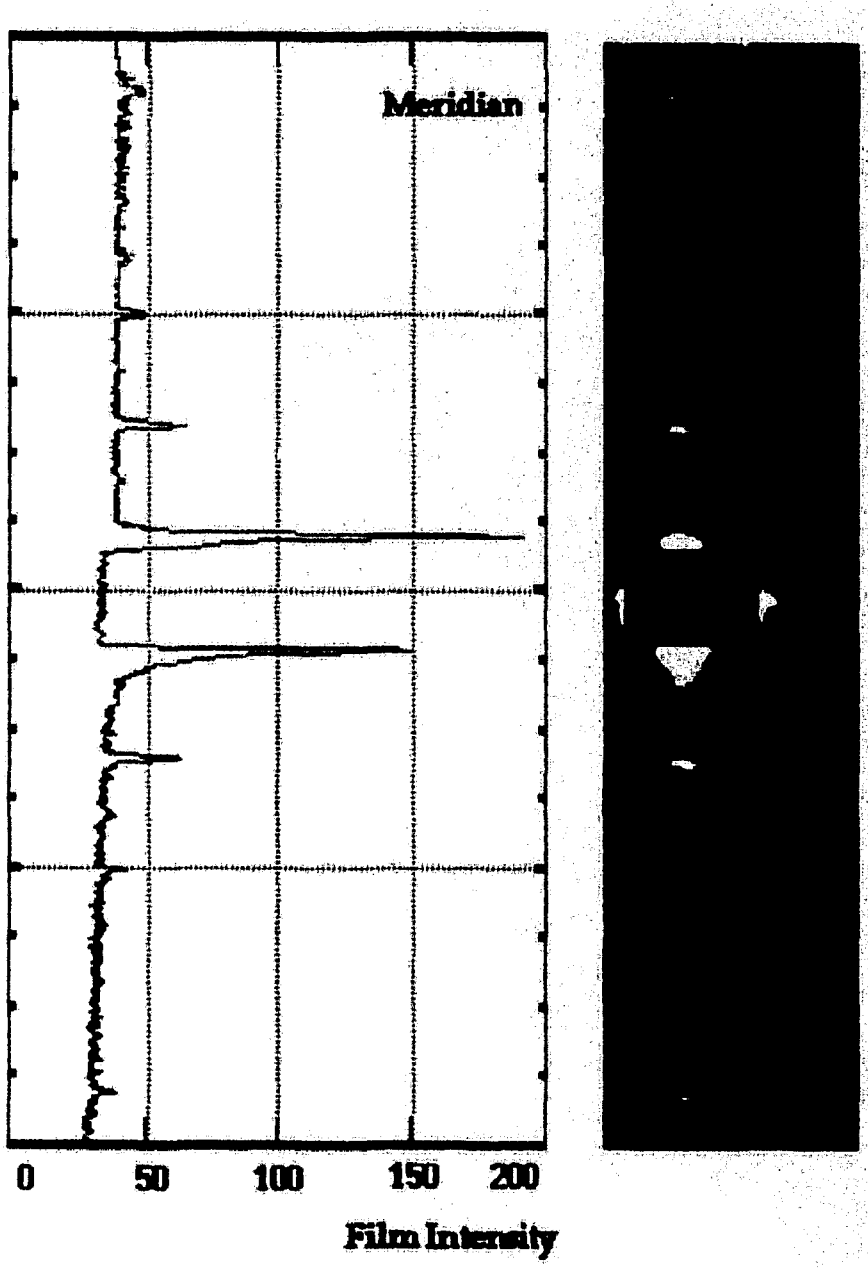

Fig. IV.6:The nine meridional orders observed for crystallite size determination in native tendon. Orders +1 and -1 seem to be larger on the right image but this is due to the choice of a logarithmic colour scale to enhance the weakest peaks.

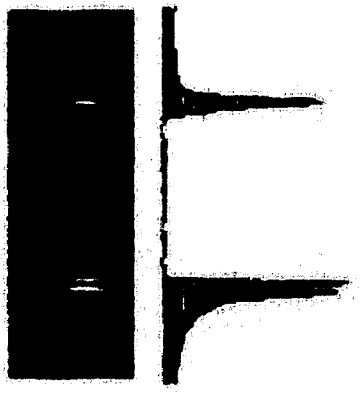

Fig. IV.7: Close view of the central region of the small angle diffraction pattern showing the beamstop and the orders 001 and 00-1 .

The radial averaged peak profile used in powder diffraction is not available in the case of tendon samples because tendon is not a crystalline powder but resembles a one dimensional powder. Therefore, peak profile is obtained by taking the projection of the meridional spots along the vertical axis. Care has been taken to first align meridional peaks so that orders are streaks which are perpendicular to the meridian.

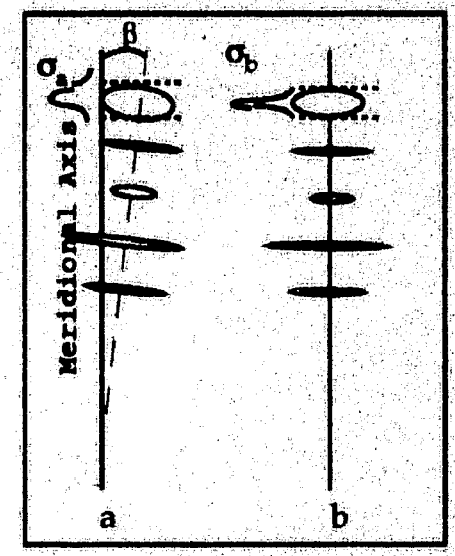

Fig. IV.8: The apparent vertical broadening of the peaks is dependent upon the relative orientation of the meridional reflections. It is correctly set by rotating the film by an angle β and taking the horizontal projection of the orders.

3. Least Squares Fitting of Data.

The basic approach for fitting a model into a set of N observed data (x_i,y_i) is to consider a simple class of functions (Gaussian or Polynomials for example) which represent the best model. This model depends on adjustable parameters and the fit supplies the appropriate set of parameters together with their accuracy. Data fitting usually requires to define a figure of merit that measures the agreement between the data and the model with a particular choice of parameters. Best fit parameters are then obtained by a process of minimisation in a multidimensional space. In summary, the results of the minimisation process provides (i) parameters (ii) error estimates on the parameters (iii) a statistical measure of the goodness-of-fit designated R in the following treatment. Supposing the model to be of the form

$$y(x)=y(x;a_1 \ldots a_M)$$

This equation has M adjustable parameters a_j , $j=1,\ldots M$ and the quantity to minimise is written

$$\chi^2 = \sum_{i=1}^{N} \left[\frac{y_i - y(x_i; a_1 \ldots a_M)}{\sigma_i}\right]^2$$

also called the Chi-square; σ_i is the standard error associated with the measurement of the y_i (here all identical and=1). When data are weighted, the equation used in calculating the linear correlation coefficient R is:

$$R=\sqrt{\frac{(1-\chi^2)}{\sum w_i (y_i-\bar{y})^2}}$$

where

R	=Pearson's R
χ^2	=chi square
w_i	=weight of actual value (set to 1 when none)
Y_i	=actual value
$\bar{Y}$	= mean of actual values

The weighs when used are the inverse of the square of standard error values.

4. Centre Determination of the Main Beam and the Meridional Diffraction Spots.

The equations of Scherrer and Stokes state that the broadening due to crystallite size is dependent on the scattering distance by the factor $1/\cos(\theta)$. Thus the origin of the patterns must be precisely determined for the direct beam and the diffraction orders from the sample. Figure IV.9 shows the first two orders fitted with a general function of the form of two symmetric Gaussian curves. The fit of the equation below, where $(\alpha x+\beta)$ is the contribution to the offset and slope of the background and X_1, a_1, X_2, a_2 being respectively the centre and the width of each Gaussian peak,

$$I = \alpha x + \beta + A \exp\left(-\frac{(X-X_1)^2}{a_1^2}\right) + B \exp\left(-\frac{(X-X_2)^2}{a_2^2}\right)$$

gives forth the centre of the pattern $Xc = (X_1+X_2)/2 = 1012$ (raster units)

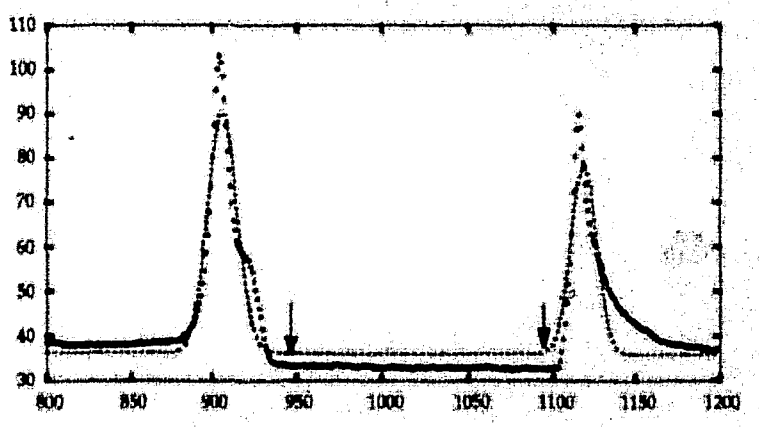

Fig IV.9: Fit of the first (and also symmetric relative to the origin) two orders 00+1 and 00-1 by a combined Gaussian curve. The edges of the beam stop are indicated by the arrows.

Figure IV.9 shows the result of the fit using standard least squares method. Due to the immediate beamstop location in the vicinity of the +1 and -1 orders the fitted Gaussian curves are not perfectly superimposed on experimental points. However, the estimated centre is a good estimate for the purpose of this work. The results of the fit are as follows:

α	β	A	X1	a1	B	X2	a2
-0.001	37.405	54.919	906	12.374	43.372	1118	10.569
±0.002	±2.141	±1.408	±0.25	±0.375	±1.526	±0.29	±0.441

A similar fit to find the origin of the main beam is shown in figure IV.10. The Gaussian fitted curve has its origin at 1022 (raster units) which is the vertical beam central position. The other parameters are :

β	A	a	Xo
25.857	107.476	5.065	1022
±0.572	±1.580	±0.091	±0.05

The correction for pattern origin is then applied so that the centre of the main beam and that of collagen meridionals match. Then, the coordinates are transformed to the 2θ-space, assuming v, the vertical coordinate of the peak (raster units) and r the distance sample-film, according to equation

$$\tan 2\theta = \frac{v}{r}$$

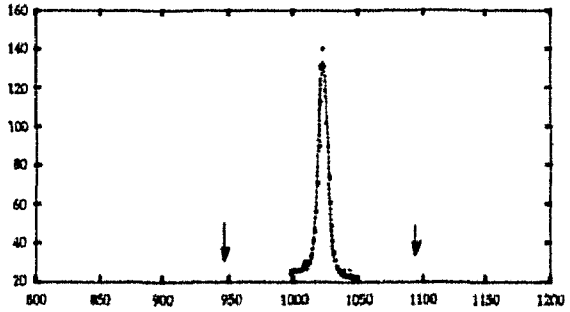

Fig IV.10:Fit of the main beam with a Gaussian curve .The peak maximum position of the fitted curve gives the centre of the pattern in raster units. Arrows indicate the estimated position of the beamstop edges obtained from figure IV.9.

Once the origin has been defined and the transform to the 2θ space calculated we further need the breadth of the primary beam (instrumental broadening) in order to determine the sample broadening for each spot on the meridian.

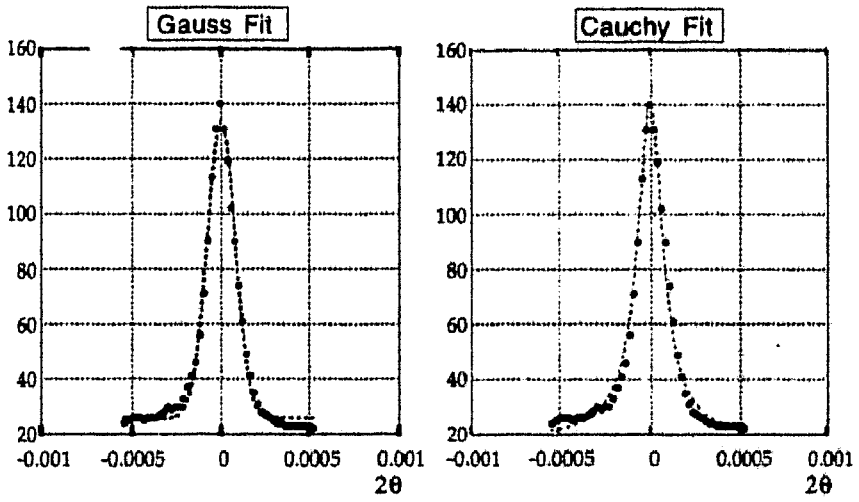

Fig. IV.11: Fit of the main beam with a Gaussian (left) and a Lorentzian curve (right). Full widths at half maximum for both curves a re listed in Table IV.4.

This is achieved by giving two analytical forms for the peaks. For a Gaussian profile with peak origin at Xo, peak height Uo and *a* the full width at half maximum

$$I=Cte+U_o\exp\left(-\frac{(X-X_o)^2}{a^2}\right)$$

where Cte is an offset value to account for the background

Whereas the Cauchy curve will be defined using the analytical form:

$$I=Cte+U_o/\left(1+\frac{(X-X_o)^2}{a^2}\right)$$

Table IV.3

000	$I=Cte+U_o\exp\left(-\frac{(X-X_o)^2}{a^2}\right)$		$I=Cte+U_o/\left(1+\frac{(X-X_o)^2}{a^2}\right)$	
Cte	25.856	0.572	18.336	0.777
Uo	107.472	1.575	122.619	1.871
Xo	0.049 10-5	0.129 10-5	-0.126 10-5	0.128 10-5
a	11.207 10-5	0.201 10-5	8.500 10-5	0.239 10-5
Area	2142.046 10-5		2940.595 10-5	
c2	441		463	
R	0.99		0.99	

The previously defined analytical forms of the Gaussian and Lorentzian curves fitted in the experimental data are given in the first row of table IV.3 and will serve as a template for all the subsequent peak fitting procedures. The area calculated in row 6 is the total area under the experimental points corrected for the background and will be useful for the calculating the integral width defined in paragraph (IV.B.2).

5. Measurement of the Broadening of Meridional Orders.

The broadening of the meridional orders is measured for the data extracted from experiment No 3 by taking the averaged intensity along the meridian. The averaged intensity is the mean value of the intensity calculated on a 3 pixel width, vertical band, to improve signal-to-noise ratio. Thus each peak represented by the graphs below is a vertical averaged section in the meridional X-ray pattern shown in figure IV.6. Following each peak fitting graph I show a table where the fitted parameters are listed. Data are only shown for l=1 to 9 and where peaks are very weak the goodness of fit is reflected by the low R parameter in the tables. The accuracy of fitted parameters is also shown and will be used to calculate the accuracy of crystallite size. Table IV.13 resumes the parameters obtained for the negative l orders displayed in Appendix 1.

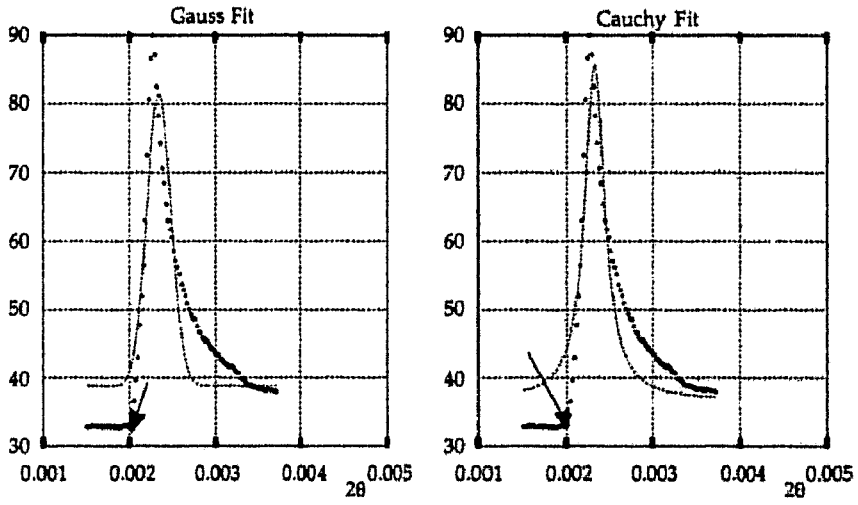

Fig. IV.12: Fit of the l=1 order with a Gaussian (left) and a Cauchy (right) curve. the resulting parameters are listed in table IV.4

Table IV.4

l=1	$I=Cte+U_0\exp\left(-\frac{(X-X_0)^2}{a^2}\right)$		$I=Cte+U_0/\left(1+\frac{(X-X_0)^2}{a^2}\right)$	
Cte	39.054	0.436	36.780	0.893
U_0	43.644	1.398	49.017	2.726
X_0	233.060 10^{-5}	0.478 10^{-5}	232.588 10^{-5}	0.767 10^{-5}
a	18.735 10^{-5}	0.726 10^{-5}	13.879 10^{-5}	1.334 10^{-5}
Area	1458.962 10^{-5}		1961.267 10^{-5}	
χ^2	1276		3506	
R	0.96		0.90	

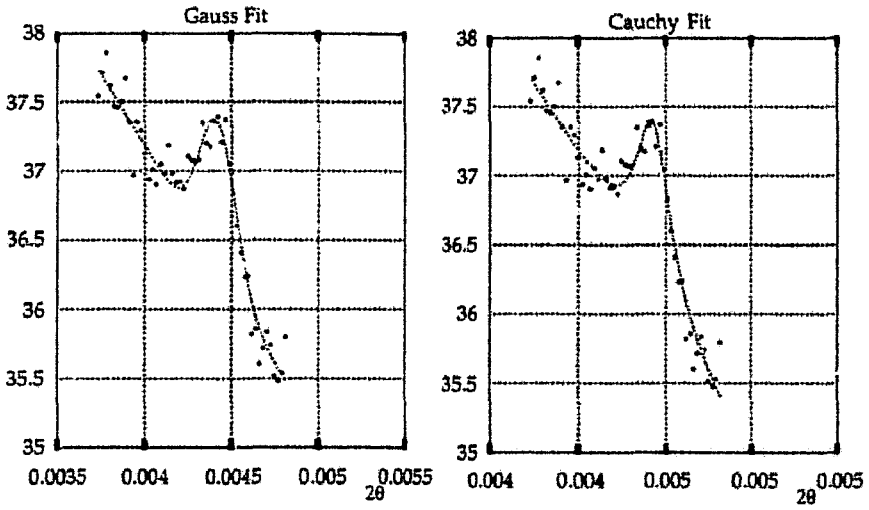

Fig. IV.13: Curve fit of the second meridional order. The fitted curve in this example was modified in order to contribute for the sloping background by adding an additional linear term (see text).

Because the second order is surrounded by some background intensity in the region 2θ≈0.004 the curves have been slightly modified by a linear term B.x and take the analytical form:

$$I=Cte+BX+U_o\exp\left(-\frac{(X-X_o)^2}{a^2}\right)$$

$$I=Cte+BX+U_o/\left(1+\frac{(X-X_o)^2}{a^2}\right)$$

The calculated R is then higher in comparison with an R value of ≈0.56 obtained without this background correction (data not shown). Moreover, the area under the curve was not calculated.

Table IV.5

l=2	Gaussian Profile		Cauchy Profile	
Cte	45.520	0.299	45.819	0.332
U_o	1.042	0.064	1.222	0.077
X_o	441.808 10^{-5}	0.718 10^{-5}	442.474 10^{-5}	0.752 10^{-5}
a	14.744 10^{-5}	1.187 10^{-5}	12.196	1.611 10^{-5}
B	-2085.083	72.0438	-2181.614	82.827
Area	na		na	
χ^2	0.88		0.96	
R	0.97		0.97	

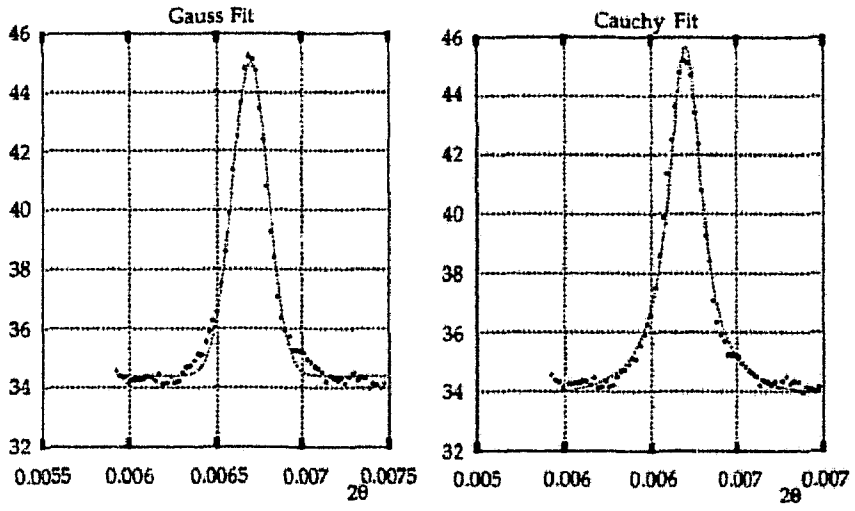

Fig. IV.14: 3rd order fit, the peak is remarkably good and one can notice the goodness-of-fit parameter R=0.99 given in Table IV.6 .

Table IV.6

l=3	Gaussian Profile		Cauchy Profile	
C_0	34.403	0.040	33.713	0.053
U_0	10.604	0.119	11.999	0.140
X_0	$668.903\ 10^{-5}$	$0.132\ 10^{-5}$	$668.961\ 10^{-5}$	$0.131\ 10^{-5}$
a	$14.918\ 10^{-5}$	$0.204\ 10^{-5}$	$11.354\ 10^{-5}$	$0.239\ 10^{-5}$
Area	$281.218\ 10^{-5}$		$388.081\ 10^{-5}$	
χ^2	5		5	
R	0.99		0.99	

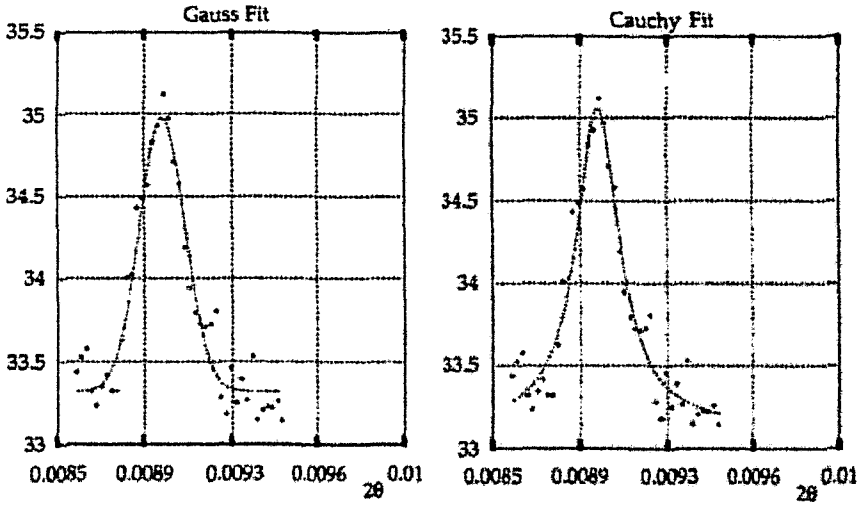

Fig. IV.15:profile fitting of the 4th meridional order .

Table IV.7

l=4	Gaussian Profile		Cauchy Profile	
Ce	33.319	0.034	33.127	0.0515
U_o	1.656	0.068	1.935	0.078
X_o	895.135 10^{-5}	0.430 10^{-5}	895.218 10^{-5}	0.420 10^{-5}
a	13.543 10^{-5}	0.727 10^{-5}	11.177 10^{-5}	0.930 10^{-5}
Area	39.837 10^{-5}		57.509 10^{-5}	
χ^2	0.78		0.77	
R	0.97		0.97	

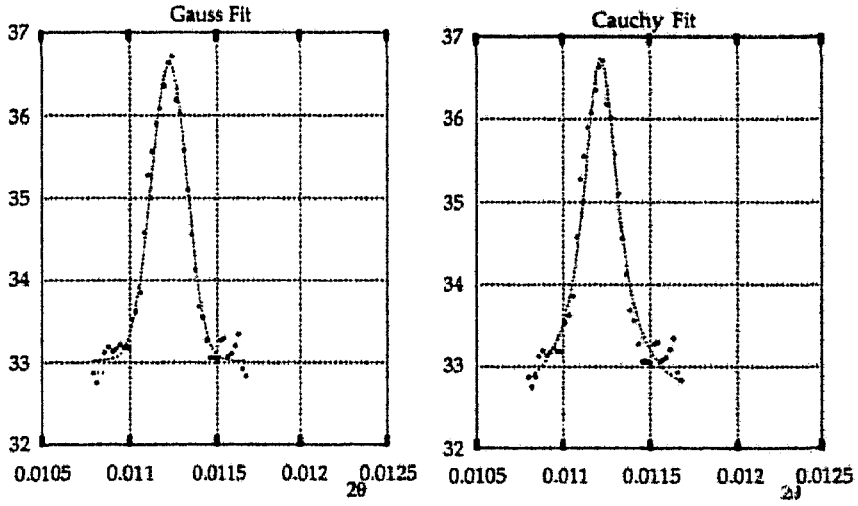

Fig. IV.16: profile fitting of the 5th order.

Table IV.8

l=5	Gaussian Profile		Cauchy Profile	
Ce	33.026	0.037	32.543	0.085
U_o	3.600	0.072	4.207	0.116
X_o	1121.784 10^{-5}	0.214 10^{-5}	1121.870 10^{-5}	0.302 10^{-5}
a	14.089 10^{-5}	0.366 10^{-5}	12.143 10^{-5}	0.714 10^{-5}
Area	90.412 10^{-5}		132.974 10^{-5}	
χ^2	0.88		1.74	
R	0.99		0.98	

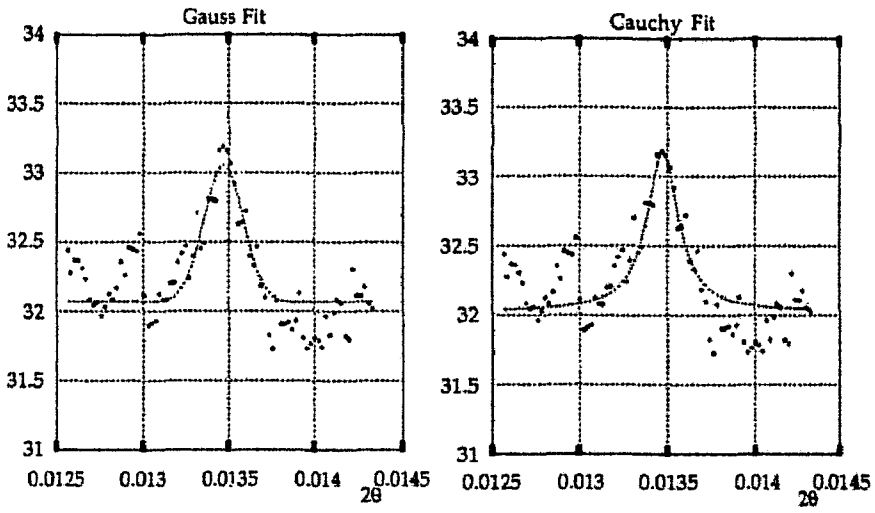

Fig. IV.17:6th order fit.

Table IV.9

l = 6	Gaussian Profile		Cauchy Profile	
Qe	32.066	0.027	32.028	0.033
U_o	0.986	0.082	1.146	0.106
X_o	1346.927 10^{-5}	1.077 10^{-5}	1347.192 10^{-5}	0.976 10^{-5}
a	16.222 10^{-5}	1.649 10^{-5}	10.581 10^{-5}	1.693 10^{-5}
Area	27.902 10^{-5}		34.679 10^{-5}	
χ^2	3.03		3.22	
R	0.83		0.82	

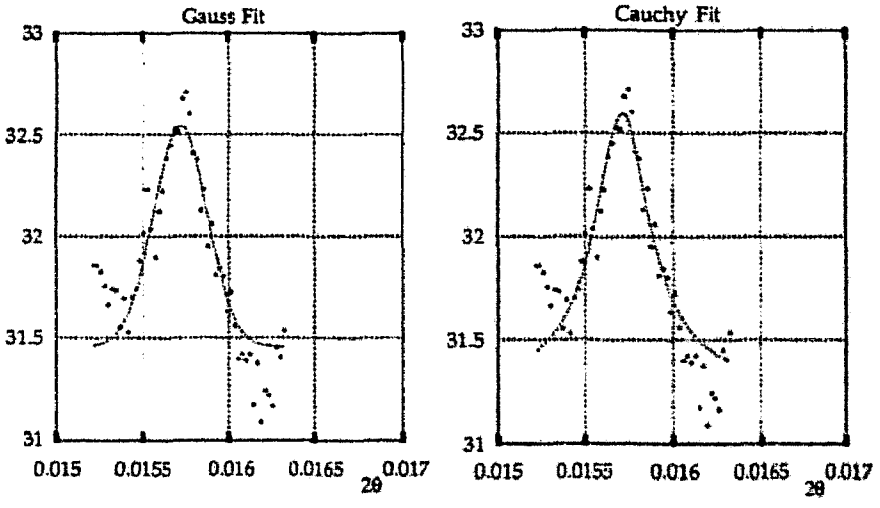

Fig. IV.18: 7th order fit.

Table IV.10

l = 7	Gaussian Profile		Cauchy Profile	
Qe	31.459	0.047	31.275	0.078
U_0	1.084	0.070	1.320	0.085
X_0	1571.586 10^{-5}	1.020 10^{-5}	1571.362 10^{-5}	0.975 10^{-5}
a	22.000 10^{-5}	1.970 10^{-5}	19.272 10^{-5}	2.676 10^{-5}
Area	41.748 10^{-5}		62.100 10^{-5}	
χ^2	1.47		1.42	
R	0.91		0.91	

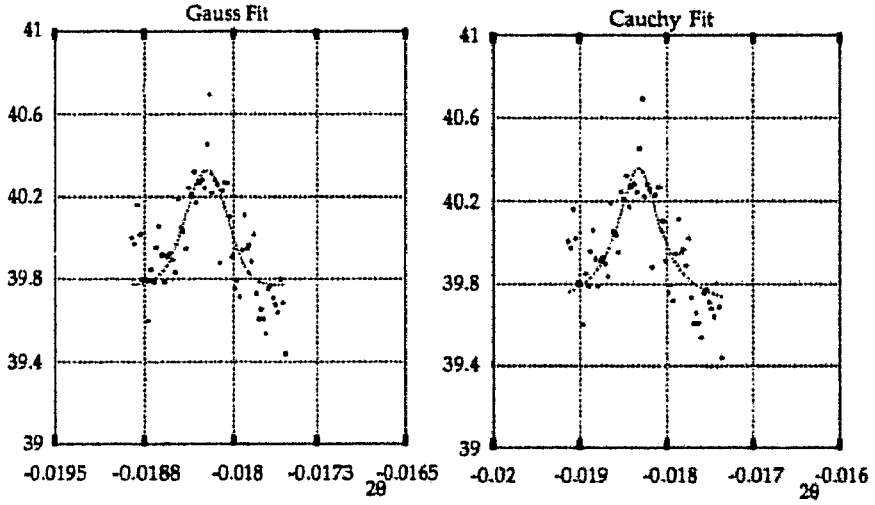

Fig. IV.19: The fitted curve shown here is that of the order 00-8 because 008 is very weak.

Table IV.11

l=-8	Gaussian Profile		Cauchy Profile	
Qe	39.776	0.036	39.682	0.060
U_0	0.554	0.057	0.674	0.068
X_0	-1823.910 10^{-5}	1.893 10^{-5}	-1824.282 10^{-5}	1.812 10^{-5}
a	24.812 10^{-5}	3.521 10^{-5}	21.796 10^{-5}	4.801 10^{-5}
Area	24.551 10^{-5}		36.967 10^{-5}	
χ^2	1.43		1.37	
R	0.78		0.79	

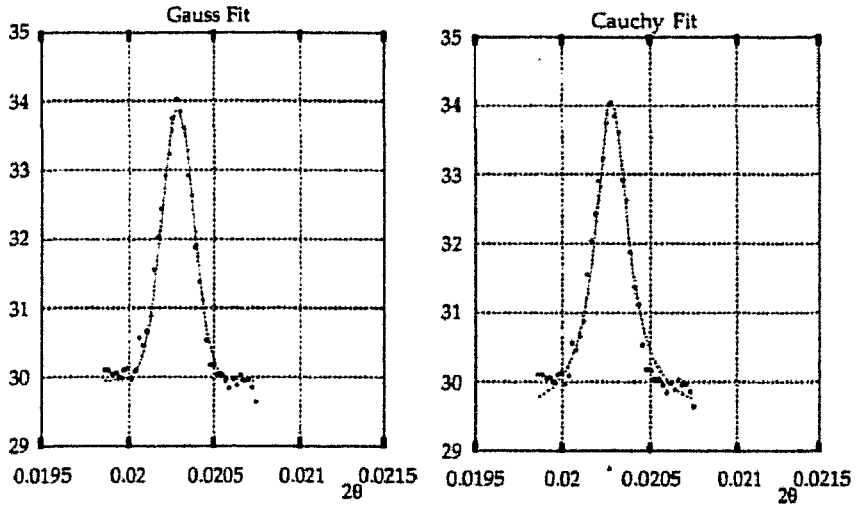

Fig. IV.20:9th order fit .

Table IV.12

I = 9	Gaussian Profile		Cauchy Profile	
Cte	29.956	0.030	29.501	0.066
U_o	3.916	0.062	4.562	0.099
X_o	2028.509 10^{-5}	0.162 10^{-5}	2028.560 10^{-5}	0.225 10^{-5}
a	13.332 10^{-5}	0.273 10^{-5}	11.004 10^{-5}	0.502 10^{-5}
Area	92.833 10^{-5}		133.246 10^{-5}	
χ^2	0.63		1.25	
R	0.99		0.99	

Table IV.13

	$I=Cte+U_o\exp\left(-\frac{(X-X_o)^2}{a^2}\right)$					$I=Cte+U_o/\left(1+\frac{(X-X_o)^2}{a^2}\right)$				
I	Cte	Uo	Xo x10^{-5}	a x10^{-5}	Area x10^{-5}	Cte	Uo	Xo x10^{-5}	a x10^{-5}	Area x10^{-5}
-1	37.204	54.685	-234.709	26.223	2544.427	33.467	65.197	-235.959	18.416	3371.078
	±0.69	±1.718	±0.645	±1.025		±0.693	±1.591	±0.442	±0.838	
-2	37.974	0.896	-463.306	15.586	24.547	37.845	1.059	-463.122	13.438	35.945
	0.027	0.046	0.607	1.085		0.047	0.058	0.641	1.586	
-3	38.123	9.592	-691.95	16.568	281.239	36.715	11.345	-691.915	14.411	415.122
	0.038	0.066	0.086	0.153		0.172	0.212	0.233	0.581	
-4	38.330	0.846	-917.239	17.323	25.85	38.17	1.024	-917.302	16.137	40.075
	0.029	0.0045	0.668	1.27		0.055	0.058	0.699	1.966	
-5	38.771	4.254	-1145.041	16.367	123.19	38.258	4.904	-1145.07	13.910	179.903
	0.039	0.081	0.241	0.404		0.097	0.144	0.379	0.855	
-6	38.93	0.894	-1373.508	24.261	38.216	38.728	1.109	-1373.812	23.597	60.462
	0.032	0.043	0.795	1.642		0.062	0.061	0.829	2.621	
-7	39.332	1.146	-1599.515	19.634	39.955	39.185	1.327	-1599.728	16.971	59.430
	0.025	0.051	0.68	1.139		0.042	0.061	0.731	1.665	
-8	39.776	0.754	-1823.91	24.812	24.551	39.682	0.674	-1824.286	21.796	36.967
	0.036	0.057	1.893	3.521		0.06	0.068	1.812	4.801	
-9	40.171	5.268	-2052.397	24.205	226.426	39.487	6.132	-2052.166	20.969	339.797
	0.0662	0.137	0.485	0.81		0.103	0.151	0.479	1.086	

6. Results and Discussion

The results of the earlier curve fits are summarised in table IV.14 and IV.15 where I show the measured peak broadening and the deduced crystal sizes calculated according to the methods of Scherrer then to Stokes-Wilson calculation. The data in table IV.14 are obtained for a Gaussian fitted profile for each peak. B(2θ) designates the broadening due to crystal size only and is obtained after subtraction of the squares of the broadening from the sample and instrumental peak. $L_{B(2\theta)}$ is the crystal size calculated from B(2θ) according to Scherrer equation. β(2θ) is the integral breadth of the curve obtained by subtracting the integral widths of the sample and instrumental peaks; then $L_{\beta(2\theta)}$ is calculated using the Stokes-Wilson equation. The data obtained for a Cauchy (also called Lorentzian curve) fits are shown in table IV.15.

Table IV.14

na=not available

ℓ	2θ 10^{-3}	$\delta(2\theta)$ 10^{-3}	$B(2\theta)$ 10^{-5}	$\delta B(2\theta)$ 10^{-5}	$L_{B(2\theta)}$ μm	$\delta L_{B(2\theta)}$ μm	$\beta(2\theta)$ 10^{-5}	$\delta\beta(2\theta)$ 10^{-5}	$L_{\beta(2\theta)}$ μm	$\delta L_{\beta(2\theta)}$ μm
1	2.331	0.005	15.013	1.057	0.964	0.068	13.497	1.057	1.141	0.115
-1	-2.347	0.006	23.707	1.230	0.611	0.032	26.597	1.230	0.579	0.038
2	4.418	0.007	9.581	2.064	1.511	0.325	na	2.064	na	na
-2	-4.633	0.006	10.806	1.774	1.340	0.220	7.440	1.774	2.070	0.480
3	6.689	0.001	9.846	0.540	1.470	0.081	6.587	0.540	2.338	0.210
-3	-6.920	0.001	12.202	0.394	1.186	0.038	9.388	0.394	1.640	0.087
4	8.951	0.004	7.604	1.593	1.904	0.399	4.116	1.593	3.741	1.175
-4	-9.172	0.007	13.209	1.837	1.096	0.152	10.598	1.837	1.453	0.264
5	11.218	0.002	8.539	0.870	1.695	0.173	5.179	0.870	2.974	0.456
-5	-11.450	0.002	11.929	0.744	1.214	0.076	9.021	0.744	1.707	0.161
6	13.469	0.011	11.728	2.475	1.234	0.260	8.344	2.475	1.846	0.588
-6	-13.735	0.008	21.518	1.957	0.673	0.061	22.817	1.957	0.675	0.070
7	15.716	0.010	18.932	2.410	0.765	0.097	18.565	2.410	0.830	0.125
-7	-15.995	0.007	16.121	1.528	0.898	0.085	14.912	1.528	1.033	0.129
8	na									
-8	-18.239	0.019	22.137	4.049	0.654	0.120	24.376	4.049	0.632	0.127
9	20.285	0.002	7.221	0.817	2.005	0.227	3.773	0.817	4.082	0.725
-9	-20.524	0.005	21.454	1.020	0.675	0.032	23.046	1.020	0.668	0.041

Table IV.15

ℓ	2θ 10^{-3}	$\delta(2\theta)$ 10^{-3}	$B(2\theta)$ 10^{-5}	$\delta B(2\theta)$ 10^{-5}	$L_B(2\theta)$ μm	$\delta L_B(2\theta)$ μm	$\beta(2\theta)$ 10^{-5}	$\delta\beta(2\theta)$ 10^{-5}	$L_\beta(2\theta)$ μm	$\delta L_\beta(2\theta)$ μm
1	2.326	0.008	5.379	1.574	2.691	0.788	16.030	1.574	0.961	0.155
-1	-2.360	0.004	9.916	1.078	1.460	0.159	27.724	1.078	0.555	0.033
2	4.425	0.008	3.696	1.851	3.917	1.962	na	1.851	na	na
-2	-4.631	0.006	4.938	1.826	2.932	1.084	9.930	1.826	1.551	0.349
3	6.690	0.001	2.853	0.479	5.073	0.852	8.361	0.479	1.842	0.164
-3	-6.919	0.002	5.911	0.821	2.449	0.340	12.608	0.821	1.221	0.102
4	8.952	0.004	2.677	1.170	5.407	2.363	5.735	1.170	2.685	0.734
-4	-9.173	0.007	7.637	2.206	1.896	0.548	15.121	2.206	1.018	0.175
5	11.219	0.003	3.643	0.954	3.974	1.041	7.624	0.954	2.020	0.328
-5	-11.451	0.004	5.410	1.095	2.676	0.541	12.703	1.095	1.212	0.138
6	13.472	0.010	2.081	1.933	6.9..	6.463	6.272	1.933	2.456	1.241
-6	-13.738	0.008	15.097	2.861	0.959	0.182	30.538	2.861	0.504	0.056
7	15.714	0.010	10.772	2.916	1.344	0.364	23.059	2.916	0.668	0.099
-7	-15.997	0.007	8.471	1.905	1.709	0.384	20.801	1.905	0.740	0.087
8	na									
-8	-18.243	0.018	13.296	5.041	1.089	0.413	30.788	5.041	0.500	0.097
9	20.286	0.002	2.504	0.742	5.781	1.712	5.222	0.742	2.949	0.568
-9	-20.522	0.005	12.469	1.326	1.161	0.124	31.432	1.326	0.490	0.027

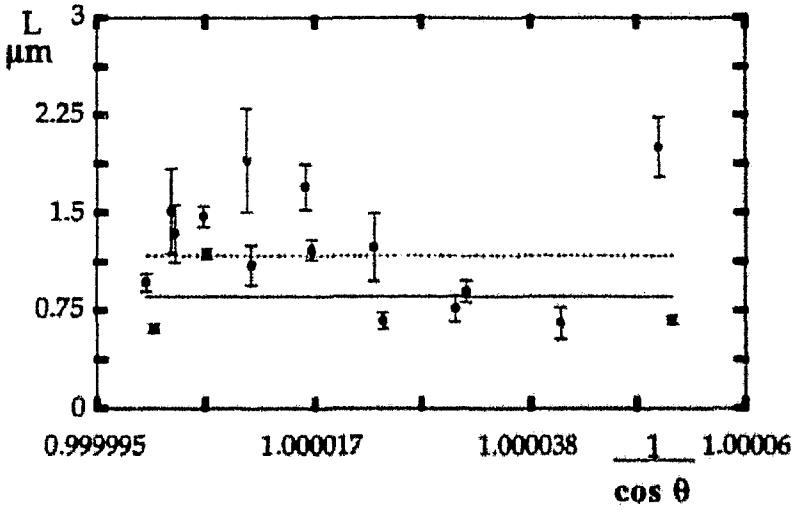

Fig. IV.21: Fitted straight line for the Gaussian assumed profiles for the orders 1 to 9. The dotted line is obtained when data are not weighted and plain line is obtained when data are weighted by the inverse of the standard error estimates. The intercept of the straight line with the y axis for the non-weighted data yields a value of 1.170±0.106μm for crystallite size whereas the weighted average crystal size is:

$L_B = 0.857 \pm 0.073 \mu m$

We now need a rather unique value to characterise the average crystallite size which is independent on the orders. Considering the Scherrer and Stokes-Wilson approach, the crystallite average size in the

direction along the fibre is independent on the scattering vector (but not the broadening of the peaks) so that a plot of the crystal average size versus $1/\cos(\theta)$ must be a constant. I, therefore, can plot the different sizes calculated for each order on a $1/\cos(\theta)$ scale and fit a horizontal straight line in the points. The intercept of the fitted line with the y axis yielded the average size of collagen crystalline domains in tendon.

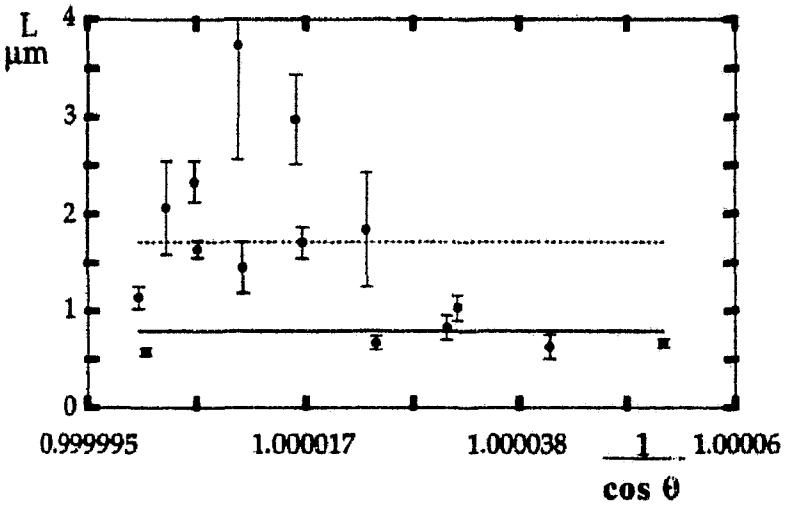

Fig IV.22: Fitted straight line for the Gaussian assumed profiles for the orders 1 to 9 using Stokes method. The dotted line yields a value of 1.713±0.274μm for average crystallite size whereas the weighted average crystal size again is :

$L_\beta = 0.796 \pm 0.101 \mu m$

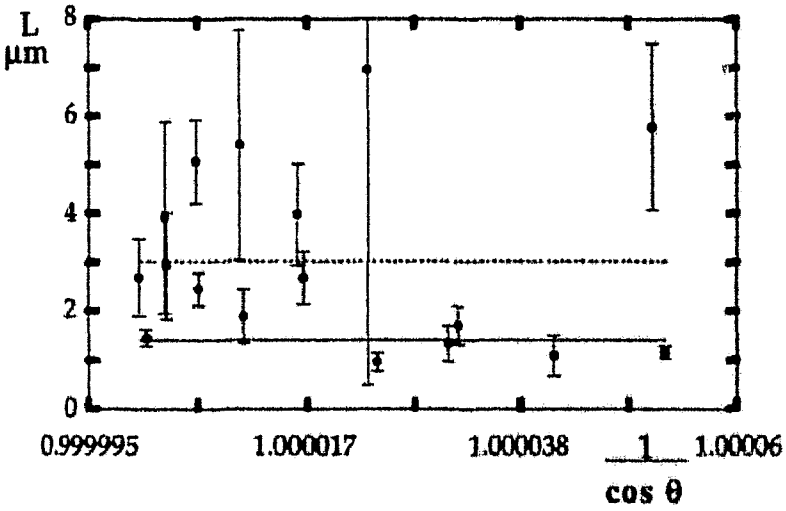

Fig IV.23: Fitted straight line for Cauchy assumed profiles using Scherrer equation. Unweighted crystal size is thus 3.027±0.449μm and weighted average crystal size is :

$L_\beta = 1.411 \pm 0.155 \mu m$

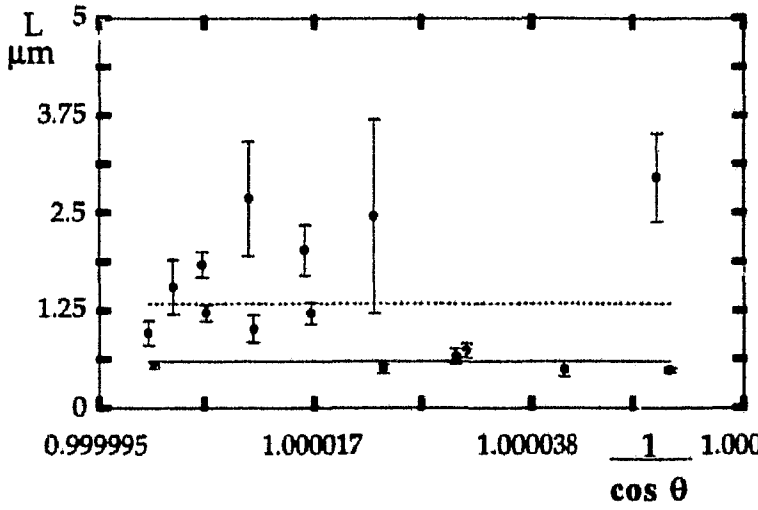

Fig IV.24: Fitted straight line for Cauchy assumed profiles using Stokes method. The intercept of the straight line with the y axis for the dotted line yields a value of 1.335±0.206µm. The weighted average crystal size is given by:

$L_\beta = 0.597 \pm 0.064 \mu m$

Table IV.16 shows the different average sizes obtained for the collagen crystallite according to Scherrer (first two rows) and to Stokes (last two rows) methods. Only the values from the straight lines weighted fits (figures IV.21 to IV.24) are considered since lower accuracy was obtained with the weakest peaks. In the third and fourth columns N and ΔN are the average number of unit cells in the c direction (c=667.9Å) contained in the small crystalline domains and the relative estimated standard deviation. n and Δn are respectively the number of molecular lengths in crystalline domain along the c axis and the error.

Table IV.16

Method ↓	L µm	ΔL µm	N	ΔN	*n*	Δ*n*
Scherrer-G	0.858	0.073	12.6	1.0	2.86	0.24
Scherrer-C	0.797	0.102	11.7	1.5	2.67	0.34
Stokes-G	1.412	0.155	20.8	2.2	4.70	0.51
Stokes-C	0.597	0.065	8.8	0.9	1.99	0.21

In conclusion, additional experimental broadening usually may also arise from the sample size that was not the subject of this work. Consequently, the value of 1µ obtained in the present study is the lower limit experimentally determined. Crystallite average size might thus have a greater value within the range of some microns. Now if we consider the length of one collagen molecule to be about 3000Å, we see that the average longitudinal crystal size of packing in tendon is on average 3.2 times the length of one collagen molecule. This number is rather unusual in macromolecular crystallography and the comparison with globular proteins where crystals are formed of thousands of regularly spaced molecules is not straightforward. One has always to keep in mind however that collagen molecules are proteins with high molecular weights e.g. containing infinite number of atoms,

belonging to the special class of fibrous proteins. We are however in the case of one of the rare proteins, the in-vivo self assembling of which is well known.

E. Fourier Deconvolution.

A rigorous method to solve the convolution problem is to use Fourier calculation by transforming each function to a complex Fourier series:

$$f(y)=\sum_{n} F(n)e^{-2\pi i n y/a}$$

$$g(z)=\sum_{n'} G(n')e^{-2\pi i n' z/a}$$

$$h(x)=\sum_{n''} H(n'')e^{-2\pi i n'' x/a}$$

Writing the convolution form of the three curves in a compact form gives

$$h(x)=g(x)\otimes f(x)$$

where $\otimes$ means a convolution product. Now, a well known mathematical result states that the Fourier transform of a convolution product is equal to the simple product of the Fourier transforms of each component

$$H(n)=F(n).G(n)$$

thus

$$F(n)=H(n)/G(n)$$

Using Fast Fourier Transform, H(n) and G(n) can thus be synthesised and the reverse Fourier calculated for f(y).

Despite the elegance of this method and its success in other powder diffraction studies, the calculation of the deconvolution for the current experimental data did not conduct to significant results .i.e. an f(y) curve with measurable broadening. This method thus turned out to be of little value what is probably due to the large broadening calculated in the preceding paragraphs.

Chapter 5
Digital Image Processing of Collagen X-Ray Patterns

The structure and packing studies of collagen in tendons require that we obtain a list of structure factors determined from X-ray experiments. Many attempts have already been made to obtain structural data from natural tendon fibres in order to understand the organisation at the molecular level in this tissue. But, unlike in usual protein crystallography where data collection now tends to be an automated process, there is to no computer programs which readily analyse fibre diffraction patterns and produce a set of structure factors suitable for crystallographic analysis. Consequently, the major and most time consuming part of this thesis was devoted to the analysis of X-ray films of native and derivative collagen in order to obtain the above required data. Integration of Bragg peaks has been carried out manually and care has been taken to obtain a convenient set of structure factors suitable for three-dimensional Fourier analysis e.g. the collected data set must contain a minimum set of Miller indices such as (0,0,l), (±1,0,l) and (0,±1,l). Furthermore the structure factors set for native and derivative collagen has to contain as much as possible of the diffracted intensity on the films in order to have a statistical (as well as a good resolution) significance. The multiple isomorphous replacement method on the other hand requires in addition, that for each measured intensity with Miller indices (h,k,l), one also has at hand the same reflection for all other derivatives in order to calculate the phase of the native F(h,k,l).

Now, whereas data integration on the meridional and on the (-1,0,l), (1,0,l) row-lines was straightforward, a special effort was done to gather correctly indexed data from the other row-lines. According to the fibre X-ray pattern predictions and peak enhancement method outlined in chapter 3, we know that for heavy atoms labelled collagen, a set of diffracted spots are present in those regions corresponding to row-lines other than the two prominent (-1,0,l) and (1,0,l) set. These row-lines intensities are relatively weak but remain necessary for a low-resolution three-dimensional structure determination. These orders can thus be obtained and correctly indexed assuming the following data analysis steps are carefully thought up:

a) the accurate determination of the pattern origin and relative orientation of different films in one pack since data must be gathered and scaled together for each derivative. Care must be taken to avoid the repeated peak integration of the same reflection on successive films or the erroneous indexing of the Bragg spots.

b) the estimation and subtraction of local background intensity surrounding each peak.

c) the checking for peak saturation and peak overlap.

d) X-ray films usually have intrinsic background inherent to the film processing conditions and chemical treatment after exposure to the X-rays. The film background in the absence of X-rays is usually designated "chemical fog". Additional problems also arise from the drying conditions where films can exhibit an altered stretching in different directions.

e) the actual tilt of the fibre relative to the X-ray beam will be shown to have a great consequence on peak indexing and is thus better estimated from the film data rather than from the goniometer value which is unsatisfactory.
f) data recorded on multiple film pack always need to be scaled and corrected for film absorption.

A. Dynamic Range of Intensities and Film Corrections

Most of the conventional crystallographic studies about proteins are performed with molecules of globular shape. The electron density distribution of globular molecules is rather isotropic when compared to fibrous proteins and consequently the molecular transform intensity function is isotropic in reciprocal space. Thus the variation in peak intensity magnitude over reciprocal space is

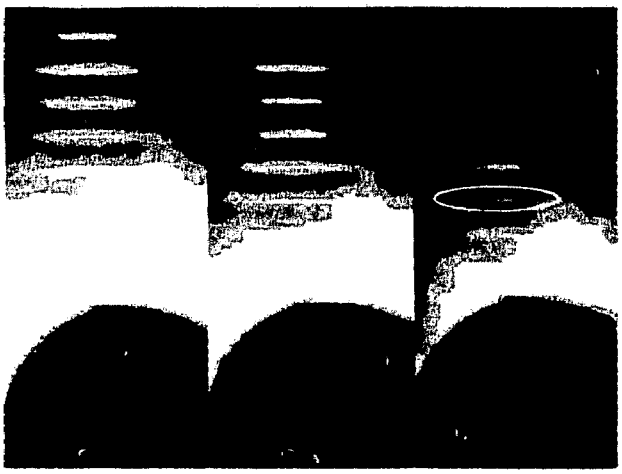

Fig. V.1 : Image of meridional native collagen patterns (small angle). The three images from the pack have been juxtaposed after a rotation and translation so that equivalent spots coincide. Then, film saturation was controlled interactively and integration carried on the non-saturated peaks.

slow for globular proteins as is shown with crystal rotating method and Laue patterns.
In most of these experiments, the X-ray films are usually uniformly crowded with the diffracted spots and there is little difference over film regions. Crystalline collagen in native and heavy atom derivative tendon is different in that it displays high anisotropy in the diffraction pattern where most of the intensity is distributed principally on the equatorial and meridional axis. This is due to the rod shaped geometry of the molecule, the molecular transform of which in reciprocal space is mostly confined on layer-lines. Meridional orders in collagen diffraction patterns for example show different order of magnitudes in the peak intensities. In chapter 4, I have already displayed a small angle X-ray diffraction pattern with collagen fibre where weak even orders compared to odd orders are shown in figure IV.6. Accordingly, the simultaneous recording of odd and even spots on the meridian requires the even orders to be sufficiently strong to allow for an estimation of their integrated intensities whereas the odd orders will be saturating for the film emulsion whenever long exposure times are

used. Another condition arises because in addition to the high continuous scattering on the equator, the off-meridional peaks are usually weaker and require long exposure times. As a consequence, the use of multiple film packs is especially required for molecules for which the diffraction patterns exhibit large variation in peak intensity in order to cover the full dynamic range of intensities. For the purpose of data collection from collagen fibres, this was achieved by using up to six X-ray films per pack with long exposure times (up to 20 minutes). Therefore, film scaling and film absorption corrections must be applied for the final set of structure factors to be correct. In conventional protein crystallography these corrections are usually obtained from the experimentally measured intensities. However, I have chosen to apply a systematic correction for intensities measured on multiple films by using the manufacturer standard value for film factor and not the usual method which consist of determining film factor from direct data measurement on successive films. The manufacturer film factor is 2.1 for the X-ray wavelength used at Daresbury (λ=1.488Å), thus writing the intensity ratio of a given Bragg reflection measured once on film No1 and once on film No2 we obtain

$$\frac{I_1}{I_2} = C_{film}$$

where C_{film} is the film factor. For a reflection measured on film number n we have

$$\frac{I_1}{I_n} = C_{film}^{\,n}$$

Since all weak reflections will generally be measured on the first film, the systematic correction we apply for film absorption when one single peak is measured on film number n is

$$I_1 = I_n \, e^{n \, \mathrm{Ln} \, C_{film}}$$

Thus, the general procedure to integrate Bragg reflections for native and derivative collagen will be carried on first films for weak reflections (off equatorial and off meridional reflections) whereas medium and bottom films will be used to integrate strong reflections (principally the equatorial and meridional reflections). Film absorption and other corrections like Lorentz factor will then be applied as required.

B. Determination of Film Orientation and Pattern Centre

I have developed, in collaboration with D. RICHARD at the Institute Laue Langevin, a software which enables a lot of interactive image processing utilities to be applied to collagen diffraction patterns. One of these tools is to determine the fibre pattern centre by calculating the intersections of two straight lines going one through the meridian and the other through the equator as shown in figure V.2. The pattern origin is thus determined in raster units for each film in the pack and was also used to calculate the predicted fibre diffraction patterns. The correct centring was then verified by inspecting the beamstop position and its shape on successive films. I thus used the image display software that was specifically developed to allow for a simultaneous comparison of different films by juxtaposing the patterns (figure V.3).

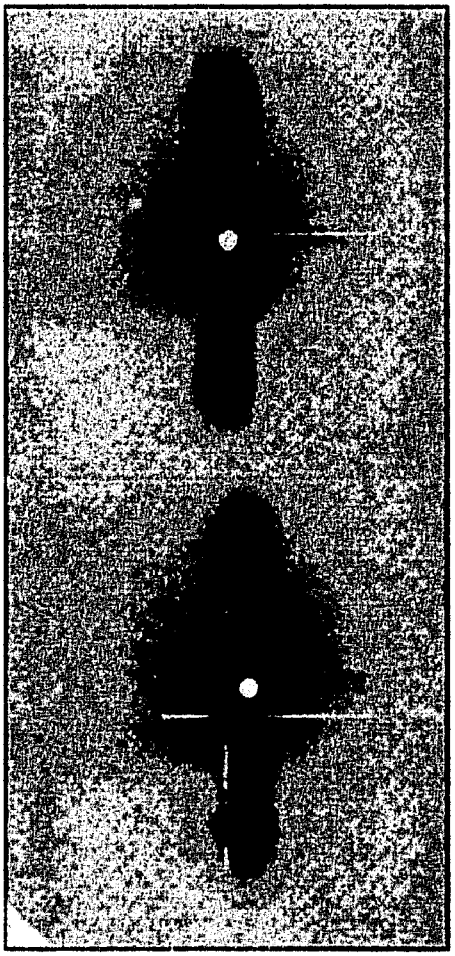

Fig V.2:The X-ray fibre diffraction centre for collagen is calculated using a graphical interactive method. The pattern origin for collagen is the intersection point of the meridional and equatorial axis. The top figure is a centred pattern obtained after rotation and translation of the pattern as explained in the text.

I first determined the pattern centres for all films in one pack using the above described method and looked for the relative position of the beamstop on all the patterns. The beamstop used in the experiment was a circular lead piece with a resulting circular shadowing of the films near the origin. When correctly centred, the beamstop marks had to be accurately coinciding on all the successive films as these are recorded all at once. The test procedure for pattern centre calculation is schematically explained in figure V.4 and has yielded a good estimate of the pattern origin for all the worked films.

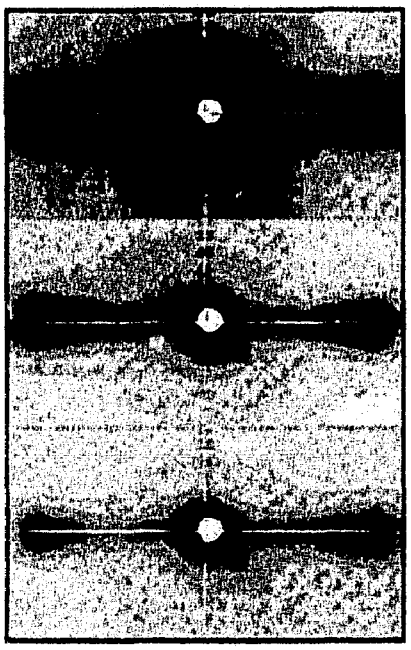

Fig. V.3 :X-ray patterns obtained with native and derivative collagen are usually scanned separately with a resulting loss of pattern origin and relative orientation. I therefore correct for it in order to obtain the correct indexing and integration of Bragg orders using all the films in the pack . This figure shows a set of three films from native collagen patterns which have been aligned and centred using the method described in the text.

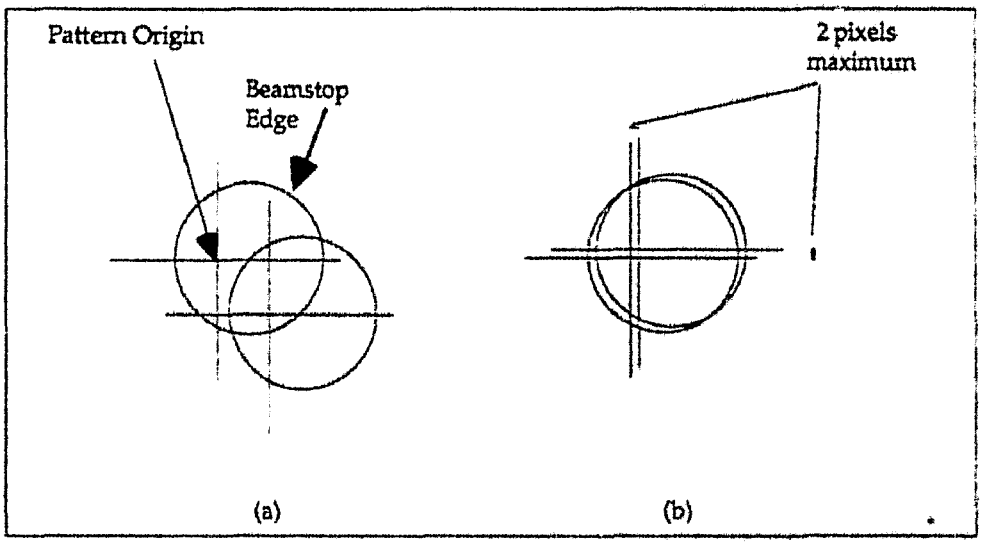

Fig. V. 4: The X-ray pattern centre is calculated using the method explained in the text. Than, one method to test for its precision is to compare between the shapes of beamstop on successive films. (a) the pattern centre and the beamstop centre do not necessarily match; whereas for a correctly calculated pattern centre the circular borders of the beamstop must be superimposed (b). The error introduced by this method was estimated to be ≤2 pixels .

C. Image Display and Handling, Integrated Intensities

The image display and handling utilities that have been developed for fibre diffraction patterns allow for fast image manipulation of one or more simultaneous films. Images can thus be compared to each other and with the predicted patterns and thus I could carefully examine every local features in the diffraction patterns. The images treated at this stage will all be represented with the corresponding simulated fibre diffraction pattern which allowed me to interactively work with the calculated and experimental data at one time. Images can also be zoomed to observe small details and weak intensities in the patterns and colour scale can be redefined to the local intensity range.

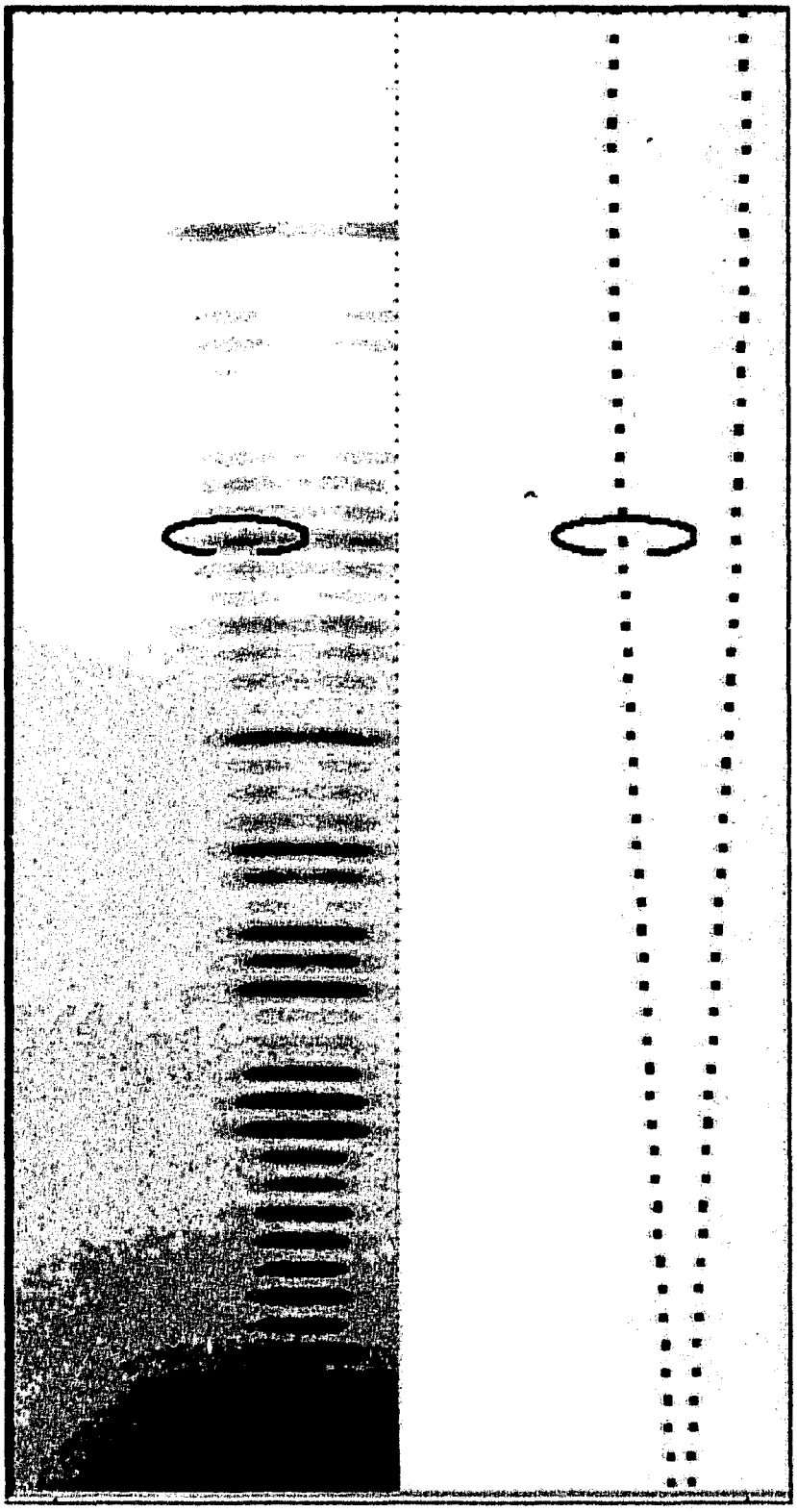

When displaying and treating images, some operations are common for all displayed films: for example if a box where the integration is to be carried is drawn on the experimental data with more than one film then the same box is simultaneously shown on all the other images. The choice of the film number where spots are integrated is thus

Fig. V.5: Meridional diffraction spots for native collagen fibres. The pattern on the right shows the predicted Bragg spots in this region. An elliptical shaped box is also drawn to indicate the area where data integration is carried. After peak integration and background subtraction, the Miller indices of the spot are obtained by comparing the coordinates of the ellipse centre with the predicted Bragg reflection.

adequately selected. I have thus ensured that saturated or strongly overlapped peaks were carefully rejected.

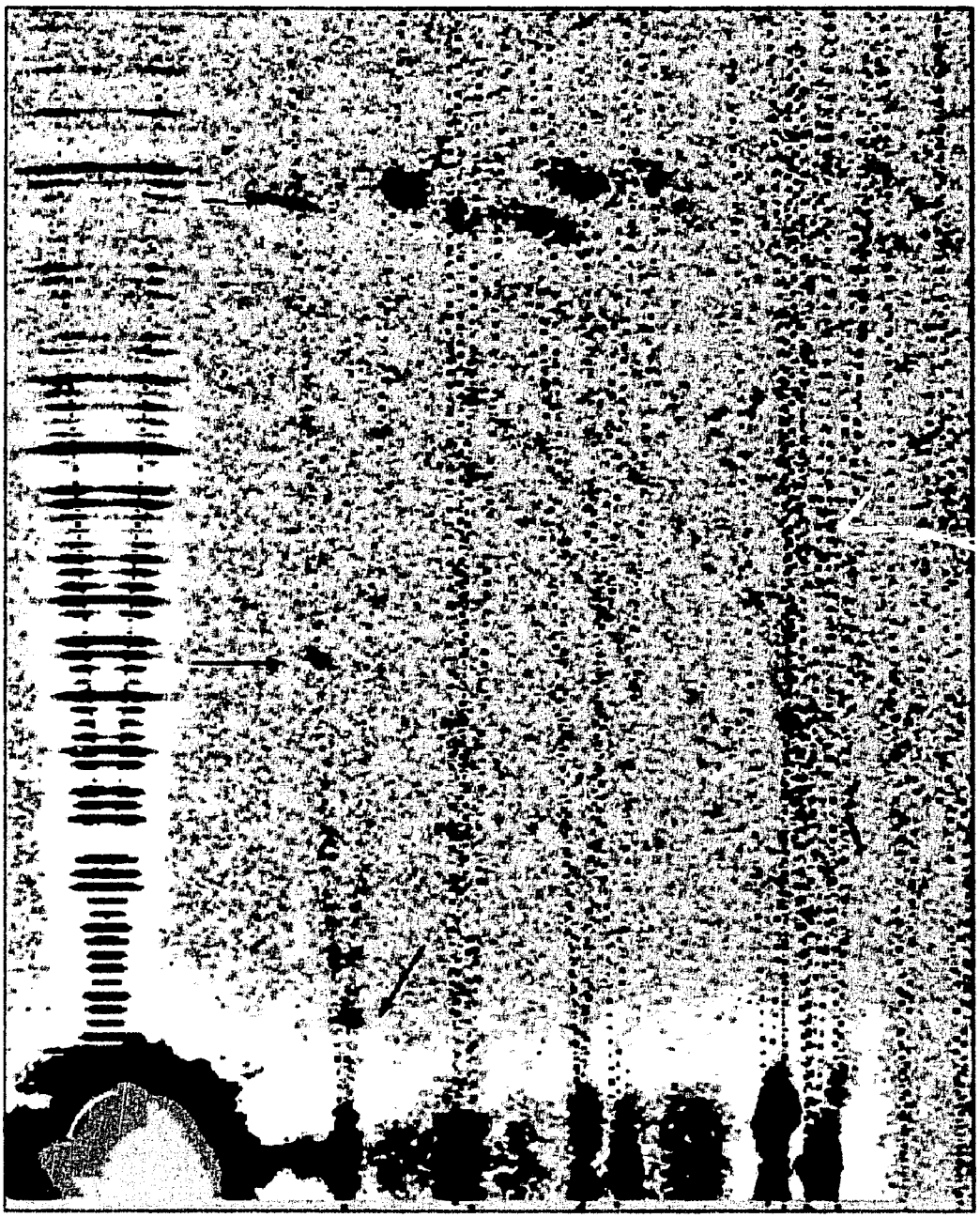

Fig. V.6 : Native fibre diffraction pattern obtained after background subtraction and overlay of the predicted fibre diffraction spots. The arrows indicate the strongest reflections on the (-1,0,l) and (1,0,l) row-lines while the topmost one indicates the intercept of the row-lines with the helix layer-line. There are also some intensities on the helix layer-line that are in good agreement with the predicted pattern in that region.

As I have explained above, the gathering of structure factors for collagen has to be done by examining every spot individually since the shape of the integration area has to be adapted to match the different orientations and extent of each Bragg reflection. The problems of background subtraction and neighbouring diffuse scattering will be discussed later on. In the next figures I show some of the

situations I encountered during peak integration. The displayed data are for native collagen fibres but the processing steps are also similar for the derivative patterns.

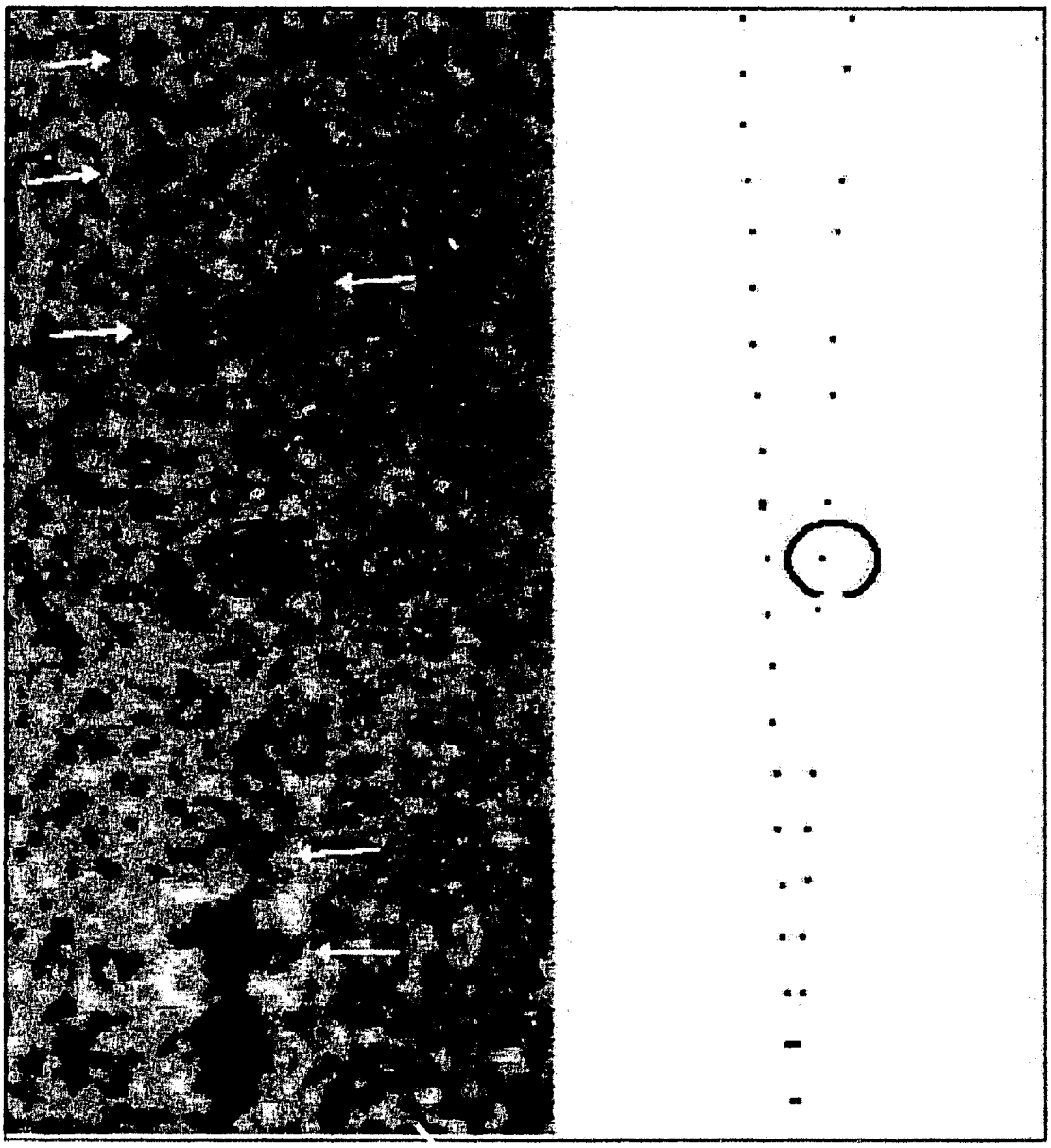

Fig. V.7: Here I show the near equatorial region of the (-1,0,l) and (1,0,l) row-lines where we can now better observe the successive orders. Some strong orders are indicated by an arrow and the circular contoured one has Miller indices h=1,k=0 and l=10. The lowest peak is particular because it has Miller indices (1,0,0) and is overlapped by the order (-1,0,0) which is equivalent to the (1,0,0) according to Friedel 's law ($|F(h\,k,l)|^2 = |F(\bar{h},\bar{k},\bar{l})|^2$). This peak is not rejected but after integration it is divided by two and assigned once to the (1,0,l) order and once to the (-1,0,l) order. The next (and obviously highest intensity) peak in the shown region of the pattern is a mixture of the orders (1,0,1) and (-1,0,1) and represent the kind of ambiguity with respect to the correct Bragg indexing.

For all data I analysed, the equatorial and near-equatorial region of the diffraction patterns contain a lot of overlapped peaks. Nevertheless, these data (which, actually, are relevant for the understanding of the lateral packing of collagen molecules) have been integrated whenever it was possible but care

has been taken to keep them apart for further processing (e.g. the indexing of these reflections can not be done automatically and require a manual processing).

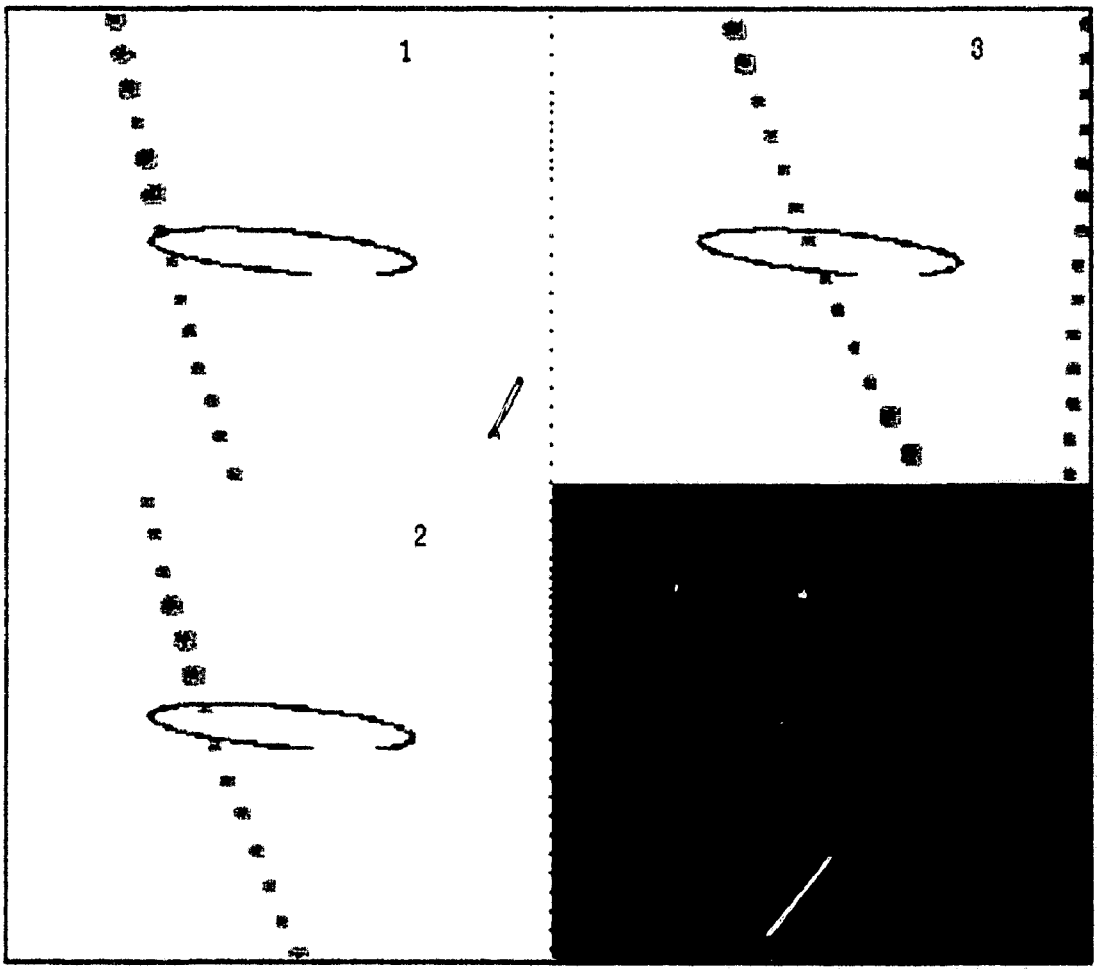

Fig. V.8: A set of three predicted diffraction patterns were calculated with a tilt angle respectively 2.00°,3.00° and 4.00°. Then, images were displayed side-by-side with the experimental diffraction pattern and a region of the diffraction pattern is shown in the vicinity of the (-1,0,-75) Bragg reflection. The elliptical box is centred at the peak maximum of the prominent reflection shown in quadrant No 4 . Thus we see that the indexing of this peak can be inaccurately determined. I thus concluded that the tilt of the fibre relative to the X-ray beam is important for the indexing of collagen Bragg spots and need to be accurately determined.

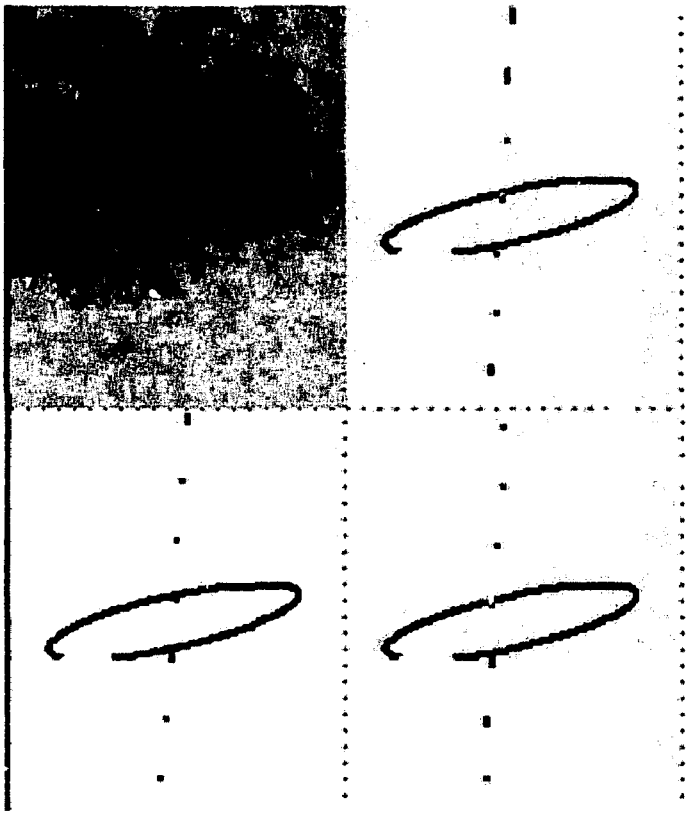

Fig. V.9: This picture shows the region in the vicinity of the (-1,0,75) order. The quadrants show respectively the experimental native spot and the predicted Bragg reflections for a fibre tilted by 2.00°,3.00° and 4.00° relative to the X-ray beam.

Fig. V.10: (below) A fibre X-ray diffraction pattern is usually symmetric relative to the meridian so one quarter of the fibre pattern contains all the necessary data for a structural determination . These 4 quarters however are only related by an exact four-fold symmetry when the fibre is perpendicular to the X-ray beam. The zero degree tilt to the X-ray beam is never achieved experimentally therefore in order to determine the fibre tilt I show a region of the pattern near the (-1,0,-75) reflection. The calculated (-1,0,l) Bragg spots are shown in the lower right quadrant of the pattern for fibre tilt respectively 2.0°,3.0°,4.0° and 4.2°.

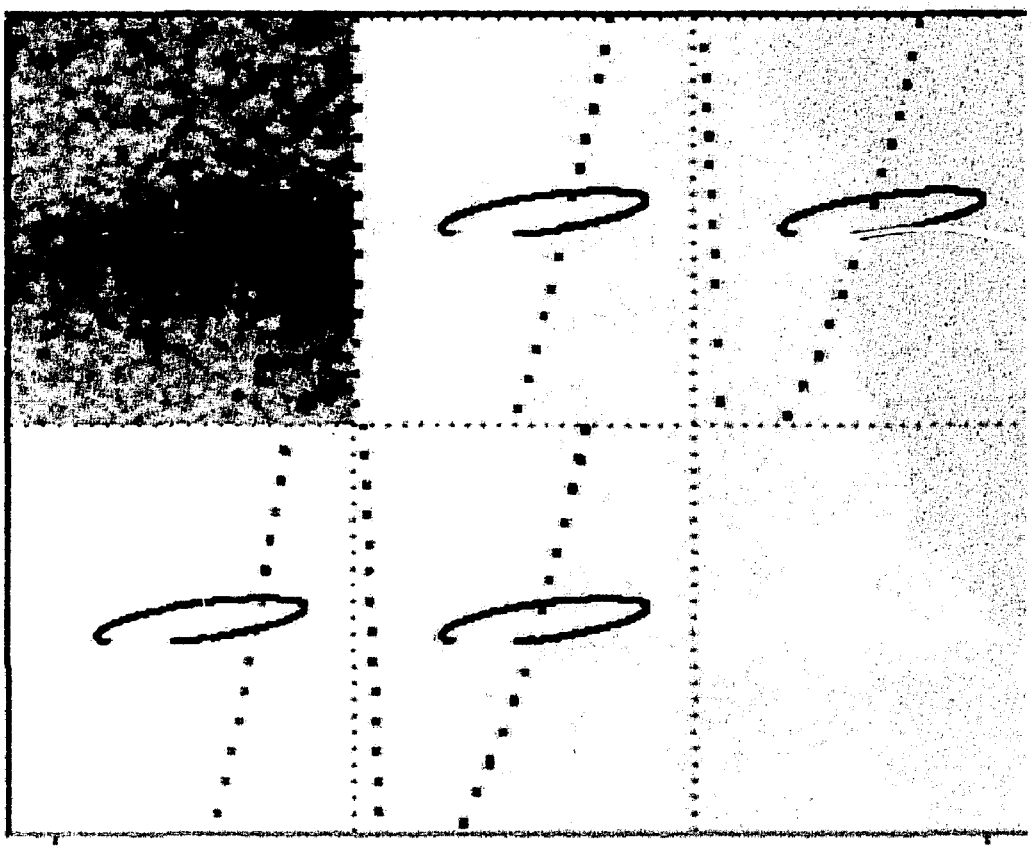

Moreover, from the data displayed in this section, I reach the conclusion that the tilt of the fibre relative to the X-ray beam is an important parameter that must be precisely determined in order to obtain the correct indexing of the integrated intensities.

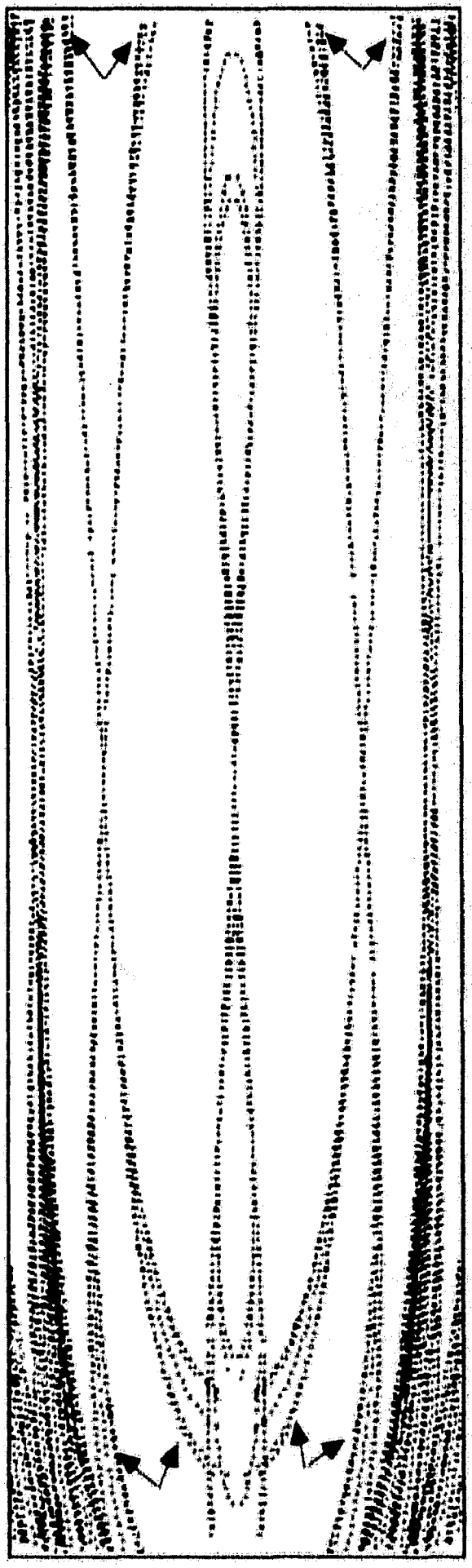

Fig V. 11: A set of predicted diffraction patterns were calculated for a fibre tilted respectively by 2.0°,2.8°,3 .2°, 4.0° and 4.2°; then patterns were added pixel by pixel. The variation in the peak predicted positions is thus followed as a function of the tilt angle. For simplicity I only show the central section of the pattern containing the meridional and some row-lines but the method is also satisfactory elsewhere on the patterns. The figure shows that the orientation effects are detectable on the extreme upper and lower (arrows) part of the patterns especially for the (-1,0,l) row line. As expected , one also notice an increase in the resolution range attainable on the meridian. On the other hand the difference in peak position on the equator is negligible for low l and up to l/l ~50.

A set of programs written by Suzuki and Rowlands, have been used to determine the tilt angle but the value so obtained was immediately used in a pattern prediction and thus tested against the experimental diffraction patterns. Unfortunately, none of the values estimated by these programs was in agreement with the experimental data and therefore I concluded that these programs were not suitable for a precise determination of the fibre tilt. I thus preferred the use of the following simple method that consists in calculating all the diffraction patterns for a set of fibre tilts. The calculation was thus done with a fibre tilted by 0° then by 0.2° and so on up to about 5° by increments of 0.2°. Figure V.11 shows an overlay of the different fibre diffraction patterns obtained with different tilt angles. The prediction is shown for a section of the pattern which contains the central part of the diffraction pattern e.g. the meridional reflections and the first row-lines, but the method is easily extended to the whole pattern. It is obtained after a calculation of the entire patterns for each tilt angle, followed by a simple addition of the binary images. Accordingly, the changes in the predicted pattern are thus continuously monitored for different fibre tilt angles by the movement of the row-lines in the film plane.

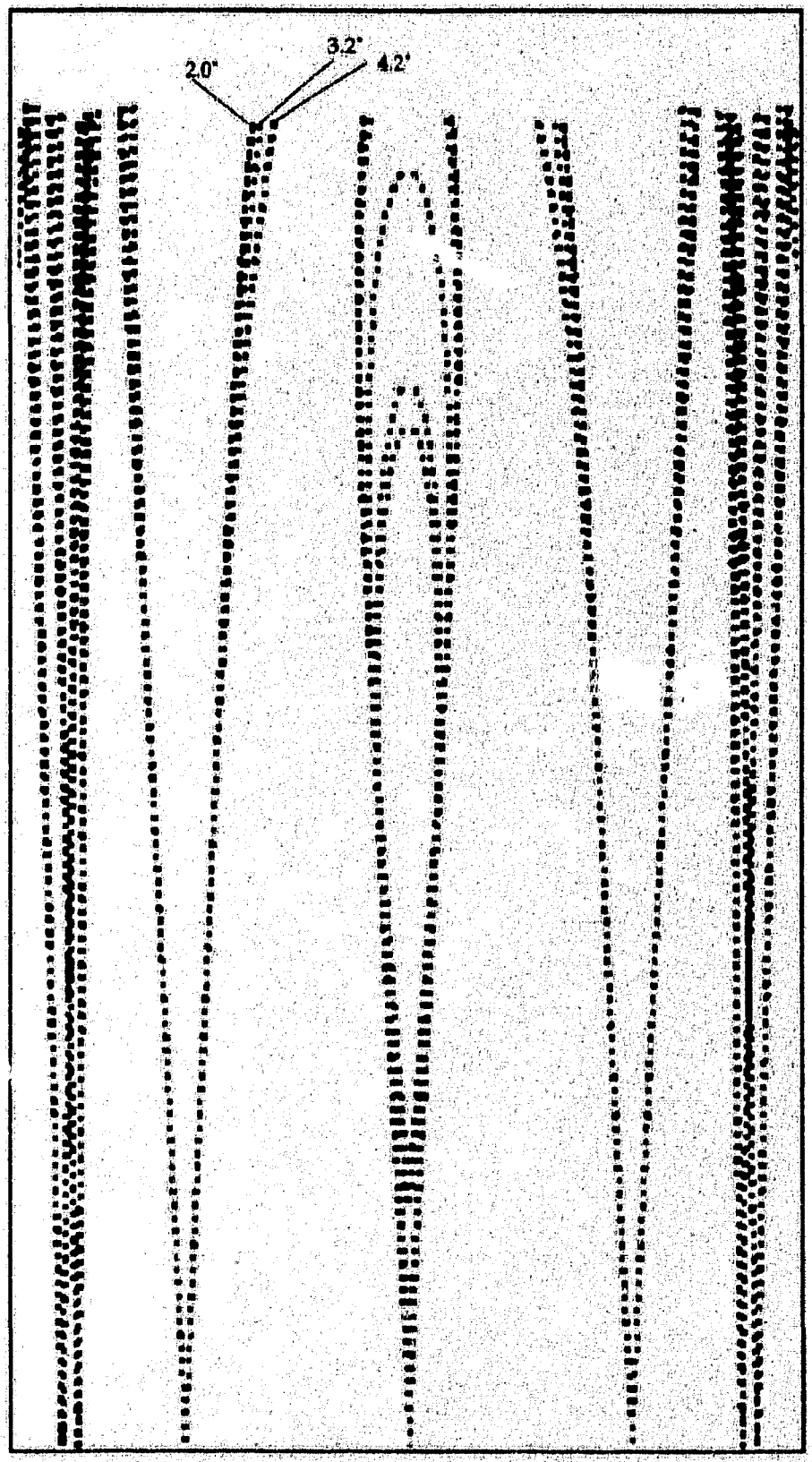

Fig V. 12: A more detailed view of the upper part of the predicted pattern where the calculated positions for a fibre tilted respectively by 2.0°,2.8°,3 .2°, 4.0° and 4.2°, are now indicated .

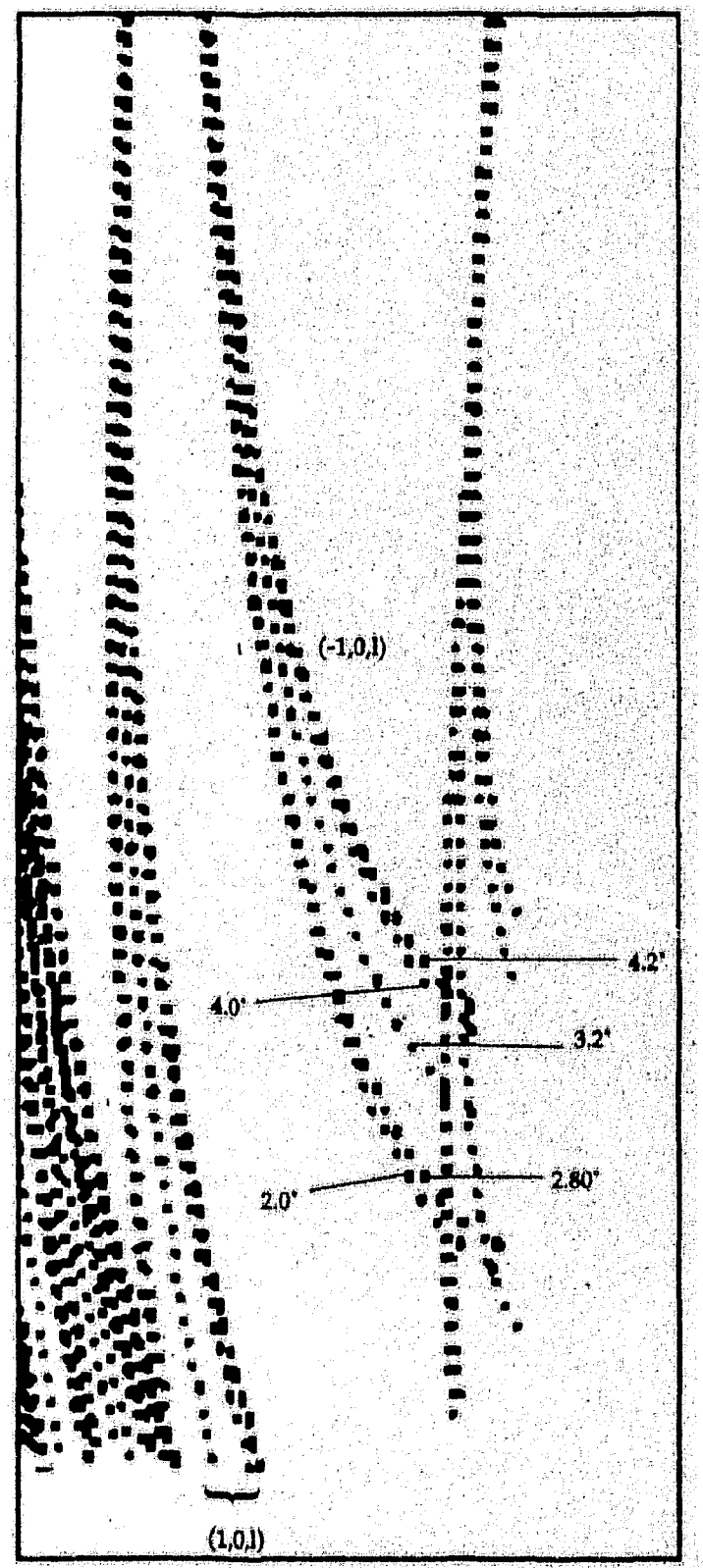

Fig V. 13: The lower part of the pattern is shown with a more detailed view on the peak position progress when the fibre is tilted. The respective values for the tilt angle are indicated on the (-1,0,l) row-line .

Figure V. 12 and V.13 also show that the tilt angle is mostly significant for the high angle values of the predicted peak positions especially in the lower part of the patterns but to a lesser extent on the upper

part of it. The actual value of the tilt angle is thus reached when the simulated pattern coincides with the upper and the lower part of the film and was estimated to 4.2° for the native data shown here.

Furthermore, the preceding figures have shown so far that data integration and indexing for the meridional and the two prominent row-lines is easily obtainable from the X-ray films where possible errors can only arise when calculating the correct l index e.g. l-1, l and l+1 might be confused. Similarly, I now further demonstrate how the integration and indexing were carried out for the other regions of the films.

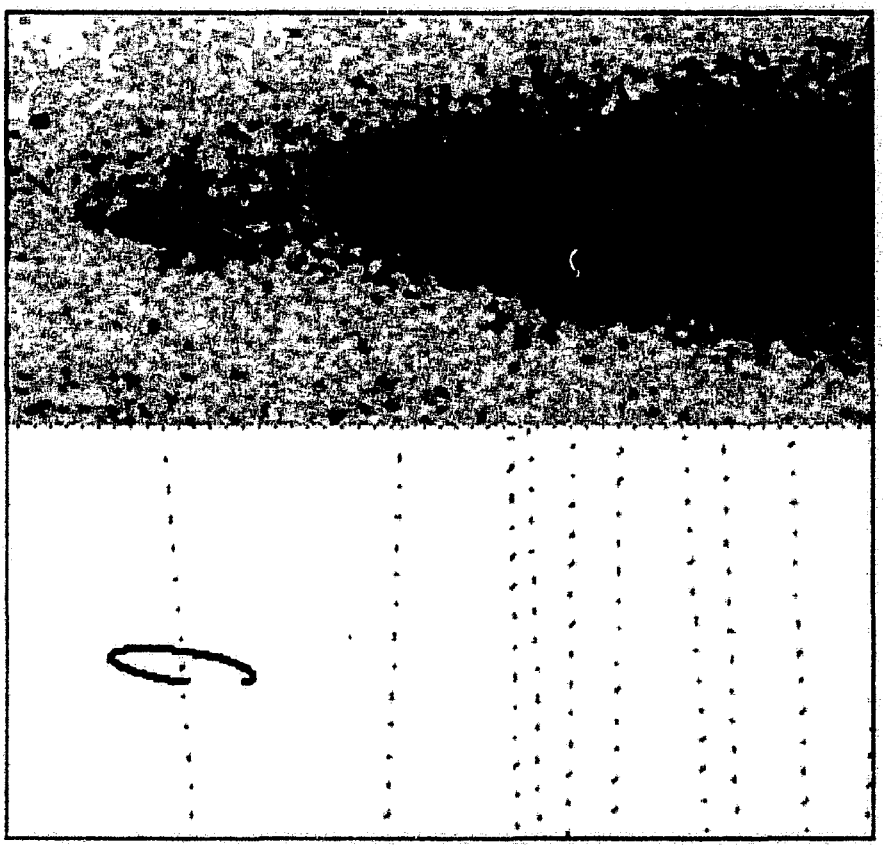

Fig. V. 14: The film region around the helix layer line display some spots superimposed on a diffuse intensity due to disorder in the crystalline packing of collagen molecules. However one can distinguish single spots as Bragg reflections for which indexes are given by the corresponding calculated spots on the bottom pattern.

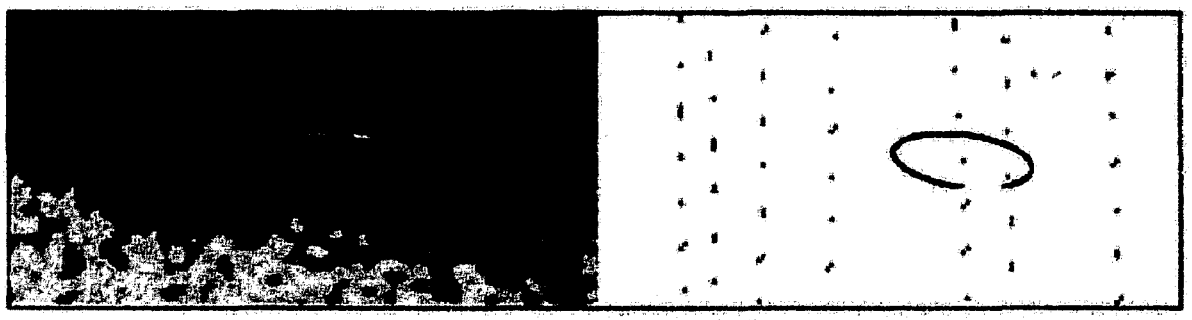

Fig. V. 15: An example of peak integration: the integration is now carried for the data on the upper helix layer-line for Bragg reflections with h,k≠1. There are clearly some weak intensity peaks for which the shapes are not well defined and otherwise too close in order to be separately integrated. These however were integrated using an appropriate elliptical box centred on the calculated Bragg position. The integrated intensity was then corrected for background by calculating the average optical density on the ellipse border and subtraction from the integrated intensity. The accuracy of a measured peak intensity is then given by the estimated standard deviation as in conventional peak integration measurement.

In order to obtain structure factors with a 3-D significance in the Fourier calculation of the electron density maps, further processing of the collagen diffraction patterns were then done by scanning all the regions in the predicted patterns. Once predicted and experimental patterns were simultaneously displayed, I centred a box around each Bragg predicted position like in figure V.15 and switched to the experimental fibre diffraction pattern looking for the presence of a discernible peak. The following rules were systematically applied:

1) for a peak which is very weak or not present a zero integrated intensity was assigned for the predicted reflection.

2) for a peak which is adjacent to another predicted one, the peak is rejected if the distance between the centres of the peak is shorter than 5 pixels on the films except if one of the peaks was strong in intensity.

3) peaks that are totally overlapped were definitely rejected from the processing to avoid the introduction of false terms in the Fourier e.g. Patterson synthesis.

4) peaks that are not well defined as regular shaped spots were included but consequently a high standard error value was expected.

5) X-ray films usually have intrinsic background due to the chemical processing and film graininess. Thus errors in interpreting film noise as a weak spot were likely to occur but integration was then strictly done since first, there was no means to decide for it and second, the same reflection might be weak for the native pattern and somewhat stronger for a derivative film. Since I am looking for intensity differences to solve the phase problem, the peak was therefore taken as it was. However a future processing is needed to discard non-isomorphous reflections.

Then, the Lorentz factor the calculation of which has been discussed in chapter 2 was systematically applied before each peak integration. The structure factor value so obtained was then written to the standard MTZ binary format for further statistical and Fourier analysis using the CCP4 crystallographic package.

Chapter 6

Data Analysis

A Collection of Native and Isomorphous Structure Factors for Collagen Crystalline Fibres

I have gathered a set of structure factors calculated from the fibre diffraction patterns of one native collagen fibre and two other heavy atom derivative fibres labelled with gold and iodine. An additional experiment is also available with PEG added to collagen fibres. PEG chemical does not contain heavy atoms but was dealt with because it produces an unusual diffraction pattern showing well resolved strong peaks on most of the row-lines. In addition, PEG stain is not supposed to label collagen molecules at specific sites for the time being. However, due to the observed increase in diffracted intensities on the row-lines one can expect that PEG is incorporated in the collagen structure with a periodic distribution within the collagen crystallites. I have processed PEG data in order to have at hand a trial set for determining the phasing capability of the other derivatives. For instance, a difference Patterson map calculated with native and PEG data would not show discernible individual peaks whereas a difference Patterson map calculated with native and heavy atom derivatives should contain such peaks (distinguishable to the available resolution limit). This chapter is intended mainly for the preliminary construction and analysis of the structure factors set, suitable for MIR difference Patterson calculation, that I could extract from the native and other derivative diffraction patterns. The data for each derivative and for the native that I have collected using the method and conditions described in chapter 5 will be grouped separately and analysed in three data categories as follows:

1) The structure factors obtained from the meridional reflections are first listed as they allow for the calculation of the one-dimensional structure of the fibre when projected down to the c-axis. Previous work (Bradshaw *et.al.*, 1989) has already been done with native and derivative meridional structure factors but the highest order obtained at that time was l≈50. In the present work I have obtained the meridional orders to a higher resolution e.g. $1/d^* \approx 8.5$Å with l≈80 for most of the native and derivatives. This allows a better resolution of the one dimensional calculated structure.

2) The structure factors obtained for the prominent (-1,0,l) and (1,0,l) row-lines, when included in the Fourier synthesis, allow for the calculation of a structure projected on the *ac* plane. The integrated intensities on the corresponding row-lines in the diffraction patterns have been obtained with a better accuracy on the Miller indices then the remaining row-lines and also with lower errors due to their discernible presence in a row and low overlap (figure VI.1). There is however a little ambiguity on the indexing of the near

equatorial reflections but this can be corrected manually at a future stage.
3) The remaining (h,k,l) reflections collected on the other vertical row-lines will be presented in the paragraphs called Other Data and in the Appendixes.

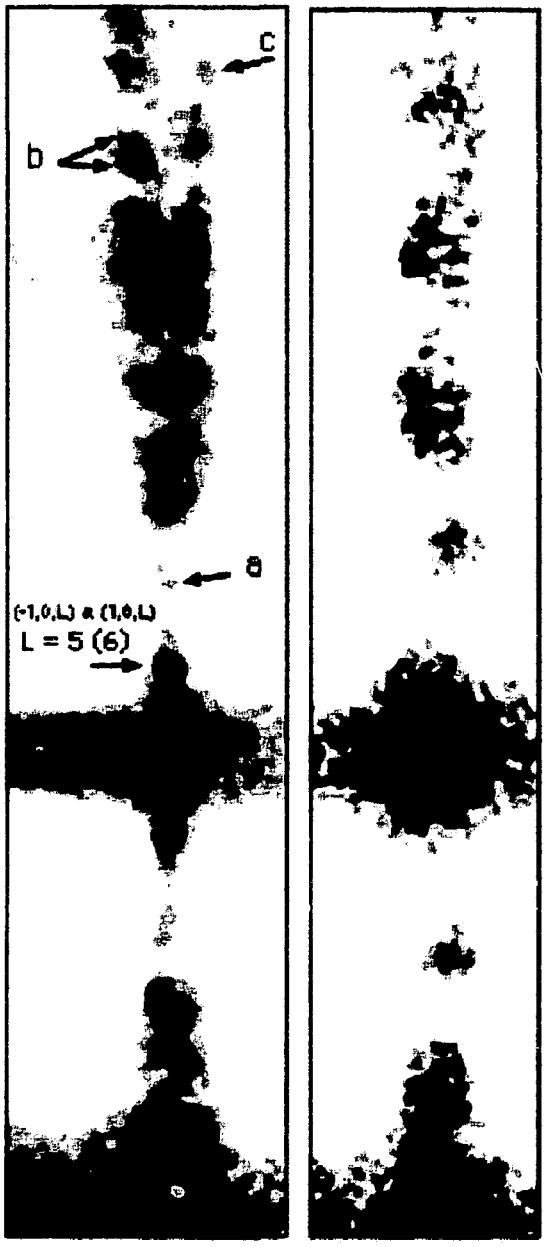

Fig. VI.1: (Left) A vertical section of the diffraction pattern with PTA labelled collagen is shown in the region containing the first row-lines. One clearly observes the presence of successive orders some of them are very weak (a) and (c) and also some strong peaks that are partially overlapped (b). This image has been obtained after orientation of six PTA experimental films and background subtraction as described before. Then the six images were added to display all the peaks all at once. In the near-equatorial region, the peaks are very strong but not separated so that I can proceed with the integration but the indexing of the reflections has to be done later manually.

(Right) PTA treated tendon also shows a set of medium (e.g. equatorial) and low intensity row-lines reflections in the region near R≈1/27Å^{-1}. These peaks are necessary for a 3-Dimensional Fourier analysis to be done but the work to integrate and index these peak is tremendous .

The diffraction spots in the film packs were integrated on one half of the patterns for native and derivative films (e.g. two quadrants, one bottom and one top containing positive and negative l indices) because of the time consuming manual processing each film pack has required. Ideally, one has to integrate the data on all four quadrants in order to obtain a better statistic when merging the data. Nevertheless, the reduced data set so obtained is sufficient to attain the required set of structure

factors and by the way to verify the Friedel's law $|F(h,k,l)|^2 = |F(\bar{h},\bar{k},\bar{l})|^2$. The Friedel law can is easily verified by comparing I(h,k,l) and I(-h,-k,-l).

A. Native Collagen Structure Factors

These are the most important data one has to obtain since electron density maps are calculated using these structure factors and the corresponding MIR calculated phases. Nevertheless, in the absence of phase information these structure factors can be used to refine a model structure by calculating the Fourier transforms and comparing with the experimental structure factors.

1. Small Angle Meridional Orders

The meridional reflections were processed manually to produce the structure factors. However, the small angle meridional reflections were missing because the low-l meridional spots are usually absent in most of the experiments with high angle diffraction patterns due to the presence of the beamstop at the film origin. Since the lowest measured l value in high-angle X-ray fibre diffraction is ≈5 to 7, the small angle experiment previously realised for peak broadening analysis (Fig. IV.6) is now convenient to measure the integrated intensities of the small angle orders (1 to 9).

Table VI.1

l	I(0,0,l)	F(0,0,l)	Imax Gauss	σImax Gauss	Imax Cauchy	σImax Cauchy	I(0,0,l)/Imax Gauss	I(0,0,l)/Imax Cauchy
-9	1841	43	5.268	0.137	6.132	0.151	2.86	3.33
-8	126	11	0.554	0.057	0.674	0.068	4.40	5.35
-7	532	23	1.146	0.051	1.327	0.061	2.15	2.49
-6	629	25	0.894	0.043	1.109	0.061	1.42	1.76
-5	1958	44	4.254	0.081	4.904	0.144	2.17	2.50
-4	390	20	0.846	0.0045	1.024	0.058	2.17	2.63
-3	7544	87	9.592	0.066	11.345	0.212	1.27	1.50
-2	796	28	0.896	0.046	1.059	0.058	1.13	1.33
-1	57618	240	54.685	1.718	65.197	1.591	0.95	1.13
1	66755	258	43.644	1.398	49.017	2.726	0.65	0.73
2	1379	37	1.042	0.064	1.222	0.077	0.76	0.89
3	7553	87	10.604	0.119	11.999	0.14	1.40	1.59
4	395	20	1.656	0.068	1.935	0.078	4.19	4.90
5	2328	48	3.6	0.072	4.207	0.116	1.55	1.81
6	928	30	0.986	0.082	1.146	0.106	1.06	1.23
7	899	30	1.084	0.07	1.32	0.085	1.21	1.47
8	176	13	no[1]	no	no	no	no	no
9	2093	46	3.916	0.062	4.562	0.099	1.87	2.18

Because of their contribution to the low resolution features in the molecular structure, the small-angle

[1] no=not observed

orders listed in table VI.1 are important for the understanding of collagen molecular packing in the unit cell and will thus be scaled and added to the native structure factors obtained with the high angle diffraction patterns. The phase calculation for these orders, obviously, will not be obtained because there was actually no meridional small angle diffraction experiment with the other derivatives.
Moreover, in chapter 4, I have already measured the peak height after the fit of Gaussian and Lorentzian curves but integrated intensities were not calculated. Thus, in order to add these reflections to the native full data set, the orders have been integrated to yield the total intensity in the peak. In the first two columns of table IV.1 are listed the integrated intensities and structure factors measured from the X-ray film shown in chapter 4. In columns 3 to 6 I report the values of the peak height calculated in chapter 4 along with the estimated errors for each small-angle order. Whereas the ratios in the last two columns indicate that the peak height intensity is a good approximation of the total integrated peak intensity. These ratios are all close to unity unless for the lowest peaks (-8, 8 and 4 ...) for which curve fits were also less accurate.

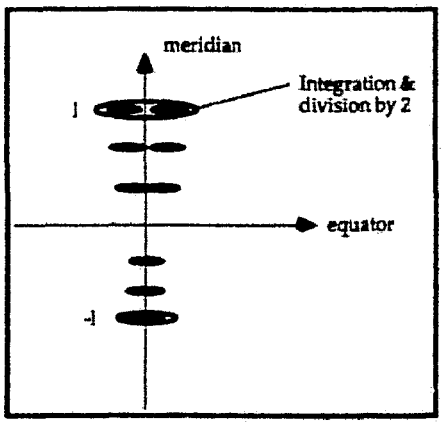

Fig. VI.2 :The integration of meridional spots was carried as usual, nevertheless due to fibre tilt the positive l orders are split into two partially separated spots. I have thus integrated the total intensity for positive l's and applied a factor 0.5 where required.

2. Meridional reflections

The data I have obtained from the meridional diffraction pattern of native collagen are listed below. The data set contains all the values for l<0 and l>0 observed on the X-ray films. Data from successive films have been corrected for film factor so that saturated peaks were integrated on bottom films in the pack. I have also added the small-angle orders obtained in the paragraph before after scaling. Now, the meridional orders on the upper part of the patterns are split gradually with increasing l due to the fibre tilt whereas the l<0 orders are not split at least to higher l values than for l>0. This kind of overlap however does not hinder the integration of these data since they belong to the same reflection. I have thus integrated reflections which were split into two spots (as a consequence of the fibre tilt) on

the upper part of the pattern only once and then, after background subtraction and Lorentz factor correction, I have divided the integrated intensity by a factor two (figure VI.2).
Reflections which were predicted but not observed on the meridian were given a zero total integrated intensity and a zero standard deviation (see table below) to allow for a native to derivative MIR differences to be estimated when orders are present in the derivative patterns. The ratio σF/F in that case was not defined and was manually set to 100%.

l	1/d*	F	σF	σF/F
-43	15.71	8	1	17
-42	16.10	8	1	13
-41	16.48	6	1	16
-40	16.90	8	1	13
-39	17.33	0	0	100
-38	17.79	6	1	15
-37	18.26	6	1	16
-36	18.76	11	1	9
-35	19.32	6	1	16
-34	19.88	16	1	9
-33	20.46	6	1	16
-32	21.13	7	1	14
-31	21.82	9	1	12
-30	22.53	19	1	7
-29	23.31	13	1	8
-28	24.11	0	0	100
-27	25.00	21	1	7
-26	25.99	16	1	9
-25	27.02	18	1	8
-24	28.17	13	2	14
-23	29.36	8	1	13
-22	30.71	10	1	10
-21	32.11	31	3	8
-20	33.71	25	2	8
-19	35.58	11	2	16
-18	37.53	9	2	19
-17	39.84	16	2	11
-16	42.26	14	2	12
-15	45.18	13	2	13
-14	48.22	14	2	12
-13	51.99	11	2	15
-12	55.90	24	2	9
-11	60.86	20	2	9
-10	67.42	19	2	10
-9	74.54	26	2	8
-8	84.52	18	2	11
-7	95.35	17	2	12
-6	111.80	20	1	5
-5	141.42	36	1	3
-4	158.11	16	1	6
-3	223.61	71	1	1
-2	316.23	23	1	4
-1	678.00	196	1	1
1	678.00	211	1	0
2	316.23	30	1	3
3	223.61	71	1	1
4	158.11	16	1	6
5	141.42	39	1	3
6	111.80	25	1	4
7	95.35	24	1	4
8	84.52	11	1	9
9	74.54	37	2	7
10	67.42	26	2	9
11	60.86	26	2	8
12	55.90	30	2	7
13	51.99	18	2	10
14	48.22	24	2	8
15	45.18	22	2	9
16	42.26	23	2	9
17	39.84	27	2	8
18	37.53	18	2	10
19	35.58	22	2	9
20	33.71	44	4	9
21	32.11	42	4	9
22	30.71	16	1	9
23	29.36	12	1	12
24	28.17	16	2	15
25	27.02	28	2	9
26	25.99	38	3	9
27	25.00	19	2	9
28	24.11	13	2	13
29	23.31	29	2	8
30	22.53	39	3	8
31	21.82	23	2	10
32	21.13	14	1	10
33	20.46	25	2	10
34	19.88	29	2	8
35	19.32	14	1	10
36	18.76	20	2	9
37	18.26	21	2	10
38	17.79	33	2	7
39	17.33	13	1	11
40	16.90	23	2	8
41	16.48	40	3	7
42	16.10	24	2	8
43	15.71	23	2	8
44	15.36	19	2	9
45	15.01	16	1	9
46	14.70	9	1	15
47	14.37	15	1	9
48	14.07	26	2	7
49	13.79	25	2	7
50	13.51	5	1	20
51	13.25	13	1	11
52	13.00	103	6	5
53	12.75	0	0	100
54	12.51	10	2	20
55	12.28	7	2	28
56	12.06	17	2	10
57	11.85	26	2	9
58	11.65	16	2	13
59	11.46	31	2	7
60	11.26	31	2	8
61	11.08	0	0	100
62	10.90	14	2	15
63	10.73	16	2	13
64	10.56	17	2	11
65	10.40	0	0	100
66	10.24	13	1	11
67	10.09	12	1	12
68	9.94	10	1	13
69	9.79	10	1	14
70	9.65	38	2	6
71	9.52	36	2	7
72	9.38	76	4	5
73	9.26	4	1	33
74	9.13	7	1	21
75	9.01	5	1	31
76	8.89	14	1	7
77	8.77	0	0	100
78	8.66	9	1	11
79	8.55	17	1	6
80	8.45	5	1	18
81	8.34	6	1	16
82	8.24	20	1	7
83	8.14	10	1	14
84	8.04	7	1	19
85	7.95	0	0	100
86	7.86	24	1	6
87	7.77	19	2	9
88	7.68	18	1	8
89	7.59	22	1	6
90	7.51	7	1	19
91	7.42	28	4	13
92	7.34	17	2	12
93	7.27	18	2	11
94	7.19	26	2	8
95	7.11	19	2	10
96	7.04	20	2	9
97	6.97	23	2	9
98	6.89	11	2	15
99	6.82	14	2	12
100	6.76	13	2	13
101	6.69	14	2	12
102	6.62	16	2	11
103	6.56	9	2	19
104	6.50	11	2	16
105	6.43	25	2	8

The above listed orders however must be checked for consistency with one of the basic crystallographic principles that is the equivalence between symmetry related reflections and also for the correct Bragg indexing. This is usually obtained by calculating the R_{sym} factor which gives a statistical measure of the data conformity to the centro-symmetry equivalent reflections. The Friedel's law states that in the absence of anomalous dispersion, centro-symmetric reflections have equal intensities . Thus in order to verify the Friedel law I have plotted in figure VI.3 the observed structure factors for the meridional reflections.

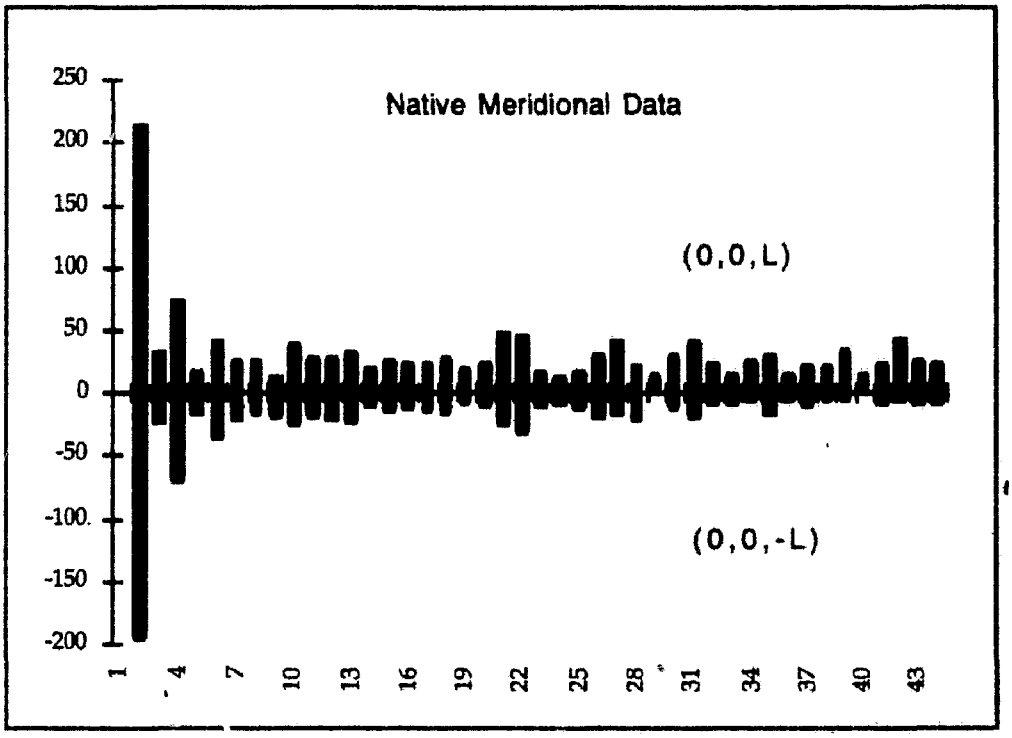

Fig VI.3: A graphical representation of Friedel's law for the meridional data obtained with native collagen. The l indices are shown on the horizontal axis up to l=43 and the structure factors amplitude on the vertical axis. The structure factors and the estimated standard deviations for l<0 are represented by their negative values to allow for a simultaneous comparison.

This simple graphical representation will be preferred to the statistical global R_{sym} factors since it allows us first to verify that structure factors amplitudes for symmetry related pairs are equal in magnitude and second, that the reflections have been correctly indexed.

3. Row-Lines

Native collagen (-1,0,l) and (1,0,l) structure factors have also been collected and are completely summarised in the list below for the first time. Here again I have associated a zero amplitude to the structure factors the prediction program has calculated but I have not observed on the X-ray films.

h	k	l	1/d*	F	σF	σF/F
-1	0	-99	6.63	0	0	100
-1	0	-98	6.69	10	2	21
-1	0	-97	6.76	13	2	15
-1	0	-96	6.83	18	3	15
-1	0	-95	6.90	12	2	15
-1	0	-94	6.97	10	2	20
-1	0	-93	7.04	0	0	100
-1	0	-92	7.11	12	2	17
-1	0	-91	7.19	19	2	10
-1	0	-89	7.34	11	2	19
-1	0	-88	7.42	0	0	100
-1	0	-87	7.50	4	2	45
-1	0	-86	7.58	7	2	28
-1	0	-85	7.67	0	0	100
-1	0	-84	7.75	0	0	100
-1	0	-83	7.84	0	0	100
-1	0	-82	7.93	12	3	24
-1	0	-81	8.02	13	2	15
-1	0	-80	8.11	16	2	12
-1	0	-79	8.21	0	0	100
-1	0	-78	8.31	6	2	35
-1	0	-77	8.41	9	2	22
-1	0	-75	8.62	8	2	24
-1	0	-74	8.73	8	2	25
-1	0	-73	8.84	0	0	100
-1	0	-72	8.96	22	2	11
-1	0	-70	9.19	35	3	9
-1	0	-69	9.31	0	0	100
-1	0	-68	9.44	17	2	12
-1	0	-68	9.44	13	2	15
-1	0	-67	9.57	0	0	100
-1	0	-65	9.84	0	0	100
-1	0	-64	9.98	29	3	10
-1	0	-63	10.12	16	2	13
-1	0	-62	10.27	13	2	15
-1	0	-61	10.43	0	0	100
-1	0	-60	10.58	13	2	15
-1	0	-59	10.75	0	0	100
-1	0	-57	11.08	21	2	10
-1	0	-56	11.26	13	2	15
-1	0	-55	11.44	0	0	100
-1	0	-54	11.62	71	2	15
-1	0	-53	11.82	0	0	100
-1	0	-52	12.02	25	3	11
-1	0	-51	12.23	15	2	13
-1	0	-50	12.44	13	2	15
-1	0	-49	12.66	18	3	16
-1	0	-48	12.89	8	2	21
-1	0	-47	13.12	0	0	100
-1	0	-46	13.36	9	2	20
-1	0	-45	13.62	0	0	100
-1	0	-44	13.88	11	3	26
-1	0	-43	14.16	12	2	14
-1	0	-42	14.43	0	0	100
-1	0	-41	14.73	17	2	12
-1	0	-40	15.02	4	2	53
-1	0	-39	15.34	0	0	100
-1	0	-38	15.67	4	2	50
-1	0	-37	16.01	0	0	100
-1	0	-36	16.35	0	0	100
-1	0	-35	16.71	10	2	20
-1	0	-34	17.10	11	2	19
-1	0	-33	17.49	12	2	19

-1	0	-32	17.90	10	3	30	-1	0	64	10.39	5	2	40	1	0	-22	25.00	13	3	22
-1	0	-31	18.35	0	0	100	-1	0	65	10.24	12	2	14	1	0	-21	25.65	8	2	22
-1	0	-30	18.80	7	2	28	-1	0	66	10.09	0	0	100	1	0	-20	26.44	13	2	15
-1	0	-29	19.25	0	0	100	-1	0	67	9.95	0	0	100	1	0	-19	27.22	11	2	15
-1	0	-28	19.73	7	2	28	-1	0	68	9.81	13	2	13	1	0	-18	27.95	15	2	13
-1	0	-27	20.24	0	0	100	-1	0	69	9.67	0	0	100	1	0	-17	28.75	11	2	15
-1	0	-26	20.76	0	0	100	-1	0	70	9.54	10	2	20	1	0	-16	29.62	23	3	13
-1	0	-25	21.32	6	2	41	-1	0	71	9.41	43	2	5	1	0	-13	32.11	9	2	22
-1	0	-24	21.87	16	3	18	-1	0	72	9.29	15	2	11	1	0	-12	32.97	6	2	28
-1	0	-23	22.47	0	0	100	-1	0	73	9.16	23	3	12	1	0	-10	34.50	8	2	22
-1	0	-22	23.12	11	3	28	-1	0	74	9.05	13	2	15	1	0	-9	35.36	0	0	100
-1	0	-21	23.77	5	2	45	-1	0	75	8.93	10	2	17	1	0	-8	36.04	6	2	34
-1	0	-20	24.40	14	2	14	-1	0	76	8.81	14	2	12	1	0	-6	37.27	7	2	31
-1	0	-19	25.08	21	3	14	-1	0	77	8.71	16	2	13	1	0	-1	38.35	29	3	9
-1	0	-18	25.82	13	3	24	-1	0	78	8.60	10	2	17	1	0	0	38.35	45	4	9
-1	0	-17	26.54	6	2	37	-1	0	79	8.49	0	0	100	1	0	1	38.07	41	3	7
-1	0	-16	27.32	7	2	30	-1	0	80	8.39	16	2	11	1	0	4	36.76	13	2	19
-1	0	-15	28.17	19	2	11	-1	0	81	8.29	17	2	11	1	0	7	34.71	0	0	100
-1	0	-14	28.99	16	2	13	-1	0	82	8.19	5	2	38	1	0	9	33.15	0	0	100
-1	0	-13	29.75	1	2	224	-1	0	83	8.10	11	2	16	1	0	11	31.47	0	0	100
-1	0	-12	30.57	17	2	12	-1	0	84	8.00	3	2	60	1	0	13	29.75	0	0	100
-1	0	-11	31.47	17	3	16	-1	0	85	7.91	11	2	15	1	0	15	28.17	12	2	19
-1	0	-9	33.15	9	4	42	-1	0	86	7.82	0	0	100	1	0	16	27.32	0	0	100
-1	0	-8	33.90	2	2	91	-1	0	87	7.73	0	0	100	1	0	20	24.40	16	2	13
-1	0	-7	34.71	13	3	24	-1	0	88	7.65	12	2	17	1	0	22	23.12	19	3	17
-1	0	-5	36.27	17	3	21	-1	0	89	7.56	7	2	27	1	0	23	22.47	14	2	14
-1	0	-4	36.76	11	3	32	-1	0	90	7.48	7	2	24	1	0	24	21.87	20	3	14
-1	0	-2	37.80	23	3	13	-1	0	91	7.40	0	0	100	1	0	25	21.32	13	2	16
-1	0	-1	38.07	55	4	8	-1	0	92	7.32	0	0	100	1	0	26	20.76	12	2	17
-1	0	3	38.35	21	4	18	-1	0	93	7.25	0	0	100	1	0	27	20.24	0	0	100
-1	0	4	38.07	27	4	17	-1	0	94	7.17	12	2	16	1	0	28	19.73	0	0	100
-1	0	5	37.80	18	5	25	-1	0	95	7.09	11	2	19	1	0	29	19.25	0	0	100
-1	0	6	37.27	0	0	100	-1	0	96	7.02	16	2	11	1	0	30	18.80	0	0	100
-1	0	7	36.76	0	0	100	-1	0	97	6.95	0	0	100	1	0	31	18.35	0	0	100
-1	0	8	36.04	0	0	100	-1	0	98	6.88	0	0	100	1	0	32	17.90	6	2	34
-1	0	9	35.36	3	2	85	-1	0	99	6.81	0	0	100	1	0	33	17.49	18	2	11
-1	0	10	34.50	10	2	20	1	0	-77	8.71	0	0	100	1	0	34	17.10	0	0	100
-1	0	11	33.71	9	3	32	1	0	-76	8.81	0	0	100	1	0	35	16.71	14	2	15
-1	0	12	32.97	5	2	38	1	0	-75	8.93	0	0	100	1	0	36	16.35	15	2	13
-1	0	13	32.11	0	0	100	1	0	-74	9.05	6	2	27	1	0	37	16.01	0	0	100
-1	0	14	31.31	3	2	65	1	0	-73	9.16	3	2	50	1	0	38	15.67	0	0	100
-1	0	15	30.43	30	3	10	1	0	-72	9.29	0	0	100	1	0	39	15.34	9	2	22
-1	0	16	29.62	12	2	16	1	0	-71	9.41	0	0	100	1	0	40	15.02	11	2	17
-1	0	17	28.75	20	2	11	1	0	-69	9.67	0	0	100	1	0	41	14.73	14	2	14
-1	0	18	27.95	24	2	9	1	0	-68	9.81	12	2	15	1	0	42	14.43	0	0	100
-1	0	19	27.22	21	2	10	1	0	-67	9.95	6	2	28	1	0	43	14.16	13	2	17
-1	0	20	26.44	16	2	13	1	0	-66	10.09	5	2	32	1	0	44	13.88	0	0	100
-1	0	21	25.65	0	0	100	1	0	-65	10.24	8	2	21	1	0	45	13.62	4	2	46
-1	0	22	25.00	19	3	15	1	0	-64	10.39	0	0	100	1	0	46	13.36	11	2	18
-1	0	23	24.25	10	2	20	1	0	-63	10.55	0	0	100	1	0	47	13.12	0	0	100
-1	0	24	23.64	19	2	10	1	0	-62	10.71	0	0	100	1	0	48	12.89	19	2	11
-1	0	25	22.94	12	2	17	1	0	-61	10.87	0	0	100	1	0	49	12.66	0	0	100
-1	0	26	22.36	0	0	100	1	0	-60	11.04	7	2	24	1	0	50	12.44	9	2	22
-1	0	27	21.77	10	2	17	1	0	-59	11.22	0	0	100	1	0	51	12.23	11	3	27
-1	0	28	21.18	0	0	100	1	0	-58	11.40	5	2	38	1	0	52	12.02	9	2	22
-1	0	29	20.67	6	2	34	1	0	-57	11.59	13	3	21	1	0	53	11.82	1	2	200
-1	0	30	20.12	0	0	100	1	0	-56	11.78	0	0	100	1	0	54	11.62	0	0	100
-1	0	31	19.65	14	2	14	1	0	-55	11.98	4	2	39	1	0	55	11.44	0	0	100
-1	0	32	19.14	10	2	21	1	0	-54	12.18	15	2	14	1	0	56	11.26	0	0	100
-1	0	33	18.70	0	0	100	1	0	-53	12.39	6	2	30	1	0	57	11.08	11	2	18
-1	0	34	18.26	14	2	14	1	0	-52	12.62	3	2	65	1	0	58	10.91	12	2	17
-1	0	35	17.82	7	2	28	1	0	-51	12.85	0	0	100	1	0	59	10.75	7	2	30
-1	0	36	17.41	9	2	23	1	0	-50	13.07	7	3	40	1	0	60	10.58	16	2	13
-1	0	39	16.29	31	3	10	1	0	-49	13.32	8	2	24	1	0	61	10.43	4	2	49
-1	0	40	15.93	0	0	100	1	0	-48	13.57	0	0	100	1	0	62	10.27	0	0	100
-1	0	41	15.60	21	2	8	1	0	-47	13.83	0	0	100	1	0	63	10.12	17	2	12
-1	0	42	15.27	10	2	21	1	0	-46	14.10	10	2	17	1	0	64	9.98	11	2	19
-1	0	43	14.96	0	0	100	1	0	-45	14.37	7	2	29	1	0	65	9.84	8	2	24
-1	0	44	14.66	0	0	100	1	0	-44	14.66	0	0	100	1	0	66	9.70	12	2	17
-1	0	45	14.37	11	2	18	1	0	-43	14.96	0	0	100	1	0	67	9.57	9	3	34
-1	0	46	14.10	0	0	100	1	0	-42	15.27	9	2	21	1	0	68	9.44	14	2	14
-1	0	47	13.83	2	2	87	1	0	-41	15.60	15	2	12	1	0	69	9.31	16	2	12
-1	0	48	13.57	18	3	16	1	0	-40	15.93	4	2	49	1	0	70	9.19	13	3	24
-1	0	49	13.32	18	3	11	1	0	-39	16.29	13	2	15	1	0	72	8.96	39	3	7
-1	0	50	13.07	8	2	26	1	0	-38	16.64	15	2	13	1	0	73	8.84	6	2	32
-1	0	51	12.85	13	2	13	1	0	-36	17.41	10	2	17	1	0	74	8.73	0	0	100
-1	0	52	12.62	10	2	17	1	0	-35	17.82	3	2	71	1	0	76	8.51	26	3	12
-1	0	53	12.39	13	2	15	1	0	-34	18.26	10	3	28	1	0	77	8.41	0	0	100
-1	0	54	12.18	14	2	15	1	0	-33	18.70	6	2	35	1	0	78	8.31	11	2	18
-1	0	55	11.98	13	2	15	1	0	-32	19.14	6	2	32	1	0	79	8.21	16	3	19
-1	0	56	11.78	0	0	100	1	0	-30	20.12	0	0	100	1	0	80	8.11	17	2	13
-1	0	57	11.59	0	0	100	1	0	-29	20.67	12	2	14	1	0	81	8.02	8	2	24
-1	0	58	11.40	27	3	10	1	0	-28	21.18	10	3	26	1	0	82	7.93	21	3	15
-1	0	60	11.04	21	3	13	1	0	-27	21.77	0	0	100	1	0	83	7.84	7	2	27
-1	0	61	10.87	11	2	16	1	0	-25	22.94	12	3	22	1	0	84	7.75	0	0	100
-1	0	62	10.71	4	2	48	1	0	-24	23.64	9	2	19	1	0	85	7.67	0	0	100
-1	0	63	10.55	9	2	23	1	0	-23	24.25	12	2	15	1	0	86	7.58	11	3	28

1	0	87	7.50	8	2	26	1	0	92	7.11	10	2	20	1	0	97	6.76	0	0	100			
1	0	88	7.42	0	0	100	1	0	93	7.04	15	3	19	1	0	98	6.69	14	2	15			
1	0	89	7.34	2	2	100	1	0	94	6.97	27	3	12	1	0	99	6.63	0	0	100			
1	0	90	7.26	10	2	20	1	0	95	6.90	0	0	100	1	0	100	6.57	0	0	100			
1	0	91	7.19	0	0	100	1	0	96	6.83	9	2	23										

The Friedel pairs are again plotted in the following two figures where I first show (figure VI.5) the near equatorial region of the pattern (e.g. reflections with $|l|<30$). One thus recognises in figure VI.5 that the Friedel law is verified only for some reflections but one have to bear in mind that strongly overlapped as well as altered peaks have been rejected from the data processing whereas, very weak reflections have been given a zero integrated intensity.

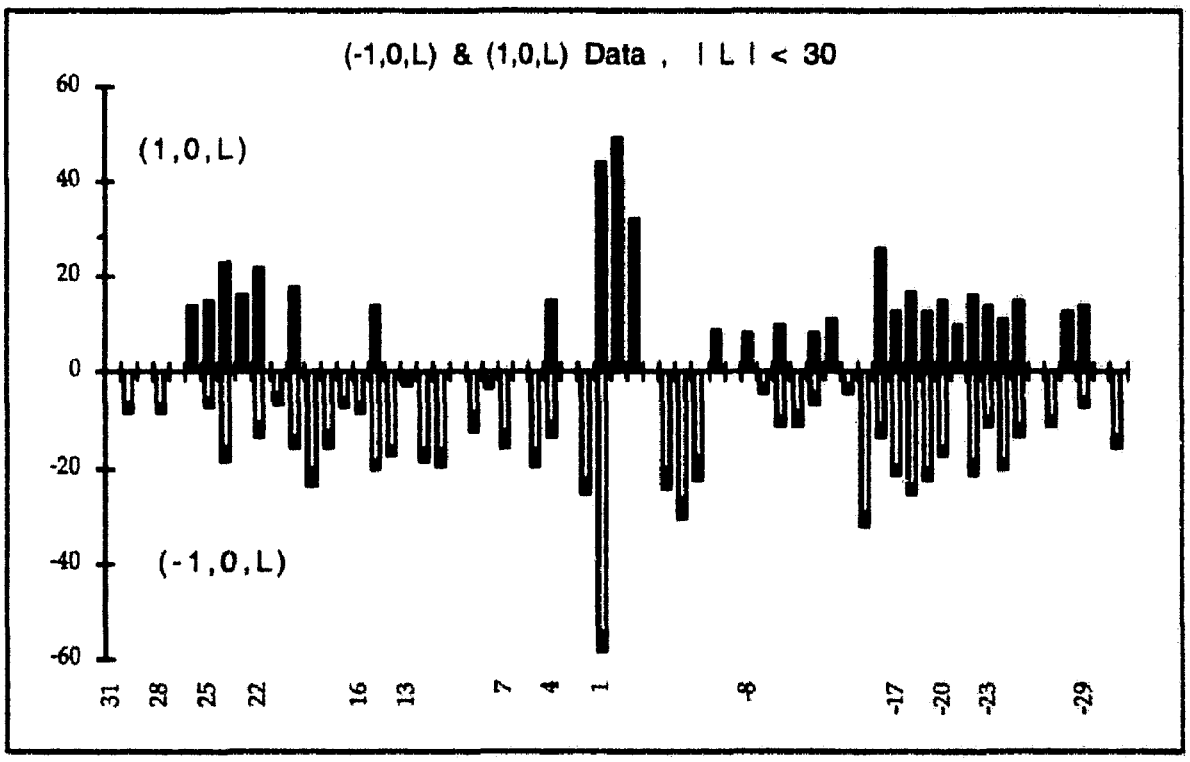

Fig. VI.5:A graphical representation of the Friedel law is shown here for native collected reflections. We observe a good agreement for some reflections like the (1,0,1) and (-1,0,-1) which is the strongest reflection on the equator.

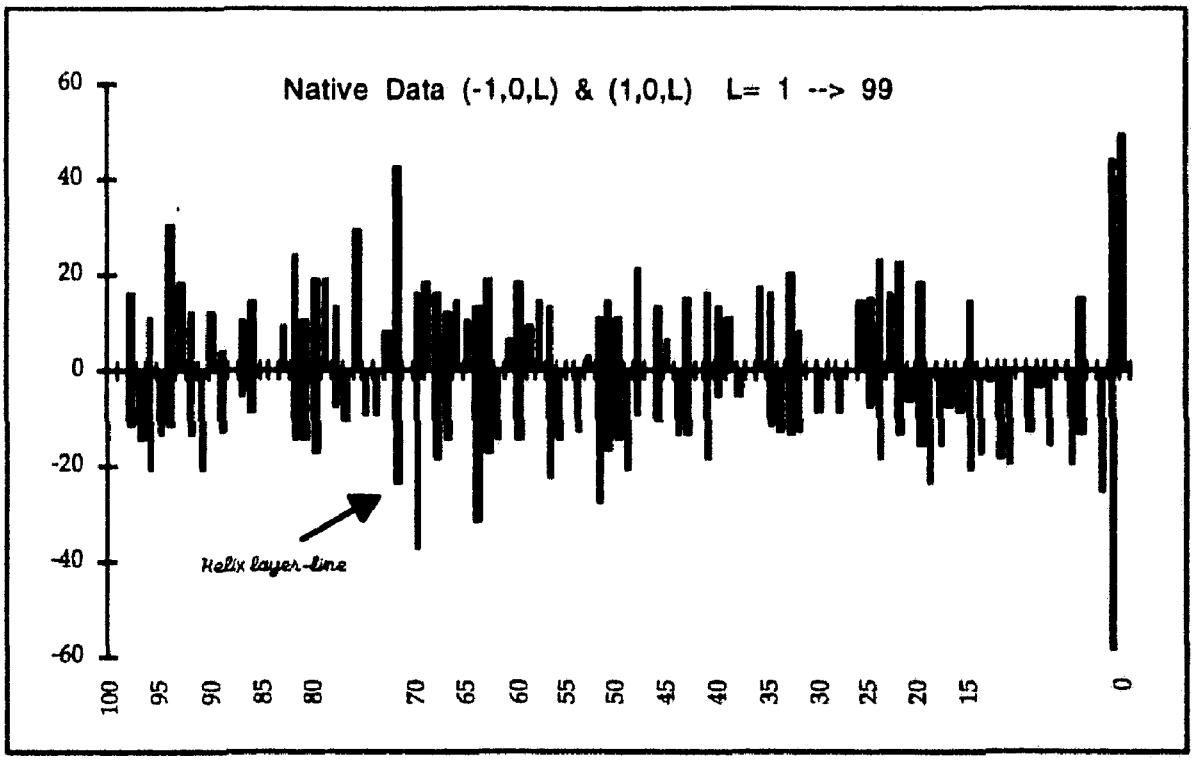

Fig. VI.6 : The Friedel plot of the (-1,0,l) and (1,0,l) row-lines is here shown for l=0 to 100. The arrow indicates the (1,0,11~73) reflections which falls at the helix layer-line intercept in the X-ray diffraction pattern.

4. Other F(h,k,l) 's

The data analysis has also yielded a set of structure factors from the other row-lines. A low-resolution 3-D Fourier analysis is thus possible assuming the gathered data are correct.

The data were checked to evaluate the reliability of the structure factors, a complete data set is provided in the appendix. Figure VI.7 shows a Friedel plot of the reflections with general indices (2,0,l) and (-2,0,l). These are again better plotted as a function of the l index. The (2,0,l) structure factors are plotted on the F>0 part of the vertical axis whereas the (-2,0,l) structure factors are plotted on the lower part of it. The "hole" between the l≈-34 to l≈50 corresponds to the region of the pattern where the reflections overlap with reflections from the other row-lines and were thus neglected. Otherwise, we see in figure VI.7 that the Friedel pairs match within the range of the experimental errors in structure factors determination.

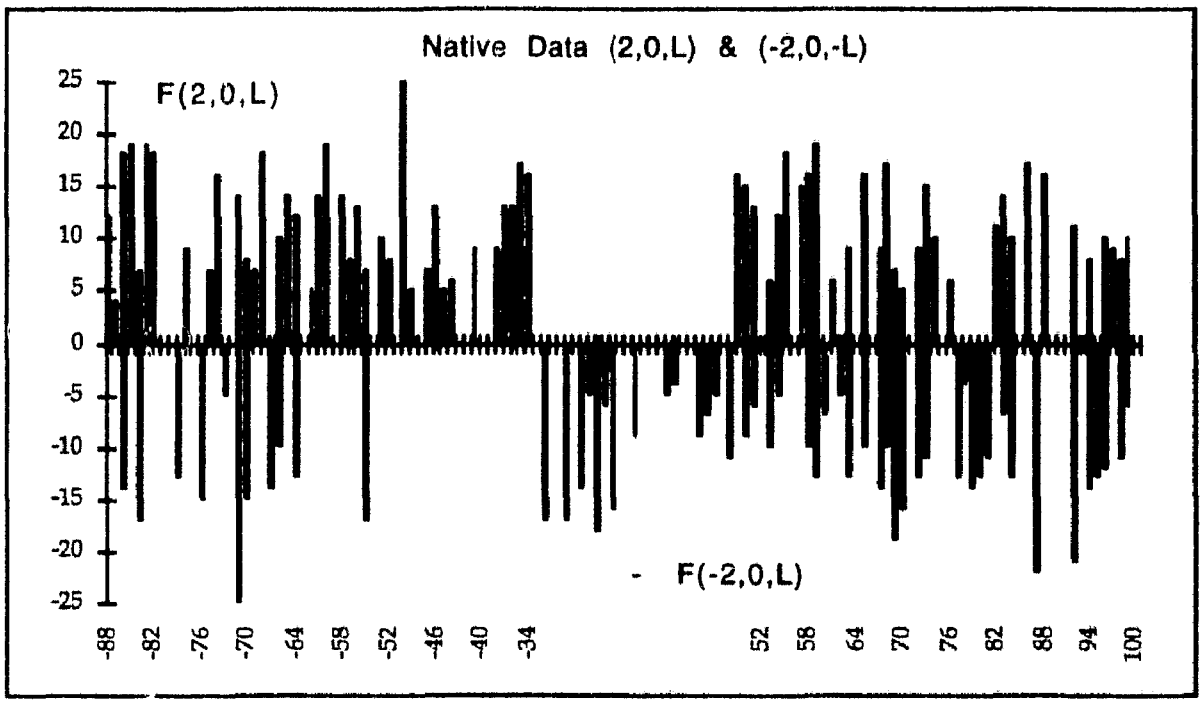

Fig. VI.7 : The Friedel law is also convincing for the set of data collected on the (-2,0,l) and (2,0,l) row-lines. There are obviously some strong reflections at l≈±70 which are obtained from reflections integrated on the helix layer-line. This plot and the others shown before give the evidence that I have obtained a reliable indexing of the reflections relative to their l index.

5. Analysis of Native Data using the CCP4 Crystallographic Programs

The above listed native structure factors are the data I have collected from X-ray films without any further processing since only film factor and Lorentz corrections were applied. However, for the purpose of electron density and Patterson calculations these data have been analysed using the CCP4 protein crystallography package. The data were first merged and scaled using the programs Agrovata & Rotavata of the CCP4 suite. Reflections recorded more then once were thus merged and equivalents are analysed to produce a unique reflection file with the new standard deviation again calculated. The output of these programs is a binary file containing a reduced unique set of structure factors (e.g. relative to the P1 crystal system) for further derivative to native scaling and other Fourier calculations. Some statistical calculations on the intensities (distribution of intensity versus resolution, calculation of R-factor versus intensities etc) are also done by the programs which are given in tables VI.2 and VI.3. The symbols used are the usual abbreviations used by CCP4 and the reader must survey the CCP4 manual for a detailed description of the symbols and algorithms used.

Table VI.2

Native Data

Analysis against resolution

N	<s>	DminÅ	Rfac	Rcum	Av_I	σ	I/σ	sd	Nmeas	Nref
1	0.0028	18.97	0.178	0.178	881.	412.4	2.1	114.06	158	79
2	0.0056	13.41	0.556	0.217	194.	255.3	0.8	92.99	82	41
3	0.0083	10.95	0.496	0.251	190.	168.1	1.1	105.52	114	57
4	0.0111	9.49	0.423	0.271	179.	147.4	1.2	107.56	131	65
5	0.0139	8.48	0.523	0.299	232.	224.7	1.0	112.88	107	52
6	0.0167	7.75	0.455	0.309	202.	160.0	1.3	103.41	76	38
7	0.0194	7.17	0.614	0.324	225.	318.5	0.7	110.74	54	27
8	0.0222	6.71	0.618	0.332	176.	232.0	0.8	93.14	40	20
9	0.0250	6.32	0.585	0.333	93.	101.3	0.9	60.79	18	9
10	0.0278	6.00	0.000	0.333	0.	0.0	0.0	0.00	0	0

Table VI.3 shows the intensity distribution of native reflections as a function of the standard deviation for the different resolution shells listed in column 1. These data have been calculated by the Rotavata program assuming the P1 space group for the collagen crystalline domains. It follows that most of the reflections have been determined with a higher σ value then the film data I have obtained only after peak integration. However these data remain convenient for low-resolution Fourier synthesis as structure factors are usually weighted by the inverse of the standard deviations in the Fourier series. I will further use these reflections with those similarly obtained for heavy atom derivatives for the purpose of difference Patterson calculation.

Table VI.3

Native Data

	Number in bin			Total	Cumulative %			
DminÅ	≤1σ	≤2σ	≤3σ		≤1σ	≤2σ	≤3σ	>3σ
18.97	37	47	27	146	25.3	57.5	76.0	24.0
13.41	55	53	32	150	36.7	72.0	93.3	6.7
10.95	48	74	30	162	29.6	75.3	93.8	6.2
9.49	69	106	50	240	28.8	72.9	93.8	6.2
8.48	43	62	38	158	27.2	66.5	90.5	9.5
7.75	33	50	25	120	27.5	69.2	90.0	10.0
7.17	25	33	26	92	27.2	63.0	91.3	8.7
6.71	18	38	18	77	23.4	72.7	96.1	3.9
6.32	8	9	5	23	34.8	73.9	95.7	4.3
6.00	0	0	0	0	0.0	0.0	0.0	100.0
Overall	336	472	251	1168.	28.8	69.2	90.7	9.3

B. Gold Derivative Structure Factors

1. Meridional Reflections

The meridional collagen diffraction data for gold derivative were also integrated using the six available films in the pack. Pattern centre and film orientation have been searched using the usual

methods.

In this paragraph I give the list of the meridional reflections I have obtained for gold meridional reflections.

l	1/d*	F	σF	σF/F
-53	12.997	20	3	13
-52	13.245	25	3	12
-51	13.509	0	0	100
-50	13.788	65	3	5
-49	14.072	35	3	9
-48	14.374	63	3	5
-47	14.696	25	3	14
-46	15.008	36	3	10
-45	15.357	67	3	5
-44	15.713	33	3	10
-43	16.096	61	4	6
-42	16.485	45	3	8
-41	16.903	103	5	4
-40	17.329	62	4	6
-39	17.789	34	3	8
-38	18.257	152	5	4
-37	18.765	46	3	7
-36	19.317	38	3	9
-35	19.881	22	3	14
-34	20.455	55	3	6
-33	21.129	68	3	5
-32	21.822	160	7	4
-31	22.53	107	5	4
-30	23.313	182	8	4
-29	24.112	64	3	5
-28	25.00	104	5	5
-27	25.994	233	10	4
-26	27.017	145	6	[illegible]
-25	27.017	[illegible]	[illegible]	4
-24	28.172	171	8	4
-23	29.361	99	5	5
-22	30.715	171	8	5
-21	32.108	174	8	5
-20	33.71	374	16	4
-19	35.578	170	10	6
-18	37.529	93	6	6
-17	39.841	68	4	6
-16	42.258	204	13	6
-15	45.175	451	28	6
-14	48.224	191	14	7
-13	51.988	87	9	10
-12	55.902	457	31	7
-11	60.858	103	9	9
-10	67.42	409	30	7
-9	74.536	397	29	7
-8	84.515	443	33	7
-7	95.346	408	31	7
-6	111.803	267	29	11
4	182.574	242	23	10
5	141.421	377	36	9
6	111.803	186	23	12
7	95.346	315	33	11
8	84.515	324	35	11
9	74.536	296	32	11
10	67.42	312	34	11
11	60.858	109	11	10
12	55.902	388	36	9
13	55.902	185	17	9
14	51.988	72	8	12
15	48.224	257	27	10
16	45.175	280	24	9
17	42.258	108	12	11
18	39.841	146	13	9
19	37.529	117	10	9
20	35.578	312	31	10
21	33.71	311	22	7
22	32.108	172	13	8
23	30.715	176	13	7
24	29.361	100	7	7
25	28.172	382	26	7
26	28.172	124	9	7
27	25.994	318	21	6
28	25.00	137	10	7
29	24.112	128	8	6
30	23.313	102	7	7
31	22.53	138	9	6
32	22.53	166	11	7
33	21.822	158	9	6
34	21.129	159	9	6
35	19.881	91	5	6
36	19.317	72	4	6
37	19.317	97	6	6
38	18.765	94	5	5
39	18.257	222	11	5
40	17.789	74	4	6
41	17.329	146	7	5
42	16.903	149	7	5
43	16.485	125	8	6
44	16.096	179	8	4
45	15.713	104	6	6
46	15.357	146	13	9
47	15.008	75	5	6
48	14.696	44	4	9
49	14.374	152	8	5
50	14.072	78	5	6
51	13.788	140	7	5
52	13.509	36	4	11
53	13.245	184	9	5
54	12.997	145	7	5
55	12.752	30	4	13
56	12.51	136	7	5
57	12.281	69	5	7
58	12.065	105	5	5
59	11.851	0	0	100
60	11.648	58	11	19
61	11.456	72	5	7
62	11.258	33	11	34
63	11.077	0	0	100
64	10.898	32	4	13
65	10.727	39	10	27
66	10.559	0	0	100
67	10.398	28	16	59
68	10.238	25	7	29
69	10.086	0	0	100
70	09.936	0	0	100
71	09.792	132	14	10
72	09.654	0	0	100
73	09.517	159	11	7
74	09.382	0	0	100
75	09.257	0	0	100
76	09.133	0	0	100
77	09.009	76	12	15
78	08.891	10	11	110
79	08.774	56	8	14
80	08.661	0	0	100
81	08.553	0	0	100
82	08.446	115	12	11
83	08.342	[illegible]	83	9

I now show a detailed graphical analysis of the meridional data. This, and the following graphical displays I will show for all the data are a redundant action that will be done for each row data since it is very important to assess for the accuracy on the structure factors determination before the data set is included in Fourier analysis. The principle however, is the same as for the native data that is, I select all the data for one simple row-line, (h,0,l) for example, and choose to plot the structure factors amplitudes as a function of one index (here the l index). The top values are those for F(h,0,l) and the bottom values for -F(-h,0,-l) whereas the X-axis values are always the l values.

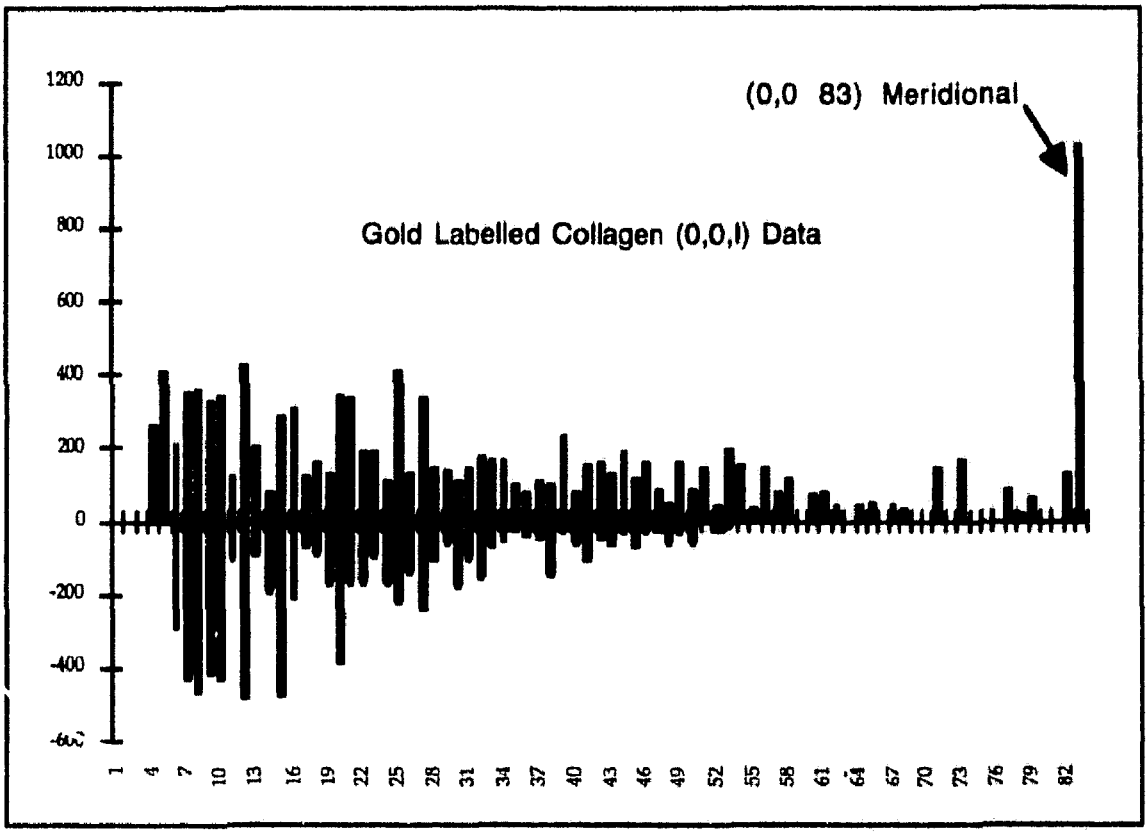

Fig. VI.8: The meridional structure factors for gold derivative are plotted here. There are obviously more orders obtained from the X-ray diffraction pattern for l>0 than for l<0 due to the fibre tilt.

Figure VI.8 shows the structure factors amplitudes obtained with meridional gold derivative data and plotted against the |l| index. The data set I show contains all the early determined structure factors I have given in the above list. There are obviously more reflections on the upper side of the graph (e.g. those with l>0) because I have observed much more orders from the upper part of the X-ray diffraction pattern (l_{max}=83) since the fibre has been tilted in a manner to bring more meridional orders into diffracting position.

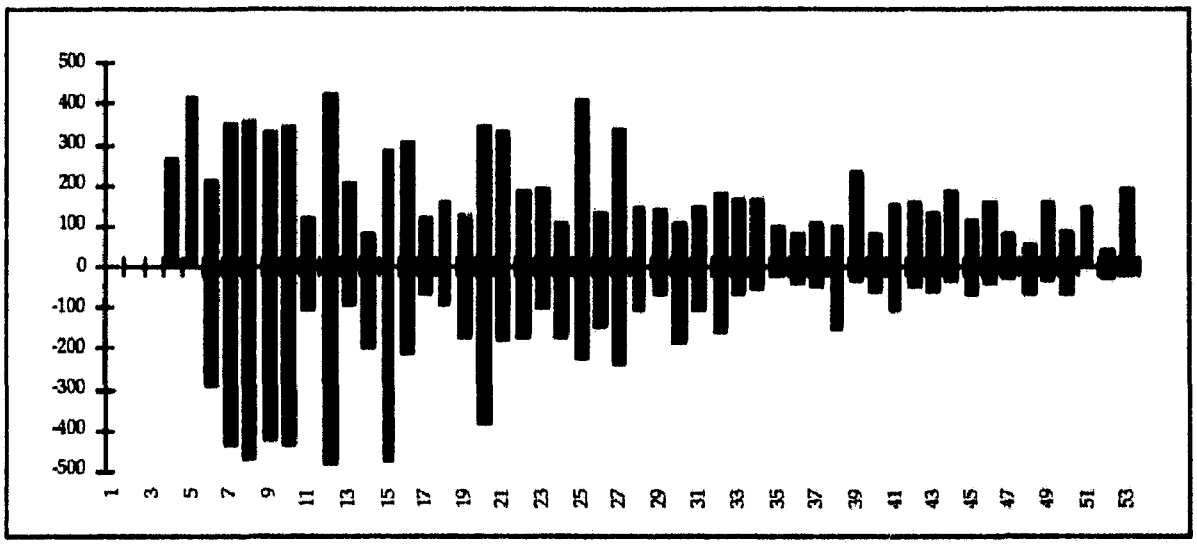

Fig. VI.9: The gold meridional data are now shown in the range |l|=[4,53] where we can now easily distinguish equivalent reflections. The reflections at low-resolution (up to l=33) are better matching in amplitude according to Friedel law but the there is a bad agreement between the amplitudes on the higher orders. There are two possible reasons for this discrepancy: the first is that the Lorentz correction I have used is not suitable for meridional reflections where R=0, and the second is that an additional correction, taking into account the fibre tilt, has been omitted.

2. Row Lines

In this paragraph, I give the sorted list of the reflections I have collected from the (-1,0,l) and (1,0,l) row-lines together with the graphical display of structure factors analysis.

h	k	l	1/d*	F	σF	σF/F
-1	0	-79	8.212	36	5	13
-1	0	-77	8.410	24	5	19
-1	0	-76	8.513	45	8	17
-1	0	-75	8.619	30	5	18
-1	0	-74	8.727	18	8	46
-1	0	-73	8.839	72	8	12
-1	0	-72	8.955	31	5	16
-1	0	-71	9.068	44	6	14
-1	0	-70	9.190	32	6	18
-1	0	-69	9.313	0	0	100
-1	0	-68	9.441	88	8	9
-1	0	-66	9.704	73	6	8
-1	0	-64	9.980	35	6	16
-1	0	-63	10.122	86	8	9
-1	0	-62	10.271	59	4	7
-1	0	-61	10.426	58	5	8
-1	0	-61	10.426	124	6	5
-1	0	-60	10.582	69	5	7
-1	0	-59	10.746	20	5	24
-1	0	-59	10.746	46	5	11
-1	0	-58	10.911	12	5	37
-1	0	-57	11.084	13	4	34
-1	0	-56	11.258	17	6	32
-1	0	-55	11.441	28	6	20
-1	0	-54	11.625	53	6	12
-1	0	-53	11.618	22	5	23
-1	0	-52	12.021	110	6	6
-1	0	-51	12.226	54	6	12
-1	0	-47	13.119	0	0	100
-1	0	-47	13.119	0	0	100
-1	0	-46	13.363	28	6	23
-1	0	-45	13.621	44	6	14
-1	0	-44	13.881	54	7	12
-1	0	-43	14.156	61	7	11
-1	0	-42	14.434	37	5	15
-1	0	-41	14.728	0	0	100
-1	0	-40	15.024	27	5	20
-1	0	-39	15.339	127	7	6
-1	0	-38	15.675	58	7	11
-1	0	-37	16.013	103	6	6
-1	0	-36	16.352	82	7	8
-1	0	-35	16.713	49	7	14
-1	0	-34	17.100	45	6	13
-1	0	-34	17.100	60	5	9
-1	0	-33	17.487	13	6	46
-1	0	-32	17.903	39	6	15
-1	0	-31	18.349	30	7	23
-1	0	-30	18.798	106	8	7
-1	0	-29	19.245	5	9	156
-1	0	-28	19.726	57	7	12
-1	0	-27	20.244	0	0	100
-1	0	-26	20.761	10	7	69
-1	0	-25	21.320	13	7	53
-1	0	-25	21.320	77	6	8
-1	0	-24	21.874	73	6	9
-1	0	-23	22.473	59	8	13
-1	0	-22	23.125	0	0	100
-1	0	-21	23.769	43	9	21
-1	0	-20	24.398	38	7	19
-1	0	-19	25.078	106	8	8
-1	0	-18	25.820	33	10	29
-1	0	-17	26.537	48	8	17
-1	0	-16	27.318	64	8	12
-1	0	-15	28.172	45	9	21
-1	0	-13	29.748	37	7	20
-1	0	-13	29.748	73	9	13
-1	0	-12	30.571	70	10	14
-1	0	-11	31.466	36	7	21
-1	0	-11	31.466	68	7	10
-1	0	-10	32.275	51	10	20
-1	0	-9	33.150	31	9	30
-1	0	-8	33.903	120	16	13
-1	0	-7	34.711	4	8	215
-1	0	-6	35.578	63	11	17
-1	0	-5	36.274	22	10	47
-1	0	-4	36.761	92	26	28
-1	0	-2	37.796	127	28	22
-1	0	2	38.348	213	26	12
-1	0	4	38.069	96	24	25
-1	0	5	37.796	175	19	11
-1	0	6	37.268	171	21	12
-1	0	7	36.761	35	8	22
-1	0	8	36.037	24	14	58
-1	0	9	35.355	26	7	29
-1	0	10	34.503	84	8	10
-1	0	11	33.710	55	8	15
-1	0	12	32.969	66	9	14
-1	0	13	32.108	84	11	13
-1	0	14	31.311	86	17	20
-1	0	15	30.429	143	9	7
-1	0	16	29.617	15	8	51
-1	0	17	28.748	82	7	8
-1	0	18	27.951	144	15	10
-1	0	19	27.217	131	17	13
-1	0	20	26.444	191	9	5
-1	0	21	25.649	99	7	7
-1	0	22	25.000	8	6	71
-1	0	23	24.254	33	5	17
-1	0	24	23.636	146	8	5
-1	0	25	22.942	148	8	5

-1	0	26	22.361	24	7	27	1	0	-63	10.547	38	4	12	1	0	11	31.466	78	10	13
-1	0	27	21.770	113	5	4	1	0	-62	10.709	13	3	26	1	0	12	30.571	148	15	10
-1	0	28	21.176	51	6	12	1	0	-61	10.872	14	4	26	1	0	13	29.748	40	9	22
-1	0	29	20.672	120	7	5	1	0	-60	11.043	36	3	9	1	0	14	28.989	92	8	9
-1	0	30	20.121	39	6	15	1	0	-59	11.223	0	0	100	1	0	16	27.318	35	9	26
-1	0	31	19.649	0	0	100	1	0	-58	11.403	45	5	11	1	0	18	25.820	73	7	10
-1	0	32	19.139	93	6	6	1	0	-57	11.586	42	5	12	1	0	20	24.398	39	14	36
-1	0	33	18.699	92	7	8	1	0	-56	11.777	5	4	77	1	0	21	23.769	51	7	14
-1	0	34	18.257	44	7	15	1	0	-55	11.973	56	5	8	1	0	22	23.125	22	7	32
-1	0	35	17.817	89	6	6	1	0	-54	12.181	20	5	22	1	0	22	23.125	5	5	112
-1	0	36	17.408	110	6	6	1	0	-53	12.394	89	6	6	1	0	23	22.473	16	7	44
-1	0	37	17.025	57	6	11	1	0	-52	12.619	0	0	100	1	0	24	21.874	59	7	12
-1	0	38	16.644	14	6	40	1	0	-51	12.846	104	5	5	1	0	25	21.320	41	7	17
-1	0	39	16.287	12	5	42	1	0	-50	13.074	48	5	11	1	0	26	20.761	54	7	13
-1	0	40	15.931	21	4	21	1	0	-49	13.316	110	5	5	1	0	27	20.244	25	6	24
-1	0	41	15.598	11	4	34	1	0	-48	13.571	69	5	8	1	0	29	19.245	31	6	20
-1	0	42	15.268	45	4	10	1	0	-47	13.828	24	4	17	1	0	30	18.798	32	6	19
-1	0	43	14.957	24	4	18	1	0	-46	14.100	88	5	6	1	0	31	18.349	77	7	9
-1	0	44	14.665	59	4	7	1	0	-45	14.374	11	6	55	1	0	32	17.903	7	6	88
-1	0	45	14.374	43	5	13	1	0	-45	14.374	5	3	61	1	0	33	17.487	46	4	10
-1	0	46	14.100	33	5	15	1	0	-44	14.665	53	5	9	1	0	34	17.100	36	6	16
-1	0	47	13.828	87	5	6	1	0	-43	14.957	17	4	26	1	0	35	16.713	58	4	8
-1	0	49	13.316	27	4	16	1	0	-42	15.268	3	5	163	1	0	36	16.352	47	5	11
-1	0	50	13.074	45	5	11	1	0	-41	15.598	43	5	12	1	0	37	16.013	80	7	8
-1	0	51	12.846	84	6	7	1	0	-40	15.931	27	5	18	1	0	38	15.675	74	5	7
-1	0	52	12.619	62	7	11	1	0	-39	16.287	24	4	16	1	0	39	15.339	38	5	14
-1	0	53	12.394	27	4	14	1	0	-38	16.644	54	5	10	1	0	40	15.024	50	5	10
-1	0	54	12.181	33	5	15	1	0	-37	17.025	86	7	8	1	0	41	14.728	0	0	100
-1	0	55	11.978	67	6	8	1	0	-36	17.408	145	7	5	1	0	42	14.434	51	4	9
-1	0	56	11.777	95	7	7	1	0	-35	17.817	115	7	6	1	0	43	14.156	53	5	10
-1	0	57	11.586	78	4	6	1	0	-34	18.257	77	7	9	1	0	44	13.881	44	5	11
-1	0	58	11.403	15	5	33	1	0	-33	18.699	34	7	22	1	0	45	13.621	12	5	45
-1	0	59	11.223	46	5	11	1	0	-32	19.139	119	7	6	1	0	46	13.363	5	4	81
-1	0	60	11.043	23	5	22	1	0	-30	20.121	25	5	19	1	0	47	13.119	23	5	22
-1	0	61	10.872	24	4	18	1	0	-29	20.672	118	7	6	1	0	48	12.888	73	5	7
-1	0	62	10.709	69	4	6	1	0	-28	21.176	59	8	13	1	0	49	12.659	49	6	11
-1	0	63	10.547	37	5	15	1	0	-27	21.770	87	7	8	1	0	50	12.442	67	5	8
-1	0	64	10.392	25	4	17	1	0	-27	21.770	69	7	10	1	0	51	12.226	14	6	42
-1	0	65	10.238	35	5	16	1	0	-26	22.361	5	5	88	1	0	52	12.021	73	7	9
-1	0	66	10.091	37	5	15	1	0	-25	22.942	126	8	6	1	0	53	11.818	55	6	10
-1	0	66	10.091	37	4	12	1	0	-24	23.636	118	8	7	1	0	54	11.625	57	6	11
-1	0	68	9.811	73	5	7	1	0	-24	23.636	83	7	8	1	0	55	11.441	60	5	9
-1	0	69	9.672	96	5	5	1	0	-23	24.254	12	7	58	1	0	56	11.258	87	5	6
-1	0	70	9.543	26	4	16	1	0	-22	25.000	86	7	8	1	0	57	11.084	23	6	26
-1	0	71	9.411	32	4	14	1	0	-21	25.649	61	7	11	1	0	58	10.911	18	5	26
-1	0	72	9.289	75	5	7	1	0	-20	26.444	121	11	9	1	0	59	10.746	50	5	9
-1	0	73	9.163	59	6	10	1	0	-19	27.217	173	8	5	1	0	59	10.746	22	5	21
-1	0	74	9.046	70	5	7	1	0	-18	27.951	67	8	12	1	0	60	10.582	42	5	11
-1	0	75	8.930	5	5	90	1	0	-17	28.748	100	7	7	1	0	60	10.582	64	5	7
-1	0	76	8.815	64	5	7	1	0	-16	29.617	31	8	25	1	0	61	10.426	57	5	9
-1	0	77	8.707	62	5	7	1	0	-14	31.311	46	6	12	1	0	62	10.271	99	5	5
-1	0	78	8.597	46	4	9	1	0	-12	32.969	43	5	12	1	0	63	10.122	94	6	6
-1	0	79	8.491	67	4	7	1	0	-11	33.710	42	7	16	1	0	64	9.980	27	6	20
-1	0	80	8.389	45	5	11	1	0	-10	34.503	66	6	10	1	0	65	9.839	39	5	14
-1	0	90	7.481	95	4	5	1	0	-9	35.355	34	7	20	1	0	66	9.704	68	6	8
-1	0	94	7.169	113	5	4	1	0	-8	36.037	81	7	9	1	0	67	9.569	97	7	7
1	0	-74	9.046	43	3	8	1	0	-7	36.761	0	0	100	1	0	68	9.441	62	8	13
1	0	-73	9.163	20	4	19	1	0	-5	37.796	90	7	7	1	0	69	9.313	143	8	6
1	0	-72	9.289	30	5	16	1	0	-4	38.069	114	28	25	1	0	70	9.190	59	9	15
1	0	-71	9.411	0	0	100	1	0	-3	38.348	107	23	21	1	0	71	9.068	140	8	6
1	0	-70	9.543	20	4	18	1	0	-2	38.348	162	28	17	1	0	72	8.955	77	7	9
1	0	-69	9.672	34	4	12	1	0	-1	38.348	92	28	31	1	0	73	8.839	62	6	10
1	0	-68	9.811	168	5	3	1	0	0	38.348	241	30	12	1	0	74	8.727	46	7	15
1	0	-67	9.950	27	4	16	1	0	2	37.796	82	23	28	1	0	75	8.619	95	7	8
1	0	-66	10.091	43	4	10	1	0	5	36.274	23	17	76	1	0	76	8.513	34	6	18
1	0	-66	10.091	24	4	16	1	0	7	34.711	35	10	28	1	0	82	7.928	99	11	11
1	0	-65	10.238	48	5	10	1	0	8	33.903	26	9	34	1	0	83	7.837	77	5	6
1	0	-64	10.392	16	4	23	1	0	10	32.275	108	11	10	1	0	99	6.630	101	6	6

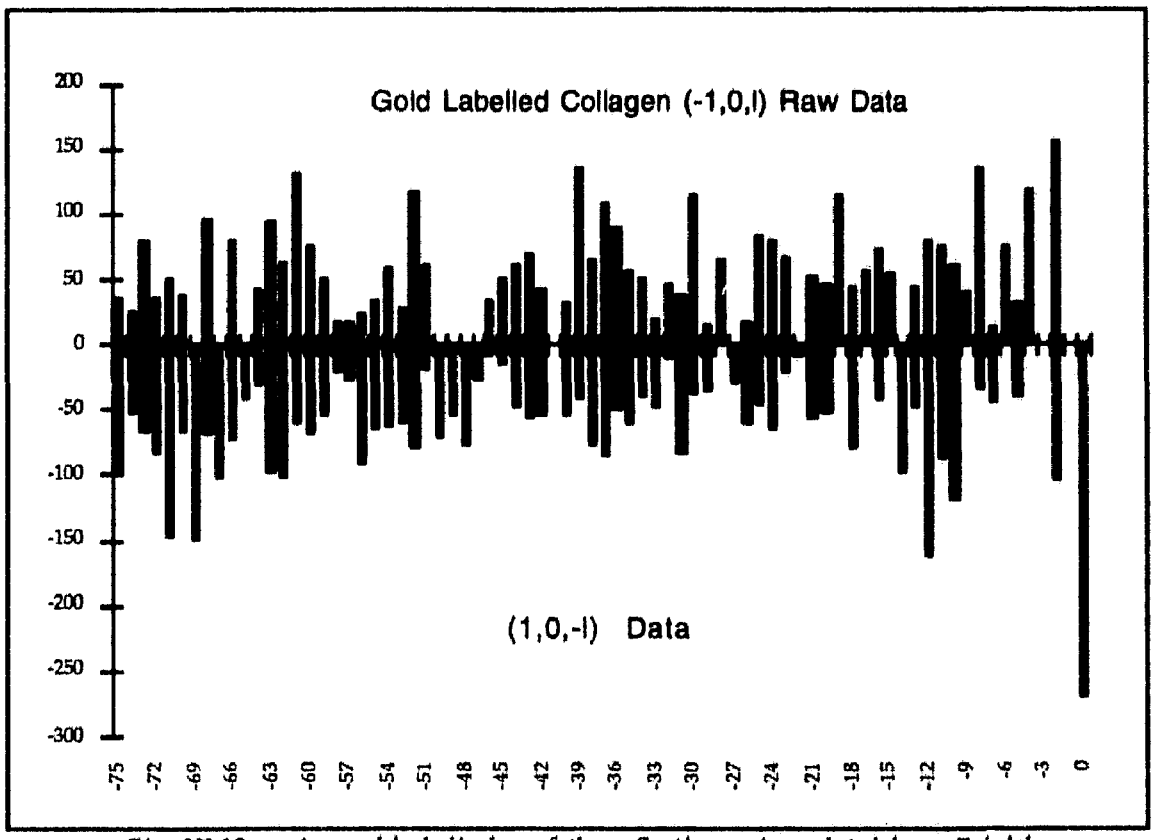

Fig. VI.10 : A graphical display of the reflection pairs related by a Friedel symmetry. The data are shown for the range of indices l=-1 to -75 for a better clarity.

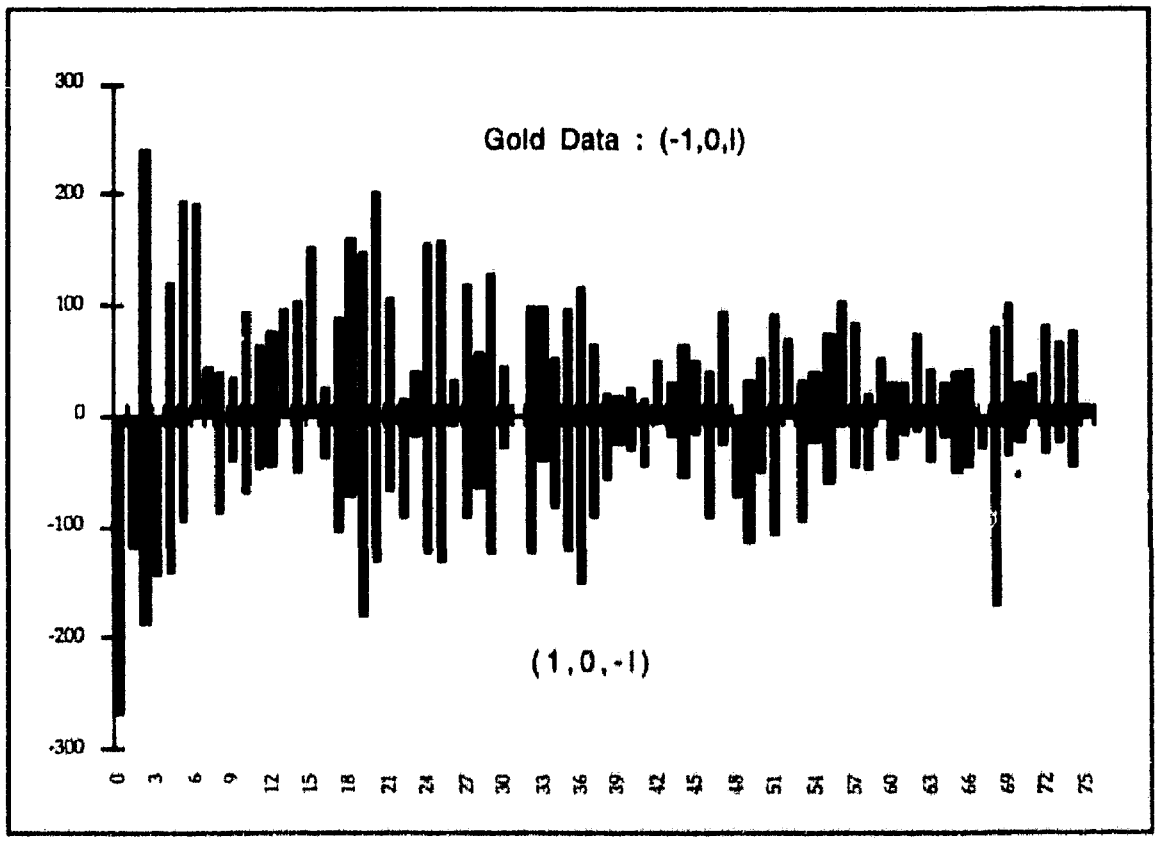

Fig. VI.11: The data shown in this figure are the row-lines (-1,0,l) and (1,0,l) with l=0 to 75.

There is obviously a good correspondence between structure factors amplitudes and indices for the reflections shown in the preceding figures. That means, the symmetric data with the same amplitude but with opposite indices can only coincide on the horizontal axis if there is no errors in the indexing otherwise a wrong indexing will show a shift between the upper and the lower structure factors.

I can finally assume that the data for the meridional reflections and the two row-lines I have already analysed are correct with respect to their amplitudes and Bragg indexing.

3. Other Structure Factors

The additional data collected on the gold derivative films are listed in the appendixes but I further show some graphical representations.

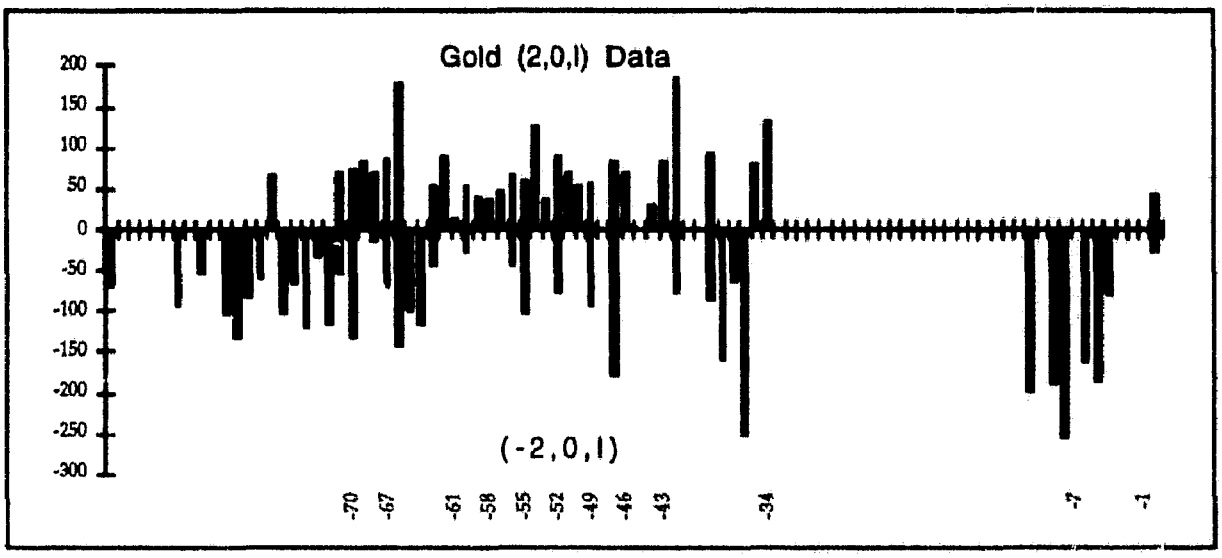

Fig. VI.12 : Data comparison for the (2,0,l) and (-2,0,l) row-lines. The missing reflections correspond to the data that have been omitted when strongly overlapped or zeroed for unobserved film intensity peaks.

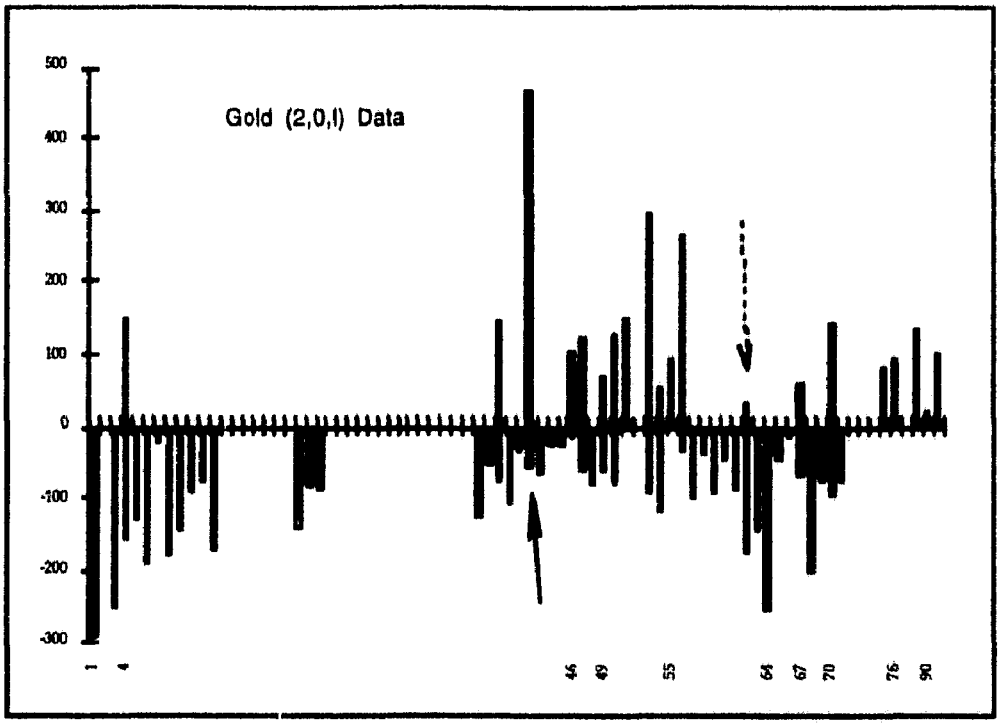

Fig. VI.13 : Data display of the (2,0,l) and (-2,0,l) row-lines. The customary steps are used as defined before, that is, on the upper side are represented the (2,0,l) reflections here l=1 to 90 , and the (-2,0,-l) reflections are drown on the lower side but the l index is represented by its opposite value. The arrows indicate reflections with bad agreement.

4. Analysis of Gold Derivative Data

I have written the data collected for gold labelled collagen to the standard format (MTZ) used by the CCP4 suite and then analysed them using the preparing programs Rotavata and Agrovata. The 3-dimensional data have been merged and searched for equivalent reflections (e.g; Friedel pairs) to produce a unique set of structure factors. I thus obtained an appropriate file for scaling with the native structure factors set. I show in the following tables the statistics on the intensity distribution as obtained by the former programs before native to derivative scaling.

Table VI.4

Gold Data

Analysis R factor against resolution

N	<s>	DminÅ	Rfac	Rcum	Av_I	σ	I/σ	sd
1	0.0028	18.97	0.372	0.372	1719.	1130.8	1.5	839.36
2	0.0056	13.41	0.164	0.181	25599.	6022.1	4.314	874.70
3	0.0083	10.95	0.144	0.170	32569.	4902.1	6.629	509.72
4	0.0111	9.49	0.492	0.182	2211.	1223.2	1.8	737.90
5	0.0139	8.48	0.914	0.204	3775.	4733.9	0.8	1315.66
6	0.0167	7.75	0.000	0.204	0.	0.0	0.0	0.00
7	0.0194	7.17	0.000	0.204	0.	0.0	0.0	0.00
8	0.0222	6.71	0.000	0.204	0.	0.0	0.0	0.00
9	0.0250	6.32	0.000	0.204	0.	0.0	0.0	0.00
10	0.0278	6.00	0.000	0.204	0.	0.0	0.0	0.00

Gold Data Completeness & multiplicity v. resolution						
N	<s>	Dmin	Nmeas	Nref	%poss	Multiplicity
1	0.003	18.97	242	238	110.7	1.0
2	0.006	13.41	254	251	63.8	1.0
3	0.008	10.95	278	277	54.4	1.0
4	0.011	9.49	219	217	36.0	1.0
5	0.014	8.48	211	210	30.7	1.0
6	0.017	7.75	117	117	15.5	1.0
7	0.019	7.17	48	48	5.8	1.0
8	0.022	6.71	37	37	4.2	1.0
9	0.025	6.32	20	20	2.1	1.0
10	0.028	6.00	1	1	0.1	1.0
	Total		1427	1416	20.8	1.0

Gold Data								
	Number in bin			Total	Cumulative %			
DminÅ	≤1σ	≤2σ	≤3σ		≤1σ	≤2σ	≤3σ	>3σ
18.97	32	55	65	238	13.4	36.6	63.9	36.1
13.41	24	63	80	251	9.6	34.7	66.5	33.5
10.95	27	84	99	277	9.7	40.1	75.8	24.2
9.49	17	56	77	217	7.8	33.6	69.1	30.9
8.48	22	60	66	210	10.5	39.0	70.5	29.5
7.75	7	24	42	117	6.0	26.5	62.4	37.6
7.17	2	6	11	48	4.2	16.7	39.6	60.4
6.71	2	7	10	37	5.4	24.3	51.4	48.6
6.32	0	4	8	20	0.0	20.0	60.0	40.0
6.00	0	0	0	1	0.0	0.0	0.0	100.0
Overall	133	359	458	1416	9.4	34.7	67.1	32.9

The scaling of gold derivative to native data was then done using the FHSCALE program of the suite.

C. Iodine Structure Factors

Fig VI.14 : A comparison of native and iodine derivative reflections. The figure on the right shows the (-1,0,l) and (1,0,l) row-line spots obtained with native collagen. The reflections on the helix layer-line (l=70) are clearly displayed. The figure on the right (not on the same scale with the native pattern) shows the prominent peaks in the same region as iodine pattern.

In a previous chapter we have already established that iodine atom is believed to label the collagen molecules at the methionine residues. Now, we know from sequence knowledge of collagen polypeptide that methionine residue occurs only at one position in the 1024 residues polypeptide chain. We have thus only one theoretical site where iodine can be fixed to the collagen chain and this limits the number of sites and the number of iodine atoms to a few that are contained in a huge protein molecule. It follows that the suitability of iodine derivative to produce MIR differences is dubious since MIR methods only yield measurable differences with heavy atoms added to reasonably high molecular weights proteins (e.g. Mr=100,000). The average additional contribution of the isomorphous signal in a derivative protein reflection was demonstrated by Crick & Magdoff (1959) to be proportional to $\sqrt{2N_H/N_P} \cdot (f_H/f_P)$, where there are N_H heavy atoms of scattering factor, f_H, and the protein is supposed to comprise N_P equal light atoms of scattering factor, f_P. This means that the addition of one or more iodine atoms to a collagen molecule with a high molecular weight (Mr ~300,000) will give a weak change in the intensity for a normal reflection.

However, from the examination of iodine fibre patterns (figures VI.14 & VI.15) we nevertheless, observe the presence of weak reflections on the row-lines with some change in the relative intensity of Bragg reflections which are discernible by eye.

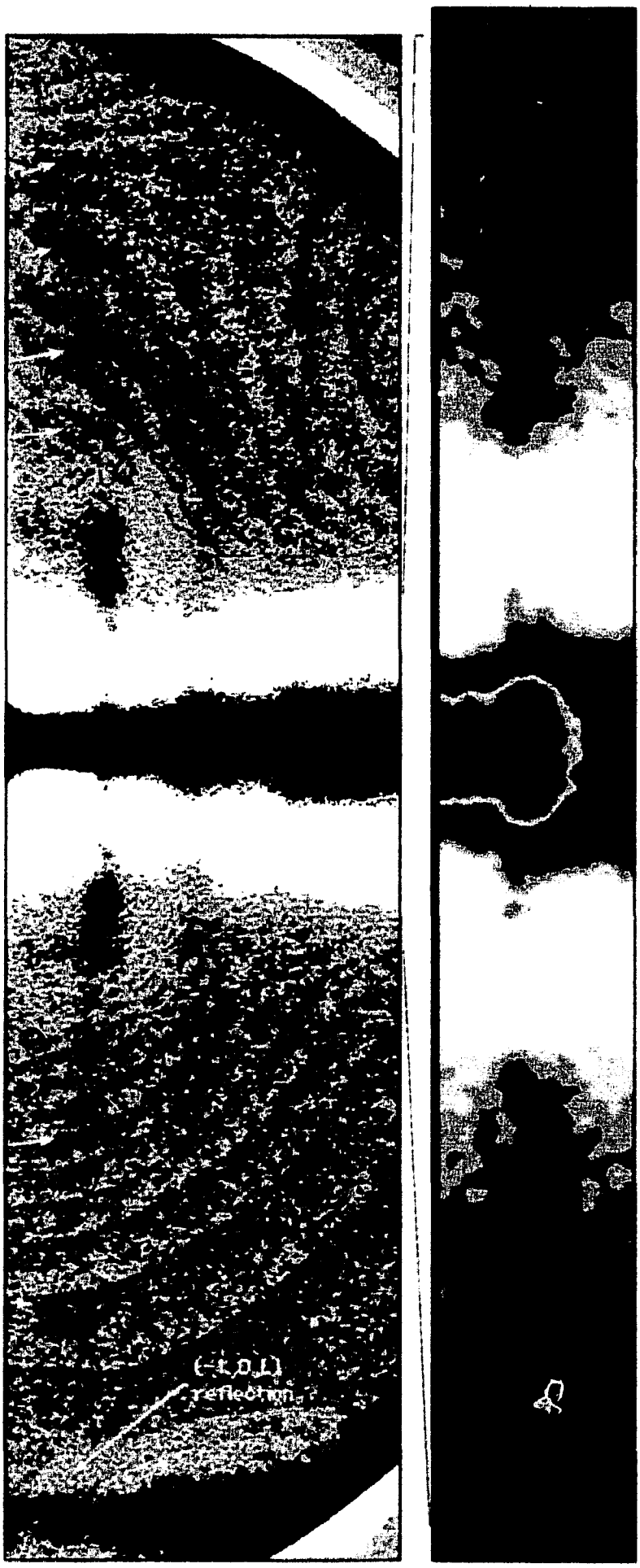

Fig. VI. 15 : The diffraction pattern of iodine derivative exhibits weak reflections on the vertical row-lines. The film section shown on the left is the region containing the (-1,0,l) and (1,0,l) row-lines and also the data-rows with R=1/27Å^{-1} and R=1/19Å^{-1}. I used the first film in the pack because it contains precisely the weakest range of intensities. The continuous background intensity was also removed to enhance the peak resolution. We thus obtain very weak spots that are roughly higher than the "film background". The Bragg peaks however have been integrated as usual and the figure on the right shows a magnified section of the R=1/39Å^{-1} near equatorial region. I also show the elliptical shaped box that is adjusted to the right orientation and used to integrate all the peak intensity.

Fig VI. 16 : Iodine patterns display weak reflections on the (1,0,l) row-line (arrows) and also some weak reflections on the row-lines with Miller indices (0,-1,l), (0,1,l) etc...

1. Meridional Reflections

l	1/d*	F	σF	σF/F
-59	11.077	93	8	8
-58	11.258	74	7	10
-57	11.456	128	7	6
-56	11.648	77	8	11
-55	11.851	141	9	6
-54	12.065	99	8	8
-53	12.281	184	9	5
-52	12.510	308	14	4
-51	12.997	27	4	16
-50	12.997	0	0	100
-49	13.245	73	4	5
-48	13.509	78	4	5
-47	14.072	64	6	9
-46	14.374	42	5	12
-45	14.696	137	9	7
-44	15.008	207	11	5
-43	15.357	150	9	6
-42	15.713	170	9	5
-41	16.096	374	19	5
-40	16.485	176	10	6
-39	16.903	297	16	5
-38	17.329	268	14	5
-37	17.789	130	9	7
-36	18.257	254	13	5
-35	18.765	92	10	11
-34	19.317	414	22	5
-33	19.881	343	20	6
-32	20.455	473	25	5
-31	21.129	266	17	6
-30	21.822	415	24	6
-29	22.530	238	16	7
-28	23.313	343	22	6
-27	24.112	470	28	6
-26	25.000	395	23	6
-25	25.994	686	39	6
-24	27.017	138	4	3
-23	28.172	76	3	4
-22	29.361	135	4	3
-21	30.715	555	19	3
-20	32.108	475	16	3
-19	33.710	269	10	4
-18	35.578	415	15	4
-17	37.529	206	8	4
-16	39.841	208	9	4
-15	42.258	475	19	4
-14	45.175	149	7	5
-13	48.224	80	3	4
-12	51.988	533	22	4
-11	55.902	259	12	5
-10	60.858	458	20	4
-9	74.536	401	19	5
-8	84.515	371	19	5
-7	95.346	363	18	5
-6		302	15	5
4		136	12	9
5		351	18	5
6		268	17	6
7	95.346	321	20	6
8	84.515	330	20	6
9	74.536	344	20	6
10	67.420	373	22	6
11	60.858	242	14	6
12	55.902	287	16	6
13	51.988	114	7	6
14	48.224	150	8	6
15	45.175	387	22	6
16	39.841	189	11	6
17	37.529	410	21	5
18	35.578	162	8	5
19	33.710	254	13	5
20	32.108	543	27	5
21	30.715	331	16	5
22	29.361	123	6	5
23	28.172	121	6	5
24	27.017	298	13	4
25	25.994	265	19	7
26	25.000	321	26	8
27	24.112	434	37	9
28	23.313	188	17	9
29	22.530	214	27	13
30	21.822	348	28	8
31	21.129	291	30	10
32	20.455	535	40	8
33	19.881	255	22	9
34	19.317	300	21	7
35	18.765	0	0	100
36	18.257	333	23	7
37	17.789	139	13	9
38	17.329	693	37	5
39	16.903	489	28	6
40	16.485	274	21	8
41	16.096	668	38	6
42	15.713	146	15	10
43	15.357	532	19	6
44	15.008	574	30	5
45	14.374	199	16	8
46	14.072	149	13	9
47	13.788	341	18	5
48	13.509	407	23	6
49	13.245	451	22	5
50	12.997	102	9	9
51	12.752	90	8	9
52	12.510	1041	50	5
53	12.251	396	23	6
54	12.065	121	9	8
55	11.851	415	20	5
56	11.648	206	12	6
57	11.456	348	18	5
58	11.258	0	0	100
59	11.077	240	11	5
60	10.898	168	11	6
61	10.727	117	9	8
62	10.559	0	0	100
63	10.398	173	10	6
64	10.238	228	11	5
65	10.086	168	10	6
66	9.936	106	9	8
67	9.792	151	9	6
68	9.517	84	8	10
69	9.382	162	8	5
70	9.257	493	30	6

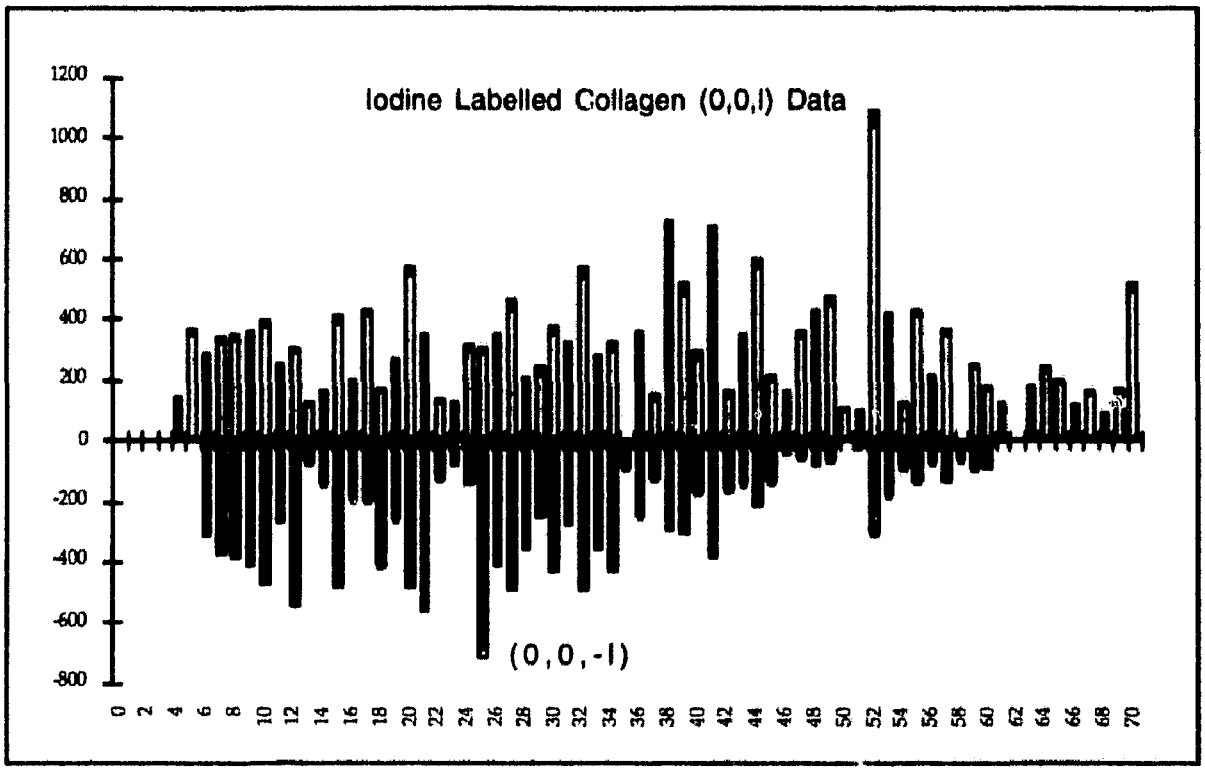

Fig. VI.17 : Iodine meridionals are here plotted versus |l| index. The agreement between Friedel's pairs seems to be acceptable everywhere unless for the {(0,0,52),(0,0,-52)} pair.

2. Row Lines

Here is the reflection list for iodine (-1,0,l) and (1,0,l) row-lines. The data have been obtained using the same method of peak integration and corrections as for the previous native and gold data set.

h	k	l	1/d*	F	σF	σF/F
-1	0	-80	8.114	0	0	100
-1	0	-79	8.212	0	0	100
-1	0	-78	8.310	40	5	13
-1	0	-77	8.410	58	5	9
-1	0	-76	8.513	0	0	100
-1	0	-75	8.619	32	6	18
-1	0	-74	8.727	150	7	5
-1	0	-73	8.839	144	7	5
-1	0	-72	8.955	121	7	5
-1	0	-70	9.190	29	5	16
-1	0	-69	9.313	3	0	0
-1	0	-68	9.441	9	3	33
-1	0	-67	9.569	34	4	11
-1	0	-66	9.704	43	4	10
-1	0	-65	9.839	25	4	16
-1	0	-64	9.980	23	4	18
-1	0	-63	10.122	21	4	18
-1	0	-62	10.271	52	4	7
-1	0	-61	10.426	36	4	11
-1	0	-60	10.582	42	4	9
-1	0	-59	10.746	38	4	9
-1	0	-57	11.084	7	3	43
-1	0	-56	11.258	0	0	100
-1	0	-55	11.441	48	4	9
-1	0	-54	11.625	58	4	7
-1	0	-53	11.818	17	4	24
-1	0	-52	12.021	11	4	36
-1	0	-51	12.226	43	4	10
-1	0	-50	12.442	41	4	9
-1	0	-49	12.659	12	4	32
-1	0	-48	12.888	53	4	8
-1	0	-47	13.119	57	5	9
-1	0	-46	13.363	43	5	11
-1	0	-45	13.621	66	5	7
-1	0	-44	13.881	53	4	8
-1	0	-43	14.156	40	4	11
-1	0	-41	14.728	20	4	20
-1	0	-40	15.024	33	4	11
-1	0	-39	15.339	9	4	48
-1	0	-38	15.675	80	5	6
-1	0	-37	16.013	59	5	9
-1	0	-35	16.713	22	6	26
-1	0	-34	17.100	0	0	100
-1	0	-33	17.487	63	5	8
-1	0	-31	18.349	23	4	19
-1	0	-30	18.798	50	4	7
-1	0	-29	19.245	0	0	100
-1	0	-28	19.726	0	0	100
-1	0	-27	20.244	17	5	32
-1	0	-26	20.761	59	7	11
-1	0	-25	21.320	72	4	6
-1	0	-24	21.874	18	4	23
-1	0	-23	22.473	31	7	21
-1	0	-22	23.125	12	5	44
-1	0	-21	23.769	55	7	13
-1	0	-20	24.396	41	6	15
-1	0	-19	25.078	42	6	15
-1	0	-18	25.820	25	6	24
-1	0	-16	27.318	6	6	89
-1	0	-15	28.172	70	6	9
-1	0	-13	29.748	107	7	7
-1	0	-12	30.571	45	5	10
-1	0	-11	31.466	44	5	11
-1	0	-10	32.275	69	7	11
-1	0	-8	33.903	0	0	100
-1	0	-7	34.711	0	0	100
-1	0	-6	35.578	21	8	40
-1	0	-5	36.274	0	0	100
-1	0	-4	36.761	53	11	21
-1	0	-3	37.268	53	12	23
-1	0	-2	37.796	11	16	139
-1	0	0	38.348	135	12	9
-1	0	2	38.348	72	11	16
-1	0	3	38.348	0	0	100
-1	0	4	38.069	0	0	100
-1	0	5	37.796	57	9	15
-1	0	6	37.268	104	9	9
-1	0	7	36.761	53	9	17
-1	0	8	36.037	17	7	40
-1	0	9	35.365	0	0	100
-1	0	10	34.503	62	5	8
-1	0	11	33.710	71	7	10
-1	0	12	32.969	15	6	38
-1	0	13	32.109	28	4	15
-1	0	14	31.311	28	5	17
-1	0	15	30.429	14	6	40
-1	0	16	29.617	145	10	7
-1	0	17	28.748	41	7	16
-1	0	18	27.951	106	7	7
-1	0	19	27.217	71	6	8
-1	0	20	26.444	24	5	21
-1	0	22	25.000	27	6	24
-1	0	23	24.254	65	6	10

-1	0	24	23.636	45	5	10	1	0	-66	10.091	59	3	6	1	0	9	33.150	0	0	100
-1	0	25	22.942	116	5	5	1	0	-65	10.238	24	3	13	1	0	10	32.275	38	8	21
-1	0	26	22.361	77	6	7	1	0	-64	10.392	32	3	10	1	0	12	30.571	0	0	100
-1	0	27	21.770	12	5	38	1	0	-63	10.547	15	3	20	1	0	13	29.748	96	6	6
-1	0	28	21.176	28	4	16	1	0	-62	10.709	22	3	14	1	0	16	27.318	65	9	13
-1	0	29	20.672	69	5	8	1	0	-61	10.872	7	3	36	1	0	18	25.820	100	6	6
-1	0	30	20.121	42	5	11	1	0	-60	11.043	13	3	23	1	0	19	25.078	0	0	100
-1	0	31	19.649	129	5	4	1	0	-59	11.223	0	0	100	1	0	20	24.398	64	6	9
-1	0	32	19.139	25	4	17	1	0	-58	11.403	0	0	100	1	0	21	23.769	102	7	7
-1	0	33	18.699	0	0	100	1	0	-57	11.586	69	4	6	1	0	22	23.125	24	5	21
-1	0	34	18.257	15	4	25	1	0	-56	11.777	89	4	4	1	0	23	22.473	9	4	46
-1	0	35	17.817	25	4	16	1	0	-55	11.978	0	0	100	1	0	24	21.874	35	6	17
-1	0	36	17.408	86	4	5	1	0	-54	12.181	87	4	4	1	0	25	21.320	86	6	7
-1	0	37	17.025	71	5	7	1	0	-53	12.394	0	0	100	1	0	26	20.761	53	5	10
-1	0	38	16.644	35	6	17	1	0	-52	12.619	0	0	100	1	0	27	20.244	39	5	12
-1	0	40	15.931	47	4	10	1	0	-51	12.846	59	4	7	1	0	28	19.726	0	0	100
-1	0	41	15.598	58	5	8	1	0	-50	13.074	0	0	100	1	0	29	19.245	27	4	16
-1	0	42	15.268	15	4	24	1	0	-49	13.316	33	5	14	1	0	30	18.798	42	4	9
-1	0	43	14.957	41	4	9	1	0	-48	13.571	76	4	5	1	0	31	18.349	35	4	13
-1	0	44	14.665	0	0	100	1	0	-47	13.828	62	4	6	1	0	32	17.903	65	5	7
-1	0	46	14.100	58	4	7	1	0	-46	14.100	104	4	4	1	0	33	17.487	70	6	8
-1	0	47	13.828	58	4	8	1	0	-45	14.374	74	4	6	1	0	34	17.100	23	5	20
-1	0	48	13.571	27	4	15	1	0	-44	14.665	34	4	11	1	0	35	16.713	35	4	12
-1	0	49	13.316	88	5	5	1	0	-43	14.957	28	4	13	1	0	36	16.352	0	0	100
-1	0	50	13.074	0	0	100	1	0	-42	15.268	45	4	8	1	0	37	16.013	0	0	100
-1	0	51	12.846	32	4	14	1	0	-41	15.598	0	0	100	1	0	38	15.675	58	5	9
-1	0	52	12.619	51	4	8	1	0	-40	15.931	38	4	11	1	0	39	15.339	41	4	9
-1	0	53	12.394	82	4	5	1	0	-39	16.287	60	6	10	1	0	40	15.024	33	4	14
-1	0	54	12.181	101	4	4	1	0	-38	16.644	183	6	3	1	0	41	14.728	67	4	6
-1	0	55	11.978	25	4	17	1	0	-37	17.025	71	5	7	1	0	42	14.434	77	4	6
-1	0	56	11.777	84	4	5	1	0	-36	17.408	77	4	5	1	0	43	14.156	17	4	26
-1	0	57	11.586	56	4	8	1	0	-35	17.817	20	4	21	1	0	44	13.881	0	0	100
-1	0	58	11.403	16	5	31	1	0	-34	18.257	27	4	16	1	0	45	13.621	57	4	7
-1	0	59	11.223	30	4	12	1	0	-33	18.699	28	4	15	1	0	46	13.363	102	5	4
-1	0	60	11.043	37	4	11	1	0	-32	19.199	46	4	9	1	0	47	13.119	43	5	11
-1	0	61	10.872	25	3	14	1	0	-31	19.649	58	5	8	1	0	48	12.888	35	5	14
-1	0	62	10.709	54	4	7	1	0	-29	20.672	27	6	22	1	0	50	12.442	72	5	7
-1	0	63	10.547	30	4	12	1	0	-28	21.176	70	4	6	1	0	51	12.226	24	4	18
-1	0	64	10.392	24	3	15	1	0	-27	21.770	68	5	7	1	0	52	12.021	22	4	20
-1	0	65	10.238	21	3	17	1	0	-26	22.361	56	6	10	1	0	54	11.625	9	4	49
-1	0	66	10.091	23	4	18	1	0	-24	23.636	89	5	5	1	0	56	11.258	44	4	10
-1	0	67	9.950	20	4	19	1	0	-23	24.254	60	6	10	1	0	57	11.084	36	5	15
-1	0	68	9.811	8	4	46	1	0	-22	25.000	76	6	7	1	0	58	10.911	35	4	13
-1	0	69	9.672	0	0	100	1	0	-21	25.649	20	6	31	1	0	59	10.746	33	4	12
-1	0	70	9.543	22	4	18	1	0	-19	27.217	6	3	60	1	0	60	10.582	34	4	12
-1	0	71	9.411	47	4	8	1	0	-17	28.748	0	0	100	1	0	61	10.426	11	4	32
-1	0	72	9.289	125	11	9	1	0	-16	29.617	45	7	16	1	0	62	10.271	0	0	100
-1	0	73	9.163	307	12	4	1	0	-15	30.429	100	6	6	1	0	63	10.122	16	4	24
-1	0	74	9.046	0	0	100	1	0	-13	32.108	83	6	7	1	0	64	9.980	55	4	8
1	0	-80	8.389	110	9	8	1	0	-12	32.969	66	7	10	1	0	65	9.839	43	4	10
1	0	-79	8.491	71	3	5	1	0	-10	34.503	53	6	11	1	0	66	9.704	60	4	7
1	0	-78	8.597	39	3	8	1	0	-8	36.037	14	7	50	1	0	67	9.569	0	0	100
1	0	-77	8.707	109	10	9	1	0	-5	37.796	67	9	14	1	0	68	9.441	0	0	100
1	0	-76	8.815	200	11	6	1	0	-3	38.348	57	14	25	1	0	68	9.441	0	0	100
1	0	-75	8.930	157	12	8	1	0	-2	38.348	80	13	16	1	0	69	9.313	74	5	7
1	0	-74	9.046	39	4	10	1	0	-2	38.348	110	13	12	1	0	70	9.190	11	4	40
1	0	-73	9.163	303	13	4	1	0	0	38.348	139	13	9	1	0	71	9.068	0	0	100
1	0	-70	9.543	30	3	11	1	0	4	36.761	48	9	19	1	0	72	8.956	36	5	14
1	0	-69	9.672	10	4	37	1	0	5	36.274	0	0	100	1	0	73	8.839	80	6	8
1	0	-68	9.811	0	0	100	1	0	6	35.578	35	10	27							
1	0	-67	9.950	35	4	11	1	0	7	34.711	82	9	11							

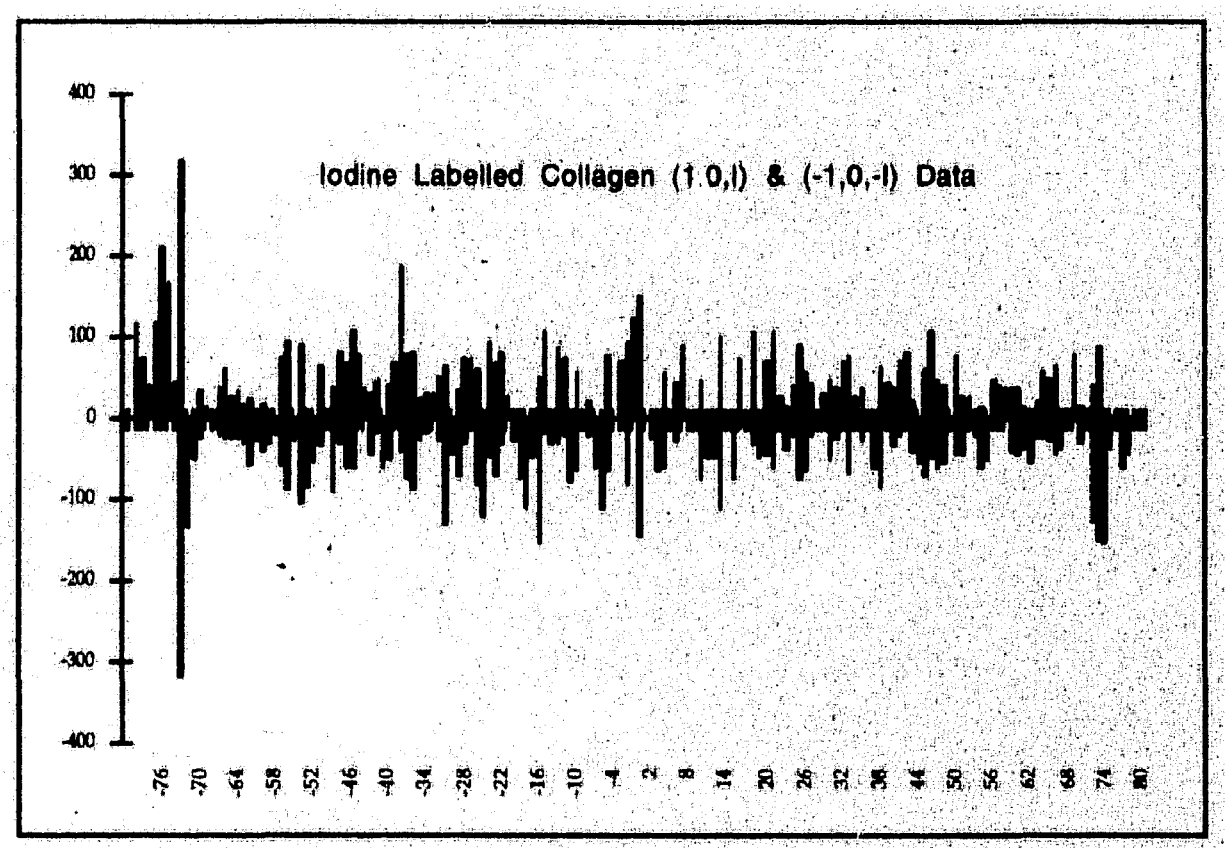

Fig. VI. 18 : This figure demonstrates the good fit of iodine (-1,0,l) and (1,0,l) row-lines to the Friedel law.

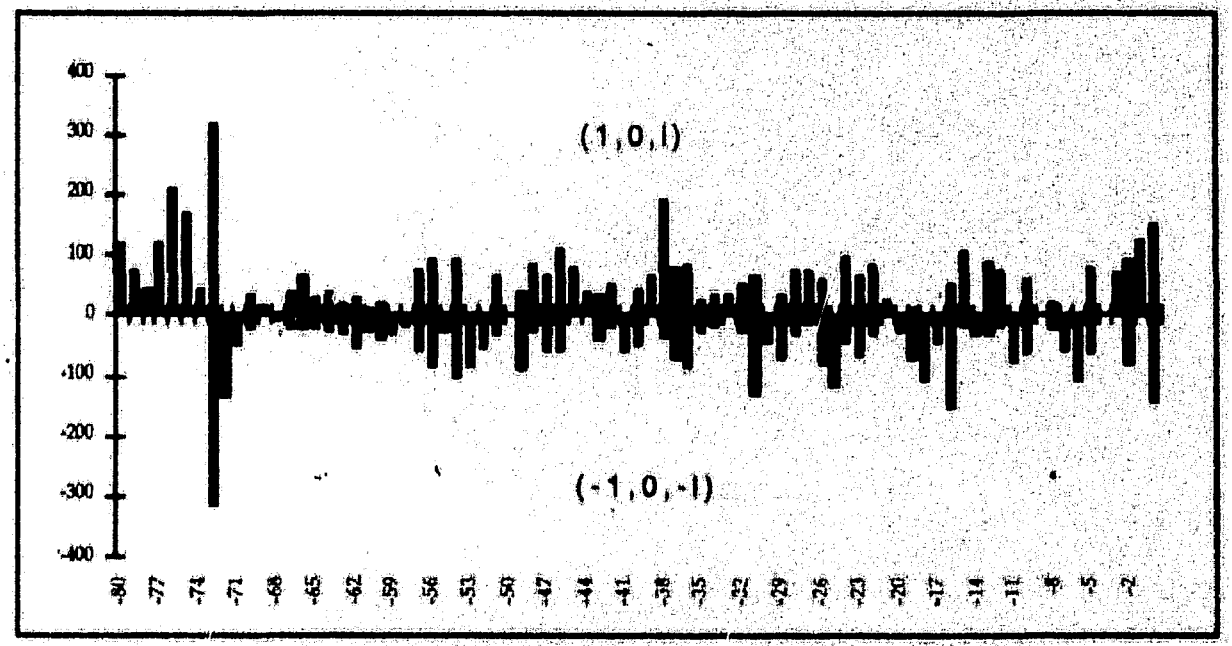

Fig. VI. 19 : Here I represent one half of the data shown in figure VI.18 .The data integration for these row-lines has been achieved correctly as it can be shown by this plot of the iodine (-1,0,l) and (1,0,l) reflections. Also notice the very good agreement between the amplitudes of the reflections (-1,0,73) and (1,0,-73).

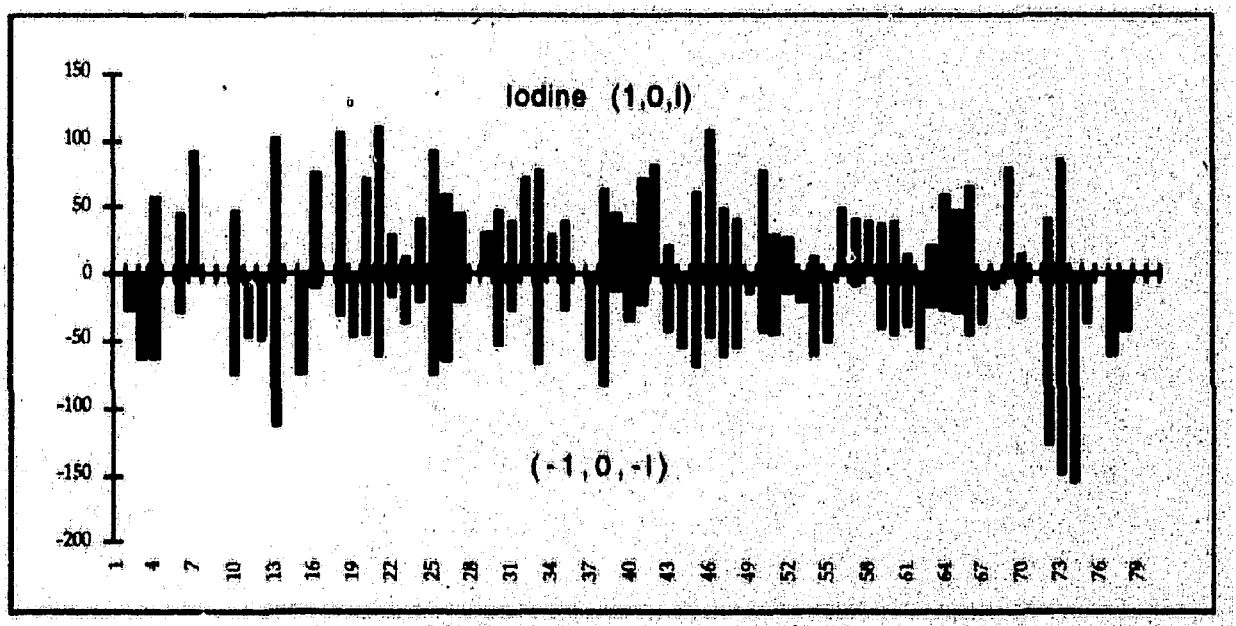

Fig. VI. 19 : The other half of the data for iodine (-1,0,l) and (1,0,l) row-lines is displayed here with more details.

3. Other Iodine Structure Factors

The complete set of iodine structure factors obtained from the current experiment are listed in the appendix. I will only show in this paragraph the graphical display of the (2,0,l) and (-2,0,l) reflections in order to evaluate the data processing method I have developed for fibre pattern analysis. However, further data analysis of the integrated intensities is needed. For instance, the (0,1,l), (0,-1,l), (1,-1,l) and (-1,1,l) analysis enables us to estimate the data goodness before the lowest resolution 3-dimensional Patterson or Fourier maps are calculated.

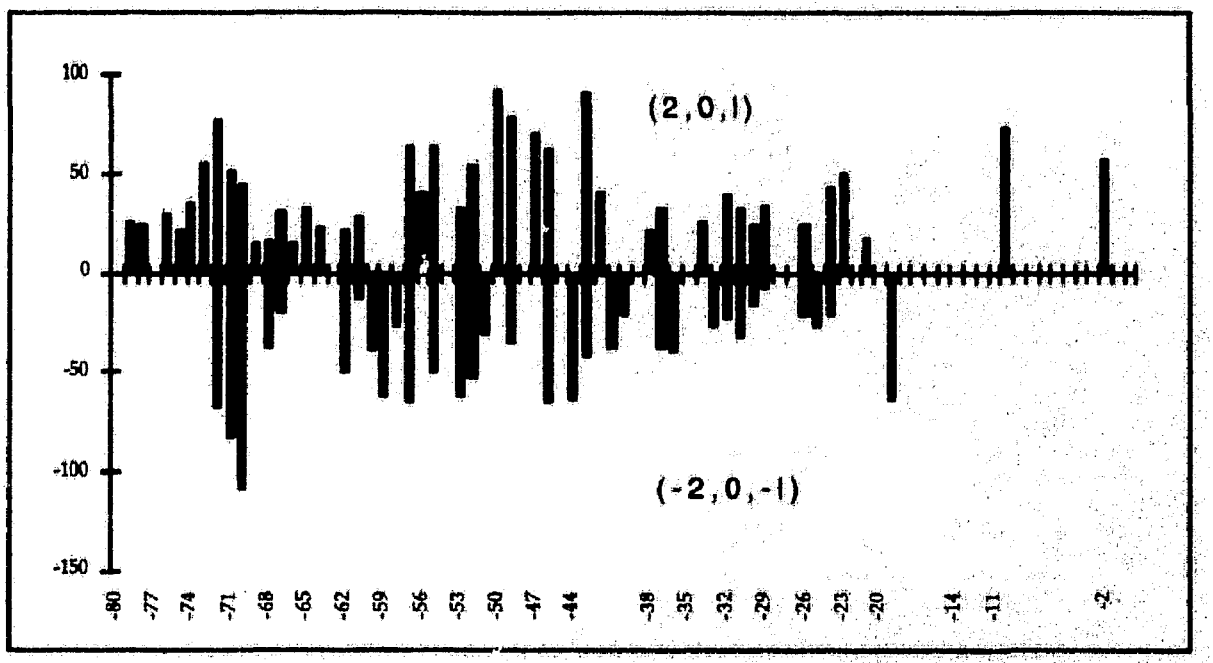

Fig. VI. 20 : Iodine (-2,0,l) and (2,0,l) Friedel plot. The only reflections shown here are the (2,0,l), l=[-1,-80], on the positive side of the structure factors amplitude axis and the reflections (-2,0,-l) on the negative side. The rest of the data is shown in figure VI.21 .

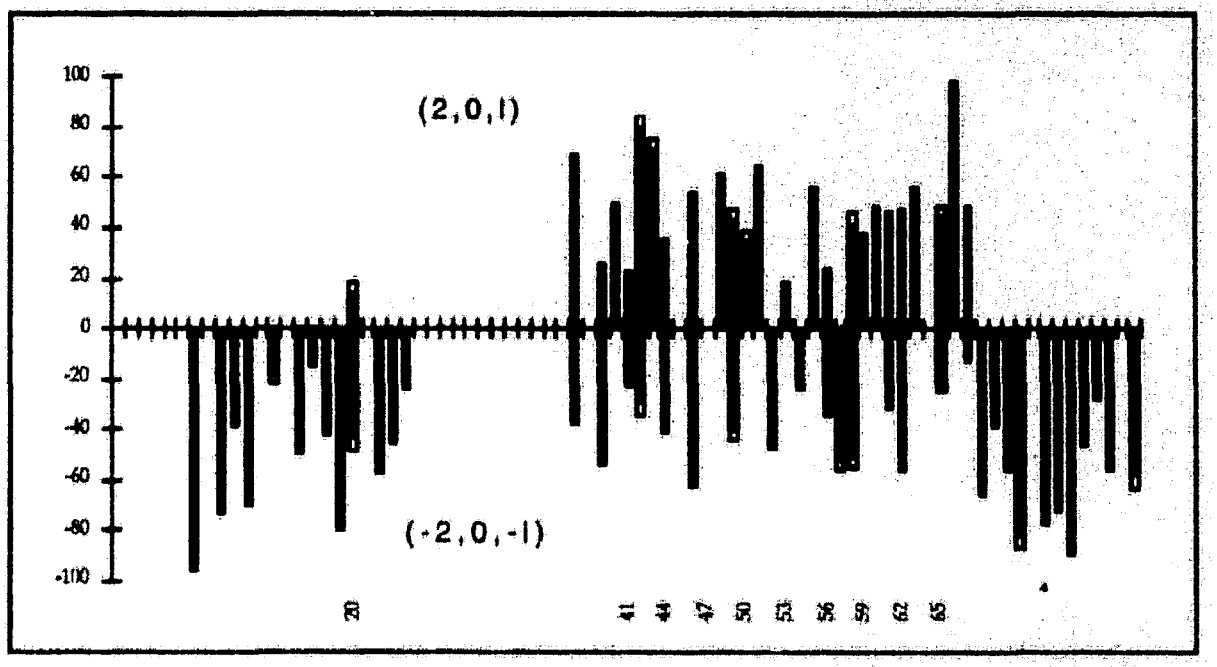

Fig. VI. 21 : Iodine (2,0,l) and (-2,0,l) Friedel plot. The data reflections shown here are the (2,0,l), l=[-10,80], on the positive vertical axis and the reflections (-2,0,-l) on the negative side.

4. Analysis of Iodine Derivative Data

The iodine reflections have been analysed using the CCP4 programs. I give in the tables below the number of measured reflections and various statistics on the intensities.

Iodine Data

Analysis R factor against resolution

N	<s>	DminÅ	Rfac	Rcum	Av_I	σ	I/σ	sd
1	0.0028	18.97	0.325	0.325	2885.	1585.8	1.8	2274.34
2	0.0056	13.41	0.000	0.325	0.	0.0	0.0	0.00
3	0.0083	10.95	0.076	0.096	32831.	4621.5	7.1	14149.8
4	0.0111	9.49	0.000	0.096	0.	0.0	0.0	0.00
5	0.0139	8.48	0.000	0.096	0.	0.0	0.0	0.00
6	0.0167	7.75	0.000	0.096	0.	0.0	0.0	0.00
7	0.0194	7.17	0.000	0.096	0.	0.0	0.0	0.00
8	0.0222	6.71	0.000	0.096	0.	0.0	0.0	0.00
9	0.0250	6.32	0.000	0.096	0.	0.0	0.0	0.00
10	0.0278	6.00	0.000	0.096	0.	0.0	0.0	0.00

Iodine Data

Completeness & multiplicity v. resolution

N	<s>	Dmin	Nmeas	Nref	%poss	Multiplicity
1	0.003	18.97	242	238	110.7	1.0
2	0.006	13.41	346	346	87.9	1.0
3	0.008	10.95	458	454	89.2	1.0
4	0.011	9.49	454	454	75.4	1.0
5	0.014	8.48	308	308	45.0	1.0
6	0.017	7.75	316	316	41.8	1.0
7	0.019	7.17	81	81	9.9	1.0
8	0.022	6.71	0	0	0.0	0.0
9	0.025	6.32	0	0	0.0	0.0
10	0.028	6.00	0	0	0.0	0.0
		Total	2205	2197	32.3	1.0

Iodine Data

	Number in bin			Total	Cumulative %			
DminÅ	≤1σ	≤2σ	≤3σ		≤1σ	≤2σ	≤3σ	>3σ
18.97	36	73	38	238	15.1	45.8	61.8	38.2
13.41	54	113	99	346	15.6	48.3	76.6	23.4
10.95	79	155	122	454	17.4	51.5	78.4	21.6
9.49	66	142	153	454	14.5	45.8	79.5	20.5
8.48	59	84	91	308	19.2	46.4	76.0	24.0
7.75	46	95	106	316	14.6	44.6	78.2	21.8
7.17	11	37	24	81	13.6	59.3	88.9	11.1
6.71	0	0	0	0	0.0	0.0	0.0	100.0
6.32	0	0	0	0	0.0	0.0	0.0	100.0
6.00	0	0	0	0	0.0	0.0	0.0	100.0
Overall	351	699	632	2197.	16.0	47.8	76.6	23.4

D. PEG Structure Factors

I have finally collected diffracted intensities from the PEG added collagen fibre. So we have at the end a complete set of reflections for the MIR method to be assessed. The data I have so far obtained are as follows: one native data set plus two heavy atoms derivative gold and iodine labelled fibres and finally a control set consisting of the PEG data I present here.

1. Meridionals

The meridional reflections from PEG diffraction pattern are listed below.

l	1/d*	F	σF	σF/F
-58	11.65	0	0	100
-57	11.85	4	1	24
-56	12.06	21	1	7
-55	12.28	0	0	100
-54	12.51	10	1	14
-53	12.75	12	1	12
-52	13	18	1	8
-51	13.25	6	1	22
-50	13.51	17	1	8
-49	13.79	10	1	15
-48	14.07	11	1	13
-47	14.37	27	1	5
-46	14.7	0	0	100
-45	15.01	23	1	6
-44	15.36	32	2	5
-43	15.71	27	1	5
-42	16.1	34	2	5
-41	16.48	2	1	58
-40	16.9	44	2	4
-39	17.33	37	2	5
-38	17.79	19	2	9
-37	18.26	63	3	4
-36	18.76	50	3	5
-35	19.32	32	2	6
-34	19.88	34	2	7
-33	20.46	33	2	5
-32	21.13	54	3	5
-31	21.82	22	2	8
-30	22.53	19	2	9
-29	23.31	21	2	8
-28	24.11	35	2	6
-27	25	98	4	5
-26	25.99	37	2	6
-25	27.02	49	3	5
-24	28.17	63	4	7
-23	29.36	55	4	8
-22	30.71	75	5	6
-21	32.11	109	7	6
-20	33.71	140	8	6
-19	35.58	89	6	7
-18	37.53	88	6	7
-17	39.84	112	7	6
-16	42.26	67	6	9
-15	45.18	91	7	8
-14	48.22	50	5	11
-13	51.99	61	6	9
-12	55.9	101	7	7
-11	60.86	73	6	9
-10	67.42	99	7	8
-9	74.54	96	7	8
-8	84.52	93	7	8
-7	95.35	97	7	8
-6	111.8	43	5	12
-5	141.4	120	7	6
-4	158.1	75	7	9
7	95.35	70	8	11
8	84.52	70	7	10
9	74.54	75	7	10
10	67.42	37	4	10
11	60.86	53	5	10
12	55.9	43	4	9
13	51.99	39	4	9
14	48.22	60	5	9
15	45.18	68	6	9
16	42.26	63	5	8
17	39.84	76	6	8
18	37.53	70	6	8
19	35.58	73	6	8
20	33.71	80	7	8
21	32.11	94	6	7
22	30.71	65	4	7
23	29.36	60	4	7
24	28.17	67	4	6
25	27.02	59	3	6
26	25.99	61	4	7
27	25	83	5	6
28	24.11	44	3	6
29	23.31	28	2	8
30	22.53	21	2	9
31	21.82	34	2	7
32	21.13	59	3	6
33	20.46	57	3	6
34	19.88	18	2	11
35	19.32	38	3	7
36	18.76	47	3	6
37	18.26	63	4	6
38	17.79	51	3	5
39	17.33	34	2	6
40	16.9	61	3	5
41	16.48	57	3	5
42	16.1	18	2	11
43	15.71	53	3	6
44	15.36	70	4	5
45	15.01	55	3	6
46	14.7	40	3	7
47	14.37	0	0	100
48	14.07	33	2	7
49	13.79	0	0	100
50	13.51	15	2	17
51	13.25	36	3	7
52	13	24	3	11
53	12.75	23	3	13
54	12.51	10	3	25
55	12.28	35	3	8
56	12.06	0	0	100
57	11.85	65	3	5
58	11.65	0	0	100
59	11.46	0	0	100
60	11.26	0	0	100
61	11.08	0	0	100
62	10.9	0	0	100
63	10.73	0	0	100
64	10.56	0	0	100
65	10.4	0	0	100
66	10.24	33	2	7
67	10.09	40	3	7
68	9.936	0	0	100
69	9.792	36	3	7
70	9.654	0	0	100
71	9.517	32	2	8
72	9.382	49	3	6
73	9.257	0	0	100
74	9.133	0	0	100
75	9.0[illegible]	0	0	100
76	8.891	24	2	10
77	8.774	17	2	15
78	8.661	21	2	11
79	8.553	30	2	8
80	8.446	15	2	17
81	8.342	0	0	100

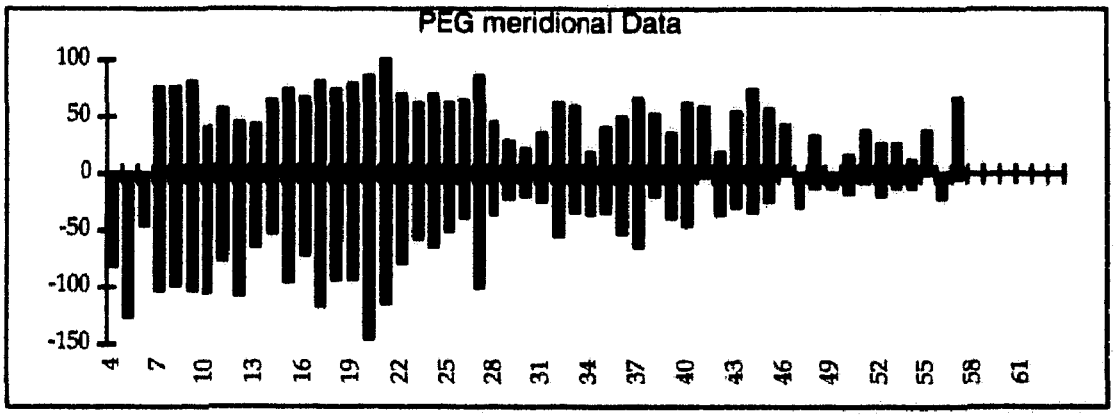

Fig. VI.22 : Friedel plot of the PEG meridional data.

2. PEG Row-Lines

The following are the (-1,0,l) and (1,0,l) row-line data I have obtained after film pack processing. The usual corrections have been applied (film factor and Lorentz correction) and the diffraction peaks have been processed by hand on one half of the films.

h	k	l	1/d*	F	σF	σF/F
-1	0	-80	8.11	12	2	15
-1	0	-79	8.21	13	1	11
-1	0	-78	8.31	0	0	100
-1	0	-77	8.41	6	2	28
-1	0	-76	8.51	8	2	22
-1	0	-75	8.62	10	2	18
-1	0	-74	8.73	9	2	20
-1	0	-73	8.84	0	0	100
-1	0	-72	8.96	8	2	23
-1	0	-71	9.07	40	3	8
-1	0	-70	9.19	45	3	7
-1	0	-69	9.31	23	3	13
-1	0	-68	9.44	0	0	100
-1	0	-67	9.57	0	0	100
-1	0	-66	9.7	0	0	100
-1	0	-65	9.84	1	1	141
-1	0	-64	9.98	0	0	100
-1	0	-63	10.1	17	2	10
-1	0	-62	10.3	9	2	19
-1	0	-61	10.4	13	2	14
-1	0	-60	10.6	0	0	100
-1	0	-59	10.7	9	2	19
-1	0	-58	10.9	8	1	18
-1	0	-57	11.1	13	2	13
-1	0	-56	11.3	8	2	22
-1	0	-55	11.4	2	2	77
-1	0	-54	11.6	10	2	17
-1	0	-53	11.8	9	2	19
-1	0	-52	12	18	2	10
-1	0	-51	12.2	0	0	100
-1	0	-50	12.4	0	0	100
-1	0	-49	12.7	12	2	15
-1	0	-48	12.9	5	2	34
-1	0	-47	13.1	14	2	12
-1	0	-46	13.4	11	2	16
-1	0	-45	13.6	7	2	24
-1	0	-44	13.9	7	2	30
-1	0	-43	14.2	7	2	25
-1	0	-42	14.4	0	0	100
-1	0	-41	14.7	17	2	10
-1	0	-40	15	17	2	10
-1	0	-39	15.3	0	0	100
-1	0	-38	15.7	0	0	100
-1	0	-37	16	0	0	100
-1	0	-36	16.4	13	2	13
-1	0	-35	16.7	10	2	20
-1	0	-34	17.1	20	2	9
-1	0	-33	17.5	0	0	100
-1	0	-32	17.9	22	2	8
-1	0	-31	18.3	13	2	14
-1	0	-30	18.8	10	2	20
-1	0	-29	19.2	16	2	13
-1	0	-28	19.7	0	0	100
-1	0	-27	20.2	21	2	9
-1	0	-26	20.8	12	2	17
-1	0	-25	21.3	20	2	12
-1	0	-24	21.9	28	2	8
-1	0	-23	22.5	19	2	11
-1	0	-22	23.1	16	2	16
-1	0	-21	23.8	19	2	13
-1	0	-20	24.4	24	3	12
-1	0	-19	25.1	24	3	11
-1	0	-18	25.8	17	3	17
-1	0	-17	26.5	6	3	51
-1	0	-16	27.3	16	3	18
-1	0	-15	28.2	32	3	11
-1	0	-14	29	29	3	11
-1	0	-13	29.7	0	0	100
-1	0	-12	30.6	25	3	14
-1	0	-11	31.5	0	0	100
-1	0	-10	32.3	32	3	10
-1	0	-9	33.1	0	0	100
-1	0	-8	33.9	8	3	40
-1	0	-7	34.7	10	4	34
-1	0	-6	35.6	27	4	15
-1	0	-5	36.3	2	4	173
-1	0	-4	36.8	18	4	25
-1	0	-3	37.3	0	0	100
-1	0	0	38.3	50	6	12
-1	0	3	38.3	41	6	15
-1	0	4	38.1	25	6	23
-1	0	5	37.8	11	6	55
-1	0	6	37.3	[illegible]	4	16
-1	0	7	36.8	23	3	14
-1	0	8	36	27	3	13
-1	0	9	35.4	17	3	17
-1	0	11	33.7	24	3	14
-1	0	12	33	21	3	16
-1	0	13	32.1	0	0	100
-1	0	14	31.3	15	3	20
-1	0	15	30.4	43	3	7
-1	0	16	29.6	0	0	100
-1	0	17	28.7	19	2	9
-1	0	18	28	22	2	9
-1	0	19	27.2	19	2	10
-1	0	20	26.4	29	2	8
-1	0	21	25.6	9	2	20
-1	0	22	25	35	3	8
-1	0	23	24.3	0	0	100
-1	0	24	23.6	39	2	6
-1	0	25	22.9	17	2	13
-1	0	26	22.4	0	0	100
-1	0	27	21.8	26	2	8
-1	0	28	21.2	30	2	7
-1	0	29	20.7	26	2	8
-1	0	30	20.1	29	2	8
-1	0	31	19.6	32	2	6
-1	0	32	19.1	21	2	8
-1	0	33	18.7	22	2	9
-1	0	34	18.3	17	2	10
-1	0	35	17.8	42	2	5
-1	0	36	17.4	11	2	18
-1	0	37	17	22	2	9
-1	0	38	16.6	34	2	6
-1	0	39	16.3	27	2	6
-1	0	40	15.9	0	0	100
-1	0	41	15.6	19	2	9
-1	0	42	15.3	27	2	6
-1	0	43	15	4	2	48
-1	0	44	14.7	6	2	28
-1	0	45	14.4	33	2	5
-1	0	46	14.1	9	2	19
-1	0	47	13.8	23	2	7
-1	0	48	13.6	11	2	16
-1	0	49	13.3	29	2	6
-1	0	50	13.1	0	0	100
-1	0	51	12.8	0	0	100
-1	0	52	12.6	23	2	7
-1	0	53	12.4	0	0	100
-1	0	54	12.2	3	2	55
-1	0	55	12	23	2	8
-1	0	56	11.8	17	2	10
-1	0	57	11.6	0	0	100
-1	0	58	11.4	21	2	8
-1	0	59	11.2	9	2	20
-1	0	60	11	8	2	22
-1	0	61	10.9	0	0	100
-1	0	62	10.7	0	0	100
-1	0	63	10.5	9	2	19
-1	0	64	10.4	9	1	16
-1	0	65	10.2	0	0	100
-1	0	66	10.1	9	2	18
-1	0	67	9.95	0	0	100
-1	0	68	9.81	3	2	61
-1	0	69	9.67	0	0	100
-1	0	71	9.41	14	2	15
-1	0	72	9.29	0	0	100

-1	0	73	9.16	0	0	100		1	0	-37	17	21	2	10		1	0	30	18.8	7	2	27
-1	0	74	9.05	17	2	10		1	0	-36	18.4	0	0	100		1	0	31	18.3	11	2	18
-1	0	75	8.93	10	2	17		1	0	-35	17.8	28	2	8		1	0	32	17.9	19	2	11
-1	0	76	8.81	14	1	10		1	0	-34	18.3	4	2	41		1	0	33	17.5	2	2	87
-1	0	77	8.71	15	1	10		1	0	-33	18.7	20	2	10		1	0	34	17.1	17	2	10
-1	0	78	8.6	0	0	100		1	0	-32	19.1	22	2	8		1	0	35	16.7	8	2	26
-1	0	80	8.39	16	2	11		1	0	-31	19.6	20	2	10		1	0	36	16.4	0	0	100
1	0	-80	8.39	7	1	20		1	0	-30	20.1	29	2	8		1	0	37	16	7	1	21
1	0	-79	8.49	10	1	14		1	0	-29	20.7	36	2	5		1	0	38	15.7	21	2	8
1	0	-78	8.6	5	1	31		1	0	-28	21.2	24	2	9		1	0	39	15.3	3	2	50
1	0	-77	8.71	4	1	33		1	0	-27	21.8	16	2	12		1	0	40	15	15	2	12
1	0	-76	8.81	10	1	14		1	0	-26	22.4	10	2	17		1	0	41	14.7	5	2	33
1	0	-75	8.93	6	1	22		1	0	-25	22.9	4	2	50		1	0	42	14.4	7	2	26
1	0	-74	9.05	12	1	11		1	0	-24	23.6	36	2	6		1	0	43	14.2	6	2	27
1	0	-73	9.16	0	0	100		1	0	-23	24.3	12	2	17		1	0	44	13.9	0	0	100
1	0	-72	9.29	0	0	100		1	0	-22	25	22	2	10		1	0	45	13.6	12	2	17
1	0	-71	9.41	22	1	6		1	0	-22	25	37	4	10		1	0	46	13.4	13	2	13
1	0	-70	9.54	0	0	100		1	0	-21	25.6	17	2	11		1	0	47	13.1	7	2	23
1	0	-69	9.67	62	2	4		1	0	-20	26.4	25	3	11		1	0	48	12.9	9	2	19
1	0	-68	9.81	0	0	100		1	0	-19	27.2	25	2	9		1	0	49	12.7	11	2	15
1	0	-67	9.95	0	0	100		1	0	-18	28	18	2	11		1	0	50	12.4	0	0	100
1	0	-66	10.1	23	1	6		1	0	-17	28.7	22	2	9		1	0	51	12.2	2	2	100
1	0	-65	10.2	0	0	100		1	0	-16	29.6	0	0	100		1	0	52	12	10	2	18
1	0	-64	10.4	15	1	10		1	0	-15	30.4	41	3	8		1	0	53	11.8	10	2	17
1	0	-63	10.5	6	1	25		1	0	-13	32.1	12	3	27		1	0	54	11.6	12	2	14
1	0	-62	10.7	0	0	100		1	0	-11	33.7	12	3	26		1	0	55	11.4	0	0	100
1	0	-61	10.9	0	0	100		1	0	-9	35.4	4	3	96		1	0	56	11.3	0	0	100
1	0	-60	11	0	0	100		1	0	-6	37.3	18	3	18		1	0	57	11.1	14	2	12
1	0	-59	11.2	16	1	9		1	0	-3	38.3	27	5	17		1	0	58	10.9	0	0	100
1	0	-58	11.4	15	2	12		1	0	-2	38.3	75	8	11		1	0	59	10.7	15	2	12
1	0	-57	11.6	0	0	100		1	0	0	38.3	19	5	24		1	0	60	10.6	0	0	100
1	0	-56	11.8	5	1	27		1	0	1	38.1	31	6	19		1	0	61	10.4	8	2	22
1	0	-55	12	3	0	100		1	0	3	37.3	29	6	22		1	0	62	10.3	12	2	14
1	0	-54	12.2	4	1	22		1	0	4	36.8	0	0	100		1	0	63	10.1	18	2	10
1	0	-53	12.4	6	2	29		1	0	5	36.3	14	4	26		1	0	64	9.98	0	0	100
1	0	-52	12.6	19	2	9		1	0	7	34.7	0	0	100		1	0	65	9.84	5	2	35
1	0	-51	12.8	14	2	13		1	0	8	33.9	0	0	100		1	0	66	9.7	6	2	27
1	0	-50	13.1	7	1	19		1	0	12	30.6	42	3	8		1	0	67	9.57	0	0	100
1	0	-49	13.3	24	2	7		1	0	13	29.7	0	0	100		1	0	68	9.44	0	0	100
1	0	-48	13.6	7	1	21		1	0	18	25.8	10	2	22		1	0	70	9.19	31	3	10
1	0	-47	13.8	14	2	12		1	0	20	24.4	29	2	8		1	0	71	9.07	21	3	17
1	0	-46	14.1	0	0	100		1	0	21	23.8	20	3	13		1	0	72	8.96	0	0	100
1	0	-45	14.4	23	2	9		1	0	22	23.1	16	2	14		1	0	73	8.84	20	3	17
1	0	-44	14.7	0	0	100		1	0	23	22.5	16	2	14		1	0	74	8.73	0	0	100
1	0	-43	15	0	0	100		1	0	24	21.9	21	2	11		1	0	75	8.62	5	2	33
1	0	-42	15.3	23	2	8		1	0	25	21.3	14	2	16		1	0	76	8.51	8	2	21
1	0	-41	15.6	7	2	23		1	0	26	20.8	0	0	100		1	0	77	8.41	0	0	100
1	0	-40	15.9	0	0	100		1	0	27	20.2	16	2	14		1	0	78	8.31	8	2	22
1	0	-39	16.3	0	0	100		1	0	28	19.7	0	0	100		1	0	79	8.21	0	0	100
1	0	-38	16.6	15	2	13		1	0	29	19.2	7	2	27		1	0	80	8.11	1	2	173

In conclusion, I have used a time consuming but nevertheless of a great utility process to gather the structure factors already given. This was an important step towards the structure and packing studies of collagen crystalline domains in tendon. The data for meridional and the two prominent row-lines were checked using a simple graphical display of the structure factors amplitudes. The graphical display has also allowed me to check for the correct indexing of reflections. These structure factors are the starting material for Fourier calculation of the structure. The phases for the meridional and row-lines reflections can also be obtained if one knows the positions of the heavy atoms in the unit cell. The one dimensional projected structure using meridional reflections can thus be obtained with a better resolution than in previous works. The (-1,0,l), (1,0,l), (-2,0,l) and (2,0,l) row-lines data allow for a the structure projected on the ac plane to be calculated. A modelled structure can also be compared against experimental native data. However the need to rapidly analyse fibre diffraction patterns is one of the conditions to obtain further structural information from X-ray experiments. Usually, large data are produced from proteins (native and derivatives) and integrated intensities are processed by automatic programs. A full automatic data processing program (e.g. peak integration, background and film factor corrections as well as Lorentz factor correction) for fibre diffraction patterns is being

under development since none exists to my knowledge. The need for such an automatic data processing software is increasing with the increasing interest in structural studies on fibrous proteins.

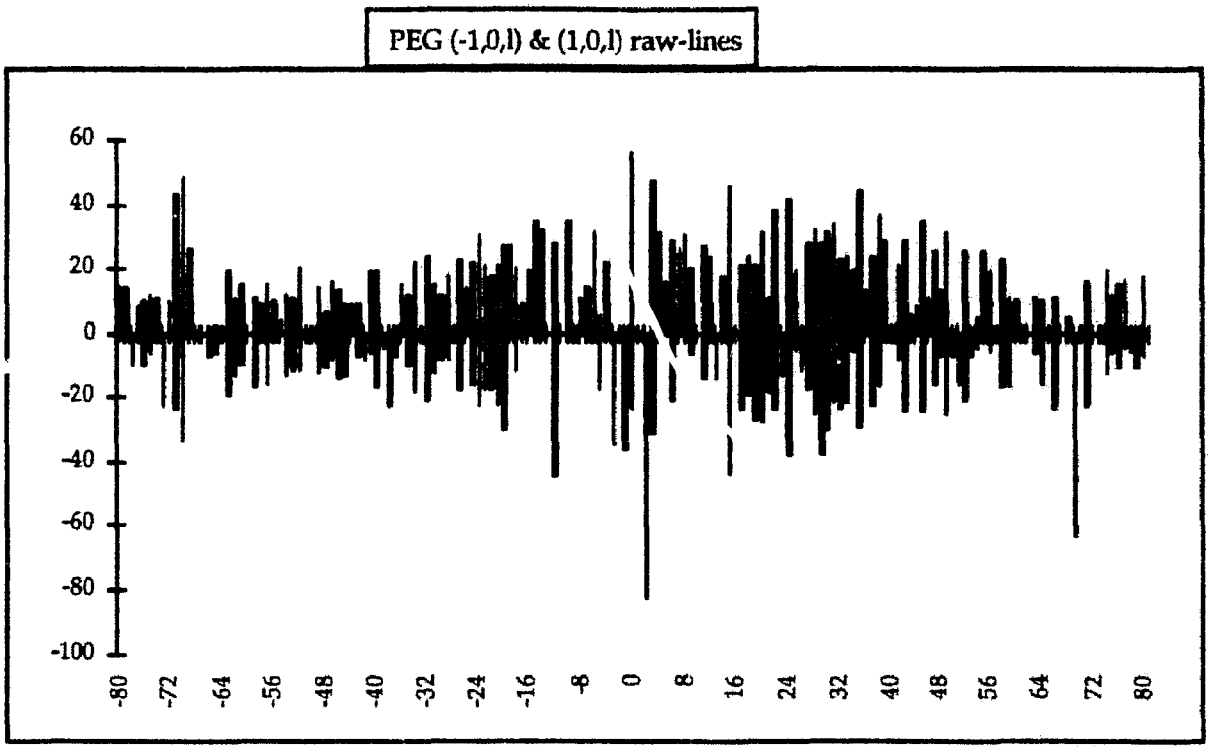

Fig. VI. 23 : This figure shows the structure factors of the (-1,0,l) and (-1,0,l) row-lines plotted against l index. thus allowing Friedel's law to be verified.

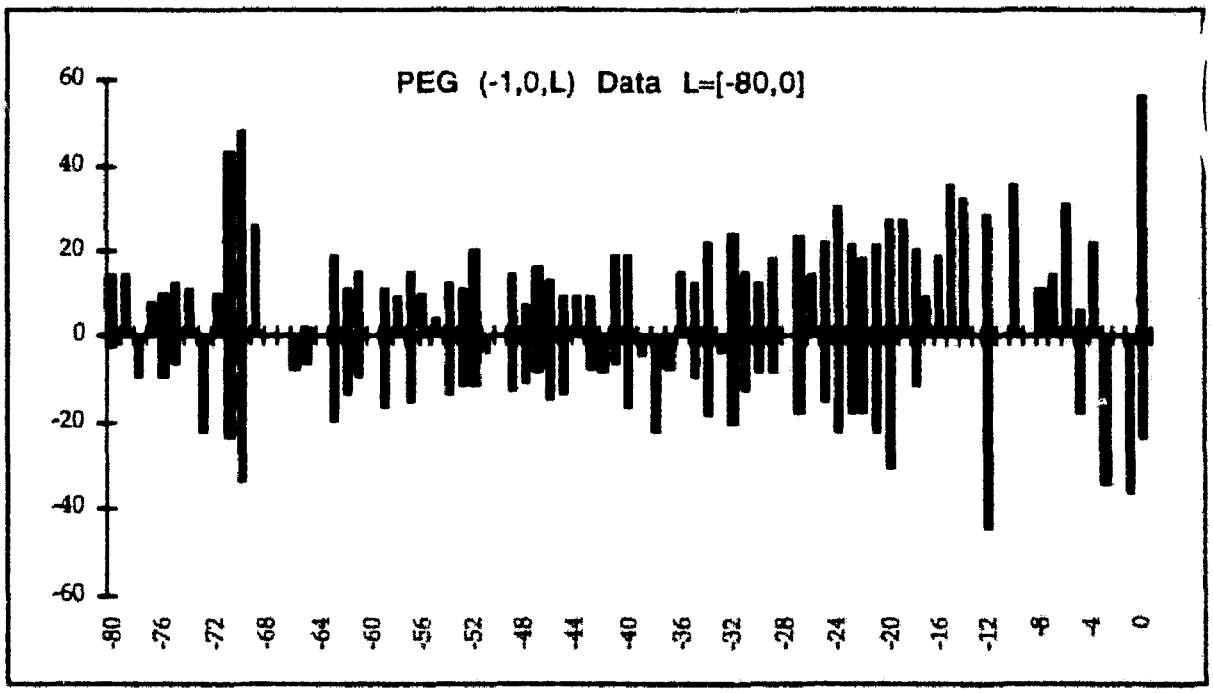

Fig. VI. 24

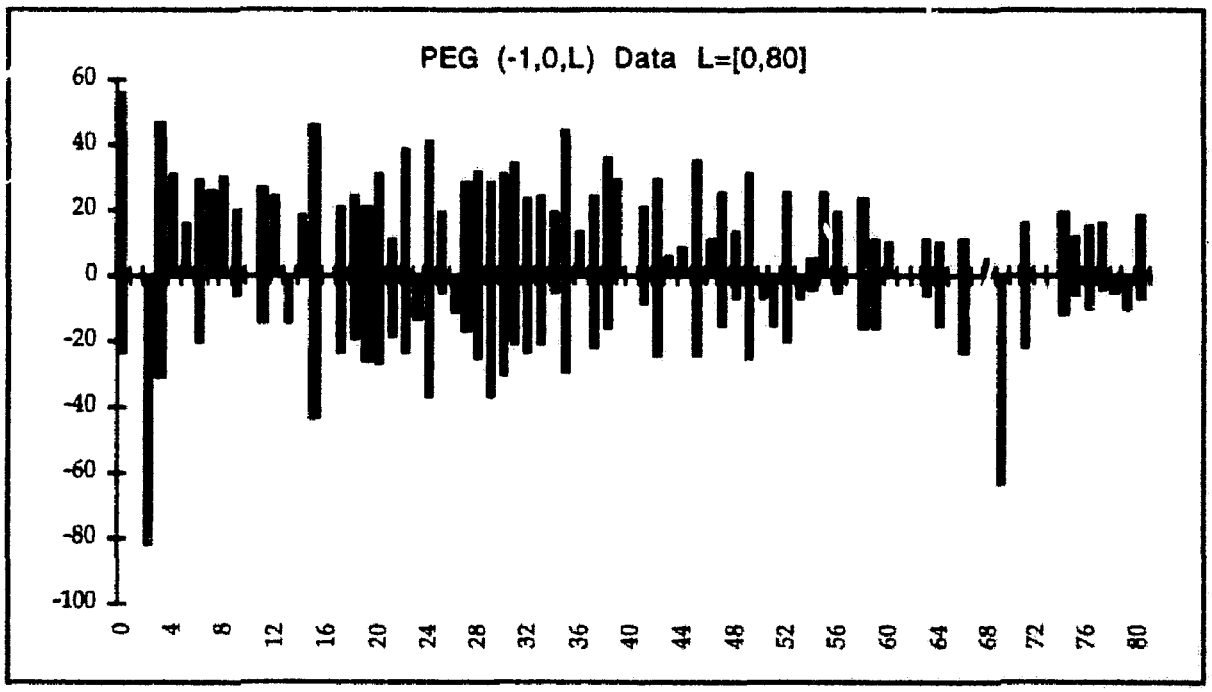

Fig. VI.25

3. Others

The reflections list of PEG added collagen is given as sorted list at the end of the thesis.

4. Analysis of PEG Derivative Data

PEG Data

Analysis R factor against resolution

N	<s>	DminÅ	Rfac	Rcum	Av_I	σ	I/σ	sd
1	0.0028	18.97	0.278	0.278	204.	61.6	3.3	118.38
2	0.0056	13.41	0.429	0.300	88.	48.5	1.8	74.97
3	0.0083	10.95	0.000	0.300	0.	0.0	0.0	0.00
4	0.0111	9.49	0.000	0.300	0.	0.0	0.0	0.00
5	0.0139	8.48	0.000	0.241	289.	0.0	0.0	113.04
6	0.0167	7.75	0.000	0.241	0.	0.0	0.0	0.00
7	0.0194	7.17	0.000	0.174	576.	0.0	0.0	157.00
8	0.0222	6.71	0.000	0.174	0.	0.0	0.0	0.00
9	0.0250	6.32	0.000	0.174	0.	0.0	0.0	0.00
10	0.0278	6.00	0.000	0.174	0.	0.0	0.0	0.00

PEG Data Completeness & multiplicity v. resolution						
N	<s>	DminÅ	Nmeas	Nref	%poss	Multiplicity
1	0.003	18.97	212	207	96.3	1.0
2	0.006	13.41	247	245	62.3	1.0
3	0.008	10.95	249	249	48.9	1.0
4	0.011	9.49	202	202	33.5	1.0
5	0.014	8.48	194	193	28.2	1.0
6	0.017	7.75	142	142	18.8	1.0
7	0.019	7.17	38	37	4.5	1.0
8	0.022	6.71	0	0	0.0	0.0
9	0.025	6.32	0	0	0.0	0.0
10	0.028	6.00	0	0	0.0	0.0
	Total	1284	1275	18.8	1.0	

PEG Data								
	Number in bin			Total	Cumulative %			
DminÅ	≤1σ	≤2σ	≤3σ		≤1σ	≤2σ	≤3σ	>3σ
18.97	25	58	40	207	12.1	40.1	59.4	40.6
13.41	64	91	47	245	26.1	63.3	82.4	17.6
10.95	67	113	43	249	26.9	72.3	89.6	10.4
9.49	61	85	37	202	30.2	72.3	90.6	9.4
8.48	40	86	38	193	20.7	65.3	85.0	15.0
7.75	34	67	29	142	23.9	71.1	91.5	8.5
7.17	9	18	6	37	24.3	73.0	89.2	10.8
6.71	0	0	0	0	0.0	0.0	0.0	100.0
6.32	0	0	0	0	0.0	0.0	0.0	100.0
6.00	0	0	0	0	0.0	0.0	0.0	100.0
Overall	300	518	240	1275.	23.5	64.2	83.0	17.0

E. MIR Difference Pattersons and Fourier Maps Calculated with Collagen Native and Derivative Data

The detailed analysis of the structure factors that I have done so far was necessary since now all the succeeding work will depend on the quality of these data. Not only I have produced the first set of structure factors including the meridional and the (-1,0,l) and (1,0,l) row-lines for the native and two derivative fibres but I have also demonstrated that our data collection method was faithful. In this paragraph , I thus will attempt to calculate 3-Dimensional maps using the whole data I have collected and I will assume that the rest of the data is correct. As stated before, a further analysis of the whole data will be necessary but some calculations (e.g. isomorphous difference Patterson maps) are readily possible.

I also first need to define some symbols used in the CCP4 file format and in the succeeding paragraphs. These symbols apply to the structure factors definition for each of the native and other derivative set and the "calculated" structure factors have been obtained from a modelled triple-helical collagen molecule described later in Chapter 7. Hence, the symbols used are defined as follows:

FNO	F_{native}, observed
FNOEQUAT	F_{native}, observed, with the near equatorial[1] data included
FGO	F_{gold}, derivative, observed
FGOEQUAT	F_{gold}, observed, with near equatorial data
FIO	F_{iodine}, derivative, observed
FGOEQUAT	F_{iodine}, observed, with near equatorial data
FEO	F_{PEG} derivative observed
FEOEQUAT	F_{PEG} observed (with near equatorial data)
FC135	$F_{calculated}$ (for the C135[2] modelled structure)
FCRAND	$F_{calculated}$ (for the random[3] collagen model)

The usefulness and purpose of the constructed C135 and Random collagen models will be discussed in chapter 7 but these are here used to calculate one model structure factors set and more specifically a set of starting model phases for the calculation of potential heavy atom sites.

1. Calculating the First Low-resolution 3-Dimensional Difference Patterson Maps

I have used the CCP4 suite to calculate three-dimensional Fourier and isomorphous difference Patterson maps using the files containing all the experimental data I have obtained. Nevertheless, all these data have not been actually used because the reflections for which I have expressly attributed a zero amplitude and a zero standard deviation were not included in the FFT routines. The CCP4 routines in fact, considers that these zero amplitude reflections as unobserved reflections. The reflections with zero amplitudes were thus definitely rejected from the statistical calculations given before and also in the derivative to native scaling and all subsequent Fourier synthesis. Hence, the calculations done hereafter are for the preliminary evaluation of the MIR (low-resolution) method only and are thus carried on a trial basis.

The general MIR structure solution after film processing and structure factors acquisition usually requires the following steps, where I also give the names of the relevant CCP4 programs:

1. Scale derivative data to native using either *Scaleit* or *Fhscal* (Kraut Scaling). The programs have been run with the native and derivative data I have obtained and

---

[1] The near equatorial reflections we have obtained are unsure due to strong intensity overlap and also to the ambiguity on the Miller indices recovery during the automatic Bragg peak identification. Therefore, we have one data set for each derivative with these equatorial reflections excluded from the scaling and subsequent Fourier calculations and another where we have included these equatorial reflections.

[2] see definition of the C135 model in Chapter 7.

[3] see definition of the Random collagen model in Chapter 7.

the program output are given in the tables below.

2. Find heavy atom sites by solving Patterson maps for one derivative and then finding the major site(s).

3. Refinement and phasing:

(a). Heavy atom refinement and phasing : *mlphare*

(Maximum Likelihood Phasing and Refinement)

(b). Heavy atom refinement: *vecref , heavy*

4. Difference Fouriers to find new heavy atom sites in the first and other derivatives: *fft* —> *peakmax* —> *npo*

5. Back to calculate and check Pattersons for other derivatives.

a) Scaling between Native and Derivative Collagen Data:

The normal procedure to scale the native and derivative data sets together is to use a Wilson plot to put the data on the same absolute scale. But this is generally a poorly reliable method especially for high resolution studies. One other method which is relatively simple and which always yield good results is the Kraut's method. The derivative scale factor is calculated by equating the Patterson origins for both native and derivative sets according to the equation:

$$\sum F_H^2 = \sum \left(K_s \, F_{PH}^2 \right) - \sum \left(F_P^2 \right)$$

where Ks is the scale factor to be applied to the derivative data set (for a review see: Kraut et al, 1962; Tickle, 1991).

Scaling Gold derivative to Native data using *FHSCALE*					
NUMBER OF REFLECTIONS READ, USED = 2145 660					
COMMON RESOLUTION RANGE = 135.14Å 6.59Å					
SHELL	1/d*(Å)	NUMBER	RMS# -FP	RMS-FPH	Ks
1	9.50	450	1040.6	1589.0	1.41884
2	7.54	181	1044.0	1579.1	1.35007
3	6.59	29	1035.5	1930.5	1.41343
Totals		660	1041.3	1602.8	1.23726
From difference *Wilson* plot :					
Overall scale and standard deviation = 1.42971 0.03840					

The results of the scaling program *FHSCAL* are given in the following tables. The program was run

RMS= Root Mean Square value

for each derivative to native scaling. The number of reflections used as well as the total number of reflections are listed in the top row of the tables given formerly. The used reflections are those actually used by the scaling process, that is, these are the common reflections between derivative and native data set. This number is unusually low but this is because the data collecting was done by hand and not systematically by an automatic process. The *FHSCAL* program also calculates a global scaling factor according to Wilson plot for each derivative. The derivative to native Wilson scale factors are given in the last table rows.

Scaling Iodine derivative to Native data using *FHSCALE*					
NUMBER OF REFLECTIONS READ, USED = 2133 793					
COMMON RESOLUTION RANGE = 135.14Å 7.42Å					
SHELL	1/d*(Å)	NUMBER	RMS-FP	RMS-FPH	Ks
1	11.78	325	1046.3	2280.9	1.93474
2	9.35	278	1027.8	1202.2	2.21574
3	8.17	140	968.6	1526.0	2.56794
4	7 42	50	1020.3	1349.1	2.72370
Totals		793	1024.9	1779.0	2.20528
From difference *Wilson* plot :					
Overall scale and standard deviation = 1.83999 0.03383					

Scaling PEG derivative to Native data using *FHSCALE*					
NUMBER OF REFLECTIONS READ, USED = 2123 627					
COMMON RESOLUTION RANGE = 135.14Å 7.40Å					
SHELL	1/d*(Å)	NUMBER	RMS-FP	RMS-FPH	Ks
1	10.68	363	1032.3	1898.8	1.52457
2	8.48	191	1024.5	1133.4	1.55401
3	7.40	73	1065.7	1189.8	1.59286
Totals		627	1033.9	1625.9	1.73300
From difference *Wilson* plot :					
Overall scale and standard deviation = 1.51086 0.00490					

b) Determination of heavy atoms positions:

The amplitude and the phase of the heavy atom contribution to the structure factor of the derivative has to be determined from the experimental data by working out the differences in scattering amplitudes caused by the introduction of heavy atoms. The different techniques usually used to do this are: Patterson searches of different kinds, direct methods and difference Fouriers.

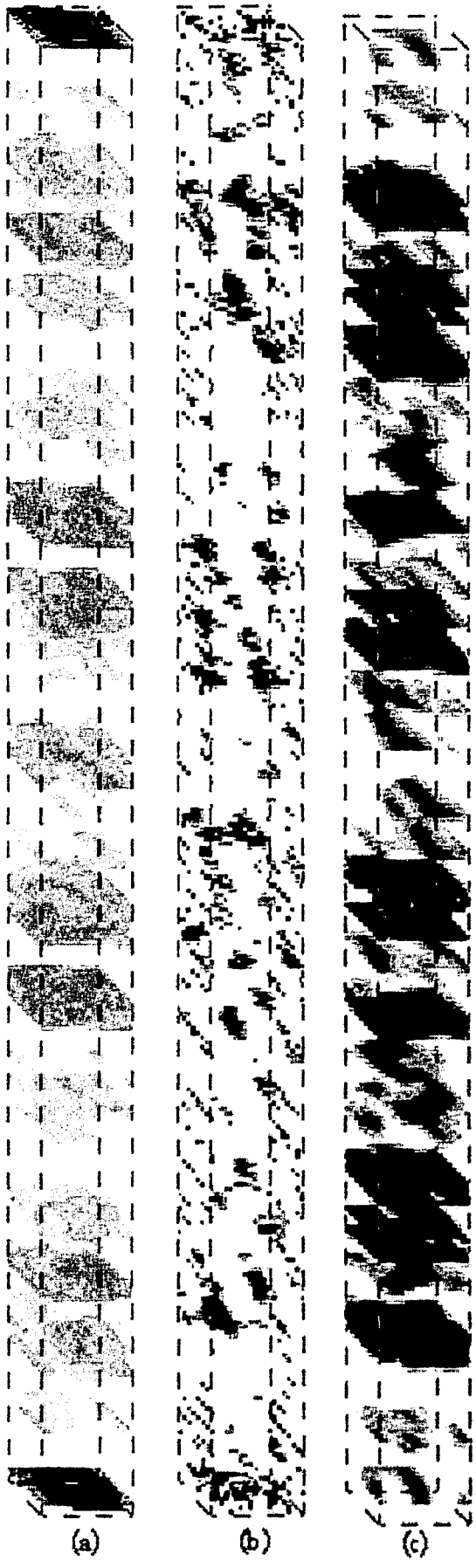

Fig. VI.26: A 3-Dimensional perspective view of the difference Patterson maps that I have calculated for each collagen heavy atom derivative using the experimental data I have gathered. The three images I have obtained were noisy so I only show the major peaks in the maps after the continuous background level was truncated. The difference Patterson maps shown here are not on the same scale because Fouriers are always calculated on arbitrary scales. These are consequently only shown to display the calculated structure in the Patterson space. (a) is a FIO-FNO difference Patterson map calculated in the reciprocal unit cell volume defined by a=[0,0.5], b=[0,0.5] and c=[0,0.5]. The vertical axis is the c-axis, b is across the paper plane and a is in the paper plane. (b) is the FGO-FNO map calculated in the same volume as (a) and (c) is the control map calculated using PEG data (e.g. FEO-FNO difference Patterson). The number of sections used to calculate the Fourier are usually set to one third of the maximum resolution of the data in each principal direction. We have thus 21 sections in the a direction (1/d=6.0Å), 9 sections in the b direction (1/d*=9.0Å) and 331 sections in the c-direction (1/d*=6.0Å).*

The conventional method to search for heavy atom peaks in a Patterson map is usually facilitated by plotting special sections (e.g. the Harker sections of an $|F_{PH}|^2$ calculated map) of the Patterson map where heavy-atom↔heavy-atom peaks are clearly distinguished. Since our aim is to search for the heavy atoms contribution to the collagen structure the first step is thus the calculation of a conventional Patterson map. The Harker method however, operates with crystals belonging to special symmetry groups other then the P1 crystal system defined for collagen. Accordingly, a Patterson map calculated with a collagen heavy atom derivative will provide the means to observe the heavy atoms contributions but its interpretation will be more complicated.

Now the transform of the P1 symmetry group is P-1 (e.g. centro-symmetric Laue group) so that a Patterson map can always be calculated over one half of the unit cell volume using each derivative data set. The difference Patterson maps $|F_{PH}|^2$

$|Pp|^2$ shown in figure VI.26 will be preferred

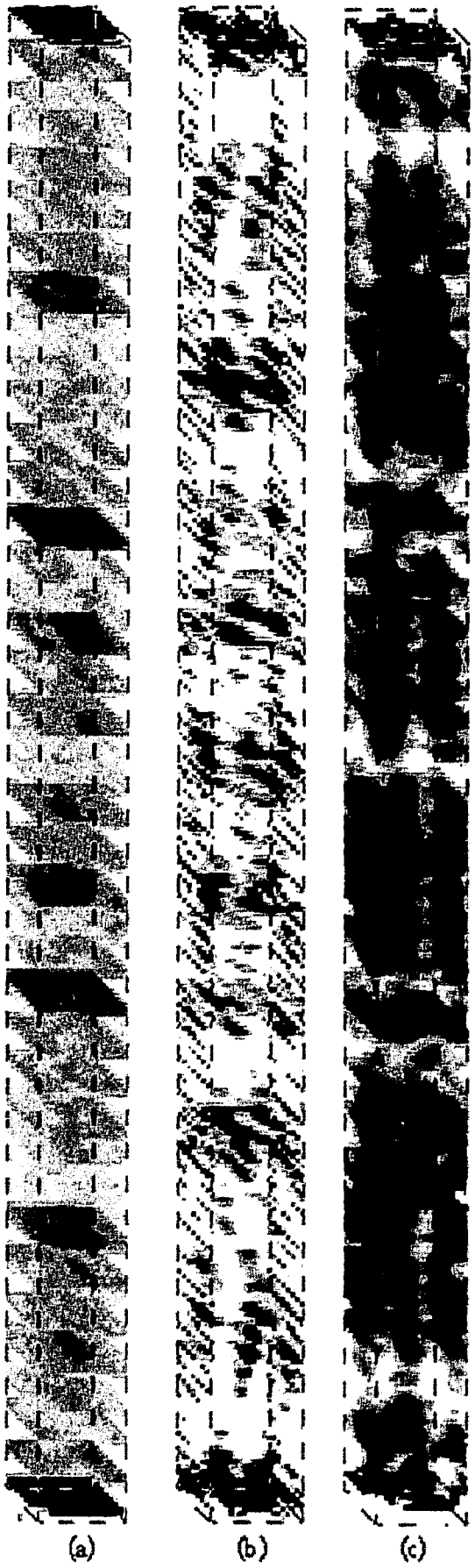

Fig. VI.27: These 3-Dimensional perspective views show the difference Patterson maps I have calculated for each collagen heavy atom derivative using the experimental structure factors. Here, the equatorial reflections have been included in the scaling and FFT calculations because of their contribution to the lateral arrangement of collagen molecules. The calculation is here shown separately because the correct indexing and peak overlap of these structure factors has not been checked. Hence, (a) is an FIOEQUAT-FNOEQUAT[1] difference Patterson map calculated in the reciprocal unit cell volume defined in figure VI.26, (b) is the FGOEQUAT-FNOEQUAT map calculated in the same volume as (a) and (c) is again the control map calculated using FEOEQUAT-FNOEQUAT data. The number of sections along each reciprocal unit cell axis is the same as figure VI.26.

to the usual $|F_{PH}|^2$ maps because the contributions of the heavy atoms are better noticed when protein↔protein peaks have been subtracted.

I have calculated the difference Patterson maps for each derivative collagen data using the *fft* programs of the CCP4 package. The maps shown in figures VI.26 & VI.27 are those obtained with difference Pattersons. The symmetry group was set to P1 so that the Patterson symmetry is P-1. The number of sections along each reciprocal unit cell axis was automatically set by the program. This number is usually chosen so that it samples the volume of the calculated map at one third of the maximum available resolution within the data set. The maps have been calculated using all

[1] the definition of structure factors FEQUAT etc... was already given.

the available data in the files (that is, all the data within the resolution range and also the data obtained with high standard deviations). But one can also choose to calculate Patterson or Fourier maps with either a resolution or an $F/\sigma F$ cutoff in order to improve the map quality. For instance, high resolution terms in Fourier synthesis introduce higher harmonic components in the summation, that is, if these terms are randomly erroneous then a global background is added to the calculated electron density or Patterson function.

The three maps shown in figure VI.26 are difference Pattersons calculated for each collagen derivative, (a) iodine-native difference Patterson, (b) gold-native difference Patterson and (c) the PEG-Native derivative that is used as control. The black zones in the maps indicate the maxima in the difference Patterson function and are represented on an 8 level grey scale.

The calculated maps (figure VI.26 & VI.27) have each a continuous level in the difference Patterson function that shows some strong peaks at different positions. In order to visualise these peaks, the continuous background has been estimated in the regions where there was no peaks and then subtracted so that only the strongest peaks are retained. The high level peaks in the c=0 plane, observed in iodine and gold derivatives are the usual peaks at the origin of Patterson maps that correspond to atom↔atom auto correlation functions. On the other hand the strong peak at the origin in the PEG-Native calculated map is obviously weaker then the ones in the heavy atoms derivatives , gold and iodine. This result, however, was expected since first, PEG added collagen does not contain heavy atoms [1] so that heavy - atom ↔ heavy - atom auto correlated peaks are entirely absent, and second the subtraction in the PEG-Native difference Patterson calculation has removed the major contribution of protein↔protein vectors to the central peak.

Iodine and PEG difference maps do not show discernible peaks in the volume represented in figures VI.26 (a) and (c) but more or less flattened peaks that are nearly parallel to the *ab* plane at different c-axis levels. Whereas the Gold-Native difference Patterson map shown in figure VI.26(b) exhibit such peaks. Considering the low resolution in the a and b direction that we have already demonstrated, the flattened peaks we observe in the Iodine and PEG difference Pattersons thus correspond to well resolved peaks in the c-direction but badly resolved peaks in the two other directions.

2. A Preliminary Fourier Calculation

In the previous paragraph, the difference Patterson maps were calculated for each derivative to see if the heavy atoms give actual contribution to them. However, difference Patterson maps usually provide the mean to find heavy atoms positions if one knows that there are a few of them in the structure. In that case the search for heavy atom position is done by hand or using automatic peak

---

[1] e.g. atoms with high Z number (see also the equation defining the heavy atom contribution to the structure factor relative differences in Paragraph C

search programs. Nevertheless, we are in the presence of a structure where one knows little about the heavy atoms number and occupancy in the unit cell. Therefore, I have built a set of 4 reasonably modelled structures of collagen like molecules in chapter 7 in order to gain an additional source of material. These models were originally constructed for the simulation of fibre diffraction patterns and will later on be demonstrated to fit the experimental patterns, but they differ in that the molecular arrangement in the unit cell was different. These models have enabled me to calculate structure factors and phases and the data so obtained were then merged and combined with the experimental data. Hence, I will use these data to calculate Fourier maps using the phases of one of the modelled structure (the so called C135 and the control model FCRAND) and the experimental structure factors I have gathered. Furthermore I will presume that the model structure is a good approximation of the native structure and thus the calculated phases are a rough guess of the realistic ones. Then, I have calculated Fourier maps for each derivative. The calculated maps are shown in figure VI.28, VI.29 and VI.30 these should in principle show strong peaks corresponding to the heavy atoms positions. I have made use of the fact that phases in Fourier calculations need not necessarily to be very precise. The following maps are thus a preliminary attempt to find heavy atom positions for the collagen derivatives.

Figure VI.28 shows the calculated map for the iodine derivative. The map on the left (a) is the one obtained with phases calculated from the FCRAND model defined above. This map displays some blackened peaks at c≈0.5 that are weaker in the map (b) on the right. The continuous background in the map has been removed using the procedure used in figures VI.27. One thus might assign these highest electron density peaks in the map to iodine atoms (or cluster of iodine atoms). One also knows that the model molecule ends up in that region, particularly with the C135 model in (b). The molecular end might however introduce some unusual behaviour in the Fourier synthesis since the electron density has a steep change to zero in that region. The figure VI.29 in turn shows the maps calculated with the gold experimental data. Both maps display a set of peaks in the unit cell volume which might correspond to gold atoms in the structure. Finally I show in figure VI.30 the maps calculated with the PEG experimental structure factors. None of these maps shows discernible discrete peaks as the structure does not contain any heavy atoms.

As I have already stated, I have calculated these Fourier maps (figure VI28 VI.29 and VI.30) on a trial basis since I have got some original material to start with (experimental structure factors and phases from model structures). The maps were analysed with automatic peak search programs that has provided a list of possible heavy atom site for the structure (data not given here). In conclusion, these maps are to be considered as is until more experimental evidence will be performed.

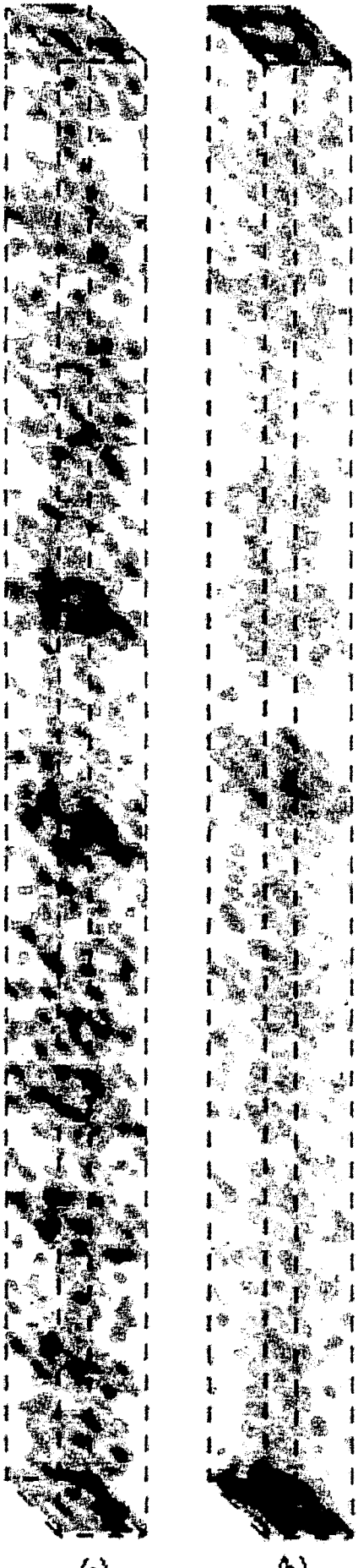

Fig. VI.28 : The phases from the modelled structures were used to calculate Fourier maps using the experimental heavy atoms structure factor amplitudes. (a) is a map calculated using iodine experimental structure factors and phases from the collagen model with atoms randomly displaced in the unit cell; (b) is a calculated map using iodine experimental structure factor amplitudes and the phases calculated with the C135 model. The volume shown represents the whole triclinic unit cell with the c axis vertical and the a axis in the plane of the paper. The resolution in each direction of the unit cell vectors is the same as in figure VI.27.

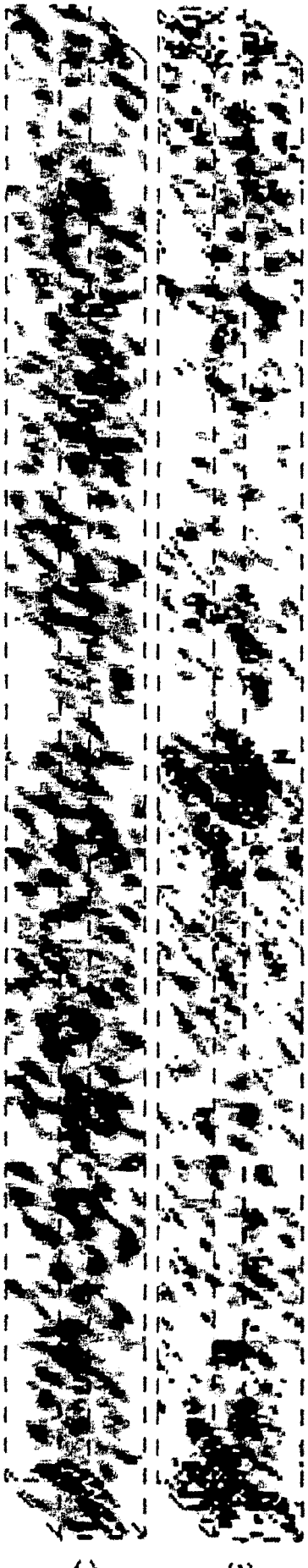

Fig. VI.29: (left) Here I show the calculated Fourier maps using the model phases and the experimental structure factors amplitudes. (c) is a map calculated using gold derivative experimental structure factors and phases from the collagen model with atoms randomly distributed in the unit cell; (d) is a calculated map using gold experimental structure factor amplitudes and the phases calculated with the C135 model. The volume shown is one unit cell.

Fig. VI.30 : (right) Finally, I show here the calculated Fourier maps for the PEG derivative: (e) is a map calculated using PEG experimental structure factors and phases from the collagen model with atoms randomly distributed in the unit cell; (f) is a calculated map using PEG experimental structure factor amplitudes and the phases calculated with the C135 model.

Chapter 7

Molecular Modelling and Computer Simulation of Collagen Fibre Diffraction Patterns

In this chapter I present the results of a computer built model of collagen molecules packed like in tendon that I have constructed from a template of a collagen triple-helical fragment found in the Brookhaven Protein Data Bank. A set of fibre diffraction patterns for the crystalline domains were then calculated for the unit cell and for different orientations of the molecule in the unit cell. This was done using the molecular modelling and data analysis packages available at the ESRF and yielded results which sustain the crystalline quality of tendon fibres.

A. $(Gly\text{-}Pro\text{-}HyPro)_n$ Sequence as a Triple-helical Model for Collagen Molecule.

An energy minimised 3-D structure of collagen molecular template was constructed by Chen et al (Chen *et.al.*, 1991), using molecular modelling methods and Kollman force fields. For this model, Chen constructed individual molecules with three identical polypeptide chains. The sequences used were a $(Gly\text{-}Pro\text{-}Pro)_{16}$, a $(Gly\text{-}Pro\text{-}Hyp)_{16}$ and a $(Gly\text{-}Ala\text{-}Ala)_{16}$, coiled into a right-handed triple-helical structure. The axial distance between adjacent amino acid residues is about 2.9Å per polypeptide chain, and the pitch of each chain is approximately 3.3 residues. These data were deposited in the PDB data bank and were retrieved from there for the purpose of model building and fibre diffraction pattern calculation.

I have chosen the $(Gly\text{-}Pro\text{-}Hyp)_{16}$ fragment because of the high content of collagen molecules of both Pro and HyPro residues since HyPro is known to stabilise collagen molecules in tendon. The fragment taken as is from the PDB has a length of ≈100Å and thus I replicated this fragment to construct the full 3000Å length model molecule. The collagen molecule in tendon is thought to have a rod shape with diameter 10-14Å and an approximate length of 4.4xD ≈3000Å. Thus, a straight molecule of the triple helical (Gly-Pro-Hyp) pattern was produced and it was then placed in a triclinic unit cell for the calculation of fibre diffraction patterns. The position and orientation of the molecule in the unit cell will be thought about later in this chapter since the exact packing of collagen crystalline domains depends on the fractional coordinates of the collagen segments in the unit cell.

B. Relevance of the Model

1. Sequence Restriction

It is obvious that the aminoacid composition and sequence in the presently prevailing model is not realistic for biochemical considerations but for the purpose of low-resolution diffraction studies it is a suitable model. The model molecule has an electron density distribution which is a rough approximation of the real one where the absence of other amino acids results in the absence of bulky

side chains. Tendon crystals also contain water molecules in the intermolecular space in addition to other substances like the carbohydrates. The organisation of these substances however is not thought to comply with any crystallographic symmetries and can be modelled by a flat homogenous electron density. There is also an additional periodicity in the Gly-Pro-HyPro sequence repeat that also restrains our representation to a simplistic model.

2. Molecular Shape

The molecular shape of native collagen molecules in tendon is not yet clear. Thus, I assume at present that all molecules in the crystalline domains are rods of straight molecules with dimensions given in the paragraph A. These molecules however, are the basic structural units and consequently all the models of packing in the unit cell have to be consistent with the wholeness of this unit (e.g. the segments arrangement in the unit cell must ensure first, the wholeness of one molecule when crystal translations are applied and second, the connectivity between molecules lying within neighbouring unit cells).

3. Thermal Motion and Molecular Disorder

Both these effects can be thought about for the X-ray diffraction calculations but these are not the subject of the study during this work. The first thermal effect can be calculated by applying a classical thermal B factor for each atom or atom groups in the model molecule whereas the second can be calculated using the appropriate random disorder effects.

4. Domains Disorientation and Crystallites Size Effects

These two important effects were mostly covered in the simulation of fibre diffraction patterns I have carried with the collagen model I have built. The complexity of the diffraction patterns obtained with fibrous materials is principally due to these two effects so that a computer simulation including these two effects is necessary for understanding the fibre diffraction patterns. The domains disorientation result is usually an arcing of the diffraction spots and was already estimated for collagen fibres to 1° or 2° . During the film processing carried in chapter 5 & 6 this has simply required that the integration area to be set in a way to fit the shape and extent of the peaks over the film regions.

Size effects in turn are also important since strong peak overlap may occur especially in the case of crystals with large c-axis. Furthermore it has been given in chapter 4 that the Bragg spots in a diffraction experiment with fibrous samples are broadened according to the Scherrer law $B(2\theta) \approx \lambda/L\cos\theta$, where L is the average crystallite size in the direction defined by the plane hkl. The Sherrer formula was derived for a powder diffraction pattern but it also holds for fibre diffraction patterns. The X-ray patterns simulations done in this chapter will be carried assuming average crystal sizes of respectively 1μ in the direction parallel to the fibre axis and 0.2μ x0.2μ in the section perpendicular to it. However, different values for the average crystal sizes will be tried in order to characterise the effects on the X-ray patterns. The above values, obtained one experimentally (along

the c axis) in the present work and from previous electron microscopy studies will be shown to fit at best the experimental patterns.

C. Molecular Orientation in the Triclinic Unit Cell

A detailed model for the molecular packing in the crystalline regions of collagen fibrils was first proposed by Miller & Parry (1973). Based on helical assemblies of collagen molecules in the form of a five-stranded rope (Smith,1968), the model was termed a microfibril, packed on a near-tetragonal lattice. Later, an alternative model based on straight collagen molecules packed in a triclinic unit cell was proposed by Hulmes & Miller (1979) and this model is presently the most agreeing with experimental data (chapter 3). In the current construct, the unit cell has dimensions a=39Å, b=26Å,

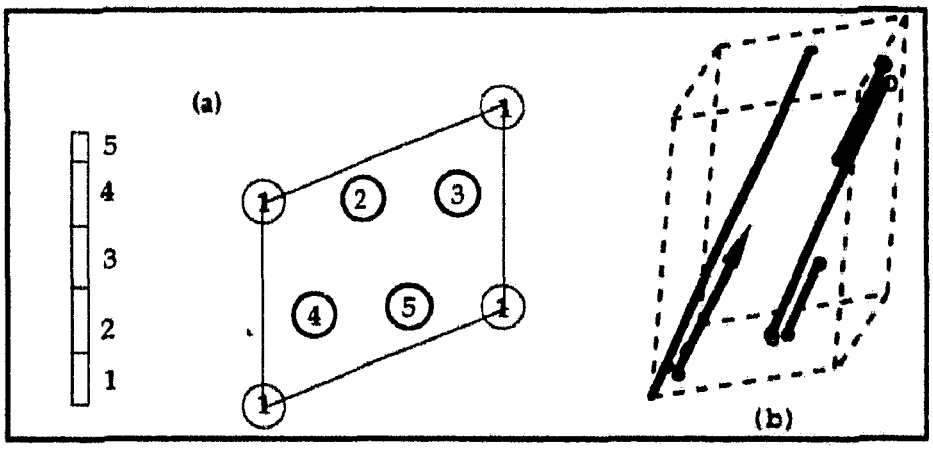

Fig. VII.1: (a) (after Miller, 1981) A collagen molecule is schematically represented by a rod divided into 5 segments labelled 1-5. Viewed in a cross section, the unit cell has thus five possible positions that define the asymmetric unit.
(b) One unit cell contains one collagen molecule and crystal 3D translations generate the whole structure by unit cell replication. This figure shows one possible structure for the collagen molecules that is defined with a fixed orientation of the segment 1 relative to the crystallographic unit cell axes. There are thus a lot of possible arrangements and orientations e.g. up and down molecules for the molecular segments 1-5 in the unit cell but this is not yet understood.

c=677Å and contains five segments of one collagen model molecule (figure VII. 1).

The content of one unit cell is thus an entire molecule. One molecule must successively proceed through cell positions 1, 2, 3, 4, 5, 1. . . with increasing z. For positive z, molecules go up and for negative z, molecules go down. The molecular path can thus be defined by looking at the intercepts of one molecule starting at an arbitrary position in the z=0 plane, with the plane z=5. These intercepts have been demonstrated (Fraser *et.al.*, 1983) to be:

(5q+1,5r+3,±5)

(5q+2,5r+1,±5)

(5q+3,5r+4,±5)

(5q+4,5r+2,±5)

where q and r are integers or zero. Considering the above coordinate set, there is a great number of possible orientations but the correct models have to agree with additional experimental observations. For instance, the gap-overlap feature of the EM micrographs and the tilt of collagen molecules relative to the fibre axis.

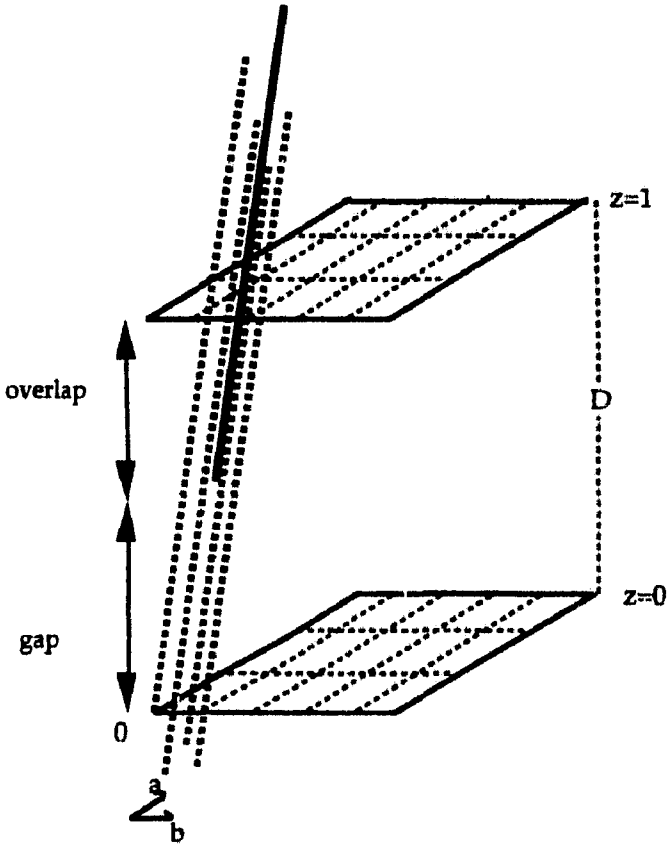

Fig. VII.2: The figures here show a region of the crystal containing 12 unit cells. The collagen molecules are thought to be bunches of parallel molecules. Only the content of one unit cell is shown for simplicity. One collagen molecule in a bunch of five molecules is shifted vertically by ≈D to give the gap-overlap banding pattern observed under electron microscope. Now if the molecules are slightly tilted to the c-axis (figure on the left) then the gap-overlap feature is normally observed. Whereas the figure below shows molecules strongly tilted to the ab plane. The ratio of gap to overlap is consequently lower than 0.4D.

The figure on the next page shows how collagen crystals were constructed using one single collagen molecule that has been replicated to generate the whole crystal. The model shown is the so called C135 collagen-like packing that I have defined in the text. One collagen molecule is represented by a thick arrow and a region of unit cells of the crystal neighbouring this collagen molecule are shown up to z=5. The other collagen molecules are hidden for the moment for clarity. The three common axis a, b and c of the triclinic unit cell and the orientation of these relative to the fibre axis are also not to scale for the moment. Hence, the molecule has it's origin at (0,0,0) (c) and it points toward a direction parallel to the direction (1,3,5) indicated by the dashed line. The molecule has thus intercepts with the different planes of the successive unit cells and portions of it that belongs to different unit cells. The different portions of the molecules are then brought into the

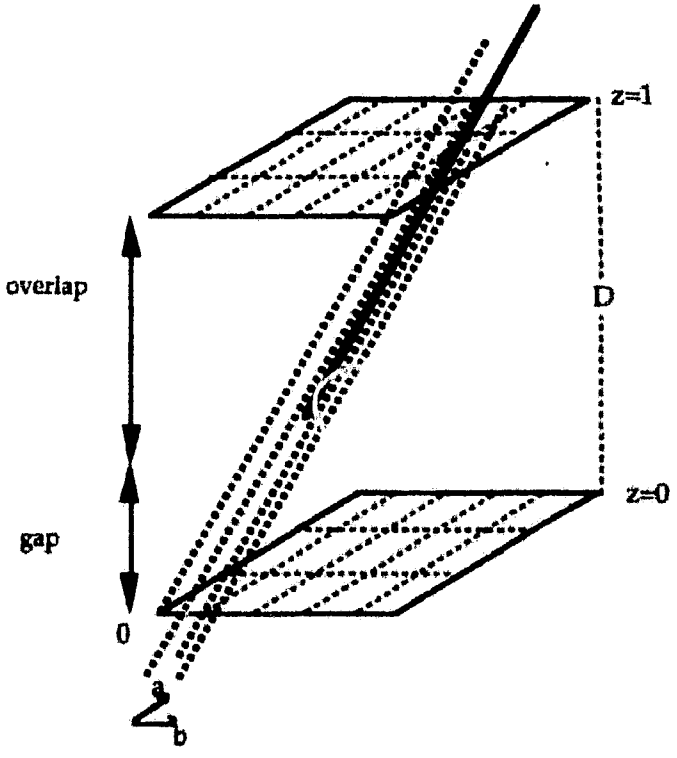

original one which was equivalent to a mathematical projection of the fractional coordinates into one single unit cell. The figure (d) shows such a projection for three consecutive unit cells. The small circles indicate the ends of each portion of the one molecule that is contained in the unit cell. A demonstration of how the gap-overlap feature of this packing is obtained will be shown later in this chapter, however, this method was used in the subsequent computer generated models of different molecular packing of collagen in tendon .

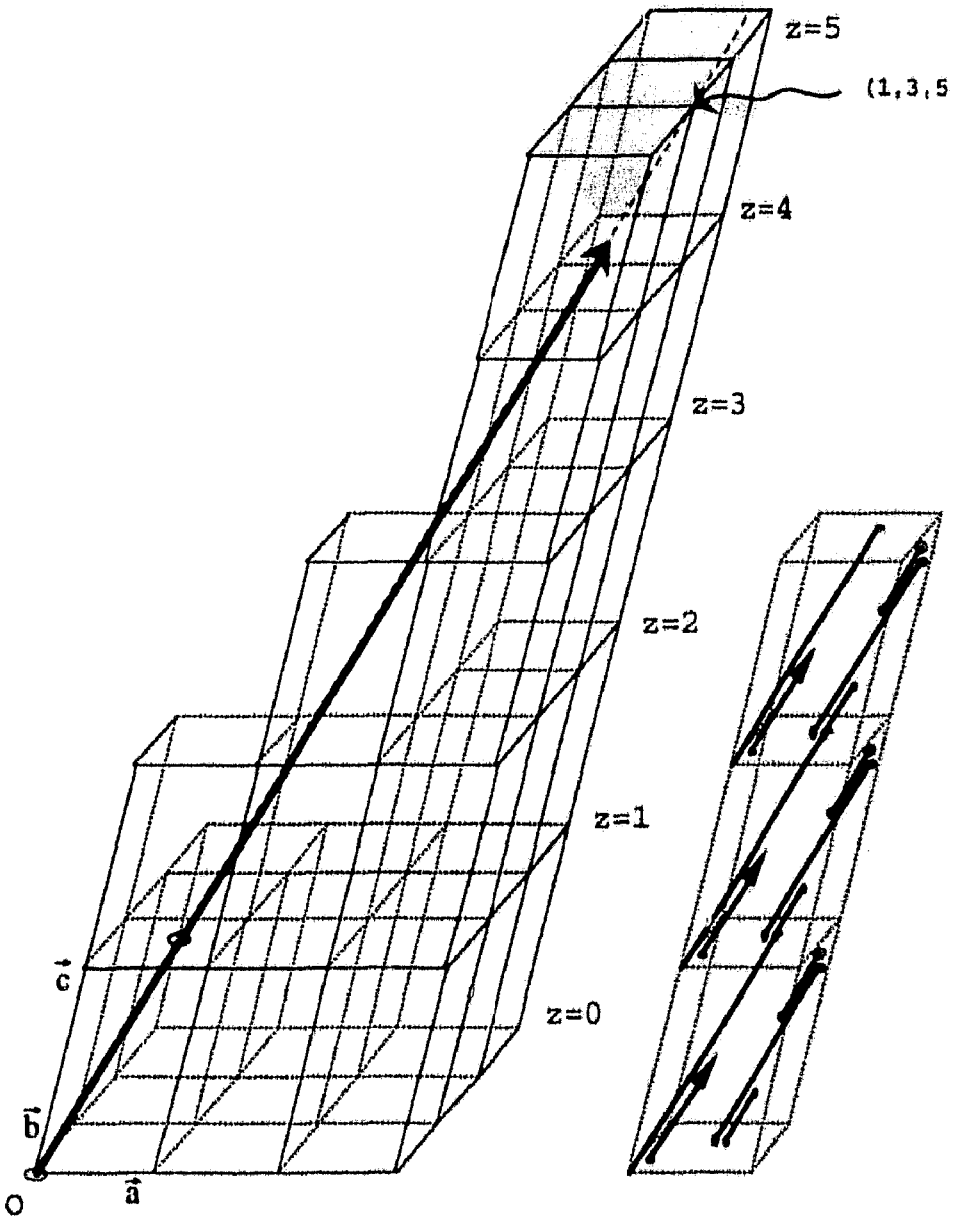

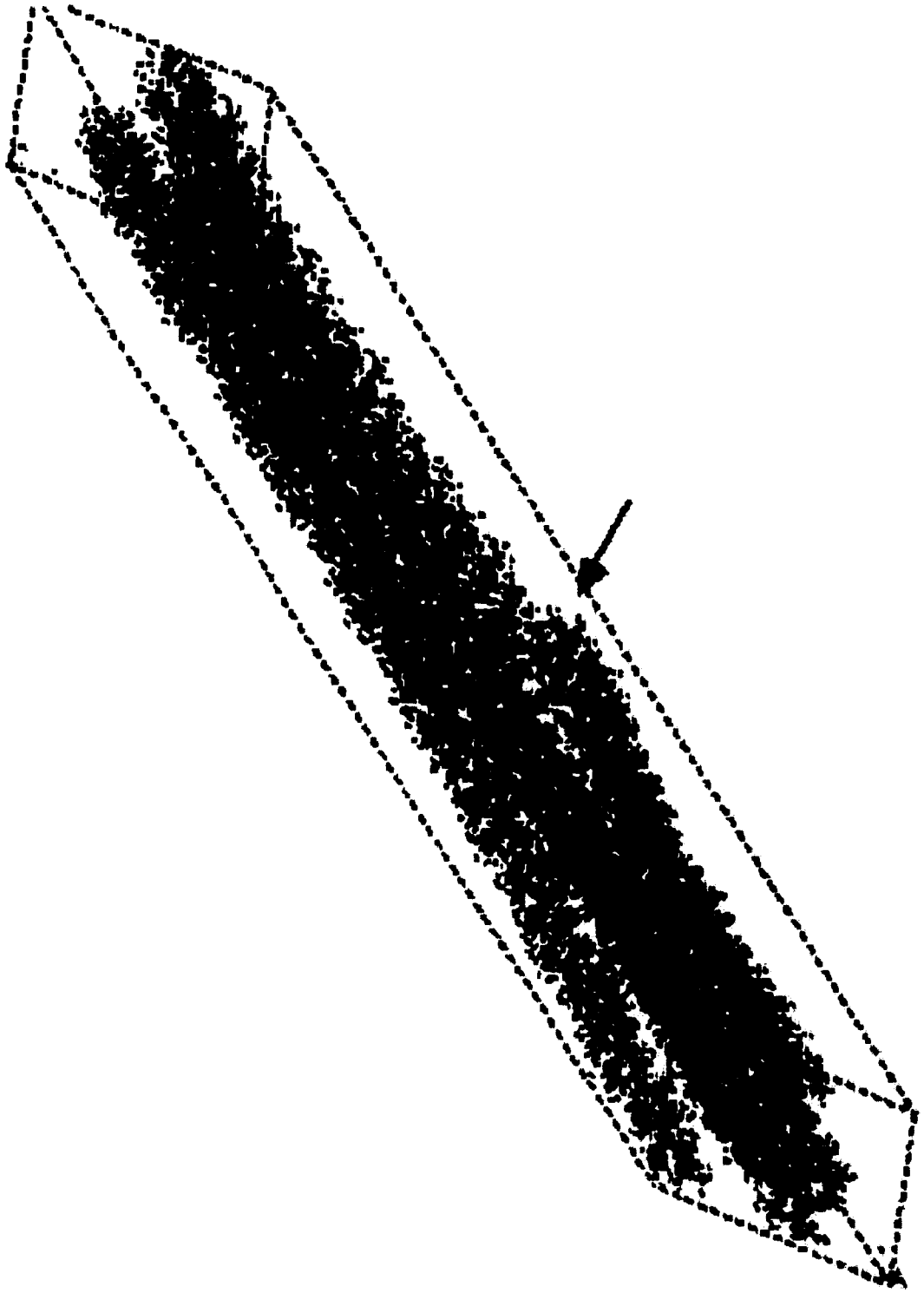

Fig. VII.3 : In the figure here I show the constructed C135 model I have defined in the text. The ~3000Å length triple-helical collagen template was first aligned parallel to a specific direction defined by the integers q=0, r=0 and then the coordinates were projected into the triclinic unit cell. The arrow indicates the position of one end of the molecule where the gap between consecutive molecules occurs.

Thus for large q or r values, the collagen molecules are too much inclined to the *ab* plane in the fibrils and consequently the gap-overlap ratio is ≠0.4D. Consequently, only low values for q and r are

MANQUE PAGE 155

2) for q=r=-1, molecules oriented down, this gives the coordinates (-4,-2,-5) of the intercept with molecules quasi-parallel to the c-axis. The model will be designated C-4-2-5.

3) for q=r=1, molecules oriented up, the coordinates of the intercept with the z=5 level are (8,6,5) with molecules significantly tilted to the *ab* plane. This model will be designated C685.

4) finally I have built a model with the C135 one but where atoms have been displaced by random amounts to generate a crystal with random distributed atoms in the unit cell. The model so obtained is not a realistic one but however it has the following advantages: first, the helical symmetry e.g. the helix periodicity is lost so that we can validate the triple-helical feature of the secondary structure of collagen molecules; second the model has enabled me to calculate a set of structure factors and phases to serve as a starting model for the experimental Fouriers calculated in chapter 6.

D. Results of Molecular Modelling and Computer Simulation of Fibre Diffraction Patterns

The four above defined models have been written to the standard PDB files after projection into the unit cell and were also used in the following fibre diffraction simulation. The pattern simulation were done using the Cerius software available at the ESRF. The rod like model molecule was first aligned parallel to the special directions in crystal space defined in the previous paragraph and then the coordinates transformed into the fractional coordinates in the unit cell. The fft routine of the CCP4 suite was then used to calculate the structure factors and phases for each model. Then a fibre diffraction pattern was simulated for each model and I show the patterns below. Additional sample characteristics can be simulated such as fibre orientation in the beam and average crystallite size in the sample. Thermal and disorder factors however were neglected as already stated because I was only looking for low resolution features in the simulated X-ray patterns. Figure VII.3 shows a simulated pattern calculated with the C135 model. The simulated pattern shows the typical features observed in experimental films such as the meridional reflections, the two prominent row lines and the helix layer-line reflections. The equatorial data are also identical to the experimental ones in that one obtain a continuous intensity distribution due to small crystallites with some off equatorial spots. The computation of the pattern shown in figure VII.3 was done with a fibre tilted to the X-ray primary beam by 3° and the crystalline size of the ordered domains was 1μm x 0.2 μm x 0.2 μm. The polar disorientation of the fibrils was approximated to 1° but higher polar disorder was introduced that produced an important arcing of the reflections. Other parameters involved in the fibre geometry were also simulated and the results are shown in the following figures. The simulated patterns are represented by one quarter of the X-ray film each for simplicity. The intensity levels are shown as intensity contours and the fibre parameters when changed are listed in the caption of each figure.

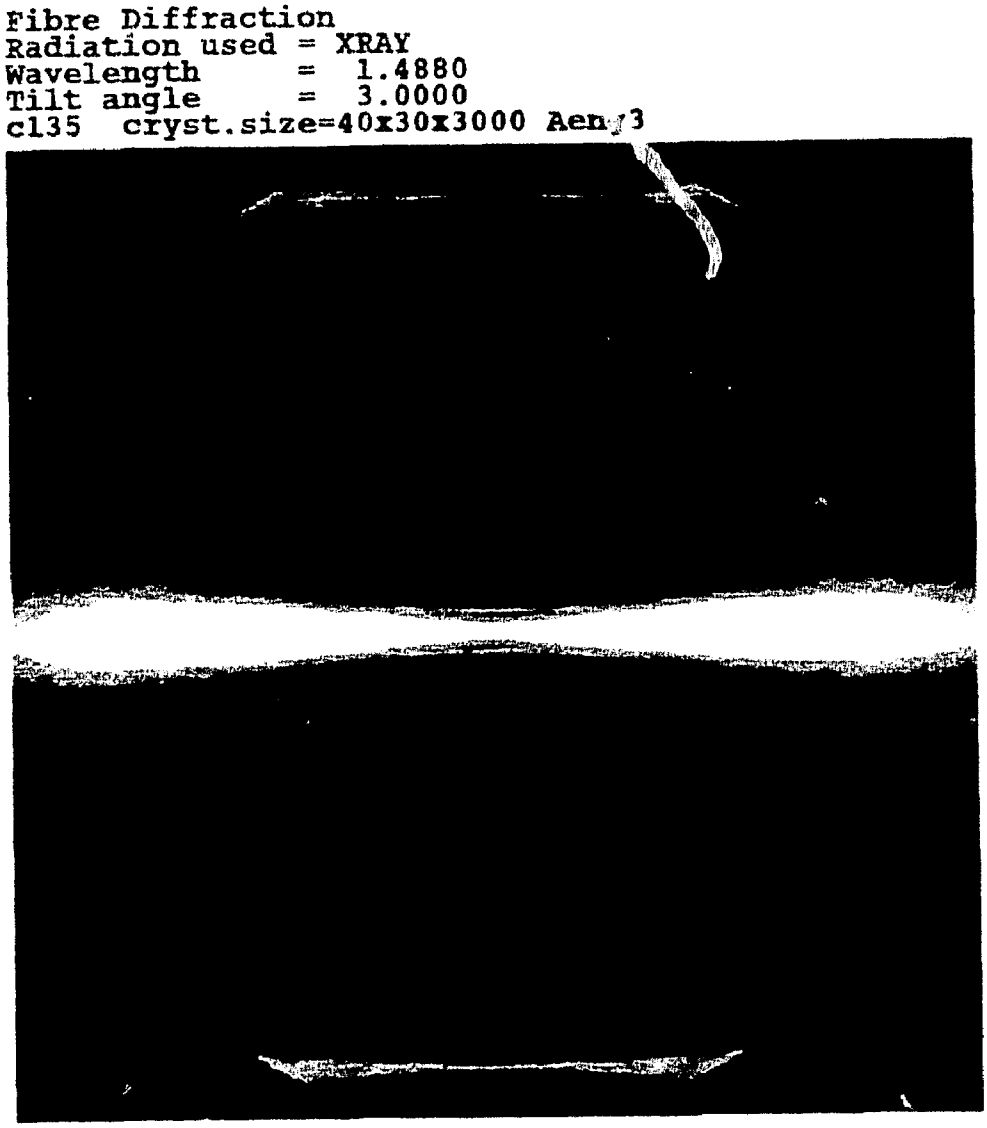

Fig. VII.5 : The high continuous intensity background on the equator and the helix layer-line is due to small crystallites in the sample as I show it in this figure. The simulated average crystalline size is here supposed to be 40 x 30 x 3000 $Å^3$, that is the crystalline domains are composed by a few number of collagen molecules where these domains are in turn randomly oriented around the fibre axis. Consequently, the actual diffraction pattern is the superposition of the intensity contribution from well ordered domains (Bragg spots) and the continuous diffuse scattering from less ordered domains that is shown here.

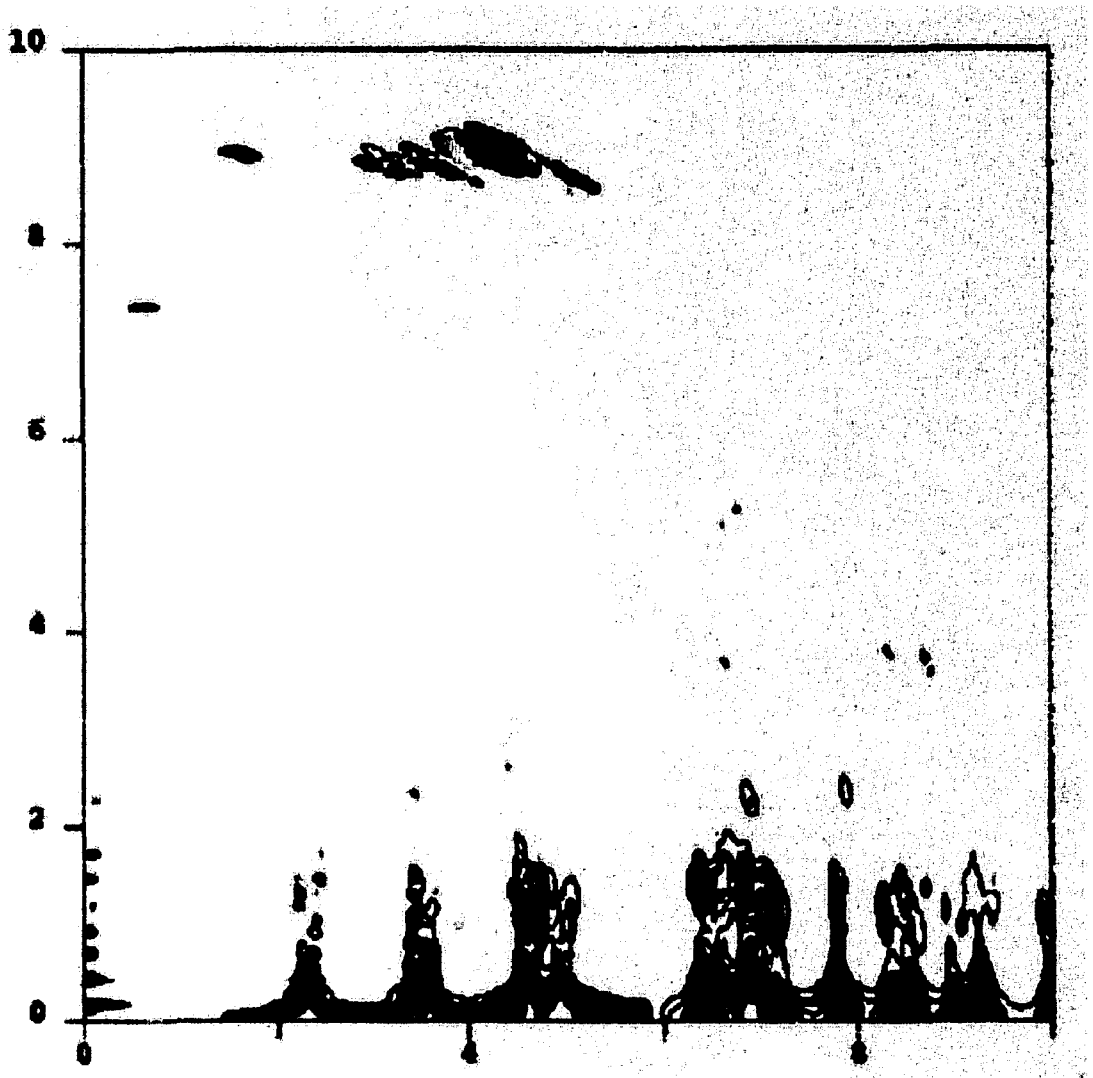

Fig. VII.6: The simulated X-ray diffraction pattern I show here is for the C135 model. The fibre is tilted by 3° to the direct beam and the fibrils have about 1° polar disorientation. The crystallites average size is 0.2μ x 0.2μ x 2.0μ which is consistent with the present study and previous electron microscopic studies. The strong intensity between the equatorial reflections is due to small crystallites that are present in the fibre whereas the arcing of the reflections on the helix layer-line is principally due to the Ewald sphere curvature and the polar disorientation of the domains. The additional strong reflections on the equator that usually are not observed in the experimental collagen diffraction patterns but these can be explained by the fact that I have built a model that diffracts well at higher resolution and also by the fact that the model molecule I have built has a radius which is smaller then the realistic one due to the absence of bulky side chains.

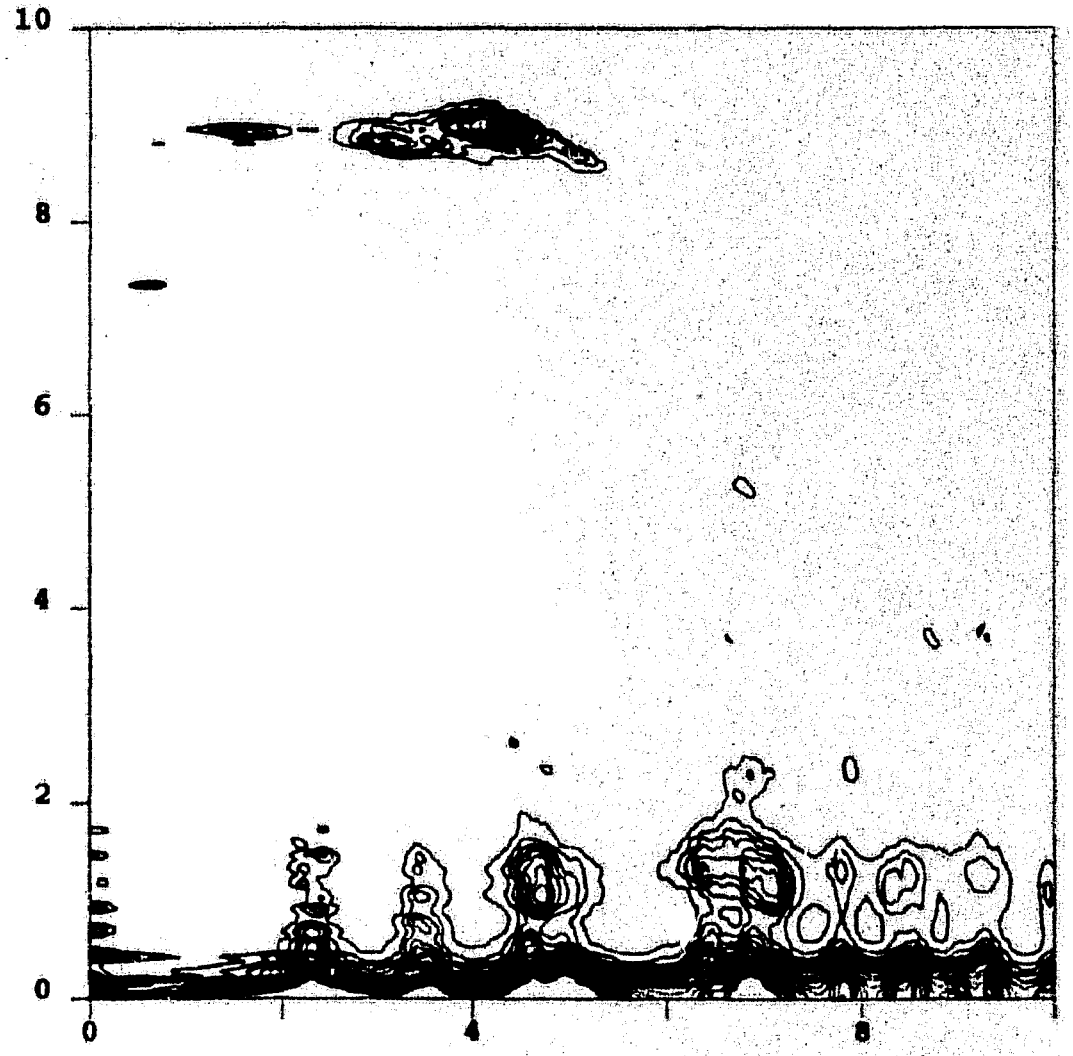

Fig. VII.7 : Here the pattern of the C135 model is simulated for a fibre tilted by 3° to the direct beam but where the crystallites average size is now smaller (0.05μ x 0.05μ x0.5μ). Thus one observes a broadening of the Bragg reflections and a stronger continuous intensity on the equator and the helix-layer line. The fibrils polar disorientation is 1°.

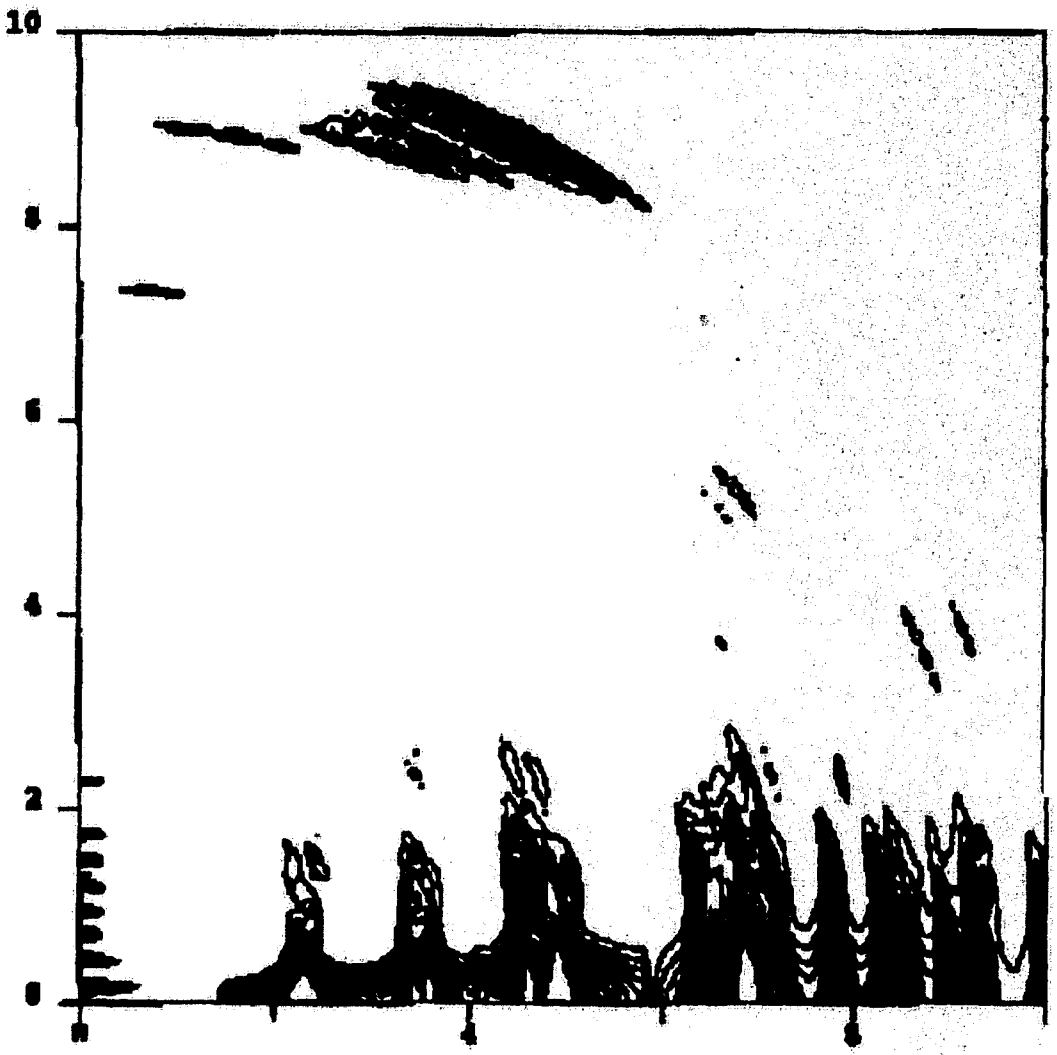

Fig. VII.8 : Here I show a simulated X-ray diffraction pattern with the C135 model where now domains polar disorientation results in an extended arcing of the reflections. The fibrils disorientation is 3° which is obviously not a realistic value in comparison to the experimental observations.

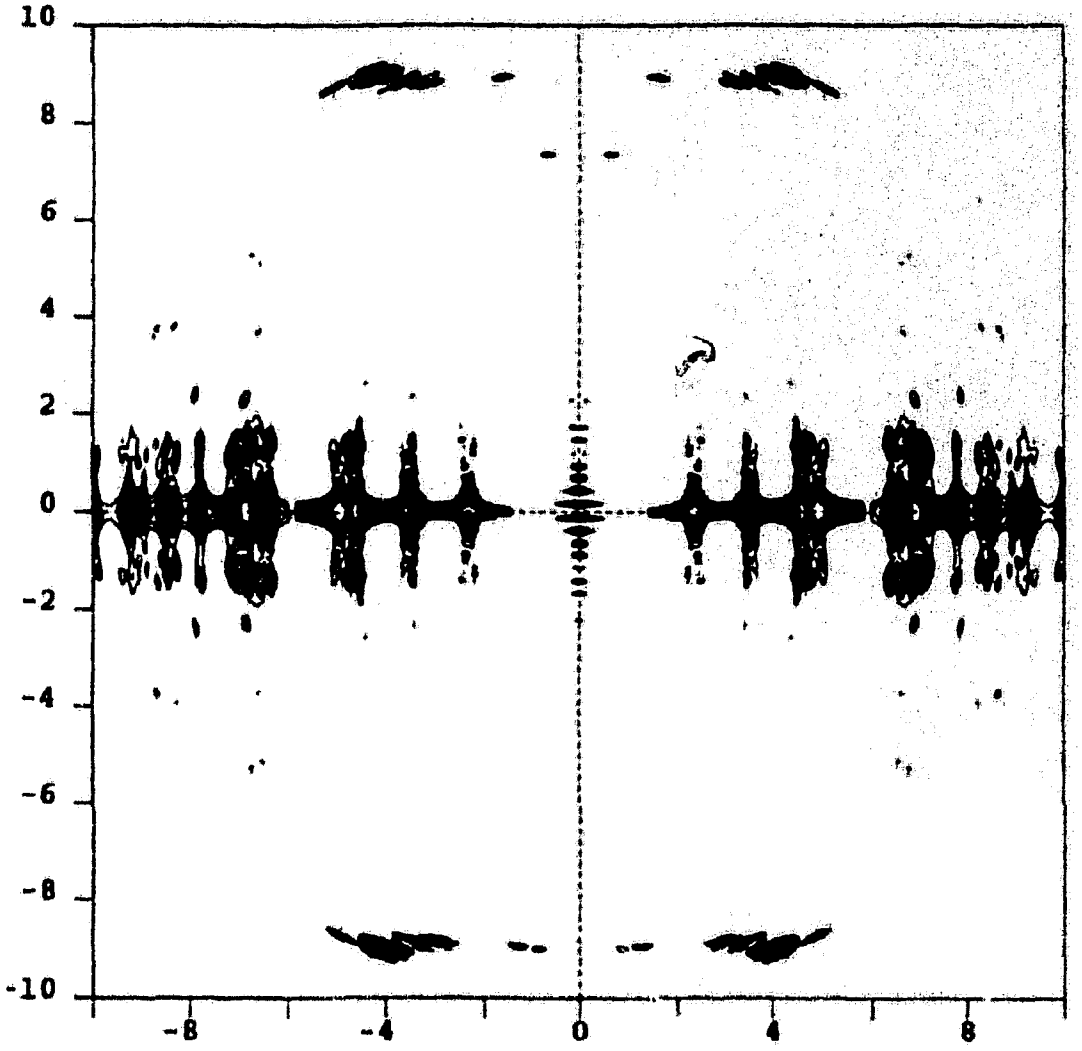

Fig. VII.9: This figure shows a whole diffraction pattern calculated for the C135 model. The fibrils polar disorientation is 1° and the domains average size is 0.2 x 0.2 x 1.0 μ^3. One principally recognises the resemblance with the experimental fibre diffraction patterns and especially the presence of helix layer-line reflections.

Fig. VII.10 : The unit cell content for the C685 model is shown here in a perspective view. The unit cell thus contains one molecule that has been first aligned parallel to the direction defined by q=1 , r=1 and then the atomic coordinates have been projected into the unit cell. One whole molecule is thus obtained when crystal translations are applied and generate bundles of staggered molecules.

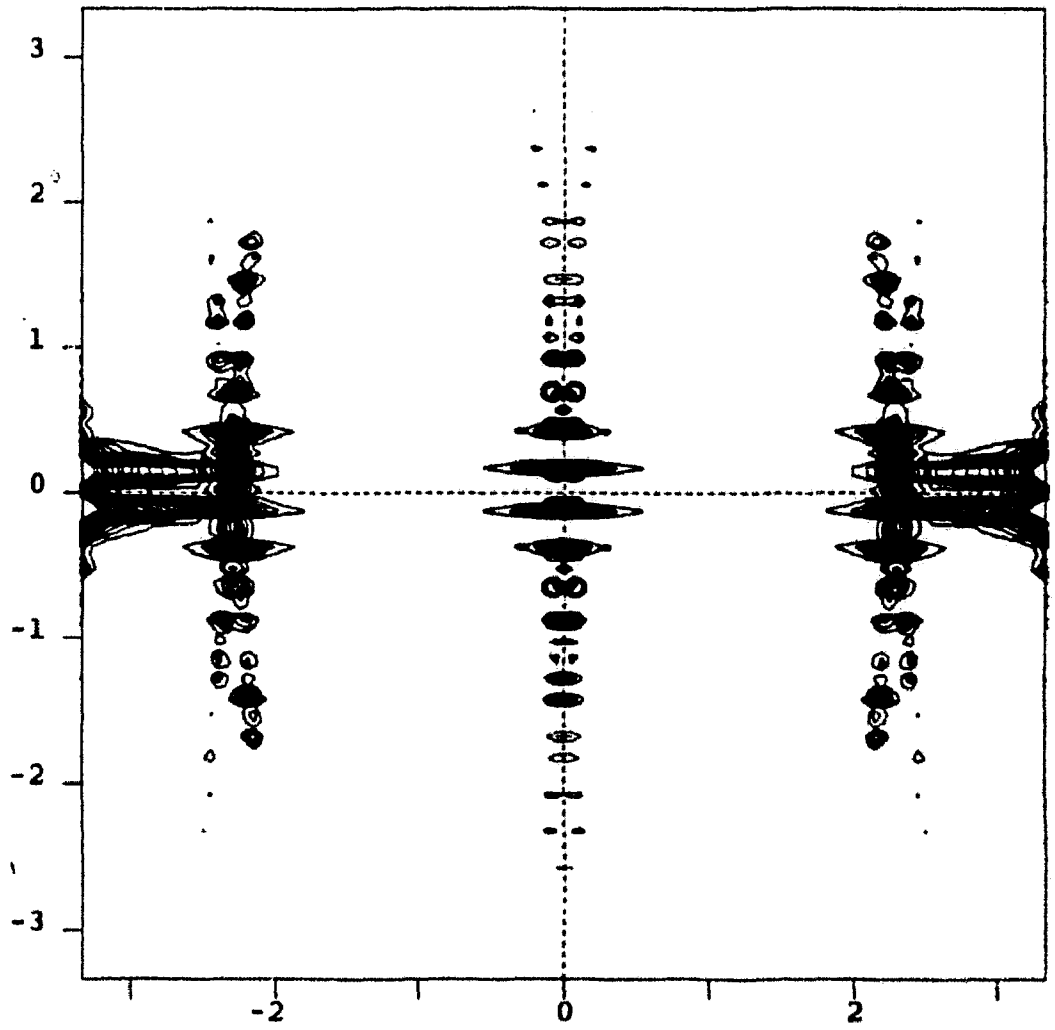

Fig. VII.11: This figure shows the central part, i.e. the meridional low angle orders and the first row-lines with $|l| \leq 30$, of the diffraction pattern calculated with the C685 model. The fibrils polar disorientation is 1° and the domains average size is 0.2 x 0.2 x 1.0 μ^3 . The figure shows that off-equatorial reflections are obtainable provided there is weak peak overlap.

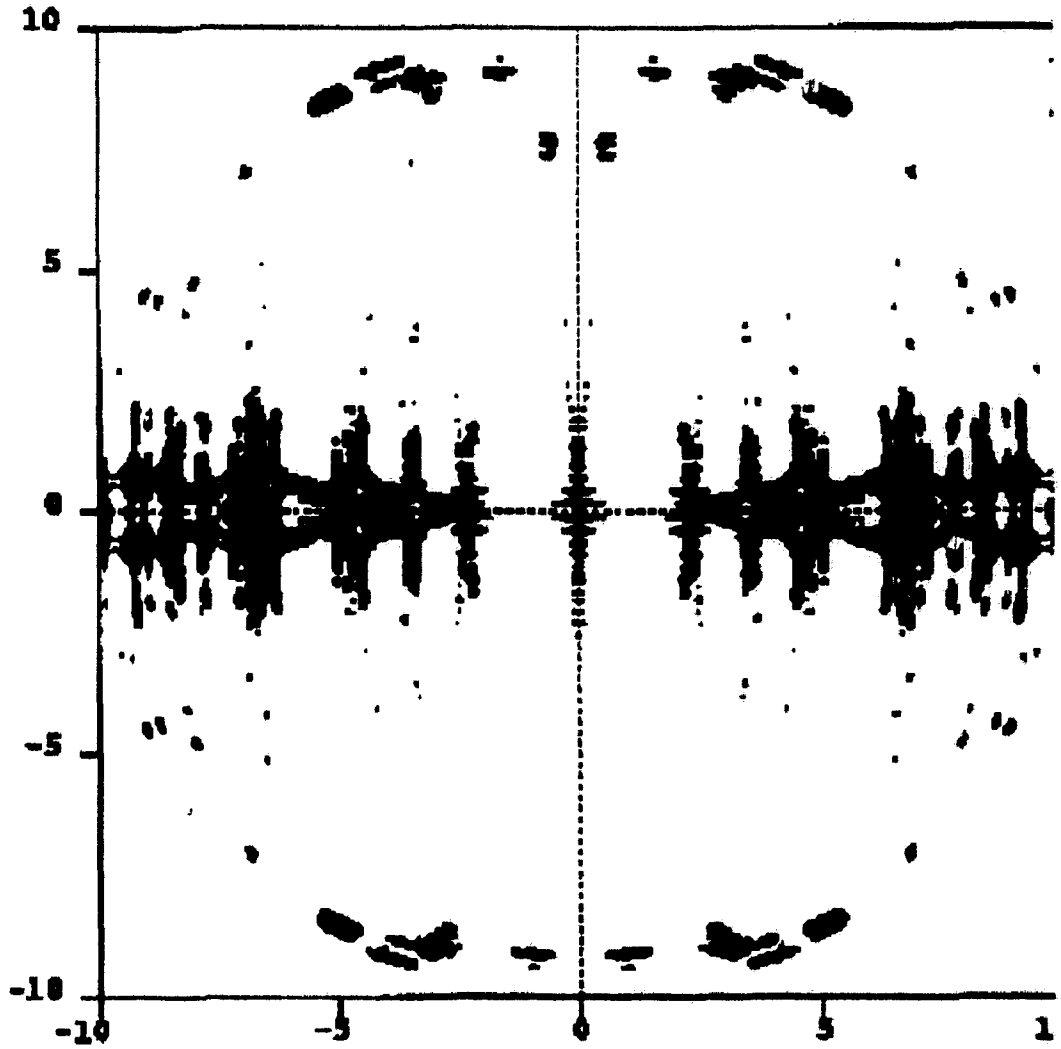

Fig. VII.12: A whole diffraction pattern calculated with the C685 model. Fibrils polar disorientation is 1° and the domains average size is 0.2 x 0.2 x 1.0 μ^3.

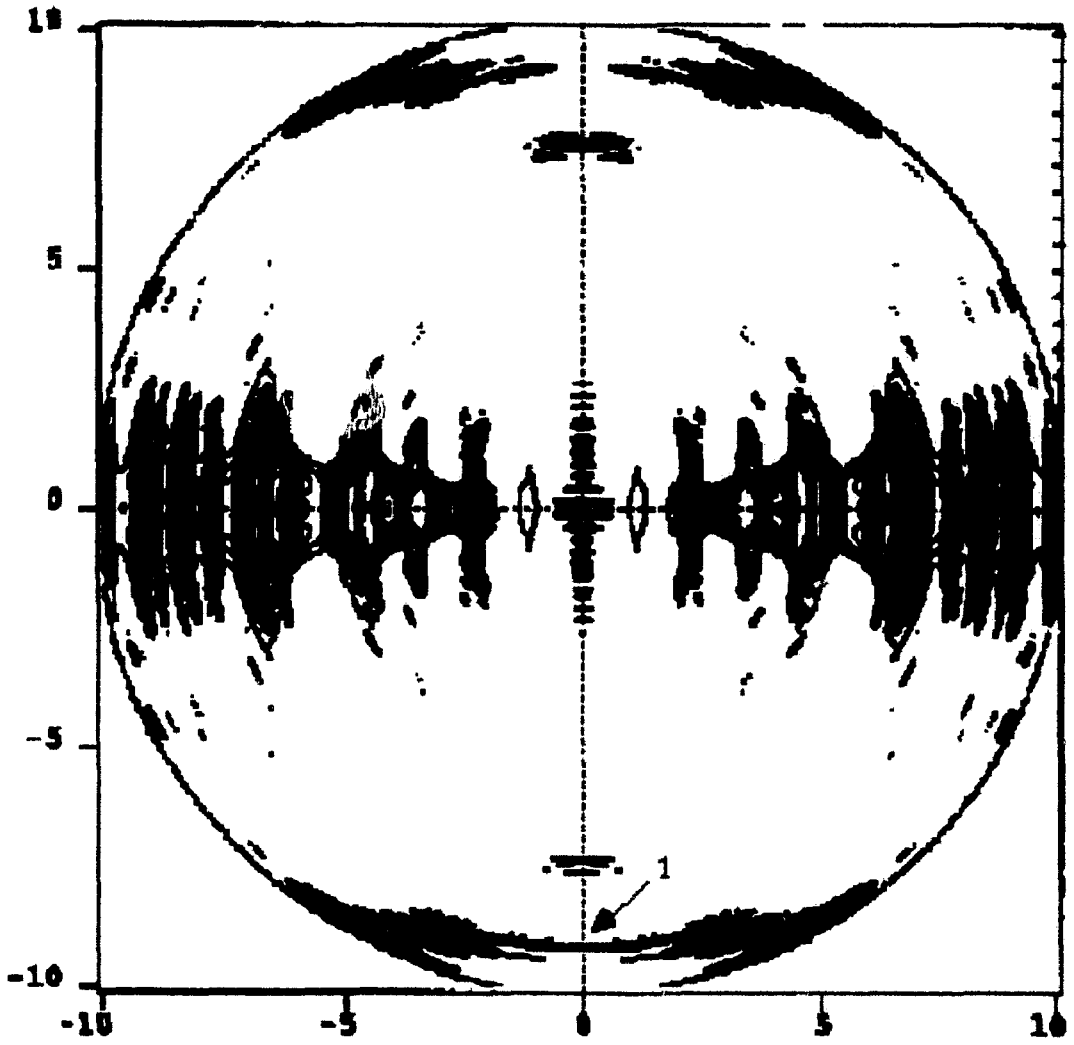

Fig. VII.13: One of the most important parameter in a fibre diffraction experiment is the average domains polar disorientation because it produces an arcing and consequently an overlap of the Bragg reflections that precludes their integration. The figure here shows such a situation with the whole diffraction pattern calculated for the C685 model. The fibrils now have higher polar disorientation ≈3° that results in an extensive arcing of the Bragg spots over the film. The arrow indicates the overlap of the meridional (0,0,l≈75) reflection with the (-1,0,l≈75) reflection.

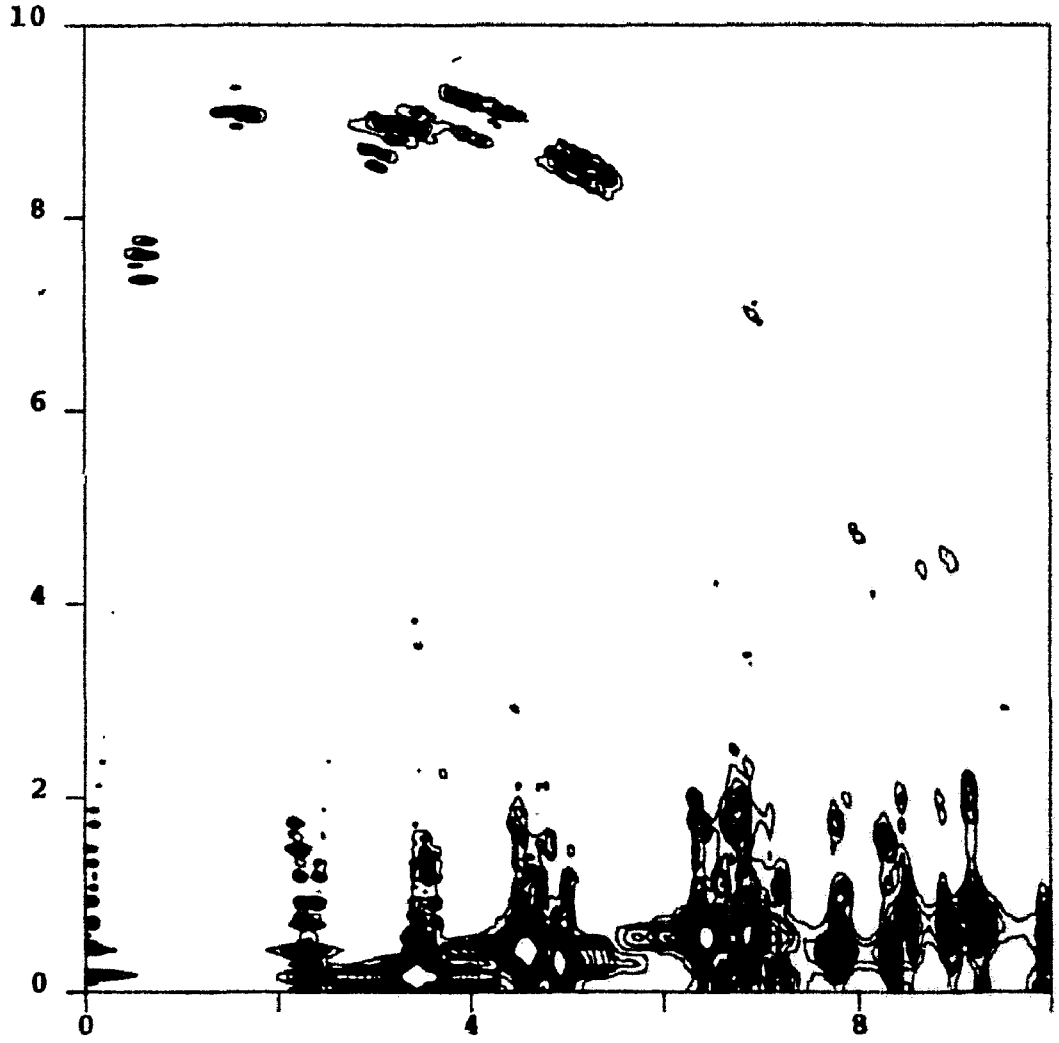

Fig. VII.14: This figure shows one quarter of the diffraction pattern calculated with the C685 model. The fibrils polar disorientation is 1°.

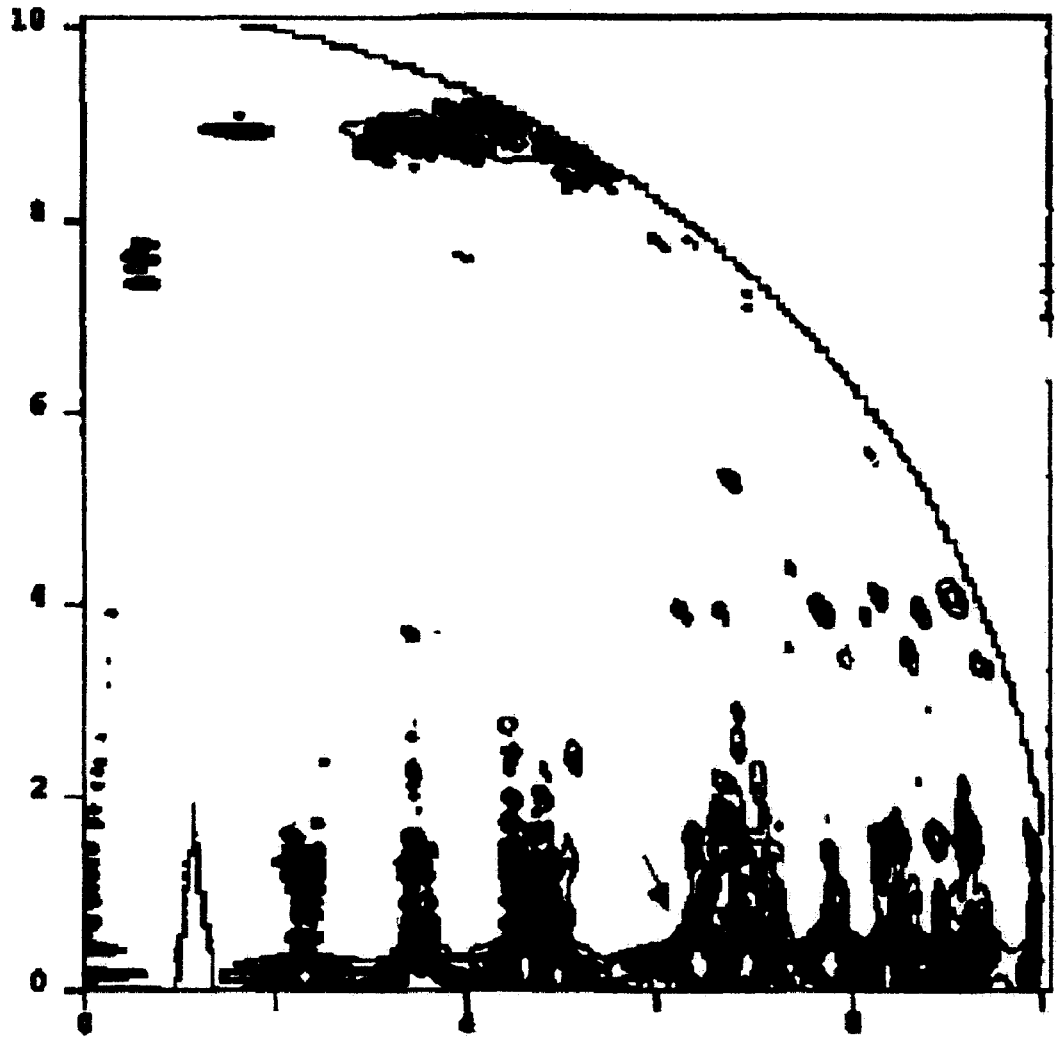

Fig. VII.15: This figure shows the diffraction pattern calculated with the C-4-2-5 model. The fibrils polar disorientation is 1°. The arrow indicates the always observed strong intensities at R≈1/13Å^{-1} that are usually designated by the triplet. Hence, this diffraction feature is the most compatible with the experimental data obtained with native collagen but quantitative structure factor analysis is more suitable to determine the exact nature of the molecular packing in tendon.

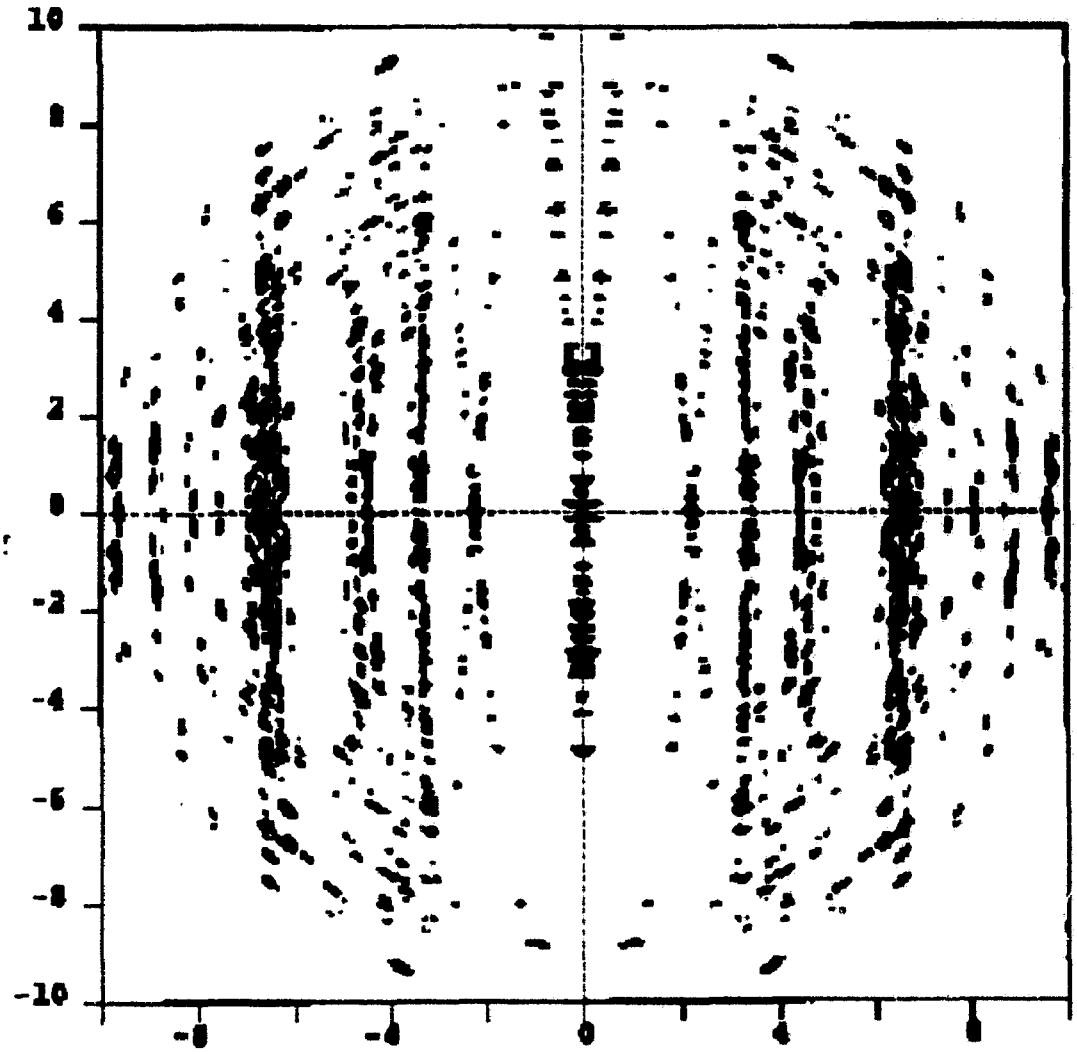

Fig. VII.16: The model with the random distributed atoms in the cell is shown here. Hence, in contrast to the previous patterns, the Bragg spots intensities are now uniformly distributed over the film space.

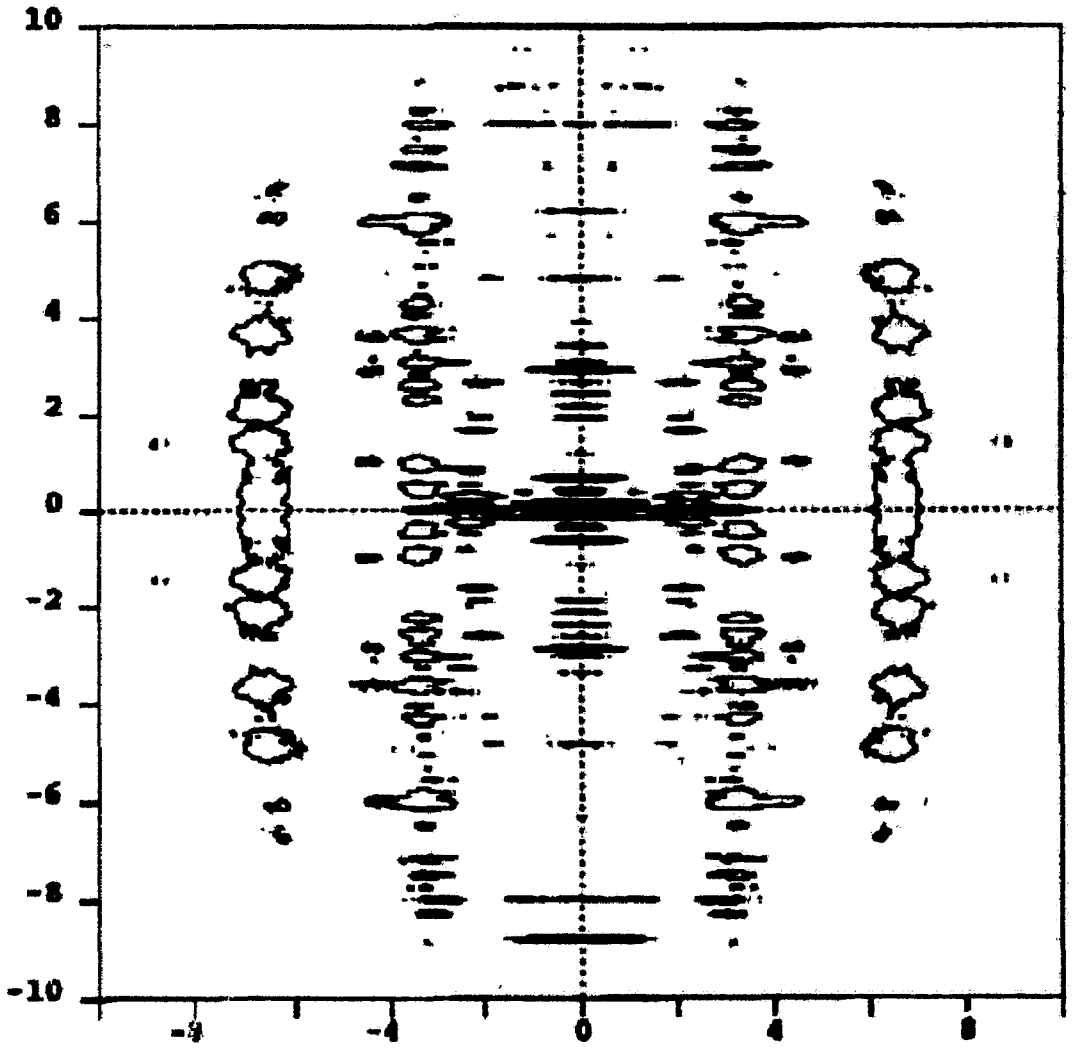

Fig. VII.17: The same random model is shown here with too small crystallites size.

E. Low Resolution Model Data

In addition to the above simulated patterns which in some cases resemble to the experimental films, I have extracted some low-resolution data from the structure factors set calculated with the previous

models. For instance, if one wishes to model a collagen structure with different packing in the unit cell than one have to ensure that the comparison between model structure factors and experimental ones is relevant. Moreover, the meridional and the two prominent row-lines reflections are the most easiest to obtain from the experiments, and has been shown to be accurate enough during this work. These data can thus be used for such a quantitative study. This in turn assumes that the different packing in the unit cell results in a noticeable relative variation of the low resolution data. Thus I present here some results which consist in comparing the relative variation in structure factors amplitudes when different packing are assumed.

In table VII.1 I show the calculated structure factors amplitudes for the 17 first meridional orders. The C135 collagen like model was taken as the reference and the last two columns show the relative difference in structure factors amplitudes when other models are assumed. We see in table VII.1 that the orders 2, 4, 6 etc... are the ones with the highest relative variation in amplitudes. These relative variations are better shown in figure VII. 18

Table VII.1

l	d	F1[1]	F2	F3	ΔF_{21} %	ΔF_{31} %
1	675.70	387	386	385	0.27	0.47
2	337.85	9	21	19	127.13	100.54
3	225.23	127	125	126	1.36	1.15
4	168.93	7	19	17	156.64	130.76
5	135.14	78	75	76	3.37	2.59
6	112.62	9	21	18	132.64	107.30
7	96.53	53	50	50	5.47	4.62
8	84.46	9	20	17	126.12	101.40
9	75.08	42	37	38	13.18	9.06
10	67.57	13	23	21	71.52	57.25
11	61.43	30	25	26	15.99	12.35
12	56.31	7	19	16	148.94	115.69
13	51.98	26	20	22	22.58	15.66
14	48.26	9	18	17	103.61	88.20
15	45.05	22	16	18	27.88	18.48
16	42.23	8	17	16	108.30	93.46
17	39.75	19	13	14	33.95	25.15

[1] F1=structure factors calculated with the C135 model

F2= C865 model

F3= C-4-2-5 model

ΔF_{21}=100*(F2-F1)/F1

ΔF_{21}=100*(F3-F1)/F1

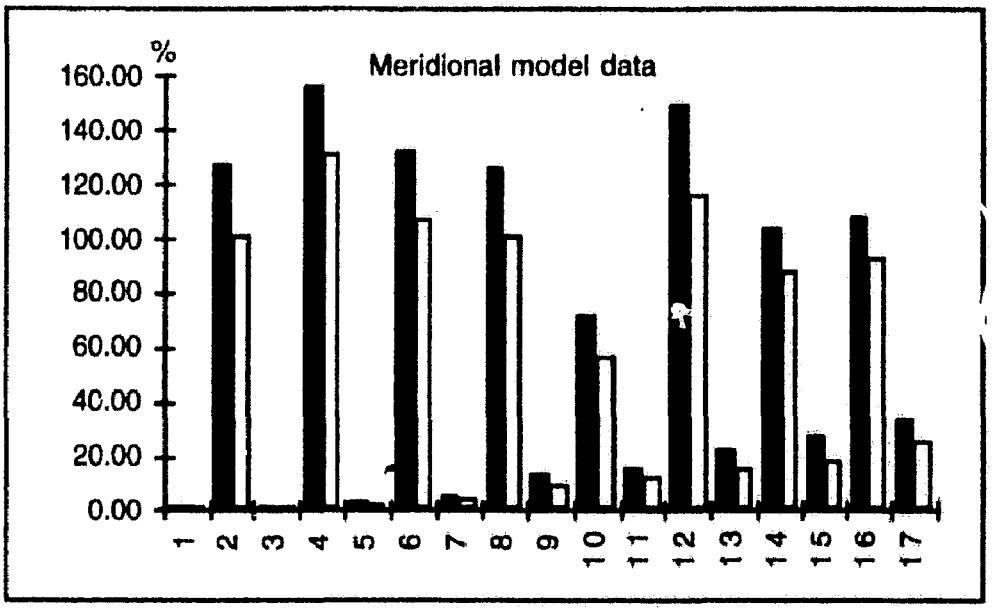

Fig VII.18 : The relative variation in the meridional structure factor amplitude is plotted here for the three calculated models. The C135 model is taken as reference. Only even orders seems to be affected (e.g. ΔF/F ≈160%) by the different packing of collagen like molecules. This figure demonstrate that low resolution meridional data can provide the means to model a structure.

The other experimental data that might contribute to the understanding of molecular packing in tendon are the row-lines reflections obtained at low-resolution. These data are relevant for the lateral packing of collagen molecules and are listed in table VII.2 for one of the row-lines with h=1, k=0 and l=-20 to 20. The equatorial and near equatorial reflections are usually overlapped on experimental films so that integrated intensities are not easily obtainable but I will give them here as an example for the method. The calculated structure factors amplitudes for the (1,0,l) row-line are listed in table VII.2.

Table VII.2

h	k	l	d	F1	F2	F3	ΔF21	ΔF31
1	0	-20	26.4209	23	7	11	69	51
1	0	-19	27.184	12	22	15	88	23
1	0	-18	27.9693	13	10	17	21	27
1	0	-17	28.7744	6	26	9	350	59
1	0	-16	29.5964	12	15	18	23	41
1	0	-15	30.4312	9	29	13	220	40
1	0	-14	31.2736	26	14	22	45	16
1	0	-13	32.1173	20	61	23	207	18
1	0	-12	32.9546	35	58	77	65	118
1	0	-11	33.7762	33	107	79	227	143
1	0	-10	34.5716	44	34	154	24	248
1	0	-9	35.3291	46	54	117	19	154
1	0	-8	36.0357	13	9	113	32	790
1	0	-7	36.6779	25	62	27	144	5
1	0	-6	37.2421	33	41	61	26	87
1	0	-5	37.715	61	139	29	127	52
1	0	-4	38.0849	75	62	152	17	104
1	0	-3	38.3419	146	337	79	131	46
1	0	-2	38.4787	216	162	441	25	104
1	0	-1	38.4915	503	410	1387	19	176
1	0	0	38.3798	3648	169	412	95	89
1	0	1	38.147	221	77	130	65	41
1	0	2	37.7995	176	65	94	63	47
1	0	3	37.3467	120	53	33	56	73
1	0	4	36.8002	91	34	66	63	28
1	0	5	36.1729	58	35	22	40	61
1	0	6	35.4783	27	31	51	12	86
1	0	7	34.7302	62	74	45	19	28
1	0	8	33.9415	45	30	55	33	23
1	0	9	33.1244	18	56	49	208	171
1	0	10	32.2895	31	43	44	39	42
1	0	11	31.4465	56	7	34	87	39
1	0	12	30.6032	14	36	20	164	48
1	0	13	29.7664	31	17	28	43	8
1	0	14	28.9414	5	33	14	595	206
1	0	15	28.1326	25	31	17	24	32
1	0	16	27.343	5	27	23	395	314
1	0	17	26.5753	19	23	25	17	31
1	0	18	25.8309	7	28	21	301	195
1	0	19	25.111	24	4	15	85	37
1	0	20	24.4162	6	18	18	181	191

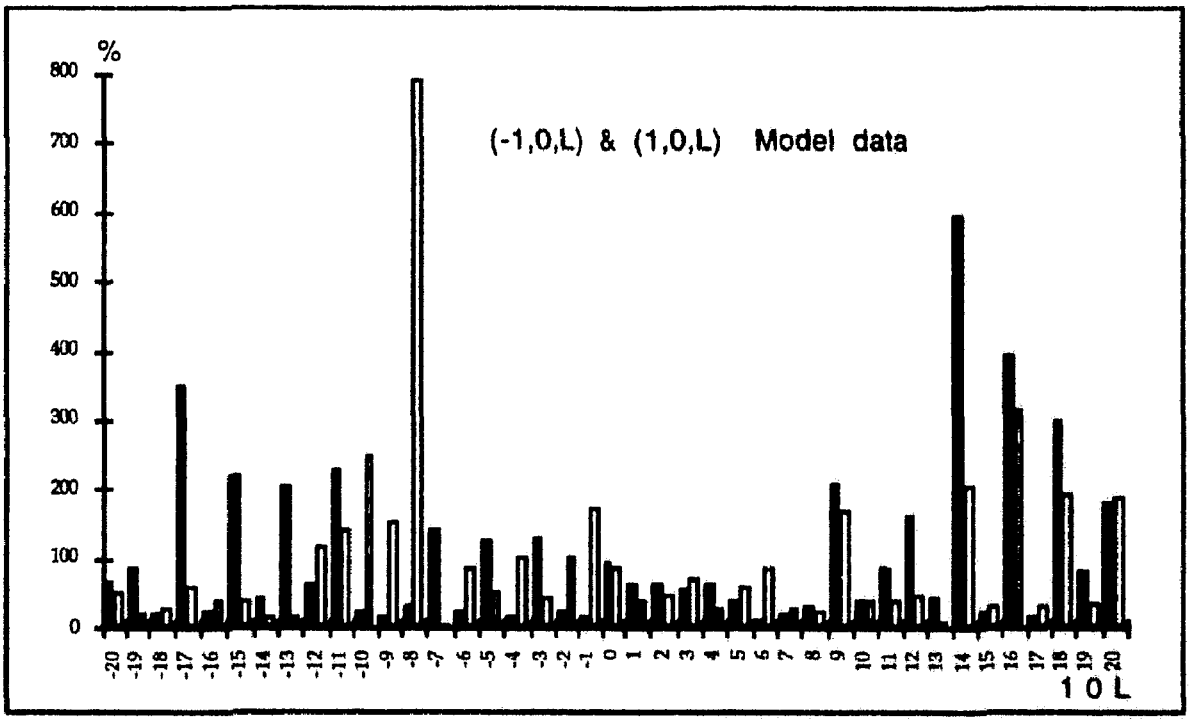

Fig VII.19: The relative deviation in the structure factor amplitude of the row-line (1,0,l) reflections is plotted here for the three constructed models. The C135 model is taken as reference. Large amplitude deviations in the structure factors (e.g. ΔF/F ≈100% to 800%) is noticeable for the different packing of collagen like molecules. These data and the low-angle meridional ones shown in figure VII.18 demonstrate that the low resolution row data can provide the means to solve the packing problem in tendon crystallites.

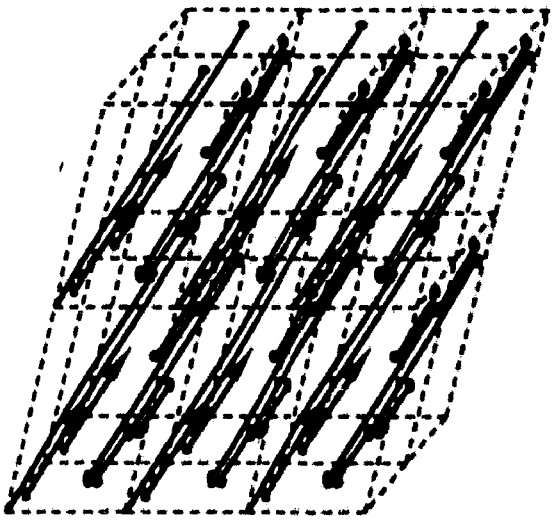

Fig. VII.20 : In this figure I show 12 adjacent unit cells from the constructed C135 crystalline model in a perspective view. The whole 3D structure and the molecular connectivity are obtained when segments from adjacent unit cells are aligned head to tail.

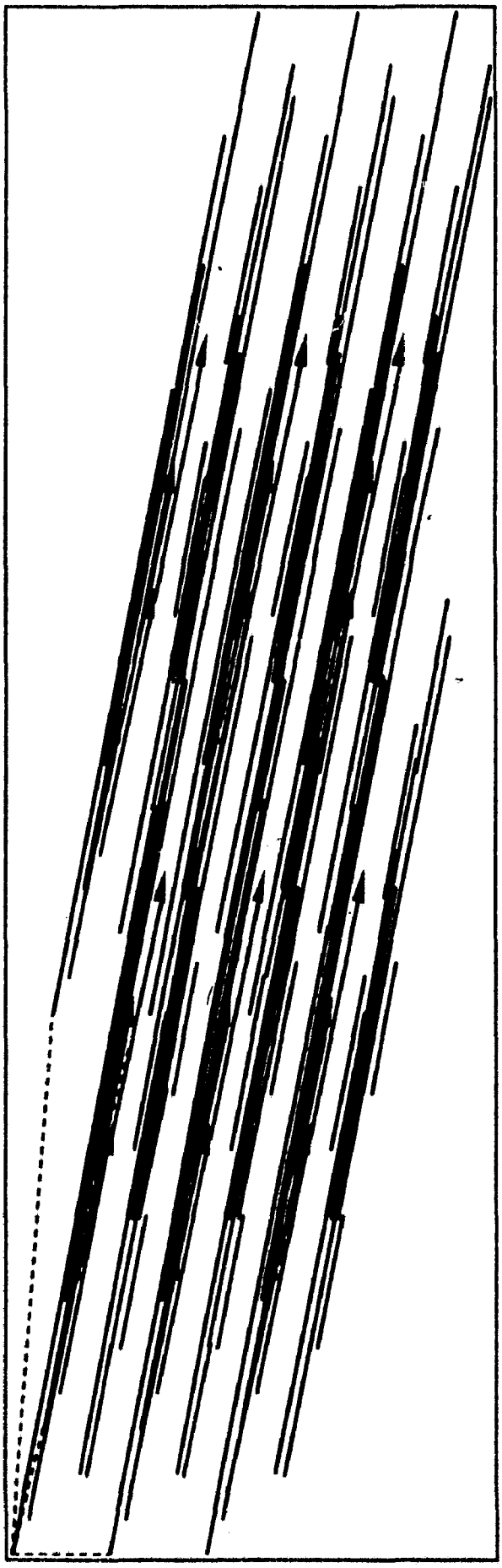

Fig. VII.21 : The structure shown in figure VII.20 was stretched longitudinally so that now the unit cell vectors are roughly on a more realistic scale. The 3D structure is thus constituted of bundles of staggered molecules shown here in perspective. The gap overlap feature is also obtained by the staggered molecules.

CONCLUSIONS

The main topic of this work has covered the data analysis aspect of fibre structure determination. Although film detector techniques are now superseded by phosphor image plates and high resolution fast area detectors, the current experiments using synchrotron radiation and X-ray films was an important work specifically designed for collagen structural investigations at the molecular level. The one dimensional structure, or axial projection, of wet collagen fibrils in rat tail tendon has been intensively studied using electron microscope, X-ray diffraction and neutron diffraction techniques over the last 25 years. However, the resolution limits of the EM and weak scattering of neutrons have provided a poor structural evidence for the three dimensional packing of molecules. Whereas the advent of synchrotron radiation X-rays now provides the potentiality for low and medium resolution studies to be undertaken because of short exposure times and less damage to the biological specimen. Moreover, the high brilliance of synchrotron radiation sources allow for weak reflections to be recorded. I have taken advantage of the high flux of the synchrotron radiation X-ray beam at the sample in order to observe and integrate very weak spots usually not obtained with classical X-ray sources. These weak spots are Bragg reflections, relevant to the 3-D structure studies of collagen crystallites and are thus necessary for the understanding of the molecular packing in tendon.

The understanding of collagen diffraction patterns has been facilitated by a computer simulation program that I have written. The Bragg peaks positions on the film were thus calculated with a good accuracy taking into consideration the fibre geometry and the unit cell parameters of the crystals. This in addition has enabled me to simultaneously compare the experimental patterns with the predicted ones, thus yielding better experimental parameters and as a consequence, has provided the way to obtain integrated background subtracted intensities.

I have started my investigation with a preliminary study of the conventional crystal unit cell that was definitely established i.e. the triclinic cell obtained by Fraser *et.al.* This was necessary for a correct indexing of the collected Bragg reflections. The new model suggested by Kajava has also been disproved as there was no experimental evidence for it. This was done using PTA labelled collagen that produces diffraction patterns with many reflections on all the row-lines.

Then, the use of small angle X-ray scattering has enabled me to measure the average crystallites size in tendons along the c-axis. I have used standard peak shape analysis known in powder diffraction methods but never used with collagen crystalline fibres and this technique was here straightforward. This characterisation was achieved in the light of the recent developments on the use of microfocused synchrotron X-ray beams for the study of ultra-small specimens. The crystal average dimension along the c-axis that came out is about 1μ whereas the average dimensions in the section of the fibre were more difficult to obtain because of fibrils polar disorientation. This result and the ones obtained by previous (Hulmes *et.al.*, 1981) electron microscopy studies which have already given an estimate of the lateral dimension of crystalline domains have been used to simulate the diffraction patterns of a collagen model built up with ultra-small crystalline domains.

I have then gathered a set of structure factors obtained from the experimental recorded patterns. The experiments were done by Dr WESS at Daresbury with native collagen fibres and a set of heavy atom derivatives for the purpose of MIR method evaluation. An additional experiment with PEG added fibre was also analysed in order to serve as a control for my data collection method and to asses for the phasing capability of the MIR methods. The data were gathered manually by carefully checking all films in a pack for each of the native and other derivative patterns. The use of pattern prediction was also of a great benefit to minimise the experimental errors and to correctly index the Bragg reflections. Peak overlap and background estimation were also considered and strongly overlapped reflections were rejected. Furthermore, due to high dynamic range in the X-ray pattern of tendon, the low intensity reflections were collected on top films whereas high intensity peaks were obtained from the bottom films to preclude saturated peaks. Then a systematic film absorption correction was applied whenever it was necessary. The data collected from the patterns were separated into three categories as follows: the meridional reflections that are the easiest to collect and to index were first given with a higher order and accuracy than never obtained, then the (-1,0,l) and (1,0,l) row-lines were obtained for the native and the derivatives, that were also systematically indexed and listed for a future use. The remaining weak reflections related to the 3D structure of collagen were also collected and listed in the Appendixes but their use requires further corrections and systematic checking. The meridional reflections were obtained with a better resolution than in all previous works and can be used for a one-dimensional structure determination to approximately 8.0Å resolution. The (ultra) small angle diffraction experiment used in chapter 4 has also provided the means to measure the amplitude of the lowest (e.g. the 1^{st} to the 9^{th}) orders of the native structure factors that, to my knowledge, have never been obtained before.

I have also collected the structure factors of the (-1,0,l) and (1,0,l) prominent row-lines with l = 0 to l ~ 75, that is up to the reflections on the helix layer-line. These Bragg reflections form a complete 2-dimensional structural data set that can be used to calculate medium resolution Fouriers with the resolution of the pitch of the basic collagen helix. The low l orders of these two row-lines were obtained for native and three derivatives but some ambiguity is still actual regarding the Miller indices since these reflections are strongly overlapped near the equator.

The remaining 3-dimensional data I have collected are of poorer quality when compared to the meridionals and the two other principal row-lines but however they have been useful for a preliminary Patterson differences and other model calculations. The whole data set were then merged and scaled together according to standard protein crystallographic algorithms provided by the CCP4 routines. Hence, an overall evaluation of the quality of the data was obtained using statistical methods on the data obtained after film processing and has revealed the poor data quality with regard to other crystallographic data. However, the data set used in the statistical analysis contained all of the data I have collected including those with low accuracy. For a better comprehensive data analysis these data were also checked for symmetry related reflections using graphical display.

Then an attempt to calculate Patterson differences was done for the purpose of the evaluation of the isomorphous intensity differences with fibre diffraction experiments. The Patterson differences were

calculated in the P-1 symmetry group using structure factors of respectively the native, gold and iodine labelled fibres and also the PEG added fibre. The gold-native Patterson difference map shows some peaks that can be related to heavy atom-heavy atom vectors whereas the iodine-native and the control PEG-native Patterson differences did not show such pronounced peaks. The absence of evident peaks in the last two maps was probably due to the lack of numerous heavy atoms in the unit cell. Despite the bad quality of these maps, they have been obtained for the first time and demonstrate that, provided an automatic film processing and ameliorated experimental conditions (e.g. microfocused synchrotron X-ray beam), one can expect a successful low-resolution structural study of collagen packing in tendon. The program I have written at the ESRF is continually improved to perform the peak prediction, the automatic intensity integration and the background subtraction tasks and has recently been applied to other biological crystalline fibres.

Finally, I have carried on an extensive fibre simulation work with a model molecule that resembles the rod shaped actual collagen molecule. I have built this model using a fragment of a collagen-like triple helical poly-Gly-Pro-HyPro segment retrieved from the PDB. This model was then used to construct a crystalline arrangement of parallel and staggered molecules to fulfil the gap-overlap feature observed under electron microscope. The model with the triclinic unit cell has been used to calculate structure factors and phases that can be further used (for example for phase refinement of observed reflections using solvent flattening techniques as well as other phase refinement methods). Diffraction patterns from the model fibrils were then calculated using the Cerius package at the ESRF, and the different fibre geometry e.g. fibre tilt, fibrils disorientation, fibrils average crystalline size, were analysed. This simulation has facilitated the understanding of the usually complicated fibre diffraction diagrams obtained experimentally. On the other hand, it clearly shows that a crystallographic analysis of collagen fibre diffraction patterns is possible provided the experimental procedure is ameliorated. However the peak overlap problem of the equatorial reflections will always be crucial.

IX. REFERENCES

- Arndt, U. W., Willis B. T. M., (1966), In "Single Crystal Diffractometry", London, Cambridge University Press.

- Atkins, E. D. T. and Keller F. R. S., (1975), In "Structure of Fibrous Polymer.", Butterwoths, London

- Blundell, T.L., Johnson, L. N., (1976), In "Protein Crystallography", Academic Press, London.

- Bradshaw, J. P., Miller A. , Wess T.J., (1992), Physica, **B180 & 181**, p. 776-778.

- Bradshaw, J. P., Miller A., Wess, T.J., (1989), J.Mol.Biol. , **205**, p. 685-694.

- Brodsky, B., Eikenberry, E.F. and Cassidy, K., (1980), Biochim. biophys. Acta, **621**, p. 162-166.

- Chen, J. M., Kung C. E. , Feairheller, S.H. and Brown, E.M., (1991), J. Protein Chem. , **10**, p. 535-552.

- Cochran, W., Crick, F. H. C. , Vand, V. , (1952), Acta Cryst., **5**, p. 581.

- Crick, F. H. C. (1952). Nature (London), p. 882.

- Crick, F. H. C. (1953), Acta Cryst., **6**,p. 685-689.

- Crick, F. H. C. (1953). Acta Cryst. , **6**, p. 689.

- Cruickshank, D. W. J., Helliwell, J.R., Moffat, K., (1987), Acta Cryst. , **A43**, p. 656-674.

- Ealick, S. E. , Walter, R. L. (1993), Current Opinion in structural Biology, **3**, p. 725-736.

- Fietzek, P.P. , Kuhn, K., (1976), In "International Review of Connective Tissue Research" , **Vol 7**, (Hall, D., and Jackson, D.S., eds.) Academic Press, New York, p. 1-60.

- Fisher, A. J. , Johnson, J. E. , (1993), Nature (London), p. 176-179.

- Franklin, R. E. , Gosling R. G., (1953), Acta Cryst., **6**, p 678-85.

- Fraser, R. D. B. , MacRae T. P. , (1981), Int. J. Biol. Macromol. , **3**, p. 9-18.

- Fraser, R. D. B., MacRae, T. P., Miller, A., (1987), J. Mol. Biol., **193**, p. 115-125.

- Fraser, R.D.B. , Suzuki, E., (1973), in "Physical principles and techniques of Protein Chemistry" (Ed S.J.Leach) Part C, Academic Press, New York.

- Fraser, R.D.B., MacRae, T.P., Miller A., Rowlands, R.J., (1976), J. Appl. Cryst. , **9**, p. 81-94.

- Fraser, R.D.B., MacRae, T.P., Miller, A., Suzuki, E., (1983), J.Mol.Biol., **167**, p. 497-521.

- Fraser, R.D.B., MacRae, T.P., Suzuki, E. and Tulloch, P.A., (1981), In "Structural aspects of recognition and assembly in biological macromolecules" (Balaban, M., ed.), Balaban, Rehovot, p. 327-340.

- Fratzl, P. and Daxer, A., (1993), Biophys. J. , **64 (4)**, p. 1210-1214.

- Helliwell, J. R., (1992), In "Macromolecular Crystallography with synchrotron Radiation", Cambridge University Press.

- Helseth, D.L., Lechner, J. H. ,Veis, A., (1979), Biopolymers, **18**, p. 3005-3014.

- Hodge, A.J. , Petruska, J. A. , (1967), in "Treatise on Collagen", (Ed. G.N. Ramachandran) Academic Press, New York.

- Holmes, D.F., Chapman, J.A., Prockop, D.J., Kadler, K. E., (1992), Proc Natl Acad Sci USA, **89** (20), p. 9855-9859.

- Hukins, D. W. L., (1992), Proc R Soc Lond [Biol] , **249**, (1326), p. 281-285.

- Hulmes, D. J. S. , Miller, A. , (1979), Nature, **282**, p. 1-3.
- Hulmes, D. J. S., Jesior J. C., Miller, A. and Berthet-Colominas C., (1981), Proc. Natl. Acad. Sci. USA, **78** (6), p. 3567-3571.
- Hulmes, D. J. S., (1992), Essays in Biochemistry, **27**, p. 49-67.
- Huxley, H. E. , Brown, W. J. , (1967), J. Mol. Biol. , **30**, p. 383.
- Jesior, J. C. , Miller, A. , Berthet-Colominas, C. , (1980) , Febs. Lett. , **113**, p. 238-240.
- Kajava, A. V., (1991), J. Mol. Biol., **218**, p. 815-823.
- Katz, E. P. and David, C.W. , (1992), J Mol Biol., **228** (3), p. 963-969.
- Klug, A., Crick, F.H.C. , Wyckoff, H. W. , (1958), Acta Cryst., **11**, p. 199-213.
- Krauss, N., Hinrichs, W., Witt, I., Fromme, P., Pritzkow, W., Dauter, Z., Betzel, C., Wilson, K.S., Witt, H. T., Saenger, W., (1993), Nature (London), p. 326-331.
- Light, N. D. and Bailey ,A. J., (1980), Biochem. J. , **185**, p. 373-381.
- Logan, D., Abu-Ghazaleh, R., Blakemore, W., Cury, S., Jackson, T., King, A., Lewis, R., Newman, J., Parry, N. et al., (1993) , Nature (London), p. 566-568.
- Millane Rick, P. and Strutter A., (1985), J. Appl. Cryst. , **18** , p. 419-423.
- Miller, A. , Parry, D.A.D. , (1973) , J. Mol. Biol. , **75**, p. 441-447.
- Miller, A. , Tocchetti D. , (1981), Int. J. Biol. Macromol. , **3** , p. 9.
- Miller, E.J., Gay, S., (1982), In "Structural and Contractile Proteins", Methods in Enzymology, **Vol 82**, Academic Press.
- Nave, C., Helliwell, J. R. , Moore, P.R., Thompson, A.W. and Worgan, J. S., (1985), J. Appl Cryst., **18**, p. 396-403.
- Nemetscheck, T., Naturwissenschaften, (1968), **55**, p. 346.
- Nemetscheck, T., Riedl, H. , Jonak, R., (1979), J. Mol. Biol. , **133**, p. 67
- North, A. C. T., Cowan, P. M. , Randall, T. J., (1954) , Nature (London) , **174**, p. 1142.
- Pauling, L. , Corey R. B. , (1953), Nature (London), p. 59.
- Pauling, L., Corey, R. B. , Branson, H. R., (1951). Proc. Nat. Acad. Sci. Wash., 37, p. 205.
- Pflugl, G., Kallen, J., Schirmer, T., Jansonius, J. N., Zurini, M. G. M. and Walkinshaw, M. D., (1993), Nature, p. 91-94.
- Ramachandran, G.N., Reddi , A. H., (1976), In "Biochemistry of collagen", Plenum Press, New York .
- Rich, A., Crick, F.H.C., (1961), J. Mol. Biol. , 3, p. 483-505.
- Scherrer, P., Nachr. Gesell. Wiss. Goet., (1918), **98**, p. 394.
- Silver, D., Miller J., Harrison. R. and Prockop D. J. , (1992), Proc Natl Acad Sci USA, **89** (20), p. 9860-9864.
- Smith, J.W. , (1968) , Nature (London) , **219**, p. 157-158.
- Smith, P.J.C. , Arnott, S. (1978), Acta Cryst., sect. A, **34**, p. 3-11.
- Stokes, A. R. , Wilson A. J. C. , (1942), Proc.Camb.Phil.Soc. , **38**, p. 313.
- Stokes, A. R. , Wilson A. J. C. , (1944), Proc.Camb.Phil.Soc. , **40**, p. 197.
- Stoss, H. , Freisinger P. , (1993), Am. J. Med. Genet. , **45** (2) , p. 257.
- Suzuki, E., Fraser, R. D. B. , MacRae, T. P., (1980), Int. J. Biol. Macromol. , 2, p. 54-56.

- Traub, W. , Piez K. A., (1971), Adv. Protein Chem. , 25 , p. 243.
- Veis, A., Yuan, L. , (1975), Biopolymers, 14 , p. 895-900.
- Vibert, P.J. , In "Fibre diffraction methods", (1987) , (Edited by Squire J. M. and Vibert P.J.), Academic Press.
- Warren, B. E. (1969), In "X-Ray Diffraction", Addison Wesley.
- Warren, B. E. (1990), In "X-Ray Diffraction", Addison Wesley, (second edition).
- Wilson, H. R. (1966), In "Diffraction of X-rays by proteins, Nucleic Acids and Viruses", London, Edward Arnold Ltd.
- Woodhead-Galloway, J. , (1984), in " Connective Tissue Matrix: topics in Molecular and Structural Biology" , Vol. 5 , (Hukins, D.W.L. , ed.), Verlag Chemie, Weinheim, p. 133-160.
- Woodhead-Galloway, J., Hukins, D.W. L., Wray, J. S., (1975), Biochem. Biophys. Res. Commun., 64, p. 1237-1244.
- Yang, C. L. L., Rui, H. F., Mosler, S., Notbohm, H., Sawaryn, A., Muller, P.K., (1993), Eur. J. Biochem., 213, p. 1297-1302.
- Yonath, A. and Traub, W. , (1969), J. Mol. Biol., 43, p. 461-477.
- Zylberberg, L., Bonaventure J. , et al. (1992), J. Cell Sci., 103 (Part 1), p. 273-285.

X. APPENDIX A

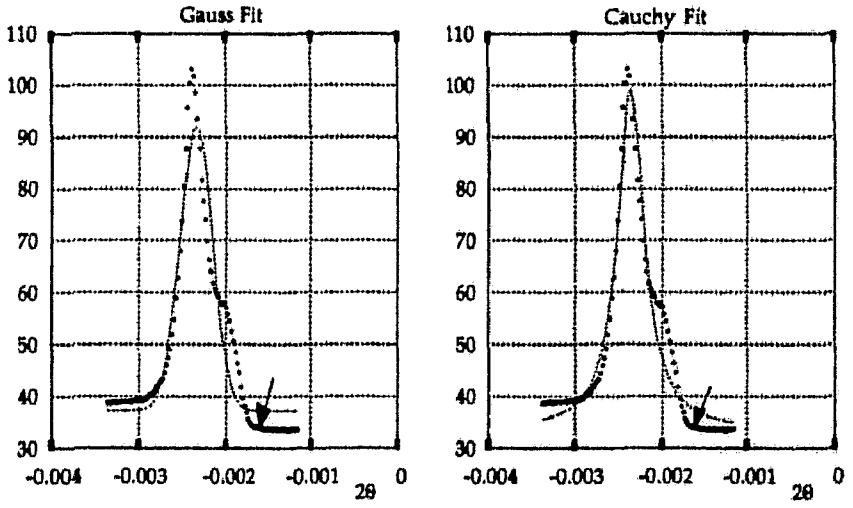

Fig. A1: Fit of the 00-1 order with a Gaussian and a Lorentzian curve. The edges of the beamstop are indicated by the arrows. Some intensity from the main beam is corrupting the base of the peak. Consequently, the best fit is obtained by the Lorentzian model which has a narrower base.

Table A1

	Gaussian Profile		Cauchy Profile	
Ce	37.204	0.690	33.467	0.693
U_0	54.685	1.718	65.197	1.591
X_0	$-234.709\ 10^{-5}$	$0.645\ 10^{-5}$	$-235.959\ 10^{-5}$	$0.442\ 10^{-5}$
a	$26.223\ 10^{-5}$	$1.025\ 10^{-5}$	$18.416\ 10^{-5}$	$0.838\ 10^{-5}$
Area	$2544.427\ 10^{-5}$		$3371.078\ 10^{-5}$	
χ^2	2607		1553	
R	0.96		0.97	

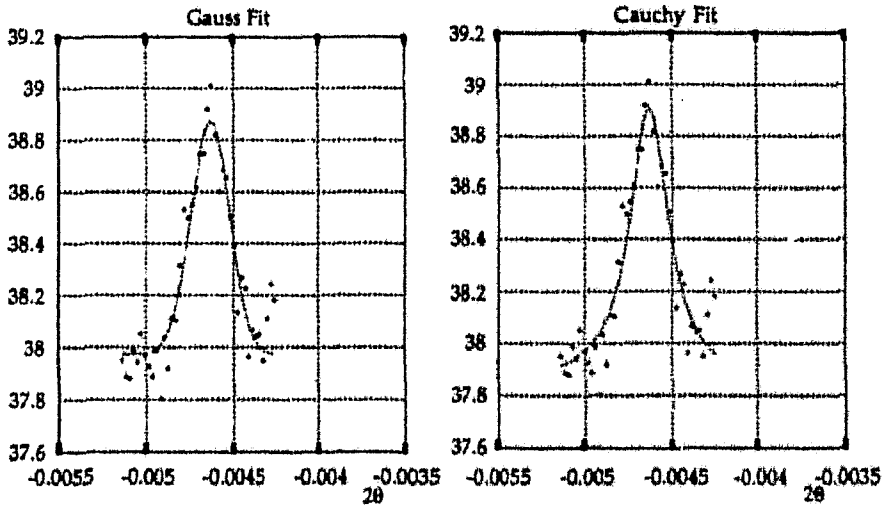

Fig. A2:Fit of the 00-2 order with a Gaussian and a Lorentzian curve. The peak is at weak height. A medium value for the goodness-of-fit parameter ~0.95 has been attained which can be explained by the high signal to noise ratio of the data.

Table A2

00-2	Gaussian Profile		Cauchy Profile	
Cte	37.974	0.027	37.845	0.047
U_o	0.896	0.046	1.059	0.058
X_o	$-463.306\ 10^{-5}$	$0.607\ 10^{-5}$	$-463.122\ 10^{-5}$	$0.641\ 10^{-5}$
a	$15.568\ 10^{-5}$	$1.085\ 10^{-5}$	$13.438\ 10^{-5}$	$1.586\ 10^{-5}$
Area	$24.547\ 10^{-5}$		$35.945\ 10^{-5}$	
χ^2	0.39		0.44	
R	0.95		0.94	

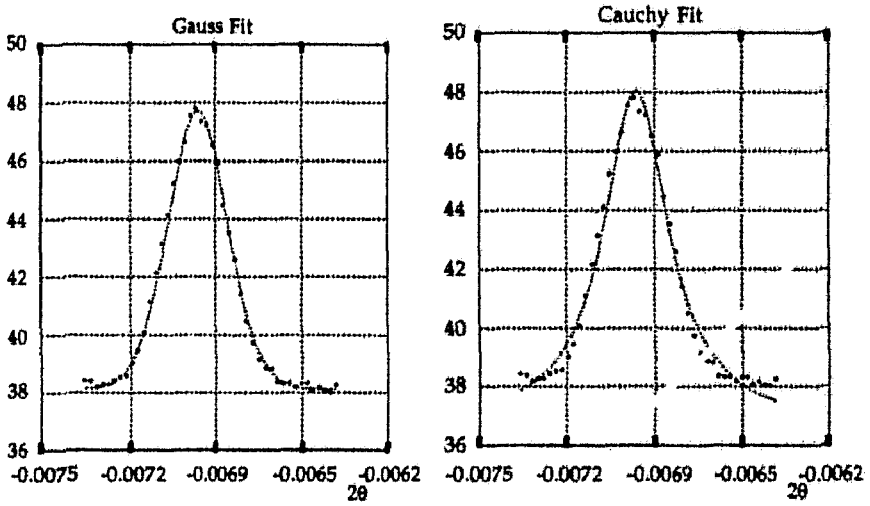

Fig. A3 : The third meridional order 00-3 fitted with the model curves. Both models yield a high (cf table A3) figure of merit factor but the Gaussian curve is more suitable to fit the wings region of the experimental data.

Table A3

	Gaussian Profile		Cauchy Profile	
Cte	38.123	0.038	36.715	0.172
U_o	9.592	0.066	11.345	0.212
X_o	$-691.950\ 10^{-5}$	$0.086\ 10^{-5}$	$-691.915\ 10^{-5}$	$0.233\ 10^{-5}$
a	$16.568\ 10^{-5}$	$0.153\ 10^{-5}$	$14.411\ 10^{-5}$	$0.581\ 10^{-5}$
Area	$281.239\ 10^{-5}$		$415.122\ 10^{-5}$	
χ^2	0.93		6.87	
R	0.99		0.99	

Table A4

	Gaussian Profile		Cauchy Profile	
Cte	38.330	0.029	38.170	0.055
U_o	0.846	0.045	1.024	0.058
X_o	$-917.239\ 10^{-5}$	$0.668\ 10^{-5}$	$-917.302\ 10^{-5}$	$0.699\ 10^{-5}$
a	$17.323\ 10^{-5}$	$1.270\ 10^{-5}$	$16.137\ 10^{-5}$	$1.966\ 10^{-5}$
Area	$25.850\ 10^{-5}$		$40.075\ 10^{-5}$	
χ^2	0.38		0.41	
R	0.95		0.94	

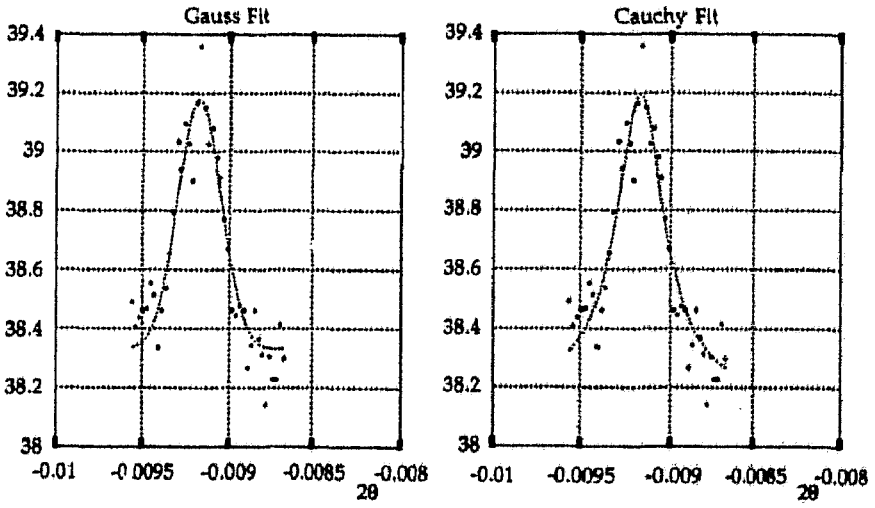

Fig. A4 : The order 00-4 is very weak (peak height<2) but one can fit the model curves and obtain an estimate of the parameters. Notice the low R value in table A4 and the relatively high standard errors on the peak broadening measurement deduced from these fits.

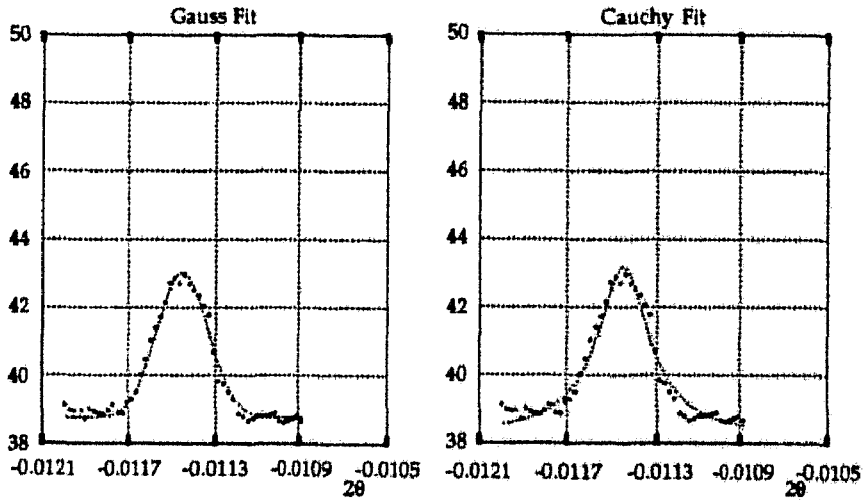

Fig. A5 : Fit of the 00-5 meridional order.

Table A5

	Gaussian Profile		Cauchy Profile	
$2\theta_0$	38.771	0.039	38.258	0.097
U_0	4.254	0.081	4.904	0.144
X_0	$-1145.041\ 10^{-5}$	$0.241\ 10^{-5}$	$-1145.070\ 10^{-5}$	$0.379\ 10^{-5}$
a	$16.367\ 10^{-5}$	$0.404\ 10^{-5}$	$13.910\ 10^{-5}$	$0.855\ 10^{-5}$
Area	$123.190\ 10^{-5}$		$179.903\ 10^{-5}$	
χ^2	1.71		4.13	
R	0.99		0.98	

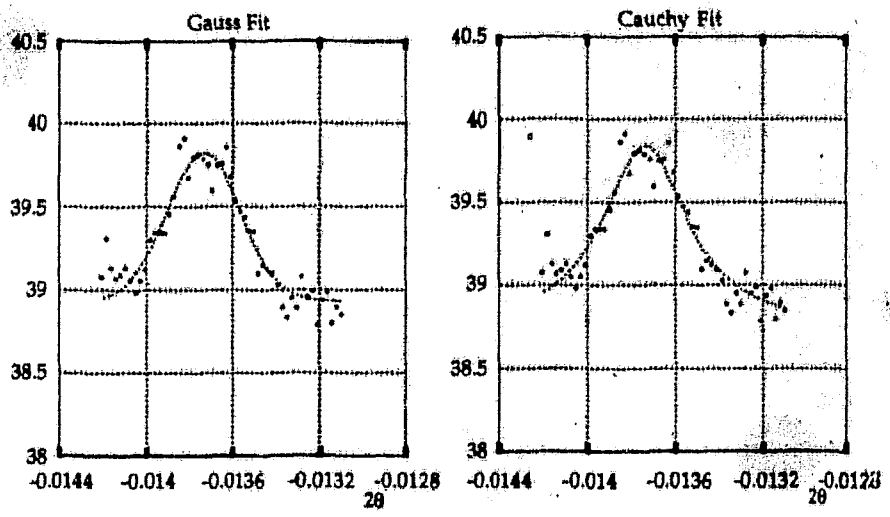

Fig. A6 : Curve fit of the meridional collagen 6th order.

Table A6

	Gaussian Profile		Cauchy Profile	
Cte	38.930	0.032	38.728	0.062
U_0	0.894	0.043	1.109	0.061
X_0	$-1373.508\ 10^{-5}$	$0.795\ 10^{-5}$	$-1373.812\ 10^{-5}$	$0.829\ 10^{-5}$
a	$24.261\ 10^{-5}$	$1.642\ 10^{-5}$	$23.597\ 10^{-5}$	$2.621\ 10^{-5}$
Area	$38.216\ 10^{-5}$		$60.462\ 10^{-5}$	
χ^2	0.55		0.58	
R	0.94		0.94	

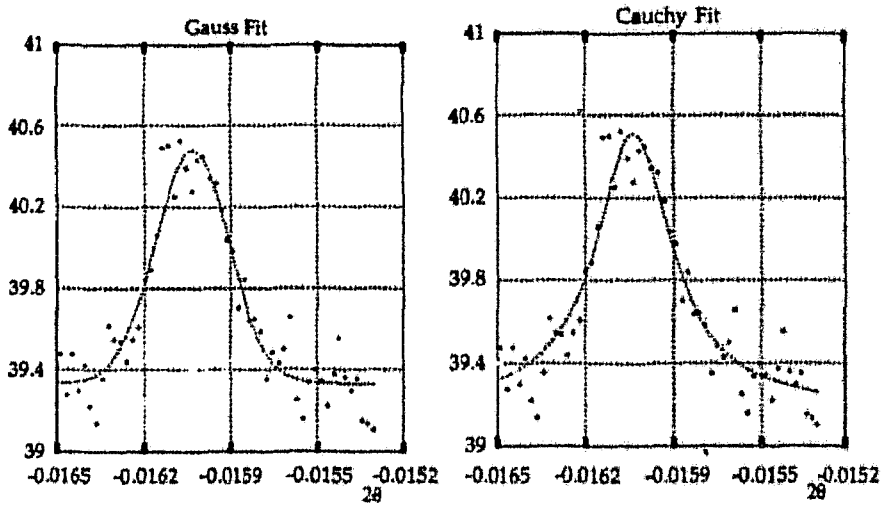

Fig. A7 :The 7th order fit.

Table A7

	Gaussian Profile		Cauchy Profile	
Cte	39.332	0.025	39.185	0.042
U_0	1.146	0.051	1.327	0.061
X_0	-1599.515 10^{-5}	0.680 10^{-5}	-1599.728 10^{-5}	0.731 10^{-5}
a	19.634 10^{-5}	1.139 10^{-5}	16.971 10^{-5}	1.665 10^{-5}
Area	39.955 10^{-5}		59.430 10^{-5}	
χ^2	1.0		1.11	
R	0.95		0.94	

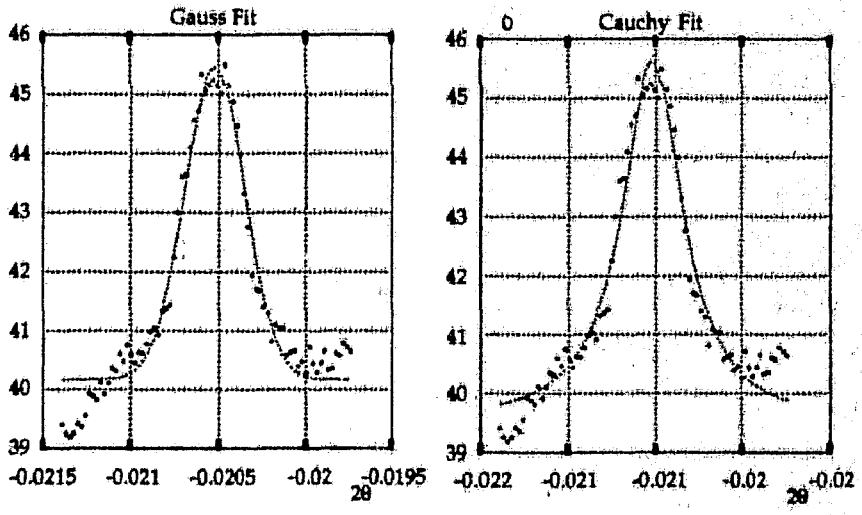

Fig. A9 :9th order fit. The drop in the intensity on the left side of the peak is due to the film edge . This explains the lower "goodness of fit" parameter in table A9 (R=0.97) but nevertheless the required data are correct.

Table A9

	Gaussian Profile		Cauchy Profile	
Cte	40.171	0.0662	39.487	0.103
U_0	5.268	0.137	6.132	0.151
X_0	-2052.397 10^{-5}	0.485 10^{-5}	-2052.166 10^{-5}	0.479 10^{-5}
a	24.205 10^{-5}	0.810 10^{-5}	20.969 10^{-5}	1.086 10^{-5}
Area	226.426 10^{-5}		339.797 10^{-5}	
χ^2	11.0		10.51	
R	0.97		0.97	

XI. APPENDIX B (Native Data)

h	k	l	F	σF	σΦ/F
-4	0	73	6	3	50
-4	0	74	2	3	129
-4	0	75	19	3	15
-4	0	76	19	3	15
-4	0	77	0	0	100
-4	1	-11	18	3	15
-4	1	-10	0	0	100
-4	1	-9	17	3	17
-4	1	-8	0	0	100
-4	1	-7	0	0	100
-4	1	8	12	3	22
-4	1	9	0	0	100
-4	1	10	25	3	13
-4	1	11	0	0	100
-4	1	12	16	3	18
-4	1	13	0	0	100
-4	1	14	0	0	100
-4	1	15	13	3	21
-4	1	16	0	0	100
-4	1	17	22	3	14
-4	1	18	0	0	100
-4	1	19	0	0	100
-4	1	20	0	0	100
-4	1	21	0	0	100
-4	1	22	0	0	100
-4	1	23	11	4	37
-4	1	24	0	0	100
-4	1	25	21	3	14
-4	1	26	0	0	100
-4	1	27	13	3	21
-4	1	28	0	0	100
-4	1	73	9	3	33
-4	1	74	11	3	24
-4	1	75	18	2	13
-4	1	76	0	0	100
-4	1	77	18	3	15
-4	1	78	14	3	20
-4	1	80	23	3	12
-3	-1	-49	0	0	100
-3	-1	-47	0	0	100
-3	-1	-46	6	3	45
-3	-1	-45	18	3	15
-3	-1	-44	20	3	17
-3	-1	-43	0	0	100
-3	-1	-26	5	3	53
-3	-1	-25	0	0	100
-3	-1	-24	0	0	100
-3	-1	-23	11	3	25
-3	-1	-22	8	3	33
-3	-1	-21	0	0	100
-3	-1	-20	0	0	100
-3	-1	-19	7	2	36
-3	-1	-18	7	3	39
-3	-1	-17	20	3	15
-3	-1	-16	0	0	100
-3	-1	-15	0	0	100
-3	-1	-14	14	3	19
-3	-1	-13	9	3	33
-3	-1	-12	15	2	17
-3	-1	-11	17	3	18
-3	-1	-10	0	0	100
-3	-1	-9	19	3	16
-3	-1	-8	0	0	100
-3	-1	-7	0	0	100
-3	-1	9	2	3	153
-3	-1	53	16	3	17
-3	0	-4	23	6	25
-3	1	-72	5	3	53
-3	1	-71	15	2	17
-3	1	-70	0	0	100
-3	1	-69	18	4	21
-3	1	-68	7	2	35
-3	1	-67	10	3	26
-3	1	-66	6	2	40
-3	1	-65	2	2	129
-3	1	-64	12	3	24
-3	1	-63	13	3	20
-3	1	-62	11	2	20
-3	1	-61	18	3	14
-3	1	-60	13	3	20
-3	1	-59	12	2	21
-3	1	-58	0	0	100
-3	1	-57	15	3	18
-3	1	-57	15	3	18
-3	1	-56	0	0	100
-3	1	-55	0	0	100
-3	1	-54	4	3	64
-3	1	-53	8	3	33
-3	1	-52	0	0	100
-3	1	-51	0	0	100
-3	1	-50	13	4	28
-3	1	-49	10	2	21
-3	1	-48	20	3	14
-3	1	-47	0	0	100
-3	1	-46	0	0	100
-3	1	-45	5	3	52
-3	1	-44	0	0	100
-3	2	-30	0	0	100
-3	2	-29	0	0	100
-3	2	-28	18	2	14
-3	2	-27	2	3	118
-3	2	-26	9	3	30
-3	2	-26	9	3	30
-3	2	-25	0	0	100
-3	2	-24	0	0	100
-3	2	-23	5	3	59
-3	2	2	12	3	28
-3	2	3	6	4	60
-3	2	4	24	5	20
-3	2	5	0	0	100
-3	2	6	0	0	100
-3	2	7	25	5	21
-3	2	8	0	0	100
-3	2	9	8	3	40
-3	2	13	7	3	45
-3	2	14	0	0	100
-3	2	15	0	0	100
-3	2	16	22	3	12
-3	2	17	0	0	100
-3	2	18	3	3	113
-3	2	19	0	0	100
-3	2	20	24	4	18
-3	2	21	18	3	14
-3	2	22	0	0	100
-3	2	24	0	0	100
-3	2	25	4	3	62
-3	2	26	0	0	100
-3	2	27	15	3	18
-3	2	28	22	3	13
-3	2	29	0	0	100
-3	2	30	12	2	18
-3	2	31	0	0	100
-3	2	32	27	3	11
-3	2	33	0	0	100
-2	-1	-14	7	3	48
-2	-1	-13	9	3	38
-2	-1	-12	0	0	100
-2	-1	-11	18	4	21
-2	-1	-10	0	0	100
-2	-1	-9	21	5	23
-2	-1	-8	6	4	71
-2	-1	-6	19	4	22
-2	-1	-3	75	9	12
-2	-1	-2	78	8	11
-2	-1	6	17	8	46
-2	-1	7	0	0	100
-2	-1	8	6	7	115
-2	-1	9	15	5	35
-2	-1	10	15	5	31
-2	-1	11	13	4	33
-2	-1	12	0	0	100
-2	-1	13	14	3	21
-2	-1	14	0	0	100
-2	-1	15	5	3	58
-2	-1	16	0	0	100
-2	-1	17	12	3	23
-2	-1	18	18	3	14
-2	-1	19	18	3	15
-2	-1	20	0	0	100
-2	-1	21	0	0	100
-2	-1	22	21	3	13
-2	-1	23	9	3	31
-2	-1	23	25	3	10
-2	-1	24	0	0	100
-2	-1	25	0	0	100
-2	-1	26	25	2	10
-2	-1	27	0	0	100
-2	-1	28	0	0	100
-2	-1	29	22	2	11
-2	-1	30	14	3	19
-2	-1	31	0	0	100
-2	-1	32	0	0	100
-2	-1	33	32	3	8
-2	-1	34	9	2	28
-2	-1	35	11	3	33
-2	-1	36	0	0	100
-2	-1	37	26	2	9
-2	-1	38	0	0	100
-2	-1	39	26	3	10
-2	-1	40	0	0	100
-2	-1	41	0	0	100
-2	-1	42	9	2	27
-2	-1	43	0	0	100
-2	-1	44	12	2	21
-2	-1	45	0	0	100
-2	-1	46	15	3	18
-2	-1	47	0	0	100
-2	-1	48	16	2	15
-2	-1	49	0	0	100
-2	-1	50	0	0	100
-2	-1	51	18	2	13
-2	-1	52	8	2	32
-2	-1	53	26	2	9
-2	-1	54	10	4	37
-2	-1	56	0	0	100
-2	-1	58	22	3	12
-2	-1	59	29	2	8
-2	-1	60	12	2	21
-2	-1	61	3	2	93
-2	-1	62	0	0	100
-2	-1	63	20	2	12
-2	-1	64	30	2	8
-2	-1	65	0	0	100
-2	-1	66	27	2	9
-2	-1	67	0	0	100
-2	-1	68	11	3	25
-2	-1	69	23	3	11
-2	-1	70	13	3	20
-2	-1	71	17	3	16
-2	-1	72	0	0	100
-2	-1	73	26	2	9
-2	-1	74	37	4	11
-2	-1	75	16	3	18
-2	-1	76	0	0	100
-2	-1	77	0	0	100
-2	-1	78	0	0	100
-2	-1	79	20	3	14
-2	-1	80	0	0	100
-2	-1	81	0	0	100
-2	-1	82	0	0	100
-2	-1	83	0	0	100
-2	-1	84	0	0	100
-2	-1	85	37	3	7
-2	-1	86	0	0	100
-2	-1	87	0	0	100
-2	-1	88	32	3	8
-2	-1	89	0	0	100
-2	-1	91	22	4	12
-2	-1	92	27	3	13
-2	0	-88	10	2	26
-2	0	-87	2	2	112
-2	0	-86	16	2	14
-2	0	-85	17	2	13
-2	0	-84	5	2	45
-2	0	-84	0	0	100
-2	0	-83	17	2	14
-2	0	-82	16	2	15
-2	0	-81	0	0	100
-2	0	-80	0	0	100
-2	0	-79	0	0	100
-2	0	-78	7	2	30

-2	0	-77	0	0	100
-2	0	-76	0	0	100
-2	0	-75	5	2	51
-2	0	-74	14	2	16
-2	0	-73	0	0	100
-2	0	-71	12	2	20
-2	0	-70	5	3	50
-2	0	-69	4	3	84
-2	0	-68	16	2	14
-2	0	-67	0	0	100
-2	0	-66	8	2	32
-2	0	-65	12	2	18
-2	0	-64	10	2	23
-2	0	-63	0	0	100
-2	0	-62	3	2	65
-2	0	-61	12	2	19
-2	0	-60	17	2	13
-2	0	-59	0	0	100
-2	0	-58	12	2	20
-2	0	-57	6	2	43
-2	0	-56	11	2	20
-2	0	-55	5	2	45
-2	0	-54	0	0	100
-2	0	-53	8	2	31
-2	0	-52	6	2	39
-2	0	-51	0	0	100
-2	0	-50	22	3	16
-2	0	-49	3	2	87
-2	0	-48	0	0	100
-2	0	-47	5	2	42
-2	0	-46	11	2	21
-2	0	-45	3	2	85
-2	0	-44	4	2	51
-2	0	-43	0	0	100
-2	0	-42	0	0	100
-2	0	-41	6	3	42
-2	0	-40	0	0	100
-2	0	-39	0	0	100
-2	0	-38	7	2	31
-2	0	-37	11	2	21
-2	0	-36	11	2	21
-2	0	-35	15	2	16
-2	0	-34	14	2	17
-2	0	-33	0	0	100
-2	0	49	14	2	16
-2	0	50	13	2	18
-2	0	51	11	2	20
-2	0	52	0	0	100
-2	0	53	4	2	61
-2	0	54	10	2	24
-2	0	55	16	2	16
-2	0	56	0	0	100
-2	0	57	13	2	17
-2	0	58	14	2	16
-2	0	59	17	2	11
-2	0	59	17	2	11
-2	0	60	0	0	100
-2	0	61	4	2	50
-2	0	62	0	0	100
-2	0	63	7	2	34
-2	0	64	0	0	100
-2	0	65	14	2	16
-2	0	66	0	0	100
-2	0	67	7	2	31
-2	0	68	15	2	16
-2	0	69	4	3	67
-2	0	69	4	3	67
-2	0	70	3	2	65
-2	0	72	7	2	37
-2	0	73	13	2	19
-2	0	74	8	2	32
-2	0	75	0	0	100
-2	0	76	4	2	53
-2	0	77	0	0	100
-2	0	78	0	0	100
-2	0	79	0	0	100
-2	0	80	0	0	100
-2	0	81	0	0	100
-2	0	82	9	2	24
-2	0	83	12	2	18
-2	0	84	8	2	27
-2	0	85	0	0	100
-2	0	86	15	2	13
-2	0	87	0	0	100
-2	0	88	14	2	17
-2	0	89	0	0	100
-2	0	90	0	0	100
-2	0	91	0	0	100
-2	0	92	9	2	22
-2	0	93	0	0	100
-2	0	94	6	2	37
-2	0	95	0	0	100
-2	0	96	8	2	24
-2	0	97	7	2	33
-2	0	98	6	2	31
-2	0	99	8	2	26
-2	0	100	0	0	100
-2	1	-87	0	0	100
-2	1	-86	0	0	100
-2	1	-85	0	0	100
-2	1	-84	0	0	100
-2	1	-82	19	2	12
-2	1	-81	0	0	100
-2	1	-80	2	2	100
-2	1	-79	0	0	100
-2	1	-78	0	0	100
-2	1	-77	2	2	129
-2	1	-76	27	4	13
-2	1	-75	21	2	12
-2	1	-74	0	0	100
-2	1	-73	0	0	100
-2	1	-72	0	0	100
-2	1	-71	25	3	10
-2	1	-70	20	2	13
-2	1	-69	25	3	10
-2	1	-68	0	0	100
-2	1	-67	8	2	32
-2	1	-66	0	0	100
-2	1	-65	0	0	100
-2	1	-64	20	2	12
-2	1	-63	0	0	100
-2	1	-62	13	3	21
-2	1	-61	0	0	100
-2	1	-60	0	0	100
-2	1	-59	17	2	13
-2	1	-58	0	0	100
-2	1	-57	0	0	100
-2	1	-56	7	2	34
-2	1	-55	11	2	22
-2	1	-54	17	3	15
-2	1	-53	13	2	18
-2	1	-52	16	2	14
-2	1	-51	0	0	100
-2	1	-50	0	0	100
-2	1	-49	0	0	100
-2	1	-48	10	2	25
-2	1	-47	11	2	21
-2	1	-46	0	0	100
-2	1	-45	0	0	100
-2	1	-44	0	0	100
-2	1	-43	7	2	36
-2	1	-42	14	2	16
-2	1	-41	0	0	100
-2	1	-40	4	2	63
-2	1	-39	0	0	100
-2	1	-38	0	0	100
-2	1	-37	12	2	18
-2	1	-36	0	0	100
-2	1	-35	10	2	24
-2	1	-34	8	2	31
-2	1	-33	8	2	29
-2	1	-32	9	2	24
-2	1	-31	0	0	100
-2	1	-30	15	3	18
-2	1	-29	17	2	15
-2	1	-28	0	0	100
-2	1	-27	0	0	100
-2	1	-26	20	3	16
-2	1	-25	14	2	16
-2	1	-24	0	0	100
-2	1	-23	0	0	100
-2	1	-22	13	2	17
-2	1	-21	0	0	100
-2	1	-20	0	0	100
-2	1	-19	0	0	100
-2	1	-18	11	2	22
-2	1	-17	17	2	15
-2	1	-16	24	3	14
-2	1	-15	28	4	13
-2	1	-14	0	0	100
-2	1	-13	7	3	37
-2	1	-12	11	3	26
-2	1	-11	14	2	17
-2	1	-10	0	0	100
-2	1	-9	20	4	22
-2	1	-8	0	0	100
-2	1	-7	27	5	19
-2	1	-6	8	4	45
-2	1	-5	7	3	44
-2	1	-4	15	6	40
-2	1	-3	13	6	51
-2	1	-1	16	5	30
-2	1	4	15	3	23
-2	1	6	0	0	100
-2	1	7	11	4	34
-2	1	8	21	5	25
-2	1	9	15	4	26
-2	1	10	10	2	24
-2	1	11	10	2	24
-2	1	12	4	3	69
-2	1	13	13	2	18
-2	1	14	9	3	30
-2	1	15	4	3	68
-2	1	16	5	3	55
-2	1	17	0	0	100
-2	1	18	7	3	36
-2	1	20	12	2	21
-2	1	21	0	0	100
-2	1	49	0	0	100
-2	1	50	0	0	100
-2	1	51	14	3	19
-2	1	53	7	2	30
-2	1	54	0	0	100
-2	1	55	19	2	12
-2	1	56	15	2	15
-2	1	57	0	0	100
-2	1	58	11	2	23
-2	1	59	14	2	17
-2	1	60	7	2	33
-2	1	61	0	0	100
-2	1	63	20	2	11
-2	1	64	15	2	16
-2	1	65	0	0	100
-2	1	66	6	2	35
-2	1	67	10	2	23
-2	1	68	0	0	100
-2	1	69	12	3	22
-2	1	70	6	2	35
-2	1	71	0	0	100
-2	1	72	17	3	16
-2	1	73	40	2	6
-2	1	74	29	4	14
-2	1	75	0	0	100
-2	1	77	2	2	91
-2	1	78	3	2	82
-2	1	79	0	0	100
-2	1	80	0	0	100
-2	1	81	0	0	100
-2	1	82	18	2	12
-2	1	83	0	0	100
-2	1	84	0	0	100
-2	1	85	0	0	100
-2	1	86	21	2	11
-2	1	87	16	2	15
-2	1	88	21	2	11
-2	1	89	0	0	100
-2	1	90	9	2	26
-2	1	91	0	0	100
-2	1	92	16	3	20
-2	1	93	19	2	12
-2	1	94	17	3	18
-2	1	95	0	0	100
-2	1	96	0	0	100
-2	1	97	3	2	65
-2	1	98	0	0	100
-2	1	99	6	2	38
-2	1	100	11	2	23
-2	2	-34	18	3	17
-2	2	-33	9	3	37
-2	2	-32	0	0	100
-2	2	-31	16	2	15
-2	2	-30	3	2	74
-2	2	-29	25	4	15
-2	2	-28	16	3	17
-2	2	-27	30	3	9
-2	2	-26	17	3	15
-2	2	-25	12	3	23
-2	2	-24	13	3	21
-2	2	-23	19	3	14
-2	2	-22	0	0	100
-2	2	-21	20	3	13

-2	2	-20	13	3	20
-2	2	-19	17	3	18
-2	2	-6	22	7	32
-2	2	-5	23	5	24
-2	2	-2	15	8	54
-2	2	-1	11	8	76
-2	2	0	0	0	100
-2	2	2	0	0	100
-2	2	3	0	0	100
-2	2	4	0	0	100
-2	2	5	0	0	100
-2	2	7	15	6	37
-2	2	9	9	6	65
-2	2	10	9	5	57
-2	2	11	23	4	19
-2	2	12	3	4	136
-2	2	13	15	4	24
-2	2	14	6	3	41
-2	2	15	28	4	14
-2	2	17	23	4	16
-2	2	48	15	2	17
-2	2	49	0	0	100
-2	2	51	0	0	100
-2	2	52	0	0	100
-2	2	53	11	3	25
-1	-2	-53	0	0	100
-1	-2	-52	20	3	14
-1	-2	-50	10	3	26
-1	-2	-49	0	0	100
-1	-2	-48	15	3	19
-1	-2	-47	0	0	100
-1	-2	-46	8	3	39
-1	-2	-45	16	3	17
-1	-2	-44	9	3	31
-1	-2	-43	12	3	22
-1	-2	-42	17	3	15
-1	-2	-41	0	0	100
-1	-2	-40	0	0	100
-1	-2	-39	17	3	17
-1	-2	-38	10	3	28
-1	-2	-37	10	3	26
-1	-2	-36	0	0	100
-1	-2	-35	18	3	17
-1	-2	-34	15	3	18
-1	-2	-33	0	0	100
-1	-2	-32	0	0	100
-1	-2	-31	9	3	29
-1	-2	-30	12	3	24
-1	-2	-29	17	2	13
-1	-2	-28	23	4	17
-1	-2	-27	7	3	37
-1	-2	-26	15	3	19
-1	-2	-25	8	3	31
-1	-2	-24	0	0	100
-1	-2	-23	12	2	21
-1	-2	-22	0	0	100
-1	-2	-21	8	3	36
-1	-2	-20	10	3	27
-1	-2	-19	13	3	22
-1	-2	-18	22	3	13
-1	-2	-17	15	4	29
-1	-2	-16	18	3	14
-1	-2	-15	14	3	23
-1	-2	-14	6	3	45
-1	-2	-13	0	0	100
-1	-2	-12	0	0	100
-1	-2	-11	0	0	100
-1	-2	-10	0	0	100
-1	-2	-1	10	4	43
-1	-2	0	19	5	27
-1	-2	1	0	0	100
-1	-2	2	13	4	35
-1	-2	3	21	5	24
-1	-2	4	16	4	25
-1	-2	5	6	3	50
-1	-2	6	25	6	25
-1	-2	7	30	4	15
-1	-2	8	16	4	25
-1	-2	9	20	3	17
-1	-2	10	0	0	100
-1	-2	11	0	0	100
-1	-2	12	11	3	29
-1	-2	13	0	0	100
-1	-2	14	6	3	53
-1	-2	15	6	3	52
-1	-2	16	16	2	16
-1	-2	17	0	0	100

-1	-2	18	9	3	29
-1	-2	19	17	3	16
-1	-2	20	0	0	100
-1	-2	21	0	0	100
-1	-2	22	0	0	100
-1	-2	23	0	0	100
-1	-2	24	[illegible]	2	62
-1	-2	[illegible]	17	3	15
-1	-2	26	10	3	26
-1	-2	27	15	2	16
-1	-2	28	18	2	14
-1	-2	29	0	0	100
-1	-2	30	0	0	100
-1	-2	31	26	3	10
-1	-2	32	0	0	100
-1	-2	33	0	0	100
-1	-2	34	6	2	41
-1	-2	35	0	0	100
-1	-2	36	0	0	100
-1	-2	37	15	3	18
-1	-2	38	0	0	100
-1	-2	39	0	0	100
-1	-2	40	0	0	100
-1	-2	41	14	3	21
-1	-2	42	0	0	100
-1	-2	43	0	0	100
-1	-2	44	0	0	100
-1	-2	45	38	4	11
-1	-2	46	0	0	100
-1	-2	47	0	0	100
-1	-2	48	0	0	100
-1	-2	49	7	3	37
-1	-2	50	19	2	13
-1	-2	51	0	0	100
-1	-2	52	12	4	29
-1	-2	53	19	3	14
-1	-2	54	0	0	100
-1	-2	55	10	4	37
-1	-2	56	0	0	100
-1	-2	57	8	3	32
-1	-2	58	16	2	16
-1	-2	59	0	0	100
-1	-2	60	13	2	19
-1	-2	61	0	0	100
-1	-2	62	23	3	12
-1	-2	63	0	0	100
-1	-2	65	12	3	23
-1	-2	66	23	3	13
-1	-2	67	45	4	9
-1	-2	69	0	0	100
-1	-2	70	36	4	12
-1	-2	71	10	2	25
-1	-2	72	20	4	18
-1	-2	73	31	3	9
-1	-1	-89	16	2	13
-1	-1	-88	0	0	100
-1	-1	-87	0	0	100
-1	-1	-86	8	2	30
-1	-1	-85	0	0	100
-1	-1	-84	8	2	30
-1	-1	-83	13	2	19
-1	-1	-82	0	0	100
-1	-1	-81	12	2	19
-1	-1	-80	10	2	23
-1	-1	-79	0	0	100
-1	-1	-78	0	0	100
-1	-1	-77	9	2	24
-1	-1	-75	6	2	35
-1	-1	-74	0	0	100
-1	-1	-73	17	2	15
-1	-1	-72	0	0	100
-1	-1	-71	4	2	56
-1	-1	-70	0	0	100
-1	-1	-69	0	0	100
-1	-1	-68	15	2	15
-1	-1	-67	0	0	100
-1	-1	-66	0	0	100
[illegible]	-1	-65	0	0	100
-1	-1	-64	13	2	19
-1	-1	-63	0	0	100
-1	-1	-61	7	3	45
-1	-1	-60	16	2	12
-1	-1	-59	5	2	42
-1	-1	-58	0	0	100
-1	-1	-57	0	0	100
-1	-1	-56	8	2	30
-1	-1	-55	8	2	28

-1	-1	-54	9	2	26
-1	-1	-53	13	2	19
-1	-1	-52	0	0	100
-1	-1	-51	8	2	26
-1	-1	-50	7	3	36
-1	-1	-46	6	2	39
-1	-1	-45	6	2	35
-1	-1	-44	5	2	42
-1	-1	-43	9	2	25
-1	-1	-42	0	0	100
-1	-1	48	0	0	100
-1	-1	49	6	2	38
-1	-1	50	13	2	15
-1	-1	51	0	0	100
-1	-1	52	0	0	100
-1	-1	53	0	0	100
-1	-1	54	0	0	100
-1	-1	55	0	0	100
-1	-1	56	0	0	100
-1	-1	57	0	0	100
-1	-1	58	0	0	100
-1	-1	59	0	0	100
-1	-1	60	11	2	21
-1	-1	61	6	2	37
-1	-1	62	0	0	100
-1	-1	63	8	2	28
-1	-1	64	9	2	27
-1	-1	65	0	0	100
-1	-1	66	0	0	100
-1	-1	67	0	0	100
-1	-1	68	13	3	21
-1	-1	69	23	2	11
-1	-1	70	18	2	14
-1	-1	71	0	0	100
-1	-1	73	15	2	16
-1	-1	74	8	2	32
-1	-1	75	13	2	19
-1	-1	76	0	0	100
-1	-1	77	17	3	15
-1	-1	78	0	0	100
-1	-1	79	15	2	15
-1	-1	80	16	2	14
-1	-1	81	14	2	16
-1	-1	82	0	0	100
-1	-1	83	6	2	40
-1	-1	84	0	0	100
-1	-1	85	12	2	19
-1	-1	86	16	2	14
-1	-1	87	15	2	15
-1	-1	88	0	0	100
-1	-1	89	9	2	25
-1	-1	90	11	2	20
-1	-1	91	10	2	20
-1	-1	92	8	2	32
-1	-1	93	15	3	18
-1	-1	94	0	0	100
-1	-1	95	11	2	18
-1	-1	96	1	2	224
-1	-1	97	4	2	60
-1	-1	98	0	0	100
-1	-1	99	0	0	100
-1	-1	100	0	0	100
-1	1	-100	7	2	31
-1	1	-99	0	0	100
-1	1	-98	10	2	20
-1	1	-97	2	2	115
-1	1	-96	12	2	17
-1	1	-95	0	0	100
-1	1	-94	14	2	14
-1	1	-93	0	0	100
-1	1	-92	7	2	30
-1	1	-91	0	0	100
-1	1	-90	3	2	63
-1	1	-89	0	0	100
-1	1	-88	13	2	17
-1	1	-87	15	2	14
-1	1	-86	4	2	45
-1	1	-85	0	0	100
-1	1	-84	19	2	12
-1	1	-83	0	0	100
-1	1	-82	14	2	16
-1	1	-81	0	0	100
-1	1	-80	10	2	20
-1	1	-79	0	0	100
-1	1	-78	7	2	30
-1	1	-77	6	2	34
-1	1	-76	19	2	12

-1	1	-75	13	2	18
-1	1	-74	4	2	58
-1	1	-73	0	0	100
-1	1	-72	11	2	20
-1	1	-71	5	2	44
-1	1	-70	29	3	11
-1	1	-69	9	2	22
-1	1	-67	12	3	26
-1	1	-66	0	0	100
-1	1	-65	0	0	100
-1	1	-64	17	2	12
-1	1	-63	0	0	100
-1	1	-62	16	3	21
-1	1	-61	0	0	100
-1	1	-60	0	0	100
-1	1	-59	14	2	15
-1	1	-58	0	0	100
-1	1	-57	13	2	18
-1	1	-56	14	2	17
-1	1	-55	0	0	100
-1	1	-54	4	2	56
-1	1	-53	0	0	100
-1	1	-52	8	2	26
-1	1	-51	20	2	11
-1	1	-50	0	0	100
-1	1	-49	17	2	13
-1	1	-48	8	2	29
-1	1	-47	7	2	30
-1	1	-46	6	2	37
-1	1	-45	8	2	24
-1	1	-44	16	2	14
-1	1	-43	10	2	22
-1	1	-42	8	2	28
-1	1	-41	19	2	12
-1	1	-40	0	0	100
-1	1	-39	13	2	16
-1	1	-38	0	0	100
-1	1	-37	9	2	25
-1	1	-36	0	0	100
-1	1	-35	17	2	13
-1	1	-34	6	2	38
-1	1	-33	0	0	100
-1	1	-32	0	0	100
-1	1	-31	0	0	100
-1	1	-30	0	0	100
-1	1	-29	0	0	100
-1	1	-28	0	0	100
-1	1	-27	10	2	21
-1	1	-26	0	0	100
-1	1	-25	0	0	100
-1	1	-24	0	0	100
-1	1	-23	8	2	26
-1	1	-22	7	2	25
-1	1	-21	0	0	100
-1	1	-20	9	2	22
-1	1	-19	16	2	14
-1	1	-18	11	3	24
-1	1	-17	13	3	22
-1	1	-16	0	0	100
-1	1	-15	0	0	100
-1	1	-14	0	0	100
-1	1	-13	6	2	42
-1	1	-12	0	0	100
-1	1	-11	0	0	100
-1	1	-10	8	2	28
-1	1	-9	0	0	100
-1	1	-8	2	2	100
-1	1	-7	0	0	100
-1	1	-6	0	0	100
-1	1	-5	5	2	48
-1	1	-4	0	0	100
-1	1	-3	7	3	40
-1	1	-2	12	3	24
-1	1	-1	16	3	16
-1	1	0	0	0	100
-1	1	1	12	3	22
-1	1	2	12	2	19
-1	1	3	11	2	23
-1	1	4	13	3	23
-1	1	5	6	3	56
-1	1	6	12	4	33
-1	1	7	10	4	43
-1	1	8	0	0	100
-1	1	8	22	4	18
-1	1	9	0	0	100
-1	1	10	18	3	15
-1	1	11	0	0	100
-1	1	12	14	2	16
-1	1	13	0	0	100
-1	1	14	6	2	36
-1	1	15	7	2	34
-1	1	16	9	2	24
-1	1	17	0	0	100
-1	1	18	11	2	20
-1	1	19	10	2	21
-1	1	20	17	2	14
-1	1	21	10	2	23
-1	1	22	2	2	115
-1	1	23	0	0	100
-1	1	33	3	2	60
-1	1	34	0	0	100
-1	1	35	10	2	23
-1	1	36	4	2	55
-1	1	37	10	3	29
-1	1	38	5	2	38
-1	1	39	0	0	100
-1	1	40	7	2	29
-1	1	41	5	2	42
-1	1	42	9	2	21
-1	1	43	4	2	50
-1	1	49	4	2	50
-1	1	50	0	0	100
-1	1	52	0	0	100
-1	1	53	19	3	16
-1	1	54	7	3	46
-1	1	55	0	0	100
-1	1	56	6	2	35
-1	1	57	0	0	100
-1	1	58	11	2	20
-1	1	59	0	0	100
-1	1	60	19	3	16
-1	1	61	12	3	23
-1	1	63	13	2	17
-1	1	64	5	2	40
-1	1	65	8	2	27
-1	1	66	4	2	55
-1	1	67	0	0	100
-1	1	68	5	2	43
-1	1	69	16	2	15
-1	1	70	11	2	18
-1	1	71	9	2	24
-1	1	72	12	3	27
-1	1	73	7	2	27
-1	1	74	4	2	56
-1	1	75	4	2	54
-1	1	76	0	0	100
-1	1	77	5	2	35
-1	1	78	2	2	91
-1	1	79	0	0	100
-1	1	80	0	0	100
-1	1	81	0	0	100
-1	1	82	0	0	100
-1	1	83	4	2	47
-1	1	84	0	0	100
-1	1	85	15	3	20
-1	1	86	0	0	100
-1	1	87	13	2	16
-1	1	88	0	0	100
-1	1	89	0	0	100
-1	1	90	6	2	35
-1	1	91	3	2	58
-1	1	92	0	0	100
-1	1	93	4	2	53
-1	1	94	12	2	17
-1	1	95	9	2	23
-1	1	96	4	2	45
-1	1	97	0	0	100
-1	1	98	0	0	100
-1	1	99	5	2	41
-1	1	100	0	0	100
-1	2	-14	0	0	100
-1	2	-13	0	0	100
-1	2	-12	5	2	46
-1	2	-11	20	4	21
-1	2	-10	10	2	25
-1	2	-9	15	3	21
-1	2	-8	12	3	26
-1	2	-6	22	6	26
-1	2	-5	15	7	43
-1	2	-4	35	7	21
-1	2	-2	27	7	25
-1	2	-1	0	0	100
-1	2	0	0	0	100
-1	2	1	29	4	14
-1	2	2	4	5	126
-1	2	3	32	7	22
-1	2	4	27	10	37
-1	2	5	59	10	16
-1	2	6	44	8	17
-1	2	7	53	10	18
-1	2	8	51	8	15
-1	2	9	18	5	31
-1	2	10	14	3	19
-1	2	11	12	3	22
-1	2	12	13	3	23
-1	2	12	15	3	22
-1	2	13	16	4	25
-1	2	14	16	4	24
-1	2	73	17	2	15
0	-2	-54	11	2	21
0	-2	-53	0	0	100
0	-2	-52	0	0	100
0	-2	-51	0	0	100
0	-2	-50	11	3	25
0	-2	-49	0	0	100
0	-2	-48	12	2	20
0	-2	-47	11	3	24
0	-2	-46	0	0	100
0	-2	-45	0	0	100
0	-2	-44	0	0	100
0	-2	-43	8	3	34
0	-2	-42	0	0	100
0	-2	-41	0	0	100
0	-2	-40	0	0	100
0	-2	-39	18	2	14
0	-2	35	24	3	12
0	-2	36	0	0	100
0	-2	37	0	0	100
0	-2	38	12	3	23
0	-2	39	0	0	100
0	-2	40	20	3	13
0	-2	41	16	2	15
0	-2	42	16	3	16
0	-2	67	29	3	10
0	-1	-100	0	0	100
0	-1	-99	8	2	24
0	-1	-98	4	2	54
0	-1	-97	0	0	100
0	-1	-96	0	0	100
0	-1	-95	11	2	18
0	-1	-94	6	2	36
0	-1	-93	0	0	100
0	-1	-92	16	2	14
0	-1	-91	0	0	100
0	-1	-90	0	0	100
0	-1	-89	0	0	100
0	-1	-88	11	2	19
0	-1	-87	0	0	100
0	-1	-86	13	2	16
0	-1	-85	12	2	16
0	-1	-84	8	2	25
0	-1	-83	0	0	100
0	-1	-82	13	2	15
0	-1	-81	2	2	100
0	-1	-80	0	0	100
0	-1	-79	0	0	100
0	-1	-78	7	2	34
0	-1	-77	0	0	100
0	-1	-76	2	2	91
0	-1	-75	15	2	13
0	-1	-74	9	2	24
0	-1	-73	0	0	100
0	-1	-72	0	0	100
0	-1	-71	4	2	56
0	-1	-70	4	2	51
0	-1	-69	5	2	49
0	-1	-68	7	2	31
0	-1	-67	0	0	100
0	-1	-66	0	0	100
0	-1	-65	0	0	100
0	-1	-64	0	0	100
0	-1	-63	9	2	23
0	-1	-62	11	2	20
0	-1	-62	13	2	17
0	-1	-61	7	2	33
0	-1	-60	24	3	13
0	-1	-59	11	2	20
0	-1	-58	0	0	100
0	-1	-57	0	0	100
0	-1	-56	9	2	25
0	-1	-55	4	2	60

0	-1	-54	0	0	100
0	-1	-53	0	0	100
0	-1	-52	6	2	40
0	-1	-50	14	3	21
0	-1	-49	12	2	17
0	-1	-48	1	2	158
0	-1	-23	0	0	100
0	-1	-22	0	0	100
0	-1	-21	0	0	100
0	-1	-20	6	2	38
0	-1	-19	13	2	17
0	-1	-18	3	2	75
0	-1	-17	0	0	100
0	-1	-16	0	0	100
0	-1	-15	9	2	25
0	-1	-14	0	0	100
0	-1	-12	0	0	100
0	-1	-11	12	2	18
0	-1	-10	0	0	100
0	-1	-9	12	3	27
0	-1	-8	5	3	50
0	-1	-7	0	0	100
0	-1	-6	38	3	8
0	-1	-5	33	3	10
0	-1	-4	23	4	16
0	-1	-3	34	4	11
0	-1	-2	0	0	100
0	-1	-1	24	3	14
0	-1	0	35	3	8
0	-1	1	29	3	11
0	-1	3	14	3	25
0	-1	4	7	3	45
0	-1	5	0	0	100
0	-1	6	5	3	60
0	-1	7	9	2	26
0	-1	9	22	3	15
0	-1	10	0	0	100
0	-1	11	3	2	75
0	-1	12	5	2	43
0	-1	13	11	2	21
0	-1	14	8	2	29
0	-1	15	4	2	50
0	-1	16	0	0	100
0	-1	17	7	2	30
0	-1	18	0	0	100
0	-1	19	9	2	25
0	-1	20	0	0	100
0	-1	21	10	2	23
0	-1	22	16	2	14
0	-1	24	1	2	200
0	-1	25	0	0	100
0	-1	26	0	0	100
0	-1	27	0	0	100
0	-1	28	2	2	91
0	-1	29	4	2	45
0	-1	30	7	2	33
0	-1	31	0	0	100
0	-1	32	11	2	18
0	-1	33	0	0	100
0	-1	35	12	2	19
0	-1	36	0	0	100
0	-1	37	9	2	23
0	-1	38	12	2	19
0	-1	39	0	0	100
0	-1	40	15	3	19
0	-1	41	0	0	100
0	-1	42	11	3	27
0	-1	43	8	2	22
0	-1	44	0	0	100
0	-1	45	0	0	100
0	-1	46	4	2	50
0	-1	47	10	2	20
0	-1	48	9	2	23
0	-1	49	8	2	26
0	-1	50	0	0	100
0	-1	51	10	2	22
0	-1	52	0	0	100
0	-1	53	0	0	100
0	-1	54	0	0	100
0	-1	55	0	0	100
0	-1	56	0	0	100
0	-1	57	8	2	24
0	-1	58	0	0	100
0	-1	59	8	3	36
0	-1	60	0	0	100
0	-1	61	0	0	100
0	-1	62	0	0	100
0	-1	63	0	0	100
0	-1	64	0	0	100
0	-1	65	0	0	100
0	-1	67	0	0	100
0	-1	68	0	0	100
0	-1	69	0	0	100
0	-1	70	10	2	23
0	-1	71	6	2	33
0	-1	72	8	2	27
0	-1	73	5	2	49
0	-1	74	0	0	100
0	-1	75	0	0	100
0	-1	76	9	2	26
0	-1	77	6	2	35
0	-1	78	0	0	100
0	-1	79	9	2	25
0	-1	80	0	0	100
0	-1	81	0	0	100
0	-1	82	12	3	24
0	-1	83	0	0	100
0	-1	84	6	3	45
0	-1	85	0	0	100
0	-1	86	0	0	100
0	-1	87	3	3	100
0	-1	89	8	2	25
0	-1	90	18	3	16
0	-1	91	2	2	115
0	-1	92	0	0	100
0	-1	93	10	2	20
0	-1	94	7	2	29
0	-1	95	6	2	35
0	-1	96	13	2	16
0	-1	97	0	0	100
0	-1	98	7	2	28
0	-1	99	6	2	33
0	-1	100	0	0	100
0	1	-100	0	0	100
0	1	-99	0	0	100
0	1	-98	0	0	100
0	1	-97	11	2	19
0	1	-96	8	2	24
0	1	-95	0	0	100
0	1	-94	8	2	26
0	1	-93	0	0	100
0	1	-92	10	3	30
0	1	-92	0	0	100
0	1	-91	0	0	100
0	1	-90	2	2	100
0	1	-89	2	2	89
0	1	-88	5	2	42
0	1	-87	0	0	100
0	1	-86	0	0	100
0	1	-85	0	0	100
0	1	-84	0	0	100
0	1	-83	0	0	100
0	1	-82	10	2	20
0	1	-81	0	0	100
0	1	-80	0	0	100
0	1	-79	0	0	100
0	1	-78	13	3	23
0	1	-76	5	2	44
0	1	-75	0	0	100
0	1	-74	0	0	100
0	1	-73	7	3	44
0	1	-72	6	2	32
0	1	-71	0	0	100
0	1	-69	8	3	36
0	1	-68	7	2	27
0	1	-67	0	0	100
0	1	-66	0	0	100
0	1	-65	6	2	32
0	1	-64	4	2	52
0	1	-63	0	0	100
0	1	-62	4	2	46
0	1	-61	16	3	19
0	1	-60	5	2	44
0	1	-59	0	0	100
0	1	-58	7	2	27
0	1	-52	0	0	100
0	1	-56	0	0	100
0	1	-55	12	2	16
0	1	-54	7	2	29
0	1	-53	8	2	24
0	1	-52	0	0	100
0	1	-51	0	0	100
0	1	-50	0	0	100
0	1	-49	0	0	100
0	1	-47	11	2	18
0	1	-45	4	2	53
0	1	-44	0	0	100
0	1	-43	13	2	17
0	1	-42	0	0	100
0	1	-42	0	0	100
0	1	-41	0	0	100
0	1	-40	11	2	18
0	1	-39	0	0	100
0	1	-38	8	2	24
0	1	-37	0	0	100
0	1	-36	8	2	25
0	1	-35	0	0	100
0	1	-34	2	2	100
0	1	-33	0	0	100
0	1	-32	0	0	100
0	1	-31	0	0	100
0	1	-30	0	0	100
0	1	-29	0	0	100
0	1	-28	17	3	18
0	1	-27	9	2	23
0	1	-26	10	3	33
0	1	-25	11	2	17
0	1	-24	2	3	129
0	1	-23	11	2	18
0	1	-22	0	0	100
0	1	-21	0	0	100
0	1	-21	0	0	100
0	1	-20	13	2	17
0	1	-19	7	2	31
0	1	-18	6	2	33
0	1	-17	10	2	22
0	1	-16	0	0	100
0	1	-15	0	0	100
0	1	-14	7	2	29
0	1	-13	0	0	100
0	1	-12	0	0	100
0	1	-11	0	0	100
0	1	-10	7	2	33
0	1	-9	7	2	26
0	1	2	15	3	18
0	1	5	6	3	54
0	1	6	10	3	29
0	1	7	0	0	100
0	1	8	0	0	100
0	1	9	2	2	100
0	1	10	0	0	100
0	1	11	0	0	100
0	1	12	0	0	100
0	1	13	23	3	14
0	1	14	0	0	100
0	1	15	9	2	25
0	1	16	12	2	17
0	1	17	2	2	115
0	1	18	0	0	100
0	1	19	0	0	100
0	1	20	0	0	100
0	1	21	12	2	19
0	1	22	6	2	35
0	1	23	10	2	22
0	1	23	10	2	22
0	1	25	17	2	13
0	1	32	0	0	100
0	1	33	10	2	20
0	1	34	6	2	28
0	1	35	0	0	100
0	1	36	7	2	28
0	1	37	10	2	21
0	1	38	4	2	55
0	1	39	5	2	38
0	1	40	8	2	25
0	1	41	8	2	26
0	1	42	13	3	22
0	1	49	14	3	21
0	1	50	14	3	22
0	1	51	10	2	20
0	1	52	0	0	100
0	1	53	0	0	100
0	1	54	4	2	45
0	1	55	15	2	15
0	1	56	15	3	20
0	1	57	0	0	100
0	1	58	0	0	100
0	1	59	0	0	100
0	1	60	0	0	100
0	1	61	13	2	15
0	1	62	0	0	100

0	1	63	0	0	100
0	1	64	0	0	100
0	1	65	11	2	17
0	1	66	0	0	100
0	1	67	6	2	36
0	1	68	0	0	100
0	1	70	0	0	100
0	1	71	13	2	18
0	1	72	5	2	46
0	1	73	6	2	32
0	1	74	13	2	15
0	1	75	0	0	100
0	1	76	3	2	67
0	1	77	0	0	100
0	1	78	0	0	100
0	1	79	0	0	100
0	1	80	0	0	100
0	1	81	2	3	122
0	1	82	0	0	100
0	1	83	0	0	100
0	1	84	18	2	12
0	1	85	0	0	100
0	1	86	19	2	12
0	1	87	8	2	29
0	1	88	12	2	19
0	1	89	0	0	100
0	1	90	10	2	20
0	1	91	0	0	100
0	1	92	0	0	100
0	1	93	0	0	100
0	1	94	5	3	65
0	1	95	0	0	100
0	1	96	0	0	100
0	1	97	0	0	100
0	1	98	17	2	13
0	1	99	0	0	100
0	1	100	0	0	100
0	2	23	3	2	75
0	2	24	6	3	41
0	2	25	0	0	100
0	2	26	0	0	100
0	2	27	17	4	21
0	2	28	0	0	100
0	2	30	0	0	100
0	2	31	0	0	100
0	2	32	9	3	30
0	2	33	0	0	100
0	2	34	10	2	23
0	2	35	0	0	100
0	2	36	13	2	18
0	2	37	10	2	24
0	2	38	6	2	44
0	2	39	0	0	100
0	2	40	0	0	100
0	2	41	0	0	100
0	2	42	14	3	21
0	2	43	0	0	100
0	2	44	14	3	19
0	2	45	15	2	16
0	2	46	7	3	37
0	2	47	0	0	100
0	2	48	10	2	25
0	2	49	12	3	24
0	2	50	15	4	24
0	2	51	12	2	19
0	2	52	7	2	37
0	2	53	0	0	100
1	-2	-15	19	3	16
1	-2	-14	5	4	82
1	-2	-13	19	3	15
1	-2	-12	0	0	100
1	-2	-11	26	6	20
1	-2	-10	18	5	27
1	-2	-9	14	7	47
1	-2	-8	26	8	30
1	-2	-7	15	5	32
1	-2	-6	27	7	26
1	-2	-5	43	7	17
1	-2	-4	37	7	19
1	-2	-2	29	5	17
1	-2	-1	12	5	42
1	-2	0	14	5	34
1	-2	1	15	6	42
1	-2	2	52	10	20
1	-2	3	61	10	17
1	-2	4	31	6	20
1	-2	5	45	7	15
1	-2	6	15	5	34
1	-2	7	33	5	17
1	-2	8	15	5	34
1	-2	9	15	6	41
1	-2	10	16	3	19
1	-2	10	27	5	17
1	-2	11	14	5	32
1	-2	12	9	2	25
1	-2	13	0	0	100
1	-2	14	0	0	100
1	-1	-100	0	0	100
1	-1	-99	2	2	82
1	-1	-98	2	2	89
1	-1	-97	0	0	100
1	-1	-96	6	2	32
1	-1	-95	0	0	100
1	-1	-94	0	0	100
1	-1	-93	13	3	22
1	-1	-92	0	0	100
1	-1	-91	0	0	100
1	-1	-90	0	0	100
1	-1	-89	2	2	115
1	-1	-88	0	0	100
1	-1	-87	8	2	24
1	-1	-86	4	2	53
1	-1	-84	4	2	46
1	-1	-83	0	0	100
1	-1	-82	5	3	52
1	-1	-81	10	2	20
1	-1	-80	8	2	24
1	-1	-79	5	2	40
1	-1	-78	9	2	21
1	-1	-77	0	0	100
1	-1	-76	0	0	100
1	-1	-75	6	2	35
1	-1	-73	21	3	14
1	-1	-71	12	2	17
1	-1	-70	0	0	100
1	-1	-69	8	2	28
1	-1	-68	0	0	100
1	-1	-67	0	0	100
1	-1	-66	10	3	29
1	-1	-65	7	2	26
1	-1	-64	5	2	37
1	-1	-63	0	0	100
1	-1	-62	0	0	100
1	-1	-61	5	2	39
1	-1	-60	0	0	100
1	-1	-59	0	0	100
1	-1	-58	16	2	12
1	-1	-57	14	2	16
1	-1	-56	6	2	34
1	-1	-55	4	2	55
1	-1	-53	16	2	14
1	-1	-52	0	0	100
1	-1	-51	2	2	91
1	-1	-50	15	3	20
1	-1	-49	7	2	30
1	-1	-32	7	2	27
1	-1	-24	0	0	100
1	-1	-23	5	2	37
1	-1	-22	0	0	100
1	-1	-21	17	2	13
1	-1	-20	0	0	100
1	-1	-19	0	0	100
1	-1	-18	5	2	41
1	-1	-17	10	2	21
1	-1	-16	7	2	31
1	-1	-15	4	2	47
1	-1	-14	8	2	25
1	-1	-13	7	2	33
1	-1	-12	12	2	17
1	-1	-11	0	0	100
1	-1	-10	0	0	100
1	-1	-9	8	2	27
1	-1	-8	7	2	28
1	-1	-7	0	0	100
1	-1	-6	0	0	100
1	-1	-5	9	3	31
1	-1	-4	6	3	50
1	-1	-3	15	3	19
1	-1	-2	10	2	24
1	-1	-1	17	3	26
1	-1	0	9	3	28
1	-1	1	8	2	29
1	-1	2	9	3	29
1	-1	3	9	3	32
1	-1	4	9	3	30
1	-1	5	0	0	100
1	-1	6	0	0	100
1	-1	8	16	3	18
1	-1	9	7	2	32
1	-1	10	8	2	29
1	-1	11	0	0	100
1	-1	12	7	2	34
1	-1	13	7	2	31
1	-1	14	0	0	100
1	-1	15	0	0	100
1	-1	16	12	2	17
1	-1	17	0	0	100
1	-1	18	0	0	100
1	-1	19	12	2	18
1	-1	20	0	0	100
1	-1	21	0	0	100
1	-1	22	0	0	100
1	-1	23	11	2	20
1	-1	24	4	2	56
1	-1	25	7	2	30
1	-1	26	0	0	100
1	-1	27	12	2	19
1	-1	28	0	0	100
1	-1	29	0	0	100
1	-1	30	5	2	37
1	-1	31	0	0	100
1	-1	31	0	0	100
1	-1	33	0	0	100
1	-1	35	9	2	23
1	-1	36	11	2	19
1	-1	37	0	0	100
1	-1	38	7	2	27
1	-1	39	15	2	15
1	-1	40	7	2	30
1	-1	41	17	2	13
1	-1	42	0	0	100
1	-1	43	0	0	100
1	-1	44	9	2	21
1	-1	45	0	0	100
1	-1	46	0	0	100
1	-1	47	8	2	24
1	-1	48	19	3	16
1	-1	49	12	2	18
1	-1	50	0	0	100
1	-1	51	12	2	19
1	-1	52	6	2	35
1	-1	53	0	0	100
1	-1	54	9	2	22
1	-1	55	14	2	15
1	-1	56	10	2	21
1	-1	57	3	2	43
1	-1	58	0	0	100
1	-1	59	4	2	56
1	-1	60	0	0	100
1	-1	61	0	0	100
1	-1	62	4	2	52
1	-1	63	0	0	100
1	-1	64	0	0	100
1	-1	64	0	0	100
1	-1	65	6	2	36
1	-1	66	10	2	19
1	-1	67	0	0	100
1	-1	68	5	2	44
1	-1	69	21	2	12
1	-1	70	4	2	53
1	-1	71	14	3	22
1	-1	72	0	0	100
1	-1	73	9	2	25
1	-1	74	10	2	24
1	-1	75	9	2	25
1	-1	76	0	0	100
1	-1	77	21	2	11
1	-1	78	23	2	10
1	-1	79	0	0	100
1	-1	80	0	0	100
1	-1	81	0	0	100
1	-1	82	0	0	100
1	-1	83	10	2	22
1	-1	84	0	0	100
1	-1	85	0	0	100
1	-1	86	7	2	32
1	-1	87	0	0	100
1	-1	88	9	2	25
1	-1	89	0	0	100
1	-1	90	12	2	19
1	-1	91	0	0	100

1	-1	92	12	2	16
1	-1	93	3	2	63
1	-1	94	10	2	22
1	-1	95	6	2	32
1	-1	96	0	0	100
1	-1	97	0	0	100
1	-1	98	10	3	26
1	-1	99	0	0	100
1	-1	100	15	2	15
1	1	-100	0	0	100
1	1	-98	0	0	100
1	1	-97	4	2	47
1	1	-95	22	3	14
1	1	-94	0	0	100
1	1	-93	0	0	100
1	1	-92	0	0	100
1	1	-91	0	0	100
1	1	-90	8	2	28
1	1	-89	5	2	43
1	1	-88	0	0	100
1	1	-87	17	3	18
1	1	-86	11	2	21
1	1	-85	14	2	16
1	1	-84	0	0	100
1	1	-83	4	3	76
1	1	-82	0	0	100
1	1	-81	7	2	30
1	1	-80	0	0	100
1	1	-79	3	2	58
1	1	-78	0	0	100
1	1	-77	0	0	100
1	1	-76	0	0	100
1	1	-76	0	0	100
1	1	-75	3	2	65
1	1	-74	9	2	26
1	1	-73	7	2	31
1	1	-72	0	0	100
1	1	-71	10	2	22
1	1	-70	20	2	12
1	1	-69	23	2	11
1	1	-68	7	2	35
1	1	-67	8	2	27
1	1	-66	6	2	38
1	1	-65	14	2	18
1	1	-64	0	0	100
1	1	-63	0	0	100
1	1	-62	16	3	19
1	1	-61	7	2	31
1	1	-60	0	0	100
1	1	-59	8	2	26
1	1	-58	5	2	44
1	1	-57	12	2	19
1	1	-56	9	2	24
1	1	-55	0	0	100
1	1	-54	0	0	100
1	1	-53	9	2	24
1	1	-52	0	0	100
1	1	-51	12	2	19
1	1	-50	0	0	100
1	1	-49	5	2	46
1	1	-48	0	0	100
1	1	-46	4	2	55
1	1	-45	0	0	100
1	1	-44	2	2	100
1	1	-43	0	0	100
1	1	-42	0	0	100
1	1	-40	11	2	20
1	1	-39	0	0	100
1	1	-38	0	0	100
1	1	-37	10	2	25
1	1	-36	4	2	60
1	1	-35	9	2	28
1	1	-34	0	0	100
1	1	-34	0	0	100
1	1	-33	5	2	51
1	1	-33	12	2	20
1	1	-32	0	0	100
1	1	-31	7	2	33
1	1	-30	0	0	100
1	1	-29	0	0	100
1	1	-28	0	0	100
1	1	-27	15	2	15
1	1	15	12	3	27
1	1	17	8	3	34
1	1	18	5	2	45
1	1	19	9	2	25
1	1	20	0	0	100

1	1	52	19	2	13
1	1	73	11	3	28
1	1	74	4	2	63
1	1	75	0	0	100
1	1	77	5	2	44
1	1	78	0	0	100
1	1	79	18	3	20
1	1	81	9	3	39
1	1	82	0	0	100
1	1	83	0	0	100
1	1	84	0	0	100
1	1	85	0	0	100
1	1	86	0	2	100
1	1	87	19	3	14
1	2	-73	6	3	46
1	2	-72	0	0	100
1	2	-71	0	0	100
1	2	-70	4	3	69
1	2	-69	19	3	15
1	2	-68	0	0	100
1	2	-67	25	3	12
1	2	-66	0	0	100
1	2	-65	25	3	11
1	2	-64	4	3	59
1	2	-63	0	0	100
1	2	-62	0	0	100
1	2	-61	0	0	100
1	2	-60	0	0	100
1	2	-59	0	0	100
1	2	-58	20	3	13
1	2	-57	0	0	100
1	2	-56	23	4	17
1	2	-55	18	2	14
1	2	-54	0	0	100
1	2	-53	14	3	18
1	2	-52	28	3	11
1	2	-51	0	0	100
1	2	-50	11	3	23
1	2	-49	21	3	13
1	2	-49	21	3	13
1	2	-48	0	0	100
1	2	-47	0	0	100
1	2	-46	15	3	18
1	2	-45	0	0	100
1	2	-44	4	3	68
1	2	-43	0	0	100
1	2	-42	17	3	16
1	2	-41	37	4	10
1	2	-40	23	4	17
1	2	-39	0	0	100
1	2	-38	18	3	16
1	2	-37	13	3	20
1	2	-36	0	0	100
1	2	-35	20	4	19
1	2	-34	0	0	100
1	2	-33	0	0	100
1	2	-32	0	0	100
1	2	-31	15	4	24
1	2	-30	0	0	100
1	2	-29	0	0	100
1	2	-28	0	0	100
1	2	-27	9	3	32
1	2	-26	10	2	25
1	2	-25	0	0	100
1	2	-24	13	3	21
1	2	-23	4	3	61
1	2	-22	15	3	19
1	2	-21	15	3	18
1	2	-20	9	2	28
1	2	-19	5	3	54
1	2	-18	27	3	10
1	2	-17	0	0	100
1	2	-16	15	3	19
1	2	-15	13	3	21
1	2	-14	9	3	30
1	2	-13	20	3	14
1	2	-12	9	3	32
1	2	-11	10	3	33
1	2	-10	9	3	38
1	2	-2	6	5	85
1	2	0	18	4	21
1	2	1	20	5	24
1	2	2	11	4	41
1	2	3	17	6	35
1	2	4	30	6	20
1	2	7	8	3	31
1	2	8	0	0	100

1	2	9	17	3	20
1	2	10	11	3	31
1	2	11	13	4	31
1	2	12	3	3	100
1	2	13	0	0	100
1	2	14	16	3	18
1	2	15	14	2	17
1	2	16	9	3	29
1	2	17	4	2	68
1	2	18	0	0	100
1	2	19	17	3	17
1	2	20	0	0	100
1	2	21	7	3	40
1	2	22	15	3	18
1	2	23	19	3	14
1	2	24	7	3	38
1	2	25	10	3	28
1	2	26	0	0	100
1	2	27	0	0	100
1	2	28	15	3	18
1	2	29	8	3	35
1	2	30	15	3	19
1	2	31	21	3	14
1	2	32	23	3	13
1	2	33	24	4	17
1	2	34	0	0	100
1	2	35	17	3	17
1	2	36	0	0	100
1	2	37	0	0	100
1	2	38	9	4	40
1	2	39	23	2	11
1	2	40	0	0	100
1	2	41	0	0	100
1	2	42	0	0	100
1	2	43	13	2	19
1	2	44	0	0	100
1	2	45	0	0	100
1	2	46	0	0	100
1	2	47	0	0	100
1	2	48	17	2	13
1	2	49	21	3	13
1	2	50	0	0	100
1	2	51	0	0	100
1	2	52	11	2	22
1	2	53	11	2	22
1	2	54	0	0	100
1	2	55	0	0	100
1	2	56	0	0	100
1	2	57	0	0	100
1	2	58	26	4	14
2	-2	-55	9	2	28
2	-2	-54	23	3	12
2	-2	-53	2	2	100
2	-2	-52	0	0	100
2	-2	-51	6	3	48
2	-2	-50	13	2	19
2	-2	-49	15	3	17
2	-2	-48	18	3	15
2	-2	-47	14	2	17
2	-2	-9	15	3	23
2	-2	-7	25	6	23
2	-2	-6	25	6	25
2	-2	-5	0	0	100
2	-2	-4	39	11	28
2	-2	-3	0	0	100
2	-2	-2	0	0	100
2	-2	-1	0	0	100
2	-2	0	0	0	100
2	-2	1	15	10	68
2	-2	2	4	8	195
2	-2	3	9	5	57
2	-2	4	8	5	68
2	-2	5	5	4	80
2	-2	6	14	6	42
2	-2	7	28	5	17
2	-2	8	16	3	20
2	-2	9	0	0	100
2	-2	11	5	5	88
2	-2	12	17	4	23
2	-2	17	0	0	100
2	-2	18	0	0	100
2	-2	20	0	0	100
2	-2	21	14	2	18
2	-2	22	16	2	16
2	-2	23	0	0	100
2	-2	24	0	0	100
2	-2	25	19	3	16

2	-2	26	25	3	10
2	-2	27	0	0	100
2	-2	28	0	0	100
2	-2	29	0	0	100
2	-2	30	15	3	18
2	-2	31	8	3	35
2	-2	32	1	4	374
2	-2	33	0	0	100
2	-1	-98	0	0	100
2	-1	-97	18	2	12
2	-1	-96	0	0	100
2	-1	-95	24	3	13
2	-1	-94	0	0	100
2	-1	-93	0	0	100
2	-1	-92	0	0	100
2	-1	-91	12	2	19
2	-1	-90	26	3	12
2	-1	-89	0	0	100
2	-1	-88	0	0	100
2	-1	-87	0	0	100
2	-1	-86	11	3	29
2	-1	-85	0	0	100
2	-1	-84	11	2	18
2	-1	-83	31	3	10
2	-1	-82	7	3	47
2	-1	-81	23	3	14
2	-1	-80	7	2	33
2	-1	-79	0	0	100
2	-1	-78	0	0	100
2	-1	-77	16	2	14
2	-1	-76	0	0	100
2	-1	-75	10	2	24
2	-1	-74	8	2	31
2	-1	-73	0	0	100
2	-1	-72	25	2	10
2	-1	-71	17	2	14
2	-1	-70	0	0	100
2	-1	-69	9	2	26
2	-1	-68	0	0	100
2	-1	-67	0	0	100
2	-1	-66	9	2	26
2	-1	-65	6	2	36
2	-1	-64	4	2	51
2	-1	-63	16	2	14
2	-1	-62	0	0	100
2	-1	-61	3	2	82
2	-1	-60	13	2	15
2	-1	-59	2	2	129
2	-1	-58	0	0	100
2	-1	-57	0	0	100
2	-1	-56	0	0	100
2	-1	-55	0	0	100
2	-1	-54	6	2	44
2	-1	-53	22	3	15
2	-1	-52	0	0	100
2	-1	-51	10	2	21
2	-1	-50	13	2	19
2	-1	-48	0	0	100
2	-1	-47	0	0	100
2	-1	-46	11	2	22
2	-1	-45	12	2	20
2	-1	-44	0	0	100
2	-1	-23	10	2	23
2	-1	-22	0	0	100
2	-1	-21	0	0	100
2	-1	-20	0	0	100
2	-1	-19	20	3	15
2	-1	-18	4	2	63
2	-1	-17	13	2	17
2	-1	-16	6	2	36
2	-1	-15	5	2	52
2	-1	-14	0	0	100
2	-1	-13	15	3	17
2	-1	-12	8	3	35
2	-1	-11	6	2	39
2	-1	-10	0	0	100
2	-1	-6	15	3	21
2	-1	-5	0	0	100
2	-1	-4	0	0	100
2	-1	5	6	3	58
2	-1	6	3	4	122
2	-1	7	16	3	20
2	-1	7	11	5	44
2	-1	8	0	0	100
2	-1	9	5	3	62
2	-1	11	4	2	53
2	-1	13	0	0	100

2	-1	14	6	2	38
2	-1	19	0	0	100
2	-1	20	6	2	41
2	-1	21	17	2	14
2	-1	22	9	2	24
2	-1	23	18	3	15
2	-1	24	0	0	100
2	-1	25	0	0	100
2	-1	26	16	2	16
2	-1	27	0	0	100
2	-1	28	12	3	22
2	-1	29	0	0	100
2	-1	30	0	0	100
2	-1	31	16	2	15
2	-1	33	15	3	20
2	-1	34	14	2	17
2	-1	35	7	2	34
2	-1	36	0	0	100
2	-1	37	18	2	14
2	-1	38	6	2	39
2	-1	39	32	4	12
2	-1	40	12	2	18
2	-1	41	0	0	100
2	-1	42	22	3	15
2	-1	43	0	0	100
2	-1	44	0	0	100
2	-1	45	0	0	100
2	-1	46	11	2	20
2	-1	47	0	0	100
2	-1	48	0	0	100
2	-1	49	15	2	14
2	-1	50	6	2	38
2	-1	51	23	2	10
2	-1	52	2	2	100
2	-1	53	16	2	14
2	-1	54	13	2	18
2	-1	55	8	2	29
2	-1	56	9	3	30
2	-1	58	0	0	100
2	-1	59	25	3	13
2	-1	60	15	3	16
2	-1	61	14	3	21
2	-1	62	0	0	100
2	-1	63	5	2	52
2	-1	64	15	2	17
2	-1	65	22	2	10
2	-1	66	0	0	100
2	-1	67	28	3	12
2	-1	68	0	0	100
2	-1	69	24	2	9
2	-1	70	12	2	18
2	-1	71	24	2	10
2	-1	72	17	4	21
2	-1	73	0	0	100
2	-1	74	0	0	100
2	-1	75	13	3	21
2	-1	76	0	0	100
2	-1	77	0	0	100
2	-1	78	9	2	25
2	-1	79	0	0	100
2	-1	80	0	0	100
2	-1	81	5	2	47
2	-1	82	0	0	100
2	-1	83	13	2	17
2	-1	84	15	2	17
2	-1	85	0	0	100
2	-1	86	13	2	17
2	-1	87	5	2	44
2	-1	89	24	3	14
2	0	-100	0	0	100
2	0	-99	4	2	55
2	0	-98	9	2	23
2	0	-97	0	0	100
2	0	-96	10	2	20
2	0	-95	11	2	18
2	0	-94	12	2	16
2	0	-93	0	0	100
2	0	-92	18	3	19
2	0	-91	0	0	100
2	0	-90	0	0	100
2	0	-89	0	0	100
2	0	-88	0	0	100
2	0	-87	20	2	11
2	0	-86	0	0	100
2	0	-85	0	0	100
2	0	-84	11	2	19
2	0	-83	5	2	39

2	0	-82	0	0	100
2	0	-81	9	2	22
2	0	-80	11	2	20
2	0	-79	12	2	19
2	0	-78	1	3	212
2	0	-77	11	2	20
2	0	-76	0	0	100
2	0	-75	0	0	100
2	0	-74	0	0	100
2	0	-73	9	2	25
2	0	-72	11	2	21
2	0	-71	0	0	100
2	0	-70	14	2	16
2	0	-69	17	2	13
2	0	-68	8	2	29
2	0	-67	12	2	19
2	0	-66	0	0	100
2	0	-65	8	2	25
2	0	-64	0	0	100
2	0	-63	11	2	20
2	0	-62	3	2	74
2	0	-61	0	0	100
2	0	-60	5	2	50
2	0	-59	11	2	20
2	0	-58	8	2	29
2	0	-57	0	0	100
2	0	-56	0	0	100
2	0	-55	0	0	100
2	0	-54	3	2	63
2	0	-53	8	2	26
2	0	-52	0	0	100
2	0	-51	3	3	80
2	0	-50	7	2	31
2	0	-49	0	0	100
2	0	-48	9	2	25
2	0	-47	0	0	100
2	0	-46	3	2	74
2	0	-45	5	2	42
2	0	-44	7	2	27
2	0	-43	0	0	100
2	0	-43	0	0	100
2	0	-42	0	0	100
2	0	-41	2	2	112
2	0	-40	3	2	65
2	0	-39	0	0	100
2	0	-38	0	0	100
2	0	-37	0	0	100
2	0	-36	7	2	30
2	0	-35	0	0	100
2	0	-34	0	0	100
2	0	-33	14	2	18
2	0	-32	4	2	58
2	0	-31	16	2	14
2	0	-30	3	2	71
2	0	14	11	3	32
2	0	15	0	0	100
2	0	16	15	2	17
2	0	17	0	0	100
2	0	19	15	2	15
2	0	55	15	2	15
2	0	64	10	3	30
2	0	65	0	0	100
2	0	66	7	3	46
2	0	67	12	2	18
2	0	69	0	0	100
2	0	70	12	3	23
2	0	71	22	3	12
2	0	73	2	3	132
2	0	75	0	0	100
2	0	76	13	2	19
2	0	77	0	0	100
2	0	78	0	0	100
2	0	79	11	2	23
2	0	80	0	0	100
2	0	81	0	0	100
2	0	82	0	0	100
2	0	83	0	0	100
2	0	84	14	3	25
2	0	85	0	0	100
2	0	86	12	2	21
2	0	87	0	0	100
2	1	15	[illegible]	3	21
2	1	-84	0	0	100
2	1	-83	0	0	100
2	1	-82	0	3	100
2	1	-81	9	3	29
2	1	-81	9	3	29

2	1	-80	10	2	24
2	1	-79	0	0	100
2	1	-78	10	2	23
2	1	-77	18	2	14
2	1	-76	0	0	100
2	1	-75	8	2	29
2	1	-74	0	0	100
2	1	-73	11	2	20
2	1	-72	23	3	12
2	1	-71	0	0	100
2	1	-70	7	2	36
2	1	-69	0	0	100
2	1	-68	10	3	26
2	1	-67	18	2	14
2	1	-66	15	3	18
2	1	-65	0	0	100
2	1	-64	11	2	22
2	1	-63	0	0	100
2	1	-62	19	2	13
2	1	-61	20	3	13
2	1	-60	11	3	23
2	1	-59	10	2	24
2	1	-58	0	0	100
2	1	-57	9	2	29
2	1	-56	5	3	53
2	1	-55	0	0	100
2	1	-54	7	3	36
2	1	-53	33	3	11
2	1	-52	7	2	33
2	1	-51	0	0	100
2	1	-50	0	0	100
2	1	-49	24	2	10
2	1	-48	15	3	19
2	1	-47	15	3	18
2	1	-46	7	3	37
2	1	-45	0	0	100
2	1	-44	7	4	56
2	1	-43	14	3	19
2	1	-42	0	0	100
2	1	-41	11	2	22
2	1	-40	0	0	100
2	1	-39	0	0	100
2	1	-38	8	3	34
2	1	-37	18	3	15
2	1	-36	14	3	18
2	1	-35	17	3	16
2	1	-34	0	0	100
2	1	-33	10	3	27
2	1	-32	7	3	40
2	1	-31	0	0	100
2	1	-30	0	0	100
2	1	-29	4	2	59
2	1	-28	0	0	100
2	1	-26	0	0	100
2	1	-24	0	0	100
2	1	-21	0	0	100
2	1	-20	10	3	27
2	1	-19	11	3	24
2	1	-18	21	3	14
2	1	-16	13	2	18
2	1	-14	20	4	18
2	1	-12	3	4	129
2	1	-9	11	4	39
2	1	-5	21	7	36
2	1	0	48	8	17
2	1	6	8	8	102
2	1	9	16	4	25
2	1	11	5	3	63
2	1	12	13	2	18
2	1	13	12	3	27
2	1	66	17	3	17
2	1	67	0	0	100
2	1	68	6	4	61
2	1	69	18	4	21
2	1	70	0	0	100
2	1	71	15	3	19
2	1	72	5	3	55
2	1	73	18	3	15
2	2	-14	19	3	15
2	2	-13	7	3	48
3	-2	-53	0	0	100
3	-2	-52	11	2	22
3	-2	-50	15	3	20
3	-2	-49	0	0	100
3	-2	-48	4	3	64
3	-2	-47	0	0	100
3	-2	-46	0	0	100
3	-2	-45	0	0	100
3	-2	-44	9	3	31
3	-2	-43	0	0	100
3	-2	-42	9	3	31
3	-2	-41	22	3	12
3	-2	-40	0	0	100
3	-2	-39	18	3	17
3	-2	-38	15	3	18
3	-2	-37	21	3	14
3	-2	-36	22	3	13
3	-2	-35	0	0	100
3	-2	-34	0	0	100
3	-2	-33	4	3	66
3	-2	-32	0	0	100
3	-2	-31	14	3	20
3	-2	-30	10	3	26
3	-2	-29	0	0	100
3	-2	-28	0	0	100
3	-2	-27	0	0	100
3	-2	-26	0	0	100
3	-2	-25	10	3	25
3	-2	-24	19	3	14
3	-2	-23	13	3	20
3	-2	-23	13	3	20
3	-2	-22	13	3	20
3	-2	-21	12	3	23
3	-2	-20	0	0	100
3	-2	-19	0	0	100
3	-2	-18	0	0	100
3	-2	-17	0	0	100
3	-2	-16	0	0	100
3	-2	-15	10	4	36
3	-2	-14	0	0	100
3	-2	-13	0	0	100
3	-2	-12	5	3	60
3	-2	-11	0	0	100
3	-2	-10	16	4	26
3	-2	-2	14	3	21
3	-2	1	16	3	18
3	-2	2	18	3	19
3	-2	3	2	3	108
3	-2	5	0	0	100
3	-2	45	0	0	100
3	-2	46	0	0	100
3	-2	47	33	4	11
3	-2	48	0	0	100
3	-2	49	0	0	100
3	-2	50	0	0	100
3	-2	69	12	3	22
3	-2	70	16	3	17
3	-1	17	19	3	14
3	-1	21	9	2	26
3	-1	23	5	3	51
3	-1	24	24	3	12
3	-1	46	22	3	13
3	-1	47	0	0	100
3	-1	49	0	0	100
3	-1	50	0	0	100
3	-1	54	0	0	100
3	-1	55	0	0	100
3	-1	56	0	0	100
3	-1	57	0	0	100
3	-1	58	23	3	11
3	-1	59	0	0	100
3	-1	60	0	0	100
3	-1	61	0	0	100
3	-1	62	9	3	30
3	-1	63	0	0	100
3	-1	64	0	0	100
3	-1	65	4	3	71
3	-1	66	0	0	100
3	-1	67	36	4	12
3	0	5	15	6	40
3	0	6	28	5	19
3	0	8	8	3	39
3	0	9	21	5	26
3	0	10	12	4	31
3	0	31	0	0	100
3	0	33	0	0	100
3	1	-53	0	0	100
3	1	-52	0	0	100
3	1	-51	0	0	100
3	1	-50	0	0	100
3	1	-49	13	3	22
3	1	-48	0	0	100
3	1	-47	13	3	22
3	1	-46	0	0	100
3	1	-44	0	0	100
3	1	-44	0	0	100
3	1	-43	0	0	100
3	1	-39	0	0	100
3	1	-36	0	0	100
3	1	-34	0	0	100
3	1	-31	0	0	100
3	1	-28	9	3	28
3	1	-27	8	3	35
3	1	-26	11	3	25
3	1	-10	16	3	18
3	1	-9	4	3	62
3	1	3	4	3	77
3	1	5	0	0	100
3	1	8	8	3	39
3	1	9	14	3	22
3	1	17	0	0	100
3	1	18	7	3	38
3	1	19	0	0	100
3	1	21	0	0	100
3	1	22	0	0	100
3	1	23	0	0	100
4	-1	-29	0	0	100
4	-1	-28	0	0	100
4	-1	-27	12	4	33
4	-1	-26	1	3	265
4	-1	-23	0	0	100
4	-1	-22	14	3	22
4	-1	-21	0	0	100
4	-1	-20	8	3	35
4	-1	-18	0	0	100
4	-1	-17	0	0	100
4	-1	-15	0	0	100
4	-1	-14	0	0	100
4	-1	-13	8	3	46
4	-1	-12	0	0	100
4	-1	5	0	0	100
4	-1	6	0	0	100
4	-1	7	10	3	28
4	-1	9	0	0	100
4	-1	11	0	0	100
4	-1	12	0	0	100

Native Data : Analysis Rfactor v Intensity

Imax	Rfac	Av_I	σ	I/σ	sd	Nmeas	Nref	Ncent
500.	0.514	191.	199.9	1.0	99.4	748.	372	0
1000.	0.322	811.	427.8	1.9	220.8	24.	12	0
1500.	0.185	1386.	331.1	4.2	274.4	4.	2	0
2000.	0.000	0.	0.0	0.0	0.0	0.	0	0
2500.	0.000	0.	0.0	0.0	0.0	0.	0	0
3000.	0.000	0.	0.0	0.0	0.0	0.	0	0
3500.	0.000	0.	0.0	0.0	0.0	0.	0	0
4000.	0.000	0.	0.0	0.0	0.0	0.	0	0
4500.	0.000	0.	0.0	0.0	0.0	0.	0	0

5000.	0.000	0.	0.0	0.0	0.0	0.	0	0
5500.	0.000	5041.	0.0	0.0	224.5	2.	1	0
6000.	0.000	0.	0.0	0.0	0.0	0.	0	0
44521.	0.074	41469.	3060.7	13.5	640.6	2.	1	0
Totals	0.333	335.	261.8	1.3	105.8	780.	388	0

Native Data : Analysis Completeness & multiplicity v. resolution

N	<s>	Dmin	Nmeas	Nref	%poss	Multiplicity
1	0.003	18.97	225	146	67.9	1.5
2	0.006	13.41	191	150	38.1	1.3
3	0.008	10.95	219	162	31.8	1.4
4	0.011	9.49	306	240	39.8	1.3
5	0.014	8.48	213	158	23.1	1.3
6	0.017	7.75	158	120	15.9	1.3
7	0.019	7.17	119	92	11.2	1.3
8	0.022	6.71	97	77	8.7	1.3
9	0.025	6.32	32	23	2.4	1.4
10	0.028	6.00	0	0	0.0	0.0
	Total		1560	1168	17.2	1.3

Native Data : Analysis of standard deviation v. Intensity

Range	Imin	Imax	Irms	No	Mean	Sigma
1	0.	500.	288.	748.	0.28	0.96
2	500.	1000.	926.	24.	0.26	1.23
3	1000.	1500.	1417.	4.	0.14	0.91
4	1500.	2000.	0.	0.	0.00	0.00
5	2000.	2500.	0.	0.	0.00	0.00
6	2500.	3000.	0.	0.	0.00	0.00
7	3000.	3500.	0.	0.	0.00	0.00
8	3500.	4000.	0.	0.	0.00	0.00
9	4000.	4500.	0.	0.	0.00	0.00
10	4500.	5000.	0.	0.	0.00	0.00
11	5000.	5500.	5041.	2.	0.00	0.00
12	5500.	6000.	0.	0.	0.00	0.00
13	6000.	41244.	41581.	2.	0.17	4.76
Totals	0.	41244.	2148.	780.	0.28	1.00

XII. APPENDIX C (Gold Data)

h	k	l	F	σF	σF/F
-1	-1	-11	149	25	17
-1	-1	-12	190	29	15
-1	-1	-13	166	27	16
-1	-1	-21	60	8	13
-1	-1	-27	94	9	9
-1	-1	-44	68	9	13
-1	-1	-46	52	7	14
-1	-1	-47	34	7	21
-1	-1	-48	30	6	20
-1	-1	-49	46	7	15
-1	-1	-50	77	6	8
-1	-1	-52	228	30	13
-1	-1	-53	38	5	14
-1	-1	-54	245	31	13
-1	-1	-55	121	7	6
-1	-1	-56	92	11	11
-1	-1	-57	111	13	11
-1	-1	-59	113	11	10
-1	-1	-60	96	10	10
-1	-1	-61	93	10	11
-1	-1	-62	51	10	19
-1	-1	-63	103	11	11
-1	-1	-64	90	18	20
-1	-1	-65	86	21	24
-1	-1	-68	304	24	8
-1	-1	-69	95	8	9
-1	-1	-7	169	29	17
-1	-1	-70	43	9	21
-1	-1	-71	85	7	9
-1	-1	-72	82	9	11
-1	-1	-73	57	8	14
-1	-1	-74	118	8	7
-1	-1	-76	41	4	11
-1	-1	-80	62	6	9
-1	-1	-81	51	6	12
-1	-1	9	105	19	18
-1	-1	41	115	8	7
-1	-1	42	69	7	10
-1	-1	46	70	6	9
-1	-1	48	51	7	14
-1	-1	49	121	12	10
-1	-1	50	64	10	16
-1	-1	57	66	7	11
-1	-1	59	57	6	11
-1	-1	61	45	6	14
-1	-1	62	88	12	14
-1	-1	63	59	8	13
-1	-1	64	90	10	12
-1	-1	66	43	7	17
-1	-1	67	53	7	13
-1	-1	68	90	8	9
-1	-1	68	104	8	8
-1	-1	71	47	9	19
-1	-1	72	56	11	19
-1	-1	75	47	7	14
-1	-1	76	45	10	21
-1	-1	76	46	10	21
-1	-1	79	127	11	9
-1	-1	80	132	10	8
-1	-1	84	98	12	12
-1	-1	85	123	12	9
-1	-1	89	98	10	10
-1	-2	11	156	26	17
-1	-2	13	154	22	15
-1	-2	14	324	30	9
-1	-2	16	294	25	9
-1	-2	18	235	25	11
-1	-2	49	106	23	22
-1	-2	50	347	27	8
-1	-2	51	206	27	13
-1	-2	52	277	24	9
-1	-2	54	301	26	9
-1	-2	55	348	26	7
-1	1	-10	40	7	19
-1	1	-11	87	11	13
-1	1	-14	35	6	18
-1	1	-15	39	7	18
-1	1	-16	104	14	14
-1	1	-17	89	12	13
-1	1	-17	102	11	11
-1	1	-18	43	9	20
-1	1	-22	64	6	10
-1	1	-25	61	7	11
-1	1	-29	64	8	13
-1	1	-3	162	29	18
-1	1	-3	165	28	17
-1	1	-30	70	8	12
-1	1	-31	91	9	10
-1	1	-32	84	7	8
-1	1	-33	28	6	22
-1	1	-34	75	8	11
-1	1	-36	68	7	10
-1	1	-39	39	7	17
-1	1	-4	112	25	22
-1	1	-40	61	9	14
-1	1	-41	75	7	9
-1	1	-42	78	9	11
-1	1	-43	64	8	12
-1	1	-44	68	6	9
-1	1	-45	97	10	10
-1	1	-46	94	10	11
-1	1	-47	36	6	18
-1	1	-5	155	25	16
-1	1	-50	61	9	15
-1	1	-51	85	11	13
-1	1	-53	152	9	6
-1	1	-54	88	10	12
-1	1	-55	82	7	9
-1	1	-56	58	7	12
-1	1	-56	81	7	9
-1	1	-57	239	25	11
-1	1	-58	167	20	12
-1	1	-60	84	5	6
-1	1	-61	57	5	9
-1	1	-63	54	6	11
-1	1	-65	50	7	14
-1	1	-66	62	5	9
-1	1	-67	32	6	18
-1	1	-7	109	24	22
-1	1	-7	188	30	16
-1	1	-71	60	8	13
-1	1	-72	54	5	9
-1	1	-77	84	7	8
-1	1	-78	54	7	12
-1	1	-79	76	8	10
-1	1	4	98	23	24
-1	1	5	121	26	22
-1	1	9	55	11	21
-1	1	10	58	8	13
-1	1	12	36	4	11
-1	1	13	26	6	22
-1	1	14	60	10	16
-1	1	15	54	11	20
-1	1	19	48	6	13
-1	1	20	55	6	11
-1	1	21	87	11	13
-1	1	23	61	10	17
-1	1	31	124	11	9
-1	1	50	24	5	19
-1	1	53	70	7	10
-1	1	53	104	7	6
-1	1	55	52	9	18
-1	1	56	50	11	22
-1	1	58	60	6	10
-1	1	63	57	9	16
-1	1	66	97	11	11
-1	1	68	42	10	24
-1	1	69	84	9	11
-1	1	74	83	10	12
-1	1	75	101	10	10
-1	1	79	89	6	7
-1	1	81	64	10	15
-1	1	92	115	11	10
-1	1	100	88	6	7
-1	1	100	100	6	6
-1	2	-1	204	43	21
-1	2	-2	244	48	20
-1	2	-58	101	10	10
-1	2	-61	79	10	13
-1	2	-63	56	6	11
-1	2	-64	58	7	12
-1	2	-65	59	6	10
-1	2	1	166	40	24
-1	2	3	345	49	14
-1	2	4	240	48	20
-1	2	4	279	45	16
-1	2	8	90	21	24
-1	2	10	159	28	17
-1	2	11	159	30	19
-1	2	33	56	8	15
-1	2	39	44	8	17
-2	-1	-63	93	11	11
-2	-1	-68	77	11	14
-2	-1	-71	205	25	12
-2	-1	-73	282	24	9
-2	-1	1	213	29	14
-2	-1	6	231	41	18
-2	-1	8	251	40	16
-2	-1	10	128	20	16
-2	-1	13	205	29	14
-2	-1	17	361	50	14
-2	-1	19	176	29	17
-2	-1	20	286	27	9
-2	-1	21	71	13	19
-2	-1	22	93	16	17
-2	-1	24	328	33	10
-2	-1	25	76	10	14
-2	-1	26	227	25	11
-2	-1	27	85	10	12
-2	-1	32	110	10	9
-2	-1	33	70	13	19
-2	-1	34	111	15	13
-2	-1	35	144	10	7
-2	-1	36	86	10	12
-2	-1	39	99	16	16
-2	-1	40	464	39	8
-2	-1	41	54	11	20
-2	-1	42	145	12	8
-2	-1	44	63	13	21
-2	-1	45	120	12	10
-2	-1	46	56	9	17
-2	-1	47	195	11	6
-2	-1	49	93	8	9
-2	-1	50	82	8	9
-2	-1	51	67	8	12
-2	-1	52	105	10	9
-2	-1	56	56	13	23
-2	-1	65	91	8	9
-2	-1	68	65	9	13
-2	-1	77	192	13	7
-2	-1	78	199	13	7
-2	-1	82	50	12	24
-2	-1	83	112	14	12
-2	-1	84	72	7	10
-2	-1	86	122	8	7
-2	-1	88	159	14	9
-2	-1	89	101	7	7
-2	-1	91	67	13	19
-2	-1	92	58	12	21
-2	-1	94	79	7	9
-2	-1	96	90	9	10
-2	-1	97	78	8	11
-2	-1	99	144	7	5
-2	1	-1	184	24	13
-2	1	-1	232	36	16
-2	1	-10	145	12	9
-2	1	-11	70	12	17
-2	1	-12	74	12	16
-2	1	-13	84	9	11
-2	1	-14	306	25	8
-2	1	-16	63	13	20
-2	1	-17	121	24	20
-2	1	-18	218	21	9

-2	1	-19	71	14	20
-2	1	-2	292	39	13
-2	1	-20	185	20	11
-2	1	-26	77	8	11
-2	1	-27	82	9	11
-2	1	-29	101	9	9
-2	1	-3	116	14	13
-2	1	-30	86	11	13
-2	1	-32	72	11	16
-2	1	-36	86	11	13
-2	1	-37	56	12	21
-2	1	-38	89	8	9
-2	1	-39	97	9	10
-2	1	-4	232	37	16
-2	1	-43	63	8	13
-2	1	-44	39	7	17
-2	1	-45	61	8	13
-2	1	-46	50	7	15
-2	1	-47	46	6	12
-2	1	-48	113	11	9
-2	1	-49	59	10	16
-2	1	-51	28	5	20
-2	1	-52	107	7	7
-2	1	-53	47	7	14
-2	1	-55	58	7	12
-2	1	-56	68	6	9
-2	1	-57	119	21	18
-2	1	-59	398	31	8
-2	1	-6	75	16	21
-2	1	-60	387	22	6
-2	1	-61	82	6	7
-2	1	-63	150	20	13
-2	1	-67	41	9	21
-2	1	-69	58	9	16
-2	1	-7	178	16	9
-2	1	-71	125	12	9
-2	1	-72	88	7	8
-2	1	-74	69	7	10
-2	1	-76	102	8	7
-2	1	-77	92	7	8
-2	1	-78	69	6	9
-2	1	-79	113	10	9
-2	1	-9	103	13	13
-2	1	1	307	38	12
-2	1	2	206	26	12
-2	1	3	163	25	16
-2	1	3	245	32	13
-2	1	6	259	30	12
-2	1	7	281	32	11
-2	1	8	103	16	16
-2	1	10	75	11	15
-2	1	11	55	11	19
-2	1	12	55	10	18
-2	1	14	88	12	14
-2	1	15	73	12	17
-2	1	17	77	14	18
-2	1	25	168	18	11
-2	1	47	87	12	14
-2	1	49	118	12	10
-2	1	50	133	7	5
-2	1	52	115	8	7
-2	1	56	93	6	7
-2	1	58	105	7	7
-2	1	59	97	6	6
-2	1	60	43	7	16
-2	1	61	88	6	7
-2	1	63	35	8	23
-2	1	64	81	9	11
-2	1	65	70	10	15
-2	1	66	76	8	11
-2	1	67	38	6	16
-2	1	68	40	6	15
-2	1	69	53	11	21
-2	1	70	83	9	11
-2	1	71	140	7	5
-2	1	73	126	8	6
-2	1	74	89	8	9
-2	1	75	130	8	6
-2	1	91	101	7	7
-2	1	92	34	6	17
-2	1	94	118	8	7
-2	2	-1	275	39	14
-2	2	-10	180	25	14
-2	2	-3	195	36	18
-2	2	3	125	30	24
-2	2	4	257	36	14
-2	2	6	147	25	17
-2	2	9	227	31	14
-2	2	46	72	8	11
-2	2	47	290	24	8
-2	2	48	344	28	8
-2	2	55	52	5	10
-2	2	56	56	7	13
-3	1	58	101	9	8
-3	1	72	72	8	11
-3	1	74	106	9	9
-3	1	75	68	13	18
-3	1	80	77	7	10
-3	1	82	94	9	9
-3	1	84	74	7	9
-3	1	85	161	13	8
-3	1	86	85	13	15
-3	1	87	152	14	9
-3	1	89	87	7	9
-3	1	90	51	12	23
-3	1	91	80	15	19
-3	1	93	65	7	11
-3	1	94	35	8	24
-3	1	96	169	21	12
0	-1	-18	88	11	13
0	-1	-2	168	25	15
0	-1	-3	127	24	19
0	-1	-31	71	10	14
0	-1	-49	87	11	13
0	-1	-56	143	25	17
0	-1	-57	202	18	9
0	-1	-58	36	5	15
0	-1	-59	63	8	12
0	-1	-60	62	7	11
0	-1	-62	41	6	15
0	-1	-64	42	7	17
0	-1	-67	58	5	9
0	-1	-68	40	6	14
0	-1	-70	37	6	17
0	-1	-71	56	6	10
0	-1	-72	47	6	13
0	-1	-76	42	5	11
0	-1	-77	38	4	12
0	-1	1	153	25	16
0	-1	8	117	24	20
0	-1	14	181	26	14
0	-1	17	63	7	11
0	-1	19	83	8	10
0	-1	20	108	8	8
0	-1	21	60	9	15
0	-1	23	68	8	12
0	-1	25	45	9	20
0	-1	26	34	7	19
0	-1	29	91	11	12
0	-1	31	66	5	8
0	-1	33	84	13	16
0	-1	34	44	7	17
0	-1	34	51	7	14
0	-1	35	91	11	12
0	-1	36	83	7	9
0	-1	38	48	6	13
0	-1	39	58	6	11
0	-1	42	94	12	12
0	-1	43	57	7	12
0	-1	43	87	8	9
0	-1	45	95	9	10
0	-1	46	88	6	7
0	-1	47	37	8	22
0	-1	48	65	9	14
0	-1	49	41	8	19
0	-1	50	33	6	18
0	-1	51	74	9	13
0	-1	53	70	9	13
0	-1	54	52	10	20
0	-1	56	51	6	11
0	-1	57	27	5	18
0	-1	63	92	8	9
0	-1	65	67	8	12
0	-1	67	45	10	23
0	-1	68	87	9	11
0	-1	76	76	10	13
0	-1	79	102	9	9
0	-1	81	78	8	10
0	-1	83	96	11	12
0	-1	83	105	11	10
0	-1	85	60	6	10
0	-2	-26	34	6	17
0	-2	-27	72	9	13
0	-2	-28	58	7	12
0	-2	-29	76	10	14
0	-2	-34	84	11	13
0	-2	30	160	17	11
0	-2	39	100	8	8
0	-2	68	70	6	9
0	-2	85	70	8	11
0	-2	86	131	15	11
0	-2	88	122	14	11
0	-2	89	123	16	13
0	-2	90	141	15	10
0	1	-10	27	4	16
0	1	-10	57	7	13
0	1	-13	43	7	16
0	1	-15	44	8	19
0	1	-18	55	7	13
0	1	-21	35	7	19
0	1	-22	39	6	16
0	1	-25	59	6	11
0	1	-26	121	11	9
0	1	-28	59	6	10
0	1	-29	41	10	24
0	1	-30	56	9	16
0	1	-31	56	7	13
0	1	-32	63	8	13
0	1	-33	30	6	20
0	1	-35	50	6	11
0	1	-37	81	7	9
0	1	-38	51	7	13
0	1	-39	62	8	13
0	1	-39	73	7	10
0	1	-4	123	24	20
0	1	-40	50	5	11
0	1	-41	59	8	13
0	1	-42	61	6	10
0	1	-43	26	6	24
0	1	-45	72	9	12
0	1	-46	310	27	9
0	1	-5	137	25	18
0	1	-5	167	24	14
0	1	-50	47	7	14
0	1	-53	67	7	10
0	1	-56	39	5	14
0	1	-58	58	7	11
0	1	-60	43	6	15
0	1	-61	32	6	17
0	1	-63	48	10	20
0	1	-64	93	9	10
0	1	-66	61	9	15
0	1	-67	60	6	11
0	1	-68	65	6	9
0	1	-70	40	5	13
0	1	-71	49	5	11
0	1	-72	34	7	21
0	1	-72	47	7	14
0	1	-73	53	6	11
0	1	-75	39	6	14
0	1	-76	34	4	12
0	1	-77	37	5	12
0	1	-78	34	4	13
0	1	-79	18	4	20
0	1	1	173	25	15
0	1	10	46	9	19
0	1	12	75	11	15
0	1	13	72	7	9
0	1	14	39	8	21
0	1	15	53	7	14
0	1	15	58	7	12
0	1	16	52	6	12
0	1	16	64	6	9
0	1	17	83	10	12
0	1	18	112	8	7
0	1	24	75	7	9
0	1	25	58	8	15
0	1	25	63	8	13
0	1	26	65	10	16
0	1	29	96	7	7
0	1	32	64	8	12
0	1	34	101	11	10
0	1	41	87	8	9
0	1	44	39	7	17
0	1	45	43	4	10
0	1	49	58	6	11
0	1	52	66	7	11
0	1	54	50	7	14
0	1	55	63	10	17
0	1	55	86	10	12
0	1	57	156	15	10

0	1	59	102	9	9
0	1	62	92	9	10
0	1	66	57	8	15
0	1	68	102	7	7
0	1	69	25	5	19
0	1	70	35	7	19
0	1	72	57	6	11
0	1	73	34	6	18
0	1	74	94	9	9
0	1	75	45	6	13
0	1	76	86	6	7
0	1	77	79	11	13
0	1	79	92	7	7
0	1	80	127	10	8
0	1	81	98	7	7
0	1	82	136	10	7
0	1	84	129	10	8
0	1	88	95	10	10
0	1	89	100	10	10
0	1	90	68	9	13
0	1	91	83	10	12
0	1	92	66	10	16
0	1	99	79	6	7
0	2	-29	100	11	11
0	2	-31	142	15	10
0	2	-32	162	15	9
0	2	-33	59	13	22
0	2	-35	95	11	11
0	2	-40	131	13	10
0	2	-41	102	13	13
0	2	-42	66	13	20
0	2	-56	84	8	9
0	2	-68	51	8	15
0	2	-7	475	50	10
0	2	-72	106	10	10
0	2	-75	111	10	9
0	2	-76	64	7	11
0	2	20	233	23	10
0	2	21	264	33	12
0	2	22	249	38	15
0	2	24	48	12	24
0	2	25	92	16	17
0	2	28	95	12	13
0	2	32	114	10	8
0	2	34	88	10	11
0	2	36	45	6	14
0	2	37	71	8	11
0	2	44	77	13	17
0	2	46	162	13	8
0	2	47	90	14	16
0	2	48	65	7	10
0	2	49	49	6	12
0	2	50	32	8	24
0	2	52	26	5	19
0	2	53	47	6	13
0	2	54	34	6	18
0	2	55	47	7	14
1	-1	-10	241	30	12
1	-1	-12	51	7	14
1	-1	-13	58	8	14
1	-1	-14	95	9	10
1	-1	-15	61	12	20
1	-1	-16	68	9	13
1	-1	-18	52	9	17
1	-1	-21	21	4	20
1	-1	-22	48	5	11
1	-1	-25	40	5	12
1	-1	-26	28	6	22
1	-1	-27	28	6	20
1	-1	-28	39	5	12
1	-1	-34	47	6	13
1	-1	-46	44	6	14
1	-1	-48	29	5	19
1	-1	-49	60	11	19
1	-1	-5	99	24	24
1	-1	-50	60	6	9
1	-1	-55	49	5	11
1	-1	-61	71	5	7
1	-1	-65	80	9	11
1	-1	-69	49	5	10
1	-1	-70	49	6	12
1	-1	-71	48	6	12
1	-1	-72	34	4	13
1	-1	-74	53	7	13
1	-1	-75	58	6	10
1	-1	-76	70	6	8
1	-1	-76	41	5	12
1	-1	-79	71	5	7
1	-1	-81	49	5	11
1	-1	10	30	5	17
1	-1	13	68	7	11
1	-1	15	58	10	18
1	-1	17	269	31	12
1	-1	18	61	10	17
1	-1	21	75	8	11
1	-1	22	71	7	10
1	-1	25	43	7	16
1	-1	26	74	12	17
1	-1	27	130	19	14
1	-1	29	100	11	11
1	-1	30	55	7	13
1	-1	31	78	9	11
1	-1	33	30	6	21
1	-1	34	55	6	11
1	-1	35	86	8	9
1	-1	38	43	6	13
1	-1	40	106	8	8
1	-1	41	46	6	14
1	-1	42	75	12	16
1	-1	43	36	5	13
1	-1	44	85	9	10
1	-1	47	54	6	12
1	-1	49	36	6	16
1	-1	50	115	10	9
1	-1	52	28	5	16
1	-1	53	73	10	14
1	-1	54	29	5	16
1	-1	56	75	5	7
1	-1	61	91	8	8
1	-1	63	60	7	12
1	-1	66	62	5	8
1	-1	67	33	7	20
1	-1	68	77	11	15
1	-1	70	80	10	12
1	-1	71	108	10	9
1	-1	72	56	5	10
1	-1	74	34	6	19
1	-1	75	108	11	11
1	-1	76	29	5	18
1	-1	79	48	11	24
1	-1	81	43	8	18
1	-1	91	113	10	8
1	-1	92	53	12	22
1	-1	93	90	11	12
1	-1	95	49	6	11
1	-2	-69	71	7	9
1	-2	7	171	27	16
1	-2	8	127	30	24
1	-2	10	141	21	15
1	-2	63	80	8	10
1	-2	66	88	11	13
1	-2	83	79	7	9
1	-2	90	94	12	13
1	1	-18	77	9	12
1	1	-20	215	25	12
1	1	-24	66	8	13
1	1	-29	73	9	12
1	1	-33	54	8	14
1	1	-39	63	10	16
1	1	-40	60	11	19
1	1	-41	110	11	10
1	1	-42	69	10	15
1	1	-44	54	11	21
1	1	-45	98	14	14
1	1	-46	64	12	18
1	1	-47	62	11	19
1	1	-48	108	12	11
1	1	-49	61	11	19
1	1	-51	37	9	24
1	1	-52	53	7	13
1	1	-53	47	7	15
1	1	-54	58	6	11
1	1	-55	116	12	10
1	1	-56	30	4	14
1	1	-58	66	7	10
1	1	-59	66	10	15
1	1	-60	49	5	10
1	1	-61	69	7	10
1	1	-62	42	7	18
1	1	-64	187	27	14
1	1	-65	160	21	13
1	1	-66	90	7	8
1	1	-67	114	8	7
1	1	-68	43	7	16
1	1	-69	112	9	8
1	1	-70	90	8	9
1	1	-71	44	7	17
1	1	-75	52	8	15
1	1	-76	88	7	8
1	1	-80	69	7	10
1	1	-9	115	13	11
1	1	2	104	20	20
1	1	3	191	31	16
1	1	11	148	34	23
1	1	14	114	12	10
1	1	17	77	12	15
1	1	40	95	14	15
1	1	44	368	40	11
1	1	45	186	38	21
1	1	49	129	13	10
1	1	56	41	6	16
1	1	57	61	6	10
1	1	58	68	7	11
1	1	60	72	7	9
1	1	62	85	8	10
1	1	63	34	5	16
1	1	65	96	11	12
1	1	67	108	12	12
1	1	68	55	10	19
1	1	69	100	13	13
1	1	70	128	11	9
1	1	72	125	13	10
1	1	73	68	13	19
1	1	76	84	7	8
1	1	82	80	7	9
1	1	83	57	8	14
1	1	84	125	11	9
1	1	86	86	9	10
1	1	87	102	13	12
1	1	88	68	7	10
1	1	90	108	8	7
1	1	91	33	7	23
1	1	96	88	7	8
1	1	98	97	6	6
1	2	-59	408	27	7
1	2	-61	295	26	9
1	2	-63	366	28	8
1	2	-64	126	27	21
1	2	8	234	26	11
1	2	9	233	31	13
1	2	45	188	28	15
1	2	48	186	27	15
1	2	49	123	28	23
1	2	51	315	24	8
2	-1	-14	78	11	15
2	-1	-15	106	11	10
2	-1	-16	65	12	18
2	-1	-17	218	24	11
2	-1	-17	238	25	10
2	-1	-2	368	29	8
2	-1	-21	93	11	12
2	-1	-22	89	13	23
2	-1	-36	137	13	9
2	-1	-46	37	7	20
2	-1	-47	44	6	18
2	-1	-48	60	9	15
2	-1	-49	71	8	11
2	-1	-50	54	10	18
2	-1	-51	21	5	23
2	-1	-52	45	8	17
2	-1	-53	30	6	20
2	-1	-55	82	13	16
2	-1	-56	28	6	23
2	-1	-58	47	7	15
2	-1	-59	106	12	11
2	-1	-6	185	33	18
2	-1	-60	60	11	18
2	-1	-61	52	10	19
2	-1	-63	90	13	14
2	-1	-64	54	11	20
2	-1	-65	94	12	13
2	-1	-68	171	18	11
2	-1	-69	135	27	20
2	-1	-70	64	6	10
2	-1	-71	65	7	11
2	-1	-72	58	7	13
2	-1	-73	56	7	12
2	-1	-8	303	38	13
2	-1	7	75	14	19
2	-1	13	86	12	14
2	-1	15	137	12	9

2	-1	18	73	13	18	2	-1	85	59	7	12	2	1	-51	45	6	14
2	-1	19	111	13	12	2	-1	89	61	6	11	2	1	-57	63	8	13
2	-1	24	63	10	15	2	-1	90	114	14	12	2	1	-59	30	5	18
2	-1	30	107	9	9	2	-1	91	69	7	10	2	1	-60	91	7	8
2	-1	31	126	12	10	2	-2	-5	157	29	18	2	1	-62	168	10	6
2	-1	32	55	12	21	2	1	-12	116	16	14	2	1	-63	91	7	8
2	-1	33	165	13	8	2	1	-13	76	13	18	2	1	-63	100	7	7
2	-1	35	81	8	10	2	1	-15	76	13	17	2	1	-64	119	8	7
2	-1	36	32	7	23	2	1	-18	92	16	18	2	1	-65	53	8	16
2	-1	41	114	12	10	2	1	-20	96	12	13	2	1	-67	90	8	8
2	-1	42	153	12	8	2	1	-21	82	14	16	2	1	-72	280	32	11
2	-1	46	49	8	16	2	1	-22	117	13	11	2	1	-73	51	7	15
2	-1	47	123	13	11	2	1	-24	158	17	11	2	1	-74	293	35	12
2	-1	50	388	40	10	2	1	-26	51	5	10	2	1	-75	449	25	6
2	-1	54	132	14	10	2	1	-28	52	12	22	2	1	-76	263	44	17
2	-1	55	96	12	13	2	1	-29	114	11	9	2	1	-77	367	23	6
2	-1	56	106	8	8	2	1	-30	70	8	11	2	1	-78	642	45	7
2	-1	58	90	12	13	2	1	-31	132	12	9	2	1	-8	405	47	12
2	-1	60	134	13	10	2	1	-32	55	10	18	2	1	-80	353	24	7
2	-1	61	105	13	12	2	1	-33	92	10	11	2	1	5	168	37	22
2	-1	64	76	11	14	2	1	-34	85	7	9	2	1	7	183	36	20
2	-1	65	140	12	8	2	1	-35	106	9	8	2	1	15	227	34	15
2	-1	66	64	12	19	2	1	-36	64	10	15	2	1	47	72	7	10
2	-1	67	122	12	10	2	1	-37	100	11	11	2	1	48	47	8	16
2	-1	68	88	12	14	2	1	-38	111	9	8	2	1	64	59	6	10
2	-1	71	98	8	8	2	1	-40	161	13	8	2	1	66	68	7	10
2	-1	75	88	6	7	2	1	-43	66	7	11	2	1	68	86	6	7
2	-1	80	73	5	8	2	1	-45	73	7	10	2	1	70	89	6	7
2	-1	81	35	7	19	2	1	-46	52	8	15	2	1	72	60	8	14
2	-1	84	106	10	10	2	1	-47	68	7	11	2	1	73	173	19	11

Gold Data : Analysis Rfactor v Intensity

Imax	Rfac	Av_I	σ	I/σ	sd
500.	0.859	1810.	2125.1	0.9	923.9
1000.	0.765	1964.	2819.4	0.7	815.9
1500.	0.246	1040.	305.3	3.4	756.7
2000.	0.000	0.	0.0	0.0	0.0
2500.	0.398	2930.	1247.9	2.3	871.4
3000.	0.000	0.	0.0	0.0	0.0
3500.	0.205	3400.	709.1	4.8	1149.2
4000.	0.083	3667.	303.4	12.1	1620.2
4500.	0.399	5409.	2409.5	2.2	1807.9
5000.	0.000	0.	0.0	0.0	0.0
5500.	0.000	0.	0.0	0.0	0.0
6000.	0.000	0.	0.0	0.0	0.0
91136.	0.148	50145.	7966.5	6.3	35352.9
Totals	0.204	11313.	3853.5	2.9	7296.4

Gold Data: Analysis of standard deviation v. Intensity

Range	Imin	Imax	Irms	No	Mean	Sigma
1	1.	500.	2386.	2.	0.78	1.14
2	500.	1000.	3151.	6.	0.59	1.42
3	1000.	1500.	1071.	2.	-0.11	0.30
4	1500.	2000.	0.	0.	0.00	0.00
5	2000.	2500.	3153.	2.	0.26	1.29
6	2500.	3000.	0.	0.	0.00	0.00
7	3000.	3500.	3471.	2.	0.06	0.60
8	3500.	4000.	3679.	2.	0.01	0.19
9	4000.	4500.	5824.	2.	0.30	1.12
10	4500.	5000.	0.	0.	0.00	0.00
11	5000.	5500.	0.	0.	0.00	0.00
12	5500.	6000.	0.	0.	0.00	0.00
13	6000.	891136.	53717.	4.	0.02	0.21
Total	1.	891136.	23115.	22.	0.28	1.03

XIII. APPENDIX D (Iodine Data)

h	k	l	F	σF	σF/F
-4	-1	8	0	0	100
-4	-1	9	62	8	14
-4	-1	10	55	9	16
-4	-1	11	0	0	100
-4	-1	12	71	8	11
-4	-1	13	0	0	100
-4	-1	14	0	0	100
-4	-1	15	110	10	9
-4	-1	16	0	0	100
-4	-1	17	87	9	10
-4	-1	19	0	0	100
-4	-1	20	0	0	100
-4	-1	21	44	7	16
-4	-1	22	61	8	13
-4	-1	23	103	9	8
-4	-1	24	54	6	11
-4	-1	25	0	0	100
-4	-1	26	74	6	8
-4	-1	27	49	6	13
-4	-1	28	10	7	67
-4	-1	29	0	0	100
-4	-1	30	0	0	100
-4	-1	31	0	0	100
-4	-1	32	76	7	9
-4	-1	33	0	0	100
-4	-1	34	90	7	7
-4	-1	35	0	0	100
-4	-1	36	51	8	16
-4	-1	37	63	8	13
-4	0	-51	0	0	100
-4	0	-50	0	0	100
-4	0	-49	87	8	9
-4	0	-48	0	0	100
-4	0	-47	50	6	12
-4	0	-46	0	0	100
-4	0	-45	59	8	13
-4	0	-44	0	0	100
-4	0	-43	80	9	11
-4	0	-42	0	0	100
-4	0	-42	101	10	10
-4	0	-41	0	0	100
-4	0	-40	0	0	100
-4	0	-39	0	0	100
-4	0	-36	36	6	18
-4	0	-35	29	6	21
-4	0	-34	68	7	11
-4	0	-33	0	0	100
-4	0	37	0	0	100
-4	0	38	16	4	25
-4	0	38	65	7	11
-4	0	39	37	6	17
-4	0	40	0	0	100
-4	0	41	32	7	21
-4	0	42	0	0	100
-4	0	43	28	6	23
-4	0	44	67	6	10
-4	0	46	32	8	24
-4	0	47	31	6	19
-4	0	48	55	8	14
-4	0	49	26	9	34
-4	0	50	63	9	14
-4	0	51	68	8	12
-4	1	-57	0	0	100
-4	1	-56	0	0	100
-4	1	-55	26	7	27
-4	1	-54	0	0	100
-4	1	-53	41	6	15
-4	1	-52	34	6	19
-4	1	-51	0	0	100
-4	1	-50	73	6	8
-4	1	-49	78	7	9
-4	1	-48	0	0	100
-4	1	-47	41	6	15
-4	1	-46	53	7	13
-4	1	-45	70	6	9
-4	1	-44	121	8	7
-4	1	-43	0	0	100
-4	1	-42	92	9	9
-4	1	-41	63	7	12
-4	1	-40	0	0	100
-4	1	-39	45	7	16
-4	1	-38	35	7	20
-4	1	-37	0	0	100
-4	1	-36	0	0	100
-4	1	-35	0	0	100
-4	1	-34	54	7	13
-4	1	-15	47	9	20
-4	1	-13	0	0	100
-4	1	-12	76	8	10
-4	1	-11	0	0	100
-4	1	-10	0	0	100
-4	1	-9	0	0	100
-4	1	-8	87	12	14
-4	1	-7	102	11	11
-4	1	-6	0	0	100
-4	1	-5	98	12	13
-4	1	-4	0	0	100
-4	1	-3	0	0	100
-4	1	-2	34	11	32
-4	1	-1	40	14	36
-4	1	0	89	13	15
-4	1	1	116	15	13
-4	1	2	59	11	19
-4	1	3	59	9	16
-4	1	5	0	0	100
-4	1	6	0	0	100
-4	1	7	26	11	44
-4	1	8	0	0	100
-4	1	9	0	0	100
-4	1	10	77	10	13
-4	1	11	0	0	100
-4	1	12	0	0	100
-4	1	13	0	0	100
-4	1	14	0	0	100
-4	1	15	0	0	100
-4	1	16	0	0	100
-4	1	17	55	10	17
-4	1	18	91	8	9
-4	1	19	0	0	100
-4	1	20	46	8	18
-4	1	21	0	0	100
-4	1	22	57	6	11
-4	1	23	77	7	9
-4	1	24	0	0	100
-4	1	25	76	9	11
-4	1	26	0	0	100
-4	1	27	19	8	43
-4	1	28	68	9	13
-4	1	29	0	0	100
-4	1	30	0	0	100
-4	1	31	0	0	100
-4	1	32	0	0	100
-4	1	42	26	8	33
-4	1	43	25	7	28
-4	1	44	57	8	14
-4	1	45	65	8	13
-4	1	46	52	7	13
-4	1	47	11	8	69
-4	1	48	0	0	100
-4	1	49	16	5	33
-4	1	50	59	8	14
-4	1	51	69	8	11
-4	1	52	49	8	16
-4	1	53	78	9	12
-4	2	29	56	6	11
-4	2	30	0	0	100
-4	2	31	0	0	100
-4	2	32	0	0	100
-4	2	33	48	7	15
-4	2	34	0	0	100
-4	2	35	0	0	100
-4	2	36	28	5	19
-4	2	37	16	6	40
-4	2	38	64	5	9
-4	2	39	0	0	100
-4	2	40	20	7	36
-4	2	41	0	0	100
-4	2	42	82	6	7
-4	2	43	91	7	8
-4	2	44	95	8	8
-4	2	45	47	8	16
-3	-2	7	0	0	100
-3	-2	8	47	10	21
-3	-2	9	27	9	34
-3	-2	10	79	9	11
-3	-2	11	0	0	100
-3	-2	12	15	8	55
-3	-2	13	110	10	9
-3	-2	14	0	0	100
-3	-2	15	83	8	10
-3	-2	16	59	8	14
-3	-2	17	0	0	100
-3	-2	18	94	9	9
-3	-2	19	0	0	100
-3	-2	20	37	7	19
-3	-1	-50	0	0	100
-3	-1	-49	26	6	24
-3	-1	-48	0	0	100
-3	-1	-46	0	0	100
-3	-1	-45	0	0	100
-3	-1	-28	75	13	17
-3	-1	-27	30	12	41
-3	-1	-27	0	0	100
-3	-1	-26	0	0	100
-3	-1	-25	83	6	8
-3	-1	-24	0	0	100
-3	-1	-23	54	6	12
-3	-1	-22	0	0	100
-3	-1	-21	0	0	100
-3	-1	-20	0	0	100
-3	-1	-19	33	7	22
-3	-1	-18	49	8	16
-3	-1	-17	100	8	8
-3	-1	-16	0	0	100
-3	-1	-15	64	7	12
-3	-1	-15	64	7	12
-3	-1	-14	58	7	12
-3	-1	-13	0	0	100
-3	-1	-12	52	9	17
-3	-1	-11	0	0	100
-3	-1	-10	67	9	14
-3	-1	-9	0	0	100
-3	-1	-8	49	11	22
-3	-1	-7	0	0	100
-3	-1	-6	40	12	30
-3	-1	-5	0	0	100
-3	-1	-4	0	0	100
-3	-1	-3	0	0	100
-3	-1	-2	0	0	100
-3	-1	5	91	15	16
-3	-1	6	90	17	18
-3	-1	7	0	0	100
-3	-1	8	0	0	100
-3	-1	9	0	0	100
-3	-1	10	0	0	100
-3	-1	11	0	0	100
-3	-1	12	57	10	17
-3	-1	13	61	12	20
-3	-1	14	0	0	100
-3	-1	24	0	0	100
-3	-1	25	0	0	100
-3	-1	26	77	13	17
-3	-1	27	129	11	9
-3	-1	28	31	11	36
-3	-1	29	35	11	33
-3	-1	30	0	0	100
-3	-1	31	61	8	13
-3	-1	32	56	8	14
-3	-1	33	92	8	9
-3	-1	34	94	9	9
-3	-1	35	61	9	14
-3	-1	36	0	0	100
-3	-1	37	109	8	8
-3	-1	38	0	0	100
-3	-1	39	0	0	100
-3	-1	40	70	7	10
-3	-1	41	0	0	100
-3	-1	42	0	0	100
-3	-1	43	55	8	14
-3	-1	44	68	9	13
-3	-1	45	0	0	100

-3	-1	46	10	8	80
-3	-1	47	0	0	100
-3	-1	48	16	8	50
-3	-1	49	0	0	100
-3	-1	50	0	0	100
-3	-1	51	37	7	19
-3	-1	52	31	7	21
-3	-1	53	0	0	100
-3	-1	54	0	0	100
-3	0	-70	87	14	15
-3	0	-69	107	14	13
-3	0	-68	103	13	13
-3	0	-45	0	0	100
-3	0	-43	58	11	19
-3	0	-41	54	11	21
-3	0	-40	0	0	100
-3	0	-39	50	10	20
-3	0	-38	105	13	12
-3	0	-37	49	7	15
-3	0	-36	0	0	100
-3	0	-35	37	8	21
-3	0	-34	44	8	17
-3	0	-33	70	8	11
-3	0	-32	0	0	100
-3	0	-31	0	0	100
-3	0	-30	46	8	17
-3	0	-17	0	0	100
-3	0	-16	61	9	15
-3	0	-15	19	9	47
-3	0	-14	0	0	100
-3	0	-13	0	0	100
-3	0	-12	44	7	16
-3	0	-11	0	0	100
-3	0	-10	0	0	100
-3	0	-9	61	11	19
-3	0	-8	0	0	100
-3	0	-7	70	16	23
-3	0	-7	81	16	20
-3	0	-6	0	0	100
-3	0	29	0	0	100
-3	0	30	0	0	100
-3	0	33	109	15	14
-3	0	36	82	15	18
-3	1	-71	0	0	100
-3	1	-70	0	0	100
-3	1	-69	0	0	100
-3	1	-67	69	11	16
-3	1	-66	54	8	15
-3	1	-65	90	8	9
-3	1	-64	22	6	28
-3	1	-63	16	6	38
-3	1	-62	31	4	14
-3	1	-61	44	5	12
-3	1	-60	39	6	15
-3	1	-59	86	7	8
-3	1	-58	55	8	15
-3	1	-57	51	8	15
-3	1	-56	45	8	17
-3	1	-55	0	0	100
-3	1	-54	0	0	100
-3	1	-53	33	8	25
-3	1	-52	0	0	100
-3	1	-51	0	0	100
-3	1	-50	0	0	100
-3	1	-49	0	0	100
-3	1	-48	39	7	19
-3	1	-47	0	0	100
-3	1	-46	110	11	10
-3	1	-45	51	11	22
-3	1	-44	84	14	16
-3	1	-43	0	0	100
-3	1	-42	0	0	100
-3	1	-41	0	0	100
-3	1	-40	0	0	100
-3	1	-39	88	12	14
-3	1	-27	74	8	11
-3	1	-26	74	8	11
-3	1	-25	56	8	15
-3	1	-24	0	0	100
-3	1	-23	0	0	100
-3	1	-22	42	7	17
-3	1	-21	0	0	100
-3	1	-20	0	0	100
-3	1	-19	0	0	100
-3	1	-18	18	8	46
-3	1	-17	0	0	100
-3	1	-16	0	0	100
-3	1	-15	54	8	15
-3	1	-14	14	9	60
-3	1	-13	8	8	97
-3	1	1	81	22	27
-3	1	29	0	0	100
-3	1	30	133	18	13
-3	1	32	0	0	100
-3	1	33	0	0	100
-3	1	35	74	17	23
-3	2	-53	0	0	100
-3	2	-52	60	6	11
-3	2	-51	0	0	100
-3	2	-50	49	6	11
-3	2	-49	45	5	11
-3	2	-48	34	5	16
-3	2	-47	90	6	7
-3	2	-46	51	6	12
-3	2	-45	0	0	100
-3	2	-44	0	0	100
-3	2	-43	63	8	12
-3	2	-42	69	7	10
-3	2	-41	0	0	100
-3	2	-40	40	7	18
-3	2	-39	0	0	100
-3	2	-38	36	7	19
-3	2	-37	17	7	42
-3	2	-36	0	0	100
-3	2	-35	0	0	100
-3	2	-34	0	0	100
-3	2	-32	0	0	100
-3	2	-31	7	7	96
-3	2	-30	88	7	8
-3	2	-29	0	0	100
-3	2	-28	0	0	100
-3	2	-27	0	0	100
-3	2	-26	0	0	100
-3	2	-25	0	0	100
-3	2	-24	0	0	100
-3	2	-23	57	7	12
-3	2	-22	0	0	100
-3	2	-11	66	11	17
-3	2	-11	11	9	75
-3	2	-10	0	0	100
-3	2	-9	27	9	32
-3	2	-8	89	11	12
-3	2	-7	0	0	100
-3	2	-6	0	0	100
-3	2	-5	36	12	32
-3	2	-4	27	15	57
-3	2	-3	35	16	46
-3	2	-2	0	0	100
-3	2	-1	78	20	26
-3	2	0	59	12	20
-3	2	1	0	0	100
-3	2	2	0	0	100
-3	2	3	109	15	14
-3	2	4	50	15	30
-3	2	6	61	11	18
-3	2	7	11	11	105
-3	2	8	87	14	16
-3	2	9	63	14	23
-3	2	10	61	13	20
-3	2	11	36	13	36
-3	2	12	0	0	100
-3	2	13	96	11	11
-3	2	14	72	14	20
-3	2	15	18	9	51
-3	2	16	38	9	24
-3	2	17	0	0	100
-3	2	18	18	10	55
-3	2	19	122	29	24
-3	2	20	74	11	14
-3	2	21	87	8	9
-3	2	22	0	0	100
-3	2	23	81	7	9
-3	2	24	0	0	100
-3	2	25	0	0	100
-3	2	26	0	0	100
-3	2	27	0	0	100
-3	2	28	76	8	10
-3	2	29	0	0	100
-3	2	30	0	0	100
-3	2	32	44	8	18
-3	2	33	77	8	11
-3	2	34	0	0	100
-3	2	35	83	8	10
-3	2	36	0	0	100
-3	2	37	0	0	100
-3	2	38	0	0	100
-3	2	39	80	8	10
-3	2	40	0	0	100
-3	2	42	36	8	21
-3	2	43	48	8	16
-3	2	44	0	0	100
-3	2	45	60	9	15
-3	2	46	0	0	100
-3	2	47	0	0	100
-3	2	48	29	6	22
-3	2	49	29	8	29
-3	2	50	0	0	100
-3	2	51	15	5	33
-3	2	52	37	7	18
-3	2	53	49	9	19
-3	2	54	33	8	25
-3	3	-38	44	10	23
-3	3	-37	88	11	12
-3	3	15	0	0	100
-3	3	16	0	0	100
-3	3	17	0	0	100
-3	3	18	0	0	100
-3	3	19	0	0	100
-3	3	20	0	0	100
-3	3	22	81	9	11
-3	3	23	0	0	100
-3	3	24	0	0	100
-3	3	25	48	7	14
-3	3	26	76	7	9
-3	3	27	48	6	13
-3	3	29	0	0	100
-3	3	30	0	0	100
-3	3	31	36	8	23
-3	3	32	32	8	25
-3	3	33	55	9	16
-3	3	34	0	0	100
-3	3	35	0	0	100
-2	-2	-54	42	6	14
-2	-2	-53	55	6	10
-2	-2	-52	13	4	34
-2	-2	-51	51	5	10
-2	-2	-50	0	0	100
-2	-2	-49	0	0	100
-2	-2	-48	0	0	100
-2	-2	-47	0	0	100
-2	-2	-46	53	7	13
-2	-2	-45	0	0	100
-2	-2	-44	0	0	100
-2	-2	-43	108	10	9
-2	-2	-42	0	0	100
-2	-2	-41	39	7	18
-2	-2	-40	30	6	21
-2	-2	-39	0	0	100
-2	-2	-38	29	6	22
-2	-2	-37	0	0	100
-2	-2	-36	0	0	100
-2	-2	-35	0	0	100
-2	-2	-34	0	0	100
-2	-2	36	74	7	10
-2	-2	37	0	0	100
-2	-2	38	12	7	64
-2	-2	39	52	6	12
-2	-2	40	68	7	10
-2	-2	41	0	0	100
-2	-2	42	61	7	12
-2	-2	43	0	0	100
-2	-2	44	73	7	10
-2	-2	45	0	0	100
-2	-2	46	0	0	100
-2	-2	47	53	8	15
-2	-2	48	0	0	100
-2	-2	49	43	4	10
-2	-1	-74	21	11	52
-2	-1	-72	67	14	22
-2	-1	-71	36	7	20
-2	-1	-68	86	7	9
-2	-1	-67	18	8	42
-2	-1	-66	0	0	100
-2	-1	-65	66	6	10
-2	-1	-64	0	0	100
-2	-1	-63	0	0	100
-2	-1	-62	56	5	10
-2	-1	-48	36	6	17
-2	-1	-47	0	0	100
-2	-1	-46	0	0	100
-2	-1	-45	0	0	100

-2	-1	-44	0	0	100
-2	-1	-43	74	12	16
-2	-1	-42	86	12	14
-2	-1	-19	0	0	100
-2	-1	-18	0	0	100
-2	-1	-17	0	0	100
-2	-1	-16	0	0	100
-2	-1	-15	116	16	14
-2	-1	-14	0	0	100
-2	-1	-13	31	10	33
-2	-1	-12	0	0	100
-2	-1	-11	46	15	32
-2	-1	-10	0	0	100
-2	-1	-9	0	0	100
-2	-1	-8	47	13	29
-2	-1	-7	31	22	70
-2	-1	-6	0	0	100
-2	-1	-5	110	22	20
-2	-1	-4	100	25	25
-2	-1	-3	18	29	165
-2	-1	-1	34	23	66
-2	-1	3	33	17	51
-2	-1	4	115	25	22
-2	-1	5	102	22	22
-2	-1	6	0	0	100
-2	-1	7	0	0	100
-2	-1	8	46	24	51
-2	-1	9	0	0	100
-2	-1	10	0	0	100
-2	-1	11	0	0	100
-2	-1	12	18	12	67
-2	-1	13	67	12	18
-2	-1	14	0	0	100
-2	-1	15	65	8	12
-2	-1	16	77	12	15
-2	-1	17	0	0	100
-2	-1	18	37	7	19
-2	-1	18	37	7	19
-2	-1	19	93	7	8
-2	-1	20	55	7	12
-2	-1	21	68	7	11
-2	-1	22	40	8	19
-2	-1	23	0	0	100
-2	-1	24	22	7	32
-2	-1	25	63	7	11
-2	-1	26	82	8	9
-2	-1	27	39	7	17
-2	-1	28	0	0	100
-2	-1	29	65	6	9
-2	-1	30	0	0	100
-2	-1	31	28	6	22
-2	-1	32	86	7	8
-2	-1	33	0	0	100
-2	-1	34	84	6	8
-2	-1	36	0	0	100
-2	-1	37	0	0	100
-2	-1	38	0	0	100
-2	-1	38	43	6	14
-2	-1	39	22	6	26
-2	-1	40	102	6	6
-2	-1	41	0	0	100
-2	-1	42	0	0	100
-2	-1	43	0	0	100
-2	-1	44	5	7	147
-2	-1	45	0	0	100
-2	-1	47	0	0	100
-2	-1	48	0	0	100
-2	-1	49	60	6	10
-2	-1	51	0	0	100
-2	-1	52	55	5	10
-2	-1	53	58	5	9
-2	-1	54	0	0	100
-2	-1	55	22	5	22
-2	-1	56	31	6	19
-2	-1	57	0	0	100
-2	-1	58	0	0	100
-2	-1	59	76	5	7
-2	-1	60	34	6	19
-2	-1	61	0	0	100
-2	-1	62	54	6	11
-2	0	-80	58	7	12
-2	0	-79	0	0	100
-2	0	-78	50	7	15
-2	0	-77	24	5	21
-2	0	-76	40	7	17
-2	0	-75	83	7	8
-2	0	-74	66	7	11
-2	0	-73	73	6	9
-2	0	-71	82	6	8
-2	0	-70	51	6	11
-2	0	-69	34	6	18
-2	0	-68	60	7	12
-2	0	-67	8	6	68
-2	0	-65	21	5	23
-2	0	-64	0	0	100
-2	0	-62	52	5	10
-2	0	-61	26	6	21
-2	0	-59	0	0	100
-2	0	-58	50	6	12
-2	0	-57	52	5	10
-2	0	-56	30	5	17
-2	0	-55	0	0	100
-2	0	-54	21	4	21
-2	0	-53	0	0	100
-2	0	-52	41	7	16
-2	0	-50	0	0	100
-2	0	-49	40	5	13
-2	0	-48	0	0	100
-2	0	-47	0	0	100
-2	0	-46	58	5	9
-2	0	-45	0	0	100
-2	0	-44	37	5	15
-2	0	-43	0	0	100
-2	0	-42	29	6	20
-2	0	-41	19	5	28
-2	0	-40	0	0	100
-2	0	-39	50	5	10
-2	0	-38	0	0	100
-2	0	-37	33	6	18
-2	0	-34	0	0	100
-2	0	-33	0	0	100
-2	0	-24	20	5	25
-2	0	-23	40	6	15
-2	0	-22	51	7	14
-2	0	-21	0	0	100
-2	0	-20	43	6	13
-2	0	-19	73	8	11
-2	0	-18	38	5	14
-2	0	-17	11	5	45
-2	0	-17	24	5	21
-2	0	-16	44	6	13
-2	0	-15	0	0	100
-2	0	-14	18	5	28
-2	0	-12	59	12	20
-2	0	-11	30	10	33
-2	0	-10	62	12	20
-2	0	-9	0	0	100
-2	0	-8	84	13	15
-2	0	-7	0	0	100
-2	0	-6	0	0	100
-2	0	19	58	6	10
-2	0	22	0	0	100
-2	0	23	0	0	100
-2	0	24	16	6	37
-2	0	25	22	5	22
-2	0	26	19	3	17
-2	0	27	0	0	100
-2	0	28	0	0	100
-2	0	29	3	5	132
-2	0	30	10	6	57
-2	0	31	28	5	17
-2	0	32	19	5	26
-2	0	33	23	4	20
-2	0	34	0	0	100
-2	0	35	0	0	100
-2	0	36	34	6	17
-2	0	37	34	4	13
-2	0	39	0	0	100
-2	0	40	16	6	41
-2	0	41	33	5	15
-2	0	42	0	0	100
-2	0	43	37	6	16
-2	0	44	58	6	10
-2	0	45	0	0	100
-2	0	46	59	6	9
-2	0	47	0	0	100
-2	0	48	0	0	100
-2	0	49	31	5	16
-2	0	50	0	0	100
-2	0	51	27	5	20
-2	0	52	49	5	10
-2	0	53	56	5	8
-2	0	54	0	0	100
-2	0	55	45	6	13
-2	0	56	0	0	100
-2	0	57	59	6	10
-2	0	58	23	5	22
-2	0	59	58	5	9
-2	0	60	35	5	14
-2	0	61	10	4	44
-2	0	62	46	5	11
-2	0	63	0	0	100
-2	0	64	0	0	100
-2	0	65	0	0	100
-2	0	66	0	0	100
-2	0	67	16	5	30
-2	0	68	34	5	15
-2	0	70	101	8	8
-2	0	71	77	7	9
-2	0	72	63	6	10
-2	1	-79	46	7	15
-2	1	-78	29	8	27
-2	1	-77	33	6	17
-2	1	-76	74	7	9
-2	1	-75	82	6	8
-2	1	-74	49	8	16
-2	1	-71	35	7	19
-2	1	-70	58	6	10
-2	1	-69	55	6	11
-2	1	-68	32	7	23
-2	1	-67	62	7	11
-2	1	-66	72	6	8
-2	1	-65	87	6	6
-2	1	-64	0	0	100
-2	1	-63	56	5	9
-2	1	-62	0	0	100
-2	1	-61	28	5	19
-2	1	-60	9	6	66
-2	1	-59	0	0	100
-2	1	-58	22	5	24
-2	1	-57	38	5	14
-2	1	-56	16	5	32
-2	1	-55	0	0	100
-2	1	-54	59	4	7
-2	1	-53	46	5	11
-2	1	-52	85	8	9
-2	1	-51	76	7	9
-2	1	-50	0	0	100
-2	1	-49	0	0	100
-2	1	-48	0	0	100
-2	1	-47	55	5	9
-2	1	-46	44	6	13
-2	1	-45	0	0	100
-2	1	-44	61	6	10
-2	1	-43	53	6	11
-2	1	-42	80	5	7
-2	1	-41	41	6	15
-2	1	-40	28	7	26
-2	1	-39	88	7	8
-2	1	-38	5	5	110
-2	1	-37	32	6	18
-2	1	-36	80	7	9
-2	1	-35	27	7	27
-2	1	-34	0	0	100
-2	1	-33	0	0	100
-2	1	-32	35	5	16
-2	1	-31	0	0	100
-2	1	-30	45	5	12
-2	1	-29	0	0	100
-2	1	-28	36	5	14
-2	1	-27	0	0	100
-2	1	-26	0	0	100
-2	1	-25	0	0	100
-2	1	-24	0	0	100
-2	1	-23	39	6	15
-2	1	-22	0	0	100
-2	1	-21	6	7	117
-2	1	-20	8	5	70
-2	1	-19	0	0	100
-2	1	-18	86	7	8
-2	1	-17	0	0	100
-2	1	-17	0	0	100
-2	1	-16	27	6	23
-2	1	-15	30	6	18
-2	1	-14	11	5	46
-2	1	-13	0	0	100
-2	1	-12	19	8	40
-2	1	-11	0	0	100
-2	1	-10	64	10	16
-2	1	-9	44	12	27
-2	1	-8	0	0	100

-2	1	-7	0	0	100
-2	1	-6	0	0	100
-2	1	-5	114	16	14
-2	1	-4	83	16	19
-2	1	-3	0	0	100
-2	1	-2	0	0	100
-2	1	-1	69	18	26
-2	1	-1	60	18	31
-2	1	0	0	0	100
-2	1	1	93	21	22
-2	1	2	0	0	100
-2	1	3	65	12	19
-2	1	4	108	15	14
-2	1	5	0	0	100
-2	1	6	0	0	100
-2	1	7	19	17	90
-2	1	8	19	13	68
-2	1	9	0	0	100
-2	1	10	84	11	13
-2	1	11	0	0	100
-2	1	12	36	10	27
-2	1	13	28	7	26
-2	1	14	0	0	100
-2	1	15	0	0	100
-2	1	16	0	0	100
-2	1	17	95	7	7
-2	1	18	0	0	100
-2	1	19	37	6	17
-2	1	20	26	6	24
-2	1	21	0	0	100
-2	1	22	64	7	10
-2	1	22	0	0	100
-2	1	24	43	4	10
-2	1	25	41	5	14
-2	1	26	0	0	100
-2	1	35	0	0	100
-2	1	36	33	6	19
-2	1	38	0	0	100
-2	1	39	0	0	100
-2	1	40	48	6	12
-2	1	41	29	6	20
-2	1	42	35	5	16
-2	1	45	52	5	10
-2	1	46	37	6	16
-2	1	47	28	6	22
-2	1	48	64	6	9
-2	1	49	24	6	24
-2	1	50	0	0	100
-2	1	51	0	0	100
-2	1	52	0	0	100
-2	1	53	0	0	100
-2	1	54	40	6	14
-2	1	55	58	7	12
-2	1	56	0	0	100
-2	1	57	13	5	40
-2	1	58	29	5	17
-2	1	59	0	0	100
-2	1	60	0	0	100
-2	1	61	37	5	14
-2	1	62	11	5	46
-2	1	63	0	0	100
-2	1	64	71	5	8
-2	1	65	74	6	8
-2	1	66	53	5	10
-2	1	67	10	5	48
-2	1	68	38	6	15
-2	1	69	0	0	100
-2	1	70	116	7	6
-2	1	71	60	7	11
-2	2	-71	80	12	15
-2	2	-69	28	10	34
-2	2	-68	0	0	100
-2	2	-45	0	0	100
-2	2	-44	36	12	32
-2	2	-43	112	11	10
-2	2	-42	0	0	100
-2	2	-41	41	12	30
-2	2	-40	77	11	14
-2	2	-39	0	0	100
-2	2	-38	0	0	100
-2	2	-37	14	7	55
-2	2	-36	0	0	100
-2	2	-34	0	0	100
-2	2	-33	41	8	19
-2	2	32	0	0	100
-2	2	-31	0	0	100
-2	2	-30	40	8	19
-2	2	-29	0	0	100
-2	2	-28	51	8	15
-2	2	-27	52	9	16
-2	2	-26	0	0	100
-2	2	-25	37	8	22
-2	2	-24	22	7	32
-2	2	-23	0	0	100
-2	2	-22	0	0	100
-2	2	-21	28	8	29
-2	2	-20	0	0	100
-2	2	-19	26	7	26
-2	2	-18	0	0	100
-2	2	-17	26	8	33
-2	2	-16	49	8	16
-2	2	-15	0	0	100
-2	2	-14	0	0	100
-2	2	-13	0	0	100
-2	2	-12	39	11	28
-2	2	-11	0	0	100
-2	2	-10	73	12	17
-2	2	-9	95	14	15
-2	2	-8	0	0	100
-2	2	-7	90	17	18
-2	2	-6	0	0	100
-2	2	-5	120	19	16
-2	2	-4	101	23	22
-2	2	-3	65	24	38
-2	2	-2	103	27	26
-2	2	-1	0	0	100
-2	2	0	170	36	21
-2	2	1	327	44	13
-2	2	2	167	36	21
-2	2	3	174	33	19
-2	2	4	0	0	100
-2	2	5	74	25	34
-2	2	6	148	24	16
-2	2	7	98	23	23
-2	2	8	0	0	100
-2	2	9	100	19	19
-2	2	10	128	20	16
-2	2	11	113	15	14
-2	2	12	18	18	100
-2	2	13	0	0	100
-2	2	14	37	7	20
-2	2	15	0	0	100
-2	2	16	70	10	15
-2	2	17	0	0	100
-2	2	18	44	11	24
-2	2	19	67	13	20
-2	2	22	122	8	7
-2	2	31	0	0	100
-2	2	32	0	0	100
-2	2	33	41	15	37
-2	2	44	0	0	100
-2	2	45	92	16	17
-2	2	46	40	9	22
-2	2	47	0	0	100
-2	2	48	67	8	13
-2	2	49	51	9	17
-2	2	50	59	8	13
-2	2	51	0	0	100
-2	2	52	78	9	11
-2	2	53	96	8	9
-2	2	54	65	8	13
-2	2	55	69	7	11
-2	2	56	25	7	29
-2	2	57	14	7	51
-2	2	58	16	7	46
-2	2	59	13	7	56
-2	2	60	9	9	96
-1	-2	-60	45	8	17
-1	-2	-59	0	0	100
-1	-2	-58	0	0	100
-1	-2	-57	0	0	100
-1	-2	-56	0	0	100
-1	-2	-55	54	6	11
-1	-2	-54	35	6	17
-1	-2	-53	20	6	30
-1	-2	-52	0	0	100
-1	-2	-51	53	6	11
-1	-2	-50	0	0	100
-1	-2	-49	0	0	100
-1	-2	-48	0	0	100
-1	-2	-47	86	6	8
-1	-2	-46	8	8	101
-1	-2	-45	97	8	8
-1	-2	-44	98	8	8
-1	-2	-43	70	7	9
-1	-2	-42	32	7	23
-1	-2	-41	0	0	100
-1	-2	-40	0	0	100
-1	-2	-39	0	0	100
-1	-2	-38	34	6	19
-1	-2	-37	0	0	100
-1	-2	-36	49	7	14
-1	-2	-35	40	6	16
-1	-2	-34	48	7	15
-1	-2	-33	43	6	15
-1	-2	-32	85	6	7
-1	-2	-31	61	7	11
-1	-2	-30	0	0	100
-1	-2	-29	49	7	14
-1	-2	-26	67	7	10
-1	-2	-25	0	0	100
-1	-2	-24	0	0	100
-1	-2	-23	46	7	15
-1	-2	-21	39	6	15
-1	-2	-20	0	0	100
-1	-2	-19	83	7	8
-1	-2	-18	0	0	100
-1	-2	-17	7	10	138
-1	-2	-16	84	10	12
-1	-2	-15	0	0	100
-1	-2	-14	0	0	100
-1	-2	-13	37	9	23
-1	-2	-12	47	9	19
-1	-2	-11	36	12	33
-1	-2	-10	0	0	100
-1	-2	-9	61	12	20
-1	-2	-8	75	13	17
-1	-2	-7	61	13	21
-1	-2	-6	42	18	44
-1	-2	-5	0	0	100
-1	-2	-4	0	0	100
-1	-2	-3	20	20	101
-1	-2	-2	0	0	100
-1	-2	-1	105	17	16
-1	-2	0	0	0	100
-1	-2	1	61	20	32
-1	-2	2	90	21	23
-1	-2	3	0	0	100
-1	-2	4	107	22	21
-1	-2	5	0	0	100
-1	-2	6	0	0	100
-1	-2	7	79	13	16
-1	-2	8	0	0	100
-1	-2	9	125	14	11
-1	-2	10	0	0	100
-1	-2	11	0	0	100
-1	-2	12	70	10	15
-1	-2	13	0	0	100
-1	-2	14	68	13	19
-1	-2	15	0	0	100
-1	-2	16	0	0	100
-1	-2	17	0	0	100
-1	-2	18	73	8	11
-1	-2	19	26	10	39
-1	-2	21	54	8	14
-1	-2	22	76	8	11
-1	-2	23	0	0	100
-1	-2	24	0	0	100
-1	-2	25	91	8	8
-1	-2	26	32	7	22
-1	-2	27	0	0	100
-1	-2	28	0	0	100
-1	-2	29	40	9	22
-1	-2	30	0	0	100
-1	-2	31	0	0	100
-1	-2	32	0	0	100
-1	-2	33	0	0	100
-1	-2	34	36	10	27
-1	-2	35	53	9	17
-1	-2	36	0	0	100
-1	-2	37	0	0	100
-1	-2	38	0	0	100
-1	-2	39	36	7	18
-1	-2	40	119	8	7
-1	-2	41	92	8	9
-1	-2	42	0	0	100
-1	-2	43	103	9	9
-1	-2	44	0	0	100
-1	-2	45	42	7	17
-1	-2	46	115	9	8
-1	-2	47	22	8	37

-1	-2	48	58	9	16
-1	-2	49	0	0	100
-1	-2	50	0	0	100
-1	-2	51	0	0	100
-1	-2	52	0	0	100
-1	-2	53	0	0	100
-1	-2	54	22	8	36
-1	-2	57	29	8	28
-1	-1	-80	58	7	12
-1	-1	-79	31	7	21
-1	-1	-78	0	0	100
-1	-1	-77	43	6	14
-1	-1	-76	17	5	31
-1	-1	-74	23	7	32
-1	-1	-73	59	7	11
-1	-1	-72	44	7	16
-1	-1	-71	50	6	12
-1	-1	-70	12	7	55
-1	-1	-69	0	0	100
-1	-1	-66	25	5	21
-1	-1	-65	45	5	11
-1	-1	-64	32	6	19
-1	-1	-63	0	0	100
-1	-1	-62	29	5	18
-1	-1	-61	54	4	8
-1	-1	-60	57	5	9
-1	-1	-59	61	5	9
-1	-1	-58	0	0	100
-1	-1	-57	44	5	11
-1	-1	-56	0	0	100
-1	-1	-55	0	0	100
-1	-1	-54	35	5	16
-1	-1	-53	62	6	10
-1	-1	-52	0	0	100
-1	-1	-51	0	0	100
-1	-1	-50	35	5	15
-1	-1	-49	0	0	100
-1	-1	-48	59	7	11
-1	-1	-47	0	0	100
-1	-1	-46	31	6	18
-1	-1	-45	0	0	100
-1	-1	-45	0	0	100
-1	-1	-44	33	5	14
-1	-1	-43	0	0	100
-1	-1	-42	0	0	100
-1	-1	-41	17	6	35
-1	-1	-40	0	0	100
-1	-1	-39	27	5	20
-1	-1	-30	15	4	26
-1	-1	-29	0	0	100
-1	-1	-28	28	5	18
-1	-1	-27	0	0	100
-1	-1	-26	38	6	15
-1	-1	-25	37	5	14
-1	-1	-24	0	0	100
-1	-1	-23	0	0	100
-1	-1	-22	34	6	17
-1	-1	-21	0	0	100
-1	-1	-20	34	8	23
-1	-1	-19	43	6	14
-1	-1	-18	11	5	50
-1	-1	-17	0	0	100
-1	-1	-15	0	0	100
-1	-1	-13	0	0	100
-1	-1	-12	59	15	25
-1	-1	-11	0	0	100
-1	-1	-10	0	0	100
-1	-1	-9	0	0	100
-1	-1	-8	62	13	20
-1	-1	-7	0	0	100
-1	-1	-6	0	0	100
-1	-1	22	0	0	100
-1	-1	23	0	0	100
-1	-1	24	0	0	100
-1	-1	25	0	0	100
-1	-1	26	28	5	18
-1	-1	27	0	0	100
-1	-1	28	25	5	19
-1	-1	29	0	0	100
-1	-1	31	57	5	9
-1	-1	32	0	0	100
-1	-1	33	0	0	100
-1	-1	34	0	0	100
-1	-1	35	0	0	100
-1	-1	36	38	5	12
-1	-1	37	0	0	100
-1	-1	38	30	6	19

-1	-1	39	0	0	100
-1	-1	40	0	0	100
-1	-1	41	56	7	13
-1	-1	42	0	0	100
-1	-1	44	27	6	21
-1	-1	45	11	5	52
-1	-1	46	0	0	100
-1	-1	47	37	5	13
-1	-1	48	0	0	100
-1	-1	49	19	5	24
-1	-1	50	0	0	100
-1	-1	51	0	0	100
-1	-1	52	28	5	17
-1	-1	53	10	5	53
-1	-1	54	0	0	100
-1	-1	55	71	7	10
-1	-1	56	42	6	14
-1	-1	57	82	7	8
-1	-1	58	30	6	19
-1	-1	59	24	6	23
-1	-1	60	0	0	100
-1	-1	61	0	0	100
-1	-1	62	38	5	14
-1	-1	63	0	0	100
-1	-1	64	60	5	8
-1	-1	65	39	5	13
-1	-1	66	0	0	100
-1	-1	68	35	6	17
-1	-1	68	0	0	100
-1	-1	69	0	0	100
-1	-1	70	60	7	12
-1	-1	71	89	6	7
-1	1	-80	48	6	13
-1	1	-79	31	7	21
-1	1	-78	20	5	26
-1	1	-77	54	5	9
-1	1	-76	2	5	316
-1	1	-75	46	5	10
-1	1	-74	68	6	9
-1	1	-73	29	5	17
-1	1	-71	21	5	26
-1	1	-70	0	0	100
-1	1	-69	0	0	100
-1	1	-68	55	5	9
-1	1	-67	53	5	9
-1	1	-66	25	5	20
-1	1	-65	33	5	15
-1	1	-64	0	0	100
-1	1	-63	16	4	25
-1	1	-62	17	4	24
-1	1	-61	64	5	7
-1	1	-60	29	4	15
-1	1	-59	0	0	100
-1	1	-58	0	0	100
-1	1	-57	0	0	100
-1	1	-56	49	6	12
-1	1	-55	0	0	100
-1	1	-54	17	5	28
-1	1	-53	0	0	100
-1	1	-52	25	5	19
-1	1	-50	4	4	100
-1	1	-49	39	4	11
-1	1	-48	0	0	100
-1	1	-47	35	4	11
-1	1	-46	51	4	9
-1	1	-45	29	6	22
-1	1	-44	47	5	10
-1	1	-43	59	5	8
-1	1	-42	13	4	35
-1	1	-42	13	4	35
-1	1	-41	32	4	14
-1	1	-40	29	5	17
-1	1	-40	0	0	100
-1	1	-39	49	4	8
-1	1	-38	12	4	30
-1	1	-37	28	4	15
-1	1	-36	54	5	10
-1	1	-35	24	5	21
-1	1	-34	32	5	17
-1	1	-33	8	5	54
-1	1	-32	15	7	46
-1	1	-31	39	6	15
-1	1	-30	39	6	14
-1	1	-29	0	0	100
-1	1	-28	32	5	16
-1	1	-27	38	5	14
-1	1	-26	13	5	42

-1	1	-25	13	5	38
-1	1	-24	54	5	10
-1	1	-23	0	0	100
-1	1	-22	23	4	18
-1	1	-21	10	5	51
-1	1	-20	0	0	100
-1	1	-19	35	6	16
-1	1	-17	0	0	100
-1	1	-16	30	5	16
-1	1	-15	0	0	100
-1	1	-14	50	5	11
-1	1	-13	36	7	20
-1	1	-12	42	8	18
-1	1	-11	37	10	26
-1	1	-10	0	0	100
-1	1	-9	38	8	21
-1	1	-8	0	0	100
-1	1	-7	0	0	100
-1	1	-6	0	0	100
-1	1	-5	0	0	100
-1	1	-4	58	13	22
-1	1	-3	47	13	27
-1	1	-2	51	14	27
-1	1	-1	58	13	23
-1	1	-1	58	13	23
-1	1	0	49	11	23
-1	1	0	0	0	100
-1	1	1	0	0	100
-1	1	1	50	13	26
-1	1	1	50	13	26
-1	1	2	62	12	19
-1	1	3	0	0	100
-1	1	4	67	18	27
-1	1	4	0	0	100
-1	1	5	0	0	100
-1	1	6	106	12	11
-1	1	7	0	0	100
-1	1	8	39	11	28
-1	1	9	49	11	22
-1	1	10	0	0	100
-1	1	11	0	0	100
-1	1	13	0	0	100
-1	1	14	17	7	39
-1	1	15	0	0	100
-1	1	16	39	5	14
-1	1	17	29	6	22
-1	1	18	0	0	100
-1	1	19	0	0	100
-1	1	20	0	0	100
-1	1	21	0	0	100
-1	1	22	227	30	13
-1	1	23	0	0	100
-1	1	24	0	0	100
-1	1	25	47	5	11
-1	1	26	45	5	11
-1	1	27	29	4	15
-1	1	28	29	6	21
-1	1	29	11	4	40
-1	1	30	34	5	16
-1	1	31	30	5	16
-1	1	32	14	5	33
-1	1	33	14	5	37
-1	1	34	0	0	100
-1	1	35	35	5	16
-1	1	36	0	0	100
-1	1	37	22	4	18
-1	1	38	20	4	21
-1	1	39	46	5	11
-1	1	40	8	4	57
-1	1	41	19	4	24
-1	1	42	33	5	16
-1	1	43	38	4	11
-1	1	44	0	0	100
-1	1	45	35	4	12
-1	1	46	0	0	100
-1	1	47	42	5	12
-1	1	48	24	6	25
-1	1	49	39	5	13
-1	1	50	37	4	10
-1	1	51	15	4	30
-1	1	52	28	5	18
-1	1	53	0	0	100
-1	1	54	0	0	100
-1	1	55	7	5	75
-1	1	56	68	5	8
-1	1	57	0	0	100
-1	1	58	0	0	100

-1	1	59	49	5	10
-1	1	60	52	5	9
-1	1	61	33	4	13
-1	1	62	35	5	14
-1	1	63	26	5	18
-1	1	65	0	0	100
-1	1	66	27	4	17
-1	1	67	36	5	13
-1	1	68	0	0	100
-1	1	69	17	5	29
-1	1	70	26	5	18
-1	1	71	31	13	42
-1	2	-75	22	12	53
-1	2	-74	58	14	24
-1	2	-73	0	0	100
-1	2	-72	34	10	30
-1	2	-70	0	0	100
-1	2	-69	0	0	100
-1	2	-69	0	0	100
-1	2	-67	54	6	12
-1	2	-66	25	7	28
-1	2	-65	25	5	22
-1	2	-64	0	0	100
-1	2	-63	31	7	22
-1	2	-62	43	6	15
-1	2	-62	32	5	17
-1	2	-61	0	0	100
-1	2	-60	0	0	100
-1	2	-59	0	0	100
-1	2	-14	0	0	100
-1	2	-13	0	0	100
-1	2	-12	21	8	40
-1	2	-11	0	0	100
-1	2	-10	54	12	22
-1	2	-9	2	13	723
-1	2	-8	0	0	100
-1	2	-7	123	17	14
-1	2	-6	99	24	25
-1	2	-5	111	22	20
-1	2	-4	214	26	12
-1	2	-3	279	24	9
-1	2	-2	217	23	10
-1	2	-1	204	21	10
-1	2	0	166	18	11
-1	2	1	145	19	13
-1	2	2	104	19	18
-1	2	3	184	19	10
-1	2	4	195	20	10
-1	2	5	168	20	12
-1	2	6	136	22	16
-1	2	7	0	0	100
-1	2	8	0	0	100
-1	2	9	77	19	24
-1	2	10	0	0	100
-1	2	11	0	0	100
-1	2	12	106	12	12
-1	2	13	23	13	57
-1	2	14	0	0	100
-1	2	15	17	10	61
-1	2	16	0	0	100
-1	2	17	79	10	13
-1	2	18	0	0	100
0	-3	-45	0	0	100
0	-3	-44	51	9	18
0	-3	-43	70	8	12
0	-3	-42	91	10	11
0	-3	-41	66	8	13
0	-3	-40	0	0	100
0	-3	-39	89	8	9
0	-3	-38	0	0	100
0	-3	-37	51	8	15
0	-3	-36	54	8	14
0	-3	-35	77	8	11
0	-3	-35	77	8	11
0	-3	-34	43	7	17
0	-3	-33	52	7	14
0	-3	-32	10	6	62
0	-3	-31	0	0	100
0	-3	-30	46	6	14
0	-3	-29	39	8	20
0	-3	-28	68	8	12
0	-3	-27	0	0	100
0	-3	-26	38	8	21
0	-3	-25	0	0	100
0	-3	-24	10	7	77
0	-3	-23	0	0	100
0	-3	-22	41	8	18
0	-3	-21	15	7	47
0	-3	-20	0	0	100
0	-3	-19	0	0	100
0	-3	23	53	7	14
0	-3	24	27	8	29
0	-3	25	21	6	29
0	-3	26	71	6	9
0	-3	27	0	0	100
0	-3	28	0	0	100
0	-3	29	63	8	12
0	-3	30	56	8	13
0	-3	31	8	7	95
0	-3	32	0	0	100
0	-3	33	0	0	100
0	-3	34	97	7	7
0	-3	35	0	0	100
0	-3	36	0	0	100
0	-3	37	0	0	100
0	-3	38	38	7	19
0	-2	-53	0	0	100
0	-2	-52	55	7	13
0	-2	-51	0	0	100
0	-2	-50	0	0	100
0	-2	-49	0	0	100
0	-2	-48	98	9	9
0	-2	-47	21	8	36
0	-2	-46	0	0	100
0	-2	-45	59	7	12
0	-2	-44	84	7	9
0	-2	-43	23	8	34
0	-2	-42	0	0	100
0	-2	-41	0	0	100
0	-2	-40	0	0	100
0	-2	-39	0	0	100
0	-2	-38	0	0	100
0	-2	-37	74	9	12
0	-2	-36	52	7	14
0	-2	-35	0	0	100
0	-2	-34	15	7	48
0	-2	-33	49	8	16
0	-2	-31	61	7	12
0	-2	-30	41	8	18
0	-2	-29	29	8	27
0	-2	-28	56	8	15
0	-2	-27	80	7	9
0	-2	-26	42	8	18
0	-2	-25	93	8	9
0	-2	-24	77	9	12
0	-2	-23	60	8	14
0	-2	-22	0	0	100
0	-2	-21	63	7	12
0	-2	-20	23	8	35
0	-2	-19	56	8	15
0	-2	-18	0	0	100
0	-2	27	44	17	38
0	-2	28	80	15	19
0	-2	29	0	0	100
0	-2	30	23	15	64
0	-2	31	75	15	20
0	-2	32	0	0	100
0	-2	33	0	0	100
0	-2	34	0	0	100
0	-2	35	0	0	100
0	-2	36	0	0	100
0	-2	37	0	0	100
0	-2	38	0	0	100
0	-2	39	15	15	101
0	-2	41	0	0	100
0	-2	42	0	0	100
0	-2	43	92	17	18
0	-1	-80	0	0	100
0	-1	-79	12	5	43
0	-1	-78	20	5	26
0	-1	-77	6	5	77
0	-1	-74	59	5	8
0	-1	-73	31	5	17
0	-1	-72	49	5	10
0	-1	-71	51	6	11
0	-1	-70	57	6	11
0	-1	-68	35	4	13
0	-1	-67	66	6	8
0	-1	-66	0	0	100
0	-1	-65	35	4	13
0	-1	-64	0	0	100
0	-1	-63	30	4	14
0	-1	-62	0	0	100
0	-1	-61	59	7	11
0	-1	-60	31	4	13
0	-1	-58	0	0	100
0	-1	-57	0	0	100
0	-1	-56	29	5	17
0	-1	-55	0	0	100
0	-1	-54	0	0	100
0	-1	-53	24	4	18
0	-1	-52	0	0	100
0	-1	-51	4	4	121
0	-1	-50	19	5	25
0	-1	-48	15	4	27
0	-1	-47	16	3	21
0	-1	-46	13	5	40
0	-1	-45	28	4	15
0	-1	-44	28	6	20
0	-1	-42	32	4	13
0	-1	-41	45	4	9
0	-1	-41	30	4	12
0	-1	-39	20	4	22
0	-1	-38	22	3	15
0	-1	-37	0	0	100
0	-1	-36	39	5	13
0	-1	-35	12	5	39
0	-1	-34	36	5	13
0	-1	-33	7	5	72
0	-1	-32	66	5	8
0	-1	-32	36	5	13
0	-1	-31	25	4	18
0	-1	-30	19	3	18
0	-1	-29	37	4	12
0	-1	-27	28	5	16
0	-1	-26	56	5	8
0	-1	-25	33	5	14
0	-1	-24	37	4	11
0	-1	-23	17	5	28
0	-1	-22	44	6	13
0	-1	-21	21	6	30
0	-1	-20	53	6	11
0	-1	-19	75	6	7
0	-1	-18	12	5	40
0	-1	-17	33	5	16
0	-1	-15	0	0	100
0	-1	-14	46	7	14
0	-1	-13	0	0	100
0	-1	-12	56	9	16
0	-1	-11	0	0	100
0	-1	-10	15	12	78
0	-1	-6	0	0	100
0	-1	-5	0	0	100
0	-1	-4	0	0	100
0	-1	-3	0	0	100
0	-1	0	36	11	29
0	-1	2	100	13	13
0	-1	3	0	0	100
0	-1	4	0	0	100
0	-1	5	39	12	31
0	-1	6	0	0	100
0	-1	10	8	10	120
0	-1	11	40	7	18
0	-1	12	0	0	100
0	-1	13	26	7	28
0	-1	14	37	5	15
0	-1	15	19	6	33
0	-1	16	0	0	100
0	-1	17	39	5	14
0	-1	18	0	0	100
0	-1	19	53	6	11
0	-1	20	64	5	8
0	-1	22	17	4	25
0	-1	23	41	5	11
0	-1	24	0	0	100
0	-1	25	27	4	16
0	-1	26	36	4	12
0	-1	27	0	0	100
0	-1	28	44	6	13
0	-1	29	0	0	100
0	-1	30	31	5	16
0	-1	31	24	4	18
0	-1	32	22	5	23
0	-1	32	43	5	12
0	-1	33	15	5	32
0	-1	34	0	0	100
0	-1	35	18	5	27
0	-1	36	46	5	11
0	-1	37	0	0	100
0	-1	38	0	0	100
0	-1	38	0	0	100

0	-1	39	20	4	20
0	-1	40	42	4	10
0	-1	41	0	0	100
0	-1	42	0	0	100
0	-1	43	0	0	100
0	-1	44	25	5	18
0	-1	45	53	4	8
0	-1	46	35	4	13
0	-1	47	14	4	29
0	-1	48	20	5	25
0	-1	49	26	5	20
0	-1	50	42	5	11
0	-1	51	0	0	100
0	-1	52	15	4	27
0	-1	53	44	5	12
0	-1	54	4	5	119
0	-1	55	0	0	100
0	-1	56	24	6	23
0	-1	57	41	6	15
0	-1	58	52	5	10
0	-1	59	0	0	100
0	-1	60	0	0	100
0	-1	61	52	5	10
0	-1	62	25	5	19
0	-1	63	0	0	100
0	-1	64	37	5	13
0	-1	65	44	5	10
0	-1	66	52	4	8
0	-1	67	38	6	15
0	-1	68	49	5	11
0	-1	70	0	0	100
0	1	-80	0	0	100
0	1	-79	0	0	100
0	1	-78	61	5	8
0	1	-77	35	5	13
0	1	-76	0	0	100
0	1	-75	10	4	44
0	1	-74	37	5	15
0	1	-73	60	6	10
0	1	-72	9	4	48
0	1	-71	27	5	20
0	1	-70	0	0	100
0	1	-69	11	4	42
0	1	-68	49	5	10
0	1	-67	43	5	12
0	1	-66	28	5	18
0	1	-65	0	0	100
0	1	-64	8	4	52
0	1	-63	44	5	11
0	1	-62	0	0	100
0	1	-61	21	4	20
0	1	-60	39	4	10
0	1	-59	0	0	100
0	1	-58	0	0	100
0	1	-57	48	5	10
0	1	-56	0	0	100
0	1	-55	0	0	100
0	1	-54	0	0	100
0	1	-52	2	5	187
0	1	-51	23	5	20
0	1	-50	18	4	23
0	1	-49	30	4	15
0	1	-48	31	4	14
0	1	-47	0	0	100
0	1	-46	37	6	16
0	1	-45	19	4	23
0	1	-43	38	4	11
0	1	-42	20	4	21
0	1	-41	0	0	100
0	1	-40	14	4	31
0	1	-39	34	5	14
0	1	-38	72	6	8
0	1	-37	7	4	59
0	1	-36	17	4	25
0	1	-35	13	5	37
0	1	-34	20	5	24
0	1	-33	24	5	19
0	1	-32	54	6	11
0	1	-31	67	6	8
0	1	-30	40	5	13
0	1	-29	0	0	100
0	1	-27	44	4	9
0	1	-26	17	5	28
0	1	-25	1	5	339
0	1	-24	30	5	16
0	1	-23	23	5	24
0	1	-22	29	6	20
0	1	-21	24	5	20
0	1	-20	0	0	100
0	1	-19	0	0	100
0	1	-18	28	6	21
0	1	-17	30	5	17
0	1	-16	64	7	12
0	1	-15	43	7	17
0	1	-14	0	0	100
0	1	-13	42	11	27
0	1	-11	0	0	100
0	1	-11	56	11	19
0	1	-10	21	12	55
0	1	-9	64	11	17
0	1	-9	30	10	34
0	1	-8	40	10	24
0	1	-6	36	13	37
0	1	-5	53	8	15
0	1	-4	33	10	31
0	1	-3	45	12	27
0	1	-2	32	13	41
0	1	-2	73	13	18
0	1	-1	0	0	100
0	1	0	0	0	100
0	1	1	60	10	17
0	1	1	70	11	15
0	1	2	0	0	100
0	1	3	77	13	17
0	1	4	0	0	100
0	1	5	0	0	100
0	1	6	110	11	10
0	1	7	48	9	18
0	1	7	0	0	100
0	1	8	58	11	20
0	1	9	0	0	100
0	1	9	41	12	28
0	1	10	38	9	25
0	1	11	0	0	100
0	1	12	0	0	100
0	1	13	37	7	20
0	1	14	28	5	19
0	1	15	39	6	16
0	1	16	41	5	13
0	1	17	0	0	100
0	1	18	0	0	100
0	1	20	50	6	12
0	1	20	45	5	11
0	1	21	0	0	100
0	1	22	0	0	100
0	1	23	15	5	36
0	1	24	8	5	57
0	1	25	0	0	100
0	1	26	17	4	25
0	1	27	40	5	12
0	1	28	33	5	16
0	1	29	0	0	100
0	1	30	18	5	28
0	1	31	38	4	12
0	1	32	33	5	15
0	1	33	24	5	21
0	1	34	41	5	13
0	1	35	0	0	100
0	1	36	34	4	11
0	1	37	25	5	19
0	1	38	0	0	100
0	1	39	43	5	12
0	1	40	0	0	100
0	1	41	0	0	100
0	1	42	35	4	12
0	1	43	28	4	15
0	1	44	0	0	100
0	1	45	39	5	13
0	1	46	20	4	19
0	1	47	49	6	13
0	1	48	43	6	14
0	1	49	49	5	10
0	1	50	26	4	15
0	1	51	42	5	11
0	1	52	34	4	13
0	1	53	51	5	11
0	1	54	43	5	11
0	1	55	0	0	100
0	1	56	44	5	11
0	1	57	43	6	13
0	1	58	0	0	100
0	1	59	0	0	100
0	1	60	0	0	100
0	1	61	24	4	17
0	1	62	0	0	100
0	1	63	14	5	32
0	1	64	40	5	11
0	1	65	43	5	11
0	1	66	0	0	100
0	1	67	0	0	100
0	1	68	17	5	30
0	1	69	32	5	14
0	2	-75	9	11	129
0	2	-74	56	12	22
0	2	-73	95	12	12
0	2	-72	14	7	48
0	2	-71	24	7	27
0	2	-70	47	6	13
0	2	-69	38	7	19
0	2	-68	117	8	7
0	2	-67	50	7	14
0	2	-66	0	0	100
0	2	-65	44	6	13
0	2	-64	17	6	32
0	2	-63	22	6	29
0	2	-49	18	6	37
0	2	-48	0	0	100
0	2	-47	74	7	9
0	2	-46	82	7	8
0	2	-45	42	6	14
0	2	-44	50	6	12
0	2	-43	0	0	100
0	2	-42	0	0	100
0	2	-41	0	0	100
0	2	-40	0	0	100
0	2	-39	0	0	100
0	2	-38	0	0	100
0	2	-37	0	0	100
0	2	-36	51	6	11
0	2	-35	20	6	32
0	2	-34	0	0	100
0	2	-33	26	6	23
0	2	-32	0	0	100
0	2	-31	41	7	17
0	2	-28	92	15	16
0	2	-27	44	17	38
0	2	-26	59	15	25
0	2	-25	124	15	12
0	2	0	32	21	65
0	2	1	50	23	47
0	2	21	23	7	30
0	2	22	64	7	11
0	2	23	0	0	100
0	2	24	71	9	12
0	2	26	0	0	100
0	2	27	32	9	29
0	2	28	0	0	100
0	2	29	0	0	100
0	2	30	0	0	100
0	2	30	0	0	100
0	2	31	0	0	100
0	2	32	99	9	9
0	2	33	0	0	100
0	2	34	41	8	20
0	2	35	50	7	14
0	2	36	70	8	12
0	2	37	0	0	100
0	2	38	53	9	16
0	2	39	0	0	100
0	2	40	26	7	28
0	2	41	0	0	100
0	2	42	69	9	13
0	2	43	79	8	10
0	2	44	65	7	10
0	2	45	0	0	100
0	2	46	85	8	10
0	2	47	49	8	16
0	2	48	0	0	100
0	2	49	0	0	100
0	2	50	81	8	10
0	2	51	83	9	11
0	2	52	0	0	100
0	2	53	0	0	100
0	2	54	50	7	14
0	2	55	0	0	100
0	2	56	35	7	21
0	2	57	42	7	17
0	2	58	53	8	15
0	2	59	52	9	16
0	3	-43	67	10	15
0	3	-42	83	10	12

0	3	-41	67	10	15
0	3	-40	58	9	16
0	3	-39	0	0	100
0	3	-38	76	9	12
0	3	-37	26	7	28
0	3	-36	63	7	11
0	3	-35	0	0	100
0	3	-34	0	0	100
0	3	-34	0	0	100
0	3	-33	66	8	12
0	3	-32	62	7	11
0	3	-31	0	0	100
0	3	-30	0	0	100
0	3	-29	49	8	16
0	3	-28	31	8	25
0	3	-27	0	0	100
0	3	-26	0	0	100
0	3	-25	0	0	100
0	3	-24	33	6	18
0	3	-23	62	8	13
0	3	-22	15	8	54
0	3	-20	62	8	13
0	3	-19	0	0	100
0	3	-18	69	9	12
0	3	24	0	0	100
0	3	25	75	7	10
0	3	26	55	6	12
0	3	27	0	0	100
0	3	28	48	8	16
0	3	29	0	0	100
0	3	30	64	7	11
0	3	31	16	8	50
0	3	32	0	0	100
0	3	33	0	0	100
0	3	34	36	6	18
0	3	35	38	8	20
0	3	36	64	7	11
0	3	37	60	7	12
1	-2	-77	79	13	16
1	-2	-76	0	0	100
1	-2	-75	109	15	14
1	-2	-74	0	0	100
1	-2	-73	43	7	18
1	-2	-71	42	6	14
1	-2	-70	0	0	100
1	-2	-69	89	7	8
1	-2	-68	0	0	100
1	-2	-67	0	0	100
1	-2	-66	0	0	100
1	-2	-65	17	6	38
1	-2	-64	0	0	100
1	-2	-63	67	5	7
1	-2	-62	79	5	7
1	-2	-61	13	6	46
1	-2	-22	100	13	13
1	-2	-17	0	0	100
1	-2	-16	0	0	100
1	-2	-15	20	7	34
1	-2	-14	11	8	75
1	-2	-13	32	8	25
1	-2	-12	38	10	25
1	-2	-11	0	0	100
1	-2	-10	87	11	13
1	-2	-9	97	17	18
1	-2	-8	87	21	24
1	-2	-8	0	0	100
1	-2	-7	172	22	13
1	-2	-6	173	22	12
1	-2	-5	230	26	11
1	-2	-4	204	23	11
1	-2	-3	221	24	11
1	-2	-2	193	18	9
1	-2	-1	0	0	100
1	-2	0	182	22	12
1	-2	1	120	17	14
1	-2	2	195	23	12
1	-2	3	183	19	10
1	-2	4	132	22	16
1	-2	5	67	21	32
1	-2	6	137	17	12
1	-2	7	196	20	10
1	-2	8	83	18	22
1	-2	9	0	0	100
1	-2	10	45	12	26
1	-2	11	91	13	15
1	-2	12	0	0	100
1	-2	13	33	12	36
1	-2	14	62	10	16
1	-2	15	0	0	100
1	-2	16	0	0	100
1	-1	-80	45	6	13
1	-1	-79	34	6	16
1	-1	-78	0	0	100
1	-1	-77	51	7	13
1	-1	-75	13	6	42
1	-1	-74	18	6	32
1	-1	-73	12	4	38
1	-1	-71	0	0	100
1	-1	-70	0	0	100
1	-1	-69	11	4	38
1	-1	-68	0	0	100
1	-1	-67	33	4	13
1	-1	-66	0	0	100
1	-1	-65	38	4	11
1	-1	-64	0	0	100
1	-1	-63	63	4	7
1	-1	-62	32	4	12
1	-1	-61	19	4	24
1	-1	-60	8	3	44
1	-1	-59	50	4	8
1	-1	-58	27	5	20
1	-1	-57	74	6	8
1	-1	-56	55	5	10
1	-1	-55	47	5	11
1	-1	-55	51	4	8
1	-1	-54	0	0	100
1	-1	-53	26	4	15
1	-1	-52	55	5	10
1	-1	-51	33	5	14
1	-1	-50	8	5	62
1	-1	-49	38	4	11
1	-1	-48	33	4	12
1	-1	-47	19	4	20
1	-1	-46	25	6	25
1	-1	-45	26	5	18
1	-1	-44	0	0	100
1	-1	-43	20	4	21
1	-1	-41	0	0	100
1	-1	-40	19	4	23
1	-1	-39	42	6	15
1	-1	-38	0	0	100
1	-1	-37	28	4	15
1	-1	-36	12	4	35
1	-1	-35	25	5	19
1	-1	-34	49	5	10
1	-1	-33	54	5	9
1	-1	-31	0	0	100
1	-1	-30	47	5	10
1	-1	-27	39	4	11
1	-1	-26	30	4	14
1	-1	-25	0	0	100
1	-1	-24	0	0	100
1	-1	-23	0	0	100
1	-1	-22	20	5	26
1	-1	-21	47	7	14
1	-1	-19	28	5	18
1	-1	-18	0	0	100
1	-1	-17	40	5	13
1	-1	-16	33	4	13
1	-1	-15	0	0	100
1	-1	-14	27	9	32
1	-1	-13	0	0	100
1	-1	-12	0	0	100
1	-1	-11	30	7	22
1	-1	-10	0	0	100
1	-1	-9	0	0	100
1	-1	-8	0	0	100
1	-1	-7	51	11	21
1	-1	-6	77	12	15
1	-1	-5	0	0	100
1	-1	-4	73	14	20
1	-1	-2	56	14	25
1	-1	1	49	10	21
1	-1	2	39	13	35
1	-1	3	61	15	24
1	-1	4	0	0	100
1	-1	5	0	0	100
1	-1	6	40	11	27
1	-1	7	0	0	100
1	-1	8	52	10	20
1	-1	8	0	0	100
1	-1	9	31	12	40
1	-1	10	0	0	100
1	-1	11	9	7	81
1	-1	12	13	5	43
1	-1	13	41	7	17
1	-1	14	4	5	116
1	-1	15	28	6	23
1	-1	16	0	0	100
1	-1	17	24	6	25
1	-1	18	16	6	36
1	-1	20	57	20	36
1	-1	21	59	5	8
1	-1	22	19	5	29
1	-1	23	38	6	15
1	-1	25	0	0	100
1	-1	26	52	7	13
1	-1	28	9	6	66
1	-1	29	0	0	100
1	-1	30	25	6	23
1	-1	31	0	0	100
1	-1	32	0	0	100
1	-1	33	12	4	38
1	-1	34	0	0	100
1	-1	34	0	0	100
1	-1	35	0	0	100
1	-1	36	0	0	100
1	-1	37	17	6	37
1	-1	38	0	0	100
1	-1	39	0	0	100
1	-1	40	0	0	100
1	-1	41	0	0	100
1	-1	43	52	5	10
1	-1	44	0	0	100
1	-1	45	13	5	43
1	-1	46	0	0	100
1	-1	47	0	0	100
1	-1	48	24	4	17
1	-1	49	28	5	19
1	-1	50	0	0	100
1	-1	51	29	5	18
1	-1	52	62	5	7
1	-1	53	33	5	14
1	-1	54	37	5	12
1	-1	55	66	6	9
1	-1	56	0	0	100
1	-1	57	0	0	100
1	-1	58	0	0	100
1	-1	59	14	5	38
1	-1	60	0	0	100
1	-1	61	60	6	10
1	-1	62	0	0	100
1	-1	63	0	0	100
1	-1	64	39	5	12
1	-1	65	19	5	28
1	-1	66	44	5	10
1	-1	67	0	0	100
1	-1	68	45	5	12
1	-1	69	32	5	17
1	-1	70	25	5	21
1	1	-80	0	0	100
1	1	-79	44	7	16
1	1	-78	25	5	20
1	1	-77	12	6	49
1	1	-76	63	6	9
1	1	-74	0	0	100
1	1	-73	0	0	100
1	1	-72	54	5	10
1	1	-71	71	6	8
1	1	-70	47	7	16
1	1	-69	0	0	100
1	1	-68	44	5	12
1	1	-67	48	5	10
1	1	-66	8	5	62
1	1	-65	0	0	100
1	1	-65	0	0	100
1	1	-64	13	5	38
1	1	-63	0	0	100
1	1	-62	0	0	100
1	1	-61	12	3	27
1	1	-60	0	0	100
1	1	-59	0	0	100
1	1	-57	0	0	100
1	1	-56	0	0	100
1	1	-55	32	6	18
1	1	-54	24	6	24
1	1	-53	30	5	16
1	1	-52	31	4	14
1	1	-51	48	4	9
1	1	-50	0	0	100
1	1	-50	35	5	15

1	1	-49	0	0	100
1	1	-48	5	6	121
1	1	-47	0	0	100
1	1	-46	0	0	100
1	1	-45	50	5	11
1	1	-44	64	6	10
1	1	-43	0	0	100
1	1	-42	39	6	15
1	1	-41	32	6	18
1	1	-39	56	7	12
1	1	-38	26	5	19
1	1	-37	50	5	10
1	1	-36	0	0	100
1	1	-35	27	5	19
1	1	-34	0	0	100
1	1	-33	16	4	26
1	1	-32	38	6	15
1	1	-31	0	0	100
1	1	-30	44	6	13
1	1	-29	0	0	100
1	1	-28	0	0	100
1	1	-27	22	7	30
1	1	-26	22	5	21
1	1	-25	33	6	19
1	1	-24	23	5	20
1	1	-23	21	6	27
1	1	-22	28	5	18
1	1	-21	21	6	28
1	1	-20	65	5	8
1	1	-19	0	0	100
1	1	-18	35	5	16
1	1	-17	0	0	100
1	1	-14	36	6	17
1	1	-13	21	12	59
1	1	-12	34	0	0
1	1	-11	0	0	100
1	1	-10	77	14	18
1	1	-9	69	12	18
1	1	-6	0	0	100
1	1	14	11	7	59
1	1	15	59	7	11
1	1	20	41	6	14
1	1	21	0	0	100
1	1	22	17	7	41
1	1	23	46	5	11
1	1	24	35	4	12
1	1	25	0	0	100
1	1	26	25	5	19
1	1	27	25	5	20
1	1	28	0	0	100
1	1	29	0	0	100
1	1	30	37	6	17
1	1	33	50	6	12
1	1	34	0	0	100
1	1	35	0	0	100
1	1	36	54	6	11
1	1	37	46	5	12
1	1	38	27	6	20
1	1	39	0	0	100
1	1	40	0	0	100
1	1	41	39	5	14
1	1	42	0	0	100
1	1	43	46	6	12
1	1	44	0	0	100
1	1	45	33	6	18
1	1	46	27	7	25
1	1	47	60	5	8
1	1	48	51	5	10
1	1	49	15	6	41
1	1	50	47	6	13
1	1	51	11	6	53
1	1	52	32	7	20
1	1	53	66	7	11
1	1	54	0	0	100
1	1	55	27	4	16
1	1	56	0	0	100
1	1	57	11	5	46
1	1	58	17	5	29
1	1	59	0	0	100
1	1	60	31	6	19
1	1	61	41	6	14
1	1	62	0	0	100
1	1	63	68	6	8
1	1	64	0	0	100
1	1	65	43	5	11
1	1	67	0	0	100
1	1	68	0	0	100

1	2	-71	64	14	22
1	2	-70	86	7	8
1	2	-69	23	8	37
1	2	-68	48	7	14
1	2	-67	76	8	10
1	2	-66	39	8	21
1	2	-65	0	0	100
1	2	-64	20	6	29
1	2	-63	77	6	7
1	2	-62	57	5	10
1	2	-61	0	0	100
1	2	-60	0	0	100
1	2	-59	63	6	10
1	2	-57	40	7	17
1	2	-56	0	0	100
1	2	-55	0	0	100
1	2	-54	79	9	11
1	2	-54	0	0	100
1	2	-53	0	0	100
1	2	-52	44	5	12
1	2	-51	51	6	12
1	2	-50	0	0	100
1	2	-49	0	0	100
1	2	-48	34	6	17
1	2	-46	0	0	100
1	2	-45	113	9	8
1	2	-44	0	0	100
1	2	-43	16	7	42
1	2	-42	0	0	100
1	2	-41	38	7	18
1	2	-40	0	0	100
1	2	-39	32	6	19
1	2	-38	65	6	10
1	2	-37	0	0	100
1	2	-36	120	7	6
1	2	-36	100	7	7
1	2	-35	67	6	10
1	2	-34	67	6	8
1	2	-33	0	0	100
1	2	-32	41	6	16
1	2	-31	83	7	8
1	2	-31	77	7	9
1	2	-30	58	6	11
1	2	-28	0	0	100
1	2	-28	51	7	13
1	2	-27	0	0	100
1	2	-25	66	9	13
1	2	-24	75	7	9
1	2	-23	88	7	8
1	2	-22	0	0	100
1	2	-21	65	8	12
1	2	-20	82	7	9
1	2	-19	55	7	13
1	2	-18	0	0	100
1	2	-17	0	0	100
1	2	-16	0	0	100
1	2	-15	0	0	100
1	2	-14	26	9	35
1	2	-13	30	9	29
1	2	-12	0	0	100
1	2	-11	30	11	38
1	2	-10	0	0	100
1	2	-9	0	0	100
1	2	-8	8	17	217
1	2	-7	69	19	27
1	2	-6	72	18	24
1	2	-5	0	0	100
1	2	-4	74	19	26
1	2	-3	0	0	100
1	2	-2	95	16	17
1	2	-1	0	0	100
1	2	0	0	0	100
1	2	1	8	16	199
1	2	2	0	0	100
1	2	3	61	16	26
1	2	4	0	0	100
1	2	5	0	0	100
1	2	6	0	0	100
1	2	7	0	0	100
1	2	8	0	0	100
1	2	9	86	10	12
1	2	10	50	16	32
1	2	11	28	11	39
1	2	12	0	0	100
1	2	13	105	14	14
1	2	14	0	0	100
1	2	15	0	0	100

1	2	16	44	8	18
1	2	17	93	9	10
1	2	19	18	8	42
1	2	20	0	0	100
1	2	21	0	0	100
1	2	22	0	0	100
1	2	23	65	7	10
1	2	24	0	0	100
1	2	25	0	0	100
1	2	26	0	0	100
1	2	27	48	7	15
1	2	28	0	0	100
1	2	29	47	8	17
1	2	30	0	0	100
1	2	31	95	8	8
1	2	32	91	9	9
1	2	33	0	0	100
1	2	34	33	8	25
1	2	35	77	9	12
1	2	36	0	0	100
1	2	37	47	7	15
1	2	38	82	8	10
1	2	39	101	8	8
1	2	40	0	0	100
1	2	41	95	7	8
1	2	42	84	9	10
1	2	43	32	9	27
1	2	44	0	0	100
1	2	45	88	9	10
1	2	46	0	0	100
1	2	47	0	0	100
1	2	48	15	9	57
1	2	49	0	0	100
1	2	50	77	8	11
1	2	51	0	0	100
1	2	52	0	0	100
1	2	53	0	0	100
1	2	54	0	0	100
1	2	55	64	8	13
2	-3	-52	52	8	15
2	-3	-51	69	9	13
2	-3	-50	94	10	11
2	-3	-49	0	0	100
2	-3	-48	0	0	100
2	-3	-47	0	0	100
2	-3	-46	46	10	21
2	-3	-42	39	6	15
2	-3	-41	17	9	54
2	-3	-40	34	7	20
2	-3	-39	0	0	100
2	-3	-38	0	0	100
2	-3	-37	72	8	11
2	-3	-36	45	8	18
2	-2	-54	54	8	15
2	-2	-53	41	10	25
2	-2	-52	0	0	100
2	-2	-51	54	11	21
2	-2	-50	0	0	100
2	-2	-49	0	0	100
2	-2	-48	66	11	17
2	-2	-47	55	13	23
2	-2	-46	82	12	14
2	-2	-44	90	11	12
2	-2	-43	105	11	11
2	-2	-42	0	0	100
2	-2	-20	42	2	17
2	-2	-19	0	0	100
2	-2	-18	0	0	100
2	-2	-17	0	0	100
2	-2	-16	28	8	29
2	-2	-15	46	7	16
2	-2	-14	67	11	16
2	-2	-13	0	0	100
2	-2	-12	80	18	22
2	-2	-11	55	18	33
2	-2	-10	0	0	100
2	-2	-9	0	0	100
2	-2	-8	0	0	100
2	-2	-7	92	20	21
2	-2	-6	73	19	26
2	-2	-5	66	28	42
2	-2	-4	45	28	61
2	-2	-3	90	37	41
2	-2	-2	267	34	13
2	-2	-1	354	43	12
2	-2	0	201	40	20
2	-2	1	110	36	33

2	-2	2	126	31	25
2	-2	3	164	26	16
2	-2	4	24	20	83
2	-2	5	63	21	34
2	-2	6	92	21	22
2	-2	7	0	0	100
2	-2	8	0	0	100
2	-2	9	0	0	100
2	-2	10	53	13	26
2	-2	11	0	0	100
2	-2	12	28	10	34
2	-2	13	60	11	18
2	-2	14	75	11	15
2	-2	15	0	0	100
2	-2	16	0	0	100
2	-2	17	0	0	100
2	-2	18	0	0	100
2	-2	19	0	0	100
2	-2	20	0	0	100
2	-2	21	71	6	9
2	-2	22	70	6	9
2	-2	23	92	6	7
2	-2	24	65	7	10
2	-2	25	0	0	100
2	-2	26	0	0	100
2	-2	27	0	0	100
2	-2	28	32	9	28
2	-2	29	41	11	26
2	-2	30	60	8	13
2	-2	31	57	9	17
2	-2	32	66	9	13
2	-2	33	27	8	31
2	-2	34	0	0	100
2	-2	38	115	13	12
2	-2	39	112	20	17
2	-2	40	96	17	18
2	-2	41	0	0	100
2	-1	-80	32	5	17
2	-1	-79	57	8	13
2	-1	-78	0	0	100
2	-1	-77	53	7	13
2	-1	-76	118	7	6
2	-1	-75	102	8	8
2	-1	-74	80	7	9
2	-1	-71	51	6	12
2	-1	-70	108	8	7
2	-1	-69	24	6	26
2	-1	-68	52	5	10
2	-1	-67	22	5	22
2	-1	-66	25	5	18
2	-1	-65	133	5	4
2	-1	-64	14	4	30
2	-1	-63	54	5	9
2	-1	-62	37	5	14
2	-1	-61	28	5	17
2	-1	-60	45	5	12
2	-1	-59	65	6	9
2	-1	-58	0	0	100
2	-1	-57	27	5	20
2	-1	-56	44	6	13
2	-1	-55	0	0	100
2	-1	-54	42	5	12
2	-1	-53	0	0	100
2	-1	-52	37	5	13
2	-1	-51	41	6	14
2	-1	-50	33	6	18
2	-1	-49	39	6	15
2	-1	-48	18	6	34
2	-1	-47	82	5	6
2	-1	-46	45	5	11
2	-1	-45	0	0	100
2	-1	-44	42	6	15
2	-1	-43	0	0	100
2	-1	-42	31	7	22
2	-1	-41	0	0	100
2	-1	-26	35	5	14
2	-1	-24	0	0	100
2	-1	-23	38	8	20
2	-1	-22	0	0	100
2	-1	-21	0	0	100
2	-1	-21	0	0	100
2	-1	-20	0	0	100
2	-1	-19	0	0	100
2	-1	-18	51	5	10
2	-1	-17	52	5	11
2	-1	-16	46	6	13
2	-1	-15	42	5	13
2	-1	-14	0	0	100
2	-1	-13	19	10	51
2	-1	-12	53	10	19
2	-1	-11	64	9	14
2	-1	-10	122	15	12
2	-1	-9	172	16	9
2	-1	-8	86	14	16
2	-1	-6	0	0	100
2	-1	-2	53	18	35
2	-1	-1	0	0	100
2	-1	1	47	15	32
2	-1	3	0	0	100
2	-1	4	68	17	25
2	-1	5	47	19	40
2	-1	8	57	11	20
2	-1	10	40	10	25
2	-1	11	40	8	20
2	-1	12	21	9	40
2	-1	13	0	0	100
2	-1	15	62	7	11
2	-1	16	0	0	100
2	-1	16	54	8	15
2	-1	17	0	0	100
2	-1	18	79	7	9
2	-1	19	0	0	100
2	-1	20	0	0	100
2	-1	21	0	0	100
2	-1	22	0	0	100
2	-1	23	10	6	57
2	-1	24	70	6	8
2	-1	25	0	0	100
2	-1	26	52	7	13
2	-1	27	15	5	32
2	-1	28	57	6	11
2	-1	29	57	7	12
2	-1	30	0	0	100
2	-1	32	63	6	10
2	-1	33	103	7	7
2	-1	34	0	0	100
2	-1	35	0	0	100
2	-1	36	45	6	13
2	-1	37	0	0	100
2	-1	38	0	0	100
2	-1	39	0	0	100
2	-1	40	0	0	100
2	-1	41	0	0	100
2	-1	42	53	6	11
2	-1	43	25	6	25
2	-1	44	63	6	9
2	-1	45	26	5	19
2	-1	46	51	6	19
2	-1	47	20	6	28
2	-1	48	35	6	16
2	-1	50	0	0	100
2	-1	51	0	0	100
2	-1	52	49	5	11
2	-1	53	0	0	100
2	-1	54	0	0	100
2	-1	55	27	5	18
2	-1	56	26	5	19
2	-1	57	13	5	41
2	-1	58	0	0	100
2	-1	59	0	0	100
2	-1	60	46	5	12
2	-1	61	0	0	100
2	-1	62	48	6	12
2	-1	63	30	6	21
2	-1	64	54	7	13
2	-1	65	128	10	8
2	-1	66	21	8	38
2	0	-80	0	0	100
2	0	-79	20	5	25
2	0	-78	18	6	33
2	0	-77	0	0	100
2	0	-76	25	5	21
2	0	-75	16	6	35
2	0	-74	29	6	21
2	0	-73	50	6	11
2	0	-72	73	5	7
2	0	-71	46	6	13
2	0	-70	38	7	19
2	0	-69	10	5	46
2	0	-68	12	4	32
2	0	-67	26	5	20
2	0	-66	11	4	36
2	0	-65	28	4	16
2	0	-64	19	4	22
2	0	-63	0	0	100
2	0	-62	17	5	31
2	0	-61	23	5	22
2	0	-60	0	0	100
2	0	-59	0	0	100
2	0	-58	0	0	100
2	0	-57	59	5	9
2	0	-56	35	6	16
2	0	-55	57	7	11
2	0	-54	0	0	100
2	0	-53	28	5	18
2	0	-53	52	5	9
2	0	-52	49	5	11
2	0	-51	0	0	100
2	0	-51	0	0	100
2	0	-50	87	5	6
2	0	-49	73	6	8
2	0	-48	0	0	100
2	0	-47	65	5	8
2	0	-46	58	5	9
2	0	-44	0	0	100
2	0	-43	85	6	7
2	0	-42	35	6	16
2	0	-40	0	0	100
2	0	-38	17	5	29
2	0	-37	27	5	17
2	0	-36	0	0	100
2	0	-35	0	0	100
2	0	-34	21	5	24
2	0	-33	0	0	100
2	0	-32	35	4	11
2	0	-31	27	5	19
2	0	-30	20	4	20
2	0	-29	29	5	16
2	0	-27	0	0	100
2	0	-26	19	5	26
2	0	-25	0	0	100
2	0	-24	39	5	14
2	0	-23	43	7	16
2	0	-21	13	5	40
2	0	-20	0	0	100
2	0	-14	0	0	100
2	0	-13	0	0	100
2	0	-11	0	0	100
2	0	-10	58	15	26
2	0	-2	43	14	31
2	0	20	13	5	38
2	0	34	0	0	100
2	0	37	63	6	9
2	0	39	20	6	30
2	0	40	44	6	13
2	0	41	18	5	28
2	0	42	79	5	6
2	0	43	70	6	8
2	0	44	30	6	21
2	0	45	0	0	100
2	0	46	48	6	12
2	0	47	0	0	100
2	0	48	56	6	11
2	0	49	42	6	15
2	0	50	33	6	18
2	0	51	59	6	11
2	0	52	0	0	100
2	0	53	13	5	38
2	0	54	0	0	100
2	0	55	50	6	11
2	0	56	18	6	32
2	0	57	0	0	100
2	0	58	40	6	14
2	0	59	33	5	15
2	0	60	44	5	12
2	0	61	41	5	12
2	0	62	42	6	13
2	0	63	50	6	13
2	0	65	43	6	13
2	0	66	90	8	8
2	0	67	41	8	19
2	1	-79	0	0	100
2	1	-78	101	8	8
2	1	-77	34	7	20
2	1	-76	21	6	30
2	1	-75	34	7	21
2	1	-74	26	6	24
2	1	-73	103	7	7
2	1	-72	45	7	15
2	1	-71	20	7	33
2	1	-70	45	6	14

2	1	-69	37	7	18
2	1	-68	57	5	9
2	1	-67	0	0	100
2	1	-66	0	0	100
2	1	-65	7	5	70
2	1	-64	35	6	18
2	1	-63	68	6	9
2	1	-62	98	6	6
2	1	-61	89	5	9
2	1	-60	62	5	8
2	1	-59	82	6	7
2	1	-58	49	6	12
2	1	-57	49	5	11
2	1	-56	0	0	100
2	1	-55	38	5	13
2	1	-54	59	5	9
2	1	-53	0	0	100
2	1	-52	0	0	100
2	1	-51	0	0	100
2	1	-50	70	7	10
2	1	-49	0	0	100
2	1	-48	65	6	10
2	1	-47	0	0	100
2	1	-45	0	0	100
2	1	-44	0	0	100
2	1	-43	0	0	100
2	1	-42	101	6	6
2	1	-41	0	0	100
2	1	-40	0	0	100
2	1	-39	52	6	12
2	1	-38	0	0	100
2	1	-37	0	0	100
2	1	-36	74	7	9
2	1	-35	65	7	11
2	1	-34	33	5	15
2	1	-33	0	0	100
2	1	-32	99	7	7
2	1	-31	58	7	13
2	1	-30	91	7	7
2	1	-29	90	7	8
2	1	-29	90	7	8
2	1	-28	80	7	9
2	1	-27	0	0	100
2	1	-26	70	7	10
2	1	-21	53	6	11
2	1	-20	0	0	100
2	1	-18	48	7	14
2	1	-17	57	8	14
2	1	-17	0	0	100
2	1	-16	0	0	100
2	1	-15	0	0	100
2	1	-14	63	9	15
2	1	-13	0	0	100
2	1	-12	0	0	100
2	1	-11	42	16	40
2	1	-10	40	19	47
2	1	-9	35	23	65
2	1	-8	80	21	26
2	1	-5	0	0	100
2	1	-2	35	19	54
2	1	-1	165	22	13
2	1	0	0	0	100
2	1	1	90	22	25
2	1	2	0	0	100
2	1	3	120	23	20
2	1	4	16	28	181
2	1	5	98	27	27
2	1	7	76	22	28
2	1	8	76	22	29
2	1	10	0	0	100
2	1	12	42	10	24
2	1	13	11	8	72
2	1	14	45	7	17
2	1	16	121	11	9
2	1	17	0	0	100
2	1	18	91	8	9
2	2	-56	21	6	31
2	2	-55	0	0	100
2	2	-54	0	0	100
2	2	-53	43	6	14
2	2	-52	64	6	9
2	2	-51	0	0	100
2	2	-50	0	0	100
2	2	-49	69	7	10
2	2	-48	0	0	100
2	2	17	0	0	100
2	2	18	76	13	17
2	2	19	69	14	20
2	2	20	0	0	100
2	2	21	100	12	12
2	2	22	108	13	12
2	2	23	0	0	100
2	2	24	0	0	100
2	2	25	0	0	100
2	2	26	41	14	34
2	2	27	0	0	100
2	2	28	0	0	100
2	2	29	65	6	9
2	2	30	57	9	15
2	2	32	0	0	100
2	2	33	26	8	31
2	2	35	85	7	8
2	2	36	0	0	100
2	2	37	49	6	13
2	2	38	0	0	100
2	2	39	46	7	15
2	2	40	21	6	30
2	2	41	0	0	100
2	2	42	49	8	16
2	2	43	40	7	16
2	2	44	0	0	100
2	2	45	19	8	44
3	-3	-45	33	8	25
3	-3	-44	70	11	16
3	-3	-43	66	10	15
3	-3	-42	0	0	100
3	-3	-41	64	9	14
3	-3	-40	0	0	100
3	-3	-39	0	0	100
3	-3	-38	0	0	100
3	-3	-37	0	0	100
3	-3	-36	0	0	100
3	-3	-35	0	0	100
3	-3	-34	0	0	100
3	-3	-33	84	8	10
3	-3	-32	40	8	19
3	-3	-31	0	0	100
3	-3	-30	62	8	13
3	-3	-29	0	0	100
3	-3	-28	36	7	19
3	-3	-27	46	7	15
3	-3	-26	0	0	100
3	-3	-25	71	7	10
3	-3	-24	0	0	100
3	-3	-23	0	0	100
3	-2	-62	0	0	100
3	-2	-61	66	8	12
3	-2	-60	0	0	100
3	-2	-59	0	0	100
3	-2	-58	22	8	35
3	-2	-57	77	7	10
3	-2	-56	19	9	48
3	-2	-55	0	0	100
3	-2	-54	0	0	100
3	-2	-53	30	6	19
3	-2	-52	37	5	15
3	-2	-51	26	5	21
3	-2	-50	0	0	100
3	-2	-49	41	5	13
3	-2	-48	52	6	11
3	-2	-47	0	0	100
3	-2	-46	0	0	100
3	-2	-45	70	9	13
3	-2	-44	0	0	100
3	-2	-43	74	7	10
3	-2	-42	0	0	100
3	-2	-41	71	7	10
3	-2	-40	50	7	14
3	-2	-39	0	0	100
3	-2	-38	0	0	100
3	-2	-37	56	8	14
3	-2	-36	0	0	100
3	-2	-35	51	7	14
3	-2	-32	0	0	100
3	-2	-31	92	7	8
3	-2	-30	0	0	100
3	-2	-29	86	7	8
3	-2	-28	0	0	100
3	-2	-27	29	6	22
3	-2	-26	65	8	12
3	-2	-25	59	7	12
3	-2	-24	47	7	15
3	-2	-23	57	9	16
3	-2	-22	50	5	11
3	-2	-21	0	0	100
3	-2	-20	36	7	20
3	-2	-19	0	0	100
3	-2	-18	21	8	37
3	-2	-17	42	6	14
3	-2	-16	0	0	100
3	-2	-15	42	9	22
3	-2	-14	0	0	100
3	-2	-13	0	0	100
3	-2	-12	56	8	15
3	-2	-11	46	9	20
3	-2	-10	0	0	100
3	-2	-9	28	11	38
3	-2	-8	0	0	100
3	-2	-7	0	0	100
3	-2	-6	0	0	100
3	-2	-5	149	21	14
3	-2	-4	67	17	25
3	-2	-3	62	19	30
3	-2	-2	45	19	43
3	-2	-1	121	18	14
3	-2	0	0	0	100
3	-2	3	78	13	16
3	-2	4	0	0	100
3	-2	5	0	0	100
3	-2	6	0	0	100
3	-2	7	0	0	100
3	-2	8	0	0	100
3	-2	9	53	10	20
3	-2	10	0	0	100
3	-2	11	65	11	18
3	-2	21	56	12	21
3	-2	22	0	0	100
3	-2	23	0	0	100
3	-2	24	53	13	24
3	-2	25	34	12	37
3	-2	26	20	8	43
3	-2	27	0	0	100
3	-2	28	55	8	14
3	-2	29	28	9	31
3	-2	30	16	5	33
3	-2	31	0	0	100
3	-2	32	29	8	27
3	-2	33	0	0	100
3	-2	34	85	7	8
3	-2	35	42	6	14
3	-2	36	8	7	84
3	-2	37	0	0	100
3	-2	38	46	6	14
3	-2	39	63	7	11
3	-2	40	44	7	15
3	-2	41	50	7	13
3	-2	43	11	7	67
3	-2	44	0	0	100
3	-2	45	19	7	37
3	-2	47	56	7	12
3	-2	48	25	9	34
3	-2	49	44	8	17
3	-2	50	0	0	100
3	-1	-27	0	0	100
3	-1	-26	0	0	100
3	-1	-24	0	0	100
3	-1	17	0	0	100
3	-1	18	63	7	11
3	-1	19	0	0	100
3	-1	20	0	0	100
3	-1	21	68	8	12
3	-1	23	17	8	45
3	-1	24	0	0	100
3	-1	25	53	16	31
3	-1	26	0	0	100
3	-1	27	84	12	14
3	-1	30	84	15	18
3	-1	41	95	17	18
3	-1	42	57	15	23
3	-1	43	37	9	23
3	-1	44	60	8	14
3	-1	45	0	0	100
3	-1	46	52	8	16
3	-1	47	71	9	12
3	-1	48	0	0	100
3	-1	49	22	7	33
3	-1	50	0	0	100
3	-1	51	0	0	100
3	-1	52	0	0	100
3	-1	53	60	10	16
3	-1	54	0	0	100

3	-1	55	33	8	24
3	-1	56	0	0	100
3	-1	57	83	9	10
3	-1	58	51	9	18
3	0	-74	75	7	10
3	0	-73	21	6	30
3	0	-72	67	7	10
3	0	-71	32	6	20
3	0	-27	76	15	20
3	0	-2	59	21	36
3	0	-1	91	22	24
3	0	0	0	0	100
3	0	3	0	0	100
3	0	5	9	25	291
3	0	6	0	0	100
3	0	9	159	18	11
3	0	13	73	8	11
3	0	14	41	12	30
3	0	16	91	9	10
3	0	32	148	15	10
3	0	33	33	15	46
3	0	39	119	15	13
3	0	40	0	0	100
3	0	41	110	18	16
3	1	-61	0	0	100
3	1	-60	56	9	16
3	1	-59	31	8	25
3	1	-58	0	0	100
3	1	-57	0	0	100
3	1	-56	0	0	100
3	1	-55	47	8	16
3	1	-54	4	5	137
3	1	-53	36	5	15
3	1	-52	25	6	23
3	1	-51	26	6	23
3	1	-50	0	0	100
3	1	-49	0	0	100
3	1	-48	0	0	100
3	1	-47	0	0	100
3	1	-44	39	7	18
3	1	-43	0	0	100
3	1	-39	67	7	11
3	1	-36	0	0	100
3	1	-33	0	0	100
3	1	-32	0	0	100
3	1	-31	7	7	108
3	1	-29	81	7	8
3	1	-26	9	7	77
3	1	-14	75	14	19
3	1	-13	100	13	13
3	1	-11	0	0	100
3	1	-7	0	0	100
3	1	-6	0	0	100
3	1	2	33	15	46
3	1	3	0	0	100
3	1	4	37	14	37
3	1	5	118	11	9
3	1	6	123	14	11
3	1	7	77	14	18
3	1	10	66	13	19
3	1	10	66	13	19
3	1	11	73	9	13
3	1	12	0	0	100
3	1	14	63	9	14
3	1	15	48	11	23
3	1	16	37	7	19
3	1	17	127	7	6
3	1	18	72	8	11
3	1	19	0	0	100
3	1	20	92	8	9
3	1	21	33	7	21
3	1	23	104	13	12
3	1	24	0	0	100
3	1	24	54	9	16
3	1	25	80	8	10
3	1	27	76	8	10
3	1	28	0	0	100
3	1	29	71	11	16
3	1	39	0	0	100
3	1	41	74	9	12
3	1	42	0	0	100
3	1	43	0	0	100
3	1	45	41	8	20
3	1	46	26	7	27
3	1	47	54	7	12
3	1	48	0	0	100
3	2	-43	40	10	24
3	2	-42	40	10	24
3	2	-41	66	9	14
4	-2	-55	47	7	15
4	-2	-54	0	0	100
4	-2	-52	57	7	13
4	-2	-51	0	0	100
4	-2	-50	70	7	9
4	-2	-49	0	0	100
4	-2	-48	75	9	12
4	-2	-47	0	0	100
4	-2	-46	0	0	100
4	-2	-45	0	0	100
4	-2	-44	0	0	100
4	-2	-43	78	7	9
4	-2	-42	20	7	37
4	-2	-41	41	6	16
4	-2	-40	0	0	100
4	-2	-39	53	8	14
4	-2	-38	11	8	71
4	-2	-37	0	0	100
4	-2	-36	70	8	11
4	-2	-35	0	0	100
4	-2	-35	0	0	100
4	-2	-34	66	8	12
4	-2	-33	52	7	14
4	-2	-32	0	0	100
4	-2	-31	15	8	52
4	-2	-30	0	0	100
4	-2	-28	21	7	33
4	-2	-27	23	7	29
4	-2	-26	52	8	15
4	-2	-25	33	8	24
4	-2	-24	55	7	13
4	-2	-23	49	7	14
4	-2	-22	87	9	10
4	-2	-21	32	7	22
4	-2	-20	0	0	100
4	-2	-19	71	8	11
4	-2	-57	37	6	15
4	-1	-56	0	0	100
4	-1	-55	88	7	7
4	-1	-54	47	5	11
4	-1	-53	0	0	100
4	-1	-52	0	0	100
4	-1	-51	0	0	100
4	-1	-50	0	0	100
4	-1	-49	70	7	10
4	-1	-48	0	0	100
4	-1	-29	55	6	12
4	-1	-28	0	0	100
4	-1	-27	33	7	22
4	-1	-26	13	7	50
4	-1	-25	0	0	100
4	-1	-24	25	7	29
4	-1	-23	53	7	14
4	-1	-21	60	9	15
4	-1	-20	0	0	100
4	-1	-19	0	0	100
4	-1	-18	29	9	31
4	-1	-17	0	0	100
4	-1	-16	80	10	12
4	-1	-15	72	7	10
4	-1	-13	59	11	19
4	-1	-12	63	11	18
4	-1	-11	0	0	100
4	-1	-10	0	0	100
4	-1	-9	0	0	100
4	-1	-8	0	0	100
4	-1	-7	87	11	13
4	-1	-6	105	12	12
4	-1	-5	81	15	18
4	-1	-3	39	12	30
4	-1	1	0	0	100
4	-1	2	94	12	13
4	-1	3	0	0	100
4	-1	4	0	0	100
4	-1	6	0	0	100
4	-1	7	0	0	100
4	-1	8	0	0	100
4	-1	9	44	9	20
4	-1	10	104	8	8
4	-1	11	0	0	100
4	-1	12	67	9	13
4	-1	12	83	10	12
4	-1	13	0	0	100
4	-1	14	0	0	100
4	-1	15	79	13	17
4	-1	16	43	15	35
4	-1	31	40	7	17
4	-1	32	17	6	39
4	-1	33	23	6	27
4	-1	34	72	7	9
4	-1	35	16	6	42
4	-1	37	0	0	100
4	-1	39	0	0	100
4	-1	40	21	8	40
4	-1	41	82	9	10
4	-1	42	0	0	100
4	-1	44	72	7	10
4	-1	45	69	8	12
4	0	-52	0	0	100
4	0	-50	0	0	100
4	0	-50	80	8	10
4	0	-49	56	8	14
4	0	17	74	15	20
4	0	21	64	9	14
4	0	25	0	0	100
4	0	28	31	7	23
4	0	30	82	7	9
4	0	31	93	6	7
4	0	32	62	7	11
4	0	35	0	0	100
4	0	36	66	7	11
4	0	39	0	0	100
4	0	40	97	8	8
4	0	41	0	0	100
4	1	-47	33	8	23
4	1	-46	46	9	19
4	1	-45	50	9	19
4	1	-44	0	0	100
4	1	-43	46	8	17
4	1	-42	50	8	17
4	1	-41	25	5	21
4	1	-40	66	8	13
4	1	-39	0	0	100
4	1	-39	0	0	100
4	1	-38	81	8	10
4	1	-37	87	8	10
4	1	-36	56	7	13
4	1	-35	42	7	17
4	1	-34	0	0	100
4	1	-33	0	0	100
4	1	-32	49	7	14
4	1	-31	55	7	13
4	1	-30	50	8	15
4	1	-28	75	8	11
4	1	-27	0	0	100
4	1	-25	0	0	100
4	1	-24	0	0	100
4	1	-23	73	7	10
4	1	11	104	9	9
4	1	12	0	0	100
4	1	13	69	8	12
4	1	14	70	8	11
4	1	15	0	0	100
4	1	16	83	7	8
4	1	17	0	0	100

Iodine Data : Analysis Rfactor v Intensity					
Imax	Rfac	Av_I	σ	I/σ	sd
500.	0.000	0.	0.0	0.0	0.0
1000.	0.000	0.	0.0	0.0	0.0
1500.	0.413	1934.	1349.8	1.4	1320.0
2000.	0.678	3177.	2532.7	1.3	2408.4
2500.	0.000	0.	0.0	0.0	0.0
3000.	0.000	2500.	0.0	0.0	2306.3
3500.	0.000	3364.	0.0	0.0	2632.9
4000.	0.000	0.	0.0	0.0	0.0
4500.	0.000	0.	0.0	0.0	0.0
5000.	0.000	0.	0.0	0.0	0.0
5500.	0.000	0.	0.0	0.0	0.0
6000.	0.145	5731.	837.6	6.8	4195.0
>6000.	0.074	62111.	6509.0	9.5	25757.0
Total	0.096	17858.	3454.9	5.2	8212.1

Iodine Data : Analysis of standard deviation v. Intensity						
Range	Imin	Imax	Irms	No	Mean	Sigma
1	1.	500.	0.	0.	0.00	0.00
2	500.	1000.	0.	0.	0.00	0.00
3	1000.	1500.	2310.	4.	0.15	0.59
4	1500.	2000.	3837.	2.	0.28	0.80
5	2000.	2500.	0.	0.	0.00	0.00
6	2500.	3000.	2500.	2.	0.00	0.00
7	3000.	3500.	3364.	2.	0.00	0.00
8	3500.	4000.	0.	0.	0.00	0.00
9	4000.	4500.	0.	0.	0.00	0.00
10	4500.	5000.	0.	0.	0.00	0.00
11	5000.	5500.	0.	0.	0.00	0.00
12	5500.	6000.	5790.	2.	0.01	0.20
13	6000.	1083681.	82567.	4.	0.00	0.13
Total	1.	1083681.	41399.	16.	0.07	0.43

XIV. APPENDIX E (PEG Data)

h	k	L	F	σ F	σF/ F
-2	-1	-72	30	5	17
-2	-1	-71	10	4	36
-2	-1	-70	15	4	30
-2	-1	-69	0	0	100
-2	-1	-68	0	0	100
-2	-1	-67	13	4	32
-2	-1	-66	11	4	35
-2	-1	-65	21	4	18
-2	-1	-64	11	4	36
-2	-1	-63	0	0	100
-2	-1	-62	0	0	100
-2	-1	-61	14	4	30
-2	-1	-60	7	4	55
-2	-1	6	42	11	26
-2	-1	7	66	14	22
-2	-1	8	53	9	16
-2	-1	9	16	8	51
-2	-1	10	21	7	32
-2	-1	11	0	0	100
-2	-1	12	0	0	100
-2	-1	13	0	0	100
-2	-1	14	21	4	21
-2	-1	15	35	4	12
-2	-1	16	9	3	37
-2	-1	17	22	3	16
-2	-1	18	0	0	100
-2	-1	19	8	3	36
-2	-1	20	0	0	100
-2	-1	21	20	3	15
-2	-1	22	15	3	18
-2	-1	23	18	2	14
-2	-1	24	4	2	59
-2	-1	25	27	2	9
-2	-1	26	37	3	7
-2	-1	27	26	2	10
-2	-1	28	0	0	100
-2	-1	29	33	2	7
-2	-1	30	0	0	100
-2	-1	31	0	0	100
-2	-1	32	29	3	9
-2	-1	33	25	2	10
-2	-1	34	3	2	87
-2	-1	35	0	0	100
-2	-1	36	35	2	6
-2	-1	37	45	3	7
-2	-1	38	19	2	13
-2	-1	39	0	0	100
-2	-1	40	31	3	9
-2	-1	41	5	2	50
-2	-1	42	20	2	11
-2	-1	43	0	0	100
-2	-1	44	22	2	11
-2	-1	45	22	2	11
-2	-1	46	10	2	25
-2	-1	47	22	2	11
-2	-1	48	40	3	7
-2	-1	49	7	3	43
-2	-1	50	19	2	13
-2	-1	51	0	0	100
-2	-1	52	13	2	18
-2	-1	53	0	0	100
-2	-1	54	17	3	17
-2	-1	55	0	0	100
-2	-1	56	0	0	100
-2	-1	57	11	2	23
-2	-1	58	17	2	13
-2	-1	59	34	2	7
-2	-1	60	0	0	100
-2	-1	61	21	2	11
-2	-1	62	24	2	8
-2	-1	63	0	0	100
-2	-1	64	0	0	100
-2	-1	65	29	3	9
-2	-1	66	23	2	11
-2	-1	67	0	0	100
-2	-1	68	18	2	14
-2	-1	69	0	0	100
-2	-1	70	22	2	10
-2	-1	71	23	2	9
-2	-1	72	0	0	100
-2	-1	73	21	3	13
-2	-1	74	14	3	19
-2	-1	75	29	3	10
-2	-1	76	0	0	100
-2	-1	77	0	0	100
-2	-1	78	18	2	14
-2	-1	79	24	2	10
-2	-1	79	24	2	10
-2	-1	80	12	2	19
-2	0	-78	19	3	17
-2	0	-77	9	4	41
-2	0	-76	0	0	100
-2	0	-75	23	3	15
-2	0	-74	29	4	13
-2	0	-73	14	3	25
-2	0	-72	24	4	16
-2	0	-71	19	3	18
-2	0	-70	16	3	22
-2	0	-69	26	4	14
-2	0	-68	20	4	18
-2	0	-67	0	0	100
-2	0	-66	0	0	100
-2	0	-65	20	3	16
-2	0	-64	19	3	15
-2	0	-63	12	2	20
-2	0	-62	17	2	13
-2	0	-61	0	0	100
-2	0	-60	0	0	100
-2	0	-59	0	0	100
-2	0	-58	2	2	100
-2	0	-57	11	2	19
-2	0	-56	0	0	100
-2	0	-55	7	2	27
-2	0	-54	7	2	34
-2	0	-53	0	0	100
-2	0	-52	16	2	13
-2	0	-51	2	2	115
-2	0	-50	0	0	100
-2	0	-49	14	2	14
-2	0	-48	7	2	27
-2	0	-47	0	0	100
-2	0	-46	4	2	51
-2	0	-45	12	2	18
-2	0	-44	16	2	13
-2	0	-43	12	2	16
-2	0	-42	0	0	100
-2	0	-41	19	2	11
-2	0	-40	13	2	17
-2	0	-39	19	2	11
-2	0	-38	0	0	100
-2	0	-37	10	3	32
-2	0	-36	0	0	100
-2	0	-35	0	0	100
-2	0	-34	0	0	100
-2	0	10	31	7	24
-2	0	19	11	3	26
-2	0	19	0	0	100
-2	0	22	7	2	34
-2	0	27	0	0	100
-2	0	28	21	3	13
-2	0	28	0	0	100
-2	0	29	16	3	17
-2	0	30	13	3	20
-2	0	30	8	2	30
-2	0	31	20	3	13
-2	0	32	0	0	100
-2	0	33	9	3	28
-2	0	34	7	3	41
-2	0	35	18	3	15
-2	0	36	7	2	36
-2	0	37	14	3	18
-2	0	38	4	2	68
-2	0	39	0	0	100
-2	0	40	0	0	100
-2	0	41	7	3	42
-2	0	42	12	2	21
-2	0	43	9	2	26
-2	0	44	19	3	15
-2	0	45	7	3	37
-2	0	46	0	0	100
-2	0	47	16	2	15
-2	0	48	0	0	100
-2	0	49	19	3	15
-2	0	50	7	2	33
-2	0	51	0	0	100
-2	0	52	0	0	100
-2	0	53	3	2	77
-2	0	54	0	0	100
-2	0	55	10	3	29
-2	0	56	15	3	19
-2	0	57	6	2	43
-2	0	58	20	2	11
-2	0	59	11	2	23
-2	0	60	0	0	100
-2	0	61	17	3	17
-2	0	62	20	2	12
-2	0	63	0	0	100
-2	0	64	0	0	100
-2	0	65	0	0	100
-2	0	66	4	3	73
-2	0	67	0	0	100
-2	0	68	23	4	16
-2	0	69	6	3	57
-2	0	70	38	4	10
-2	0	71	18	3	19
-2	0	72	15	3	21
-2	0	73	16	3	22
-2	0	74	9	3	38
-2	0	75	7	2	28
-2	0	76	4	2	56
-2	0	77	15	2	14
-2	0	78	7	2	27
-2	0	79	15	2	13
-2	0	80	0	0	100
-2	1	-80	18	3	18
-2	1	-76	16	3	20
-2	1	-75	24	3	14
-2	1	-74	0	0	100
-2	1	-73	0	0	100
-2	1	-71	18	4	22
-2	1	-70	0	0	100
-2	1	-69	32	4	12
-2	1	-68	25	4	15
-2	1	-67	1	3	346
-2	1	-66	24	4	15
-2	1	-65	22	4	16
-2	1	-64	0	0	100
-2	1	-63	0	0	100
-2	1	-62	14	2	14
-2	1	-61	12	2	16
-2	1	-60	0	0	100
-2	1	-59	7	2	30
-2	1	-58	0	0	100
-2	1	-57	17	2	12
-2	1	-56	15	2	13
-2	1	-55	16	2	14
-2	1	-54	12	2	16
-2	1	-53	16	2	12
-2	1	-52	4	2	53
-2	1	-51	0	0	100
-2	1	-50	0	0	100
-2	1	-49	17	2	12
-2	1	-48	13	2	17
-2	1	-47	0	0	100
-2	1	-46	0	0	100
-2	1	-45	6	2	39
-2	1	-44	16	2	13
-2	1	-43	6	2	33
-2	1	-42	16	2	12
-2	1	-41	2	2	89
-2	1	-40	5	2	42
-2	1	-39	0	0	100
-2	1	-38	12	2	18
-2	1	-37	0	0	100
-2	1	-36	0	0	100
-2	1	-35	0	0	100
-2	1	-34	12	2	20
-2	1	-33	0	0	100
-2	1	-32	0	0	100
-2	1	-31	8	2	26

-2	1	-30	0	0	100
-2	1	-29	22	3	12
-2	1	-28	0	0	100
-2	1	-27	11	2	21
-2	1	-26	0	0	100
-2	1	-25	20	2	10
-2	1	-24	14	2	16
-2	1	-23	5	2	49
-2	1	-22	0	0	100
-2	1	-21	0	0	100
-2	1	-20	17	2	14
-2	1	-19	0	0	100
-2	1	-18	6	2	35
-2	1	-17	17	2	13
-2	1	-16	11	2	23
-2	1	-15	17	2	13
-2	1	-14	9	2	28
-2	1	-13	10	2	22
-2	1	-12	0	0	100
-2	1	-11	24	4	15
-2	1	-10	0	0	100
-2	1	-9	0	0	100
-2	1	-8	0	0	100
-2	1	-5	0	0	100
-2	1	-4	49	6	12
-2	1	-3	71	8	11
-2	1	-2	0	0	100
-2	1	-1	78	9	11
-2	1	0	76	7	9
-2	1	1	58	7	11
-2	1	2	71	6	9
-2	1	3	44	5	12
-2	1	4	58	8	14
-2	1	5	0	0	100
-2	1	6	23	5	22
-2	1	6	0	0	100
-2	1	7	0	0	100
-2	1	8	33	6	17
-2	1	9	15	5	31
-2	1	10	15	5	33
-2	1	11	10	4	44
-2	1	12	0	0	100
-2	1	13	24	3	15
-2	1	14	25	3	12
-2	1	15	0	0	100
-2	1	16	4	3	69
-2	1	17	22	3	13
-2	1	18	0	0	100
-2	1	19	10	3	32
-2	1	20	11	3	23
-2	1	21	4	3	73
-2	1	44	12	3	21
-2	1	45	2	2	100
-2	1	46	10	2	24
-2	1	47	13	3	20
-2	1	48	12	3	23
-2	1	49	5	3	53
-2	1	50	0	0	100
-2	1	51	0	0	100
-2	1	52	8	2	24
-2	1	53	0	0	100
-2	1	54	0	0	100
-2	1	55	6	2	33
-2	1	56	0	0	100
-2	1	57	17	2	12
-2	1	58	19	2	11
-2	1	59	5	2	46
-2	1	60	0	0	100
-2	1	61	21	2	11
-2	1	62	0	0	100
-2	1	63	16	2	14
-2	1	64	20	2	10
-2	1	65	16	2	14
-2	1	66	0	0	100
-2	1	67	19	2	13
-2	1	68	35	3	9
-2	1	69	0	0	100
-2	1	70	26	4	15
-2	1	71	20	4	18
-2	1	72	14	4	25
-2	1	73	12	3	28
-2	1	74	0	0	100
-2	1	75	7	4	55
-2	1	76	12	3	24
-2	1	77	0	0	100
-2	1	78	0	0	100
-2	1	79	0	0	100
-2	1	80	0	0	100
-2	2	53	25	4	17
-2	2	54	5	4	85
-2	2	55	12	4	32
-2	2	56	18	4	23
-2	2	57	21	4	18
-2	2	58	22	4	20
-1	-1	-80	0	0	100
-1	-1	-79	7	3	49
-1	-1	-78	21	4	17
-1	-1	-77	13	4	28
-1	-1	-76	20	4	20
-1	-1	-75	9	4	41
-1	-1	-74	14	3	24
-1	-1	-73	0	0	100
-1	-1	-72	15	4	23
-1	-1	-71	0	0	100
-1	-1	-70	19	3	18
-1	-1	-69	0	0	100
-1	-1	-68	29	4	12
-1	-1	-67	0	0	100
-1	-1	-66	23	3	14
-1	-1	-65	0	0	100
-1	-1	-64	0	0	100
-1	-1	-63	0	0	100
-1	-1	-62	22	3	16
-1	-1	-61	7	3	38
-1	-1	-60	10	2	18
-1	-1	-59	0	0	100
-1	-1	-58	11	2	20
-1	-1	-57	3	2	52
-1	-1	-56	9	2	19
-1	-1	-55	12	2	18
-1	-1	-54	11	2	18
-1	-1	-53	7	2	30
-1	-1	-52	10	2	21
-1	-1	-51	0	0	100
-1	-1	-50	0	0	100
-1	-1	-49	11	2	15
-1	-1	-48	18	3	20
-1	-1	-47	20	4	20
-1	-1	-46	0	0	100
-1	-1	-45	18	4	20
-1	-1	-44	2	3	141
-1	-1	-43	15	2	14
-1	-1	-42	0	0	100
-1	-1	-41	16	2	13
-1	-1	-29	13	3	21
-1	-1	21	20	3	13
-1	-1	28	0	0	100
-1	-1	30	13	3	21
-1	-1	31	0	0	100
-1	-1	32	0	0	100
-1	-1	33	16	3	16
-1	-1	34	0	0	100
-1	-1	35	13	2	18
-1	-1	36	0	0	100
-1	-1	37	0	0	100
-1	-1	38	0	0	100
-1	-1	39	0	0	100
-1	-1	40	8	2	32
-1	-1	41	5	2	45
-1	-1	42	0	0	100
-1	-1	43	22	3	13
-1	-1	44	7	3	40
-1	-1	45	20	3	15
-1	-1	46	0	0	100
-1	-1	47	6	2	41
-1	-1	48	12	2	21
-1	-1	49	0	0	100
-1	-1	50	0	0	100
-1	-1	51	14	3	19
-1	-1	52	19	3	15
-1	-1	53	16	3	16
-1	-1	54	6	2	41
-1	-1	55	0	0	100
-1	-1	56	11	2	23
-1	-1	57	0	0	100
-1	-1	58	13	2	17
-1	-1	59	12	2	20
-1	-1	60	19	2	13
-1	-1	61	3	2	87
-1	-1	62	7	2	34
-1	-1	63	16	3	17
-1	-1	64	21	3	13
-1	-1	65	0	0	100
-1	-1	66	8	3	32
-1	-1	67	0	0	100
-1	-1	68	32	3	11
-1	-1	69	30	4	12
-1	-1	70	0	0	100
-1	-1	71	22	4	17
-1	-1	72	18	4	21
-1	-1	73	21	3	17
-1	-1	74	5	3	69
-1	-1	75	0	0	100
-1	-1	76	6	2	35
-1	-1	77	14	2	15
-1	-1	78	11	2	16
-1	-1	79	9	2	22
-1	-1	80	0	0	100
-1	1	-80	12	3	24
-1	1	-79	18	3	19
-1	1	-78	11	3	30
-1	1	-77	0	0	100
-1	1	-76	32	3	10
-1	1	-75	0	0	100
-1	1	-74	24	2	8
-1	1	-73	0	0	100
-1	1	-72	16	2	13
-1	1	-71	11	3	27
-1	1	-70	15	3	22
-1	1	-69	14	3	25
-1	1	-68	14	3	24
-1	1	-67	0	0	100
-1	1	-66	11	3	30
-1	1	-65	14	3	20
-1	1	-64	15	2	14
-1	1	-63	0	0	100
-1	1	-62	0	0	100
-1	1	-61	11	2	16
-1	1	-60	16	2	11
-1	1	-59	10	2	17
-1	1	-58	0	0	100
-1	1	-57	13	2	14
-1	1	-56	9	2	20
-1	1	-55	6	2	29
-1	1	-54	4	2	48
-1	1	-53	7	2	26
-1	1	-52	6	2	28
-1	1	-51	9	2	20
-1	1	-50	10	2	20
-1	1	-49	10	2	21
-1	1	-48	9	2	20
-1	1	-47	2	2	82
-1	1	-46	15	2	14
-1	1	-45	0	0	100
-1	1	-44	8	2	21
-1	1	-43	0	0	100
-1	1	-42	9	2	20
-1	1	-41	0	0	100
-1	1	-40	0	0	100
-1	1	-39	10	2	20
-1	1	-38	0	0	100
-1	1	-37	0	0	100
-1	1	-36	9	2	19
-1	1	-35	0	0	100
-1	1	-34	11	2	18
-1	1	-33	4	2	46
-1	1	-32	0	0	100
-1	1	-31	3	2	71
-1	1	-30	11	2	19
-1	1	-29	0	0	100
-1	1	-28	0	0	100
-1	1	-27	7	2	28
-1	1	-26	0	0	100
-1	1	-26	0	0	100
-1	1	-25	0	0	100
-1	1	-24	14	2	14
-1	1	-23	8	2	25
-1	1	-22	8	2	21
-1	1	-21	0	0	100
-1	1	-20	0	0	100
-1	1	-19	0	0	100
-1	1	-18	11	2	18
-1	1	-17	4	2	45
-1	1	-16	8	2	25
-1	1	-15	0	0	100
-1	1	-14	0	0	100
-1	1	-13	0	0	100
-1	1	-12	7	3	38
-1	1	-11	0	0	100
-1	1	-10	10	2	19
-1	1	-9	0	0	100

-1	1	-9	22	7	32
-1	1	-8	14	6	48
-1	1	-8	0	0	100
-1	1	-7	21	6	28
-1	1	-7	0	0	100
-1	1	-6	44	6	15
-1	1	-6	3	7	251
-1	1	-5	13	5	36
-1	1	-5	0	0	100
-1	1	-4	19	5	27
-1	1	-3	0	0	100
-1	1	-2	41	5	11
-1	1	-1	37	6	17
-1	1	0	77	9	11
-1	1	1	15	6	41
-1	1	2	0	0	100
-1	1	3	19	7	35
-1	1	4	45	7	17
-1	1	5	46	7	15
-1	1	6	0	0	100
-1	1	7	11	3	31
-1	1	7	0	0	100
-1	1	8	15	3	23
-1	1	8	18	4	20
-1	1	9	19	4	21
-1	1	10	0	0	100
-1	1	10	9	4	42
-1	1	11	8	3	35
-1	1	11	14	2	17
-1	1	12	0	0	100
-1	1	13	18	3	17
-1	1	14	20	3	14
-1	1	15	11	2	22
-1	1	16	10	2	22
-1	1	17	7	3	39
-1	1	18	0	0	100
-1	1	19	7	2	33
-1	1	20	5	2	37
-1	1	21	5	2	50
-1	1	22	0	0	100
-1	1	23	15	2	15
-1	1	24	13	3	20
-1	1	25	8	3	34
-1	1	26	10	2	23
-1	1	27	12	2	17
-1	1	28	0	0	100
-1	1	29	11	2	22
-1	1	30	12	2	21
-1	1	31	12	2	19
-1	1	32	12	2	19
-1	1	33	3	2	52
-1	1	35	6	2	30
-1	1	36	2	2	100
-1	1	37	0	0	100
-1	1	38	10	2	24
-1	1	39	7	2	30
-1	1	40	0	0	100
-1	1	41	0	0	100
-1	1	42	7	3	38
-1	1	43	0	0	100
-1	1	44	0	0	100
-1	1	45	13	2	19
-1	1	46	13	2	18
-1	1	48	1	2	173
-1	1	49	12	2	21
-1	1	50	7	2	35
-1	1	51	7	2	36
-1	1	52	11	2	23
-1	1	53	0	0	100
-1	1	54	0	0	100
-1	1	55	0	0	100
-1	1	56	9	2	24
-1	1	57	3	2	75
-1	1	58	17	3	16
-1	1	59	12	2	21
-1	1	59	13	2	19
-1	1	60	18	2	13
-1	1	61	14	2	16
-1	1	62	6	2	40
-1	1	63	0	0	100
-1	1	64	0	0	100
-1	1	65	6	2	41
-1	1	66	0	0	100
-1	1	67	0	0	100
-1	1	68	14	3	22
-1	1	69	20	3	16
-1	1	70	13	3	27
-1	1	71	15	4	24
-1	1	72	0	0	100
-1	1	73	21	3	17
-1	1	74	0	0	100
-1	1	75	0	0	100
-1	1	76	0	0	100
-1	1	77	9	3	34
-1	1	78	0	0	100
-1	1	79	6	3	48
-1	1	80	11	3	27
-1	2	-76	0	0	100
-1	2	-75	23	4	16
-1	2	-74	12	4	35
-1	2	-73	22	4	17
-1	2	-72	6	4	61
-1	2	-71	0	0	100
-1	2	-70	25	3	14
-1	2	-69	23	4	18
-1	2	-68	0	0	100
-1	2	-67	0	0	100
-1	2	-66	14	4	25
-1	2	-65	0	0	100
-1	2	-64	0	0	100
-1	2	-63	2	4	168
-1	2	-62	11	4	34
-1	2	-61	13	4	30
-1	2	-4	24	11	47
-1	2	-2	29	9	31
-1	2	-1	0	0	100
-1	2	0	0	0	100
-1	2	1	0	0	100
-1	2	2	29	8	29
-1	2	3	49	10	21
-1	2	4	0	0	100
-1	2	4	30	11	35
-1	2	5	0	0	100
-1	2	6	0	0	100
-1	2	7	0	0	100
-1	2	8	47	10	21
-1	2	9	0	0	100
-1	2	9	10	10	104
-1	2	9	28	6	20
-1	2	10	0	0	100
-1	2	11	6	5	79
-1	2	12	18	4	25
-1	2	13	27	4	15
-1	2	14	9	4	50
-1	2	15	6	4	66
0	-2	-40	6	3	50
0	-2	-39	20	3	16
0	-2	-38	0	0	100
0	-2	-37	0	0	100
0	-2	-36	21	3	14
0	-2	-35	20	3	15
0	-2	-34	15	3	18
0	-2	-33	0	0	100
0	-2	36	32	4	12
0	-2	37	24	4	16
0	-2	37	25	4	17
0	-2	38	0	0	100
0	-2	39	21	4	18
0	-2	40	32	4	12
0	-2	41	6	4	61
0	-1	-80	9	3	34
0	-1	-79	12	3	29
0	-1	-78	0	0	100
0	-1	-77	19	3	18
0	-1	-76	0	0	100
0	-1	-75	12	3	27
0	-1	-74	3	3	87
0	-1	-73	15	3	22
0	-1	-72	0	0	100
0	-1	-71	16	3	19
0	-1	-70	8	3	36
0	-1	-69	14	3	22
0	-1	-68	11	3	30
0	-1	-67	15	4	23
0	-1	-66	0	0	100
0	-1	-65	0	0	100
0	-1	-64	10	2	17
0	-1	-63	7	2	24
0	-1	-62	0	0	100
0	-1	-61	6	2	29
0	-1	-60	0	0	100
0	-1	-59	0	0	100
0	-1	-58	11	2	16
0	-1	-57	6	2	27
0	-1	-56	2	2	100
0	-1	-55	7	2	24
0	-1	-54	0	0	100
0	-1	-53	8	2	26
0	-1	-44	0	0	100
0	-1	-43	0	0	100
0	-1	-41	14	4	32
0	-1	-40	17	5	26
0	-1	-39	23	4	19
0	-1	-38	18	7	38
0	-1	-37	0	0	100
0	-1	-35	24	6	26
0	-1	-34	55	7	12
0	-1	-33	45	6	14
0	-1	-32	36	7	19
0	-1	-30	55	6	12
0	-1	-29	23	6	28
0	-1	-28	15	5	32
0	-1	-27	0	0	100
0	-1	-26	30	7	23
0	-1	-25	0	0	100
0	-1	-24	25	7	28
0	-1	-23	17	7	39
0	-1	-22	31	6	21
0	-1	-20	15	2	13
0	-1	-18	28	6	23
0	-1	-17	11	2	19
0	-1	-16	0	0	100
0	-1	-15	31	6	21
0	-1	-13	10	2	22
0	-1	6	29	7	23
0	-1	14	10	2	25
0	-1	16	16	2	15
0	-1	17	0	0	100
0	-1	18	12	2	14
0	-1	19	9	2	19
0	-1	20	18	2	10
0	-1	21	15	2	13
0	-1	22	9	2	26
0	-1	23	12	2	19
0	-1	24	7	2	24
0	-1	25	0	0	100
0	-1	26	15	2	13
0	-1	27	11	2	21
0	-1	28	0	0	100
0	-1	29	0	0	100
0	-1	30	9	2	23
0	-1	31	14	2	16
0	-1	32	14	2	14
0	-1	33	19	2	12
0	-1	34	6	2	34
0	-1	35	11	2	15
0	-1	36	11	2	15
0	-1	37	8	2	25
0	-1	38	0	0	100
0	-1	38	8	2	30
0	-1	39	0	0	100
0	-1	40	9	2	18
0	-1	41	7	2	25
0	-1	42	16	2	13
0	-1	43	8	2	24
0	-1	44	0	0	100
0	-1	45	14	2	14
0	-1	46	8	2	23
0	-1	47	14	2	12
0	-1	48	11	2	18
0	-1	49	4	2	53
0	-1	50	13	2	16
0	-1	51	11	2	18
0	-1	52	17	2	10
0	-1	53	0	0	100
0	-1	54	0	0	100
0	-1	55	10	2	21
0	-1	56	0	0	100
0	-1	57	13	2	16
0	-1	58	13	2	17
0	-1	59	5	2	47
0	-1	60	0	0	100
0	-1	61	10	2	22
0	-1	62	0	0	100
0	-1	63	0	0	100
0	-1	64	13	2	17
0	-1	65	14	2	17
0	-1	65	14	2	18
0	-1	66	15	2	17
0	-1	67	15	3	22
0	-1	68	16	3	20

0	-1	69	0	0	100
0	-1	70	13	3	26
0	-1	71	9	3	34
0	-1	72	0	0	100
0	-1	73	3	3	95
0	-1	74	0	0	100
0	-1	75	0	0	100
0	-1	76	16	3	19
0	-1	77	0	0	100
0	-1	78	11	3	29
0	-1	79	0	0	100
0	-1	80	21	3	15
0	1	-80	0	0	100
0	1	-79	15	3	21
0	1	-78	13	3	24
0	1	-77	14	3	21
0	1	-76	18	3	19
0	1	-75	0	0	100
0	1	-74	9	3	38
0	1	-73	12	3	25
0	1	-72	15	4	24
0	1	-71	16	3	19
0	1	-70	18	3	18
0	1	-69	10	3	32
0	1	-68	0	0	100
0	1	-67	9	3	40
0	1	-66	0	0	100
0	1	-65	0	0	100
0	1	-64	0	0	100
0	1	-63	12	2	14
0	1	-62	12	2	17
0	1	-61	9	2	18
0	1	-60	2	2	77
0	1	-59	0	0	100
0	1	-58	2	2	77
0	1	-57	5	2	38
0	1	-56	6	2	31
0	1	-55	11	2	16
0	1	-54	7	2	24
0	1	-53	0	0	100
0	1	-52	8	2	21
0	1	-51	0	0	100
0	1	-50	11	2	18
0	1	-49	0	0	100
0	1	-48	14	2	12
0	1	-47	11	2	16
0	1	-46	0	0	100
0	1	-45	12	2	14
0	1	-44	5	2	33
0	1	-43	0	0	100
0	1	-42	15	2	12
0	1	-41	0	0	100
0	1	-40	15	2	12
0	1	-39	0	0	100
0	1	-38	6	2	31
0	1	-37	18	2	10
0	1	-36	9	2	23
0	1	-35	0	0	100
0	1	-34	8	2	21
0	1	-33	8	2	21
0	1	-32	5	2	32
0	1	-31	12	2	17
0	1	-30	9	2	22
0	1	-29	7	2	24
0	1	-28	5	2	39
0	1	-27	12	2	16
0	1	-26	15	2	14
0	1	-25	16	2	12
0	1	-24	0	0	100
0	1	-23	11	2	17
0	1	-22	4	2	58
0	1	-21	31	7	22
0	1	-21	15	2	13
0	1	-20	4	2	53
0	1	-19	36	7	20
0	1	-19	0	0	100
0	1	-18	0	0	100
0	1	-17	25	6	25
0	1	-16	10	2	22
0	1	-15	0	0	100
0	1	-14	0	0	100
0	1	-14	43	7	15
0	1	-13	10	2	20
0	1	-12	0	0	100
0	1	-12	9	2	21
0	1	-11	26	7	25
0	1	-11	19	7	36

0	1	-10	24	6	26
0	1	-10	29	7	23
0	1	-9	15	4	29
0	1	-8	14	6	46
0	1	-7	13	5	37
0	1	-6	17	4	25
0	1	-5	25	4	18
0	1	-4	27	5	17
0	1	-3	40	4	11
0	1	-2	29	5	16
0	1	-1	16	4	29
0	1	0	41	6	16
0	1	0	0	0	100
0	1	1	0	0	100
0	1	2	27	6	23
0	1	3	23	6	25
0	1	4	43	8	18
0	1	4	20	6	32
0	1	5	0	0	100
0	1	5	0	0	100
0	1	6	4	6	180
0	1	7	11	7	68
0	1	7	0	0	100
0	1	8	16	4	29
0	1	8	36	6	17
0	1	9	0	0	100
0	1	9	21	6	30
0	1	10	0	0	100
0	1	10	7	4	57
0	1	11	14	2	17
0	1	11	6	3	50
0	1	12	0	0	100
0	1	12	11	3	23
0	1	13	0	0	100
0	1	13	13	3	20
0	1	14	21	3	14
0	1	15	7	2	34
0	1	15	10	3	27
0	1	16	0	0	100
0	1	17	3	2	71
0	1	18	10	2	19
0	1	19	9	2	23
0	1	20	13	3	20
0	1	21	10	2	25
0	1	22	4	3	68
0	1	23	8	3	34
0	1	24	13	2	19
0	1	25	4	2	56
0	1	26	13	2	18
0	1	27	0	0	100
0	1	28	17	2	15
0	1	29	0	0	100
0	1	30	14	2	17
0	1	31	7	2	35
0	1	32	11	2	20
0	1	33	9	2	25
0	1	33	6	2	37
0	1	34	6	2	35
0	1	35	11	2	18
0	1	36	9	2	19
0	1	37	9	2	25
0	1	38	11	2	22
0	1	39	0	0	100
0	1	40	4	2	65
0	1	41	8	2	29
0	1	42	10	2	24
0	1	43	0	0	100
0	1	44	8	2	28
0	1	45	3	2	85
0	1	46	13	3	21
0	1	46	0	0	100
0	1	47	9	2	24
0	1	48	14	3	19
0	1	49	7	2	33
0	1	50	11	2	20
0	1	51	0	0	100
0	1	52	12	2	20
0	1	53	0	0	00
0	1	54	0	0	100
0	1	55	5	2	51
0	1	56	18	2	12
0	1	57	0	0	100
0	1	58	18	2	19
0	1	59	15	2	14
0	1	60	0	0	100
0	1	61	0	0	100
0	1	62	15	2	17

0	1	63	0	0	100
0	1	64	0	0	100
0	1	65	11	2	23
0	1	66	0	0	100
0	1	67	10	3	27
0	1	68	15	3	22
0	1	69	23	2	11
0	1	70	10	3	34
0	1	71	18	3	18
0	1	72	14	3	24
0	1	73	25	3	10
0	1	74	5	2	33
0	1	75	16	2	12
0	1	76	0	0	100
0	1	77	18	2	12
0	1	78	7	2	29
0	1	79	0	0	100
0	1	80	0	0	100
0	2	-76	0	0	100
0	2	-75	0	0	100
0	2	-74	0	0	100
0	2	-73	0	0	100
0	2	-72	9	4	44
0	2	-71	7	4	56
0	2	-70	0	0	100
0	2	-69	0	0	100
0	2	-68	0	0	100
0	2	-67	30	5	16
0	2	-66	0	0	100
0	2	-65	0	0	100
0	2	-64	36	4	11
0	2	-63	26	4	16
0	2	-62	0	0	100
0	2	-61	0	0	100
0	2	-32	21	3	15
0	2	-31	0	0	100
0	2	-30	13	3	26
0	2	-29	0	0	100
0	2	37	14	4	29
0	2	49	8	4	48
0	2	50	18	4	22
0	2	51	0	0	100
0	2	52	11	4	35
0	2	53	11	4	35
0	2	54	14	4	31
0	2	55	0	0	100
0	2	56	2	4	153
0	2	57	0	0	100
0	2	58	17	4	26
1	-2	-80	0	0	100
1	-2	-79	19	4	21
1	-2	-78	18	4	21
1	-2	-77	0	0	100
1	-2	-76	14	4	26
1	-2	-75	18	4	23
1	-2	-74	6	4	66
1	-2	-73	23	4	17
1	-2	-72	0	0	100
1	-2	-71	11	4	37
1	-2	-70	22	4	18
1	-2	-69	24	4	16
1	-2	-68	22	4	20
1	-2	-67	26	4	17
1	-2	-5	0	0	100
1	-2	-4	0	0	100
1	-2	-3	0	0	100
1	-2	-2	0	0	100
1	-2	-1	26	8	32
1	-2	0	27	8	31
1	-2	1	43	10	23
1	-2	3	24	10	43
1	-2	4	33	7	22
1	-2	5	31	10	32
1	-2	6	82	9	12
1	-2	9	22	4	20
1	-2	10	16	5	28
1	-2	11	16	4	26
1	-2	12	31	4	14
1	-2	13	20	4	20
1	-1	-80	0	0	100
1	-1	-79	0	0	100
1	-1	-78	0	0	100
1	-1	-77	0	0	100
1	-1	-76	0	0	100
1	-1	-75	16	3	19
1	-1	-74	0	0	100
1	-1	-73	16	3	22

1	-1	-72	15	3	22
1	-1	-71	0	0	100
1	-1	-70	12	3	26
1	-1	-69	0	0	100
1	-1	-68	7	3	51
1	-1	-67	15	3	20
1	-1	-66	0	0	100
1	-1	-65	0	0	100
1	-1	-65	0	0	100
1	-1	-64	0	0	100
1	-1	-64	0	0	100
1	-1	-63	8	2	22
1	-1	-62	6	2	27
1	-1	-61	12	2	14
1	-1	-60	3	1	50
1	-1	-59	0	0	100
1	-1	-58	6	2	28
1	-1	-57	6	2	29
1	-1	-56	0	0	100
1	-1	-55	12	2	15
1	-1	-54	0	0	100
1	-1	-53	6	2	28
1	-1	-51	5	2	34
1	-1	-46	26	5	18
1	-1	-45	17	4	26
1	-1	-44	7	5	63
1	-1	-43	10	4	44
1	-1	-42	14	5	33
1	-1	-42	9	4	50
1	-1	-41	31	4	15
1	-1	-40	26	5	18
1	-1	-39	0	0	100
1	-1	-38	38	7	19
1	-1	-37	8	6	85
1	-1	-37	12	2	14
1	-1	-36	19	5	24
1	-1	-35	26	6	25
1	-1	-34	0	0	100
1	-1	-33	29	6	22
1	-1	-32	52	7	14
1	-1	-31	25	7	28
1	-1	-31	46	7	15
1	-1	-30	17	6	36
1	-1	-29	0	0	100
1	-1	-28	23	4	19
1	-1	-27	30	6	21
1	-1	-26	10	2	17
1	-1	-25	4	2	39
1	-1	-24	36	7	19
1	-1	-23	9	6	68
1	-1	-22	16	6	40
1	-1	-21	6	2	35
1	-1	-20	19	2	12
1	-1	-19	0	0	100
1	-1	-18	8	2	23
1	-1	-17	8	2	28
1	-1	-16	0	0	100
1	-1	-15	12	2	20
1	-1	-14	12	2	17
1	-1	-13	11	2	17
1	-1	-12	6	2	39
1	-1	-11	14	2	16
1	-1	8	19	4	22
1	-1	11	13	3	20
1	-1	12	15	2	16
1	-1	13	4	3	76
1	-1	14	14	3	19
1	-1	15	0	0	100
1	-1	16	19	3	15
1	-1	17	0	0	100
1	-1	18	0	0	100
1	-1	19	4	2	49
1	-1	20	12	2	16
1	-1	21	12	2	17
1	-1	22	0	0	100
1	-1	23	0	0	100
1	-1	24	8	2	22
1	-1	25	11	2	18
1	-1	26	0	0	100
1	-1	27	0	0	100
1	-1	28	13	2	14
1	-1	29	15	2	14
1	-1	30	0	0	100
1	-1	31	16	2	13
1	-1	32	17	2	12
1	-1	33	11	2	17
1	-1	34	6	2	34
1	-1	35	0	0	100
1	-1	36	12	2	17
1	-1	37	0	0	100
1	-1	38	24	2	9
1	-1	39	4	2	53
1	-1	40	19	2	11
1	-1	41	11	2	18
1	-1	42	0	0	100
1	-1	43	15	2	13
1	-1	44	16	2	14
1	-1	45	12	2	16
1	-1	46	15	2	11
1	-1	47	3	2	58
1	-1	48	0	0	100
1	-1	49	23	2	8
1	-1	50	10	2	21
1	-1	51	0	0	100
1	-1	52	10	2	19
1	-1	53	12	2	17
1	-1	54	0	0	100
1	-1	55	0	0	100
1	-1	55	0	0	100
1	-1	56	8	2	23
1	-1	57	7	2	28
1	-1	58	0	0	100
1	-1	59	3	2	87
1	-1	60	9	3	33
1	-1	61	8	2	27
1	-1	62	0	0	100
1	-1	63	6	2	30
1	-1	64	18	2	10
1	-1	65	11	2	23
1	-1	66	0	0	100
1	-1	67	0	0	100
1	-1	68	0	0	100
1	-1	69	19	2	13
1	-1	70	25	2	10
1	-1	71	5	2	50
1	-1	72	15	2	13
1	-1	73	6	2	35
1	-1	74	17	2	14
1	-1	75	8	2	23
1	-1	76	7	2	27
1	-1	77	2	2	100
1	-1	78	9	2	20
1	-1	79	10	2	21
1	-1	80	3	2	65
1	1	-80	5	3	64
1	1	-79	23	3	15
1	1	-78	16	3	21
1	1	-77	30	3	11
1	1	-76	11	3	29
1	1	-75	20	3	16
1	1	-74	0	0	100
1	1	-73	17	3	19
1	1	-72	36	3	10
1	1	-71	25	3	14
1	1	-70	0	0	100
1	1	-69	22	3	16
1	1	-68	32	3	10
1	1	-67	22	4	19
1	1	-66	3	3	104
1	1	-65	7	3	45
1	1	-64	0	0	100
1	1	-63	0	0	100
1	1	-62	5	2	33
1	1	-61	8	2	29
1	1	-60	0	0	100
1	1	-59	0	0	100
1	1	-58	9	2	27
1	1	-57	6	2	39
1	1	-56	14	2	18
1	1	-55	6	2	35
1	1	-54	10	2	23
1	1	-53	0	0	100
1	1	-52	13	2	15
1	1	-51	14	2	12
1	1	-50	7	2	25
1	1	-49	11	3	24
1	1	-48	0	0	100
1	1	-47	17	2	14
1	1	-46	0	0	100
1	1	-45	0	0	100
1	1	-44	13	2	19
1	1	-43	2	2	110
1	1	-42	0	0	100
1	1	-41	0	0	100
1	1	-40	0	0	100
1	1	-39	11	2	23
1	1	-38	0	0	100
1	1	-37	0	0	100
1	1	-36	3	3	94
1	1	-35	8	2	32
1	1	-34	14	3	20
1	1	-33	0	0	100
1	1	-32	8	2	31
1	1	-31	0	0	100
1	1	-30	0	0	100
1	1	-29	8	4	49
1	1	-28	0	0	100
1	1	-27	0	0	100
1	1	-27	15	4	23
1	1	-26	16	4	22
1	1	-25	11	4	32
1	1	-24	0	0	100
1	1	-24	9	4	41
1	1	-23	26	4	15
1	1	-23	0	0	100
1	1	-22	17	3	20
1	1	-15	14	7	51
1	1	-14	10	5	50
1	1	-13	10	5	45
1	1	-5	40	8	19
1	1	2	60	8	13
1	1	3	56	8	15
1	1	11	25	4	16
1	1	26	13	3	22
1	1	27	0	0	100
1	1	29	21	3	13
1	1	42	6	3	42
1	1	43	0	0	100
1	1	44	10	3	27
1	1	45	0	0	100
1	1	46	16	3	17
1	1	47	0	0	100
1	1	48	18	3	16
1	1	49	22	3	14
1	1	50	15	3	18
1	1	51	9	3	29
1	1	52	14	3	20
1	1	53	19	3	14
1	1	54	4	3	66
1	1	55	0	0	100
1	1	56	6	3	49
1	1	57	20	3	14
1	1	58	14	3	20
1	1	59	13	3	21
1	1	60	0	0	100
1	1	61	17	2	15
1	1	61	17	2	15
1	1	62	17	3	15
1	1	63	21	3	13
1	1	64	4	4	83
1	1	65	0	0	100
1	1	66	26	3	13
1	1	67	10	3	32
1	1	68	16	4	23
1	1	69	11	3	32
1	1	70	24	3	14
1	1	71	0	0	100
1	1	72	6	3	55
1	1	73	25	4	15
1	1	74	17	3	20
1	1	75	0	0	100
1	1	76	16	2	14
1	1	77	10	2	21
1	1	78	0	0	100
1	1	79	11	2	20
1	1	80	11	2	20
1	2	-42	25	3	10
1	2	-61	0	0	100
1	2	-60	0	0	100
1	2	-59	4	2	54
1	2	-58	0	0	100
1	2	-57	0	0	100
1	2	-56	0	0	100
1	2	-55	12	2	20
1	2	-54	12	2	20
1	2	-53	19	2	12
1	2	-52	12	2	18
1	2	-51	15	2	16
1	2	-50	22	2	11
2	-2	-73	26	2	9
2	-1	-80	20	4	18

2	-1	-79	12	3	27
2	-1	-78	10	3	35
2	-1	-77	0	0	100
2	-1	-76	24	3	14
2	-1	-75	0	0	100
2	-1	-74	26	4	15
2	-1	-73	20	3	17
2	-1	-72	26	2	9
2	-1	-71	24	2	9
2	-1	-70	0	0	100
2	-1	-69	0	0	100
2	-1	-68	0	0	100
2	-1	-67	25	2	10
2	-1	-66	0	0	100
2	-1	-65	0	0	100
2	-1	-64	0	0	100
2	-1	-63	11	3	30
2	-1	-62	13	2	15
2	-1	-61	15	2	14
2	-1	-60	9	2	25
2	-1	-59	0	0	100
2	-1	-58	4	2	51
2	-1	-57	0	0	100
2	-1	-56	11	2	19
2	-1	-55	7	2	30
2	-1	-54	5	2	52
2	-1	-53	7	2	31
2	-1	-52	0	0	100
2	-1	-51	4	2	40
2	-1	-50	6	2	41
2	-1	-49	8	3	31
2	-1	-48	0	0	100
2	-1	-47	10	3	27
2	-1	-46	15	3	19
2	-1	-45	16	3	17
2	-1	-44	17	3	20
2	-1	-43	22	3	15
2	-1	-24	0	0	100
2	-1	-23	12	3	25
2	-1	-22	13	3	20
2	-1	-21	0	0	100
2	-1	-20	0	0	100
2	-1	-19	5	3	55
2	-1	-18	21	3	14
2	-1	-17	0	0	100
2	-1	-16	0	0	100
2	-1	-15	0	0	100
2	-1	-14	0	0	100
2	-1	-13	12	3	26
2	-1	-12	0	0	100
2	-1	-11	4	3	87
2	-1	-9	0	0	100
2	-1	-8	53	5	10
2	-1	5	31	6	19
2	-1	12	10	3	32
2	-1	13	5	3	58
2	-1	14	0	0	100
2	-1	15	9	3	32
2	-1	17	0	0	100
2	-1	18	10	3	27
2	-1	19	8	3	32
2	-1	20	15	2	15
2	-1	21	23	2	9
2	-1	22	17	2	14
2	-1	23	18	2	13
2	-1	24	12	2	21
2	-1	25	25	2	10
2	-1	26	0	0	100
2	-1	27	0	0	100
2	-1	28	18	2	12
2	-1	29	19	2	13
2	-1	30	8	2	28
2	-1	31	5	2	51
2	-1	32	9	2	29
2	-1	33	7	2	36
2	-1	34	4	2	65
2	-1	35	0	0	100
2	-1	36	0	0	100
2	-1	37	0	0	100
2	-1	38	0	0	100
2	-1	39	20	2	12
2	-1	40	0	0	100
2	-1	41	0	0	100
2	-1	42	22	2	9
2	-1	43	0	0	100
2	-1	44	22	2	10
2	-1	45	0	0	100
2	-1	46	20	2	11
2	-1	47	6	2	34
2	-1	48	21	2	11
2	-1	49	21	2	11
2	-1	50	9	2	26
2	-1	51	13	2	19
2	-1	52	9	2	23
2	-1	53	0	0	100
2	-1	54	15	2	16
2	-1	55	13	2	18
2	-1	56	0	0	100
2	-1	57	0	0	100
2	-1	58	14	2	18
2	-1	59	14	2	15
2	-1	60	9	2	24
2	-1	61	16	2	14
2	-1	62	13	2	17
2	-1	63	0	0	100
2	-1	64	0	0	100
2	-1	65	8	2	29
2	-1	66	8	2	28
2	-1	67	23	4	16
2	-1	68	40	4	10
2	-1	69	35	4	12
2	-1	70	0	0	100
2	-1	71	14	4	29
2	-1	72	18	4	21
2	-1	73	0	0	100
2	-1	74	20	4	18
2	-1	75	0	0	100
2	-1	76	16	2	14
2	-1	77	13	2	15
2	-1	78	0	0	100
2	-1	79	19	2	12
2	-1	80	23	2	9
2	0	-80	0	0	100
2	0	-79	16	3	21
2	0	-78	16	3	19
2	0	-77	11	3	30
2	0	-76	11	3	29
2	0	-75	9	3	33
2	0	-74	9	3	37
2	0	-73	20	4	18
2	0	-72	12	3	30
2	0	-71	9	3	37
2	0	-70	15	3	22
2	0	-69	13	4	27
2	0	-68	33	4	12
2	0	-67	9	4	40
2	0	-66	16	4	23
2	0	-65	19	3	18
2	0	-64	8	4	44
2	0	-63	3	3	100
2	0	-62	0	0	100
2	0	-61	0	0	100
2	0	-60	3	2	52
2	0	-59	11	2	19
2	0	-58	0	0	100
2	0	-57	0	0	100
2	0	-56	0	0	100
2	0	-55	11	2	22
2	0	-54	12	2	20
2	0	-53	0	0	100
2	0	-52	17	2	15
2	0	-51	13	2	18
2	0	-50	16	3	17
2	0	-49	0	0	100
2	0	-48	18	3	16
2	0	-47	14	3	19
2	0	-46	10	3	27
2	0	-45	8	2	30
2	0	-44	13	3	20
2	0	-43	12	3	24
2	0	-42	0	0	100
2	0	-41	3	3	84
2	0	-40	0	0	100
2	0	-39	13	3	21
2	0	-38	0	0	100
2	0	-37	10	2	21
2	0	-36	11	2	21
2	0	-35	0	0	100
2	0	-34	3	2	82
2	0	-33	8	3	36
2	0	-32	20	3	13
2	0	-31	10	2	24
2	0	-15	24	5	19
2	0	-6	38	7	19
2	0	39	0	0	100
2	0	40	11	2	22
2	0	41	9	2	26
2	0	42	0	0	100
2	0	43	17	3	15
2	0	44	9	3	28
2	0	45	11	3	23
2	0	46	5	2	52
2	0	47	12	3	22
2	0	48	13	3	22
2	0	49	0	0	100
2	0	50	0	0	100
2	0	51	17	3	15
2	0	52	7	2	35
2	0	53	0	0	100
2	0	54	0	0	100
2	0	55	0	0	100
2	0	56	14	3	21
2	0	57	10	3	28
2	0	58	0	0	100
2	0	59	13	3	20
2	0	60	13	3	22
2	0	61	0	0	100
2	0	62	0	0	100
2	0	63	0	0	100
2	0	64	14	4	27
2	0	65	11	3	28
2	0	66	0	0	100
2	0	67	0	0	100
2	0	68	17	4	21
2	0	69	25	4	15
2	0	70	27	4	13
2	0	71	24	4	15
2	0	72	20	3	17
2	0	73	31	4	12
2	0	74	18	4	20
2	0	75	25	2	9
2	0	76	0	0	100
2	0	77	22	2	10
2	0	78	0	0	100
2	0	79	11	2	18
2	0	80	0	0	100
2	1	-80	15	2	13
2	1	-79	24	3	12
2	1	-78	0	0	100
2	1	-77	14	2	17
2	1	-76	26	2	9
2	1	-75	29	2	8
2	1	-74	8	2	29
2	1	-73	15	2	15
2	1	-72	11	2	19
2	1	-71	12	2	20
2	1	-70	9	2	23
2	1	-69	0	0	100
2	1	-68	22	2	11
2	1	-67	0	0	100
2	1	-66	17	2	13
2	1	-65	3	2	75
2	1	-64	7	2	31
2	1	-63	16	2	14
2	1	-62	0	0	100
2	1	-61	13	2	15
2	1	-60	0	0	100
2	1	-59	15	2	15
2	1	-58	9	2	24
2	1	-57	19	2	12
2	1	-56	28	2	8
2	1	-55	0	0	100
2	1	-54	0	0	100
2	1	-53	26	2	9
2	1	-52	22	2	9
2	1	-51	0	0	100
2	1	-50	11	3	25
2	1	-49	22	3	16
2	1	-48	0	0	100
2	1	-47	0	0	100
2	1	-46	21	3	14
2	1	-45	9	3	31
2	1	-44	13	3	23
2	1	-43	0	0	100
2	1	-42	21	3	15
2	1	-41	16	3	17
2	1	-40	12	3	27
2	1	-39	18	3	17
2	1	-38	0	0	100
2	1	-37	18	3	19
2	1	-36	0	0	100

2	1	-35	3	3	95
2	1	-34	22	3	13
2	1	-33	0	0	100
2	1	-32	0	0	100
2	1	-31	0	0	100
2	1	-30	16	3	19
2	1	-29	21	3	13
2	1	-28	0	0	100
2	1	-27	16	3	19
2	1	-26	0	0	100
2	1	-25	0	0	100
2	1	-24	0	0	100
2	1	-23	0	0	100
2	1	-22	12	3	23
2	1	-21	18	3	19
2	1	-20	15	3	22
2	1	-18	0	0	100
2	1	-17	0	0	100
2	1	-15	25	3	13
2	1	-14	0	0	100
2	1	2	78	8	10
2	1	3	82	10	13
2	1	5	29	9	32
2	1	7	33	6	18
2	1	8	26	7	25
2	1	9	5	6	110
2	1	12	10	4	37
2	1	52	37	4	11
3	-1	-77	37	4	11
3	0	-80	17	4	24
3	0	-79	0	0	100
3	0	-78	21	4	19
3	0	-76	0	0	100
3	0	-75	12	4	34
3	0	-74	20	3	17
3	0	5	0	0	100
3	0	6	22	6	26
3	0	7	45	11	24
3	0	9	0	0	100
3	0	10	27	6	20

PEG Data : Analysis Rfactor v Intensity

Imax	Rfac	Av_I	σ	I/σ	sd
500.	0.241	185.	54.4	3.4	106.9
1000.	0.000	576.	0.0	0.0	157.0
1500.	0.000	0.	0.0	0.0	0.0
2000.	0.000	0.	0.0	0.0	0.0
2500.	0.000	0.	0.0	0.0	0.0
3000.	0.000	0.	0.0	0.0	0.0
3500.	0.000	0.	0.0	0.0	0.0
4000.	0.000	0.	0.0	0.0	0.0
4500.	0.000	0.	0.0	0.0	0.0
5000.	0.000	0.	0.0	0.0	0.0
5500.	0.000	0.	0.0	0.0	0.0
6000.	0.000	0.	0.0	0.0	0.0
19600.	0.000	0.	0.0	0.0	0.0

PEG Data : Analysis of standard deviation v. Intensity

Range	Imin	Imax	Irms	No	Mean	Sigma
1	1.	500.	227.	16.	0.08	0.52
2	500.	1000.	576.	2.	0.00	0.00
3	1000.	1500.	0.	0.	0.00	0.00
4	1500.	2000.	0.	0.	0.00	0.00
5	2000.	2500.	0.	0.	0.00	0.00
6	2500.	3000.	0.	0.	0.00	0.00
7	3000.	3500.	0.	0.	0.00	0.00
8	3500.	4000.	0.	0.	0.00	0.00
9	4000.	4500.	0.	0.	0.00	0.00
10	4500.	5000.	0.	0.	0.00	0.00
11	5000.	5500.	0.	0.	0.00	0.00
12	5500.	6000.	0.	0.	0.00	0.00
13	6000.	19600.	0.	0.	0.00	0.00
Total	1.	19600.	287.	18.	0.07	0.49